A gold rush of artifacts from melting ice *p. 157*

The dynamic lung cancer genome *pp. 169, 251, & 256*

New brain neurons made from astrocytes *p. 237*

Science

$10
10 OCTOBER 2014
sciencemag.org

AAAS



SPECIAL ISSUE

The social life of robots

From automatons to co-workers and companions *p. 178*

CONTENTS



168
Combatting parasitic worms

10 OCTOBER 2014 • VOLUME 346 • ISSUE 6206



SPECIAL SECTION
Robots

INTRODUCTION

178 The social life of robots

NEWS

180 Meet your new co-worker
By J. Bohannon

182 Minds of their own
By R. F. Service

184 Getting a feel for the world
By H. DuRant and J. You

186 Helping robots see the big picture
By J. Bohannon

188 In our own image
By D. Normile

190 Humans need not apply
By H. DuRant and J. You

192 The accidental roboticist
By A. Cho

195 Q&A: Robots and the law
By D. Normile

REVIEW

196 Biorobotics: Using robots to emulate and investigate agile locomotion
A. J. Ijspeert

SEE ALSO

- ▸ PERSPECTIVE P. 160
- ▸ REPORT P. 224
- ▸ PODCAST
- ▸ VIDEO
- ▸ SLIDESHOW
- ▸ *SCIENCE TRANSLATIONAL MEDICINE*: 3 RELATED ARTICLES; 8 OCT 2014
- ▸ *SCIENCE* CAREERS
- ▸ WORKING LIFE P. 274
- ▸ sciencemag.org/special/robotics

ON THE COVER



Robotics engineer Hiroshi Ishiguro and his mechanical doppelgänger "Geminoid." No matter how uncannily human some of today's robots may seem, the resemblance is skin deep. An ongoing challenge is endowing robots with the capability to sense their environment and the wits to comprehend it. See page 178. *Photo: Osaka University*

NEWS

IN BRIEF

146 Roundup of the week's news

IN DEPTH

148 **STEM CELL RECIPE OFFERS DIABETES HOPE**
Researchers coax stem cells into becoming long-sought insulin-producing β cells *By G. Vogel*

149 **THE BRAIN'S GPS FINDS TOP HONOR**
Three earn physiology or medicine Nobel for discovering "place" and "grid" cells *By E. Underwood*

149 **PHYSICISTS CHANGE THE LIGHT BULB**
Blue LEDs win 2014 physics Nobel
By D. Normile

150 **A CALL FOR AN NIH YOUTH MOVEMENT**
Wariness greets congressman's proposal to require agency to reduce average age at first grant *By J. Kaiser*

151 **IMAGINING EBOLA'S NEXT MOVE**
Scientists look beyond the models to envision how the epidemic might unfold
By K. Kupferschmidt

152 **CONGRESS, NSF SPAR ON ACCESS TO GRANT FILES**
Grantees wonder what science panel will do with private award details *By J. Mervis*

FEATURES

154 **DON'T BLAME THE BEETLES**
Beetle-killed trees aren't necessarily fueling more severe fires in the west
By C. Carswell

157 **RACING THE THAW**
A trove of artifacts is emerging from alpine ice *By A. Curry*

INSIGHTS

PERSPECTIVES

160 **OF SNAKES AND ROBOTS**
How can snakes and robots move up sandy slopes? *By J. J. Socha*
▸ ROBOTS SECTION P. 178; REPORT P. 224

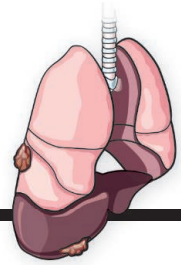
162 **PLANT SYNTHETIC BIOLOGY TAKES ROOT**
Applying the basic principles of synthetic biology to plants shows progress *By J. I. Medford and A. Prasad*

163 **ADJUSTING TO THE FERTILITY BUST**
What is the best response to declining populations? *By T. M. Smeeding*
▸ REPORTS PP. 229 & 234

165 **CATCHING THE QUANTUM SOUND WAVE**
A superconducting qubit built to listen as well as see *By R. Ruskov and C. Tahan*
▸ RESEARCH ARTICLE P. 207

Published by AAAS

CONTENTS



169, 251, & 256
Intratumoral heterogeneity in lung cancer

10 OCTOBER 2014 • VOLUME 346 • ISSUE 6206

166 TAKING THE MEASURE OF CHANGE
Predictive models of biodiversity change are required to inform conservation policy decisions *By B. Collen and E. Nicholson*

168 HALTING HARMFUL HELMINTHS
Vaccines and new drugs are needed to combat parasitic worm infections
By K. F. Hoffmann et al.

169 ATTACK OF THE CLONES
What makes lung cancer so resilient?
By R. Govindan
▸ REPORTS PP. 251 & 256

171 AMPLIFY SCIENTIFIC DISCOVERY WITH ARTIFICIAL INTELLIGENCE
Many human activities are a bottleneck in progress *By Y. Gil* et al.

BOOKS *ET AL.*

173 MARS UP CLOSE
By M. Kaufman, reviewed by M. Moerchen

173 THE ISLAND OF KNOWLEDGE
By M. Gleiser, reviewed by M. A. Goldman

174 THE REMEDY
By T. Goetz, reviewed by M. Maheu-Giroux

LETTERS

175 ALGAL BLOOMS: NOTEWORTHY NITROGEN
By H. W. Paerl et al.

175 ALGAL BLOOMS: PROACTIVE STRATEGY
By M. Qu et al.

176 OCEAN ACIDIFICATION FOILS CHEMICAL SIGNALS
By T. D. Wyatt et al.

176 TECHNICAL COMMENT ABSTRACTS

RESEARCH

IN BRIEF

204 From *Science* and other journals

RESEARCH ARTICLE

207 QUANTUM PROCESSING
Propagating phonons coupled to an artificial atom *M. V. Gustafsson* et al.
▸ PERSPECTIVE P. 165

REPORTS

212 PLANETARY DYNAMICS
A class of warm Jupiters with mutually inclined, apsidally misaligned close friends *R. I. Dawson and E. Chiang*

216 EARLY UNIVERSE
A local clue to the reionization of the universe *S. Borthakur* et al.

219 ORGANIC SYNTHESIS
Asymmetric syntheses of sceptrin and massadine and evidence for biosynthetic enantiodivergence *Z. Ma* et al.

224 ANIMAL MOTION
Sidewinding with minimal slip: Snake and robot ascent of sandy slopes
H. Marvi et al.
▸ PERSPECTIVE P. 160; ROBOTS SECTION P. 178; VIDEO

229 ECONOMIC DEMOGRAPHY
Is low fertility really a problem? Population aging, dependency, and consumption *R. Lee* et al.
▸ PERSPECTIVE P. 163



234 WORLD POPULATION
World population stabilization unlikely this century *P. Gerland* et al.
▸ PERSPECTIVE P. 163

237 ADULT NEUROGENESIS
A latent neurogenic program in astrocytes regulated by Notch signaling in the mouse *J. P. Magnusson* et al.

241 CONSERVATION TARGETS
A mid-term analysis of progress toward international biodiversity targets
D. P. Tittensor et al.

244 CELL-FREE ASSAYS
Spatial organization of cytokinesis signaling reconstituted in a cell-free system *P. A. Nguyen* et al.

248 YEAST MEIOSIS
Sister kinetochores are mechanically fused during meiosis I in yeast
K. K. Sarangapani et al.

LUNG CANCER EVOLUTION

251 Spatial and temporal diversity in genomic instability processes defines lung cancer evolution
E. C. de Bruin et al.

256 Intratumor heterogeneity in localized lung adenocarcinomas delineated by multiregion sequencing *J. Zhang* et al.
▸ PERSPECTIVE P. 169

DEPARTMENTS

145 EDITORIAL
Five years of translation
By Katrina L. Kelner and Marcia McNutt

274 WORKING LIFE
Building the Bionic Woman
By Ayanna Howard
▸ ROBOTS SECTION P. 178

Science Staff 144
New Products 261
Science Careers 262

SCIENCE (ISSN 0036-8075) is published weekly on Friday, except the last week in December, by the American Association for the Advancement of Science, 1200 New York Avenue, NW, Washington, DC 20005. Periodicals mail postage (publication No. 484460) paid at Washington, DC, and additional mailing offices. Copyright © 2014 by the American Association for the Advancement of Science. The title SCIENCE is a registered trademark of the AAAS. Domestic individual membership and subscription (51 issues): $153 ($74 allocated to subscription). Domestic institutional subscription (51 issues): $1282; Foreign postage extra: Mexico, Caribbean (surface mail) $55; other countries (air assist delivery) $85. First class, airmail, student, and emeritus rates on request. Canadian rates with GST available upon request, GST #1254 88122. Publications Mail Agreement Number 1069624. **Printed in the U.S.A.**
Change of address: Allow 4 weeks, giving old and new addresses and 8-digit account number. **Postmaster:** Send change of address to AAAS, P.O. Box 96178, Washington, DC 20090–6178. **Single-copy sales:** $10.00 current issue, $15.00 back issue prepaid includes surface postage; bulk rates on request. **Authorization to photocopy** material for internal or personal use under circumstances not falling within the fair use provisions of the Copyright Act is granted by AAAS to libraries and other users registered with the Copyright Clearance Center (CCC) Transactional Reporting Service, provided that $30.00 per article is paid directly to CCC, 222 Rosewood Drive, Danvers, MA 01923. The identification code for *Science* is 0036-8075. *Science* is indexed in the *Reader's Guide to Periodical Literature* and in several specialized indexes.

IMAGE (BOTTOM) : PHILIP KRANTZ, KRANTZ NANOART

Published by AAAS

Science
AAAS
1200 New York Avenue, NW, Washington, DC 20005
Bateman House, 82-88 Hills Road, Cambridge, UK CB2 1LQ

Editor-in-Chief Marcia McNutt
Executive Editor Monica M. Bradford **News Editor** Tim Appenzeller
Managing Editor, Research Journals Katrina L. Kelner
Deputy Editors Barbara R. Jasny, Andrew M. Sugden(UK), Valda J. Vinson, Jake S. Yeston

Research and Insights

SR. EDITORS Caroline Ash(UK), Gilbert J. Chin, Lisa D. Chong, Maria Cruz(UK), Julia Fahrenkamp-Uppenbrink(UK), Pamela J. Hines, Stella M. Hurtley(UK), Paula A. Kiberstis, Marc S. Lavine(Canada), Kristen L. Mueller, Ian S. Osborne(UK), Beverly A. Purnell, L. Bryan Ray, Guy Riddihough, H. Jesse Smith, Jelena Stajic, Peter Stern(UK), Phillip D. Szuromi, Brad Wible, Nicholas S. Wigginton, Laura M. Zahn **ASSOCIATE EDITORS** Brent Grocholski, Melissa R. McCartney, Margaret M. Moerchen, Sacha Vignieri **ASSOCIATE BOOK REVIEW EDITOR** Valerie B. Thompson **ASSOCIATE LETTERS EDITOR** Jennifer Sills **CHIEF CONTENT PRODUCTION EDITOR** Cara Tate **SR. CONTENT PRODUCTION EDITORS** Harry Jach, Trista Wagoner **CONTENT PRODUCTION EDITORS** Jeffrey E. Cook, Chris Filiatreau, Cynthia Howe, Lauren Kmec, Barbara P. Ordway **SR. EDITORIAL COORDINATORS** Carolyn Kyle, Beverly Shields **EDITORIAL COORDINATORS** Ramatoulaye Diop, Joi S. Granger, Lisa Johnson, Anita Wynn **PUBLICATIONS ASSISTANTS** Aneera Dobbins, Jeffrey Hearn, Dona Mathieu, Le-Toya Mayne Flood, Shannon McMahon, Scott Miller, Jerry Richardson, Rachel Roberts(UK), Alice Whaley(UK), Brian White **EXECUTIVE ASSISTANT** Anna Bashkirova **ADMINISTRATIVE SUPPORT** Janet Clements(UK), Lizanne Newton(UK), Maryrose Madrid, John Wood(UK)

News

NEWS MANAGING EDITOR John Travis **INTERNATIONAL EDITOR** Richard Stone **DEPUTY NEWS EDITORS** Daniel Clery(UK), Robert Coontz, Elizabeth Culotta, David Grimm, David Malakoff, Leslie Roberts **CONTRIBUING EDITORS** Martin Enserink(Europe), Mara Hvistendahl (Asia) **SR. CORRESPONDENTS** Jeffrey Mervis, Elizabeth Pennisi **NEWS WRITERS** Adrian Cho, Jon Cohen, Jennifer Couzin-Frankel, Carolyn Gramling, Eric Hand, Jocelyn Kaiser, Kelly Servick, Robert F. Service, Erik Stokstad, Emily Underwood **INTERNS** Xochitl Rojas-Rocha, Jia You **CONTRIBUTING CORRESPONDENTS** Pallava Bagla(South Asia), Michael Balter(Paris), John Bohannon, Ann Gibbons, Sam Kean, Richard A. Kerr, Eli Kintisch, Kai Kupferschmidt(Berlin), Andrew Lawler, Christina Larson(Beijing), Mitch Leslie, Charles C. Mann, Eliot Marshall, Virginia Morell, Dennis Normile(Tokyo), Heather Pringle, Tania Rabesandratana(Brussels), Gretchen Vogel(Berlin), Lizzie Wade(Mexico City) **CAREERS** Jim Austin(Editor), Donisha Adams **COPY EDITORS** Kara Estelle, Nora Kelly, Jennifer Levin **ADMINISTRATIVE SUPPORT** Scherraine Mack

Executive Publisher Alan I. Leshner
Publisher Beth Rosner **Chief Digital Media Officer** Rob Covey

BUSINESS OPERATIONS AND ADMINISTRATION DIRECTOR Deborah Rivera-Wienhold **BUSINESS SYSTEMS AND FINANCIAL ANALYSIS DIRECTOR** Randy Yi **MANAGER OF FULFILLMENT SYSTEMS** Neal Hawkins **SYSTEMS ANALYST** Nicole Mehmedovich **ASSISTANT DIRECTOR, BUSINESS OPERATIONS** Eric Knott **MANAGER, BUSINESS OPERATIONS** Jessica Tierney **BUSINESS ANALYSTS** Cory Lipman, Cooper Tilton, Celeste Troxler **FINANCIAL ANALYST** Jeremy Clay **RIGHTS AND PERMISSIONS ASSISTANT DIRECTOR** Emilie David **PERMISSIONS ASSOCIATE** Elizabeth Sandler **RIGHTS, CONTRACTS, AND LICENSING ASSOCIATE** Lili Kiser

MARKETING DIRECTOR Ian King **MARKETING MANAGER** Julianne Wielga **MARKETING ASSOCIATE** Elizabeth Sattler **SR. MARKETING EXECUTIVE** Jennifer Reeves **SR. ART ASSOCIATE, PROJECT MANAGER** Tzeitel Sorrosa **ART ASSOCIATE** Seil Lee **ASSISTANT COMMERCIAL EDITOR** Selby Frame **MARKETING PROJECT MANAGER** Angelissa McArthur **SR. WRITER** Bill Zimmer **PROGRAM DIRECTOR, AAAS MEMBER CENTRAL** Peggy Mihelich **FULFILLMENT SYSTEMS AND OPERATIONS** membership@aaas.org **MANAGER, MEMBER SERVICES** Pat Butler **SPECIALISTS** LaToya Casteel, Javia Flemmings, Latasha Russell **MANAGER, DATA ENTRY** Mickie Napoleoni **DATA ENTRY SPECIALISTS** JJ Regan, Jaimee Wise, Fiona Giblin

DIRECTOR, SITE LICENSING Tom Ryan **DIRECTOR, CORPORATE RELATIONS** Eileen Bernadette Moran **SR. PUBLISHER RELATIONS SPECIALIST** Kiki Forsythe **PUBLISHER RELATIONS MANAGER** Catherine Holland **PUBLISHER RELATIONS, EASTERN REGION** Keith Layson **PUBLISHER RELATIONS, WESTERN REGION** Ryan Rexroth **MANAGER, SITE LICENSE OPERATIONS** Iquo Edim **FULFILLMENT ANALYST** Lana Guz **ASSOCIATE DIRECTOR, MARKETING** Christina Schlecht **MARKETING ASSOCIATES** Thomas Landreth, Minah Kim

DIRECTOR OF WEB TECHNOLOGIES Ahmed Khadr **SR. DEVELOPER** Chris Coleman **DEVELOPER** Dan Berger **SR. PROJECT MANAGER** Trista Smith **SYSTEMS ENGINEER** Luke Johnson **PRODUCT MANAGER** Walter Jones

CREATIVE DIRECTOR, MULTIMEDIA Martyn Green **DIRECTOR OF ANALYTICS** Enrique Gonzales **SR. WEB PRODUCER** Sarah Crespi **WEB PRODUCER** Alison Crawford **VIDEO PRODUCER** Nguyen Nguyen **SOCIAL MEDIA PRODUCER** Meghna Sachdev

DIRECTOR OF OPERATIONS PRINT AND ONLINE Lizabeth Harman **PRINT PRODUCTION DIRECTOR** Wendy K. Shank **PREFLIGHT MANAGER** Marcus Spiegler **ASSISTANT MANAGER ONLINE** Lisa Stanford **ASSISTANT MANAGER PRINT** Rebecca Doshi **SR SPECIALISTS** Steve Forrester, Jason Hillman, Antoinette Hodal, Tara Kelly, Anthony Rosen **SPECIALISTS** Jacob Hedrick, Nichele Johnston, Lori Murphy, Kimberley Oster

DESIGN DIRECTOR Beth Rakouskas **ASSOCIATE ART DIRECTOR** Laura Creveling **SR. ILLUSTRATORS** Chris Bickel, Katharine Sutliff **ILLUSTRATOR** Valerie Altounian **SR. ART ASSOCIATES** Holly Bishop, Preston Huey **ART ASSOCIATES** Kay Engman, Garvin Grullón, Chrystal Smith **SR. PHOTO EDITOR** William Douthitt **PHOTO EDITOR** Leslie Blizard

DIRECTOR, GLOBAL COLLABORATION, CUSTOM PUBLICATIONS, ADVERTISING Bill Moran **EDITOR, CUSTOM PUBLISHING** Sean Sanders: 202-326-6430 **ASSISTANT EDITOR, CUSTOM PUBLISHING** Tianna Hicklin: 202-326-6463 **ADVERTISING MARKETING MANAGER** Justin Sawyers: 202-326-7061 science_advertising@aaas.org **ADVERTISING MARKETING ASSOCIATE** Javia Flemmings **ADVERTISING SUPPORT MANAGER** Karen Foote: 202-326-6740 **ADVERTISING PRODUCTION OPERATIONS MANAGER** Deborah Tompkins **SR. PRODUCTION SPECIALIST/GRAPHIC DESIGNER** Amy Hardcastle **PRODUCTION SPECIALIST** Yuse Lajiminmuhip **SR. TRAFFIC ASSOCIATE** Christine Hall **SALES COORDINATOR** Shirley Young **ASSOCIATE DIRECTOR, COLLABORATION, CUSTOM PUBLICATIONS/CHINA/TAIWAN/KOREA/SINGAPORE** Ruolei Wu: +86-186 0822 9345, rwu@aaas.org **COLLABORATION/CUSTOM PUBLICATIONS/JAPAN** Adarsh Sandhu + 81532-81-5142 asandhu@aaas.org **EAST COAST/E. CANADA** Laurie Faraday: 508-747-9395, FAX 617-507-8189 **WEST COAST/W. CANADA** Lynne Stickrod: 415-931-9782, FAX 415-520-6940 **MIDWEST** Jeffrey Dembksi: 847-498-4520 x3005, Steven Loerch: 847-498-4520 x3006 **UK EUROPE/ASIA** Roger Goncalves: TEL/FAX +41 43 243 1358 **JAPAN** Katsuyoshi Fukamizu(Tokyo): +81-3-3219-5777 kfukamizu@aaas.org **CHINA/TAIWAN** Ruolei Wu: +186-0082-9345

WORLDWIDE ASSOCIATE DIRECTOR OF SCIENCE CAREERS Tracy Holmes: +44 (0) 1223 326525, FAX +44 (0) 1223 326532 tholmes@science-int. co.uk **CLASSIFIED** advertise@sciencecareers.org **U.S. SALES** Tina Burks: 202-326-6577, Nancy Toema: 202-326-6578 **SALES ADMINISTRATOR** Marci Gallun **EUROPE/ROW SALES** Axel Gesatzki, Sarah Lelarge **SALES ASSISTANT** Kelly Grace **JAPAN** Hiroyuki Mashiki(Kyoto): +81-75-823-1109 hmashiki@aaas.org **CHINA/TAIWAN** Ruolei Wu: +86-186 0082 9345 rwu@aaas.org **MARKETING MANAGER** Allison Pritchard **MARKETING ASSOCIATE** Aimee Aponte

AAAS BOARD OF DIRECTORS RETIRING PRESIDENT, CHAIR Phillip A. Sharp **PRESIDENT** Gerald R. Fink **PRESIDENT-ELECT** Geraldine (Geri) Richmond **TREASURER** David Evans Shaw **CHIEF EXECUTIVE OFFICER** Alan I. Leshner **BOARD** Bonnie L. Bassler, May R. Berenbaum, Carlos J. Bustamante, Claire M. Fraser, Laura H. Greene, Elizabeth Loftus, Raymond Orbach, Inder M. Verma

SUBSCRIPTION SERVICES For change of address, missing issues, new orders and renewals, and payment questions: 866-434-AAAS (2227) or 202-326-6417, FAX 202-842-1065. Mailing addresses: AAAS, P.O. Box 96178, Washington, DC 20090-6178 or AAAS Member Services, 1200 New York Avenue, NW, Washington, DC 20005

INSTITUTIONAL SITE LICENSES 202-326-6755 **REPRINTS:** Author Inquiries 800-635-7181 **COMMERCIAL INQUIRIES** 803-359-4578 **PERMISSIONS** 202-326-6765, permissions@aaas.org **AAAS Member Services** 202-326-6417 or http://membercentral.aaas.org/discounts

Science serves as a forum for discussion of important issues related to the advancement of science by publishing material on which a consensus has been reached as well as including the presentation of minority of conflicting points of view. Accordingly, all articles published in *Science*—including editorials, news and comment, and books reviews—are signed and reflect the individual views of the authors and not official points of view adopted by AAAS or the institutions with which the authors are affiliated.

INFORMATION FOR AUTHORS See pages 680 and 681 of the 7 February 2014 issue or access www.sciencemag.org/about/authors

SENIOR EDITORIAL BOARD
A. Paul Alivisatos, *Lawrence Berkeley Nat'l. Laboratory,* **Ernst Fehr,** *U. of Zürich*
Susan M. Rosenberg, *Baylor College of Medicine,* **Michael S. Turner,** *U. of Chicago*

BOARD OF REVIEWING EDITORS (Statistics board members indicated with **(S)**)
Adriano Aguzzi, *U. Hospital Zürich*
Takuzo Aida, *U. of Tokyo*
Leslie Aiello, *Wenner-Gren Foundation*
Judith Allen, *U. of Edinburgh*
Sonia Altizer, *U. of Georgia*
Virginia Armbrust, *U. of Washington*
Sebastian Amigorena, *Institut Curie*
Kathryn Anderson, *Memorial Sloan-Kettering Cancer Center*
Peter Andolfatto, *Princeton U.*
Meinrat O. Andreae, *Max-Planck Inst. Mainz*
Paola Arlotta, *Harvard U.*
Johan Auwerx, *EPFL*
David Awschalom, *U. of Chicago*
Jordi Bascompte, *Estación Biológica de Doñana CSIC*
Facundo Batista, *London Research Inst.*
Ray H. Baughman, *U. of Texas, Dallas*
David Baum, *U. of Wisconsin*
Mark Bear, *Massachusetts Inst. of Technology*
Kamran Behnia, *ESPCI-ParisTech*
Yasmine Belkaid, *NIAID, NIH*
Philip Benfey, *Duke U.*
Stephen J. Benkovic, *Penn State U.*
Gabriele Bergers, *U. of California, San Francisco*
Christophe Bernard, *Aix-Marseille U.*
Bradley Bernstein, *Massachusettes General Hospital.*
Peer Bork, *EMBL*
Bernard Bourdon, *Ecole Normale Supérieure de Lyon*
Chris Bowler, *École Normale Supérieure*
Ian Boyd, *U. of St. Andrews*
Emily Brodsky, *U. of California, Santa Cruz*
Ron Brookmeyer, *U. of California Los Angeles* **(S)**
Christian Büchel, *U. Hamburg-Eppendorf*
Joseph A. Burns, *Cornell U.*
William P. Butz, *Population Reference Bureau*
Gyorgy Buzsaki, *New York U. School of Medicine*
Blanche Capel, *Duke U.*
Mats Carlsson, *U. of Oslo*
David Clapham, *Children's Hospital Boston*
David Clary, *U. of Oxford*
Joel Cohen, *Rockefeller U., Columbia U.*
Jonathan D. Cohen, *Princeton U.*
James Collins, *Boston U.*
Robert Cook-Deegan, *Duke U.*
Alan Cowman, *Walter & Eliza Hall Inst.*
Robert H. Crabtree, *Yale U.*
Roberta Croce, *Vrije Universiteit*
Janet Currie, *Princeton U.*
Jeff L. Dangl, *U. of North Carolina*
Tom Daniel, *U. of Washington*
Frans de Waal, *Emory U.*
Stanislas Dehaene, *Collège de France*
Robert Desimone, *MIT*
Claude Desplan, *New York U.*
Ap Dijksterhuis, *Radboud U. of Nijmegen*
Dennis Discher, *U. of Pennsylvania*
Gerald W. Dorn II, *Washington U. School of Medicine*
Jennifer A. Doudna, *U. of California, Berkeley*
Bruce Dunn, *U. of California, Los Angeles*
Christopher Dye, *WHO*
Todd Ehlers, *U. of Tuebingen*
David Ehrhardt, *Carnegie Inst. of Washington*
Tim Elston, *U. of North Carolina at Chapel Hill*
Gerhard Ertl, *Fritz-Haber-Institut, Berlin*
Barry Everitt, *U. of Cambridge*
Ernst Fehr, *U. of Zurich*
Anne C. Ferguson-Smith, *U. of Cambridge*
Michael Feuer, *The George Washington U.*
Peter Fratzl, *Max-Planck Inst.*
Elaine Fuchs, *Rockefeller U.*
Daniel Geschwind, *UCLA*
Andrew Gewirth, *U. of Illinois*
Karl-Heinz Glassmeier, *TU Braunschweig*
Julia R. Greer, *Caltech*
Elizabeth Grove, *U. of Chicago*
Kip Guy, *St. Jude's Children's Research Hospital*
Taekjip Ha, *U. of Illinois at Urbana-Champaign*
Christian Haass, *Ludwig Maximilians U.*
Steven Hahn, *Fred Hutchinson Cancer Research Center*
Michael Hasselmo, *Boston U.*
Martin Heimann, *Max-Planck Inst. Jena*
Yka Helariutta, *U. of Finland*
James A. Hendler, *Rensselaer Polytechnic Inst.*
Janet G. Hering, *Swiss Fed. Inst. of Aquatic Science & Technology*
Michael E. Himmel, *National Renewable Energy Lab.*
Kai-Uwe Hinrichs, *U. of Bremen*
Kei Hirose, *Tokyo Inst. of Technology*
David Hodell, *U. of Cambridge*
David Holden, *Imperial College*
Lora Hooper, *UT Southwestern Medical Ctr. at Dallas*
Thomas Hudson, *Ontario Inst. for Cancer Research*
Raymond Huey, *U. of Washington*
Steven Jacobsen, *U. of California, Los Angeles*
Kai Johnsson, *EPFL Lausanne*
Peter Jonas, *Inst. of Science & Technology (IST) Austria*
Matt Kaeberlein, *U. of Washington*
William Kaelin Jr., *Dana-Farber Cancer Inst.*
Daniel Kahne, *Harvard U.*
Daniel Kammen, *U. of California, Berkeley*
Masashi Kawasaki, *U. of Tokyo*
Joel Kingsolver, *U. of North Carolina at Chapel Hill*
Robert Kingston, *Harvard Medical School*
Alexander Kolodkin, *Johns Hopkins U.*
Roberto Kolter, *Harvard Medical School*
Alberto R. Kornblihtt, *U. of Buenos Aires*
Leonid Kruglyak, *UCLA*
Thomas Langer, *U. of Cologne*
Mitchell A. Lazar, *U. of Pennsylvania*
David Lazer, *Harvard U.*
Thomas Lecuit, *IBDM*
Virginia Lee, *U. of Pennsylvania*
Stanley Lemon, *U. of North Carolina at Chapel Hill*
Ottoline Leyser, *Cambridge U.*
Marcia C. Linn, *U. of California, Berkeley*
Jianguo Liu, *Michigan State U.*
Luis Liz-Marzan, *CIC biomaGUNE*
Jonathan Losos, *Harvard U.*
Ke Lu, *Chinese Acad. of Sciences*
Christian Lüscher, *U. of Geneva*
Laura Machesky, *CRUK Beatson Inst. for Cancer Research*
Anne Magurran, *U. of St. Andrews*
Oscar Marin, *CSIC & U. Miguel Hernández*
Charles Marshall, *U. of California, Berkeley*
C. Robertson McClung, *Dartmouth College*
Graham Medley, *U. of Warwick*
Yasushi Miyashita, *U. of Tokyo*
Richard Morris, *U. of Edinburgh*
Alison Motsinger-Reif, *NC State U.* **(S)**
Sean Munro, *MRC Lab. of Molecular Biology*
Thomas Murray, *The Hastings Center*
James Nelson, *Stanford U. School of Med.*
Karen Nelson, *J. Craig Venter Institute*
Daniel Neumark, *U. of California, Berkeley*
Timothy W. Nilsen, *Case Western Reserve U.*
Pär Nordlund, *Karolinska Inst.*
Helga Nowotny, *European Research Advisory Board*
Ben Olken, *MIT*
Luke O'Neill, *Trinity College, Dublin*
Joe Orenstein, *U. of California Berkeley & Lawrence Berkeley National Lab*
Harry Orr, *U. of Minnesota*
Andrew Oswald, *U. of Warwick*
Steve Palumbi, *Stanford U.*
Jane Parker, *Max-Planck Inst. of Plant Breeding Research*
Giovanni Parmigiani, *Dana-Farber Cancer Inst.* **(S)**
Donald R. Paul, *U. of Texas, Austin*
John H. J. Petrini, *Memorial Sloan-Kettering Cancer Center*
Joshua Plotkin, *U. of Pennsylvania*
Philippe Poulin, *CNRS*
David Randall, *Colorado State U.*
Colin Renfrew, *U. of Cambridge*
Felix Rey, *Institut Pasteur*
Trevor Robbins, *U. of Cambridge*
Jim Roberts, *Fred Hutchinson Cancer Research Ctr.*
Barbara A. Romanowicz, *U. of California,Berkeley*
Jens Rostrup-Nielsen, *Haldor Topsoe*
Mike Ryan, *U. of Texas, Austin*
Mitinori Saitou, *Kyoto U.*
Shimon Sakaguchi, *Kyoto U.*
Miquel Salmeron, *Lawrence Berkeley National Lab*
Jürgen Sandkühler, *Medical U. of Vienna*
Alexander Schier, *Harvard U.*
Randy Seeley, *U. of Cincinnati*
Vladimir Shalaev, *Purdue U.*
Robert Siliciano, *Johns Hopkins School of Medicine*
Joseph Silk, *Institut d'Astrophysique de Paris*
Denis Simon, *Arizona State U.*
Alison Smith, *John Innes Centre*
Richard Smith, *U. of North Carolina* **(S)**
John Speakman, *U. of Aberdeen*
Allan C. Spradling, *Carnegie Institution of Washington*
Jonathan Sprent, *Garvan Inst. of Medical Research*
Eric Steig, *U. of Washington*
Paula Stephan, *Georgia State U. and National Bureau of Economic Research*
Molly Stevens, *Imperial College London*
V. S. Subrahmanian, *U. of Maryland*
Ira Tabas, *Columbia U.*
Sarah Teichmann, *Cambridge U.*
John Thomas, *North Carolina State U.*
Christopher Tyler-Smith, *The Wellcome Trust Sanger Inst.*
Herbert Virgin, *Washington U.*
Bert Vogelstein, *Johns Hopkins U.*
Cynthia Volkert, *U. of Göttingen*
Douglas Wallace, *Dalhousie U.*
David Wallach, *Weizmann Inst. of Science*
Ian Walmsley, *U. of Oxford*
David A. Wardle, *Swedish U. of Agric. Sciences*
David Waxman, *Fudan U.*
Jonathan Weissman, *U. of California, San Francisco*
Chris Wikle, *U. of Missouri* **(S)**
Ian A. Wilson, *The Scripps Res. Inst.* **(S)**
Timothy D. Wilson, *U. of Virginia*
Rosemary Wyse, *Johns Hopkins U.*
Jan Zaanen, *Leiden U.*
Kenneth Zaret, *U. of Pennsylvania School of Medicine*
Jonathan Zehr, *U. of California, Santa Cruz*
Len Zon, *Children's Hospital Boston*
Maria Zuber, *MIT*

BOOK REVIEW BOARD
David Bloom, *Harvard U.,* **Samuel Bowring,** *MIT,* **Angela Creager,** *Princeton U.,* **Richard Shweder,** *U. of Chicago,* **Ed Wasserman,** *DuPont*

Published by AAAS

EDITORIAL

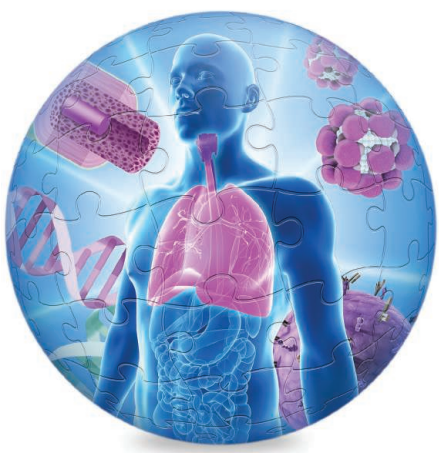
Five years of translation

In October 2009, the Nobel committee awarded prizes for basic research on ribosomes and telomeres. In the same month, AAAS launched a new journal with a different focus—*Science Translational Medicine* (*SciTM*)—staking out a clear role for the organization in advancing clinical medicine. One year later, awards at the pinnacle of science also recognized more translational achievements.*

Worldwide, scientists are thinking more about the translational value of their work, and big efforts have been funded to create institutes that bridge basic research and clinical practice. Over the past 5 years, there has been an exciting outgrowth of research programs and funding resources focused on discoveries at this interface. With the guidance of Elias Zerhouni, *SciTM*'s founding Chief Scientific Advisor and former director of the U.S. National Institutes of Health, the journal shaped its mission: to provide an interdisciplinary forum for research that makes tangible progress toward improvements in clinical medicine by applying basic biological research and engineering science. Then and now, with Chief Scientific Advisors Elazer R. Edelman and Garret A. FitzGerald at the helm, *SciTM* publishes findings from all areas of biomedicine, including those with roots in engineering and the physical sciences.

On this 5-year anniversary of *SciTM*, the journal's progress and support of this exciting and vital "bench-to-bedside" enterprise can be traced through its published papers that have spurred encouraging translational progress. Early success was reported in 2011 with the treatment of two advanced leukemia patients with T lymphocytes engineered to attack tumor cells.† These therapeutic immune cells—decorated with chimeric antigen receptors—seemed to be long-lasting memory T cells, raising hopes that remission would be permanent. Today, these patients remain cancer-free. Numerous biotech and pharma firms are now genetically engineering T cells, and the approach appears to work for other blood cancers. At present, 52 clinical trials employ these engineered receptors for targeting cancers ranging from leukemias to neuroblastoma. Cancer immunotherapy was chosen as *Science*'s 2013 Breakthrough of the Year, and the field is poised to make more major leaps.

SciTM also published a key resource for exploring the links between disease and the human microbiota—a mouse model in which microbes of the human gut set up residence in the mouse gut for study under controlled conditions.‡ Since then, this model has shown that intestinal microbes transferred from obese or malnourished people confer these maladies to recipients and that gut microbes contribute to colon cancer and fatty liver disease. Further elucidation of microbe-disease associations using this model will lead to treatments and preventions that improve health.



"Worldwide, scientists are thinking more about the translational value of their work..."

In an early application of bioengineering to cancer, *SciTM* reported an implantable vaccine depot built from a polymer matrix.§ Loaded with a soluble signal to attract immune cells, the polymer triggers an immune response in the host, just like a natural infection. Mice carrying the implant produce lymphocytes that kill cancer cells and squelch undesirable immune cells, resulting in tumor regression and longer survival. This fruitful collaboration among materials scientists, bioengineers, and immunologists has led to a clinical trial of a small disklike sponge inserted under the skin of patients with melanoma—the first test of the system in humans.

Recently, Stephen Palumbi, a prominent marine biologist, commented that the rise of the conservation mission at aquariums provided the perfect outlet to bring marine ecosystem research to an audience that is larger and more powerful than a few dozen academic peers. Although awards and citations are intellectually gratifying, little compares with the satisfaction of knowing that one's research has had an impact on the well-being of society. As a science community, we should be creating more opportunities for facilitating the transfer of science in the service of society.

– Katrina L. Kelner and Marcia McNutt



Katrina L. Kelner
Editor
Science
Translational
Medicine



Marcia McNutt
Editor-in-Chief
Science *journals*

IMAGES: (INSET) MOKOM 01; (TOP RIGHT) C. SMITH/*SCIENCE*; (BOTTOM RIGHT) STACEY PENTLAND PHOTOGRAPHY

*S. Desmond-Hellman, *Sci. Transl. Med.* **2**, 63ed9 (2010). †M. Kalos *et al.*, *Sci. Transl. Med.* **3**, 95ra73 (2011).
‡P. J. Turnbaugh *et al.*, *Sci. Transl. Med.* **1**, 6ra14 (2009). §O. A. Ali *et al.*, *Sci. Transl. Med.* **1**, 8ra19 (2009).

10.1126/science.1262034

Published by AAAS

Downloaded from www.sciencemag.org on October 9, 2014

NEWS

> “Just because someone says something confidently doesn’t mean it’s true.”
>
> **Psychologist Elizabeth Loftus** of the University of California, Irvine, on a National Research Council report calling for a more scientific approach to eyewitness identifications of suspects in a lineup. **http://scim.ag/eyewitID**

IN BRIEF

Ancient cave art in Indonesia



These hand stencils in an Indonesian cave may be among the oldest rock art in the world.

At least 40,000 years ago, prehistoric artists were stenciling their hands and painting images of primitive pigs on the walls of a cave on the Indonesian island of Sulawesi, according to a study published in *Nature* this week. The new dates came from the decay of uranium in the mineral crusts that formed over time atop the paintings in seven caves. If the dates are accurate, this would be some of the oldest rock art in the world, challenging the view that Europeans were the first to paint figurative rock art. Eerily similar stencils of hands and paintings of animals in France date to almost the same time and have long been thought to be the first examples of such sophisticated figurine art. The finding suggests that humans might have created rock art independently on both continents at the same time—or that modern humans brought this sensibility with them as they swept out of Africa and spread around the globe in the past 60,000 years. **http://scim.ag/cavepaint**

AROUND THE WORLD

Stem cell trial is off

ROME | The Italian government won’t proceed with plans for a human study of a stem cell treatment that has led to fierce debates the past 3 years. On 3 October, an expert panel appointed by Health Minister Beatrice Lorenzin concluded that the treatment, developed by the Stamina Foundation in Turin and widely criticized by scientists, hasn’t been shown to be safe and should not undergo the formal clinical trial ordered by law in 2013 (*Science*, 31 May 2013, p. 1028). The panel’s verdict led Lorenzin to scrap the study immediately. “The decision has left me amazed,” says Stamina Foundation President Davide Vannoni, who says he will appeal the verdict at a court in Rome. **http://scim.ag/ltstemcell**

First commercial CCS plant opens

ESTEVAN, CANADA | A Saskatchewan-based company has opened the first commercial-scale coal-fired power plant to include carbon capture and storage technology. SaskPower’s CA$1.4 billion Boundary Dam project, hailed by proponents of “clean coal” technology, went online 2 October. The company plans to capture and sell as much as 90% of its emissions, amounting to 1 million tonnes of CO_2 each year, to oil company Cenovus Energy. Cenovus will then transport the compressed gas via pipeline to an enhanced oil recovery site 66 kilometers away.

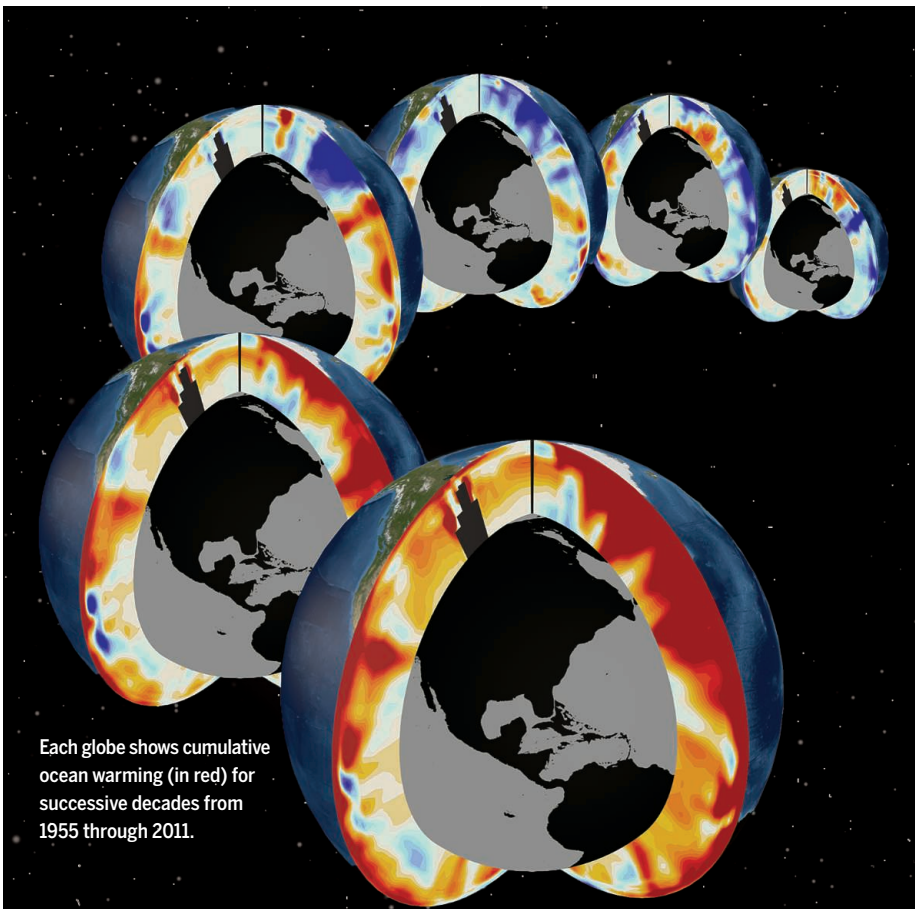
Construction on TMT begins

MAUNA KEA, HAWAII | With the untying of the maile lei and the turning of dirt with the O’o stick, construction of the $1.4 billion Thirty Meter Telescope (TMT) officially began this week on the sacred summit. TMT will comprise a primary mirror 30 meters across made up of 492 hexagonal segments, and two smaller mirrors; together, they will give about 10 times better resolution than the Hubble Space Telescope. An international consortium from the United States, Canada, Japan, China, and India, TMT is the third to join the extremely large telescopes club; the

PHOTO: KINEZ RIZA

Downloaded from www.sciencemag.org on October 9, 2014

Published by AAAS



Each globe shows cumulative ocean warming (in red) for successive decades from 1955 through 2011.

Overheated oceans

The oceans store more than 90% of the warming caused by greenhouse gases. But a new study argues scientists may have underestimated how much heat the upper oceans have actually absorbed over the past 40 years, due to the lack of ocean data in the Southern Hemisphere. The team compared a new analysis of heat content in the region, inferred from satellite data and models, to measurements from buoys and other devices in the water—and found a large inconsistency. Past global estimates of long-term warming could be 25% or more too low, they report this week in *Nature Climate Change*. The findings also suggest the oceans may be considerably more sensitive to greenhouse warming than thought. **http://scim.ag/oceanwarm**

CREDITS: (LEFT TO RIGHT) TIMO BREMER/LLNL; THE UNIVERSITY OF HONG KONG/COMMUNICATIONS AND PUBLIC AFFAIRS OFFICE

25-meter Giant Magellan Telescope and the 40-meter European Extremely Large Telescope are under construction in Chile. All three are scheduled to collect first light in 2022.

Students fight degree downgrade

MEXICO CITY | After days of protests, the Mexican government has agreed to reverse a controversial change to the degrees granted by the country's National Polytechnic Institute (IPN). On 24 September, IPN released new bylaws that downgraded some of its professional engineering degrees to technical degrees. Many students and professors felt the move was kowtowing to businesses that employ IPN graduates, because technicians cannot command the higher salaries engineers earn. On 3 October, interior minister Miguel Ángel Osorio Chong, appearing before thousands of student protesters, agreed to cancel the bylaw changes. "Like you, we're invested in making sure IPN continues to offer a quality education," he said. IPN's director and secretary-general have both since resigned.

Drug trial data to be shared

LONDON | After an 18-month saga, the European Medicines Agency on 2 October approved the details of a new system opening clinical trial data to public scrutiny. Proponents of open sharing praised the decision, which will allow scientists to download and reanalyze data. Earlier proposals would have allowed data to be viewed only on screen (*Science*, 23 May, p. 784). But campaigners still worry that information could be redacted before the reports are shared. To take effect in 2016, the new rules will apply to data submitted after 1 January 2015 as part of applications to market drugs. The policy will serve as a bridge until the rollout of a revamped E.U. clinical trial regulation, which will include new provisions for the release of clinical trial results.
http://scim.ag/EMAdatashare

NEWSMAKERS

Three Q's



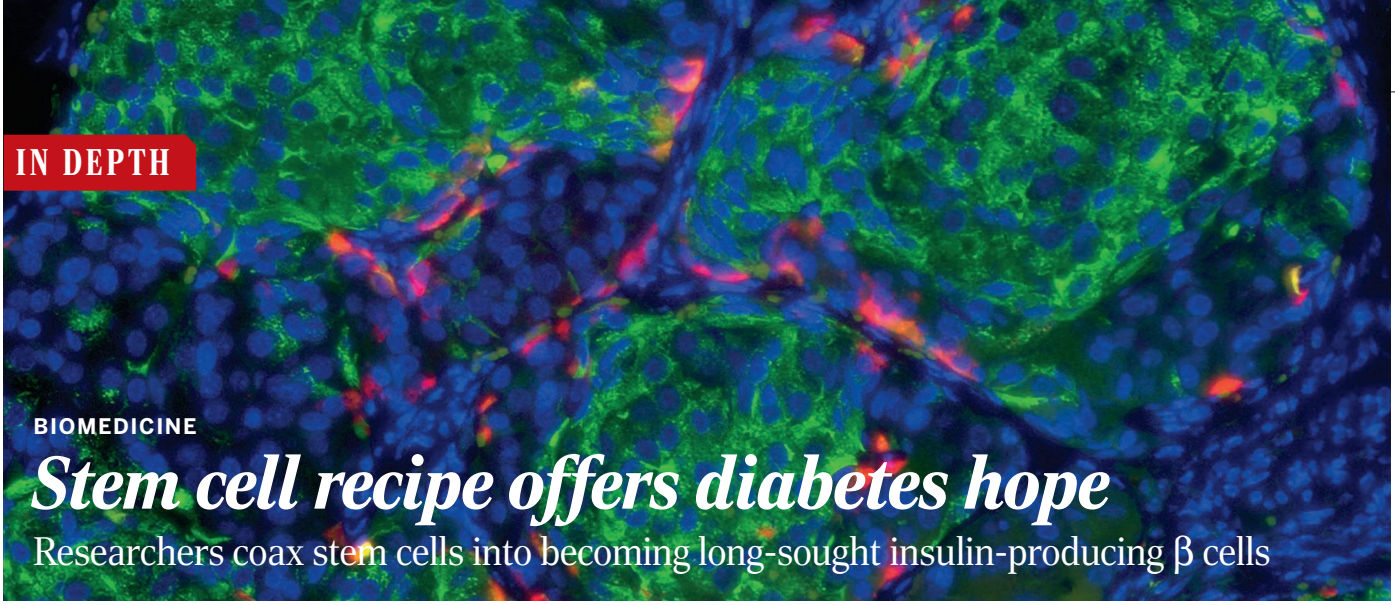
Hong Kong is in the throes of a confrontation between the government and a pro-democracy movement over proposed electoral restrictions. University students are playing a leading role, boycotting classes to demonstrate. **Peter Mathieson**, a kidney researcher and the University of Hong Kong's vice chancellor, discussed the situation.

Q: How is your university being affected?
A: The students have become very significant figures in the deliberations with the government. I imagine this is going to have an effect for years to come in terms of student activism.

Q: If democratic principles are compromised, would that affect your ability to attract faculty and students from abroad?
A: It makes me concerned that people might be put off in the short term by a feeling that Hong Kong is now a place of great uncertainty.

Q: Do you worry that as mainland China's influence grows in Hong Kong, academic freedom might be curtailed?
A: At the moment, there is manifestly freedom of speech and freedom of association being practiced in the streets of Hong Kong. A critical part of my role is to do everything that I can to defend academic freedom and freedom of speech in the future.

Published by AAAS



IN DEPTH

BIOMEDICINE

Stem cell recipe offers diabetes hope

Researchers coax stem cells into becoming long-sought insulin-producing β cells

By **Gretchen Vogel**

Douglas Melton is as impatient as anyone for a cure for diabetes. His son developed the disease as an infant, and his daughter was diagnosed at age 14. For most of the past 2 decades, the developmental biologist at the Harvard Stem Cell Institute has focused his research on finding a cure. This week, he and his colleagues report a potentially significant step toward that goal: a recipe that can turn human stem cells into functional pancreatic β cells—the cells that are destroyed by an autoimmune attack in type 1 diabetes patients such as Melton's son and daughter. The cells his group made respond to glucose by producing insulin, just as normal β cells do. And when implanted into mice with a form of diabetes, the cells can cure the disorder.

"The diabetes research community has been waiting for ages for this type of breakthrough," says Jorge Ferrer, who studies the genetics of β cells at Imperial College London. The lab-generated cells should be a valuable tool for studying diabetes and, Melton hopes, could eventually be used to treat patients.



Douglas Melton

Throughout the day, the pancreas regulates the body's blood sugar levels, responding to an increase in glucose after a meal by secreting insulin, which helps cells take up the sugar. In type 1 diabetes, the body's immune system mistakenly kills the β cells for still-unknown reasons, and the body is left without insulin. People control their diabetes by injecting carefully calibrated doses of insulin. But matching the precise insulin control achieved by the healthy pancreas is almost impossible, so researchers have hoped for decades to find a way to replace the missing cells.

When scientists isolated human embryonic stem (ES) cells in 1998, hopes soared. ES cells are pluripotent, which means that in theory they can turn into any of the body's cell types—including β cells. Indeed, one of the first things researchers tried to make from ES cells was pancreatic β cells. Later, they tried with so-called induced pluripotent stem (iPS) cells, made by reprogramming adult cells into an embryo-like state. Either way, "it's proved to be an extraordinarily complicated undertaking," says Mark Magnuson of Vanderbilt University in Nashville, who studies pancreatic development.

Several teams have turned stem cells into precursors of β cells, which mature when placed into experimental animals. But the cells take 6 weeks to become fully functional β cells, and they can't be easily studied outside the body.

In *Cell* this week, Melton and his colleagues report a complex recipe that can transform either human ES cells or iPS cells directly into functional β cells. The breakthrough is based on more than a decade of tenacious work in Melton's lab. He and his colleagues have painstakingly studied the signals that guide pancreas development, applying what they and others have found to develop their method. "There's no magic to this," Melton says. "It's not a discovery so much as applied developmental biology."

The protocol "is reproducible, but it is tedious," Melton adds. The stem cells are grown in flasks and require five different growth media and 11 molecular factors, from proteins to sugars, added in precise combinations over 35 days to turn them into β cells. On the bright side, Melton says, the technique can produce 200 million β cells in a single 500 ml flask—enough, in theory, to treat a patient. Melton says the protocol seems to work equally well with ES and iPS cell lines.

Two weeks after transplant into a diabetic mouse, human pancreatic β cells made in the lab produce enough insulin (green) to cure the animal.

Before the cells can be used to treat type 1 diabetes, researchers need to find a way to protect them from immunologic rejection. The same autoimmune response that triggered the disease would likely attack new β cells derived from the patient's own iPS cells, and a normal immune response would destroy ES-derived β cells, which would appear foreign. (That has been a challenge for efforts to treat type 1 diabetes with transplants of β cells from deceased organ donors.) Melton and colleagues are now exploring how to physically encapsulate their stem cell–derived β cells, as well as ways to modify the β cells to enable them to ward off immune attack.

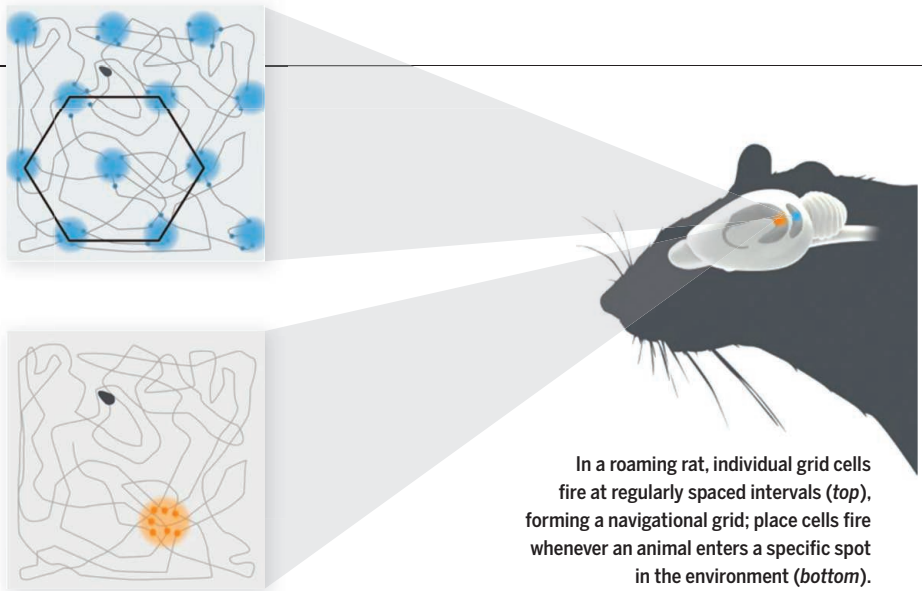
In the meantime, the cells should help the study of both type 1 and type 2 diabetes. (In type 2, β cells are present but can't keep up with the body's insulin demands.) The technique "potentially provides ways to create model systems for studying the genetic basis of diabetes, or to discover novel therapies to enhance existing β cells," Ferrer says. For example, using iPS cell lines from people with type 1 and type 2 diabetes and healthy controls, Melton's lab is generating β cells to look for differences that explain the distinct forms of the disease. They also will screen for chemicals that can stop or even reverse the damage diabetes does to β cells.

Melton says his son and daughter—now 23 and 27 years old, respectively—were pleased but unsurprised by his group's progress. Reversing the parent-child role, they gently nagged him to "get going and solve the [immune-rejection] problem." ■

PHOTOS: (TOP TO BOTTOM) DOUGLAS MELTON; B. D. COLEN/HARVARD UNIVERSITY

Downloaded from www.sciencemag.org on October 9, 2014

Published by AAAS



In a roaming rat, individual grid cells fire at regularly spaced intervals (*top*), forming a navigational grid; place cells fire whenever an animal enters a specific spot in the environment (*bottom*).

ILLUSTRATION: MATTIAS KARLEN

NOBEL PRIZES

Brain's GPS finds top honor

"Place" and "grid" cells help explain how we navigate

By **Emily Underwood**

Here's a valuable lesson for neuroscientists everywhere: Give your test subjects a little freedom to roam.

In the 1970s, when neuroscientist John O'Keefe was at McGill University in Montreal, Canada, he recorded rat brain activity in a region called the hippocampus as the animals meandered freely about enclosures. He and colleagues spotted a group of neurons that fired only when the animals passed by a particular spot. Together, these "place cells" acted as a mental GPS, enabling the rats to create a mental map of their surroundings, O'Keefe says. Now director of the Sainsbury Wellcome Centre for Neural Circuits and Behaviour at University College London, O'Keefe learned this week that his discovery won him one half of the 2014 $1.1 million Nobel Prize in physiology or medicine.

PHYSIOLOGY NOBEL

"for their discoveries of cells that constitute a positioning system in the brain"

John O'Keefe

May-Britt Moser

Edvard Moser

Place cells "set in motion an entire field" within neuroscience, says Loren Frank, a neuroscientist at the University of California, San Francisco. "Hundreds, if not thousands" of neuroscientists interested in how the brain perceives, remembers, and plans movement through space flocked to study the hippocampus's role in spatial memory after O'Keefe's original find, adds Lynn Nadel, a neuroscientist at the University of Arizona in Tucson, who collaborated with O'Keefe on a 1978 book about place cells.

Among those drawn to the nascent field was the couple who shared the Nobel Prize with O'Keefe: May-Britt Moser, now director of the Centre for Neural Computation in Trondheim, Norway, and Edvard Moser, now director of the Kavli Institute for Systems Neuroscience in Trondheim. The husband-wife team, who briefly worked in O'Keefe's lab as postdocs, also monitored the brain activity of roaming rodents, chemically inactivating the hippocampus to identify other brain regions involved in spatial navigation. In 2005, they published their Nobel-winning finding: a set of "grid cells" in a brain region called the entorhinal cortex. Unlike place cells, which signal a specific point in the environment, individual grid cells fire in a roaming rodent at multiple, regularly spaced locations, which form a honeycomblike pattern. They may provide a set of reference points for navigation, though more research is needed to determine their precise role.

Recently, researchers have begun to manipulate these navigational neurons. A team earlier this year altered the positive and negative associations that mice had formed with specific locations, by triggering hippocampal place cells with lasers while simultaneously stimulating other brain cells. And although grid and place cells remain a focus of fundamental neuroscience research, there are hints of clinical relevance: The hippocampus and entorhinal cortex are among the first brain regions damaged in neurodegenerative diseases such as Alzheimer's. There may yet be a place for place and grid cells in medicine. ■

NOBEL PRIZES

Physicists change the light bulb

Blue light-emitting diodes, critical to white LED lighting, win this year's prize

By **Dennis Normile**

In a choice that surprised Nobel watchers, this year's physics prize is going to three Japanese scientists not for a basic discovery but rather for an invention: the blue light-emitting diode (LED). The Nobel Committee recognized three researchers as contributing equally to the breakthrough: Isamu Akasaki of Meijo University in Nagoya and Nagoya University; Hiroshi Amano of Nagoya University; and Shuji Nakamura, now of the University of California, Santa Barbara.

LEDs appeared in commercial applications in the 1960s. But until the early 1990s they only came in such colors as red and green. They were used as indicator lights in electronic devices and in electronic displays and, later, in auto brake lights. But without a blue LED, there was no way to create the white light needed for general-purpose lighting.

The challenge was in the materials. LEDs are semiconductor constructions that rely on an applied voltage to drive electrons and positive carriers called holes through different layers of a crystal sandwich. When electrons and holes come together in the so-called active layer of the sandwich, they give off photons—light. The wavelength of the light, and thus the color, depends on the properties of the crystal and embedded impurities, called dopants. For years, major corporations tried to find the right combination of semiconductor materials and dopants to produce blue light, but they failed.

This trio of Japanese researchers began experimenting with gallium nitride. Theoretically, gallium nitride had the right stuff to produce blue light, but it was notoriously finicky to work with. "People thought [a blue LED] wouldn't be achieved during the 20th century," Akasaki said during a 7 October press conference in Nagoya. "Other researchers gave up but I didn't think of doing so—I was doing what I liked," he said.

Downloaded from www.sciencemag.org on October 9, 2014

Published by AAAS

Akasaki and Amano, working together at Nagoya University, tried different ways of growing the semiconductor crystal and made the first breakthrough, coaxing faint blue light from a gallium nitride semiconductor in 1986. While Akasaki and Amano continued improving their blue LED, Nakamura, who then had only a master's degree and was working at Nichia Corp., a maker of phosphors located in a small town in rural Shikoku, pursued his own effort. He tried different ways of growing the needed gallium nitride layers and in 1993 got a device emitting very bright, very blue light.

Japanese politicians heaped praise on the trio on evening newscasts. But Nakamura may have mixed feelings. He had a falling out with Nichia and after a nasty legal spat won a share of the profits the company earned from his invention. He also decided to move to the United States after failing to find an academic position in Japan. During a January 2005 press conference after the settlement of his suit, Nakamura blasted Japan's courts, educational system, and treatment of researchers (*Science*, 21 January 2005, p. 337). "Basically, Japanese society doesn't value the contributions of individuals," he said. He is now an American citizen.

PHYSICS NOBEL

"for the invention of efficient blue light-emitting diodes which has enabled bright and energy-saving white light sources"

Isamu Akasaki

Hiroshi Amano

Shuji Nakamura

The breakthroughs initiated a still-ongoing revolution in lighting. LED lighting is far more efficient than previous forms of lighting, which involve heating a filament or a gas and waste most of the input energy. "With 20% of the world's electricity used for lighting, it's been calculated that optimal use of LED lighting could reduce this to four per cent. Akasaki, Amano and Nakamura's research has made this possible and this prize recognises this contribution," said Frances Saunders, president of the U.K. Institute of Physics, in a statement. "This is physics research that is having a direct impact on the grandest of scales, helping protect our environment, as well as turning up in our everyday electronic gadgets."

LEDs' efficiency also means that they can be run on low-cost solar power and simple batteries, bringing light to the 1.5 billion people who are not connected to energy grids. The usefulness of this invention is something that would make Alfred Nobel "really happy about this prize," said Per Delsing, chair of the Nobel Committee for Physics. ■

BIOMEDICAL RESEARCH

A call for NIH youth movement

Wariness greets congressman's proposal to require agency to reduce average age at first grant

By **Jocelyn Kaiser**

Representative Andy Harris (R–MD) spent 12 years as a physician-researcher at Johns Hopkins University in Baltimore, Maryland, before venturing into politics. He likes to note that he is the only serving member of Congress who has been funded by the National Institutes of Health (NIH). And he believes that experience gives him practical insight into the plight of young biomedical scientists, who now are often in their 40s before they win their first NIH grant.



Last week, Harris offered a radical solution to this graying of U.S. biomedical science: Congress should order NIH to reduce the average age at which new investigators receive their first grant by 4 years within a decade, he argued in an opinion piece in *The New York Times*. "I saw firsthand how the most innovative thinking frequently came from younger scientists," he wrote, warning that current NIH practices are damping innovation. He has drafted a bill to turn his prescription into law.

The idea is getting a wary reception from research advocates. "Mandating NIH to come up with a specific outcome is a dangerous and risky position … given the complexity of the situation," says Howard Garrison, deputy executive director for policy for the Federation of American Societies for Experimental Biology in Bethesda, Maryland.

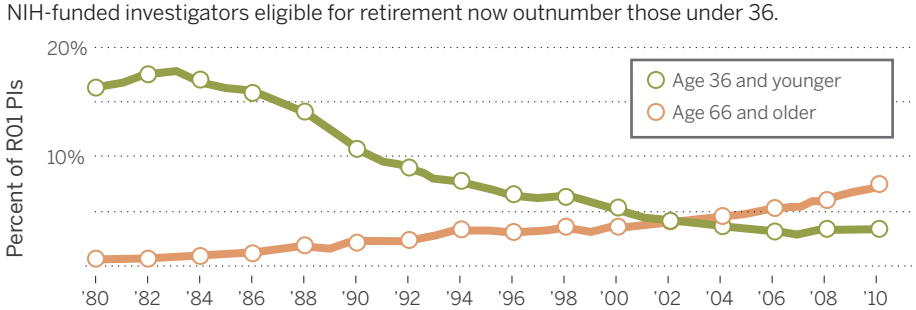
Harris, 57, a conservative who represents a semirural district in Maryland, spent his early career as an obstetric anesthesiologist and division chief at Hopkins. Starting at age 30, he became a co-investigator on three successive NIH grants studying cerebral blood flow in the developing fetus. At the time, the age distribution of Harris's peers who were principal investigators (PIs) winning their first grant clustered around the late 30s. But today, he notes, the median age at which a Ph.D. researcher receives his or her first NIH R01, the agency's bread-and-butter grant, has increased to 42, up from an average of 36 in 1980.

The biomedical community has long lamented the rising age of first-time investigators, which many attribute to ever-longer graduate studies and postdocs and a dearth of new faculty positions. In 2008, then-NIH Director Elias Zerhouni crafted a policy ensuring that "early stage investigators" (defined as those no more than 10 years out from finishing their Ph.D. or medical residency) have the same success rate as established investigators submitting a new grant. Many NIH institutes achieve this by setting a more generous "payline" for proposals from new applicants. The policy helped stop but not reverse the rise in the average age for first R01s for Ph.D. researchers.

Although NIH is aware of the problem, Harris says the agency "does not have a serious plan to fix it." Simply giving NIH

In with the old, out with the young

NIH-funded investigators eligible for retirement now outnumber those under 36.



CREDITS: (PHOTO) AP PHOTO/STEVE RUARK; (DATA SOURCE) NIH

Downloaded from www.sciencemag.org on October 9, 2014

Published by AAAS

more money won't help, he argues: The proportion of NIH grants going to young scientists dropped even during the 1999 to 2003 doubling of the NIH budget and didn't increase after NIH received a burst of funding from the 2009 stimulus spending.

To devise a legislative solution, Harris says he spent a year and a half meeting with biomedical leaders, including regular interactions with NIH Director Francis Collins. The result: a draft bill (shared with *Science*) that says the NIH director "shall ensure" that the median age of investigators receiving their first R grant (which includes R01s and other research grants) falls to under 40 by 2019; under 39 by 2022; and under 38 by 2025.

To prime the fountain of youth, Harris—who serves on the spending panel that oversees NIH's budget—wouldn't divert money from existing grants. Instead, he would redirect a pool of about $700 million (in 2013)—known as the tap—that NIH hands over to its parent agency, the Department of Health and Human Services, for other activities. A separate draft bill would channel this funding to the NIH director's office, to be used for "emerging scientists"—defined as those who finished their training within the last 15 years and are seeking their first or second research grant. Harris hopes the two bills will become part of legislation expected to emerge early next year from a bipartisan effort in the U.S. House of Representatives—known as 21st Century Cures—to support NIH and speed drug development.

NIH officials are hesitant. Sally Rockey, the agency's deputy director for extramural research, says Harris's mandate might not achieve much unless scientists' training can be shortened so that more are ready to compete for NIH grants at a younger age. For now, there may be too few proposals coming from scientists in their 30s to meet Harris's targets without dramatically propping up their success rates, says Jeremy Berg of the University of Pittsburgh in Pennsylvania, a former director of the National Institute of General Medical Sciences. "You really need to look at what's driving the numbers and understand the whole system before doing things that might be harmful in the long run," he says. Too much special treatment for young researchers could create problems down the road, worries Jessica Polka, a postdoctoral researcher at Harvard Medical School in Boston. "The glut of new [young] PIs would only further strain the funding system in the future," she predicts.

Harris stands by his plan. Researchers "at the age of peak innovation" deserve "a leg up," he says. And "if they continue to have good ideas … they will be able to compete." ■



A son and his sick father in Monrovia.

PHOTO: JOHN MOORE/GETTY IMAGES

INFECTIOUS DISEASES

Imagining Ebola's next move

As containment efforts fall short, scientists look beyond the models to envision how the epidemic might unfold

By **Kai Kupferschmidt**

When a traveler from Liberia came down with Ebola in Dallas on 24 September, it was a warning to the world: As the number of cases in West Africa keeps rising, so does the risk the disease will spread beyond Guinea, Sierra Leone, and Liberia. The United States was the third country, after Nigeria and Senegal, to catch a spark from the growing conflagration; it was followed by Spain, which reported the first case of Ebola contracted outside of Africa on 6 October. The patient, a nurse, had taken care of a priest who became infected in Sierra Leone.

None of these cases has triggered a widespread outbreak, and most experts are confident that wealthy nations can contain introduced cases. "My first reaction was: Well, it had to be somewhere. Better Dallas than Mumbai," says Peter Sandman, an adviser on risk communication based in Brooklyn, New York, about the U.S. case. But developing countries may not be so lucky when Ebola arrives on their doorstep. That could result in entirely new chapters in the disease's spread.

On 3 October, the World Health Organization (WHO) had reported 7470 cases and 3431 deaths in the three affected countries. Those numbers, believed to be gross underestimates, are rising exponentially, and models show they could reach the hundreds of thousands in a matter of months. But models can't forecast unpredictable things like viral mutations, changes in human behavior, the impact of new vaccines and drugs, or where and how the disease will next become entrenched. So researchers are looking beyond the models, and at possible scenarios, to prepare for what might happen. Scientists are naturally loath to speculate, Sandman says, but "risk communication and crisis communication are all about what-ifs."

On the optimistic picture, an effective vaccine could finally check the rise in cases—something classic control methods such as isolation and quarantine have failed to do. Without a vaccine, "I think the best we can hope for is that the spread slows down a little bit," says Alessandro Vespignani, a physicist at Northeastern University in Boston who has modeled the spread of the Ebola virus. "Increasing public health measures will have a huge impact, but I believe it has gotten to the stage where we will need a vaccine as well to stop this outbreak," says Jeremy Farrar, an epidemiologist who heads the Wellcome Trust in London.

One candidate vaccine is already in phase I safety tests, and another will be soon; at a meeting at WHO on 29 and 30 September, experts discussed how to speed vaccine development and how to cope with the thorny ethical issues involved in testing a vaccine for efficacy in the affected countries (http://scim.ag/Ebolavac). But those tests are unlikely to start until January, and they may not yield results until April.

In the meantime, some researchers fear the virus could mutate. In an op-ed piece in *The New York Times* on 11 September, Michael Osterholm, director of the Center for Infectious Disease Research and Policy at the University of Minnesota, Twin Cities,

Published by AAAS

argued that Ebola might change in such a way "that just breathing would put one at risk of contracting" it. He was widely criticized for fear mongering. "I do not know of a viral infection whose mode of transmission has changed in this way," Farrar says. WHO put out a statement on 6 October, calling the idea "speculation, unsubstantiated by any evidence." Osterholm retorts that "it may be a very remote possibility, but we have to be prepared for even that."

What is more plausible, some researchers say, is a change that makes the virus less deadly, but also harder to get rid of. The Ebola virus most likely lurks in bats and apes, occasionally spilling over into the human population, probably when infected animals are hunted and consumed. In the past, outbreaks tended to burn out in the face of aggressive containment efforts and Ebola's sheer deadliness. In essence, human beings remain dead ends for the virus. That could change if it becomes less fatal. "There is an evolutionary advantage to reducing virulence and adapting to your host," Farrar says. "This has happened with many other diseases."

If it happens with Ebola, the only way to get rid of it this time around could be a massive vaccination effort similar to those used in the eradication campaigns against smallpox and polio. "We would be looking at vaccinating hundreds of millions of people in Africa," Farrar says.

Even if the virus does not change, the sheer size of the epidemic will lead to new challenges. As the number of beds in treatment units falls short, more and more patients will be taken care of at home, where they pose a major risk to others. That could speed up Ebola's spread and make it harder to chart its epidemiology. Home care kits, which include basic protective equipment such as gloves and bleach, have never been widely used before to fight Ebola, but they could become important for controlling infection. They would need to be accompanied by an education campaign however, and nobody is sure how much protection they will offer.

As the already crippled health care systems in the affected countries buckle under the strain, people are also more likely to die in larger numbers of other diseases like malaria, or during childbirth. "We need to start looking beyond Ebola," Farrar says. Food shortages may occur if harvests are missed or trade is paralyzed. "The whole region might become a failed state," Osterholm says.

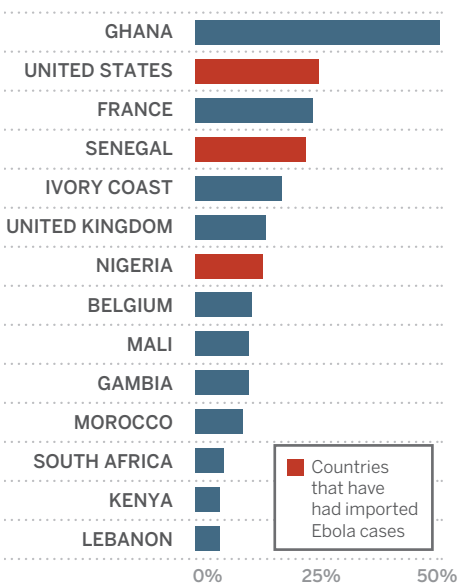
Meanwhile, the risk of spread beyond the three countries is growing, says Northeastern's Vespignani, who listed the countries most at risk in a paper published in *PLOS Currents: Outbreaks* in September (see table). The three countries where the virus has since landed—Senegal, Nigeria, and the United States—were in his top 16. His most recent calculations also put the chance of a case occurring in nearby Ghana by 24 October at close to 50%, even with an anticipated 80% decrease in travel. Mali and Ivory Coast are at high risk, too. If the virus gains a new foothold elsewhere, a huge effort would be needed to prevent a second firestorm, Osterholm says—even if that means diverting some resources from West Africa.

Scientists are debating the use of travel bans, which many worried U.S. citizens have called for after the Dallas case. WHO and the Centers for Disease Control and Prevention have strongly advised against closing borders because it would make it difficult to bring people and materials into the affected countries. Bans are also difficult to implement, Vespignani says, because many countries would have to agree; otherwise Ebola carriers could just fly to a country that doesn't impose restrictions and move on from there. Those who manage to circumvent a ban might then be more likely to lie about their contact history if they became sick. In the end, Vespignani says, travel bans would probably increase the risk for everyone.

But Sandman says the idea shouldn't be dismissed entirely. "It is quite reasonable for people to ask how best to reduce the number of sparks flying out of Africa and threatening to ignite elsewhere," he says. The world may need to buy time to test vaccine candidates, so it should look for practical ways to reduce the number of travelers carrying Ebola to other places, Sandman says. "These are discussions we need to have." ■

Probability of Ebola importation

For October, using data through 23 September



DATA: MOBS LAB, NORTHEASTERN UNIVERSITY

U.S. POLICY

Congress, NSF spar on access to grant files

Grantees wonder what House science panel will do with private award details

By **Jeffrey Mervis**

Four times this past summer, in a spare room on the top floor of the National Science Foundation (NSF), two congressional staffers spent hours poring over confidential material relating to 20 research projects that NSF has funded over the past decade. The staffers work for the U.S. House of Representatives committee that oversees NSF. And their visits were an unprecedented—and some say bizarre—intrusion into the much admired process that NSF has used for more than 60 years to award research grants.

Unlike the experts who normally review proposals, the congressional staffers weren't really there to judge their scientific merits. The Republican aide was looking for anything that Representative Lamar Smith (R–TX), his boss as chair of the House Committee on Science, Space, and Technology, could use to demonstrate how the $7 billion research agency is wasting taxpayer dollars on frivolous or low-priority projects, particularly in the social sciences. The Democratic staff member wanted to make sure that her boss, Representative Eddie Bernice Johnson (D–TX), the panel's senior Democrat, knew enough about each grant to rebut any criticism that Smith might levy.

The peculiar exercise is part of a long-running and bitter battle pitting Smith and many of his panel's Republican members against Johnson and the panel's Democrats, NSF's leadership, and the academic research community. There's no end in sight: The visits are expected to continue into the fall, because NSF has agreed to Smith's request to turn over information on an additional 27 awards. (A spreadsheet of the requested grants and more details are at http://scim.ag/NSFgrants.)

Indeed, the feud appears to be escalating. Last week, Johnson wrote to Smith accusing him "of go[ing] after specific peer-reviewed grants simply because the Chairman personally does not believe them to be of high

Downloaded from www.sciencemag.org on October 9, 2014

Published by AAAS

value." Smith, however, argues he is simply taking seriously Congress's oversight responsibility. And he promises to stay the course: "Our efforts will continue until NSF agrees to only award grants that are in the national interest," he e-mailed *Science* after being asked to respond to Johnson's letter.

Over the past 18 months, Smith has repeatedly ridiculed specific NSF awards, championed legislation that would alter the agency's peer-review system and slash funding for its social science programs, and berated NSF officials for providing what he considers to be inadequate explanations of their funding decisions. He's also kept up a stream of correspondence with NSF about examining the awards in question, first with acting Director Cora Marrett and then with the new NSF Director, France Córdova.

Federal lawmakers have a long tradition of taking potshots at grants they don't like, but Smith's 7 April request for material on the 20 grants was unprecedented, and it created a major dilemma for NSF. On the one hand, Córdova knows that Congress has the authority to demand the information. On the other hand, NSF has promised scientists that every aspect of the peer-review process will remain confidential.

Smith wanted the material shipped to his offices on Capitol Hill. But Córdova made a counteroffer that the Texas legislator grudgingly accepted. First, the names of the outside reviewers would be redacted. Second, the material would remain at NSF headquarters in Arlington, Virginia. Third, none of the information could be photocopied or otherwise reproduced. Judy Gan, head of public and legislative affairs at NSF, says the arrangement "preserves the integrity of the merit review process."

Working under those conditions, committee staff spent 25 hours this summer at NSF headquarters. On 11 September, Smith gave NSF a list of the 27 additional grants; NSF is still processing that request. The arrangement required NSF to print out more than 100 pages of confidential information on each award, including the initial application, reviewer comments, and correspondence between program officers and principal investigators.

Before the committee staffers began their visits, NSF officials sent letters explaining what was going on to the president of every university with a grant on Smith's hit list. In many cases, NSF staffers had already sounded the alarm.

Steven Folmar, a cultural anthropologist at Wake Forest University in Winston-Salem, North Carolina, found out from his program manager about the science committee's pending review of his 2012 grant, titled "Oppression and Mental Health in Nepal." Folmar, who has worked on and off in Nepal since 1979, says the country's economic and cultural divisions are so striking that it's an ideal place to measure the impact of discrimination on those in the lowest caste.

Folmar's first reaction after hearing that his 3-year, $160,000 award had been singled out was to hunker down and keep quiet. "I felt like somebody in a war movie, with bullets whizzing over my head." But after further reflection, he decided to express his views.

Information on how social inequality can cause depression and anxiety is useful to governments everywhere, he believes. The project was a bargain, he adds: Three senior researchers and their graduate students spent several months in the field "for about $50,000 a year. That's pretty cheap science."

It's hard to find a pattern among the $26 million in grants Smith has chosen to examine. One of them goes back to 2005, and 13 have expired. The smallest is a $20,000 grant for a doctoral dissertation by an anthropology student working in Bolivia; the largest, for $5.65 million, aims to use innovative education methods to educate Arctic communities about climate change and related issues. Nearly two-thirds were supported by NSF's social, behavioral, and economic sciences directorate, the program that has taken the brunt of Smith's criticism. Slightly more than half of the grants involve work outside the United States.

A committee representative declined to answer repeated queries about the criteria used to select the grants. In his written statement to *Science*, Smith said only that "there are many grants that no taxpayer would consider in the national interest, or worthy of how their hard-earned dollars should be spent. … The public deserves an explanation for why the NSF has spent hundreds of thousands of dollars on musicals about climate change, bicycle designs, and a video game that allows users to relive prom night."

Mont Hubbard is the "bicycle designs" grantee on Smith's intended list of shame. A professor emeritus of mechanical engineering at the University of California, Davis, Hubbard received $300,000 in 2009 to study the feedback system that allows humans to control a moving vehicle, in this case a bicycle. And he thinks the work clearly meets Smith's definition of research in the national interest. Substitute "pilot" for "rider" and "airplane" for "bicycle," he says, and it's clear that helping humans do a better job of manipulating machines has the potential to greatly improve performance, reduce safety risks, and even defend the country.

In a 27 August letter to Córdova, Smith declares that "the current review work is 5% complete, which implies that this oversight initiative will span at least 12 months." He accuses her of reneging on a promise to provide the committee with everything it requested. "To the contrary," Córdova responded 2 weeks later, "NSF has provided the Committee full and complete access to our files for each of the grants of interest."

Given the strong rhetoric on both sides, it's hard to see a quick ending to this confrontation. In the meantime, scientists are bracing to find out what Smith plans to do with his trove of information from NSF's confidential records. ■

With reporting by David Shultz.



How a rider controls a bicycle is an old puzzle—and the subject of a disputed NSF grant.

PHOTO: LAWRENCE SCHILLER/POLARIS COMMUNICATIONS/GETTY IMAGES

Published by AAAS



Don't blame the beetles

Bark beetles have devastated western forests, but that may not mean more severe fires

By **Cally Carswell**

When the evergreen trees turned red, it was hard not to worry. The die-offs started in Alaska about 20 years ago, and soon conifers were perishing en masse across western North America. Life drained from millions of hectares of forest so quickly it was as if they had been abruptly unplugged, like a Christmas tree before bedtime.

The killers: tiny insects called bark beetles. Many people worried that the dead, dry trees would give birth to huge, damaging wildfires. To prevent infernos, some U.S. lawmakers pushed expensive, controversial policies to aggressively log beetle-damaged trees. "We are battling a huge insect epidemic that is destroying our forests" and creating "prime real estate for forest fires," warned then-Representative John Salazar, a Democrat from Colorado, on the floor of the U.S. House of Representatives in 2006. To some casual observers, the prediction seemed to come true as blazes such as the 2012 High Park Fire near Fort Collins, Colorado, set records for hectares burned and homes destroyed.

But that fire, like others, burned green forest as well as beetle-killed trees. And now, a growing body of research—including a study published last week—is challenging the notion that beetle-killed forests are more vulnerable to severe fires than forests that have escaped infestation. The findings are highlighting the complex causes of western wildfires and raising new questions about policies that promote the removal of insect-damaged trees to reduce fire risks. Contrary to popular belief, says forest ecologist Thomas Veblen of the University of Colorado (CU), Boulder, the science suggests that "healthy forests [can] include fire, and bark beetles, and lots of dead trees."

THE RECENT BARK BEETLE OUTBREAKS aren't the first to grip North America. Some 15 major species of these insects, about equal in size and appearance to a fleck of mouse poop, kill trees in western forests. The beetles, which are native, attack mostly weak, old trees, boring in and cutting off

PHOTO: MATT OLSON

Downloaded from www.sciencemag.org on October 9, 2014

Published by AAAS





Bark beetles, including mountain pine beetles (*above*, *left*), have damaged trees throughout the west (opposite page), but their role in intensifying fires has been hard to pin down.

the flow of nutrients. In the past, their populations boomed periodically, overwhelming patches of even healthy forest. But the recent epidemics seem different, researchers say. Beetles have devastated stands of ancient whitebark pine, for instance, which was not a common past target. And although historical data are scarce, the outbreaks appear to be unusually extensive and synchronized, with many species erupting simultaneously in all sorts of forests (see graphic, p. 156). The booms have been aided by warmer winters and summers, as well as tree-weakening drought, leading scientists to wonder if massive attacks could become a new normal. "With climate change, we're essentially seeing bark beetle outbreaks on steroids," says Brian Harvey, a forest ecologist at the University of Wisconsin (UW), Madison.

Among the most visible victims have been towering, lanky lodgepole pines (*Pinus contorta*), a common tree that defines many Rocky Mountain landscapes. Hillsides of mature lodgepoles faded from green to red to gray in just 3 or 4 years—the telltale sign of death by beetle. As the mountains flushed red, fears mounted that they would soon erupt in flames.

That perception is understandable, says ecologist Monica Turner of UW Madison. "It's normal for most of us to think that the more dead wood we have, the worse fires will be," she says. Campers, for instance, don't fuel bonfires with green trees still supple with water and sap—they use dead, dry wood.

Early qualitative studies did hypothesize that beetle-killed forests would ignite more easily and burn more fiercely. But as early as the 1990s, work led by Veblen suggested that a massive spruce beetle outbreak in Colorado in the 1940s hadn't had a major influence on subsequent fire frequency, extent, or severity.

Interest in better understanding the insect-fire connection grew, Turner says, as the recent epidemics spread. One research target: lodgepole stands, where she and others began to tally up fuel characteristics and feed the data into fire behavior models. They hoped to learn whether beetle kill raises the risk of blazes developing into "ecologically severe" crown fires, which burn hotter and kill more trees than fires that crawl across the forest floor.

In a provocative 2011 study that modeled fire potential in forests in the Greater Yellowstone ecosystem, Turner was part of a team that found that during the "gray stage," when beetle-killed trees have lost their needles, the risk of crown fires actually decreases. That's because the fine fuels that help fire spread through the canopy, such as twigs and needles, were scarce. More surprisingly, their model suggested that even during the "red stage," when dead trees are clad in dry, easy-to-light needles, the risk of crown fires was no greater than in green forests.

> ***"We shouldn't let the bark beetles drive major management decisions."***
>
> **Thomas Veblen**, University of Colorado, Boulder

But models are imperfect, and some researchers cautioned against drawing sweeping conclusions from them. The models couldn't accurately account for tree-to-tree differences in needle moisture and flammability in mixed stands of living and dead trees, for instance. Such complexity can influence important fire behaviors, such as how quickly it spreads, how frequently it "spots" (shooting embers that ignite new fires), and how difficult it is for firefighters to control, says Matt Jolly, a research ecologist with the U.S. Forest Service's Missoula Fire Sciences Laboratory in Montana. After the fact, fires in beetle-killed and unaffected forests may look the same, he says, "but the actual fire behavior could have been vastly different." Such details are important to officials who must decide how to spend hundreds of millions of dollars on fighting wildfires every year, and whether to risk lives to stop a blaze or let it burn.

NAILING DOWN SUCH NUANCES was difficult until recently, Turner says, because few researchers "had real fires to work in." But six fires in 2011, including the Salt and Saddle Complex fires in Idaho and Montana, respectively, offered Harvey, one of Turner's doctoral students, an ideal chance to study how mountain pine beetles influenced the ecological impact of fire. In the sweltering summer of 2012, he led field teams into the charred remains of lodgepole stands relatively untouched by beetles and those where the insects had killed up to 84% of the trees. Drenched in sweat and smudged with soot, they counted dead trees in dozens of plots, determining whether they had been killed by fire or beetles before the fire by looking under bark for the tunnels the bugs dig. The researchers also determined fire severity by measuring the depth of char on tree trunks, how many needles and small branches were consumed, and how much duff and topsoil had burned off the forest floor. And they evaluated recovery, counting each green seedling popping from the blackened soil in plots where most or all trees were dead.

Harvey's results, published online on 29 September in the *Proceedings of the National Academy of Sciences*, highlight

PHOTOS: (LEFT TO RIGHT) © DAVID PARSONS/GETTY IMAGES; MATT OLSON

Published by AAAS

the sometimes counterintuitive dynamics between beetles and fire. In general, his group found that the insect-killed forests weren't more severely burned than greener stands. Other factors, including topography, wind, humidity, and air temperature, turned out to be more important in determining a fire's ecological severity.

That conclusion, based on real-world data and not models, is "a very important finding," says CU Boulder's Veblen, who was not involved in the study. It demonstrates that beetles didn't fundamentally change the impact that fire had on lodgepole forests: "They burn naturally at high severity, with or without beetles."

Harvey also saw hopeful signs of life, concluding that the prefire severity of a beetle outbreak didn't necessarily compromise the forests' capacity to regenerate. One key is a lodgepole adaptation called serotiny, in which resin seals and protects seeds within pinecones until wildfire melts the resin and releases the seeds. Beetle-killed trees can hold on to viable serotinous cones. "They've still got seeds locked up in the canopy," Harvey says.

Extreme fires can destroy the seeds, which are particularly vulnerable in red stage trees, where dead needles and branches make it more likely that whole treetops—cones, seeds, and all—will burn. But Harvey found that enough seeds survived in beetle-killed forests after severe fires to spur regrowth. Beetles didn't kill every tree, and "sometimes all you need are a few trees to get really high postfire seedling densities."

The recovery findings come with caveats, Harvey notes. They apply to just one forest type, lodgepole pine; in another study, he saw significantly lower postfire regrowth in beetle-killed forests dominated by Douglas fir, a nonserotinous species. And puzzles remain even in lodgepole forests. For instance, how long their cones protect seeds on dead trees isn't entirely understood, says Monique Rocca of Colorado State University, Fort Collins. This past summer, she did fieldwork similar to Harvey's in Colorado's High Park Fire scar and observed "large areas with very little regeneration," perhaps due to the severity of the beetle kill or the time between the tree deaths and the fire.

Harvey's study also suggests beetle damage can influence fire behavior—lending credence to what firefighters in the United States and Canada have reported. On hot, dry, and windy days, for instance, he found that crown fires were more likely to burn dead trees down to pencil-like sticks. (In contrast, crown fires in green lodgepoles often consume only needles and twigs.) That behavior may have minimal ecological impact, but Jolly of the Missoula Fire Sciences Laboratory notes it can pose serious threats and challenges to firefighters. Abundant dead wood also lends wildfires extra energy to create powerful and potentially dangerous air currents. One fire Harvey studied in a beetle-killed forest sucked in air with so much force that it toppled ponderosa pines more than 3 kilometers away, Jolly recalls. "We saw thousands of trees literally flattened."

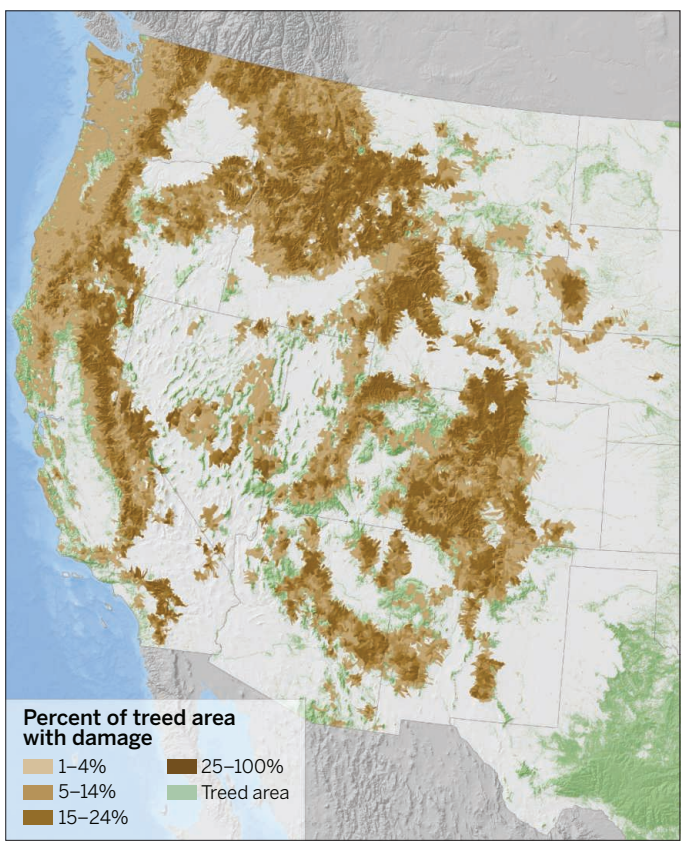
FOREST ECOLOGISTS SAY there is still plenty to learn about fire-insect interactions, but the new findings strengthen the idea that beetles may receive too much blame for fire risks. The bigger challenge for forests, many researchers say, is the changing global climate and the ways in which it is simultaneously altering numerous ecological processes. A hotter climate is expected to increase drought and fire frequency, for instance, both of which could make it harder for seedlings to gain a foothold. "Really droughty conditions directly after [a fire] are probably going to be the most significant challenge for these forests," predicts fire ecologist Tania Schoennagel of CU Boulder.

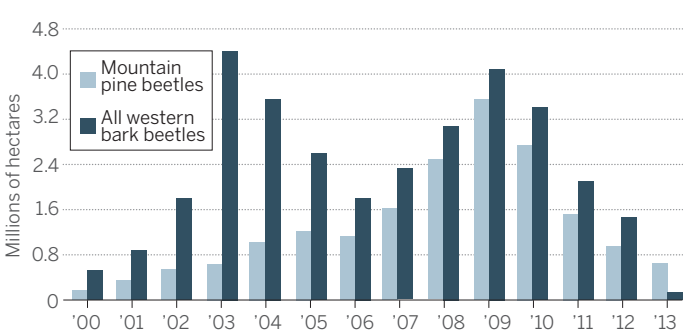
And with heat and drought eclipsing beetles as major factors in fire and forest resilience, some researchers question periodic proposals to remove beetle-killed trees from significant swaths of forest. Earlier this year, for instance, U.S. officials cited improving forest health and reducing fire risks as their goals in designating 18 million hectares as priority areas for "treatment," which can include removing dead or threatened trees. (So far, however, specific plans aren't set.) Thinning can reduce fire risks around communities, roads, and in recreation areas by reducing available fuel, whether or not beetles have killed trees. But many fire ecologists argue that aggressively thinning dead wood in forests far from human use and infrastructure is unnecessary and unlikely to "improve" forest health or prevent climate-driven fires. The research, Veblen says, suggests "we shouldn't let the bark beetles drive major management decisions" throughout forests. ■

Cally Carswell is a freelance science and environment writer in Santa Fe.

The beetles that won the west

Bark beetles have attacked some 17 million hectares of U.S. forest since 1996 and killed at least 5.2 million hectares of trees. The mountain pine beetle (*Dendroctonus ponderosae*), which often attacks lodgepole pines, is responsible for more than half of the damage.





CREDITS: ADAPTED FROM FOREST SERVICE/UNITED STATES DEPARTMENT OF AGRICULTURE

Published by AAAS



This Bronze Age leather shoe, found by a hiker in 2006, was perfectly preserved in Norway's alpine ice for thousands of years.

PHOTO: MUSEUM OF CULTURAL HISTORY/VEGARD VIKE

Racing the thaw

Archaeologists scramble to recover artifacts emerging from alpine ice

By **Andrew Curry**

For Norway's ice, the trouble began with a warm, dry winter. Then summer started early. By July, temperatures had crested 17°C atop the 2000-meter-high Jotunheimen mountains, part of the great range that runs like a spine down the middle of the country. By August, roaring meltwater streams and blue ice on the mountainsides signaled that the glaciers and ice patches that crown central Norway's highest peaks were in full retreat, exposing ice and rock not seen in up to 6000 years.

But what was bad for the ice has spurred a miniboom in archaeology. The ice patches—up to 30 meters thick and 50 hectares in size—formed when layers of snow compacted into ice over thousands of winters. The layer cake of ice trapped and preserved everything ancient people dropped into the snow, from reindeer and horse dung to leather, wood, and metal artifacts. As the ice melts, a trove of exquisitely preserved artifacts is suddenly released. Cloth and leather are intact and supple after millennia; Stone Age arrowheads still bear the resin used to haft them.

Across Norway, this summer was a "hectic season," says archaeologist Martin Callanan of the Norwegian University of Science and Technology (NTNU) in Trondheim. The large Juvfonne ice patch receded 30 meters this year—as much as it had in the previous 5 years—revealing arrows and other ancient artifacts. In Oppland county in southern Norway, Lars Pilø, an archaeologist with the county preservation office, and a team of archaeologists and glaciologists scoured the edges of other melting patches, using a helicopter to reach remote mountainous sites. In less than a month, they found nearly 400 objects, ranging from a complete horse skull to what might be a Viking walking stick and Stone Age arrows.

That haul makes Norway ground zero for ice melt archaeology today, but in the past 20 years rising temperatures have exposed frozen artifacts worldwide (*Science*, 19 April 2002, p. 454). Ötzi, the Stone Age mummy discovered in the Alps in 1991, may be the best-known ice patch find. Today, archaeologists hover over the Yukon in helicopters, identifying shrinking ice patches by the scent and sight of acres of ancient caribou dung. In the peaks of the Andes, mountaintop mummies frozen since the days of the Inca are now at risk.

Archaeologists are working to build a specialty from these frozen finds, with papers, conferences, and a new journal that debuts in November. The discoveries encompass a wide swath of Europe's history, from the time of hunter-gatherers to that of medieval trav-

Downloaded from www.sciencemag.org on October 9, 2014

Published by AAAS

elers on skis. In the short term, the priority is to rescue fragile artifacts quickly. But already researchers are beginning to use them to refine climate records and to understand how people in the icy parts of the globe used the landscape and dealt with past climate change since a global warm spell some 7000 years ago. "This whole thing has grown," Callanan says. "Now it's not just about the artifacts themselves, it's about how people have used and moved in the frozen portion of the planet."

NORWAY'S ICE PATCHES are a product of climate cooling that began about 7000 years ago. Unlike glaciers, which move and flow like rivers in slow motion, crunching boulders and artifacts as they go, ice patches form stable layers, like the silt at the bottom of a still lake. So although objects recovered from glaciers are a few centuries old at most, those in ice patches may go back to the time of the oldest ice. "If the artifacts had been under a glacier, they would have been destroyed," says Atle Nesje, a glaciologist at the University of Bergen in Norway.

At 1900 meters, the Oppland ice patches are high above the region's tree line, typically perched atop a layer of permafrost and jagged glacial scree. But they leave a clear mark of their retreat. A stable ice patch is edged with lichen, which takes centuries to establish, but retreating ice leaves a zone of bare, lichen-free rock, marking terrain revealed anytime from last week to 3 centuries ago.

In 2006, Pilø and his colleagues identified an ice patch called Lendbreen, on the north side of a jagged ridge, as one likely to produce artifacts, in part because in the 1970s it produced a complete Viking spear. To find more artifacts, they hike up to the base of the 400,000-square-meter patch and camp, sometimes for weeks at a time. Each day they scour the area between the lichen and the ice, making their way slowly across the exposed stone. Anything that's not stone, ice, lichen, or reindeer antler is by definition an artifact, brought there by human activity. When they find one, they log its location with a GPS device and photograph it, then collect it to carry back down the valley.

Once they thaw, millennia-old organic artifacts must be recovered quickly or they will decompose, dry out, and blow away. Leather and fabric are particularly fragile. Some artifacts are one-of-a-kind: In the warm summer of 2006, a sharp-eyed hiker brought a Bronze Age leather shoe to a local museum, sending archaeologists scrambling into the mountains. "The ice was bleeding artifacts everywhere," Pilø says of that summer. "We were just trying to extinguish fires."

In 2011, an intact woolen tunic, expertly patched and last worn 1700 years ago by a slender man about 170 centimeters tall, was found in a sodden heap in ice water at Lendbreen's upper edge. One of just a handful of European garments that old, the tunic's excellent preservation allowed curators to figure out the weave and the type of wool used to produce it, which came from an ancient sheep breed. Fragments of fabric woven in the same diamond twill pattern have been found in northern European bogs and at Roman forts, suggesting that the hunters here were in contact with the Roman world—or at least shared their fashion sense. "It was patched several times, and used for a long time," says Marianne Vedeler, a curator at the Museum of Cultural History at the University of Oslo and co-author on a 2013 paper in *Antiquity* on the tunic. "But why did [he] leave the tunic at 1900 meters?"

AS AUGUST DREW TO A CLOSE, searches near Lendbreen yielded several long, smooth sticks whose purpose is unknown. Packing a stick carefully in paper on the expedition's last day, archaeologist Elling Utvik Wammer furrowed his brow as he passed the artifact to Pilø. "Well, it's a goddamned runic inscription," Pilø said, peering at scratched letters running lengthwise along the stick. Such inscriptions often indicate ownership, though the researchers haven't yet deciphered the runes. Radiocarbon dating confirms that they were carved around 1000 C.E., during the Viking Age.

Other finds this summer show that people traversed these mountains on horseback. At Lendbreen, cairns of piled stone mark a mountain pass; the ankle-breaking scree along the route would have been passable only when covered by snow. Now clear of snow and ice, the path is littered with artifacts, from scraps of discarded leather moccasins to horseshoes and nails. Icelandic zooarchaeologist Rúnar Leifsson of the Cultural Heritage Agency of Iceland in Reykjavík found a complete horse skull that



Treasures from the ice. A horse skull from a small Viking breed shows how people once crossed a treacherous mountain pass; archaeologists retrieved a pocketknife dropped by an ancient traveler, and an iron arrowhead from the Viking Age, lost perhaps 1000 years ago, emerged from an icy pool.

PHOTOS: GLACIER ARCHAEOLOGY PROGRAM/OPPLAND COUNTY COUNCIL (3)

Published by AAAS

resembles modern Icelandic horses—small, tough descendants of imported Viking steeds—rather than larger modern European breeds. "The organic remains are so well preserved, it's unbelievable they're as old as they are," he says.

The evidence of horses was so thick on the ground that the team named one spot Dung Island. "We have thousands of kilos of horse shit. A lot of it could have been deposited last week," says James Barrett, an archaeologist at the University of Cambridge in the United Kingdom. "It doesn't sound all that exciting, but it opens up all kinds of avenues of analysis," including DNA investigations into ancient horse breeding.

But reindeer, not horses, are at the center of most Norwegian finds. In the Scandinavian summers, reindeer seek shelter on ice patches and glaciers to avoid biting flies. In the past, hunters followed. More than half of the objects discovered in Oppland so far are "scare sticks," wooden rods with a thin, square flag of wood attached to one end with a string. A historical account from 18th century Greenland illustrates similarly constructed sticks and explains that ancient hunters used lines of scare sticks fluttering in the breeze to guide skittish reindeer across the ice toward hunting blinds, Pilø says.

The sticks were used intensively from about 300 C.E. to 1000 C.E., according to Pilø, but the oldest go back to before the ice reached its full extent. Some scare sticks are found jammed upright between rocks or in hunting blinds, just as ancient hunters placed them, indicating that the area was ice-free then. Carbon dates for these sticks put that time at more than 1500 years ago. Conversely, "if they are lying flat on the ice, you know the hunters put them in the snow," until they melted out and toppled in the modern heat, Nesje says.

Scare stick numbers seem to peak at periods when trade was liveliest in Europe, for example during the Viking Age, when the Norse traveled from Scandinavia to as far as Turkey, England, and France. That suggests that reindeer hides and antler from the highlands were important trade goods tying the region to the rest of Europe. More scare sticks could mean more reindeer hunting to satisfy rising demand. "Activity in the high mountains was connected to long-distance demand," Barrett says. "They are not isolated, marginal phenomena—they're happening because of drivers from elsewhere."

SIGNS OF THIS DISTINCTIVE hunting method were scarce this summer, perhaps a sign that an era has melted away: "That ice is now gone, and the sticks have all melted out," Pilø says. "Now we're finding other types of older artifacts." In August, not far from Langfonne ice patch, the team found 23 arrows, one with a stone tip and another tipped with shell. In mid-September, Pilø got the first radiocarbon dates back: One arrow was lost by a hunter 5900 years ago in the early Neolithic, 6 centuries before Ötzi; it is the oldest arrow yet dated in Norway and only a few centuries younger than the ice patches themselves.

Further north, too, "we're now at the really old layers," Callanan says. Equally old arrows and part of a bow emerged from the ice at a site called Storbreen in central Norway, studied by the Snow Patch Archaeology Research Cooperation project, based at NTNU. The well-preserved arrows—some with sinew threads still clinging to their heads—are helping Callanan study how hunting technology changed over the course of the Stone Age.

Despite the overall warming trend, the ice is fickle. In Switzerland, the Schnidejoch glacier melted dramatically between 2003 and 2008, yielding hundreds of artifacts ranging from a Roman brooch to a bow that could have been carried by an Ötzi contemporary. The finds showed how people traveled across the Alpine pass for millennia. Then in 2010, just as researchers thought the patch would melt completely, a wet, cold winter covered it with new snow. Since then, Swiss ice finds have slowed to a trickle, says archaeologist Leandra Naef of the University of Zurich in Switzerland. After 2 weeks of rain and snow in August, she had to call off her planned ice patch search. "It was the worst summer ever," she said.

In the Andes, a handful of exquisitely preserved Incan mummies, likely human sacrifices, have been discovered half-thawed at high altitudes since 1985 (*Science*, 18 May 2012, p. 834). Any mummies still undiscovered are now at risk, says archaeologist Constanza Ceruti of the Catholic University of Salta in Argentina. "Mummies that stay on the mountainsides will definitely be affected," she says. Melting ice and permafrost also threaten frozen sites in Siberia and in the Altai Mountains on the border between Russia and Mongolia.

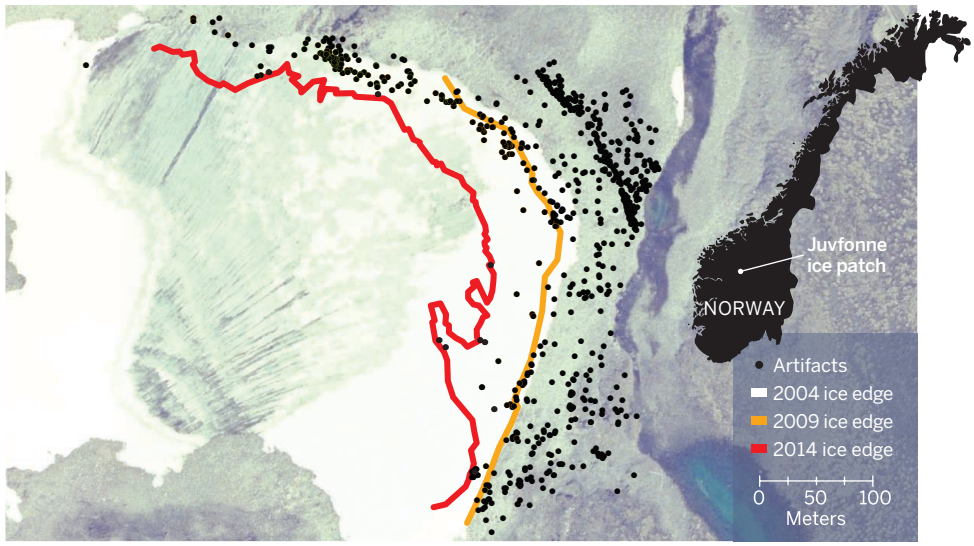
In Canada's far north, years of melting in the 1990s yielded a partially preserved human body from just before Europeans reached this part of North America, as well as hundreds of throwing darts and arrows that document 9000 years of caribou hunting. DNA from the body, dubbed "long-ago person found" in the local language, was matched to 17 people still living nearby. But the avalanche of finds has slowed, says Greg Hare, an archaeologist with the Government of Yukon in Whitehorse, Canada. "We're not experiencing the dramatic melting we were seeing 10 or 12 years ago," he says. Global warming may be pushing more moisture into the air in the Yukon, meaning snowier winters and less melting.

As climate warming continues, archaeologists must move swiftly when a warm summer strikes. As the first snow fell on the Norwegian highlands in late September, Pilø contemplated summers to come. "The ice is going, so we need to continue this work until the oldest ice is melted," he says. "It's like a story where you know the ending but not the plot. Is it going to go quickly, or is it going to take its time?" ■

Andrew Curry is a freelancer in Berlin.

Going, going ...

Norway's Juvfonne ice patch is shrinking fast, rapidly releasing hundreds of artifacts.

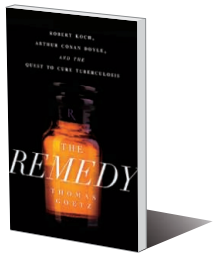


MAP: MIMISBRUNNR KLIMAPARK2469 RESEARCH GROUP

Published by AAAS

Research, rivalries, and the quest for a remedy *p. 174*

Capturing biodiversity change *p. 166*



PERSPECTIVES



Survival skill. Sidewinder rattlesnakes are one of a few snake species that can move sideways up sandy slopes, helping them to survive in deserts.

APPLIED PHYSICS

Of snakes and robots

How can snakes and robots move up sandy slopes?

By **John J. Socha**

As anyone who has run up a sand dune can attest from burning calves, climbing a sandy slope is demanding. The root of the struggle—in animal and vehicle alike—comes from the behavior of the sand, a granular medium that can slip, slide, and flow like a fluid. Yet, desert-dwelling snakes can ascend sandy slopes with grace and energetic ease (*1*) through a process called sidewinding. Having no limbs to push off should make the matter worse, yet the snakes make it look simple. How do they do it? On page 224 of this issue, Marvi *et al.* (*2*) explore the physics of sidewinding in animal and robot, revealing how limbless locomotors can move up sandy slopes.

Among animals, only snakes sidewind, a behavior found mostly in vipers and a few other snake species that live in desert or muddy environments (*3*). Sidewinding gets its name from the orientation of the snake while slithering, appearing to move to the side rather than toward the head (see the figure) (*4*). As with most other forms of serpentine movement, the snake produces force by curving its body, but in sidewinding the body does not slide. Instead, it rolls and peels like a wheel (*4*, *5*), maintaining static rolling contact along a few points while the rest of the body is lifted in the air (*6*). Marvi *et al.* show that this contact and lifting are key to successful sand slope climbing in the sidewinder rattlesnake *Crotalus cerastes* (see the first photo) and in a snakelike robot composed of 17 modular segments (see the second photo).

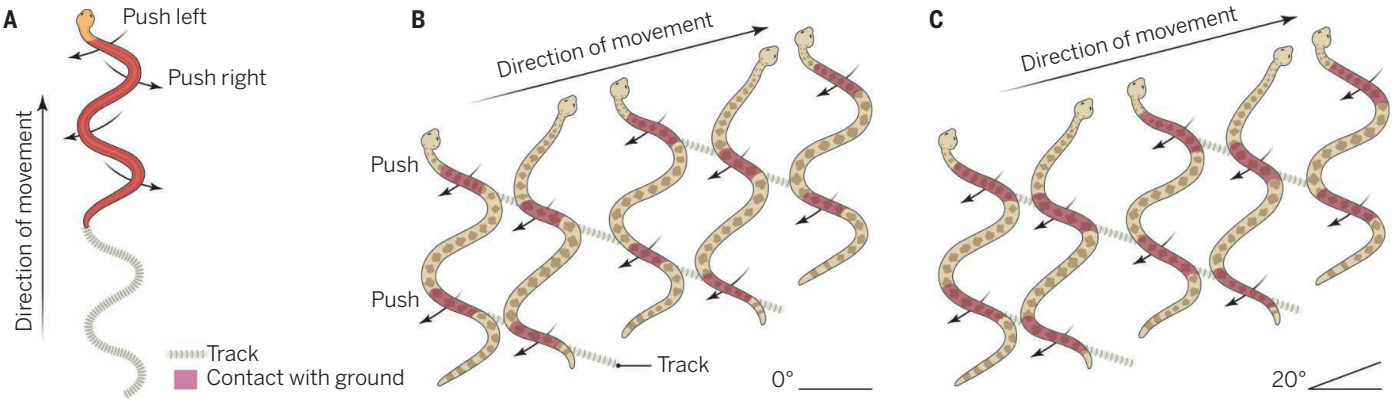
Studying the snake and robot together was a reciprocally illuminating process: The robot was used as a model to probe the snake, and the snake was used to understand and improve the robot. Part of the motivation for working with this particular robot (dubbed "Elizabeth") arose from a real-world experience. On an archaeological mission in Egypt, Elizabeth was tasked to explore a sandy room with a slope, but failed miserably in its attempt to move forward, slipping and pitching over. Coauthor Choset had developed a long line of snakelike robots over the course of two decades, achieving various locomotor styles including sidewinding (*7*) and pole climbing (*8*), but sand climbing had remained elusive.

To determine patterns of movement in a controlled environment, the team investigated the robot and snakes on a custom-made, tiltable bed of sand. Built in the Zoo Atlanta for easy access to a broad range of

Biomedical Engineering and Mechanics, Virginia Tech, 495 Old Turner Street, Blacksburg, VA 24061, USA. E-mail: jjsocha@vt.edu

PHOTO: ADAM THOMPSON

Published by AAAS



Sidewinding explained. Rather than moving in the direction of the head as do other snakes (**A**), sidewinding snakes move sideways both on level ground (**B**) and up slopes (**C**). Marvi *et al*. show that when snakes sidewind up a slope, they increase the body length that is in contact with the ground, thereby reducing slip.

snake species for comparison, the bed was tilted from level to 20°, just below the critical incline where the sand will flow with any perturbation. The sand was air-fluidized, producing a repeatably uniform volume and flat surface before each trial and thus enabling precise measurement of intrusion depth, contact length, and body lifting by the sidewinding locomotors.

The properties of granular media vary with features like particle size and shape, friction, and compaction (*9*). Mindful of this depend ence, Marvi *et al*. went the extra mile to provide the snakes with a realistic substrate. In an unprecedented feat of experimental rigor and determination, they trucked hundreds of pounds of sand in from the Yuma Desert of Arizona to ensure that the experimental conditions matched those of the native environment of the sidewinder rattlesnake.



Sidewinding robot. By studying snakes and robots, Marvi *et al*. were able to elucidate how snakes sidewind and to modify a robot so that it could also achieve this feat.

The authors discovered that the sidewinding snakes create two waves of bending, one horizontal and one vertical, which move simultaneously from head to tail with an offset of a quarter period. Elizabeth also used two orthogonal waves to sidewind on level ground (*7*), but could not sidewind up a slope. What was the missing ingredient?

Marvi *et al*. found that the snakes dealt with the challenge of increasing slope not by digging in deeper, but by increasing the length of body contact with the sand, correspondingly decreasing the amount of body lifted in the air (see the figure). Effectively, as the slope became steeper, the snake laid down more body, increasing its purchase on the sand until nearly half the body was in contact. By modifying the robot, the authors found a range of contact lengths that produced sidewinding up the slope, but as the slope became steeper, fewer options resulted in effective climbing. This suggests that the snakes are physically constrained to certain movement patterns to move up a slope.

Why do the snakes not dig in deeper? It is energetically costly to displace level sand (*10*), but the important question is how yield force changes with increasing slope. (Yield occurs when the deformed sand cannot return to its original state when the force is removed.) In follow-up experiments, the authors dragged a flat plate through sand and showed that yield occurred with smaller forces at greater inclines. This means that the maximum force that the snake can generate without slipping becomes smaller with greater slope. The snake has to do something to compensate, and what it does is increase its contact length. This led to a new model of sidewinding locomotion: the snake produces two offset waves of bending—a neuromechanical "template" (*11*)—and varies contact length to prevent slip.

The team also tested 13 other closely related species of pit vipers. Although only some specialized snake species excel at sidewinding, many others were thought able to adopt this mode given the right conditions (*3*, *6*, *12*, *13*). Yet, none of the other snake species switched to sidewinding when presented with the sandy substrate. Some could move forward haltingly using other means of locomotion, but when the bed was tilted at a small angle, all but one were stopped in their tracks, with some flailing helplessly. This suggests that the evolution of sidewinding may have required a change in neuromotor control (*14*), shifting the timing of muscle activation to match the required template for sidewinding.

The work of Marvi *et al*. demonstrates the strength of integrating biology, engineering, and physics, providing the finest example to date of the reciprocal use of animals and robots for mutual illumination. The drive to understand the mechanics of sidewinding has brought us one step closer to achieving lifelike locomotion in robots. The upshot seems to be that going up slippery slopes with no legs simply requires a double wave to target the right pattern of contact. ■

REFERENCES

1. S. M. Secor *et al*., *J. Exp. Biol.* **163**, 1 (1992).
2. H. Marvi *et al*., *Science* **346**, 224 (2014).
3. H. W. Greene, *Snakes: The Evolution of Mystery in Nature* (Univ. of California Press, Berkeley, 1997).
4. W. Mosauer, *Am. Nat.* **64**, 179 (1930).
5. J. Gray, *J. Exp. Biol.* **23**, 101 (1946).
6. C. Gans, H. Mendelssohn, in *Toxins of Animal and Plant Origin*, A. de Vries, E. Kochva, Eds. (Gordon and Breach Science, London, 1972), vol. 1, pp. 17–38.
7. R. L. Hatton, H. Choset, in *Robotics and Automation (ICRA), 2010 IEEE International Conference on Robotics and Automation*, pp. 691–696.
8. F. Enner, D. Rollinson, H. Choset, in *Robotics and Automation (ICRA), 2013 IEEE International Conference on Robotics and Automation*, pp. 5168–5173.
9. R. M. Nedderman, *Statics and Kinematics of Granular Materials* (Cambridge Univ. Press, New York, 2005).
10. A. G. Winter *et al*., *Bioinspir. Biomim.* **9**, 036009 (2014).
11. R. J. Full, D. E. Koditschek, *J. Exp. Biol.* **202**, 3325 (1999).
12. B. C. Jayne, *Copeia* **1986**, 915 (1986).
13. H. B. Lillywhite, *How Snakes Work: Structure, Function and Behavior of the World's Snakes* (Oxford Univ. Press, New York, 2014).
14. A. R. V. Rivera, R. W. Blob, *Biol. Lett.* **9**, 20130471 (2013).

10.1126/science.1259970

ILLUSTRATION: P. HUEY/*SCIENCE*; PHOTO: NICO ZEVALLOS

Published by AAAS

PLANT SCIENCE

Plant synthetic biology takes root

Applying the basic principles of synthetic biology to plants shows progress

By **June I. Medford**[1] *and* **Ashok Prasad**[2]

The evolution of computers and electronics from bulky room-size devices to the sleek devices of today has relied on a well-honed strategy: Use parts whose behaviors are quantitatively defined and assemble complex systems from simpler modules. Synthetic biology aims to bring this approach to living organisms (*1*, *2*), and it is already starting to happen in plants. A sensor and response system can be designed, sensor proteins programmed in a computer, encoded in a plant, and empowered with such properties as memory and amplification (*3*). Using genetic information and mathematical analysis allows one to design predictable and quantitative functions in plants, comparable to those of integrated electronic circuits. Just as integrated circuits can be reused in diverse electronic devices, from cell phones to aircraft, synthetic biology components should function predictably in different synthetic circuits and plants.

What sets synthetic biology apart from "engineering" plants through transgenic technology is that the former aims for predictable biological functions through the use of mathematical analyses, modeling, and orthogonal parts. It therefore relies on quantitatively characterized gene components such as transcriptional promoters, terminators, and proteins (e.g., translational modifiers). Like electronics, synthetic biology assembles quantitatively defined parts in particular ways (with standard rules for their connections) to produce biological functions such as memory, amplification, and precise switches.

Synthetic gene circuits are designed to act independently of the organism's natural systems. They can be designed in silico and then assembled to yield the correct behavior (*4*). For example, gene circuits that use Boolean logic (values are reduced to "true" or "false") have been produced in bacteria by modeling behavior in silico and producing simple logic gate functions to control biological signals and responses. Thus, in *Escherichia coli*, many synthetic circuits starting from a genetic toggle switch (*5*) to genetic programs using layered logic gates (*6*) have been engineered by this procedure.

[1]Department of Biology and [2]Department of Chemical and Biological Engineering, Colorado State University, Fort Collins, CO 80523, USA. E-mail: june.medford@colostate.edu

If genetic toggle switches and genetic logic gates could be produced in plants, precise control of plant traits would be feasible. A bioenergy crop such as sorghum could devote its resources to biomass production prior to activating a synthetic toggle switch that diverts the plant's resources to oil accumulation. Basic plant studies also could benefit from a synthetic toggle switch to help elucidate complex gene functions. Such logic circuits in plants have not yet been achieved.



Sentinel plant. A sensor protein was computationally designed and linked to downstream gene components to enable a plant (*Nicotiana tabacum* shown) to detect an external ligand (100 nM TNT) and respond with a visual display (such as loss of chlorophyll) (*3*).

The vast majority of synthetic genetic circuits have been produced in bacteria, and designing similar circuits for plant platforms faces the greater complexity of plant genomes and protein networks. Moreover, there are currently only a handful of quantitatively characterized plant components with different rules for assembling them into functional expression units in monocots and dicots. In addition, unlike bacterial plasmids, plant components may be affected by the contextual information provided by the chromosome position.

Plant biologists have long understood positional effects from variable transfer DNA (T-DNA) insertion in the chromatin. The tumor-inducing plasmid of bacteria such as *Agrobacterium tumefaciens* has been used in plant genetic engineering in which tumor-promoting genes are removed and a gene of interest inserted for stable integration into plants (*7*). Less well appreciated is the need for chromatin insulators within a synthetic gene circuit to rigorously isolate one gene-encoded function from another. These positional effects are just beginning to be understood through approaches such as the use of unique chromosomal positions or "landing pads" to use when quantitatively characterizing plant components. Multiple technologies for targeted chromosomal integrations such as zinc fingers, TALENS, and CRISPRs exist for this type of approach in plants (*8*, *9*).

A further challenge in addressing the context-dependent behavior of synthetic circuits in plants is the unavoidable interaction of synthetic proteins and genes with the host system. For example, host DNA can act as a load on a synthetic gene circuit and show altered behavior (e.g., slower switching in a toggle switch) (*10*). Similarly, orthogonal synthetic circuits may be coupled to the host system through their dependence on the host system for synthesis and degradation. Hence, if a synthetic circuit functions correctly in a model plant like *Arabidopsis thaliana*, the effects of the context should be considered when transferring that circuit to a species such as soybean or corn.

One approach to manage the challenges of using plants as a synthetic biology platform is to refactor the genetic process of interest, that is, to simplify design parameters and remove inefficiencies while still accomplishing the desired function. For example, the nitrogen fixation pathway from *Klebsiella oxytoca* was refactored by removing noncoding DNA and nonessential genes, connecting the remaining genes to orthogonal promoters, and altering the DNA sequences to be as different from the original as possible while still coding for the same proteins (*11*). The synthetic nitrogen fixation cluster could then be introduced into a plant's chloroplast or mitochondria.

Published by AAAS

Whereas electrical circuits are physically connected with wires, gene functions often require diffusible factors (e.g., proteins). Hence, producing a predictable function is more challenging in biological systems and subcellular compartmentalization must also be considered. Simplifying complex signaling systems in plants allowed the production of the first synthetic signal transduction system (*12*), linking the presence of external substances [such as trinitrotoluene (TNT)] to internal responses with only two or three genes; when coupled with computational protein redesign, the result was "computerized" detection technology in plants, which may have applications as environmental sensors (*3*, *13*) (see the figure).

Another major challenge is that quantitative characterization of genetic components for a multicellular plant in isolated plant cells (such as mesophyll protoplasts) has limitations, particularly because cultured plant cells do not have the cell-cell interactions found in differentiated tissues. Nonetheless, progress has been made in transient expression methods that enable the efficient expression of multiple genes within the same plant cell over a time scale of days (*14*, *15*). This has led to the production of macromolecular complexes, such as virus-like particles that have potential use in nanotechnology and as vaccines. However, it is important that genetic controls be introduced into whole plants to assess their behaviors under "real life" conditions.

By applying theory-driven engineering approaches developed for electronics to plant biology, we can not only uncover the natural genetic circuits behind complex gene regulations in plants, but we could also design traits that are new to evolution and beneficial to humanity. The future is looking green. ■

REFERENCES

1. D. Endy, *Nature* **438**, 449 (2005).
2. E. Andrianantoandro *et al.*, *Mol. Syst. Biol.* **2**, 2006.0028 (2006).
3. M. S. Antunes *et al.*, *PLOS ONE* **6**, e16292 (2011).
4. J. A. Brophy, C. A. Voigt, *Nat. Methods* **11**, 508 (2014).
5. T. S. Gardner, C. R. Cantor, J. J. Collins, *Nature* **403**, 339 (2000).
6. T. S. Moon, C. Lou, A. Tamsir, B. C. Stanton, C. A. Voigt, *Nature* **491**, 249 (2012).
7. C. N. Stewart *et al.*, Eds., *Plant Transformation Technologies* (Blackwell, West Sussex, UK, 2011).
8. V. K. Shukla *et al.*, *Nature* **459**, 437 (2009).
9. Z. Feng *et al.*, *Proc. Natl. Acad. Sci. U.S.A.* **111**, 4632 (2014).
10. S. M. Lyons, W. Xu, J. Medford, A. Prasad, *PLOS Comput. Biol.* **10**, e1003533 (2014).
11. K. Temme, D. Zhao, C. A. Voigt, *Proc. Natl. Acad. Sci. U.S.A.* **109**, 7085 (2012).
12. M. S. Antunes *et al.*, *Mol. Syst. Biol.* **5**, 270 (2009).
13. K. J. Morey *et al.*, *Methods Enzymol.* **497**, 581 (2011).
14. S. D. Yoo, Y. H. Cho, J. Sheen, *Nat. Protoc.* **2**, 1565 (2007).
15. F. Sainsbury, G. P. Lomonossoff, *Curr. Opin. Plant Biol.* **19**, 1 (2014).

10.1126/science.1261140

ECONOMICS

Adjusting to the fertility bust

What is the best response to declining populations?

By **Timothy M. Smeeding**

Fertility in the United States is at an all-time low, having reached a rate of 1.86 children per woman of child-bearing age in 2013 (*1*). Researchers warn of the worldwide "low-fertility trap" (*2*), and the population of Europe is projected to decline in the next 25 years (*3*). Should we be worried? On page 229 of this issue, Lee *et al.* (*4*) argue that moderately low fertility and modest population decline favor a higher living standard. They are not alone in urging restraint to concerns about population aging (*5*) but have painstakingly assembled a new data set to make their point very clearly. Meanwhile, Gerland *et al.* contend on page 234 of this issue (*6*) that the world population will still grow substantially and is unlikely to stop growing in this century. However, almost all of the projected population increase by 2100 is confined to sub-Saharan Africa, with almost all other continents and major countries experiencing declining rates of population growth and rising ratios of elders to workers.

There was once a "demographic dividend" from high fertility that has now largely disappeared. Substantial reductions in child and infant mortality rates meant that women and families needed to have fewer children to reach their desired number of offspring. Falling child mortality led to a higher life expectancy and, at least initially, a larger working-age population. More workers led to higher fiscal balances in intergenerational transfer systems, such as most social retirement systems in rich countries. For a time there were more workers than elders, raising revenue per elder and benefiting one generation (the older one) at the expense of another.

The policy problem of an aging population is surely one to be recognized. The U.S. "baby boom" between 1946 and 1960 created a huge demographic dividend for the parents of these children, not to mention a larger number of offspring to care for these persons in old age. But then fertility declined rapidly, and the number of elders (now the early baby boomers) became large relative to the number of workers as lower fertility reduced the growth rate of the labor force. At the same time, continuing improvements in old-age mortality led to faster growth of the elderly population. This U.S. baby bust has led to projections of substantial long-term changes in federal spending priorities and shortages in trust funds for Social Security and Medicare (*7*).

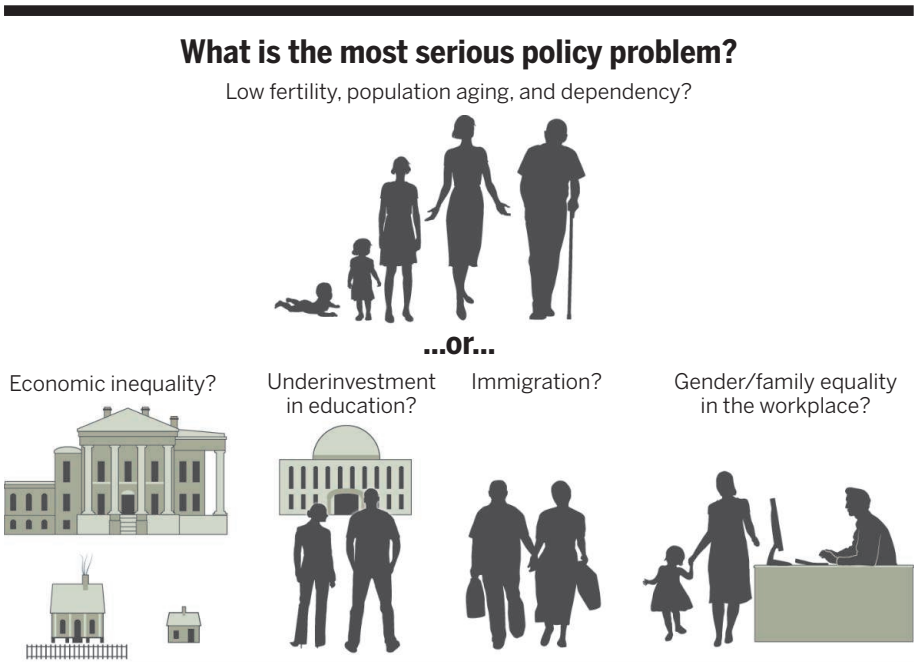
In addition to this common policy problem, what else matters in aging populations (see the figure)? Well, in a word, behavior. First, savings, work, and both physical and human capital formation may change. Older generations, with an extended period of retirement and fewer workers to support them, can and often do save more and work longer. That saving will lead to faster economic growth if it increases physical productive capital. This growth dividend can produce a larger economic pie for all, especially if greater education investments are made to increase human capital in the younger and smaller generation to complement the technological change that comes with physical capital growth. But this is not always the case; in fact, the United States may be losing the race between investments in human capital (education) and physical capital (technology) (*8*). And so we have a different worry: underinvestment in education.

"... as governments confront population aging, they must also address a number of related policy issues: immigration, inequality, education, and gender/family equity in the workplace ..."

Second, private transfers from the old to the young can offset many of these intergenerational imbalances. The generation who feels their living standards are highest—that is, current elders—may transfer more money and educational opportunity to those who are younger, as has been the case in many rich nations in recent decades. These transfers do, however, depend on the distribution of wealth among the older populations compared to younger ones. Growing wealth inequality (*9*) means that wealthy households

Department of Public Affairs and Economics, University of Wisconsin, Madison, WI 53706, USA. E-mail: smeeding@lafollette.wisc.edu

Published by AAAS



The consequences of falling fertility. As fertility falls and populations age in most parts of the world, numerous policy issues arise.

are much more able to protect their generationally disadvantaged children—for example, through payments for college tuition and other "strategic transfers." Less-well-off households have fewer resources to devote to their children, exacerbating inequality.

Third, immigration is both important and controversial in rich countries (*10*). In emigrant nations, a "good son" is one who leaves, at least temporarily, to earn more money and transfer it back to his family in the home country, a different type of intergenerational transfer. Both temporary and permanent immigrants from poorer to richer nations are usually the youngest and most productive, and those immigrants who stay usually have higher fertility rates than the native population. Of course, eventually these permanent migrants grow old, too. And so, we are back to investing in the productivity of the younger generation, but now a growing immigrant generation.

The United States faces this issue right now—with the aging white population being asked to invest in the education of a growing nonwhite child population, many of whom are the children of immigrants. These investments will be made all the harder at the state and local level by the diversion of state taxes into health insurance for the poor and the elderly. Similar issues may follow in Europe and other parts of the rich world as African populations grow and African migration increases.

And then there is fertility itself (*1*). Sometimes falling fertility is an unmitigated good thing. For instance, American fertility has reached its record low through falling birthrates among teens and women in their early 20s. This is good news for improving the upward mobility of children, keeping young women out of poverty, and bringing the U.S. teen pregnancy rate closer to that in other rich countries. But in other cases, falling fertility among older, more stable couples is exactly the baby bust that concerns demographers (*2*).

Finally, fertility decline is a direct product of greater rights and opportunities for women. But fertility can rise again with policy that encourages and supports family formation. Most young women want motherhood to be a part of their lives (*11*). But the deferral of child bearing to older ages, later marriages for the well-educated, and the reduction of births in rich nations is part and parcel of the higher educational attainment and career aspirations of young women. Fertility recently rebounded in Sweden and France. Both nations now have birth rates above those in the United States. Both nations provide subsidized day care for children on a sliding scale based on family income. Paid parental leave and flexible work schedules also help support and nurture family growth. Indeed, there is a national family and parental leave policy in every rich country except the United States (*12*, *13*). Gender equity is thus another policy issue to consider.

Lee *et al.* (*4*) conclude that the problem of population aging in rich and middle income countries is tractable: Low fertility can challenge government social retirement programs, but those programs can adjust by reducing benefits for the old or raising taxes on the young. And moderately low fertility and population decline favor the broader material standard of living for all. But as governments confront population aging, they must also address a number of related policy issues: immigration, inequality, education, and gender/family equity in the workplace (see the figure). Such considerations can enhance economic growth, raise fertility, dampen or reverse population decline, and produce a fairer and better world for all generations.

So what about Africa? Gerland *et al.* (*6*) acknowledge that greater investments in family planning programs and girls' education might cause a decline in population growth this century in Africa, just as it has in most of Asia in the 20th century. But just like population aging has its set of problems, the authors suggest that rapid population growth in high-fertility countries can create its own environmental, economic, and health-related challenges as public and private sector investments lag in health, education, and infrastructure.

The simple moral is that whether population increases or declines, adjustments will have to be made. Sub-Saharan Africa has a wide range of issues such as racism and genocide to contend with also, but the rest of the world will continue to experience population aging and, in some areas, continued population decline. The time to respond to these challenges is now. ■

REFERENCES

1. B. E. Hamilton *et al.*, *Births: Preliminary data for 2013. National Vital Statistics Reports,* vol. 63, no. 2 (National Center for Health Statistics, Hyattsville, MD, 2014).
2. W. Lutz, V. Skirbeck, M. R. Testa, *Vienna Yearbook of Population Research*, 167 (Austrian Academy of Sciences, Vienna, 2006).
3. European Union, The 2012 Ageing Report: Underlying Assumptions and Projection Methodologies, *European Economy* **4**, 10.2765/15373 (2011).
4. R. Lee *et al.*, *Science* **346**, 229 (2014).
5. M. S. Teitelbaum, J. Winter, *The Global Spread of Fertility Decline: Population, Fear, and Uncertainty* (Yale University Press, 2013).
6. P. Gerland *et al.*, *Science* **346**, 234 (2014).
7. D. W. Elmendorf, *Shifting Priorities in the Federal Budget* (Congressional Budget Office, Washington, DC, 2014); www.cbo.gov/publication/45700?utm_source=feedblitz&utm_medium=FeedBlitzEmail&utm_content=812526&utm_campaign=0.
8. C. Goldin, L. Katz, *The Race Between Technology and Education* (Harvard Univ. Press, Cambridge, MA, 2008).
9. T. Piketty, *Capital in the 21st Century* (Harvard Univ. Press, Cambridge, MA, 2014).
10. C. Parsons, T. M. Smeeding, *Immigration and the Transformation of Europe* (Cambridge Univ. Press, Cambridge, UK, 2006).
11. G. Livingston, "Birth rates lag in Europe and the U.S., but the desire for kids does not," Factank, Pew Research Center, 11 April 2014.
12. J. C. Gornick, A. Hegewisch, in *Lessons from Europe? What Can Americans Learn from European Public Policies*, Daniel Kelemen, Ed. (Congressional Quarterly Press, Washington, DC, 2014), pp. 17–41.
13. C. Goldin, *Am. Econ. Rev.* **104**, 1091 (2014).

10.1126/science.1260504

ILLUSTRATION: P. HUEY/*SCIENCE*

Published by AAAS

QUANTUM PROCESSING

Catching the quantum sound wave

A superconducting qubit built to listen as well as see

By **Rusko Ruskov** *and* **Charles Tahan**

An ultrasound transducer ("the wand") both creates and detects sound waves that travel through the body to create images of internal organs or precious cargo (see the figure, panel A). This compact device is made possible with piezoelectric crystals that expand or contract in response to an applied voltage and thus interconvert sound waves and electrical signals. Because sound travels relatively slowly, there is time to process the reflected pulses and display an image in real time. These measurements are in the realm of classical physics, but sound could also play a useful role in quantum-based devices. On page 207 of this issue, Gustafsson *et al.* (*1*) take a major step toward that goal, demonstrating a system in which a specially engineered artificial atom in the form of a superconducting quantum bit (qubit) couples to propagating surface acoustic waves on a chip. This sound-matter system shows evidence of quantum behavior.

A fundamental concept of quantum physics is the wave-particle duality of elementary particles; for example, a photon behaves like a particle or a wave depending on the measurement being made. The quantum nature of light is especially evident in experiments that couple moving photons with atoms (quantum optics) or quantize a confined light field, placing an atom between two mirrors (cavity quantum electrodynamics, or cavity QED). That light is composed of photons is made clear when a single atom is shown to radiate one photon at a time (*2*).

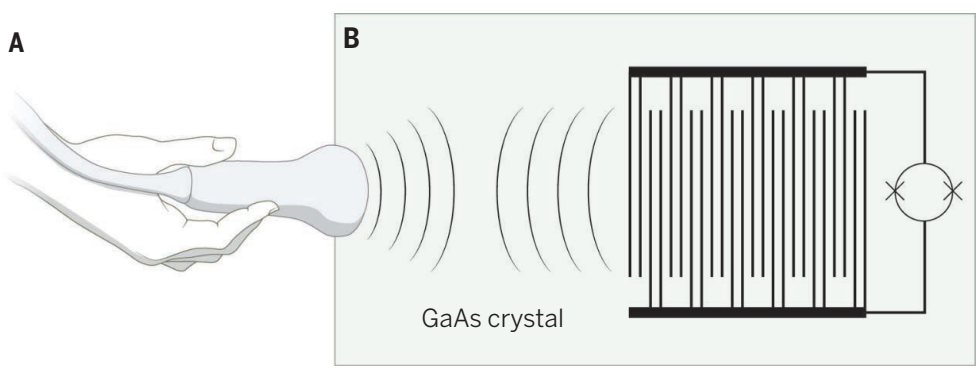
Although sound waves in solid-state systems such as a crystal are the collective excitation of many atoms, quantum mechanics tells us that these too behave at the smallest level as quantized particles called phonons. Mechanical systems have received renewed attention, especially in the study of nanomechanical resonators as nanofabrication and quantum control techniques have improved (*3*–*7*).

The work of Gustafsson *et al.* introduces a new test bed to investigate the quantum properties of sound that is reminiscent of the earliest quantum optics experiments. In recent years, the essential physics of quantum optics and cavity QED have been replicated with superconducting circuits (circuit QED) (*8*). In circuit QED, the photons are in the microwave regime, and anharmonic ("atom-like") superconducting qubits that use the loss-less nonlinear element of the Josephson junction take the place of the atoms. Whereas atoms are microscopic and provided by nature, superconducting circuits are macroscopic, can be made artificially on a chip, and offer exceptional design choice. These artificial atoms can be tuned to be very sensitive to electromagnetic fields, and this capability has been used to create strong light-qubit coupling, both in a cavity and with itinerant photons.

Gustafsson *et al.* took advantage of the flexibility of superconducting circuits to design a transmon-type qubit (designed to minimize sensitivity to charge noise) that couples strongly with surface acoustic waves (SAWs) in the crystal on which the qubit sits. First, they deliberately fabricated a qubit on a gallium-arsenide piezoelectric crystal. In a piezoelectric crystal, strain and electric fields are directly coupled, the latter being a natural interaction mechanism for superconducting qubits. They then integrated a SAW transducer into the qubit, which can act as both a speaker and a microphone for SAWs. By fabricating metal wires in an interdigitated finger arrangement and applying an oscillating voltage, the electric field drives the strain field via the piezoelectric effect to produce sound waves on the surface of the crystal.

In this manner, Gustafsson *et al.* constructed a beautifully straightforward experiment. A standalone interdigitated transducer (IDT) (analogous to the wand shown in panel A of the figure) generates SAWs directed toward the sound-sensitive transmon qubit (see the figure, panel B). This IDT also detects acoustic waves that reflect back from or are generated by the sound-sensitive qubit, which one might call a "soundmon". The IDT attached to the qubit translates the incoming sound wave to an electrical signal that can act as an input signal for the qubit. This qubit is designed to interact with phonons of precisely the same frequency as those produced by the IDT.

The critical question is whether the artificial atom really couples to sound in a quantum way. The qubit can be used to probe the quantum nature of sound because its energy levels are not equally spaced. In particular, the energy splitting between the ground and first excited states is greater than the splitting between the first and second excited states. The phonon quanta that make up the sound wave can be registered by the qubit, which starts out in its ground state given the very low temperatures of the experiment. When the sound wave's energy is in resonance with the qubit (which can be tuned with an external magnetic field), a phonon can be absorbed as a whole, and the qubit will be excited from its ground state to the first excited state. A subsequently impinging second phonon of the same frequency can-



Classical and quantum sound. (**A**) Ultrasound imaging works by creating and detecting sound waves with piezoelectric crystals in the handheld "wand." (**B**) A schematic of the superconducting device of Gustafsson *et al*. that operates in the quantum regime at cryogenic temperatures. An acoustic transducer coupled to a superconducting qubit is fabricated on a piezoelectric substrate. Surface acoustic waves are shown to interact in a quantum way with the artificial atom.

Laboratory for Physical Sciences, College Park, MD 20740 USA. E-mail: charlie@tahan.com

ILLUSTRATION: P. HUEY/*SCIENCE*

Published by AAAS

not scatter until the first phonon is "released" from the qubit, because it does not match the splitting between the first and second excited states. Gustafsson *et al.* showed this by continuously changing the rate of impinging phonons from a much lower to a much higher rate with respect to the qubit relaxation time. Their artificial atom reflected sound on resonance and did not for nonresonant conditions, in a manner similar to that seen in circuit QED (*9*).

Gustafsson *et al.* also used microwave radiation to independently excite and drive the qubit without sound. The excited artificial atom is expected to relax by emitting phonons that will travel to and induce a characteristic signal at the IDT. The time the phonons take to get to the IDT definitively differentiates sound from purely electrical signals. A cross-talk signal on the IDT was seen when the electrical pulse to the qubit was turned on (and even when the qubit was off resonance). Then, ~40 ns later, the sound wave was detected, and this delay corresponded to the sound-wave propagation time. Further experiments that used both acoustic and microwave drives on the qubit showed additional analogs of atomic physics, specifically the Autler-Townes splitting related to the Stark effect.

A next step would be to confirm phonon antibunching of the driven qubit in this system, which would definitively "prove" the existence of phonons. But more questions can be asked. How long will an acoustic phonon stay coherent in a specific crystal? Can phonons be entangled with each other? Can sound-sensitive qubits and cavity quantum phonodynamics be realized in other systems, for example, via the deformation potential (*10*, *11*)? With the ability to make artificial atoms much larger than the wavelength of the phonon or to perform several qubit operations (including classical processing and feedback) while the slow phonon is still traveling, the space of available quantum experiments grows. Look out, quantum optics; the future seems loud for quantum sound. ■

REFERENCES

1. M. V. Gustafsson *et al.*, *Science* **346**, 207 (2014).
2. H. J. Kimble, M. Dagenais, L. Mandel, *Phys. Rev. Lett.* **39**, 691 (1977).
3. M. D. LaHaye, J. Suh, P. M. Echternach, K. C. Schwab, M. L. Roukes, *Nature* **459**, 960 (2009).
4. M. Eichenfield, J. Chan, R. M. Camacho, K. J. Vahala, O. Painter, *Nature* **462**, 78 (2009).
5. A. D. O'Connell *et al.*, *Nature* **464**, 697 (2010).
6. P. Rabl *et al.*, *Nat. Phys.* **6**, 602 (2010).
7. R. W. Andrews *et al.*, *Nat. Phys.* **10**, 321 (2014).
8. A. Blais, R.-S. Huang, A. Wallraff, S. Girvin, R. Schoelkopf, *Phys. Rev. A* **69**, 062320 (2004).
9. O. Astafiev *et al.*, *Science* **327**, 840 (2010).
10. O. O. Soykal, R. Ruskov, C. Tahan, *Phys. Rev. Lett.* **107**, 235502 (2011).
11. R. Ruskov, C. Tahan, *Phys. Rev. B* **88**, 064308 (2013).

10.1126/science.1260180

CONSERVATION

Taking the measure of change

Predictive models of biodiversity change are required to inform conservation policy decisions

By **Ben Collen**[1] *and* **Emily Nicholson**[2]

Over the past decade, numerous metrics for biodiversity—including species abundance, extinction risk, distribution, genetic variability, species turnover, and trait diversity—have been used to create indicators to track how biodiversity has changed (*1*–*3*). These indicators have made it clear that biodiversity loss, however it is measured, is showing little sign of abatement (*1*, *4*) and that humans must respond to safeguard the provision of natural services on which we all rely (*5*, *6*). But which metrics provide the most informative indicators under which circumstances? And how can the growing list of indicators best serve conservation policy decisions?



CONSERVATION SERIES

ALIGNMENT OF TARGET AND INDICATOR. If we are interested in the status of an economy, we measure its performance over time using metrics such as cost of goods, income, and employment numbers. Those metrics are then used to produce indicators such as GDP and RPI. Similarly, metrics such as species abundance are used to create indicators of the health of biodiversity.

For an indicator to help achieve a particular conservation target, the indicator and the target must be closely aligned (*4*). There is little point in measuring progress toward a target with an indicator based on a metric that is only loosely related to the desired outcome. For example, ensuring that protected areas maintain their biodiversity is a fundamental goal of conservation. Targets are frequently centered on the extent of area under protection [e.g., 17% of land should be under protection by 2020 (*6*)]. The implicit assumption is that the greater the area protected, the more biodiversity will prosper. However, this ignores factors such as governance, funding, and the type of species within the protected area that influence its effectiveness. Protected areas differ greatly in the protection they afford species, but management effectiveness indicators are only available for less than 5% of protected areas (*4*). Using just one metric as an indicator may not achieve the desired outcome.

Ideally, the chain between metric, indicator, and policy should start with specific targets. In fisheries management, targets are often explicit, typically relating to the sustainability of fish stocks; this helps to guide fisheries policy and management interventions and to detect fishing impacts on marine biodiversity (*7*). Targets can vary widely in scale; metrics such total biomass, catch, and mean trophic level are used to evaluate sustainability targets for ecosystem management (*8*), whereas changes in recruitment and abundance are used to construct indicators for managing specific fish stocks (*9*).

In contrast, global biodiversity targets such as those agreed to in the Convention on Biological Diversity (CBD) (*6*) tend to be less specific, and the alignment of metric, indicator, and target can be poor. For example, one CBD target calls for pollution to be reduced to levels that are not detrimental to ecosystem function or biodiversity. This laudable target does not detail which pollutants, ecosystem functions, or particular aspects of biodiversity should be addressed. The distinction is important because many functions will trade off with one another, and prioritizing some aspects of biodiversity will be at the cost of others. Efforts to measure progress toward this target, hold polluting countries and industries to account, and diagnose which interventions work best are made more difficult.

The outcomes of global biodiversity targets are perhaps inevitably less focused than those in specified circumstances such as fisheries management. However, with greater demand and scrutiny placed on biodiversity indicators (*4*) through targets such as CBD, how can they better support conservation efforts? One way forward is improved prediction.

PROJECTING FORWARD. Effective conservation policy decisions require an explicit understanding of the links between desired outcomes of conservation, how those outcomes can be measured, and the proposed actions needed to achieve them (*10*). One way to accomplish this is to project forward the impacts of a prospective policy. In doing so, both the impact of the policy and the ability of indicators to detect change in

ILLUSTRATION: C. SMITH/*SCIENCE*

Published by AAAS

biodiversity can be measured. By assessing alternative policies against a suite of metrics, the best combination of metrics and indicators for evaluating policy impacts can be identified.

In a recent study, Kelly *et al.* showed how indicators can provide a link between broad conservation targets and local-scale implementation (*11*). The authors applied abundance metrics to decisions on wildfire management in Australia. The results showed that optimizing fire management using an indicator based on geometric mean abundance of the vertebrate community resulted in improved biodiversity outcomes relative to following the conventional wisdom of maximizing the prevalence of different fire management regimes. This approach demonstrates that clearly defined management goals are necessary to maximize biodiversity in fire-prone ecosystems.

In fisheries science, substantial emphasis has been placed on ensuring that indicators respond in predictable ways to particular interventions or pressures, enabling decision makers to tease apart the impacts of different drivers of change (*12*). In-depth knowledge of such indicator behavior is lacking from analyses of most global biodiversity indicators. Put simply, any useful indicator must be able to pick up the impact of a management intervention.

RIGOROUS TESTING. Two factors that affect indicator performance are the design of the indicator and the quality of the data that underpin it. An indicator may perform badly because data to calculate it are difficult to obtain or are biased geographically or taxonomically, rendering it unrepresentative of the components of biodiversity the indicator is designed to reflect (*10*). In other cases, excellent data may be available but the metric may be a poor proxy for the aspects of biodiversity of interest. For example, the rate of forest loss is often cited as a chief driver of decline of wildlife populations (*5*, *6*), but the impact of bushmeat hunting, also recognized to be a key driver, is rarely measured. Biodiversity declines in forested areas can thus continue undetected even when the forest loss is slowed or halted.

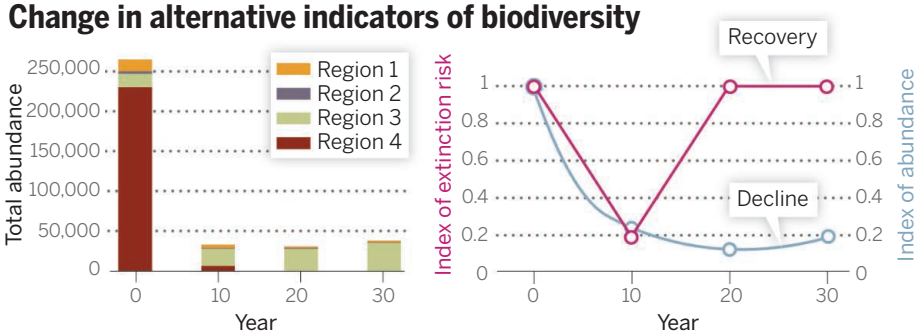
Different metrics can give varying impressions of conservation success. For example, imagine that a wildlife population collapses, leaving a much smaller population surviving in only one region. Tracking abundance then yields a picture of decline, whereas tracking extinction risk suggests recovery (see the figure). One problem lies in adapting metrics designed for another purpose: Extinction risk assessments provide a snapshot and were not designed to evaluate change through time (*10*). Another problem is expectation: The risk to the species is diminished toward the end of the example because the population is now stable, albeit at a much lower level than before.

Several fisheries indicators have been subjected to rigorous evaluation of whether or not they reliably predict changes in marine ecosystems (*7*, *8*), but few biodiversity indicators have been tested in this way. There are exceptions; tests of indicator performance have shown that data biases can give a misleading impression of policy impacts (*7*, *10*). Other recent studies favorably related the Living Planet Index's underlying metric (geometric mean abundance) to models of species viability from ecological theory (*13*) and explored its mathematical properties (*14*), showing it to be suitable for measuring trends in species extinction risk.

More extensive stress testing of biodiversity indicators would enhance knowledge of how biodiversity is changing, show whether the existing indicators can measure that change, and help identify the most appropriate policies to counteract biodiversity declines. Predictive modeling will help to ensure that biodiversity indicators can support conservation policy. For example, sampling data from model systems to mimic current monitoring programs allows indicators to be compared with a "truth" not available to real-world data sets. This framework has been used to test indicators for fisheries management (*7*, *8*) and to evaluate other biodiversity indicators (*10*), showing that while some indicators perform well, others need rethinking.

TOWARD A MEANINGFUL SET OF METRICS. Because of the inconsistency in delivery of measures of biodiversity change, a set of agreed metrics of biodiversity is urgently required (*2*). If the right information to guide conservation policy cannot be gleaned from existing metrics, gathering global-level data for an array of new metrics would be a necessary but costly endeavor. Striking the right balance between expanding existing data sets and developing new, more appropriately designed monitoring programs and metrics will be vital if measures of biodiversity change are to robustly support conservation decisions.

In doing so, conservation science must be rigorous. Testing the modeled performance of alternative management actions prior to implementation should be the gold standard for conservation decision-making. Indicators of change must also be subjected to rigorous performance tests. Such evaluation was mentioned in the selection of indicators of the CBD 2010 target, with all indicators "identified for immediate testing." Yet, with few exceptions, the indicators remain largely unevaluated in their capacity to report meaningfully on conservation targets and the means of achieving them; this remains a critical task for predictive conservation science if it is to influence conservation progress. ■



Recovery or decline? Two metrics lead to different conclusions following the regional extirpation of a hypothetical species to a low but stable population size.

[1]*Centre for Biodiversity & Environment Research, University College London, London WC1E 6BT, UK.* [2]*School of Botany, University of Melbourne, Melbourne, VIC 3010, Australia. E-mail: b.collen@ucl.ac.uk*

REFERENCES AND NOTES

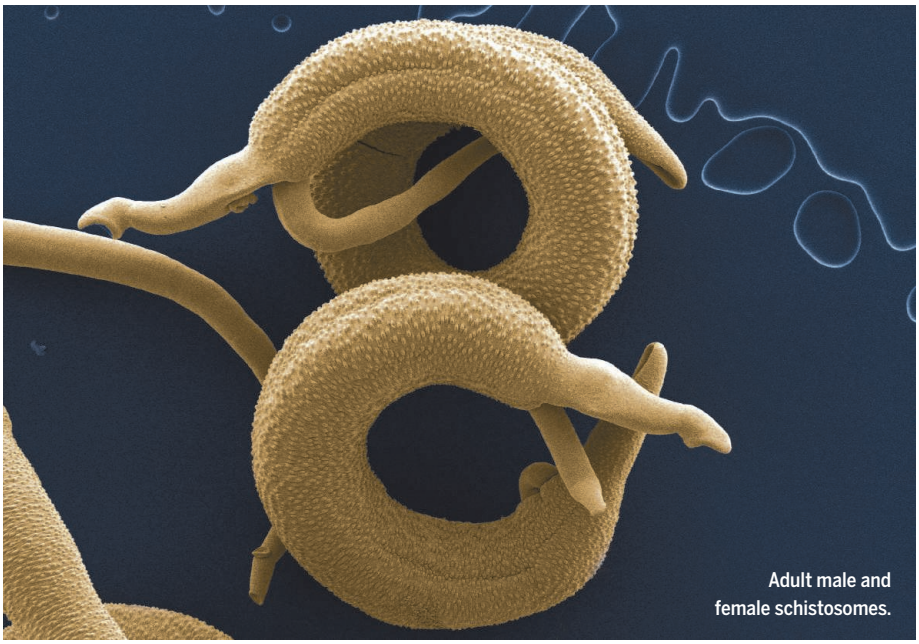
1. S. H. M. Butchart *et al.*, *Science* **328**, 1164 (2010).
2. H. M. Pereira *et al.*, *Science* **339**, 277 (2013).
3. B. Collen *et al.*, *Conserv. Biol.* **23**, 317 (2009).
4. D. P. Tittensor *et al.*, *Science* **346**, 241 (2014).
5. G. M. Mace *et al.*, *Biodiversity: Millennium Ecosystem Assessment: Current State and Trends: Findings of the Condition and Trends Working Group. Ecosystems and Human Well-Being* (Island, Washington, DC, 2005).
6. Secretariat of the Convention on Biological Diversity, *Global Biodiversity Outlook 3* (2010).
7. T. A. Branch *et al.*, *Nature* **468**, 431 (2010).
8. E. Fulton *et al.*, *ICES J. Mar. Sci.* **62**, 540 (2005).
9. F. J. Mueter *et al.*, *ICES J. Mar. Sci.* **68**, 1284 (2011).
10. E. Nicholson *et al.*, *PLOS ONE* **7**, e41128 (2012).
11. L. T. Kelly *et al.*, *Conserv. Biol.* 10.1111/cobi.12384 (2014).
12. J. S. Link *et al.*, *ICES J. Mar. Sci.* **67**, 787 (2010).
13. M. McCarthy *et al.*, *Conserv. Biol.* 10.1111/cobi.12308 (2014).
14. S. T. Buckland *et al.*, *Ecosphere* **2**, art100 (2011).

ACKNOWLEDGMENTS

Both authors thank the ARC Centre of Excellence for Environmental Decisions.

10.1126/science.1255772

Published by AAAS



Adult male and female schistosomes.

MEDICINE

Halting harmful helminths

Vaccines and new drugs are needed to combat parasitic worm infections

By **Karl F. Hoffmann,[1] Paul J. Brindley,[2] Matthew Berriman[3]**

More than 300 million people are infected each year with parasitic flatworms such as hydatid tapeworms and blood fluke schistosomes. The diseases caused by such parasitic helminths, including alveolar/cystic echinococcosis and hepatosplenic/urogenital schistosomiasis, are typically chronic but frequently deadly. They are among the 17 neglected tropical diseases listed by the United Nations World Health Organization, and infections by these flatworm pathogens cause ~4 million disability-adjusted life years to be lost annually, although this vastly underestimates the true impact that such long-term and chronic illnesses can have (*1*). Historically considered restricted to the tropics and subtropics, suitable habitats for transmission of these parasites are now expanding into Europe (*2*), and conditions are right for similar expansions to other continents (*3*, *4*). The lack of vaccines perpetuates the unsustainable over-reliance on single-drug chemotherapies, a potentially catastrophic situation unless new solutions are found.

To accelerate the discovery of vaccines, drugs, and exploitable insights into pathogenesis, there has been a drive to apply state-of-the-art technologies to parasitic helminth research. With mammals, great strides have been made in these arenas by harnessing technologies in stem cell research for large-scale mutagenesis studies (*5*). More recently, there has been a shift to develop cell-focused approaches coupled with genome editing (*6*). These strategies—especially the bacterial clustered regularly interspaced short palindromic repeats (CRISPR)–Cas9 endonuclease system—have revolutionized the way in which genetic-mutational-phenotypic analyses in eukaryotic species are performed. By contrast, comparable research on helminths has lagged far behind. The difficulty in maintaining parasitic flatworms in the laboratory due to their complex life cycles (typically alternating between two obligate hosts) and their recalcitrance to genetic and cellular manipulations present major bottlenecks for adapting technologies.

Despite these hurdles, progress in the areas of schistosome (blood fluke) transgenesis (*7*), organ isolation (*8*), and stem cell characterization (*9*), coupled with advances in echinococcal (hydatid tapeworm) primary cell cultures (*10*, *11*), portends a transformation in the ability to manipulate and study parasitic flatworms. As a prelude to whole organism or cellular transgenesis, techniques have been honed over the past 15 years to perform loss-of-function studies in schistosomes using posttranscriptional gene silencing (*12*). However, this approach is only transient, often not fully penetrant, and difficult to translate to other parasitic flatworms. Gain-of-function manipulation, based on overexpressing transgenes in schistosomes with plasmid-based vectors, is possible (*13*), but suffers from the same challenges as post-transcriptional gene silencing.

A breakthrough in developing a stable system for manipulating gene function came recently with the discovery that pseudotyped retroviruses (murine leukemia viruses) and, to a lesser degree, transposons (*piggyBac*) can introduce transgenes into all eight schistosome chromosomes, including those found in germ cells (*7*). Translating this to other parasitic flatworms, as well as applying methods for selective targeting of transgene genome integration, should spur investigation of individual gene function.

Coincident with these developments in transgenesis are innovations in parasitic flatworm cell culture. Attention has focused on stem cells (also called germinative cells or neoblasts) and the tissues in which they reside because these cells self-replicate as well as differentiate and, hence, endow the evolutionary and developmental plasticity of parasitic flatworms. It is now feasible to isolate gonads enriched in stem cells (*8*), identify somatic proliferating stem cells (*9*), and initiate limited-passage cell cultures from schistosomes (*14*). Also promising are advances in cell cultivation systems for echinococcal tapeworms, where continuous cultures enriched for replicative and differentiating stem cells can be derived from *Echinococcus multilocularis* (*10*) and "immortal" cell lines can be produced from the closely related species *E. granulosus* (*11*). Although still being refined, it is clear that immortalized cell lines based on the proliferation and differentiation capacity of flatworm stem cells will alleviate the need for maintaining complex parasitic life cycles.

By applying genome editing and knowledge about cell biology and cell culture to blood flukes and hydatid tapeworms, the aspiration of developing stable transgenic parasitic helminths and manipulable cell lines derived from these pathogens is now a near-future certainty. Retroviruses engineered to deliver CRISPR-Cas9-RNA cargos represent the most feasible approach in

[1]*Institute of Biological, Environmental and Rural Sciences (IBERS), Aberystwyth University, Aberystwyth SY23 3DA, UK.* [2]*Department of Microbiology, Immunology and Tropical Medicine and Research Center for Neglected Diseases of Poverty, School of Medicine and Health Sciences, George Washington University, Washington, DC 20037, USA.* [3]*Wellcome Trust Sanger Institute, Wellcome Trust Genome Campus, Hinxton, Cambridge CB10 1SA, UK. E-mail: krh@aber.ac.uk*

IMAGE: FLORIAN SESSLER AND DAVID GOULDING/WELLCOME TRUST SANGER INSTITUTE

Published by AAAS

generating permanent transgenic helminths (*15*). By adopting this technology, the assessment of gene function in these parasites—by gene deletion or disruption or by exchanging codons—should be possible. Developing both transgenic parasitic worms and stable cell lines will functionally equip investigators with game-changing tools to keep pace with other, more tractable areas of biology.

For the first time, these resources will enable the field to address fundamental evolutionary, biomedical, and immunological questions that have stymied the development of new treatments. How does immortality in parasitic flatworms operate? That is, how do parasite stem cells contribute to the developmental plasticity involved in the complex life cycles of these animals (including both asexual and sexual components) within obligate hosts? And, in the case of *Echinococcus*, for example, do the highly proliferative asexually reproducing larvae present new opportunities for interventions? Also mysterious is how long-term host-parasite relationships develop and are maintained to the mutual benefit of both symbiotic species. Once infected, helminth-mediated host immunomodulation and host-mediated parasite elimination compete, continuously striving to gain the upper hand. For example, age-dependent immunity is seen in schistosome-infected humans, where children harbor the vast majority of parasites in endemic areas. What are the molecular mechanisms underlying these processes, and what opportunities do they offer for developing new intervention strategies?

Adapting breakthrough biotechnologies to these neglected pathogens hopefully will drive the innovations needed to more fully understand their intriguing biology and pathogenesis. This could open up an exciting new frontier of translational options needed to control the damage caused by these harmful helminths. ■

REFERENCES AND NOTES

1. P. J. Hotez *et al.*, *PLOS Negl. Trop. Dis.* **8**, e2865 (2014).
2. M. Holtfreter *et al.*, *Euro Surveill.* **19**, 153 (2014).
3. G. Majoros *et al.*, *Emerg. Infect. Dis.* **14**, 1812 (2008).
4. P. R. Torgerson, C. N. Macpherson, *Vet. Parasitol.* **182**, 79 (2011).
5. A. Ayadi *et al.*, *Mamm. Genome* **23**, 600 (2012).
6. P. Mali *et al.*, *Nat. Methods* **10**, 957 (2013).
7. V. H. Mann *et al.*, *Transgenic Res.* **23**, 539 (2014).
8. S. Hahnel *et al.*, *PLOS Negl. Trop. Dis.* **7**, e2336 (2013).
9. J. J. Collins 3rd *et al.*, *Nature* **494**, 476 (2013).
10. U. Koziol *et al.*, *Evodevo* **5**, 10 (2014).
11. C. M. Albani *et al.*, *Acta Trop.* **128**, 124 (2013).
12. R. Bhardwaj *et al.*, *Methods Mol. Biol.* **764**, 223 (2011).
13. S. Beckmann *et al.*, *Exp. Parasitol.* **117**, 292 (2007).
14. Q. Ye *et al.*, *Biotechnol. Adv.* **31**, 1722 (2013).
15. A. Malina *et al.*, *Genes Dev.* **27**, 2602 (2013).

ACKNOWLEDGMENTS

We thank K. Brehm, C. G. Grevelding, C. Grunau, and L. Vallier for helpful discussions.

10.1126/science.1261139

ILLUSTRATION: V. ALTOUNIAN/*SCIENCE*

CANCER

Attack of the clones

What makes lung cancer so resilient?

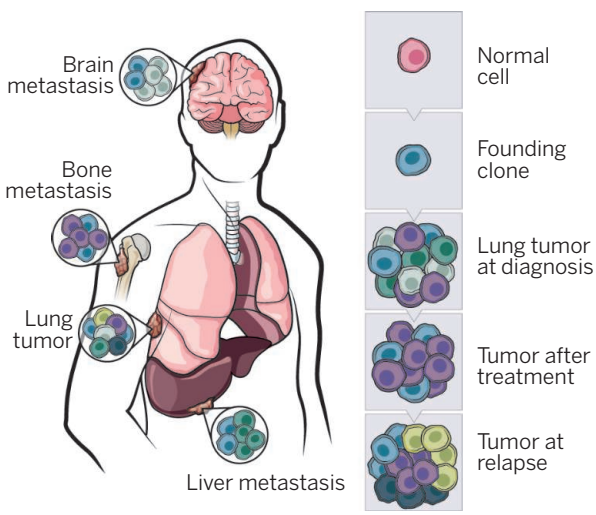
By **Ramaswamy Govindan**[1,2]

Nearly 40 years ago, it was presciently observed (*1*) that each patient's cancer would require individual therapy and that this would be "thwarted" by the emergence of resistant cells. This prediction has proven to be depressingly true in various malignancies. It is now evident that malignant clones and subclones evolve not only through gradual acquisition of mutations but are also secondary to abrupt catastrophic events (such as massive chromosomal rerarrangement), leading to genomic heterogeneity in a tumor over time. The advent of next-generation sequencing has enabled these processes to be studied in unprecedented detail. Considerable intratumoral heterogeneity has been demonstrated in certain hematological malignancies and cancers of the breast, ovary, bladder, prostate, pancreas, and kidney (*2*–*8*). On pages 256 and 251 of this issue, Zhang *et al.* (*9*) and de Bruin *et al.* (*10*), respectively, describe the universal prevalence of intratumoral heterogeneity in lung cancer, with important implications for future research.

Lung cancer is one of the leading causes of cancer-related death globally. Non–small cell lung cancer (NSCLC) is the most common type, accounting for nearly 85% of all newly diagnosed cases. A sizable minority of patients with lung cancer, ranging from 10 to 40% depending on the region of the world, reports no history of tobacco smoking (*11*). More than half report quitting tobacco smoking years before the diagnosis of lung cancer. Most patients with NSCLC either present with metastatic disease or their cancer recurs despite undergoing treatment for seemingly localized disease, underscoring the systemic nature of this disease. Cytotoxic chemotherapy regimens developed over the past few decades have produced only modest improvements in survival in patients with metastatic NSCLC. However, a small subset of patients (15%), with tumors driven by activating mutations in the gene encoding epidermal growth factor receptor (*EGFR*) or rearrangements in the gene coding for anaplastic lymphoma kinase (*ALK*), benefit substantially from specific targeted therapies. Even these patients eventually succumb to tumor progression within a few years of diagnosis. It is critical to understand fully the molecular events leading to the initiation, maintenance, and progression of lung cancer to improve these outcomes.

The complex genomic landscape of NSCLC related to tobacco smoking is characterized by innumerable single-nucleotide variations, gene amplifications, insertions, deletions, and structural rearrangements (*12*, *13*). By contrast, there are strikingly fewer mutations and genomic alterations in the lung cancer specimens from nonsmokers (*14*). Almost all genomic studies in lung cancer reported to date have been conducted with samples obtained from a single region of the tumor, limiting knowledge about the extent of intratumoral heterogeneity and clonal evolution.

Tumors evolve either in a linear fashion, by acquiring progressively fitter clones that outpace the founding clones, or more com-

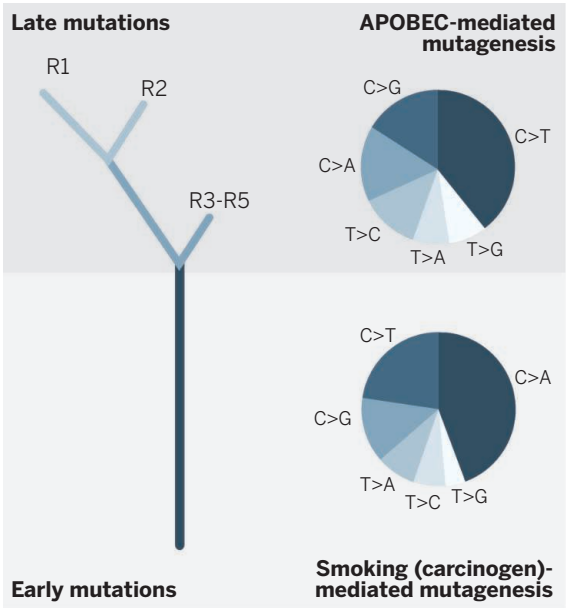


Lung cancer resilience. A model is shown of how a tumor may acquire progressively fitter clones, giving rise to subclonal populations and tumor heterogeneity.

[1]*Department of Medicine, Washington University School of Medicine, St. Louis, MO 63110, USA.* [2]*Alvin J. Siteman Cancer Center, Washington University School of Medicine, St. Louis, MO 63110, USA. E-mail: rgovinda@dom.wustl.edu*

Published by AAAS

monly follow a branched pattern where multiple subclones thrive simultaneously, resulting in a complex heterogeneous tumor (see the first figure). Identification of key "driver" mutations—those that confer a selective growth advantage to a cancer cell—contributing to these branch points in NSCLC is vitally important from the therapeutic standpoint. Zhang *et al.* used multiregion whole-exome sequencing on 11 lung adenocarcinomas whereas de Bruin *et al.* applied whole-exome sequencing and/or whole-genome sequencing on 25 spatially distinct regions from seven localized NSCLC tumor samples. Intratumoral heterogeneity was universal in all the 18 primary tumors. About a third of all nonsilent mutations analyzed by de Bruin *et al.* were present in at least one region but not in all regions of individual tumors. De Bruin *et al.* found evidence of branched evolution with key driver mutations present before, and even after, subclonal diversification, raising the uncomfortable possibility that single-region sampling, as is currently being done in clinical diagnosis, could miss key driver mutations present in specific subclones. By contrast, Zhang *et al.* identified 20 out of 21 known cancer genes in all regions of the individual tumors. As these two studies are too small to allow any definite conclusions to be drawn on this topic, for now, the practice of single-region biopsy should continue for clinical diagnostic purposes. Multiregion, multisite biopsies of metastatic lesions carry considerable risks, and the evidence has to be more persuasive to change this practice.



Clonal evolution. An example of a phylogenetic tree showing the clonal evolution of lung cancer. Pie charts show the spectrum of six types of mutations during early tumor evolution (smoking-induced mutations) and late evolution (APOBEC mediated) (*10*). R indicates regions of the tumor.

More work is needed to understand the prevalence of regionally dominant subclones with known driver mutations and their role in metastases and drug resistance. Zhang *et al.* noted that three patients with a larger fraction of subclonal populations developed recurrent disease after surgery, an observation that deserves further attention with regard to the use of intratumoral heterogeneity itself as a biomarker of poor prognosis.

Two interesting observations made by de Bruin *et al.* suggest the possibility that smoking-related genomic events occur fairly early in the disease, together with early driver events and single-nucleotide variations (see the second figure). Genome-doubling events incorporating characteristic signatures of smoking occurred long before the development of clinical disease in former smokers, suggesting prolonged latency from the first driver events to clinical presentation. Even in the presence of continued tobacco smoking, carcinogen-related genomic events decreased over time along with a concomitant increase in mutagenesis related to activation of a class of enzyme called apolipoprotein B mRNA editing, enzyme-catalytic, polypeptide-like cytidine deaminases (APOBEC).

Clearly, more work needs to be done to understand the clinical implications of clonal evolution and intratumoral heterogeneity. Studies on intratumoral heterogeneity so far have relied mostly on DNA alterations, whereas genomic events contributing to clonal evolution likely extend beyond single-nucleotide variations and copy-number alterations. Multiregion analyses need to incorporate sample procured from metastatic sites along with their corresponding primary lesions to identify the subclones enriched in metastatic foci. In addition, a better understanding of clonal evolution at metastatic sites, perhaps under selective pressures from local tissue environments, could help identify patients at risk for recurrence and distant metastases, and perhaps lead to specific therapies to halt the inexorable spread of cancer to other organs.

The distorted cancer genome landscape is sculpted continually by stochastic events and therapy-induced alterations. Understanding this process requires serial biopsies to characterize clonal evolution both spatially and temporally. Emerging technologies would hopefully facilitate comprehensive genomic analyses of circulating cell-free DNA (so-called liquid biopsies) to obviate the need for invasive core biopsies. Further, statistical methods and algorithms should be developed to elucidate the interplay between dysfunctional gene and protein networks using an integrated multilayered "omics" approach.

To accomplish these goals, clinical trial infrastructure must be optimized to incorporate genomic studies along with interventional clinical studies. For example, the Adjuvant Lung Cancer Enrichment Marker Identification and Sequencing (ALCHEMIST) trial will screen ~8000 patients with surgically resected NSCLC to test for the presence of *EGFR* mutations and *ALK* rearrangements and determine the efficacy of targeted drugs in the postoperative setting. The trial will include studies to identify genomic alterations in NSCLC. Attempts will be made to collect samples at the time of relapse to study clonal evolution following postoperative therapy. A large prospective effort, Tracking NSCLC Evolution Through Therapy (TRACERx), and its sister study, Deciphering Anti-tumor Response and Evolution with Intratumor heterogeneity (DARWIN), will also contribute to understanding intratumoral heterogeneity and clonal evolution.

It is critical to develop a national infrastructure to conduct comprehensive multiregional and multisite genomic studies with samples procured through "warm autopsies" from patients with a wide variety of malignancies. An organized program could collect a large amount of highly informative samples in a relatively short period. Developing new cancer therapies may still be a long and arduous process. A better understanding of genomic alterations is key to develop more rational and effective therapies. ■

REFERENCES AND NOTES

1. P. C. Nowell, *Science* **194**, 23 (1976).
2. D. A. Landau *et al.*, *Cell* **152**, 714 (2013).
3. J. G. Lohr *et al.*, *Cancer Cell* **25**, 91 (2014).
4. K. Anderson *et al.*, *Nature* **469**, 356 (2011).
5. B. E. Johnson *et al.*, *Science* **343**, 189 (2014).
6. M. Gerlinger *et al.*, *Nat. Genet.* **46**, 225 (2014).
7. M. J. Walter *et al.*, *N. Engl. J. Med.* **366**, 1090 (2012).
8. L. Ding *et al.*, *Nature* **481**, 506 (2012).
9. J. Zhang *et al.*, *Science* **346**, 256 (2014).
10. E. C. de Bruin *et al.*, *Science* **346**, 251 (2014).
11. J. Subramanian, R. Govindan, *Lancet Oncol.* **9**, 676 (2008).
12. Cancer Genome Atlas Research Network, *Nature* **489**, 519 (2012).
13. Cancer Genome Atlas Research Network, *Nature* **511**, 543 (2014).
14. R. Govindan *et al.*, *Cell* **150**, 1121 (2012).

ACKNOWLEDGMENTS

I thank M. Walter and P. Ranganathan for critical feedback and J. Duke for administrative assistance.

10.1126/science.1259926

Published by AAAS

ARTIFICIAL INTELLIGENCE

Amplify scientific discovery with artificial intelligence

Many human activities are a bottleneck in progress

By **Yolanda Gil,[1] Mark Greaves,[2] James Hendler,[3]* Haym Hirsh[4]**

Technological innovations are penetrating all areas of science, making predominantly human activities a principal bottleneck in scientific progress while also making scientific advancement more subject to error and harder to reproduce. This is an area where a new generation of artificial intelligence (AI) systems can radically transform the practice of scientific discovery. Such systems are showing an increasing ability to automate scientific data analysis and discovery processes, can search systematically and correctly through hypothesis spaces to ensure best results, can autonomously discover complex patterns in data, and can reliably apply small-scale scientific processes consistently and transparently so that they can be easily reproduced. We discuss these advances and the steps that could help promote their development and deployment.

POLICY

Applying AI to the practice of science is not new. AI pioneer and Nobel laureate Herbert Simon hypothesized that cognitive mechanisms involved in scientific discovery are a special case of general human capabilities for problem-solving and, with colleagues, developed systems in the 1970s and 1980s that demonstrated reasoning capabilities for analyzing scientific data (*1*). Also in the 1970s, Joshua Lederberg (another Nobel winner) and colleagues developed the DENDRAL system for analyzing mass spectrometry data in order to hypothesize molecular structures (*2*). More recent breakthroughs, such as robot scientists and software that formulates laws for complex dynamical systems, demonstrate broader applicability of AI techniques for scientific discovery (*3*).

Over the past two decades, AI has seen accelerating scientific advances and concomitant commercial-sector successes because of advances on three fronts: steady scholarly advances, especially as success has increased the numbers of interested participants; Moore's law and steady exponential increases in computing power; and exponential increases in, and broad availability of, relevant data in volumes never previously seen. Those scientific efforts that have leveraged AI advances have largely harnessed sophisticated machine-learning techniques to create correlative predictions from large sets of "big data." Such work aligns well with the current needs of peta- and exascale science. However, AI has far broader capacity to accelerate scientific discovery, and AI-based systems that can represent hypotheses, reason with models of the data, and design hypothesis-driven data collection techniques can reduce the error-prone human bottleneck in scientific discovery.



Schematic of Hanalyzer. Hanalyzer is an example of a modern scientific discovery system. It integrates assertions from biomedical databases and then reasons about the resulting semantic information to suggest novel correlations from which scientists can generate testable hypotheses.

SEARCHING AND SYNTHESIZING. What do these intelligent systems look like today? AI techniques are amplifying existing tools in identifying relevant results from the broader scientific community. Search engines are some of the most important and frequently used tools in the general scientific arsenal. Major search engines all use AI techniques for tasks like query suggestion and result customization. Increasingly, scientists in many fields are augmenting the power of search by using machine-readable ontologies and Semantic Web technology (*4*) to tag not just scientific articles but also figures and videos, blogs, data sets, and computational services, which allow information-finding beyond current search limitations.

We can project a not-so-distant future where "intelligent science assistant" programs identify and summarize relevant research described across the worldwide multilingual spectrum of blogs, preprint archives, and discussion forums; find or generate new hypotheses that might confirm or conflict with ongoing work; and even rerun old analyses when a new computational method becomes available. Aided by such a system, the scientist will focus on more of the creative aspects of research, with a larger fraction of the routine work left to the artificially intelligent assistant.

New types of intelligent systems that can enhance scientific efforts in this manner are transitioning from academic and industrial research laboratories. A term gathering popularity for systems that intelligently process online information beyond search is "cognitive computing," used by IBM in describing the Watson system that beat the best human players in the televised *Jeopardy!* game (*5*). One kind of cognitive system includes language-based programs like Watson, which is now being used by IBM and a number of prominent medical centers in developing tools for improving medical treatment by helping doctors keep up with constantly changing medical literature. To enhance these capabilities, the U.S. Defense Advanced Research Projects Agency (DARPA) recently announced a major effort to synthesize new systems-biology models of cancer by knitting together fragmentary causal hypotheses gathered by automatically reading papers in the literature (*6*). Another group of cognitive systems, based largely on advances in neural networks and neurologically inspired computation, is beginning to show promise in the analysis of nontextual processing, especially of online images and video, across a wide range of areas including

[1]*Information Sciences Institute, University of Southern California, Marina del Rey, CA 90292, USA.* [2]*Pacific Northwest National Laboratory, Richland, WA 99354, USA.* [3]*Information Technology and Web Science, Rensselaer Polytechnic Institute, Troy, NY 12203, USA.* [4]*Cornell University, Ithaca, NY 14850, USA.* **E-mail: hendler@cs.rpi.edu*

ILLUSTRATION: P. HUEY/*SCIENCE*

Downloaded from www.sciencemag.org on October 9, 2014

Published by AAAS

biological imaging (*7*), species preservation (*8*), and quantum chemistry (*9*).

DIGESTING DATA. AI techniques have accelerated the pace and quality of analysis of the huge quantities of data that can stream from modern laboratory equipment. To derive scientific insight from data at this scale, standard methods include applying dimensionality-reduction techniques and feature extractors to create high-speed classifiers based on machine-learning approaches, such as Bayesian networks or support-vector machines. Because the phenomena under study often exist in nonstationary environments or in contexts with only small quantities of labeled data that can be used for training—complex, unsupervised, and reinforcement machine-learning techniques are critical for data analysis. These types of approaches are being used in recent projects in data-rich areas as diverse as chemical structure prediction, pathway analysis and identification in systems biology, the processing of large-scale geophysics data, and others.

Another, more ambitious class of intelligent systems is being developed under the rubric of Discovery Science or, increasingly, Discovery Informatics (*10*). These systems enhance the intelligent assistants described earlier with the capability to attack scientific tasks that combine rote work with increasing amounts of adaptivity and freedom. These systems use encoded knowledge of scientific domains and processes in order to assist with tasks that previously required human knowledge and reasoning. In fact, several sciences have significant investments in the representation of vast amounts of scientific knowledge and are poised to explore new intelligent systems that exploit that knowledge for discovery.

For example, the Hanalyzer (short for high-throughput analyzer) uses natural language processing to automatically extract a semantic network from all PubMed papers relevant to a specific scientist, uses Semantic Web technology to integrate assertions from other biomedical sources, and reasons about the network to find new correlations that suggest new genes to investigate (*11*) (see the figure). The Wings system uses Semantic Web technologies and AI planning to reason about specific choices of models and algorithms for water-quality data and customizes workflows automatically for daily conditions (*12*). Eureqa, usable in many scientific fields, searches a vast space of hypotheses consistent with given data observed in an experiment, selects those most promising, and designs experiments to test them (*13*). Sunfall incorporates usability principles and cognitive load considerations in the design of a visual analytics interface; this reduces scientists' workload and false-positive rates in identifying supernovae (*14*).

These four systems are representative of the ways that more advanced AI can serve scientific ends. They are based on explicit representations of science processes, and they reason about these to automate processes and assist the human scientist. Development of the explicit representations of scientific processes on which they are based is complex. When successful, the computer can become a real (although junior) participant in the science process, doing what it does best: applying algorithmic methods and bringing knowledge to bear in a consistent, systematic, and complete manner.

A VIRTUOUS CIRCLE. Developing systems like these is not just an exercise in AI application—it affects the direction of AI research. Addressing real challenges of science pushes the AI envelope in many areas, including knowledge representation, automatic inference, process reasoning, hypothesis generation, natural language processing, machine learning, collaborative interaction, and intelligent user interfaces. This interaction creates a virtuous circle where advances in science go hand in hand with advances in AI. This virtuous circle can only work well if balanced and well oiled.

"AI-based systems that can represent hypotheses … can reduce the error-prone human bottleneck in … discovery."

What are the best ways to immerse AI research into scientific practice so that it can deliver on this promise? First, and perhaps most obviously, is conceiving new means of bringing interdisciplinary research teams together at an earlier stage of research and in a sustainable manner. Increasingly, there is a realization in academia that scientists must gain broad knowledge and skills in computation and programming. This should include AI components—training and supporting students and young researchers. In addition, basic research to advance AI in domains of science practice needs to be facilitated and rewarded in academia, as standard criteria for research merit focus primarily on theoretical advances in computing per se and thus do not transfer well to this kind of multidisciplinary research.

A significant challenge that appears to be specific to AI is to attract scientific researchers to engage in this joint research. Scientists have made significant investments in the past in advanced computing technologies, such as high-end computing, distributed databases, and sensor networks. However, their interest in AI seems relatively limited. With AI systems having impacts in the consumer sector (e.g., speech recognition systems, real-time automated language translation, and self-driving cars and self-navigating drones), why are scientists not enthusiastic about embracing AI?

One hypothesis is the lack of clear methods to measure the impact of AI in science. There are exceptions in some areas of AI, such as machine learning and language processing, where metrics to compare systems have been defined and improvement has been measured. But there has been little research into such measurement more generally, especially for the heuristic methods of the reasoning field. Methods to quantify significant advances because of the use of new AI technologies in scientific fields are needed to validate the impact of AI on scientific discovery.

Another reason may be the limited work of the AI community in disseminating and marketing ideas to scientists. Although many non-AI scientists attend supercomputing and database conferences, few are compelled to attend an AI conference. Possibly, researchers are influenced by the unrealistic science fiction images of super-smart machines, rather than the realities of current technological advances. Understanding the sources of hesitation of scientists to embrace AI will be a first step toward changing the culture and bringing these communities together.

The world faces deep problems that challenge traditional methodologies and ideologies. These challenges will require the best brains on our planet. In the modern world, the best brains are a combination of humans and intelligent computers, able to surpass the capabilities of either one alone. ■

REFERENCES AND NOTES

1. P. Langley, H. A. Simon, G. L. Bradshaw, J. M. Zytkow, *Scientific Discovery: Computational Explorations of the Creative Processes* (MIT Press, Cambridge, MA, 1987).
2. R. K. Lindsay *et al.*, *Applications of Artificial Intelligence for Organic Chemistry: The DENDRAL Project* (McGraw-Hill, New York, 1980).
3. D. Waltz, B. G. Buchanan, *Science* **324**, 43 (2009).
4. J. Hendler, *Science* **299**, 520 (2003).
5. J. Kelly III, S. Hamm, *Smart Machines* (Columbia Univ. Press, New York, 2013).
6. Information Innovation Office, DARPA; www.darpa.mil/Our_Work/I2O/Programs/Big_Mechanism.aspx.
7. S. N. Deepa, B. Aruna Devi, *Indian J. Sci. Technol.* **4**, 1538 (2011).
8. M. Martialay, "Citizen Scientist," The Approach; http://approach.rpi.edu/2014/04/25/citizen-scientist-your-safari-photos-are-the-data/.
9. C. Caetano *et al.*, *Int. J. Quantum Chem.* **111**, 2732 (2011).
10. S. M. Leach *et al.*, *PLOS Comput. Biol.* **5**, e1000215 (2009).
11. Y. Gil *et al.*, *IEEE Intell. Syst.* **26**, 62 (2011).
12. Eureqa desktop, www.nutonian.com/products/eureqa/.
13. C. R. Aragon, S. J. Bailey, S. Poon, K. Runge, R. C. Thomas, *J. Phys. Conf. Ser.* **125**, 012091 (2008).

10.1126/science.1259439

Published by AAAS



Readers are invited to explore Mars with the Curiosity rover in National Geographic's *Mars Up Close*.

SPACE EXPLORATION

The illustrated Mars

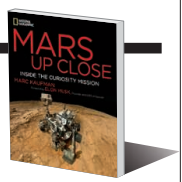
By **Margaret Moerchen**

An outsider could easily gape at Curiosity and its images without knowing the planning and innovation required to gently deliver a 2000-pound robot laden with 10 instruments to Mars. But journalist Marc Kaufman spent two years embedded with the team at NASA's Jet Propulsion Laboratory to bring this dramatic journey to life for the reader of *Mars Up Close*. The goal of Curiosity's mission—to characterize the habitability of Mars—is no simple task, and it relies on the myriad expertise of several hundred scientists and engineers. Snapshot profiles of 13 of these "Mission Makers" are woven throughout the book and include experts with diverse expertise and skill sets—from geologists to robot drivers to astrobiologists.

The presentation of Curiosity's journey, landing, and instrumentation, depicted in large format, recalls the works of author and illustrator David Macaulay, whose books deconstruct complex systems in a visually stunning manner. Curiosity's design and execution are presented as similarly monumental.

However, unlike static monuments, only through movement can Curiosity fulfill the mission's key aim: to find out whether Mars ever had the capacity to support life as we know it. Detailed satellite maps show the path of more than five miles between the rover's safe landing site and its intended destination, the three-mile-high Mount Sharp (Aeolis Mons).

With Curiosity's array of cameras and novel image-processing techniques, we see how different Mars is from Earth. Photographs taken by Curiosity show the marked sedimentary stratification of the mountain, which mission scientists hope to read like a timeline of the Martian environment. At times, however, photos of Mount Sharp and other landscapes shown throughout the book are difficult to distinguish from more-familiar Earth terrain. The layout of the photos offers the dramatic presentation for which its publisher, National Geographic, is known.



Mars Up Close
Inside the Curiosity Mission
Marc Kaufman
National Geographic Books, 2014. 304 pp.

Two exciting findings from the Curiosity mission detailed in the book are the discoveries that Mars was much wetter than previously thought and that wet conditions lasted until as recently as 3.5 billion years ago. Using drills, ovens, and lasers to sample the planet's surface for chemical and mineral analysis, Curiosity has revealed an apparent lake bed where water pooled for at least hundreds, and possibly tens of thousands, of years. Other tools on board the Curiosity offer further tantalizing hints at the building blocks of life, as detailed in the chapter "In search of organics."

Interviews with those at the periphery of the mission provide a broader context for the history. For example, Jet Propulsion Laboratory chief engineer Gentry Lee, who directed the Mars Viking landers, is a passionate advocate for improving understanding of Curiosity's importance to our society, and SpaceX founder Elon Musk entreats us to push our frontiers of exploration while we can. This book lays out both the inspiration and the justification for maintaining support for the Mars program.

10.1126/science.1260482

ILLUSTRATION: KENN BROWN

PHILOSOPHY OF SCIENCE

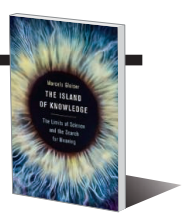
The edge of science

By **Michael A. Goldman**

To Dartmouth cosmologist Marcelo Gleiser, scientific knowledge is an island in an infinite sea, expanding as we discover, and with an ever-expanding shore of new questions and mysteries. The question he poses in *Island of Knowledge* is whether or not our failure to know everything is just the technical limitation of the moment, or if there is a point at which something is just plain unknowable. Whatever the answer, he assures us that we should feel neither defeated nor smug; the excitement is in the challenge.

The author provides a sweeping didactic and historical introduction to astronomy and physics. It stretches in size from the outer reaches of the universe to the too small to measure and in time from before the Big Bang to the end of eternity.

Gleiser has a gift for telling a story grandly and clearly. His history is nothing if not thorough, beginning in early superstition and mythology and methodically working up to current scientific questions in cosmology and physics. Along the way, he touches on everything from philosophy to optics to artificial intelligence.



The Island of Knowledge
The Limits of Science and the Search for Meaning
Marcelo Gleiser
Basic Books, 2014. 359 pp.

Throughout the book, Gleiser wrestles with the two extremes of the physical world, at times exploring the limitations associated with understanding the vastness of the physical universe and, at others, describing the challenges associated with understanding objects on the quantum scale. I don't fear a "spoiler" here, as the careful cases Gleiser builds in elegant language can't be summarized in this space. But I also warn that the depth of Gleiser's philo-

The reviewer is at the Department of Biology, San Francisco State University, San Francisco, CA 94132-1722, USA. E-mail: goldman@sfsu.edu

Downloaded from www.sciencemag.org on October 9, 2014

Published by AAAS

sophical thought, his analytical approach to history, and his refusal to whitewash technical detail make this a demanding, though stimulating, read.

Gleiser paints a clear picture of the way in which our knowledge is dependent on the tools currently at our disposal. He illustrates this idea by describing the limits imposed by the power of the first microscopes and telescopes. Today, he argues, it's the power of our particle accelerators that determines what we can perceive. On the other hand, he maintains that new tools have the power to reveal the breadth of our ignorance, prompting new questions that were previously inconceivable. With the invention of the microscope came the discovery of microscopic life, for example, prompting a slew of new questions about the origins and evolution of life.

Of course, science still has some difficulty in grappling with its own provisional nature. It was the religious right that opposed Galileo, but it was clearly the scientific establishment that challenged DNA as the genetic material in the 1940s and later would challenge any idea to the contrary (like Prusiner's prions). It seems the more we endeavor to teach the public about the exquisite process of science, the more we ourselves forget its dependence on confirmation and self-correction.

Ambiguity is at the very heart of quantum physics, which Gleiser illustrates with a description of the aptly named Heisenberg uncertainty principle. At least right now, this is a fundamental, physical limit to knowledge. This idea of inherent uncertainty is, perhaps, one of the most humbling limits associated with our quest for understanding.

The book is mistitled in that it deals primarily with the limits to the science of physics, rather than science in general, dabbling just a bit in neural science and artificial intelligence. Although the unknown now courses into every branch of science and mathematics, it is arguable whether the true, ultimate bounds of knowledge will indeed be reached in the realm of physics and cosmology.

Coming to grips with the ever-changing landscape of fact, and the possibility that some things cannot, by their very nature, be known, is fundamental to our understanding of science and the scientific method. But, as Gleiser argues, this needn't be cause for despair. "To avoid the funk of a modern scientific nihilism, we must find joy in what we are able to learn of the world, even if knowing that we can only be certain of very little."

10.1126/science.1256987

HISTORY OF MEDICINE

How medicine became modern

By **Mathieu Maheu-Giroux**

In 19th-century Europe and North America, consumption, as tuberculosis was then known, was the most common cause of death. It was so common and disease progression so torpid—patients could often expect to live years, if not decades, with this malady—that the idea that consumption was contagious was unfathomable. A diagnosis of tuberculosis was considered a death sentence, and, although many cures had been proposed, from cod-liver oil to sanatoriums, none of them worked. In *The Remedy*, science journalist Thomas Goetz describes much more than the fascinating quest to find a cure for tuberculosis. He chronicles the emergence of modern medical science through the pioneering work of Robert Koch and the life of author Arthur Conan Doyle.



The story begins in the 1870s with Robert Koch, then a young provincial doctor in Germany, performing his first experiments to demonstrate that bacteria were the causative agents of anthrax. His meticulous work would lead to the widespread acceptance of the germ theory, the then-radical proposition that diseases are caused by microorganisms (and not by miasma, a pernicious form of "bad air"). The author exposes how breakthroughs do not occur in a vacuum, that discoveries are attributed to those who succeed in convincing others, and how scientists themselves often resist innovation.

The book also goes to lengths in describing Koch's rivalry with Louis Pasteur, fueled by French-German antagonism and personal ambition, and how it catalyzed research efforts leading to Koch's discovery of tuberculosis's infective cause, *Mycobacterium tuberculosis*. This finding was hailed as a revolution as it finally opened the door for a cure. There was even more excitement when Koch announced, a few years later, the discovery of a remedy.

This is where Koch and Conan Doyle, also a physician by training, crossed paths. The latter traveled to Berlin and visited patients receiving this mysterious treatment. "Using Koch's own model of logic and analysis," Conan Doyle attacked this remedy as spoof, noting that Koch's substance had no effect in treating the disease.

Goetz posits that Koch "provided the template for Sherlock Holmes's fascination with minuscule detail." As much as the author would like to convince us, his case remains disputable, as the two men never actually met. Conan Doyle himself said that his inspiration for the famous detective was his former professor, Joseph Bell. That and some digressions on the antivivisectionist and modern antivaccination movements are the book's shortcomings.

Despite this, Goetz's pungent account of some of the 19th century's landmark medical discoveries, from antiseptic surgery to the anthrax vaccine, is definitely worth a read. Hopscotching through time and countries, he brilliantly narrates the rise of the two protagonists and how their embrace of deductive logic and scientific methods embodied the spirit of the time.

10.1126/science.1255877

The reviewer is at the Department of Global Health and Population, Harvard School of Public Health, 665 Huntington Avenue, Boston, MA 02115, USA. E-mail: m.maheu.giroux@mail.harvard.edu

The Remedy
Robert Koch, Arthur Conan Doyle, and the Quest to Cure Tuberculosis
Thomas Goetz
Gotham Books, 2014. 320 pp.

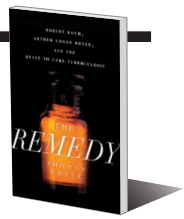


PHOTO: THINKSTOCK

Published by AAAS

Edited by **Jennifer Sills**

Algal blooms: Noteworthy nitrogen

NUTRIENT OVER-ENRICHMENT in lakes drives water-quality deterioration. The August 2014 water supply shutdown from Lake Erie to over 500,000 residents in Toledo, Ohio (*1*), highlights this problem, which has been historically addressed by controlling phosphorus (P) inputs. Management and research are based on the premise that P is the limiting factor in freshwater productivity and harmful algal bloom (HAB) formation (*2*, *3*). However, reducing P is no longer adequate for many lakes. Recent studies indicate algal proliferation in response to combined nitrogen (N) and P additions, or in some cases, the addition of only N (*4*–*8*). This shift in the freshwater nutrient management paradigm has important implications.

The toxic cyanobacterial genus *Microcystis* often dominates in nutrient-sensitive systems despite P-focused controls. Members of this genus cannot fix atmospheric N_2 (i.e., convert N_2 to ammonia), so they require combined N sources (such as ammonium, organic N, or nitrate) to support growth. Burgeoning usage of N fertilizers, urban and agricultural N wastes, and atmospheric N deposition have increased bioavailable N in receiving waters (*9*). This global pattern coincides with growing eutrophication issues, especially toxic, non–N_2-fixing cyanobacterial blooms, as exemplified by China's third-largest lake, Tai; in 2007, massive *Microcystis* blooms cut off drinking-water supplies to approximately 10 million local residents (*10*).

N occurs in gaseous forms, unlike P, and N is "lost" to the atmosphere through denitrification and other N sinks, whereas P is recycled internally (along with some N), perpetuating N-limitation (*8*). In-lake N_2 fixation does supply bioavailable N, but this input does not compensate for N loss (*8*, *11*). External N input is thus a key driver of eutrophication. Therefore, the "P-only" management paradigm should be amended to incorporate N-driven eutrophication and HAB abundances.

New nutrient reduction strategies should incorporate point and non-point sources, including N removal in wastewaters, optimization of fertilizer application, and erosion controls. This investment in joint P and N controls will counter the very high costs of HAB events and losses of freshwater resources in Toledo and worldwide.



Bloom of the toxic, non–N_2-fixing cyanobacteria *Microcystis* spp. in eutrophic Lake Tai, China.

CREDIT: H. PAERL, UNC-CHAPEL HILL, INSTITUTE OF MARINE SCIENCES

Hans W. Paerl,[1]* Wayne S. Gardner,[2] Mark J. McCarthy,[2] Benjamin L. Peierls,[1] Steven W. Wilhelm[3]

[1]Institute of Marine Sciences, University of North Carolina at Chapel Hill, Morehead City, NC 28557, USA. [2]Marine Science Institute, University of Texas at Austin, Port Aransas, TX 78373, USA. [3]Department of Microbiology, University of Tennessee, Knoxville, TN 37996-0845, USA.

*Corresponding author. E-mail: hpaerl@email.unc.edu

REFERENCES

1. G. Tanber, "Toxin leaves 500,000 in northwest Ohio without drinking water," *Reuters* (2 August, 2014); www.reuters.com/article/2014/08/02/us-usa-water-ohio-idUSKBN0G20L120140802.
2. D. W. Schindler *et al.*, *Proc. Nat. Acad. Sci. U.S.A.* **105**, 11254 (2008).
3. D. Scavia *et al.*, *J. Great Lakes Res.* **40**, 226 (2014).
4. J. J. Elser *et al.*, *Ecol. Lett.* **10**, 1124 (2007).
5. W. M. Lewis, W. A. Wurtsbaugh, H. W. Paerl, *Environ. Sci. Technol.* **45**, 10030 (2011).
6. H. W. Paerl *et al.*, *Wat. Res.* **45**, 1973 (2011).
7. J. D. Chaffin, T. B. Bridgeman, D. L. Bade, *Adv. Microbiol.* **3**, 16 (2013).
8. H. W. Paerl, J. T. Scott, *Environ. Sci. Technol.* **44**, 7756 (2010).
9. U.S. Environmental Protection Agency, "Reactive Nitrogen in the United States: An Analysis of Inputs, Flows, Consequences, and Management Options" (EPA-SAB-11-013, Washington, DC, 2011).
10. B. Qin *et al.*, *Environ. Manag.* **45**, 105 (2010).
11. J. T. Scott, M. J. McCarthy, *Limnol. Oceanogr.* **55**, 1265 (2010).

Algal blooms: Proactive strategy

CYANOBACTERIAL HARMFUL algal blooms (CHABs) are increasing in severity on a worldwide basis. Combining nutrient-source control with post-bloom control is currently considered the best strategy for dealing with CHABs (*1*). However, huge investments in this strategy have proven ineffective in China, as demonstrated by yet another massive bloom last summer in Lake Tai despite over 100 billion RMB (more than US$16.25 billion) invested since 2007 (*2*). Further afield, four decades of strict phosphorus loading regulations have not prevented massive CHAB events in Lake Erie of the Laurentian Great Lakes of North America and the adjacent water bodies (*3*).

The current strategy apparently has limited effectiveness. Furthermore, nutrient-source control may not be feasible for many developing countries because of increasing population pressure and pollution, and elevated CO_2 influx into aquatic systems and climate change will intensify algal blooms (*4*). Once CHABs have occurred, even the most effective methods to date of removal of cyanobacteria and cyanotoxins cannot eliminate their adverse impacts on ecosystems and human health (*5*).

We firmly believe that the missing key component in the current strategy is proactive CHAB control. By implementing this approach over the past 15 years, we have achieved effective long-term prevention of CHABs in several severely eutrophic lakes and reservoirs in Eastern China (*6*), thus showing that this approach is entirely possible and practical. Our strategy also affords valuable time for the implementation of nutrient-source control.

Proactive CHAB control requires appropriate technical expertise aimed at inhibiting algal growth during the spring season, when cyanobacteria is vulnerable to foraging species. This would involve developing new tools to trace pre-bloom algal distribution so that proactive treatments only need to be implemented within algae concentrated areas and in a cost-effective manner. Continuous monitoring and assessment of water bodies would maximize treatment efficacy.

Downloaded from www.sciencemag.org on October 9, 2014

Published by AAAS

Moreover, supportive laws and government policies are necessary. In particular, governments from different jurisdictions should reallocate resources to where CHABs originate; implement an appropriate merit system for proactive CHAB prevention and other measures related to eco-service enhancement; and curtail counterproductive human practices such as illegal fishing by enhancing law enforcement and providing alternative livelihoods and social learning to affected communities.

Mingzhi Qu,[1] Daniel D. Lefebvre,[1] Yuxiang Wang,[1] Yunfang Qu,[2] Donglin Zhu,[3] Wenwei Ren[4]*

[1]Department of Biology, Queen's University, Kingston, ON, K7L 3N6, Canada. [2]Ministry of Education Key Laboratory for Biodiversity Science and Ecological Engineering, School of Life Sciences, Fudan University, Shanghai, 200433, China. [3]Jiangsu Engineering Consulting Center, Nanjing, Jiangsu Province, 210003, China. [4]Key Laboratory of Yangtze Water Environment, Ministry of Education, The College of Environment Science and Engineering, Tongji University, Shanghai, 200092, China.

*Corresponding author.
E-mail: wenwei.ren.tongji@gmail.com

REFERENCES

1. H. W. Paerl, J. Huisman, *Science* **320**, 57 (2008).
2. D. Yu, H. Xiang, in *New Cent. Wkly*. (Caixin Media, Beijing, 2014), vol. 22.
3. A. M. Michalak *et al.*, *Proc. Natl. Acad. Sci. U.S.A.* **110**, 6448 (2013).
4. J. M. H. Verspagen *et al.*, *PLOS ONE* **9**, e104325 (2014).
5. H. K. Hudnell, *Toxicon* **55**, 1024 (2010).
6. W. Ren, M. Qu, Y. Qu, Y. Lin, Q. Wu, *New Theory and Technology in Harmful Algae Bloom Control* (SciTech Education Press, Shanghai, 2012) [in Chinese].

Ocean acidification foils chemical signals

THE CRUCIAL IMPORTANCE of chemical cues to reef resettlement was elegantly demonstrated by D. L. Dixson *et al.* ("Chemically mediated behavior of recruiting corals and fishes: A tipping point that may limit reef recovery," Research Article, 22 August, p. 892). Similarly, waterborne chemical signals (pheromones) and cues are essential for mediating marine species' behaviors, including those associated with mating, foraging, recruitment, and alarm (*1*).

Responses to these chemical signals and cues are in danger of global disruption by the effect of rising atmospheric CO_2 levels on aquatic pH. At current rates, ocean pH will drop from the current and historic pH of 8.15 to 8.25 to about 7.8 or below by 2100 (*2*). Quite apart from effects on calcification, reduced pH has the capability to affect both the signaling (semiochemical) molecules themselves and their interaction with chemosensory receptor proteins. The interaction of semiochemical ligands with chemosensory receptors changes with pH, through the number, type, and alignment of intermolecular forces (e.g., hydrogen bonding, electrostatic potential, and hydrophilic/hydrophobic regions) on both ligand and chemosensory receptor (*3*, *4*). Examples of the pH-affected semiochemicals are pheromones and cues, including peptides, nucleosides, thiols, and organic acids in nereid polychaete worms, *Aplysia* sea hares, crustaceans, and fish (*3*).

The current rate of oceanic pH decline is occurring faster than chemosensory systems can evolve; today's systems have evolved over 50 million years under relatively constant pH (*2*). Every marine species, at every trophic level, is potentially affected by disruption of chemical cues and signals, including responses to predator odors [e.g., (*5*)], sexual reproduction, sperm attraction, fertilization, social interactions, feeding, and larval settlement (*1*). Studies into not only the effects of disruption but also the mechanisms of action and resulting predictive ecological models are urgently needed. We risk widespread ecosystem damage by this additional silent danger from rising anthropogenic CO_2 levels.

Tristram D. Wyatt,[1]* Jörg D. Hardege,[2] John Terschak[2]

[1]Department of Zoology, University of Oxford, Oxford, OX1 3PS, UK. [2]School of Biological, Biomedical, Environmental Sciences, University of Hull, Hull, HU6 7RX, UK.

*Corresponding author.
E-mail: tristram.wyatt@zoo.ox.ac.uk

REFERENCES

1. T. D. Wyatt, *Pheromones and Animal Behavior: Chemical Signals and Signatures* (Cambridge Univ. Press, Cambridge, ed. 2, 2014).
2. S. C. Doney *et al.*, *Ann. Rev. Mar. Sci.* **4**, 11 (2012).
3. J. D. Hardege, J. M. Rotchell, J. Terschak, G. M. Greenway, *Trends Analyt. Chem.* **30**, 1320 (2011).
4. J. Reisert, D. Restrepo, *Chem. Senses* **34**, 535 (2009).
5. D. L. Dixson, P. L. Munday, G. P. Jones, *Ecol. Lett.* **13**, 68 (2010).

TECHNICAL COMMENT ABSTRACTS

Comment on "Oxytocin-mediated GABA inhibition during delivery attenuates autism pathogenesis in rodent offspring"

Victorio Bambini-Junior, Gustavo Della Flora Nunes, Tomasz Schneider, Carmem Gottfried

Tyzio *et al.* (Reports, 7 February 2014, p. 675) reported that bumetanide restored the impaired oxytocin-mediated γ-aminobutyric acid (GABA) excitatory-inhibitory shift during delivery in animal models of autism, ameliorating some autistic-like characteristics in the offspring. However, standard practices in the study of these models, such as the use of sex-dimorphic or males-only analyses and implementation of tests measuring social behavior, are lacking to definitely associate their findings to autism.

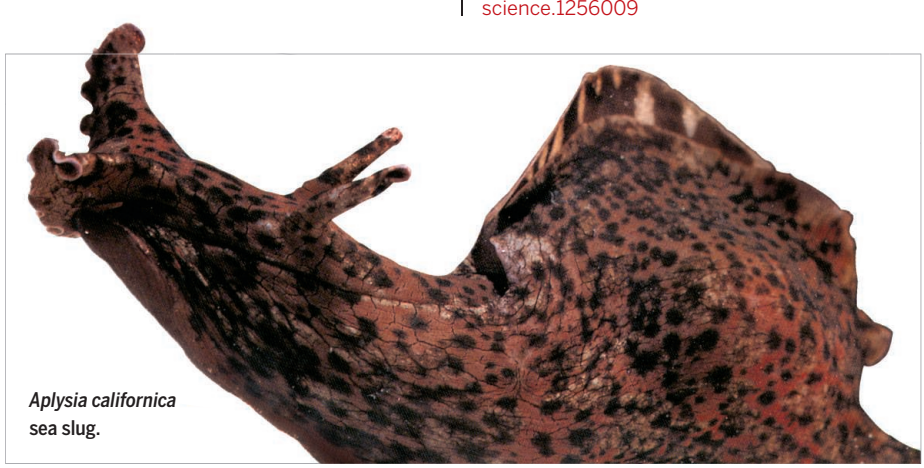
Full text at http://dx.doi.org/10.1126/science.1255679

Response to Comment on "Oxytocin-mediated GABA inhibition during delivery attenuates autism pathogenesis in rodent offspring"

Sanaz Eftekhari, Amene Shahrokhi, Vera Tsintsadze, Romain Nardou, Corinne Brouchoud, Magali Conesa, Nail Burnashev, Diana C. Ferrari, Yehezkel Ben-Ari

Bambini-Junior *et al.* questioned whether our treatment in two rodent models of autism has a long-lasting effect into adulthood. In response, we show that bumetanide treatment around delivery attenuates autistic behavioral features in adult offspring. Therefore, the polarity of γ-aminobutyric acid (GABA) actions during delivery exerts long-lasting priming actions after birth.

Full text at http://dx.doi.org/10.1126/science.1256009



Aplysia californica sea slug.

CREDIT: COLUMBIA UNIVERSITY, NEW YORK

Published by AAAS

TECHNICAL COMMENT

DEVELOPMENTAL NEUROLOGY

Comment on "Oxytocin-mediated GABA inhibition during delivery attenuates autism pathogenesis in rodent offspring"

Victorio Bambini-Junior,[1,2]* Gustavo Della Flora Nunes,[1,2] Tomasz Schneider,[3] Carmem Gottfried[1,2]

Tyzio *et al*. (Reports, 7 February 2014, p. 675) reported that bumetanide restored the impaired oxytocin-mediated γ-aminobutyric acid (GABA) excitatory-inhibitory shift during delivery in animal models of autism, ameliorating some autistic-like characteristics in the offspring. However, standard practices in the study of these models, such as the use of sex-dimorphic or males-only analyses and implementation of tests measuring social behavior, are lacking to definitely associate their findings to autism.

Autism spectrum disorders (ASD) are a group of neurodevelopmental disabilities characterized by sociability impairments, communication deficits, and stereotyped behavioral patterns (*1*). The etiology of autism is still not known, and current treatment options provide only a mild relief to some aspects of this condition. Nevertheless, there is mounting evidence that an excitation/inhibition imbalance plays a crucial role in the pathology of ASD (*2*). Tyzio *et al*. (*3*) recently reported that bumetanide maternal pretreatment was able to restore physiological levels of intracellular chloride in CA3 hippocampal neurons in two different animal models of autism: rats prenatally exposed to valproate (VPA) and Fmr1 knock-out mice (FRX). As a consequence, excitatory actions of γ-aminobutyric acid–mediated (GABAergic) signaling were reduced and electroencephalographic patterns were normalized. In addition, bumetanide treatment of pregnant females reversed aberrant maternal-separation–induced ultrasonic vocalization in the offspring. The authors also stressed the importance of oxytocin in the developmental GABA switch from excitatory to inhibitory, because prenatal treatment with the oxytocin receptor antagonist SSR126768A in naïve animals triggered alterations similar to those observed in VPA rats and FRX mice. The use of both genetic and drug-induced autism models strengthen their discovery, which is also supported by their previous finding of bumetanide efficacy in a clinical trial in children with autism (*4*). However, we strongly feel that some technical issues of their work remained unaddressed and that the final conclusions of this work would be greatly improved by resolving those issues.

One of the most relevant features of autism is the difficulty to establish and maintain reciprocal social interactions with peers. These disabilities in social skills are mimicked in both VPA rats (*5*) and FRX mice (*6*) and can be detected by behavioral testing. Tyzio *et al*. did not evaluate social parameters in the rodents used in their work. We understand that, in principle, impaired ultrasonic vocalizations (USV) can lead to sociability deficits, but this has not been proved yet, and changes in USV in pups may be modulated by several factors not related to social domain—for example, temperature, sensitivity to pain, or general distress (*7*). Because social behavior requires the integration of a wide variety of neural circuits related to diverse aspects of sensory and cognitive functions (*8*), they have to be studied in much more elaborate ways—for example, using reciprocal social interaction or social preference tests, possibly in combination with USV recording. We believe that analyses of social behavior and USV emitted during social tasks are necessary to improve the quality and confidence of their data.

It is also important to verify whether the effects of bumetanide and SSR126768A persist over time. To clarify whether those are temporary or long-lasting modifications, the authors should extend the evaluation of the behavioral and electrophysiological phenotypes into different developmental stages, including adulthood and, possibly, the end of the first postnatal week as a rough equivalent of birth-stage development in humans (*9*).

Another factor that needs to be taken into consideration to fully understand the relevance of Tyzio *et al*.'s results for autism is the use of both male and female rodents in all experiments. The higher prevalence of ASD in males is very well established, and some animal models of autism also show this male bias. The VPA animal model of autism has demonstrated solid evidence of sex-specific behavioral and morphological outcomes. The VPA rats were extensively analyzed, and most of the autistic-like features, including sociability deficits, were not detected in females (*10*, *11*). In fact, VPA female rats are sometimes used in comparison to males to determine gender-specific alterations, which are likely to be more relevant to autism pathophysiology (*11*, *12*). In addition, there is no complete characterization of autistic-like features in female FRX mice, because the vast majority of researchers use only males in their experiments (*13*–*15*). Thus, the authors should consider sex, including in embryos, as a factor in their data analysis, and therefore increase the number of animals per sex per group. Without taking this into account, the results are affected by the possibility of misbalanced numbers of males and females per group.

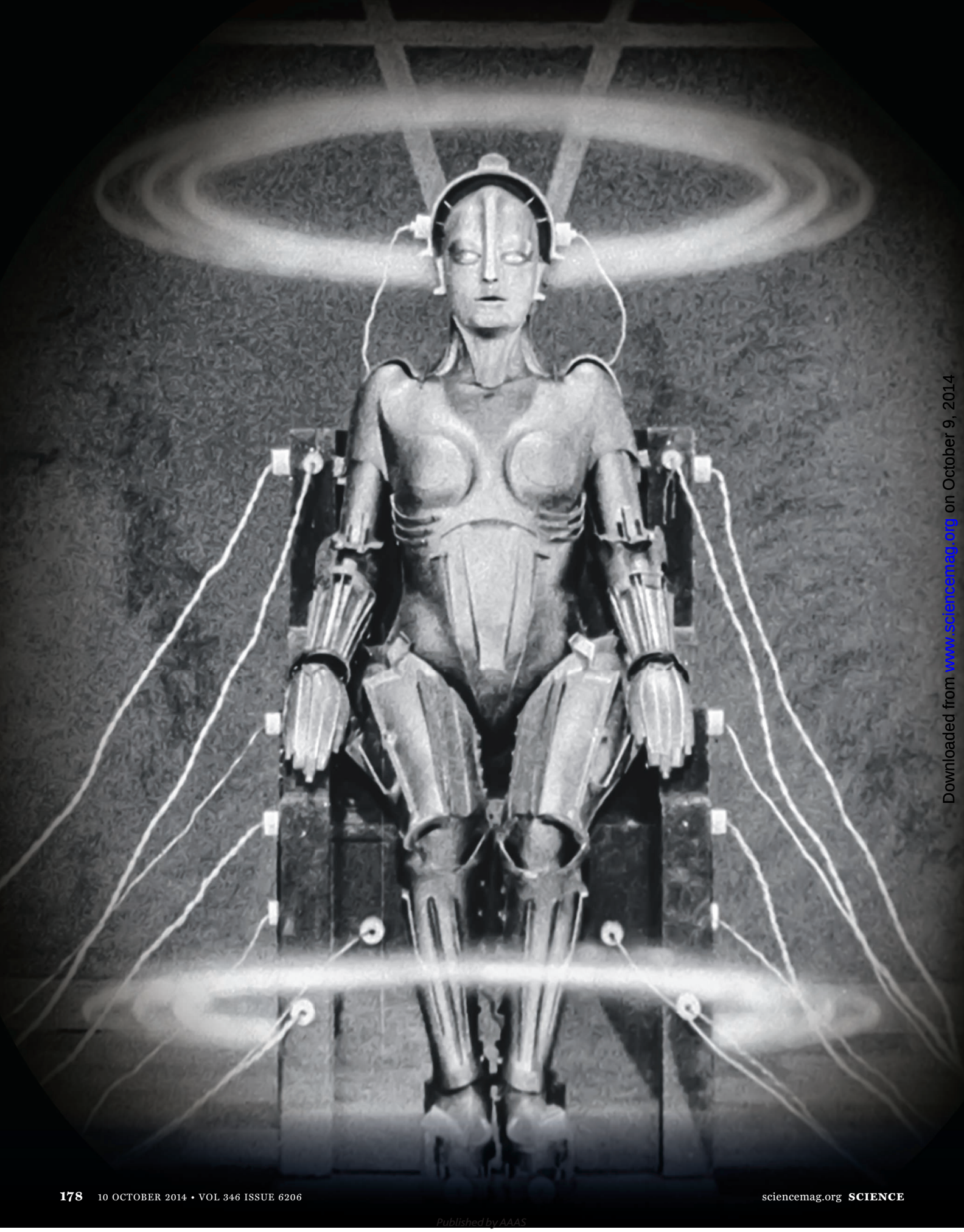
The concepts analyzed by Tyzio *et al*. have an enormous potential to help the development of future studies and can represent a turning point in the research of the etiology of ASD. However, giving the topic's prominence and impact, we believe that our suggestions are important to clarify key aspects discussed by them. It is still premature to think of bumetanide as a prenatal intervention for ASD, but it can be regarded as a meaningful research tool of the molecular underpinnings of this condition.

[1]Federal University of Rio Grande do Sul, Research Group in Neuroglial Plasticity at the Department of Biochemistry, Institute of Health's Basic Science, Porto Alegre, Rio Grande do Sul, Brazil. [2]Federal University of Rio Grande do Sul, Translational Research Group in Autism Spectrum Disorders (GETTEA), Porto Alegre, RS, Brazil. [3]School of Medicine, Pharmacy and Health, TS17 6BH, Durham University, Durham, UK.
*Corresponding author. E-mail: victoriobambini@gmail.com

REFERENCES

1. M. W. State, N. Šestan, *Science* **337**, 1301–1303 (2012).
2. O. Yizhar *et al*., *Nature* **477**, 171–178 (2011).
3. R. Tyzio *et al*., *Science* **343**, 675–679 (2014).
4. E. Lemonnier *et al*., *Transl. Psychiatry* **2**, e202 (2012).
5. V. Bambini-Junior *et al*., *Brain Res.* **1408**, 8–16 (2011).
6. M. A. Mines, C. J. Yuskaitis, M. K. King, E. Beurel, R. S. Jope, *PLOS ONE* **5**, e9706 (2010).
7. M. L. Scattoni, L. Ricceri, J. N. Crawley, *Genes Brain Behav.* **10**, 44–56 (2011).
8. D. A. Stanley, R. Adolphs, *Neuron* **80**, 816–826 (2013).
9. B. D. Semple, K. Blomgren, K. Gimlin, D. M. Ferriero, L. J. Noble-Haeusslein, *Prog. Neurobiol.* **106-107**, 1–16 (2013).
10. T. Schneider *et al*., *Psychoneuroendocrinology* **33**, 728–740 (2008).
11. K. C. Kim *et al*., *J. Neurochem.* **124**, 832–843 (2013).
12. Y. Hara *et al*., *J. Pharmacol. Sci.* **118**, 543–546 (2012).
13. B. M. Dolan *et al*., *Proc. Natl. Acad. Sci. U.S.A.* **110**, 5671–5676 (2013).
14. S. Pietropaolo, A. Guilleminot, B. Martin, F. R. D'Amato, W. E. Crusio, *PLOS ONE* **6**, e17073 (2011).
15. C. M. Spencer *et al*., *Autism Res.* **4**, 40–56 (2011).

6 May 2014; accepted 12 September 2014
10.1126/science.1255679



Downloaded from www.sciencemag.org on October 9, 2014

Published by AAAS

the social life of Robots

By **Richard Stone** *and* **Marc Lavine**

Autonomous machines have gripped our imagination ever since the first robot flickered on the silver screen, Maria (left) in the 1927 film *Metropolis*. Most of the robots we know today—unglamorous devices like robotic welders on car assembly lines and the Roomba vacuum cleaner—fall short of those in science fiction. But our relationship with robots is about to become far more intimate. Would you be comfortable with a robot butler, or a self-driving car? How about a robo-scientist toiling away next to you at the bench, not only pipetting but also formulating hypotheses and designing experiments?

As robots become more sophisticated, psychological paradoxes are coming into sharper relief. Robots that look human strike many of us as downright creepy (as this week's cover attests), while robots that act human—when they are programmed, for example, to cheat at cards—somehow put us at ease. And no matter how uncannily lifelike some of today's robots may seem, the resemblance is skin-deep. A stubborn challenge has been endowing robots with not only the capability to sense their environment, but also the wits to make sense of it. Robots will get there eventually, and when that happens we'll be confronted with a new array of ethical and moral questions. Questions like: Should robots be accorded rights as sentient beings? The rise of the machines will be anything but predictable.

PHOTO: FRIEDRICH-WILHELM-MURNAU STIFTUNG, WIESBADEN, GERMANY

INSIDE

NEWS

Meet your new co-worker *p. 180*

Minds of their own *p. 182*

Getting a feel for the world *p. 184*

Helping robots see the big picture *p. 186*

In our own image *p. 188*

Humans need not apply *p. 190*

The accidental roboticist *p. 192*

Q&A: Robots and the law *p. 195*

REVIEW

Biorobotics: Using robots to emulate and investigate agile locomotion *p. 196*

RELATED ITEMS

- **PERSPECTIVE p. 160**
- **REPORT p. 224**
- **PODCAST**
- **VIDEO**
- **SLIDESHOW**
- ***SCIENCE TRANSLATIONAL MEDICINE:* 3 RELATED ARTICLES; 8 OCT 2014**
- **CAREERS**
- **WORKING LIFE**
- **sciencemag.org/special/robotics**

Published by AAAS

Meet your new co-worker

At the vanguard of human-robot interactions is Baxter, a bot quick on the uptake that even knows how to cheat

By **John Bohannon**, *in Boston*



"We are pleased to confirm receipt of your order for fifteen thousand robots," says the industrialist Harry Domin in the opening scene of *R.U.R.*, a 1920 play written by Karel Čapek. Čapek coined the word "robot" from *robota*, which in Czech means forced labor or drudgery. He imagined a future in which the global economy runs on humanoid automatons. Things get stirred up when an activist named Helena appears at Domin's company, demanding equal rights for robots. He dismisses her concerns. Once in a while a robot working on an assembly line goes crazy, "smashing up all the moulds and models," admits one of the company's human employees, but Domin assures Helena that the robots are soulless and have no desire for rights or freedoms.

Nearly a century later, at least some of Čapek's vision is starting to come true. Machines are now capable of carrying out certain tasks on an assembly line—such as welding car frames or spray-painting parts—far more efficiently than humans. And they are now developing some of the dexterity and awareness needed to serve as pets and helpers in homes, as caregivers in hospitals, and as co-workers in factories (see p. 188). But for people to truly embrace bots in their daily lives, the machines will need social smarts. "These are exciting times for human-robot interaction," says Brian Scassellati, a roboticist at Yale University.



Baxter has a variety of "hands" adapted to specific tasks.

Like many others in his field, Scassellati has adopted a robot, called Baxter by its manufacturer, as his research subject. The company behind Baxter, Rethink Robotics, is selling it to manufacturing companies. The hope is that assembly lines are poised for disruption by a versatile robot that can take over repetitive, mind-numbing tasks. In the meantime, Baxter is serving as a test subject for robot psychology. In the past, experiments in human-robot interaction were limited to custom-built bots that required careful supervision to avoid harming human or robot. Baxter was built to interact safely with humans. "I can even let my high school interns work with it unsupervised," Scassellati says. And crucially, Baxter, by design, learns from people.

WHEN I ASK CHRIS HARBERT if I can play with one of the $25,000 humanoids in the Rethink Robotics offices here, he doesn't flinch. "Go for it," he says, taking a step back from Baxter. The big cartoon eyes on the robot's face—a computer screen mounted on a swivel neck—stare down at an unmoving conveyor belt cluttered with objects. Its hulking red arms hang open in a shrug, as if to say, "I'm ready for whatever."

Nearby is a box of white plastic widgets that look like giant nipples. The goal, I decide, is for Baxter to pick them up and place them on the conveyor belt. Baxter learns by example, so I grab one of the robot's arms and pull it into position over one of the widgets. The plastic-cased steel limb is as thick as a human leg, but moving it requires surprisingly little strength. The robot is paying attention: Its head turns, and its cartoon eyes track my hand. I lower Baxter's hand into position and press a button on the arm, making it seize the widget with its pincer grabber, which is reminiscent of the robot from the 1960s TV show *Lost in Space*.

With a gentle tug, I guide the arm to the far side of the conveyor belt, lower the hand, press the button again, and Baxter drops the widget. Scaling up this task takes me a few more steps, with minimal guidance from Harbert. Holding Baxter's hand, I trace an imaginary square over the widgets and then over the destination, defining the pickup and drop-off areas. And then, with an actual nod of its computer-screen head, Baxter gets to work, mimicking my movements and—except for one dropped nipple—efficiently transferring them from box to conveyor belt.

As I will soon hear from Rodney Brooks, the legendary roboticist who founded the company, getting a robot even to this level of success on tasks like these normally takes an engineer weeks or even months of work. I did it in 5 minutes without an engineering degree. If I can teach Baxter, surely the average factory manager can, too. But would the average factory employee be comfortable with a robot co-worker?

MAKING A ROBOT that collaborates with people is at least as much about human psychology as it is about robot engineering.

Just the appearance of a robot can be a barrier—especially if it falls within the uncanny valley, a term introduced by Japanese roboticist Masahiro Mori in 1970. A zone of discomfort lies somewhere between robots that are obviously nonhuman—something cute like the late 1990s toy Furby—and robots like the replicants from the 1982 film *Blade Runner*, so humanlike that you can't perceive the difference. Robots that look almost-but-not-quite human creep us out, and no one knows why. According to one theory, they are similar to corpses.

A machine's movements are another barrier. The challenge is to create robots that are less *robotic*, says Guy Hoffman, a roboticist at the Interdisciplinary Center Herzliya in Israel. Just like the "user interface" that enabled the personal computer revolution, a movement-based "robot user interface" is needed, he says. In some circumscribed domains, progress has been impressive. For

PHOTOS: (LEFT TO RIGHT) BENJAMIN ECKSTEIN; RETHINK ROBOTICS

Downloaded from www.sciencemag.org on October 9, 2014

Published by AAAS



Humans can infer Baxter's intentions from "emotions" expressed on the bot's flat panel display "face."

example, Hoffman created the world's first robot that can play improvisational jazz in an ensemble with humans. But to live and work side by side with humans, he says, a robot must understand your intentions and act appropriately, "looking you in the eyes, touching your shoulder, coming closer or shying away."

Baxter has none of those social graces. But the scientists using the robot in their labs are trying to create a road map to get there. Scassellati is working with a simple system. Baxter has only six facial expressions, ranging from sleepy and content to confused and surprised, each of which signals a different internal state. "The important thing is that you should be able to work with Baxter with as little special training as possible," says Miri Bauman, the designer of Baxter's user interface.

One ongoing experiment has generated surprising results. "We've been having Baxter play checkers with humans," Scassellati says. At a certain point in the game, Baxter cheats. The social dynamics change abruptly. "People interact with the robot like a person," he says. Without realizing that they're doing it, the subjects start talking to the robot, making eye contact, and maintaining human-appropriate social distance. "It's a powerful effect," he says. "If you want people to treat a robot like a person, have the robot cheat." Roboticists hope that more sociable tricks like joking and sarcasm will achieve the same effect.

With some human subjects, no subterfuge is necessary to elicit profound effects. For example, Scassellati has been working with a 12-year-old boy with autism spectrum disorder. "He is high-function, but if you met him on the street, you'd immediately recognize him as autistic," he says. The boy avoids eye contact, has difficulty communicating, and makes repetitive movements. "But we put him in a room with the robot and he changes." The boy gazes right into Baxter's eyes, using his gaze to signal what he's thinking. "We take the robot away and the effect lasts maybe 15 minutes and it's gone," Scassellati says. "We don't understand what's going on, but dozens of labs have replicated this effect."

Scassellati is also using Baxter to study the other side of the equation: getting robots to read our minds. In one experiment, Baxter works with people at a tabletop to assemble Ikea furniture. The robot knows the blueprint, but it also must anticipate what the human will do next. Fellow humans find it effortless to guess why you're looking for all the pieces of a particular shape, but that represents a steep challenge for Baxter. It requires what psychologists call the theory of mind, which has yet to be captured in computer code. "This is the frontier of human-robot interaction," Scassellati says. At this point, humans are better off muddling through Ikea furniture assembly on their own.

"I TAUGHT BAXTER a task," I tell Brooks. "He's impressive."

"It's an it. Or if anything, a she," Brooks says in his broad Australian accent. The original meaning of the word "baxter" is a female baker, he explains. "But everyone makes this mistake." The misattribution isn't bad news—it indicates that Baxter's "robot user interface" is working—but Brooks worries that "robots shouldn't make promises they can't keep." Baxter isn't designed to have much of a personality, let alone a gender.

There is one promise that Baxter is programmed to keep, at all costs: It will do its utmost not to hurt you. (Unlike Čapek's robots, which rise up and exterminate humanity.) "Robots are extremely dangerous," explains Brooks, whose lab at the Massachusetts Institute of Technology in nearby Cambridge has churned out a large proportion of today's leading roboticists, including Scassellati. The industrial robots on assembly lines today simply aren't safe to be around. "The robots work in their own room, people work in another, and the two don't mix," he says. "Baxter is meant to bridge that gap."

Brooks's team has built several layers of safety into Baxter. It constantly searches for the presence of humans with a 360° sonar system, halting if anything gets too close. If a human insists on getting in the way of the arms, Baxter's plastic armor and control system—the key is a special spring called a series elastic actuator—soften the blow. "When I'm giving demonstrations I like to stick my head in the way to show that it doesn't hurt," Brooks says. He knows that if Baxter were to cause a single serious injury, its days would be numbered.

And what about harming livelihoods? "It's not about taking people's jobs," Brooks says before I even ask the question. Rather than replacing workers, he says, Baxter will free people to do higher level tasks. "Robots have a long way to go before they can completely replace someone working in a factory." For a start, he says, robots lack "dexterous manipulation." To demonstrate, Brooks stands up and pulls his keys out of his pocket. "What I just did is nearly impossible for a robot," he says. Another impediment is robot vision (see p. 186). "And then there's the problem of mobility," Brooks says. "Stairs are a nightmare for robots."

After chatting with Brooks, I walk down the hall to see how Baxter is doing. At the end of my robot tutorial, I'd asked Harbert to instruct Baxter to do something that would drive a human insane: After placing the widgets on the conveyor belt, put them back in the box, and repeat that in an infinite loop. I find Baxter toiling away, unsupervised, delicately moving widgets onto the belt, one at a time, and then putting them back. Like Sisyphus, but without the suffering. ■

Published by AAAS



EyeRover negotiates obstacles, guided by software that emulates the brain.

Downloaded from www.sciencemag.org on October 9, 2014

Minds of their own

Novel neuromorphic chips and software should provide robots with unrivaled perceptual skills

By **Robert F. Service**, *in San Diego, California*

Like a miniature Segway with eyes, a robot built from 3D printed plastic does laps around a cubicle here at Brain Corporation, having learned in a matter of minutes to avoid bumping into walls as it roams. As eyeRover scoots away, Peter O'Connor, a staff scientist at the robotics software company, steps into its route. Using a remote control unit, he briefly takes control of the foot-tall robot and steers it around his feet, much as a parent might help a toddler learn to avoid a coffee table. On the next lap, eyeRover whisks around the obstacle all by itself.

EyeRover may look like a toy, but it's packed with some of the most advanced robotic technology ever devised, including a prototype computing platform designed to emulate the human brain. Unlike conventional computer chips and software, which execute a linear sequence of tasks, this new approach—called neuromorphic computing—carries out processing and memory tasks simultaneously, just as our brains do for complex tasks such as vision and hearing.

Many researchers believe that neuromorphic computing is at the threshold

PHOTO: BRAIN CORPORATION

Published by AAAS

of endowing robots with perceptual skills they've never had before, giving them an unprecedented level of autonomy. It "has the potential to be a real revolution" in robotics, says Michele Rucci, a robotics vision expert at Boston University. At the same time, robots could provide the perfect demonstration of the power of neuromorphic computing, helping persuade scientists in fields ranging from computer vision to environmental data analysis to embrace the approach. "We think robotics is the killer app for neuromorphic computing," says Todd Hylton, Brain Corporation's senior vice president for strategy.

IF YOUR EYES ROLL at yet another claim that we are on the cusp of a golden age of robotics, you're forgiven. The dream of autonomous robots predates even the dawn of computing. But it has never been realized because of the difficulty of programming robots to learn and adapt. Decades of work in artificial intelligence, computer architectures, and Bayesian statistics—a technique for weighing the likelihood of different outcomes to unfolding events—have failed to produce robots capable of managing more than a handful of mundane tasks in everyday environments.

Building robots that can make sense of their surroundings is "a particularly tough computational problem," Hylton says. Take vision, the primary way most of us analyze our environment. "Robotic vision is far behind what we promised 20 to 30 years ago," Rucci says.

Teams have come up with various strategies for enabling robots to process and react to what they see (see p. 186). Rucci, for one, has given robots the same type of tiny, involuntary eye movements that humans perform; by providing our brains with constantly shifting images, they help us judge depth and track objects. Still, Rucci's best flitting-eye bots are hampered by their brains, which process information 10 times slower than we do.

The human eye works so well, in part, because of the sheer complexity of the computer inside our skulls. Our brains contain an estimated 100 billion neurons connected by 100 trillion synapses, and they can distribute different perceptual tasks to different groups of neurons and different brain regions, explains Brain Corporation CEO Eugene Izhikevich. In vision, for example, separate groups of neurons respond to vertical and horizontal features and pass those signals up the chain to other neurons that integrate the signals.

Brain Corporation's neuromorphic software, called BrainOS, mimics that approach. Like our brains, the operating system segregates visual functions into different networks, analogous to the retina, the brain's lateral geniculate nucleus (a relay station for visual signals), and the layers of the visual cortex. Integrating the output of these networks results in a robotic visual system able to focus automatically on salient features that stand out from background, such as a brightly colored ball rolling across a gray carpet or the shoes of a person crossing a robot's path.

Another innovation of BrainOS is that it doesn't require a supercomputer to run. A previous neuromorphic software program, developed by IBM in 2012, did run on a supercomputer, using it to mimic the firing patterns of an animal brain containing 500 billion neurons and 100 trillion synapses. But even with an array of 1.5 million computer chips, the program couldn't produce those firing patterns in anywhere close to real time.

> ***"We think robotics is the killer app for neuromorphic computing."***
> **Todd Hylton**, Brain Corporation

BrainOS, on the other hand, is integrated into a coaster-sized computer circuit board called bStem (short for "brainstem") that's powered by a Snapdragon mobile phone processor from Qualcomm. Unlike conventional computer chips, mobile phone chips minimize power use by distributing tasks, such as memory, graphics processing, and communication, to specialized sub-processors. That "distributed" architecture dovetails well with the neuromorphic approach.

A truly neuromorphic architecture, with memory and processing elements distributed throughout the chip, may be coming soon. Qualcomm researchers who sit just upstairs from Brain Corporation have built a neuromorphic chip they call their Zeroth processor—named after science fiction writer Isaac Asimov's Zeroth Law of Robotics, which states that robots are not allowed to harm humans. M. Anthony Lewis, who heads neuromorphic computing efforts at Qualcomm, says the company is nearing commercialization of the processor, which they plan to integrate into their mobile chips to improve handheld devices' audio and visual processing skills.

Qualcomm has plenty of competition. Just up Interstate 5, researchers at HRL Laboratories LLC in Malibu are working on their own neuromorphic chip, which they've recently shown can process visual data fast enough to pilot a palm-sized helicopter inside an office building and recognize and explore rooms it has never seen before. And in August, a team led by researchers at IBM's Almaden Research Center in San Jose reported a titanic neuromorphic chip, dubbed TrueNorth, that contains 5.4 billion transistors wired to behave like 1 million neurons connected by 256 million synapses (*Science*, 8 August, p. 614).

These neuromorphic chips are inspired not only by the architecture of the brain but also by its energy efficiency—the brain, which bests supercomputers on many tasks, uses roughly 20 watts of power. Whereas conventional computer circuits regularly bleed electricity even when they're not sending a signal, neuromorphic circuits use power only when active. And by distributing memory and processing modules throughout the chip, they minimize the power required to send data back and forth during computations. TrueNorth, for example, uses only 1/1000 the energy of a conventional chip to carry out the equivalent visual perception tasks.

Which real-world applications for neuromorphic robots will emerge first? Last fall, Qualcomm engineers demonstrated that a meter-high neuromorphic robot called Dragon could adeptly clean up scattered toys, sorting blocks into one bin and stuffed animals into another. For his part, Izhikevich believes that neuromorphic hardware and software will at long last give robots enough perceptual skills to be valuable home companions: able to take out the trash, clean the house, and pick vegetables from a garden. Neuromorphically heightened perception, adds IBM's neuromorphic team leader Dharmendra Modha, will give robots the wherewithal to navigate hazardous environments, such as a damaged nuclear reactor, without guidance from a human operator, beaming back data on radiation and other conditions in real time.

The energy efficiency of neuromorphic computing could open the way to new functions, Lewis says. Efficient chips can run complex—and normally power-hungry—algorithms that enable robots to learn. The Internet, in turn, will allow far-flung robots to share those lessons and skills. A robot that learns how to pick a strawberry without crushing it, for instance, could uplink that skill for the benefit of its kind around the globe. That means neuromorphic computing could offer robots something far more profound than enhanced perceptual skills. When humans collectively pass along life lessons, we call that culture. ■

Published by AAAS



Touch

In 2003, a stroke left Henry Evans mute and quadriplegic. Last year, Georgia Institute of Technology researcher Charlie Kemp developed a robotic arm that Evans directs by moving his head. It uses tactile "skin" to feel its way without damaging the environment. Software tunes the robot's sense of touch, allowing it to gently make contact with an object and intelligently maneuver within clutter. Kemp says that giving robots the sensation of touch "humanizes" them.

Smell

As we breathe, molecules of all sorts are drawn into the nasal passage, tickling receptors in our mucous membrane that match an odor to a learned scent. A Swedish creation called the Gasbot has the robot version of a nose, though it knows just one smell. Equipped with a laser beam tuned to the wavelength of light commonly absorbed by methane, Gasbot can detect gas leaks at concentrations as low as 5 parts per million.

Taste

Alcohol doesn't give robots a thrill, but one in Spain has an electronic tongue that differentiates between six types of beer. A Japanese team has built a bot capable of distinguishing wines by bathing them in infrared light and analyzing the absorption patterns. The same robot also "tasted" human body odor and pronounced it to be closest to bacon.



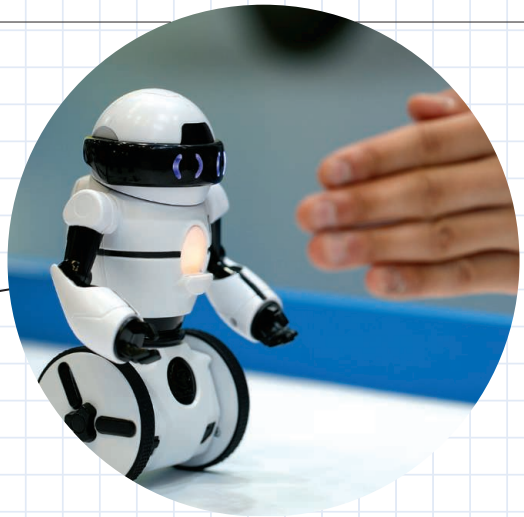
GETTING A FEEL FOR THE WORLD

To be fully autonomous, robots must be able to make sense of their surroundings. Forget *joie-de-vivre* sensations like Robert Browning's "yellow half-moon large and low" over a "warm sea-scented beach." Designing mundane, practical sensors for robots has proven to be a formidable challenge.

Design by Garvin G. Grullón; reporting by Hassan DuRant and Jia You

Downloaded from www.sciencemag.org on October 9, 2014

Published by AAAS



Sight

Roboticists once thought that of all the senses, sight would be the easiest to recreate. How wrong they were. Image acquisition is not the issue: Robots can "see" with far more acuity than the 20/20 standard by which we measure our fluid-filled eyeballs. The challenge is getting machines to make sense of what they are seeing. Two new powerful approaches—deep learning (p. 186) and neuromorphic computing, which emulates the human brain (p. 182)—could finally equip robots with the processing firepower to size things up.

Hearing

Imagine yourself at a noisy cocktail party, trying to tune in to the guy in the corner inveighing against an inevitable robot uprising. That's a cinch for our brains, which are wired to filter signal from noise. Japanese roboticists have hit upon a sound localization algorithm that disentangles up to four simultaneous sound sources. Our ears also filter out many sounds inside the body, such as breathing and heartbeat. Robot ears have to contend with the whine and whir of machinery.

Balance

Humans effortlessly stay upright with continual, minute adjustments of our bodies. Researchers in Massachusetts have endowed Atlas, a humanoid robot, with a similar dynamic sense of balance. Moving its body with high-powered hydraulics, the robot can walk across unsteady debris and stay balanced on one leg when whacked with a 9-kilogram wrecking ball. But Atlas is still prone to falling, breaking its right ankle during a 2013 walking demonstration in Hong Kong.

Published by AAAS

Helping robots see the big picture

A computational approach called deep learning has transformed machine vision

By **John Bohannon**,
in San Francisco, California

If you want to see the state of the art in machine vision, says artificial intelligence researcher D. Scott Phoenix, "you should watch the YouTube video of the robot making a sandwich." The robot in question is a boxy humanoid called PR2. It was built less than an hour away at Willow Garage in Menlo Park, California, one of the most influential robotics companies in the world. But Phoenix is being ironic. When PR2 finally manages to pick up a piece of bread, it drops the slice on the toaster; the bread caroms off, and a human rushes in to help. After stabbing a slice of salami with a fork, PR2 holds it in the air for what seems like an eternity. The sandwich does eventually get assembled, but it happens so slowly that the video is sped up 10-fold to make it watchable. And that was in an experimental kitchen in which "everything is carefully laid out," Phoenix says. "There's exactly one plate. Exactly one knife."

Robots are clumsy because they struggle to make sense of all the data coming in from their cameras. "Vision is the biggest challenge," Phoenix says. Depending on their angle of view, objects can appear to have millions of different shapes. Change the lighting and each of those millions multiplies again—and this is the simplest case. A cluttered scene with overlapping objects is a nightmare. Although machines easily surpass human ability for certain constrained visual tasks, such as identifying a face among thousands of passport photos, as soon as they venture out "in the wild," as roboticists call the everyday human environment beyond the lab, machines flounder.

Two years ago, a powerful new computational technique, called deep learning, took the field of machine vision by storm. Inspired by how the brain processes visual information, a computer first learns the difference between everyday objects by creating a recipe of visual features for each. Those visual recipes are now incorporated into smart phone apps, stationary computers, and robots including PR2, giving them the capability to recognize what is in their environment. But roboticists worry that deep learning can't give machines the other visual abilities needed to make sense of the world—they need to understand the 3D nature of the objects, and learn new ones quickly on the fly—and researchers are already looking beyond deep learning for the next big advance.

PHOENIX CO-FOUNDED A STARTUP here called Vicarious, one of the myriad trying to capture human sight in code. Their optimism is surging. Over the past 2 years, deep learning has propelled machine vision by leaps and bounds. Where computers once struggled to detect the presence of something like a dog in a photo, with the help of deep learning they can now not only recognize a dog but even discern its breed.

"The theoretical side of deep learning was actually worked out decades ago," says Yann LeCun, a machine vision researcher at New York University in New York City who was one of its pioneers. He traces back its inspiration to the research of David Hubel and Torsten Wiesel, who shared a Nobel Prize in 1981 for research on biological vision. Working mostly with anesthetized cats in the 1960s and 1970s, Hubel and Wiesel discovered a hierarchical system of neurons in the brain that creates representations of images, starting with simple elements like edges and building up to complex features such as individual human faces. Computer scientists set about trying to capture the essence of this biological system. After all, LeCun says, "the brain was the only fully functioning vision system known."

The deep learning architecture that emerged is called a deep convolutional neural network. Information flows between virtual neurons in a network. And like the real neurons in the brain's visual system, they are arranged in hierarchical layers that detect ever more complex features based on information from the previous layer. For example, the network would first break down a photo of a dog into edges between dark and light areas and then pass that information to the next layer for processing. By the time the last layer is reached, the system can apply a mathematical function to answer the question: Is this a dog or not a dog?

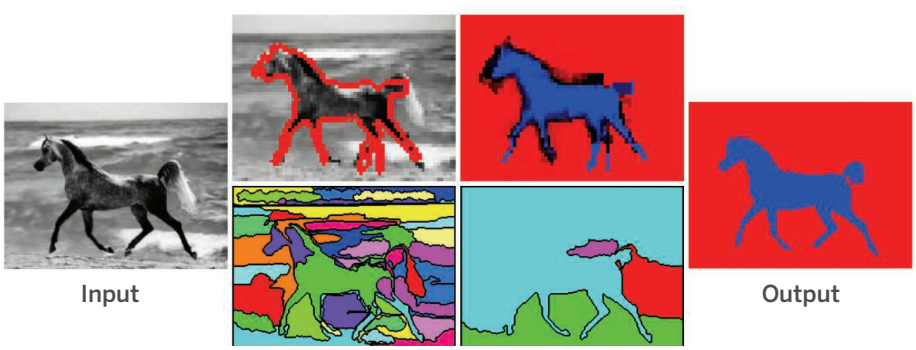
The problem was getting the dog-detecting function. "We just did not have the computers that we needed," LeCun says, nor the data. A network needed to process millions of labeled images of a dog to learn what a generic dog looks like, and in the 1980s even supercomputers did not have the speed or memory to handle this training. So researchers turned away from deep learning. Machine vision improved only incrementally—until 2012.

That year, a team led by computer scientist Geoffrey Hinton of the University of Toronto in Canada entered the ImageNet Challenge, an annual event in which competing computer programs must identify which objects —people, animals, vehicles—are present in thousands of photographs. Hinton's team used a deep convolutional neural network, trained on massive sets of labeled images. Unlike the computers of the 1980s, today's cheap computers have more than enough speed and memory for the calculations. Their system blew the competition out of the water.

"That changed everything," LeCun says. "The accuracy was so good that everyone in machine vision dropped what they were doing and switched to deep learning." Since then, billions of dollars have flooded into deep learning research. Hinton now develops deep learning applications at Google,

Looking beyond deep learning

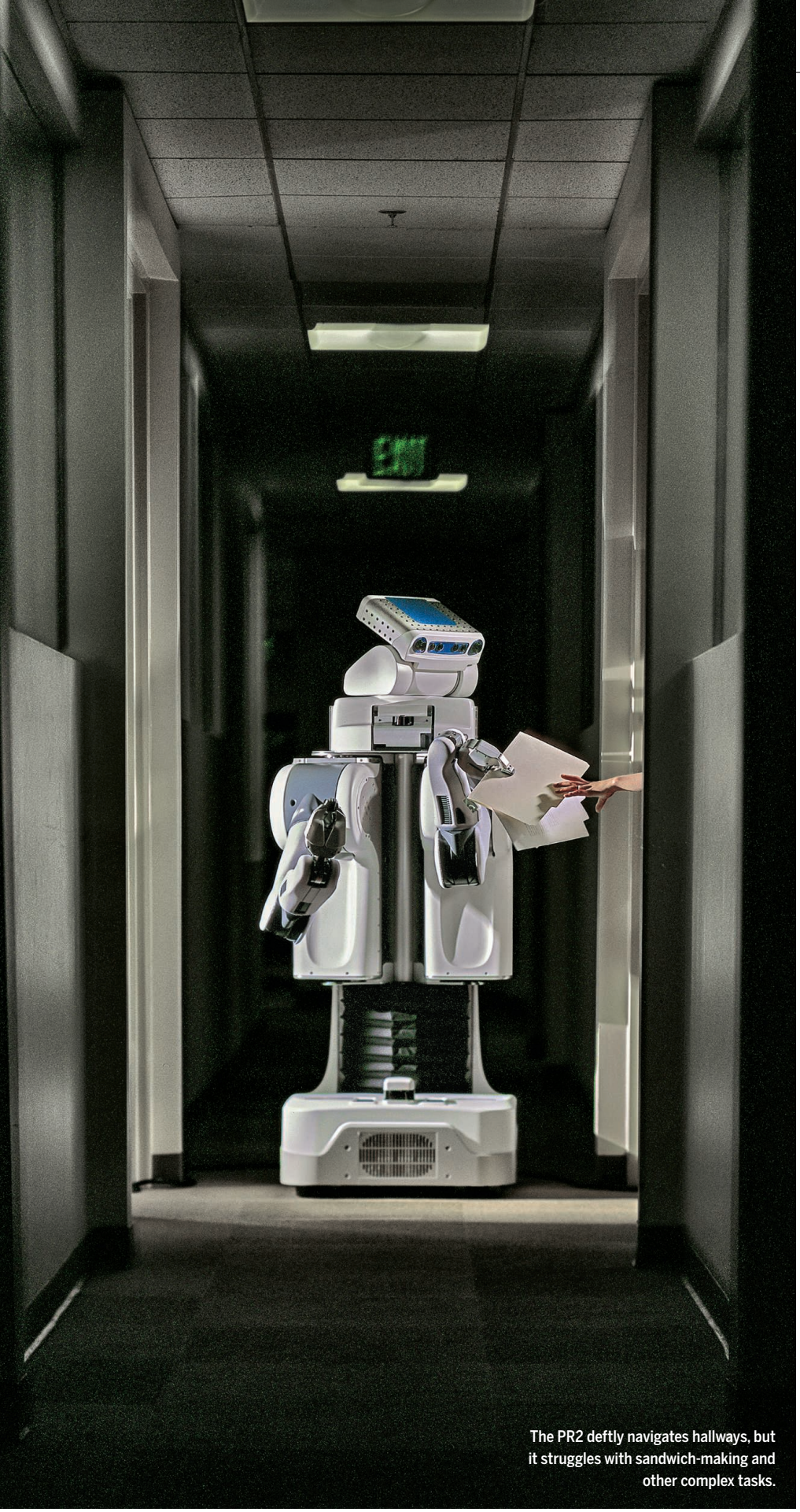
A technique developed in the lab of Shimon Ullman uses a feedback system inspired by the brain's visual system to identify a horse in an image and locate it—missing only part of the tail.



IMAGES: (LEFT) SHIMON ULLMAN; (RIGHT) MAX AGUILERA-HELLWEG

Downloaded from www.sciencemag.org on October 9, 2014

Published by AAAS



The PR2 deftly navigates hallways, but it struggles with sandwich-making and other complex tasks.

which is hoping to use the technique to create cars that can drive themselves. And at Facebook, where LeCun now heads the company's artificial intelligence efforts, a project called DeepFace aims to automatically identify any face in any photograph. (Whether the face's owner consents to being identified is another question.)

But amid the deep learning gold rush, some researchers are skeptical about the technique's prospects. Take PR2's epic struggle to make a sandwich. Deep learning enables the robot to recognize the objects around it—bread, salami, toaster—but it also needs to know exactly where those objects are in relation to its moving hand. Predicting where the bread will go when it drops requires physics. And what if the toaster is unplugged? The robot wouldn't have a clue why the bread wasn't toasting. "We have a long way to go before machines can see as well as humans," says Tomaso Poggio, who studies both machine and biological vision at the Massachusetts Institute of Technology in Cambridge.

The U.S. National Science Foundation (NSF) agrees. Poggio now heads an NSF-funded initiative called the Center for Brains, Minds and Machines. Most of the center's research is focused on understanding how human vision works and emulating it with computers. For example, Poggio says, "I can show a child a couple of examples of something and he will identify it again easily without having to train on millions of images." He calls this trick object invariance—a representation of an object that allows humans to identify it in any setting, from any angle, in any lighting—and his research focuses on capturing it as a computer algorithm.

Tech companies aren't waiting on the sidelines. Some are exploring new biologically inspired computer hardware (see p. 182). Phoenix and his colleagues at Vicarious are focusing on a software solution to visual intelligence. Last year, they announced that their algorithms had surpassed deep learning by cracking CAPTCHA, the visual puzzles made up of distorted letters that are used on websites to confound Web-crawling software. Vicarious has kept the details under tight wraps, but according to the company's co-founder, Dileep George, it is not based on deep learning at all. "We are working from how the human brain processes visual information."

When asked for something more tangible, George, like all entrepreneurs working furiously in secret, demurs. "It will be a few years before we pull it together," he says. And what is the goal? "A robot with the visual abilities of a 3-year-old." That would give robots the ability to do far more than make a sandwich. ■

Published by AAAS



In our own image

Will humans be more comfortable living with robots that look less like machines and more like pets—or ourselves?

By **Dennis Normile**, *in Nara and Osaka, Japan*

The creators of Robovie, a boxy robot the size of a child, had a pretty good idea what would happen when they rolled it out as a conversation partner for the elderly at a Nara day care center in 2009. They expected the humanoid robot with its buglike eyes and mechanical voice would lift the seniors' spirits with cheery greetings, a sympathetic ear for their health woes, and encouraging words while they exercised. But a surprise came after the 14-week experiment ended: The seniors missed Robovie so much that they wanted to visit it in the lab.

The seniors knew they were participating in an experiment, but they assumed Robovie is autonomous. In fact, a 29-year-old researcher was at work in a control room, steering the wheeled robot through the hallways, triggering its hand waves, and feeding Robovie its lines. The researchers, based at the Advanced Telecommunications Research Institute International (ATR) in Nara, were not engaging in deception for fun. Rather, says Hiroshi Ishiguro, an engineer who heads both the ATR team and a second robotics group at Osaka University, they were studying how humans will interact with the sophisticated robots of the future.

For 2 decades, Ishiguro's teams have deployed various robots—some with vaguely human forms, others crafted to look indistinguishable from people—as customers in cafes, clerks in stores, guides in malls and museums, teachers in schools, and partners in recreational activities. The roboticists, who use both autonomous robots and ones under human remote control, have come to some startling conclusions. In some situations, people prefer to speak with an android instead of another person, and they feel that robots should be held accountable for mistakes and treated fairly. And as the seniors here showed, humans can quickly form deep emotional bonds with robots.

Ishiguro's approach is "pretty brilliant," says Kate Darling, who studies robot ethics at the Massachusetts Institute of Technology's (MIT's) Media Lab in Cambridge. Some find the implications of the work worrisome, however. If interactions with robots can substitute for interactions with other humans, says Peter Kahn, a psychologist who studies the relations between humans and technology at the University of Washington, Seattle, "we'll dumb ourselves down socially even as our technologies advance." But Ishiguro and others believe robots are more likely to expand rather than narrow our horizons.

The debate is no longer academic. Simpler robots are creeping into daily life, serving as pets, vacuuming houses, and comforting dementia patients. A new wave of more sophisticated social robots is about to hit the mass market. In the coming days, for example, semiconductor giant Intel is expected to start selling a $1600 bipedal robot kit called Jimmy, for which hobbyists can design a body and fabricate it on a 3D printer. Intel claims Jimmy will be able to fetch a beer from a fridge and play games with a kid.

In February, a child-sized rolling bot called Pepper will go on the market in Japan. Able to recite stories to children and banter with adults, Pepper has microphones to track the direction of voices, an infrared sensor to measure distances, two cameras to recognize faces, touch sensors scattered over its body, nimble five-fingered hands, and Internet connectivity. And the $2000 price tag means "this is a robot for you," said Masayoshi Son, CEO of technology conglomerate SoftBank in Tokyo, which developed Pepper, at its unveiling in June. He claimed that Pepper "marks a turning point for humankind."

LIKE THEIR MAKER, the Geminoid HI robots dress in black, wear tinted glasses, and are perpetually scowling. The androids bear an uncanny resemblance to Ishiguro, who has won renown among roboticists for his Geminoids. But the robot falls short of fully capturing Ishiguro's stern demeanor, as an experiment in Linz, Austria, showed. On different days, either Ishiguro or Geminoid HI-1 sat at a table in a cafe. Random passersby rated the android friendlier than they did the real Ishiguro.

The latest Geminoids have 50 motors

PHOTO: HARUYOSHI YAMAGUCHI/CORBIS

Downloaded from www.sciencemag.org on October 9, 2014

Published by AAAS

Hiroshi Ishiguro's strikingly humanlike Geminoids speak during a press preview at the Miraikan museum in Tokyo in June.

controlling facial expressions; head motions; and even subconscious movements like breathing, blinking, and shifting position. As they cannot walk, they are typically seated. And, as I learned when coming face to face with a female android, Geminoid F, in Ishiguro's Osaka lab, they can, for a brief unsettling moment, be taken for human—before their slightly unnatural movements and off-the-mark eye contact erase any doubts.

It's out in the field, however, where Geminoids truly are conversation starters. In one experiment conducted over 2 weeks last fall, Ishiguro's group installed Geminoid F as a sales clerk in an Osaka department store. Operating autonomously, the android answered customer questions and made suggestions regarding a selection of $100 cashmere sweaters. Geminoid F handled 45 customers a day, versus 20 on average for the human sales clerks, in part because the android never took breaks and was a novelty. Some customers also sought out the android—apparently to avoid a human clerk's subtle pressure to make a purchase. "With the android it was easy to reject the [sales] offer," Ishiguro says. (As a result, Geminoid F's sales success did not match that of the store's best human salespeople.) In an upcoming trial, the Geminoid F will offer to help male customers choose gifts for wives and girlfriends.

Longer encounters can forge emotional bonds between human and machine. In the experiment at the elderly care center, some participants said it was more pleasant to converse with Robovie than with relatives. One remarked that the robot never talked back—unlike her grandchildren. For others, Robovie was a welcome substitute for grandchildren they rarely saw. "Even when I felt sad, I could feel brighter by talking with Robovie," one senior told the researchers. When the trial ended, the seniors held a farewell party for Robovie, giving it a card with handwritten notes of thanks and best wishes for the future. A month later, they visited the robot in the ATR labs.

Ishiguro's team has noted a similar phenomenon in dementia patients. Many people with brain impairments find it difficult to talk with other people, Ishiguro says, perhaps out of fear of what the healthy conversation partner may be thinking. "But they love to talk to robots," he says, after observing dementia patients interact with a humanoid robot that his team developed called Telenoid, which has a minimalistic human form and is held on a lap like a small child.

That's also the premise of PARO, a robotic baby harp seal intended to comfort dementia patients. Developed by Takanori Shibata of Japan's National Institute of Advanced Industrial Science and Technology in Tsukuba, PARO chirps when stroked and looks in the direction of a voice. Many reports from around the world indicate that interacting with it improves dementia patients' mood and social interactions and reduces agitated behavior.

Such emotional ties with robots disturb some researchers. PARO and similar robots "push our Darwinian buttons, by making eye contact, for example, which causes people to respond *as if* they were in a relationship," wrote Sherry Turkle, a sociologist at MIT, in a 2007 paper. Turkle, who studied PARO's use in a Boston-area nursing home, wondered whether it is ethical to encourage relationships based on such a "fundamentally deceitful interchange."



Dementia patients form emotional bonds with PARO, a robotic baby harp seal.

Still, widespread use of social robots as assistants is inevitable in many countries, including Japan, where more and more elderly will need care while the number of young people dwindles, says ATR roboticist Takayuki Kanda. Endowing these robot caregivers with social skills will improve acceptance and effectiveness, he says.

THE RISE OF SOCIAL ROBOTS raises other ethical issues, including whether the bots should be accorded rights and responsibilities deemed irrelevant for less interactive machines. In one experiment probing the ethical frontier, Kahn's team had a remotely operated Robovie interact one-on-one with children in three age groups: 9-, 12-, and 15-year-olds. To break the ice, the kids and the robot exchanged greetings and chatted as they examined the contents of a room. Then Robovie thought of an object in the room and gave clues for the child to guess what it was. When the roles were reversed and it was Robovie's turn to guess, a moderator suddenly interrupted and, over the robot's objections, ordered it into a closet.

As the team reported in *Developmental Psychology* in 2012, 89% of the children enjoyed spending time with Robovie, and a majority believed the robot is intelligent and has feelings. Most also said that the moderator acted unfairly in stopping the game when it was Robovie's turn, and 54% thought it improper to put the robot into a closet against its wishes.

In a second experiment, Kahn's group invited undergraduates to participate in a scavenger hunt, in which they searched a room for specified items while Robovie kept count. Identifying seven netted a participant $20. But Robovie, as programmed, invariably miscounted and denied the prize to those who found seven objects. As the team reported at a robotics conference in Boston in 2012, 65% of participants held the robot "morally accountable" for its miscount. Whereas participants also said they would hold a fellow human more at fault for the same infraction, very few said they would judge a vending machine morally responsible for short-changing someone.

According to Kahn, these experiments show that humans are already thinking of autonomous robots as being alive technologically—though not biologically—and according them moral rights and responsibilities they would never extend to nonhumanoid machines. Kahn thinks more work needs to be done to understand the implications of living and working with social robots.

Darling, of MIT's Media Lab, agrees. Fears about an impact on human relationships are "an argument that is made with every new technology that comes along," she says. As social robots become common, she says interactions with these new, artificial companions should become second nature—like using the telephone. ■

PHOTO: KAREN KASMAUSKI

Published by AAAS

HUMANS NEED NOT APPLY

It's hard enough these days landing a job as a flesh-and-blood human. Soon we may be competing with robots. In a 2013 report, the University of Oxford's Oxford Martin School estimated that 47% of U.S. jobs could be taken over by machines in the next decade or two. Here are a few careers where robots may have the inside track.

Design by Garvin G. Grullón; reporting by Hassan DuRant and Jia You



Rescuers

Tough, strong, and fearless, robots could make ideal first responders to a natural disaster. In December, 16 teams worldwide competed in a Defense Advanced Research Projects Agency Robotics Challenge trial that required the machines to complete eight tasks including driving into a disaster site, moving debris, breaking down walls, and turning valves. The 11 qualified teams will face off in a final round in June 2015.



Downloaded from www.sciencemag.org on October 9, 2014

Bellhops

Don't be surprised if a robot greets you at a hotel lobby. The Aloft hotel in Cupertino, California, is testing Botlr, a robotic bellhop that can shuttle razors, snacks, and morning papers from the lobby desk to guest rooms in 2 to 3 minutes. Cameras and other sensors enable the bot to recognize opened room doors, and users can enter reviews of the service on the robot's flat panel display. The bot even does a small dance before trundling off.



Reporters

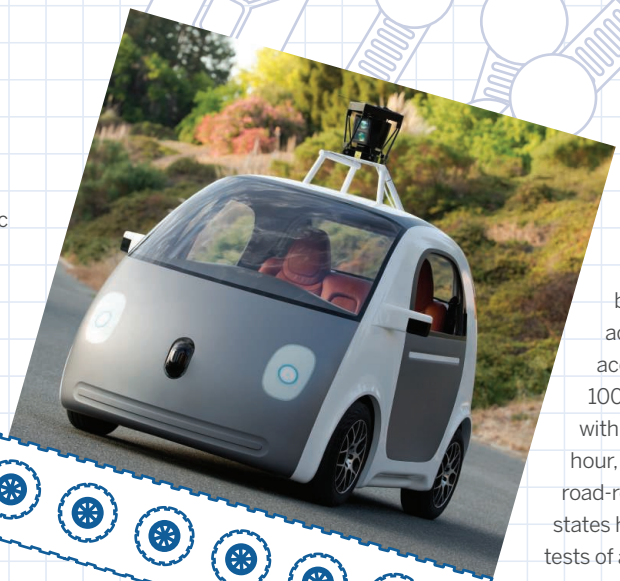
Untroubled by writer's block or caffeine cravings, robots are already writing data-based stories in some newsrooms. Algorithm, developed by Chicago, Illinois–based Narrative Science, now churns out corporate earnings reports for *Forbes*, and the *Los Angeles Times* employs similar technology to cover earthquakes. A study earlier this year found that readers could not reliably tell the difference between robot-generated and human-written sports articles.



Published by AAAS

Pharmacists

Researchers estimate that medication errors by health practitioners or pharmacists kill 7000 people in the United States alone each year. In 2011, the University of California, San Francisco, Medical Center introduced a robotic pharmacy that took over all manual tasks associated with filling prescriptions. Computers receive medication orders electronically, then command machines to assemble and dispense barcoded prescriptions.



Chauffeurs

Putting a robot instead of flesh and blood behind the wheel could save hundreds of thousands of lives a year by eliminating human error, which accounts for 95% of automobile accidents. Google is building at least 100 fully autonomous, two-seat test cars with a maximum speed of 40 kilometers per hour, which the company expects to be road-ready by early next year—and several states have already opened their roads to tests of autonomous cars.

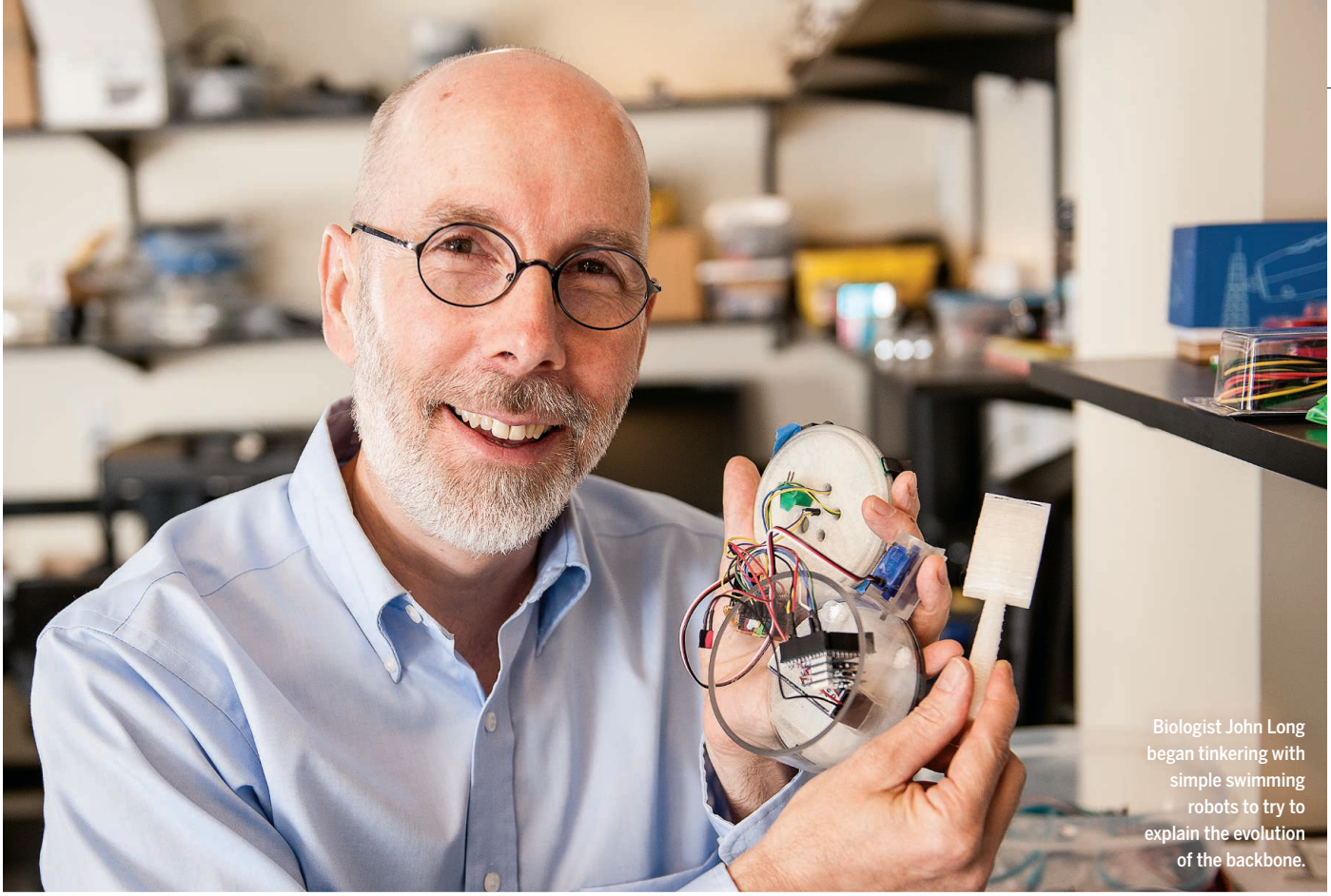


Scientists

Robots already carry out repetitive lab tasks like pipetting uncomplainingly, but they can make discoveries, too. At the University of Manchester, a lab bot named Adam used algorithms to formulate hypotheses and design experiments to identify genes involved in yeast metabolism, without any human input. At Cornell University, another team devised a robot that observed the swinging of interconnected pendulums and deduced their "laws of motion."



Published by AAAS



Biologist John Long began tinkering with simple swimming robots to try to explain the evolution of the backbone.

PHOTO: KARL RABE

The accidental roboticist

John Long wondered how life developed the capacity to evolve—so he unloosed a fleet of robot tadpoles

By **Adrian Cho**, *in Poughkeepsie, New York*

The Tadro is a primitive creation. The robotic tadpole's palm-sized cylindrical body contains a few wires and resistors and a reprogrammable chip. An electric motor wags the tail, a simple plastic cone tapering to a square fin. On either side of the robot's head perch two light sensors, with a third in the center. That's it. Yet when placed in its environment—for now, a kiddie pool in a darkened locker room here at Vassar College—the Tadro does something that most complex machines cannot: Unlike your car or computer, it guides itself and behaves like a living creature.

A flood lamp hangs a meter or so over the pool, supplying light that serves as Tadro's "food." Tipping slightly forward, the robot churns toward the lamp, its motor squeaking *weekee weekee weekee*, and then circles under it, feeding on the glow. As the Tadro wriggles toward the light again and again, it's hard *not* to think it's alive.

And like living things, Tadros evolve. With help from their makers, they change from generation to generation in response to a form of survival-of-the-fittest selection. They are the brainchildren of John Long, a Vassar biologist with a cheerful smile and a scholar's little round glasses who peppers his conversation with references to books and movies. ("Pay no attention to the man behind the curtain!") He has used Tadros to study the evolution of backbones, testing the idea that by making ancient fish stiffer, backbones made them faster and hence better at collecting food or evading predators.

Now, he and his team are gearing up for an even more ambitious effort. They plan to use Tadros to probe the font of all life's diversity: the ability to evolve, or evolvability. One key to that ability, he and his collaborators think, may be modular design, especially in the brain. In animals, distinct neural circuits control different functions, such as vocalization and vision. "The grand hypothesis is that modularity will enhance evolvability," Long says. "It's this capacity for future change that we're trying to get our hands around." If he is right, modularity itself should evolve within the Tadro's control circuits, under the right conditions.

That may be a lot to ask of toy tadpoles, but others say that experiments with robots can lay bare the nuts and bolts of evolution in ways that observations with living things cannot. "You're able to set up and test hypotheses that couldn't be tested otherwise," says Robert Pennock, a philosopher of science and evolutionary biologist at Michigan State University in East Lansing. A. E. "Gusz" Eiben, an evolutionary computer scientist at VU University Amsterdam, agrees. Long's work, he says, "deserves to be more widely known, especially among biologists."

IN THE YOUNG FIELD of evolutionary robotics, Long's research swims against the prevailing current. Most researchers use evolution as a tool to develop better robots. They construct otherwise identical robots with a variable trait—say, the length of a limb or some aspect of the robot's circuitry—which is specified in an abstract numerical "gene." They set the robots loose in some environment to determine, according to some previously decided criterion related to their behavior, which ones are fitter and get to pass their winning traits to more offspring.

There's no hot sex for the robots, however. Instead, mating occurs entirely within a computer using a "genetic algorithm" to determine the traits of the next generation of robots. To mimic biological reproduction, each numerical gene is divided by two, the

Published by AAAS

Downloaded from www.sciencemag.org on October 9, 2014

algorithm randomly "mutates" the results, and they're stored in virtual eggs and sperm. The program then pairs up the virtual gametes—with fitter robots providing a larger share—to concoct "genomes" for the next generation.

Often evolutionary roboticists don't build physical robots at all. Instead, computers simulate the robots and their behavior to determine which are fitter. Researchers quickly plow through thousands or millions of generations to optimize the design for a physical robot.

Long, however, likes to keep his evolving robots real, immersed in a physical environment. He grew up in Rochester, Michigan, but, as a descendent of New England whalers, felt the call of the sea at an early age. Hoping to become a marine biologist, he attended the tiny College of the Atlantic—enrollment 362—in Bar Harbor, Maine, where he worked for Sentiel "Butch" Rommel, a bioengineer who would take students out to slice up beached whales.

In graduate school at Duke University in Durham, North Carolina, Long studied fish, in particular the blue marlin, which can swim 80 kilometers per hour. He built a rig that would hold marlin backbones, begged from fish shops in Hawaii, and bend them back and forth. He expected that at higher bending frequencies, the backbones would become springier and absorb less energy. Instead he saw the opposite, suggesting the backbone works a bit like a shock absorber at high speeds.

Long was still pondering backbones when he arrived at Vassar in 1991. He wondered how the chainlike spine of vertebrates evolved from the sinewy notochord of invertebrates—an innovation that has happened at least three times in evolutionary history. Stiffer than a notochord, a backbone may have helped early fish swim faster and gather more food than their floppier peers, he hypothesized. Long had started to build mechanical models of fish, but his collaborator Kenneth Livingston, a cognitive scientist at Vassar, suggested developing them into autonomous robots.

To try to replicate backbone evolution, Long decided to mimic the tadpolelike larva of invertebrates of the genus *Botrylloides*, commonly called sea squirts. The larva resembles ancient invertebrate fish, such as the extinct eel-like *Haikouichthys*. Other researchers had traced the neural circuits that make sea squirt larvae spiral toward light, so the robots could be wired accurately and provide a reasonable model of the larva, which would stand in for the fish.

Thus the Tadro—short for tadpole robot—was hatched, in 2004. Its simplicity hit the sweet spot for research with undergraduates, who can't afford to spend years constructing a complex robot. Long's team built the first Tadros out of food containers, says Nicholas Livingston, chief engineer in Long's lab and Kenneth Livingston's son. "I remember feeling both clever and silly when I went to the local grocery store and bought a lot of Tupperware and plastic wrap," he says.

Thinking inside the box

Researchers hope to make their swimming robot evolve distinct control circuits (right) instead of one spaghettilike tangle (left).

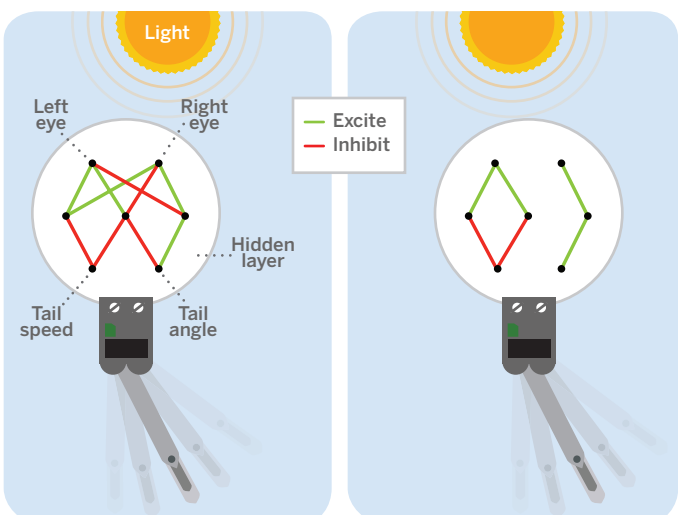


ILLUSTRATION: G. GRULLON/*SCIENCE*

COMPARED WITH COMPUTER MODELS or biological studies, robots have advantages for reprising evolution. Unlike a computer simulation, a real robot cannot leave out some subtle interaction with its environment or break the laws of physics. And robot experiments can be much faster than biological experiments, at least those with larger animals, says Jodi Schwarz, a bioinformaticist and collaborator at Vassar. "Even with mice, each generation is months," she says, "so it would take you forever."

Even so, studying evolution with robots can be tricky. In his first experiment, Long varied the length and stiffness of the Tadro's tail, molding new tails for each generation out of a tunable polymer. Researchers ran trials with three Tadros programmed to find and circle a light and assessed their fitness. Because the robots did not actually live or die—the gold standard for measuring fitness—the researchers had to find some other measure of fitness. They settled on a metric based on how fast and straight a Tadro swam, as assessed in a frame-by-frame video analysis.

But over 10 generations they observed no clear trend toward longer, stiffer tails. Instead, the tails' characteristics varied almost randomly. Why? Long and company had tripped on a pitfall of evolutionary robotics. They had defined their fitness metric to reward a Tadro for speed and penalize it for wobble. But in reality, faster Tadros wobbled more than slower ones—so, paradoxically, the fitness measure both rewarded and penalized a Tadro for being fast.

Even after correcting for that error and reanalyzing their data, they found that in some generations, selection favored bendy, slower Tadros. So Long's hypothesis was wrong: The race for food alone probably did not create a need for speed and account for the evolution of vertebrae, as he explains in his 2012 book, *Darwin's Devices: What Evolving Robots Can Teach Us About the History of Life and the Future of Technology*.

That negative result only spurred Long on. By 2007, he had revised his hypothesis. Perhaps vertebrae evolved not only to enable a fish to gather more food, but also to help it dash away from predators, he thought. To test that idea, Long and colleagues deployed a new version of Tadro, this time modeled after the extinct jawless fish *Drepanaspis gemuendenensis*, a vertebrate that also appeared to have had to fend off predators, as it had a hard shell. And this time researchers made two kinds of Tadros: predators and prey. The prey would still seek the light. However, they would also have infrared sensors that would trigger them to flee whenever a predator got too close.

The results of the new experiment were more in keeping with expectations. To keep the experiment manageable, tail length was fixed, but prey Tadros' tails could have different numbers of vertebralike rings. More vertebrae meant more stiffness, which presumably meant more speed. The researchers ran two trials of five and 11 generations each. And the Tadros did indeed evolve to have more vertebrae, from a starting average of 4.5 to an average of 5.5 or more—bolstering Long's hypothesis.

Published by AAAS

Both experiments were limited to a handful of generations and couldn't replicate the dramatic effects in the fossil record. Nevertheless, the results were clear, says Eiben, the computer scientist from VU University Amsterdam. "I'm amazed that they found such developments in just this few generations," he says. He credits Long's group with not just observing a trend, but also digging deeper and "asking themselves why."

NOW, LONG AND COLLABORATORS aim to study the evolution of the Tadro's "brain," hoping to induce the appearance of the distinct neural network circuits that they believe may aid further evolution. This time, the experiment also promises a practical payoff, says Josh Bongard, a computer scientist from the University of Vermont in Burlington who is collaborating with Long.

Bongard uses simulations to develop control circuitry for robots. But he has been frustrated to find that the process runs out of steam: The circuits become so interconnected that changing one connection requires rewiring the whole thing. Nature avoids that tangle by evolving modular circuits, and he hopes to learn how do to that, too. "The roadblock isn't that we don't have big enough computers," he says. "The roadblock is intellectual—we're not simulating evolution in the right way."

The new Tadro's neural network is rudimentary (see figure, p. 193). Inscribed on a reprogrammable chip, it has two "neurons" that take input from the eyelike light sensors on either side of the head. Two output neurons control, independently, the tail's angle and flapping rate. Inputs connect to outputs through a "hidden layer" of neurons. The map of that circuitry will be the heritable trait, and researchers hope Tadros will evolve distinct circuits for controlling tail speed and angle.

Learning from previous work, Long's team will simplify the experiment. Each Tadro will ply the water alone, and fitness will be determined by how much light it collects as measured by the light sensor in the middle of the head. The researchers may eventually allow some aspect of the Tadro's body, such as its tail, to evolve, too, as modularity may arise from the interplay of body function and the environment, Bongard says.

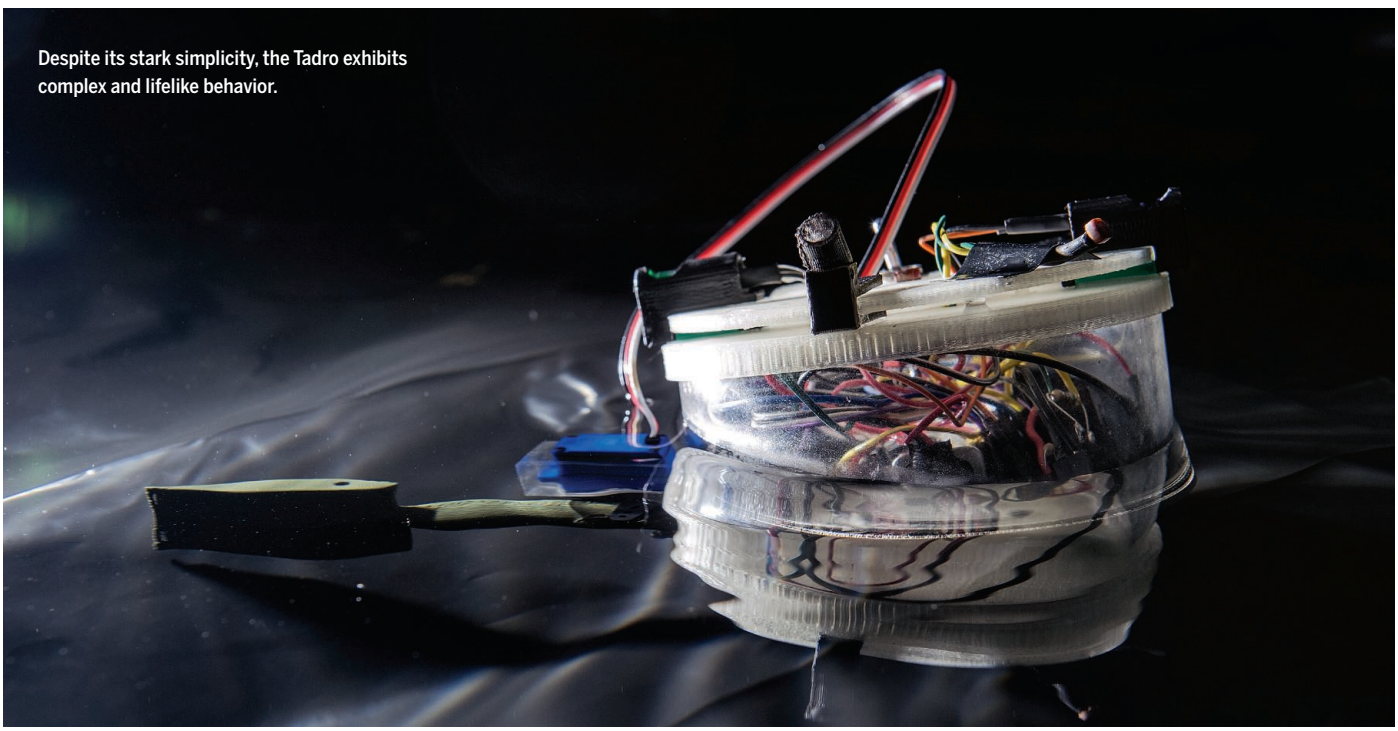
But first, the team must get the new Tadros running—a challenge for the four undergrads who will work for 2 years on the project. They had planned to make the Tadros entirely with a 3D printer over the summer. But the printed bodies leaked and sank, even after researchers tried to seal them with paint. "We had five different bodies painted with five different spray paints, and they all leaked," says Jessica Ng, a biology major at Vassar. "So we just gave up." The team is now using bodies machined from clear acrylic.

Long's students also face the daunting task of taking the data during the school year. Long, a passionate teacher who arrives at work at 7 a.m. and likes to squeeze in instruction whenever he can—he regularly reads aloud to his wife and two teenaged daughters at dinner—says he strives to help students succeed on their own terms. "My line to them is 'You're no good to us if you fail,'" he says. Instead of committing a number of hours per week to the project, the students will aim for monthly research milestones. If that's a recipe for periodic all-nighters, so be it, says John Loree, a physics major at Vassar: "Hey, it's college!"

It's tantalizing to imagine that Long's modest robots will evolve wildly. If they do, they might even provide insight into deep philosophical issues about the genome, says Kenneth Livingston, the cognitive scientist. "The genome is a set of instructions to do something, but it's not pure because it's about a particular world," he says. So, he says, the connection between the environment and the genome is "the beginning of meaning."

But it's also imaginable that things won't go so swimmingly. For example, the Tadros' evolution will depend in part on randomly tweaking connections within their neural networks. But most randomly wired networks may not work at all, leaving the Tadro dead in the water and evolution at a standstill—although simulations suggest that won't be a showstopper, Bongard says.

"We really have no idea what will happen," says Schwarz, the Vassar bioinformaticist. But that's part of the attraction of studying evolution with robots, says Pennock, the philosopher of science at Michigan State. "The thing that is underappreciated in this approach is that it's truly experimental," he says. "You're often surprised." ■



Despite its stark simplicity, the Tadro exhibits complex and lifelike behavior.

PHOTO: KARL RABE

Published by AAAS

Q&A: Robots and the law

As robots take on societal roles that were once the province of humans, they are creating new legal dilemmas

By **Dennis Normile**

Should driverless cars be allowed on the roads? Should robots capable of thought be accorded rights as sentient beings? Ryan Calo, a lawyer at the University of Washington School of Law in Seattle, tackles these and other questions in "Robots and the Lessons of Cyberlaw," a paper that will appear in the *California Law Review* next spring. In a report for the Brookings Institution last month, he called for the creation of a Federal Robotics Commission that would oversee the integration of robotics technologies into U.S. society. *Science* caught up with Calo recently on the murky questions surrounding robo rights and responsibilities. His remarks have been edited for brevity.

Q: The law tends to see a clear dichotomy between persons and objects. Do robots fall in between, and therefore are new laws needed?
A: Robots tend to undermine this clean distinction between a thing and a person. For example, you get compensated differently when someone else's negligence results in injury to property than to a person. When property is involved, you get market value. With people you have been deprived of that person's companionship. To the extent that people become heavily enmeshed socially with robots, the law will have to decide into what category to sort them.

Q: Should robots be given legal status as "beings"?
A: I don't think we'll have stand-alone rights for robots. Rather, the rights of owners may extend to robots in certain ways. Already lawmakers have struggled with cases where a software agent makes a deal on your behalf. Personally, I think we should hold people to contracts formed by their software unless something about the transaction makes it look objectively implausible.

Q: Robots already generate speech. Does the First Amendment protect this speech? And what if a robot makes defamatory statements?
A: If an artist creates an art bot that does surprising things, maybe we'll think about free speech as attaching to the creation of that art bot. There are news bots that wait for an event to happen and then report it without human intervention. What if it gets something wrong? Legal precedent requires not just that you intend defamation but that you have actual malice. You're not going to have defamation attach to news bots.

Q: Will we need laws to protect robots from abuse the way we protect animals from abuse?
A: I don't see laws actually protecting robots. But the link is so strong between animal abuse and child abuse that a number of jurisdictions have policies saying that if you respond to an animal abuse case and there are children in the same household, you immediately call child welfare services. You could imagine tweaking those policies to apply if you were to have reports that someone was kicking their robot dog.

Q: If a robot inadvertently injures someone following a command from its owner enabled by third-party software, who is liable?
A: In the early days of computers, people did sue when the computer froze and they lost something of value. The courts were very quick to say it's just data, so we are going to limit liability to the cost of the computer or software. Once you have platforms that are physical, if they harm someone, victims will sue not just the user, and not just the apps developer, but they'll sue the platform manufacturer. I think the solution will probably end up being statutory limitations on liability.

Q: Do companion robots raise new privacy issues?
A: Anything that collects, processes, and shares information is going to have an impact on privacy. No one really cares how you use your dishwasher. But how you ask your robot to interact with you has a great deal of sensitivity around it. Much privacy law is worded broadly enough to encompass these new problems.

Q: Personal robots may send information on interactions with users back to developers to improve functionality. Could this be abused?
A: What I worry about is the prospect of manipulating people in the interest of the company, for example getting someone really invested with a virtual girlfriend and then getting the user to buy things for her. We should think creatively about how to interrupt corporate incentives to exploit consumers.

Q: Could robots be programmed to alert police if they witness their owner commit a crime?
A: Absolutely! One thing to bear in mind is that anything a robot records could be subpoenaed. And then, what if a robot gets good enough that it can tell if you're doing something unlawful? It might have chemical sensors to help you cook. Could the government direct those sensors also to tell if someone is cooking meth? That's a question the Constitution doesn't obviously answer. ■

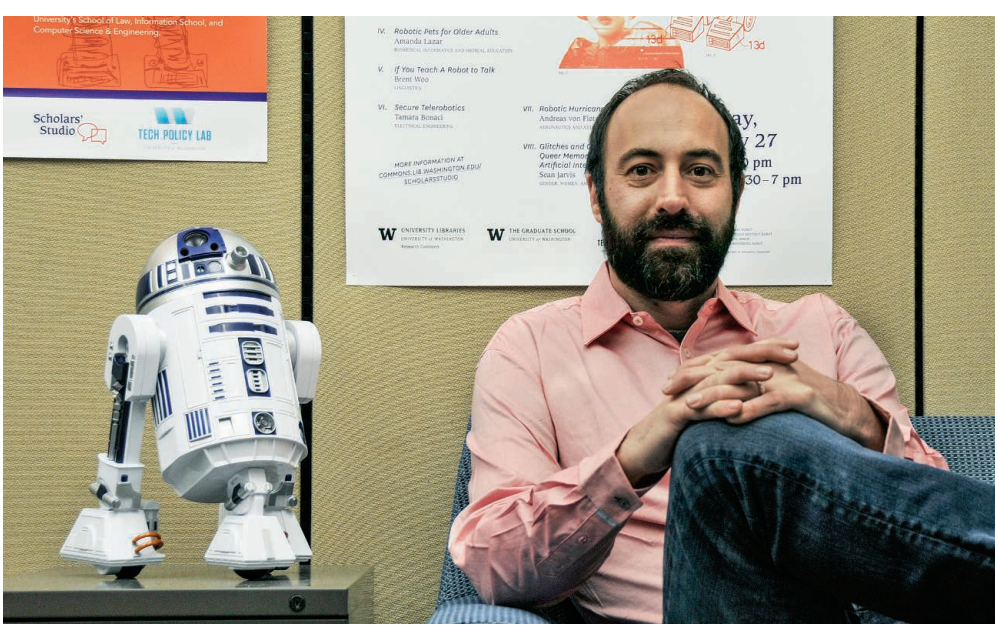


PHOTO: DEVON KELLEY

Downloaded from www.sciencemag.org on October 9, 2014

Published by AAAS

REVIEW

Biorobotics: Using robots to emulate and investigate agile locomotion

Auke J. Ijspeert

The graceful and agile movements of animals are difficult to analyze and emulate because locomotion is the result of a complex interplay of many components: the central and peripheral nervous systems, the musculoskeletal system, and the environment. The goals of biorobotics are to take inspiration from biological principles to design robots that match the agility of animals, and to use robots as scientific tools to investigate animal adaptive behavior. Used as physical models, biorobots contribute to hypothesis testing in fields such as hydrodynamics, biomechanics, neuroscience, and prosthetics. Their use may contribute to the design of prosthetic devices that more closely take human locomotion principles into account.

A cat running, climbing, jumping, and rapidly catching moving objects is fascinating to watch. Performing these agile motor behaviors requires complex interactions among the central nervous system, the peripheral nervous system, the musculoskeletal system, and the environment. Such good locomotion abilities are fundamental for animals and are also useful for robots. The field of biorobotics—the construction of biologically inspired or biomimetic robots—takes inspiration from biological principles to design robots with sensorimotor skills that approach those of animals. This has led to fish-like (*1*–*4*), snake-like (*5*–*7*), cat-like (*8*–*12*), and humanoid robots (*13*, *15*) (Fig. 1), with possible applications in search and rescue, environmental monitoring, agriculture, transport, and construction.

Biorobotics is increasingly contributing back to biology in fields such as biomechanics and neuroscience. Indeed, biorobots are becoming important scientific tools (*4*, *16*, *17*) and can be used to investigate locomotion and to test hypotheses about the underlying interactions of body, control, and environment. Robots have multiple properties to complement animal studies: Their actions are repeatable, they offer access to variables or quantities that would be difficult to measure on animals, they can perform movements that are unnatural or dangerous for animals, and their morphology can be systematically changed. Biorobots are providing useful contributions to biomechanics (*10*, *14*, *18*), neural control of movement (*9*, *19*), prosthetics (*20*, *21*), and environmental interaction mechanics; such as hydrodynamics (*1*, *3*), and the new field of terradynamics, the dynamics of sand and other granular media (*22*), that was established with the use of biorobots.

As a first approximation, animal locomotion is based on two key principles: (i) the generation of periodic movements using muscles (which is quite different from the rotational movement of electromagnetic motors), and (ii) the generation of asymmetries in the interaction forces with the environment, such that periodic movements of muscles are transformed into a forward acceleration (as opposed to back-and-forth movements in place). Depending on the ecological niche, nature has evolved a large variety of different morphologies and ways of generating these asymmetries: elongated bodies with traveling waves for swimming, scales in snakes that provide asymmetric friction for crawling, and limbs that alternate between (high-friction) stance and (low-friction) swing for walking (*23*, *24*).

Although the underlying principles appear simple at first glance, understanding animal locomotion is complex because it is a problem that (i) involves complex dynamic interaction among many elements (multiple neurons, muscle fibers, bones, tissues, and all elements in the environment), (ii) is therefore high-dimensional, (iii) is highly nonlinear (e.g., doubling the contraction of a single muscle at a given time will not lead to a doubling of the locomotion speed), and (iv) is multidisciplinary. The biomechanics of locomotion requires the investigation of all the internal forces in the high-dimensional musculoskeletal system and also all the complex interaction forces with the (unstructured) environment—with the further complication that the interaction will change the environment itself, such as when a motion displaces water or sand.

Understanding locomotion therefore requires a systems-level approach that explores the interaction of all involved components (*23*, *25*), in addition to studying components in isolation. Such an approach comes naturally in robotics, which is by essence the science of integration of many components (materials, actuators, sensors, and control loops). Biorobots can play a key role in animal locomotion studies by offering an "understanding by building" approach (*26*). Complementing other reviews in biorobotics (*12*, *15*–*17*, *25*, *27*–*29*), the focus here will be on locomotion, on vertebrate animals, and on the use of robots as scientific tools to explore the biology of locomotion.

Biorobotics Laboratory, Ecole Polytechnique Fédérale de Lausanne, CH-1015 Lausanne, Switzerland.
E-mail: auke.ijspeert@epfl.ch

Swimming

Swimming involves complex interactions between a deformable body (e.g., a fish undulating its body and/or flapping its fins) and water motion. The interaction forces generate complex water displacements and can lead to surprising behavior, such as a dead trout swimming upstream when placed downstream of a fixed cylinder (*30*), or Gray's paradox: Using an estimated drag coefficient of a rigid body, Gray concluded that the ratio between drag power and muscle power appeared too large by almost an order of magnitude for a dolphin to reach its observed swimming speed (*31*, *32*). It is now known that fish swimming strongly depends on the interaction of the body with vortices (i.e., spinning motion of water)—in particular, periodic patterns of vortices called Karman streets—and that fish "exert precise and effective control of the flow around their bodies to extract energy from waves, turbulence and even their own wakes" (*32*). Gray's paradox therefore appears to be due to an overestimation of the drag because of the rigid body assumption as well as an underestimation of the peak muscle power of dolphins (*31*, *32*).

Biorobotics can play an important role in exploring the underlying physical phenomena and in testing hypotheses about the mechanisms of fish swimming (*1*, *4*, *33*). It can also benefit from the impressive swimming skills of fishes in terms of agility [e.g., the ability to rapidly turn without losing much speed (*32*)] and energy efficiency [e.g., the ability of eels to swim thousands of kilometers with little or no food (*34*)]. Different types of robotic devices have been used in these studies: (i) robotic devices with actuated fins that are attached to a fixed or (externally) moving basis, typically in a flow tank (*32*); (ii) robotic devices that are self-propelled while being attached to a low-friction rail (Fig. 1A) (*1*, *35*); or (iii) freely moving fish-like robots (*2*–*4*, *36*–*40*).

A self-propelled robotic pectoral fin was used in studies of the interaction between deformable fins and water (*1*). Three different fin motions were compared while recording interaction forces with water at the base of the fin. One of the motions, "cup and sweep," closely resembled the motion of a sunfish and led to the highest thrust forces. The forces closely match predicted force patterns from a computational fluid dynamics simulation based on the actual movements of the sunfish pectoral fins (*41*) and were in agreement with particle image velocimetry analyses of water flow around the fish (*1*). The authors also designed a device made of two foils to investigate the interaction between dorsal and anal fins (first foil) and the caudal fin (second foil). It was shown that the interaction of two foils can be beneficial for thrust enhancement, with the first foil shedding a distinct vortex wake that markedly alters incoming flow to the second foil and causes increased leading-edge suction, in agreement with predictions from a computational study (*42*).

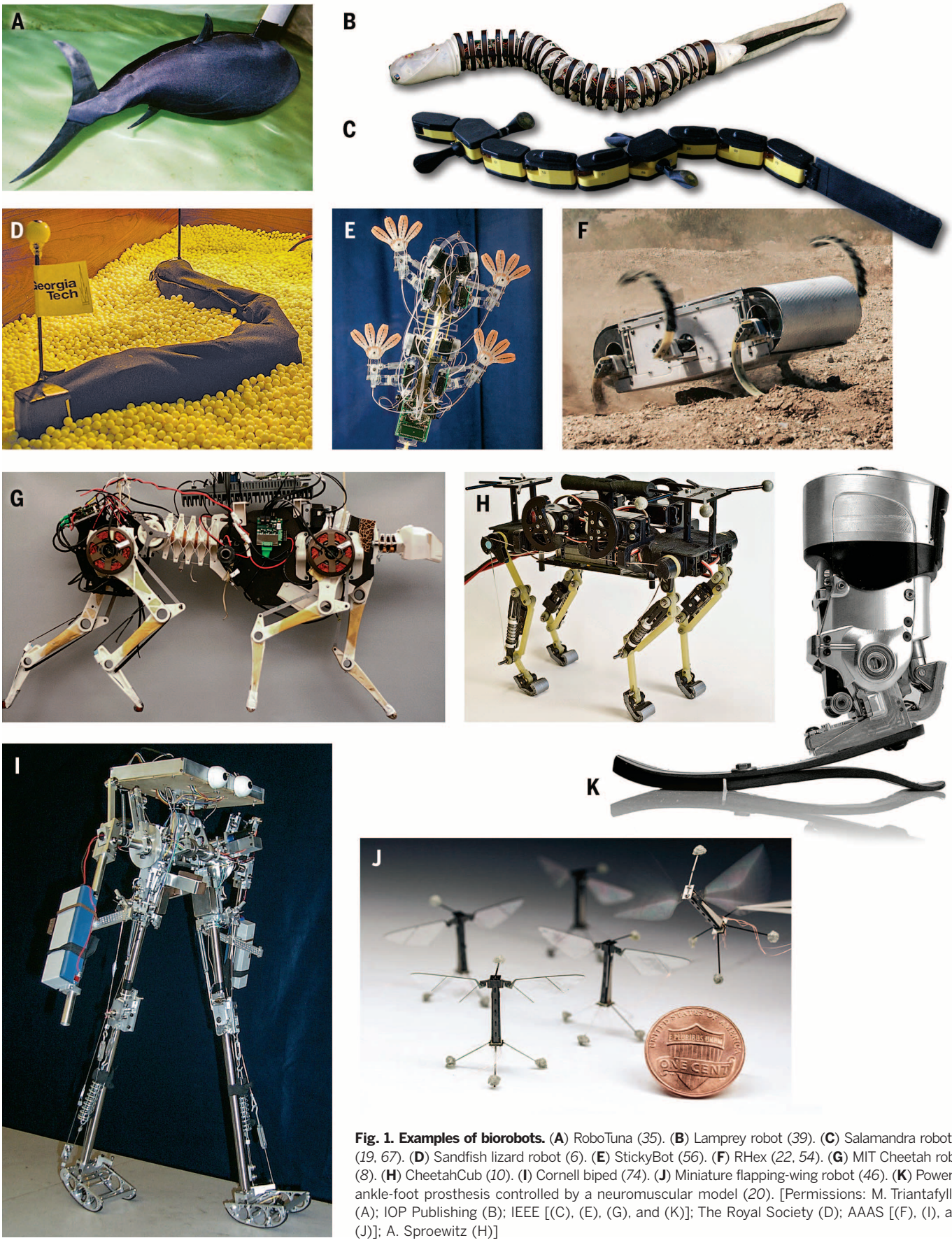


Fig. 1. Examples of biorobots. (**A**) RoboTuna (*35*). (**B**) Lamprey robot (*39*). (**C**) Salamandra robotica (*19*, *67*). (**D**) Sandfish lizard robot (*6*). (**E**) StickyBot (*56*). (**F**) RHex (*22*, *54*). (**G**) MIT Cheetah robot (*8*). (**H**) CheetahCub (*10*). (**I**) Cornell biped (*74*). (**J**) Miniature flapping-wing robot (*46*). (**K**) Powered ankle-foot prosthesis controlled by a neuromuscular model (*20*). [Permissions: M. Triantafyllou (A); IOP Publishing (B); IEEE [(C), (E), (G), and (K)]; The Royal Society (D); AAAS [(F), (I), and (J)]; A. Sproewitz (H)]

Some fishes, like the glass knifefish, perform fin movements that generate forces in other directions than necessary for forward locomotion, sometimes even against it, which looks like a waste of energy (*2*). The hypothesis is that these movements are performed to enhance the control of locomotion and to reduce the trade-off between stability (e.g., the ability to keep a steady speed and heading) and maneuverability (the ability to accelerate and turn) that animals and robots face. The glass knifefish uses a single elongated ventral fin to hover and rapidly change direction (Fig. 2A). The fin performs undulatory movements in opposite directions along different parts of the body, typically with two inward-traveling waves that meet at a nodal point (Fig. 2C). It was observed that the position of the nodal point was modified depending on the speed of swimming, moving toward the tail for higher forward speed. This was then tested using a mathematical model and a robot (Fig. 2B), and it was found that the resulting thrust force varied linearly with the shift of the nodal point. It was also found that the counteracting waves lead to a passive damping effect that helps rejecting perturbations of swimming velocities (that could be due to perturbations of the water around the robot) and can be adjusted by the frequency of the undulation. Together, these two mechanisms nicely enhance both the maneuverability (by shifting the nodal point) and stability (by adjusting the damping) of glass knifefish swimming, relative to a swimming mode that uses a single wave along the whole fin with changes of frequency for changing direction. The increase of maneuverability is especially striking for small-amplitude movements.

Flying

There is currently a boom in flying robots, in particular robots with rotating wings (such as quadropters) and fixed-wing robots (*43*). Self-propelled flapping-wing robots, also called ornithopters, are less common (*44*). They range from miniature robots (*45*–*47*) to the SmartBird by Festo (a flying robot inspired by the herring gull), toys (such as a flying pigeon-like robot by E-Bird and the Flytech Dragonfly by WowWee), and large-scale ornithopters capable of carrying a person (*48*).

Flapping-wing robots have been very useful as physical models to investigate insect and bird flying. Similarly to Gray's paradox for swimming, the wings of insects appear unable to generate sufficient lift when maintained statically in air flows at constant velocities (in the same range of velocities as those of flapping) (*49*), which suggests that the flapping and rotational movements of the wings, as well as the vortices shed by the wings, are important to generate the lift forces necessary for flight (*50*). Taking advantage of the similarities of fluid dynamics in air and in water, studies of the physics of insect flapping wings have used dynamically scaled robotic wings in mineral oil (with adjusted dimensions, frequencies, and oil viscosity to match the Reynolds number of the insect flight) (*50*). By equipping the actuated wings with force sensors, it was possible to investigate how lift can be generated by flapping wings, and it was found that insect flight could be explained by the interaction of three mechanisms: delayed stall (during stroke), rotational circulation, and wake capture during stroke reversal (*50*). The mechanisms of wake capture, in which a wing benefits from the vortices generated by the previous stroke, are similar to those found with fish robots (*42*). Furthermore, by simply modifying the timing of the rotational movements, the direction of forces can be adjusted and hence the direction of flying can be modulated, both for left-right yawing and up-down movements. These changes of timing resemble the changes of movements observed during steering behaviors in *Drosophila* (*50*). Similarly, it was found that yaw movements can be obtained with small adjustments of the stroke plane angle and the stroke amplitude (*51*) and that forward speed could be regulated by wing movements that alter pitch (*52*). Like the findings of the glassfish study described above, propulsion and steering are therefore closely merged and obtained by subtle modulations of propulsive movements; this is quite different from most fixed-wing and propeller-based aerial or underwater robots, where some motors are dedicated for propulsion and others for steering (e.g., using rudders).

Although flying based on flapping wings is currently outperformed by propeller-based flying for robots of the weight of birds or more, it is well suited for robots of the size and weight of insects. An impressive miniature 80-mg flapping-wing robot has been designed (*45*, *46*) (Fig. 1J). The authors note that "conventional technologies for macroscale aircraft propulsion and manufacturing are not viable for millimeter-scale robots because of inefficiencies that arise from force scaling, suggesting a biologically inspired solution based on flapping wings." The robot could exhibit stable hovering and simple flight maneuvers. The rotational motion of the wings was obtained by combining active flapping with passive pitch rotation thanks to passive compliant flexures. The resulting movements resemble those described above (*50*) and similarly generate sufficient lift forces for flight. For future work, the authors note that such robots could be used to study the mechanics and control of insect flying, and may enable the measurement of forces and torques during free flight that could be difficult to simulate in scaled models.

Crawling and terradynamics

Many animals locomote on granular media such as dry sand or gravel. Granular media are complex media that can exhibit both solid-like and fluid-like features (*22*, *53*). Some animals can even swim through sand; the sandfish lizard uses a large-amplitude traveling wave (*53*) not unlike the swimming of water snakes. The modeling of locomotion in granular media has led to the new field of terradynamics, in which robots play a big role (*6*, *22*). More generally, a range of snake robots have been constructed that, like their biological counterparts, perform motion through multiple contacts with the environment (*5*, *7*).

High-speed x-ray imaging revealed that the lizard swims in sand by means of body undulations, without the help of limbs. Making the hypothesis that the animal swims in a so-called "frictional fluid" in which grain-grain and grain-animal friction determine drag and thrust forces, the authors developed an empirical model of sand swimming that shares similarities with swimming in liquids with low Reynolds numbers (e.g., with negligible inertia effects), but with a mechanism for drag that is frictional (i.e., velocity-independent) instead of viscous (*53*). The model showed good agreement with the experiments and could predict the wave efficiency and optimal kinematics. A robot model of the lateral undulations of the lizard was later developed to further validate the model (Fig. 1D) (*6*). The robot was useful for systematic testing of different types of body undulations, in particular with different ratios between amplitude and wavelength. The robot proved to be good match with the empirical model. Interestingly, they both obtained maximal speeds when the ratio between amplitude and wavelength was 0.2, the same as that used by the sandfish.

The same group extended their terradynamics model to predict interaction forces induced by arbitrarily shaped legs and bodies moving freely in granular media (*22*). A RHex-like robot (*54*) with six rotary legs was tested with different types of leg shapes in different types of granular media (Fig. 1F). The authors obtained a remarkable match between experimental data and the model—for instance, in terms of the interaction forces of rotating legs of different shapes with the granular media, and in terms of locomotion speeds of the robot with different leg shapes and different stride frequencies. Such a terradynamics model can be useful to understand how lizards run in the sand (*55*) and to design leg shapes and control laws for robots that move in sand and gravel.

Climbing

Climbing has also been studied in robots (*56*–*60*), in particular the impressive climbing abilities of gecko lizards that exhibit directional dry adhesion under their feet (*61*). On the basis of an analysis of the feet and the small hairs that provide directional adhesive to the gecko, the toes of a lizard-like robot (Fig. 1E) were equipped with arrays of small-angled polymer hairs manufactured using shape deposition (*56*). Despite being at least two orders of magnitude larger than gecko hairs, this led to similar directional adhesion that was sufficient to carry the robot on vertical surfaces of glass or other smooth surfaces. Together with the compliance of the feet, the robotic toes adhere to a surface when pulled toward the ankle and are easily released when pulled in the other direction. Relative to non-directional adhesives, the foot required much less pulling force to detach from the surface. This explains the ease and rapidity with which geckos can climb on walls and ceilings (*61*). For proper climbing, the robot required movements and postures such that feet are always pulled toward

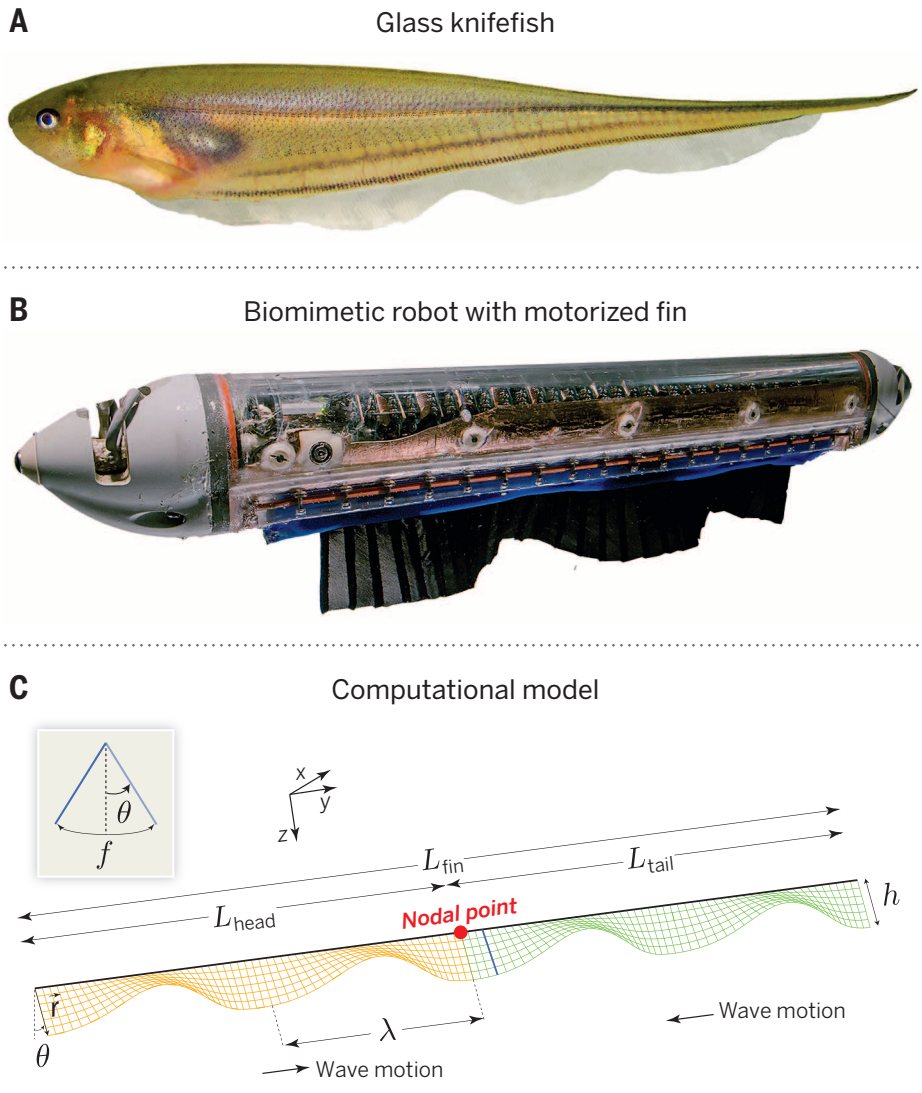


Fig. 2. A biomimetic robot that emulates the hovering performance of the glass knifefish. (*2*). (**A** and **B**) To mimic the kinematics of the glass knifefish (A), the motorized fin was programmed to produce two inward-traveling waves that meet at a nodal point (B). (**C**) Experiments with the fish and robot were explained by a computational model. By shifting the nodal point and altering the frequency of the undulation, both the direction of thrust and the damping of perturbations can be adjusted, offering a way to simultaneously adjust maneuverability and stability, respectively. [Reproduced with permission: N. Cowan]

each other—something that has been observed in geckos that reorient their feet as they climb in different directions.

Quadruped walking and running

A range of quadruped (*8*–*12*, *62*) and multilegged robots (*54*, *63*) have been constructed to date, including robots developed by companies for which no scientific reports exist [e.g., BigDog and WildCat by Boston Dynamics; see (*12*, *15*) for reviews]. Many of these were designed to emulate the walking and running skills of tetrapods, such as climbing over complex uneven terrain and crossing terrain with limited footholds (e.g., stones in a river); they benefit from the advantages offered by discrete contacts with the ground, versus continuous contact through wheels or tracks.

One drawback of many legged robots is their low energy efficiency, as illustrated, for instance, by their large costs of transport (CoT, the ratio of power consumption to the product of weight and speed), a dimensionless measure of energy efficiency for locomotion (*8*). Several principles for reducing these energy costs were proposed by Kim and colleagues (*8*, *18*): the "employment of high torque density motors, low impedance transmission, energy regenerative electronics and a design architecture that minimizes the leg inertia." The last principle has led the authors to design a lightweight leg that followed the hypothesis that vertebrate legs are organized such that bones carry only compressive loads while the muscles, tendons, and ligaments carry tensile loads in order to reduce bending torques (*64*). The robotic legs were constructed using Kevlar cables for tendons and lightweight bone-like structures made of foam-core composite fabrication (Fig. 1G). By using the principle of tendon-bone colocation, stress on the bone during a stride could be reduced by up to 59% relative to a leg configuration without a tendon (*18*). Combined with actuators that have low gear ratios (and therefore low friction) and electronics that allow recapture of energy when the motor brakes, the robot is capable of fast locomotion (2.51 m/s) at a CoT of 0.51; according to the authors, this is significantly lower than that of BigDog (estimated CoT of 15) and is comparable to running animals at the same scale.

In related work, it was shown that replicating the pantograph-like structure of a mammal limb and approximating its viscoelastic properties (Fig. 1H) can lead to surprisingly robust and dynamic gaits purely with open-loop control (*10*). Relatively big perturbations, such as walking down a step, did not require sensory feedback nor complex closed-loop control, but were in fact dampened out by the mechanical properties of the robot. Similar mechanical self-stabilization mechanisms have been identified in running cockroaches (*65*).

Quadruped robots have also been used for testing hypotheses related to the neural control of motion, for instance in the cat (*9*) and the salamander (*19*). The salamander uses an anguilliform swimming gait in water and a walking-trot gait on the ground. The locomotor patterns are generated by neural circuits in the spinal cord called central pattern generators. Gait transitions between the two modes of locomotion can be induced in a decerebrated animal by electrical stimulation of a region in the brainstem, with walking-like patterns at low stimulation and swimming-like patterns at high stimulation (*66*). This illustrates that spinal cord circuits not only can produce well-coordinated movements but can even generate gait transitions under simple descending control signals. A salamander-like robot (Fig. 1C and Fig. 3A) was used to test the hypothesis that the salamander central pattern generator is based on an ancestral lamprey-like swimming neural circuit for its axial musculature, extended during evolution by specialized and slower neural oscillators for the limbs (*19*). The model and the robot could replicate the gait transition induced by electrical stimulation. It also provided an explanation of why walking gaits (Fig. 3B) are systematically performed at lower frequencies than swimming gaits (Fig. 3C) in the animal. Finally, the robot demonstrated that the particular body-limb coordination used by salamanders on the ground is the one among several options that optimizes its locomotion speed (*67*).

The mechanisms of interlimb coordination, and in particular the respective role of neural coupling versus mechanical coupling, have also been investigated using a quadruped robot (*68*). It was shown that stable gaits could be generated without direct coupling between limb oscillators and with only indirect coupling through

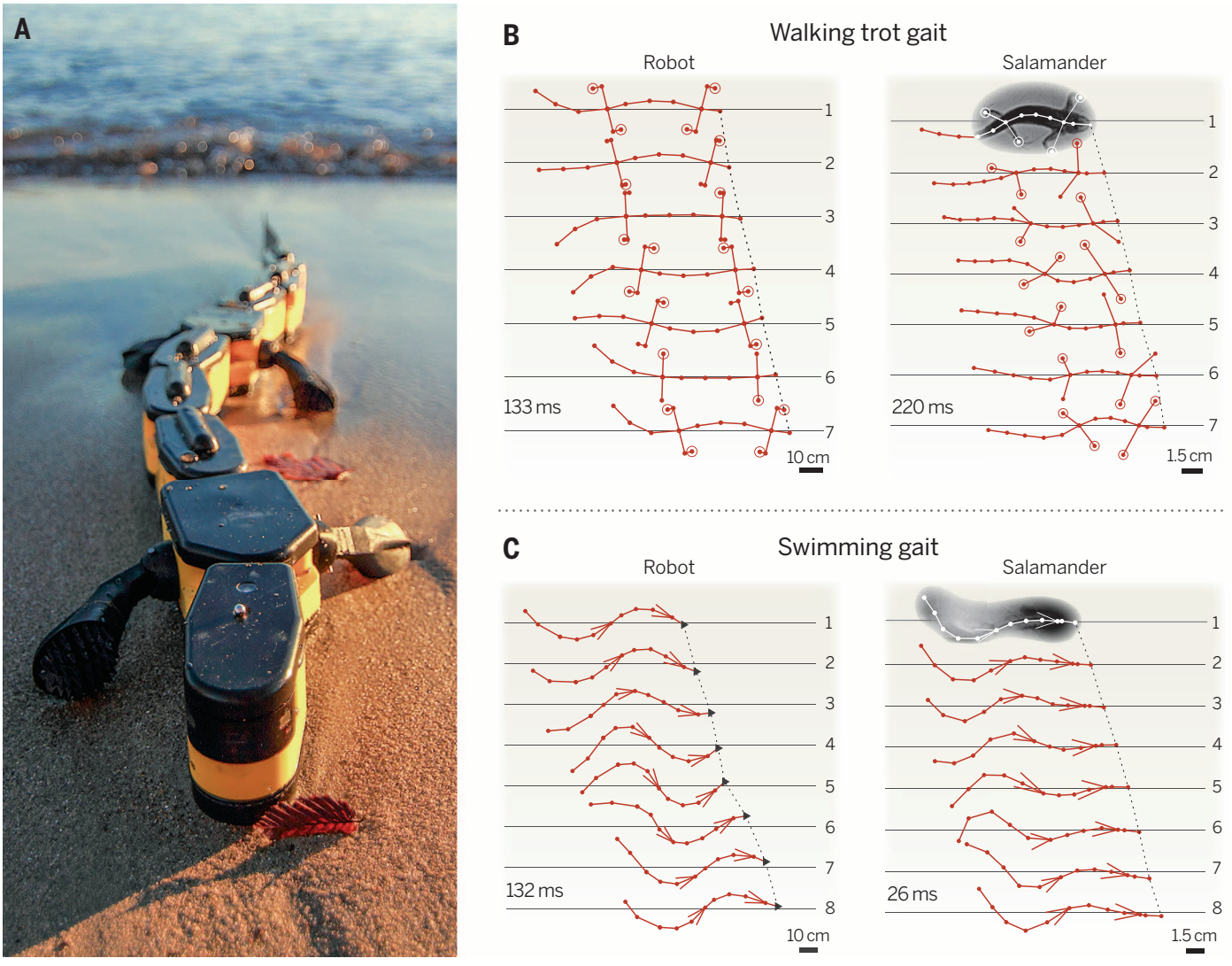


Fig. 3. Salamandra robotica, a salamander robot that can swim and walk. This robot was designed to test hypotheses about the organization of salamander spinal circuits and the mechanisms of gait transition (*19*, *67*). (**A**) The waterproof robot is equipped with eight motors for spine undulations, and four motors, one per leg, for leg rotation. (**B**) Comparison of the walking trot gait of the robot (left) and the salamander, as recorded with x-ray videos (right). (**C**) Comparison of the swimming gait of the robot (left) and the salamander (right) (*67*).

sensory feedback and mechanical coupling, similar to what has been observed in the stick insect (*69*). The robot was a useful tool to demonstrate that different gaits could be obtained depending on the mass distribution in the robot. When the mass was placed more in the front, as in camels, or more to the rear, as in monkeys, the same gaits emerged as in their biological counterparts.

Biped locomotion

Two broad classes of biped and humanoid robots can be distinguished: (i) robots that are designed to be versatile, and (ii) passive-dynamic robots that are designed to be energy-efficient. Versatile robots use multiple high-torque actuators and sophisticated control algorithms to carefully control all joints at any given time. This has led to impressive machines such as Asimo (Honda), Qrio (SONY), Atlas (Boston Dynamics), Shaft's biped, and HRP (AIST and Kawada Industries) [see (*15*) for a review]. However, from a biomechanical point of view, these robots are far from human-like because they require actuation to perform any motion, as opposed to human walking that relies extensively on natural dynamics of the musculoskeletal system (such as pendulum-like swinging movements of the limb). Such robots are therefore highly inefficient from an energy point of view.

Passive-dynamic walking robots are more human-like in terms of biomechanical aspects and energetics, and are interesting tools for exploring the biomechanics of human locomotion (*13*, *14*, *70*). This type of locomotion is called passive because it relies on passive dynamical properties of the body such as free-swinging motions (as opposed to motions that are actuated at all times), and dynamic because it is dynamically stable (i.e., a notion of stability over time) as opposed to statically stable (i.e., with the center of gravity remaining at any time over the support polygons shaped by the contact points of the feet on the ground). Note that most versatile robots also perform dynamic locomotion.

Inspired by ramp-walking toys and abstracting walking as a wheel without a rim, McGeer (*14*), using nonlinear stability analysis and by building prototypes, demonstrated how a passive-dynamic walking machine could be constructed to get down a ramp without actuation and control. With a well-tuned body morphology made of two straight legs with round feet, swinging motions of the limbs and stable walking could be obtained thanks to gravity and inertia alone, without the need for careful control of limb motions. This led to a paradigm shift in biped locomotion, going away from trajectory-based control toward locomotion that is tightly based on passive properties of the body, much like humans are believed to do (*71*–*73*).

For instance, a more human-like 3D passive-dynamic walker with knees and counterswinging

arms produced strikingly human-like features (*13*). Subsequent developments included the addition of actuation to remove the necessity of a ramp, and of learning algorithms to learn suitable control policies online (i.e., while walking) (*74*). This has led to three robots (the Cornell, Delft, and MIT bipeds) that "use less control and less energy than other powered robots, yet walk more naturally, further suggesting the importance of passive dynamics in human locomotion" (*74*). The Cornell biped (Fig. 1I) was designed to minimize energy loss that happens in human and robot walking when the foot hits the ground and when actuators actively brake movements and perform negative work. By completely avoiding negative work, the robot could walk with a low CoT of ~0.2, which is equivalent to human walking (CoT of 0.2) and is an order of magnitude lower than Honda's Asimo (estimated CoT of 3.2). Further, the locomotion of the robots required very little control effort relative to trajectory-based control. The Cornell and Delft bipeds used very simple control laws directly linking ground contact sensors to on/off motor commands sent once per step. The MIT biped used online reinforcement learning to optimize a control policy during locomotion. Because the intrinsic mechanical stability simplified the learning problem, the learning was sufficiently rapid that the robot could continuously adapt to the terrain during walking. This work showed that with the right mechanics, human locomotion is energy-efficient and possibly less difficult to control than originally thought. The passive-dynamic walking robot Ranger (1 m high, 9.9 kg) could walk 65 km over 31 hours on a single battery charge (~500 W·hours, CoT of 0.28)—an impressive feat (*75*).

The interaction between passive-dynamic walking and neuronal control with simulated synaptic plasticity has been further explored (*76*). It was shown that a robot maintained in the sagittal plane could walk with high speed and could learn to walk on different terrains with only a few learning iterations. The authors concluded that "the tight coupling of physical with neuronal control, guided by sensory feedback from the walking pattern itself, combined with synaptic learning may be a way forward to better understand and solve coordination problems in other complex motor tasks" (*76*).

The versatile and passive-dynamic approaches can to some extent be merged in robots that exploit torque control in addition to position control (*77*–*81*). Such robots typically use whole-body model-based control together with optimization algorithms. By taking into account natural dynamics in the dynamic model of the robot, and by adding energy criteria in the optimization, it is in principle possible to generate locomotion that is both versatile and energy-efficient. Torque-controlled robots also offer the opportunity to easily test biomechanical hypotheses without having to rebuild all the mechanics (*82*). They can emulate muscle models using active impedance, while the real physics is still taking care of the part that is difficult to simulate (i.e., the contacts and interactions with the environment).

Active exoskeletons and prostheses

Active exoskeletons (for limb support) and prostheses (for limb replacement) are fields in which robotics, biomechanics, and human motor control converge (*83*). In order to restore or augment human locomotion, a series of actuated exoskeletons have been designed, including BLEEX (*84*), HAL (*85*), Sarcos' exoskeleton, MIT Exoskeleton (86), MINDWALKER (87), and RoboKnee (*88*) [see (*83*, *89*) for reviews]. Several can be bought as commercial products, such as the ReWalk from ReWalk Robotics and Ekso from Ekso Bionics. Potential users are soldiers, workers, or persons with a locomotor handicap (for instance, due to a spinal cord lesion).

To reduce the size and weight of fully actuated exoskeletons, researchers have investigated the energetics of human locomotion. Closely linked to the passive-dynamics walking studies mentioned above, numerical models and optimization have shown that purely passive exoskeletons made of elastic tendons should in principle be capable of reducing the metabolic cost of locomotion for specific movements (*90*). Such ideas have led to the design of exoskeletons for helping to carry a load with little actuation—for instance, in an exoskeleton equipped with springs at the hip and ankle, and a variable damper at the knee (*86*).

Going even further, it is possible to harvest energy from human walking. One example is the use of a knee brace that collects energy at specific movements during the walking cycle, during late swing when knee muscles normally perform negative work to prevent hitting the joint-angle limit (*91*). Such a device can produce an average of 5 W of electricity with little extra effort by the wearer. Alternative methods include harvesting the energy lost in shoe soles at impacts with the ground (*92*) or in periodic movements of backpacks (*93*).

Similarly to exoskeletons, powered prostheses for ankles and knees have been developed and have become commercial products from companies such as Ottobock, Össur, and SpringActive. An interesting approach used a simulated neuromuscular model to drive a powered ankle-foot prosthesis (Fig. 1K) (*20*). The controller was based on a simulated Hill-type muscle with a positive-force feedback reflex, replicating the reflexive muscle response based on feedback signals from muscle spindles and Golgi tendon organs in human walking (*94*). Compared to other approaches that play a fixed torque pattern, the motivation is to adjust the torque produced by the prosthesis depending on the slope of the terrain and the size of steps. The system was tested with a transtibial amputee walking on level ground and up and down a ramp. It was found that the energy provided by the prosthesis was adapted to the type of terrain and was directly correlated to the ground slope angle. Also, the gait characteristics were close to those of intact locomotion in terms of the measured ankle torque and ankle angle profiles. In subsequent work, it was found that the approach could successfully be used for speed adaptation (*95*) and that it decreases metabolic cost by 8% and increases preferred walking speed by 23% relative to using a passive-elastic prosthesis (*21*).

Conclusion, future prospects, and implications

Biorobotics is an exciting research area with two main objectives: (i) taking inspiration from biological principles to design robots that match the agility of animals, and (ii) using robots as scientific tools to investigate animal adaptive behavior. Although the two objectives share many common aspects and methods, they also differ in some subtle but important points. First, the evaluation of success is different. A contribution to robotics (i.e., to the first objective) will be considered successful if it provides a method that is better (according to some performance metric, such as speed or energy efficiency of locomotion) or simpler to implement than alternative methods. The RHex robot (*54*) is a nice example of such a contribution. A contribution to biology (second objective) will be considered successful if it contributes to a scientific theory either by formulating new hypotheses, proposing new experimental methods, validating experiments against animal data, and/or providing new theories (e.g., mathematical formulation)—for instance, the studies of terradynamics of the sandfish lizard (*6*, *53*) and of the tradeoff between stability and maneuverability in the glassfish (*2*). It is important for a project to properly define which of the two (or sometimes both) objectives it is aiming at. Otherwise, there is the risk that a project does not contribute to robotics (because it does not outperform other methods) nor to biology (because it does not satisfy scientific standards of well-established hypotheses, methods, and experiments).

A second important point is the choice of the level of abstraction and which features of an animal should be replicated in the robot. Researchers are mostly aware that animal locomotion is not "optimal" in any sense, but just "good enough" from an evolutionary perspective, and that animals and evolution need to satisfy many constraints such as growth, reproduction, metabolism, etc., that are not relevant for robot locomotion. Therefore, it is important to only replicate the key relevant features. For instance, a multisegmented leg can be approximated with a rotary leg driven by a single rotational motor (*19*, *54*, *96*), and a simple wheeled robot with an active tail can be a useful tool to investigate active tail stabilization in lizards (*97*). To formalize the choice in the level of abstraction, Full and colleagues introduced the useful concepts of templates and anchors (*25*, *98*). A template is "the simplest model (least number of variables and parameters) that exhibits a targeted behavior" (*98*). For instance, the spring-loaded inverted pendulum model of running (*99*) is a template. An anchor is a more elaborate model that takes into account many more aspects of the musculoskeletal and the nervous systems (e.g., with

multisegmented legs, multiple muscles, and multilayered neural control loops). Depending on the type of scientific questions, the right level of abstraction between template and anchor should be carefully chosen [see (*16*, *25*) for in-depth discussions].

From robotics to biology

Biorobots can give something back to biology. Like numerical models that are now routinely used in any field of science, robots can become part of the scientific cycle of making hypotheses and predictions, testing them in experiments, and iteratively adjusting them toward a scientific theory (*16*).

Robots can be programmed to make repeatable, parameterized experiments (*1*). They can be equipped with multiple sensors to monitor relevant variables/quantities that would be difficult to measure on an animal [e.g., internal forces (*11*, *62*)]. Their morphology can be modified in systematic ways (*22*). They can perform movements that would be dangerous for animals. They can perform movements that animals typically not do (*1*, *67*), allowing one to explore whether animal movements are optimizing some criteria [see the salamander study that showed that the walking trot gait of salamander optimizes speed (*67*)]. Given today's computer and communication technologies, they can be controlled by numerical models (controllers) that replicate some parts of the central nervous system in great detail. With the right type of actuators and materials, they can properly approximate viscoelastic properties of the musculoskeletal system [e.g., with virtual muscles and torque-controlled motors (*82*), or with muscle-like actuation (*70*)]. In short, robots can be used to perform some experiments that would be difficult or even impossible to make with animals. In the long run, they could even reduce the need for some types of animal experimentation.

Webb extensively discussed the use of robots as physical models and proposed seven dimensions (relevance, level, generality, abstraction, structural accuracy, performance match, and medium) to characterize and compare models (*16*). As pointed out by Long, the classification is not perfect (e.g., the dimensions are rather qualitative and lack scales) but is very useful to challenge "researchers to explicitly justify their use of robots to make and test biological hypotheses" (*4*).

Why use robots and not simply numerical simulation?

Robots and numerical simulations are complementary, and in many cases numerical simulations precede robotic experiments (*6*, *19*). There is a long history of mathematical and numerical models of animal locomotion (*25*); biped locomotion has been modeled using simple abstract models (i.e., templates) like the spring-loaded inverted pendulum model (*99*), as well as by complex neuromechanical (anchor) models (*94*).

Robots are better than numerical simulations when real (as opposed to simulated) physics is important. This is often the case with locomotion that involves complex physical interactions with the environment: swimming in water (*1*–*3*), crawling on sand (*6*), and walking on mud or gravel. Mechanical simulations are now very good at computing the dynamics of articulated rigid bodies but are less good at correctly simulating compliant structures and interaction forces with a complex environment. Such problems are very complex for various reasons: They involve complex geometries, complex physics, deformations of whole structures, multiple materials, nonstationary phenomena with often abrupt changes, and induced changes in the environment (e.g., motion of water, sand, or gravel). For instance, consider a salamander robot that swims in water in contact with a rocky ground, then crosses mud and climbs over a grassy terrain. Properly formulating all the underlying equations of motion and boundary conditions is tremendously hard. Finally, as visible from the many impressive robots designed by hobbyists, constructing a robot allows for tinkering—itself a powerful iterative design process based on intuition that can lead to impressive constructions and that is quite different from creating a numerical model on a computer (*13*).

There are, however, a number of difficulties in using robots for investigating animal locomotion that should not be underestimated [as discussed in (*29*) and briefly reported here]. It is difficult to properly replicate the biomechanical properties of animal musculoskeletal system (e.g., the same number of degrees of freedom, the viscoelastic properties, and the mass distribution). There is therefore a tradeoff between the benefits of real physics and the risk of designing a robot that has significantly different dynamics from that of the modeled animal. This relates to choosing the right level of abstraction between anchors and templates (*25*, *98*). Also, some biological sensor modalities such as touch and proprioception are still difficult to properly replicate with current sensor technology. Finally, using robots is sometimes more cumbersome than using numerical simulation because robots are less adjustable, require a large overhead and expertise for construction and maintenance, and are less amenable to extensive experiments.

Future challenges and opportunities

There remain multiple challenges that roboticists and biologists can tackle together. Some of the main challenges include designing and controlling robots that are really field-ready, designing robots capable of multimodal locomotion, studying non–steady-state behavior, and quantifying and achieving agility.

Apart from a few exceptions [e.g., (*7*, *67*) and robots from BostonDynamics such as RHex (*54*) and BigDog], most biorobots are not yet field-ready; they are not sturdy enough to resist water, dust, mud, and falls, and cannot adapt their locomotion to complex environments. A lot of scientific and engineering work is still needed to make robots field-ready, not only in terms of mechanics and actuation [e.g., with muscle-like variable impedance actuators (*70*, *100*)], but also in terms of integrating multimodal sensing for perceiving unstructured terrain (e.g., identifying the right footholds for walking and climbing), adding better proprio- and tactile information (e.g., to identify when stuck), and improving control. An interesting approach toward sturdiness and more animal-like mechanical properties comes from the rising field of soft robotics [see (*101*) for a review], with the design of robust robots that can move in multiple terrains and survive harsh conditions (*102*). Progress toward outdoor tests will not only help to make robots more useful for applications in search and rescue, environmental monitoring, agriculture, transport, and construction, but will also help (and be guided by) research on animal locomotion in their natural ecological niches.

Unlike their biological counterparts (*103*), few robots are capable of multimodal locomotion, the ability to switch between different gaits and motor behaviors (e.g., a cat running, jumping, crawling, climbing, standing up, etc.). Exceptions include RHex (and AQUA, its aquatic version) that can walk and swim (*54*, *104*), and the salamander robot than can swim, crawl, and walk (*19*). For many outdoor applications, the ability to perform multimodal locomotion will be important for crossing many types of environments without getting stuck. Interesting scientific questions remain to be addressed with robots to better understand the interplay (and necessary tradeoffs) of morphology, energetics, and control in multimodal locomotion.

Studying non–steady-state behavior is difficult. Except possibly for flying (*50*, *51*), most studies in biology and in robotics have so far focused on steady-state behavior (e.g., analyzing periodic gaits of straight-line locomotion at a given speed). The main reason for this is that making experiments and collecting data for non–steady-state behavior is much more difficult than for steady-state behavior. But freely moving animals are rarely in a steady state: They continuously accelerate or decelerate, turn, switch between gaits and different motor behaviors, superimpose motor behaviors, etc. From a dynamical systems point of view, they are mostly in transient mode rather than in a steady state. Biorobots, being more amenable to experiments than animals, can become key tools to study non–steady-state locomotion.

Related to this, there is still a lack of quantitative metrics to measure agility, both in animals and in robots. Steady-state locomotor performance can be assessed using measures such as speed of locomotion normalized by body length, the cost of transport, the Froude number, and the Stroudhal number (*24*). But the concept of agility still has to be properly defined and quantified. For instance, it would be very useful to define normalized agility scores that assess and compare how well an animal or a robot turns, accelerates, jumps, stands up, etc. A useful attempt to quantify versatility for robots (defined as the ability to cross different types of terrains)

can be found in (*105*). This represents an exciting opportunity for roboticists and biologists to define various agility metrics together, not only for assessing existing animals and robots, but also for setting targets for the design of the next generations of biorobots.

REFERENCES AND NOTES

1. G. V. Lauder, E. J. Anderson, J. Tangorra, P. G. A. Madden, *J. Exp. Biol.* **210**, 2767–2780 (2007).
2. S. Sefati *et al*., *Proc. Natl. Acad. Sci. U.S.A.* **110**, 18798–18803 (2013).
3. M. Porez, F. Boyer, A. Ijspeert, *Int. J. Robot. Res.* **33**, 1322–1341 (2014).
4. J. H. Long, *Proc. Inst. Mech. Eng. C* **221**, 1193–1200 (2007).
5. S. Hirose, *Biologically Inspired Robots: Snake-Like Locomotors and Manipulators* (Oxford Univ. Press, Oxford, 1993).
6. R. D. Maladen, Y. Ding, P. B. Umbanhowar, A. Kamor, D. I. Goldman, *J. R. Soc. Interface* **8**, 1332–1345 (2011).
7. M. Tesch *et al*., *Adv. Robot.* **23**, 1131–1158 (2009).
8. S. Seok *et al*., in *2013 IEEE International Conference on Robotics and Automation (ICRA)* (2013), pp. 3307–3312.
9. H. Kimura, Y. Fukuoka, A. H. Cohen, *Int. J. Robot. Res.* **26**, 475–490 (2007).
10. A. Spröwitz *et al*., *Int. J. Robot. Res.* **32**, 932–950 (2013).
11. C. Semini *et al*., *J. Systems Control Eng.* **225**, 831–849 (2011).
12. X. Zhou, S. Bi, *Bioinspir. Biomim.* **7**, 041001 (2012).
13. S. H. Collins, M. Wisse, A. Ruina, *Int. J. Robot. Res.* **20**, 607–615 (2001).
14. T. McGeer, *Int. J. Robot. Res.* **9**, 62–82 (1990).
15. S. Kajita, B. Espiau, in *Handbook of Robotics* (Springer, Berlin, 2008), pp. 361–389.
16. B. Webb, *Behav. Brain Sci.* **24**, 1033–1050 (2001).
17. B. Webb, *Nature* **417**, 359–363 (2002).
18. A. Ananthanarayanan, M. Azadi, S. Kim, *Bioinspir. Biomim.* **7**, 046005 (2012).
19. A. J. Ijspeert, A. Crespi, D. Ryczko, J.-M. Cabelguen, *Science* **315**, 1416–1420 (2007).
20. M. F. Eilenberg, H. Geyer, H. Herr, *IEEE Trans. Neural Syst. Rehabil. Eng.* **18**, 164–173 (2010).
21. H. M. Herr, A. M. Grabowski, *Proc. R. Soc. B* **279**, 457–464 (2012).
22. C. Li, T. Zhang, D. I. Goldman, *Science* **339**, 1408–1412 (2013).
23. M. H. Dickinson *et al*., *Science* **288**, 100–106 (2000).
24. R. M. Alexander, *Principles of Animal Locomotion* (Princeton Univ. Press, Princeton, NJ, 2003).
25. P. Holmes, R. Full, D. Koditschek, J. Guckenheimer, *SIAM Rev.* **48**, 207–304 (2006).
26. R. Pfeifer, J. Bongard, S. Grand, *How the Body Shapes the Way We Think: A New View of Intelligence* (MIT Press, Cambridge, MA, 2007).
27. R. Pfeifer, M. Lungarella, F. Iida, *Science* **318**, 1088–1093 (2007).
28. M. Sitti, A. Menciassi, A. Ijspeert, K. H. Low, S. Kim, *IEEE/ASME Trans. Mechatron.* **18**, 409–418 (2013).
29. A. J. Ijspeert, *Neural Netw.* **21**, 642–653 (2008).
30. D. N. Beal, F. S. Hover, M. S. Triantafyllou, J. C. Liao, G. V. Lauder, *J. Fluid Mech.* **549**, 385–402 (2006).
31. F. E. Fish, *Bioinspir. Biomim.* **1**, R17–R25 (2006).
32. M. S. Triantafyllou, G. S. Triantafyllou, *Sci. Am.* **272**, 64–71 (March 1995).
33. M. Sfakiotakis, D. M. Lane, J. B. C. Davies, *IEEE J. Oceanic Eng.* **24**, 237–252 (1999).
34. V. van Ginneken *et al*., *J. Exp. Biol.* **208**, 1329–1335 (2005).
35. M. S. Triantafyllou, G. S. Triantafyllou, D. K. P. Yue, *Annu. Rev. Fluid Mech.* **32**, 33–53 (2000).
36. J. M. Anderson, N. K. Chhabra, *Integr. Comp. Biol.* **42**, 118–126 (2002).
37. J. Liu, H. Hu, *J. Bionics Eng.* **7**, 35–48 (2010).
38. N. Kato, *IEEE J. Oceanic Eng.* **25**, 121–129 (2000).
39. C. Stefanini *et al*., *Bioinspir. Biomim.* **7**, 025001 (2012).
40. M. C. Leftwich, E. D. Tytell, A. H. Cohen, A. J. Smits, *J. Exp. Biol.* **215**, 416–425 (2012).
41. R. Mittal, H. Dong, M. Bozkurttas, G. Lauder, P. Madden, *Bioinspir. Biomim.* **1**, S35–S41 (2006).
42. I. Akhtar, R. Mittal, G. V. Lauder, E. Drucker, *Theor. Comput. Fluid Dyn.* **21**, 155–170 (2007).
43. E. Feron, E. N. Johnson, in *Handbook of Robotics* (Springer, Berlin, 2008), pp. 1009–1029.
44. B. M. Kulfan, A. J. Colozza, in *Biomimetics: Nature-Based Innovation*, Y. Bar-Cohen, Ed. (CRC Press, Boca Raton, FL, 2011), pp. 525–674.
45. R. J. Wood, *IEEE Trans. Robot.* **24**, 341–347 (2008).
46. K. Y. Ma, P. Chirarattananon, S. B. Fuller, R. J. Wood, *Science* **340**, 603–607 (2013).
47. L. Hines, D. Campolo, M. Sitti, *IEEE Trans. Robot.* **30**, 220–232 (2014).
48. J. D. DeLaurier, *Can. Aeronaut. Space J.* **45**, 72–82 (1999).
49. C. P. Ellington, *Philos. Trans. R. Soc. London Ser. B* **305**, 1–15 (1984).
50. M. H. Dickinson, F.-O. Lehmann, S. P. Sane, *Science* **284**, 1954–1960 (1999).
51. S. N. Fry, R. Sayaman, M. H. Dickinson, *Science* **300**, 495–498 (2003).
52. M. J. Elzinga, F. van Breugel, M. H. Dickinson, *Bioinspir. Biomim.* **9**, 025001 (2014).
53. R. D. Maladen, Y. Ding, C. Li, D. I. Goldman, *Science* **325**, 314–318 (2009).
54. U. Saranli, M. Buehler, D. E. Koditschek, *Int. J. Robot. Res.* **20**, 616–631 (2001).
55. C. Li, S. T. Hsieh, D. I. Goldman, *J. Exp. Biol.* **215**, 3293–3308 (2012).
56. S. Kim *et al*., *IEEE Trans. Robot.* **24**, 65–74 (2008).
57. O. Unver, A. Uneri, A. Aydemir, M. Sitti, in *Proceedings 2006 IEEE International Conference on Robotics and Automation, 2006 (ICRA 2006)* (2006), pp. 2329–2335.
58. M. Carlo, S. Metin, *J. Bionics Eng.* **3**, 115–125 (2006).
59. M. J. Spenko *et al*., *J. Field Robot.* **25**, 223–242 (2008).
60. G. A. Lynch, J. E. Clark, P.-C. Lin, D. E. Koditschek, *Int. J. Robot. Res.* **31**, 974–996 (2012).
61. K. Autumn *et al*., *J. Exp. Biol.* **209**, 260–272 (2006).
62. M. Hutter *et al*., in *15th International Conference on Climbing and Walking Robot (CLAWAR 2012)* (2012); http://infoscience.epfl.ch/record/181042).
63. B. Klaassen, R. Linnemann, D. Spenneberg, F. Kirchner, *Robot. Auton. Syst.* **41**, 69–76 (2002).
64. K. E. Rudman, R. M. Aspden, J. R. Meakin, *Biomed. Eng. Online* **5**, 12 (2006).
65. T. M. Kubow, R. J. Full, *Philos. Trans. R. Soc. London Ser. B* **354**, 849–861 (1999).
66. J.-M. Cabelguen, C. Bourcier-Lucas, R. Dubuc, *J. Neurosci.* **23**, 2434–2439 (2003).
67. A. Crespi, K. Karakasiliotis, A. Guignard, A. J. Ijspeert, *IEEE Trans. Robot.* **29**, 308–320 (2013).
68. D. Owaki, T. Kano, K. Nagasawa, A. Tero, A. Ishiguro, *J. R. Soc. Interface* **10**, 20120669 (2012).
69. H. Cruse, *Trends Neurosci.* **13**, 15–21 (1990).
70. B. Verrelst *et al*., *Auton. Robots* **18**, 201–213 (2005).
71. F. C. Anderson, M. G. Pandy, *Gait Posture* **17**, 159–169 (2003).
72. A. D. Kuo, *J. Biomech. Eng.* **124**, 113–120 (2002).
73. D. Renjewski, A. Seyfarth, *Bioinspir. Biomim.* **7**, 036005 (2012).
74. S. Collins, A. Ruina, R. Tedrake, M. Wisse, *Science* **307**, 1082–1085 (2005).
75. P. A. Bhounsule *et al*., *Int. J. Robot. Res.* **33**, 1305–1321 (2014).
76. P. Manoonpong, T. Geng, T. Kulvicius, B. Porr, F. Wörgötter, *PLOS Comput. Biol.* **3**, e134 (2007).
77. G. Hirzinger, A. Albu-Schaffer, M. Hahnle, I. Schaefer, N. Sporer, in *IEEE International Conference on Robotics and Automation (ICRA 2001)* (IEEE, 2001; http://ieeexplore.ieee.org/xpls/abs_all.jsp?arnumber=933136), vol. 4, pp. 3356–3363.
78. L. Sentis, O. Khatib, *Int. J. Humanoid Robot.* **2**, 505–518 (2005).
79. L. Righetti, J. Buchli, M. Mistry, S. Schaal, in *IEEE International Conference on Robotics and Automation (ICRA 2011)* (IEEE, 2011; http://ieeexplore.ieee.org/xpls/abs_all.jsp?arnumber=5980156), pp. 1085–1090.
80. N. G. Tsagarakis, S. Morfey, G. M. Cerda, L. Zhibin, D. G. Caldwell, in *IEEE International Conference on Robotics and Automation* (ICRA 2013), pp. 673–678.
81. S. Faraji, S. Pouya, A. Ijspeert, in *Robotics Science and Systems (RSS)* (2014); www.roboticsproceedings.org/rss10/p28.html
82. C. Semini, V. Barasuol, T. Boaventura, M. Frigerio, J. Buchli, in *International Symposium of Robotics Research (ISRR)* (2013); http://e-citations.ethbib.ethz.ch/view/pub:124391.
83. D. P. Ferris, G. S. Sawicki, M. A. Daley, *Int. J. Humanoid Robot.* **4**, 507–528 (2007).
84. A. B. Zoss, H. Kazerooni, A. Chu, *IEEE/ASME Trans. Mechatron.* **11**, 128–138 (2006).
85. H. Kawamoto, S. Lee, S. Kanbe, Y. Sankai, in *IEEE International Conference on Systems, Man and Cybernetics* (IEEE, 2003; http://ieeexplore.ieee.org/xpls/abs_all.jsp?arnumber=1244649), vol. 2, pp. 1648–1653.
86. C. J. Walsh, K. Endo, H. Herr, *Int. J. Humanoid Robot.* **4**, 487–506 (2007).
87. J. Gancet *et al*., in *4th IEEE RAS & EMBS International Conference on Biomedical Robotics and Biomechatronics (BioRob)* (IEEE, 2012; http://ieeexplore.ieee.org/xpls/abs_all.jsp?arnumber=6290688), pp.1794–1800.
88. J. E. Pratt, B. T. Krupp, C. J. Morse, S. H. Collins, in *IEEE International Conference on Robotics and Automation (ICRA 2004)* (IEEE, 2004; http://ieeexplore.ieee.org/xpls/abs_all.jsp?arnumber=1307425), vol. 3, pp. 2430–2435.
89. A. Dollar, H. Herr, *IEEE Trans. Robot.* **24**, 144–158 (2008).
90. A. J. van den Bogert, *Biomed. Eng. Online* **2**, 17 (2003).
91. J. M. Donelan *et al*., *Science* **319**, 807–810 (2008).
92. J. A. Paradiso, T. Starner, *IEEE Pervasive Comput.* **4**, 18–27 (2005).
93. L. C. Rome, L. Flynn, E. M. Goldman, T. D. Yoo, *Science* **309**, 1725–1728 (2005).
94. H. Geyer, H. Herr, *IEEE Trans. Neural Syst. Rehabil. Eng.* **18**, 263–273 (2010).
95. J. Markowitz *et al*., *Philos. Trans. R. Soc. London Ser. B* **366**, 1621–1631 (2011).
96. R. T. Schroer, M. J. Boggess, R. J. Bachmann, R. D. Quinn, R. E. Ritzmann, in *IEEE International Conference on Robotics and Automation (ICRA 2004)* (2004), vol. 4, pp. 3288–3293.
97. T. Libby *et al*., *Nature* **481**, 181–184 (2012).
98. R. J. Full, D. E. Koditschek, *J. Exp. Biol.* **202**, 3325–3332 (1999).
99. R. Blickhan, R. J. Full, *J. Comp. Physiol. A* **173**, 509–517 (1993).
100. B. Vanderborght *et al*., *Robot. Auton. Syst.* **61**, 1601–1614 (2012).
101. S. Kim, C. Laschi, B. Trimmer, *Trends Biotechnol.* **31**, 287–294 (2013).
102. M. T. Tolley *et al*., *Soft Robot.* **1**, 213–223 (2014).
103. R. J. Lock, S. C. Burgess, R. Vaidyanathan, *Bioinspir. Biomim.* **9**, 011001 (2014).
104. C. Georgiades *et al*., in *IEEE/RSJ International Conference on Intelligent Robots and Systems (IROS 2004)* (2004), vol. 4, pp. 3525–3531.
105. C. Nie, X. Pacheco Corcho, M. Spenko, *IEEE Robot. Autom. Mag.* **20**, 72–82 (2013).

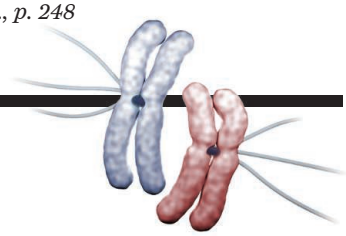
ACKNOWLEDGMENTS

I thank M. Ajallooeian, J. Buchli, P. Eckert, N. van der Noot, and D. Renjewski for useful comments on the manuscript. Supported by the Swiss National Center of Competence in Research in Robotics, the Swiss National Science Foundation, the Swiss NanoTera program, the EU-funded WalkMan project (FP7-ICT 611832), and the EU-funded Symbitron project (FP7-ICT 661626).

10.1126/science.1254486

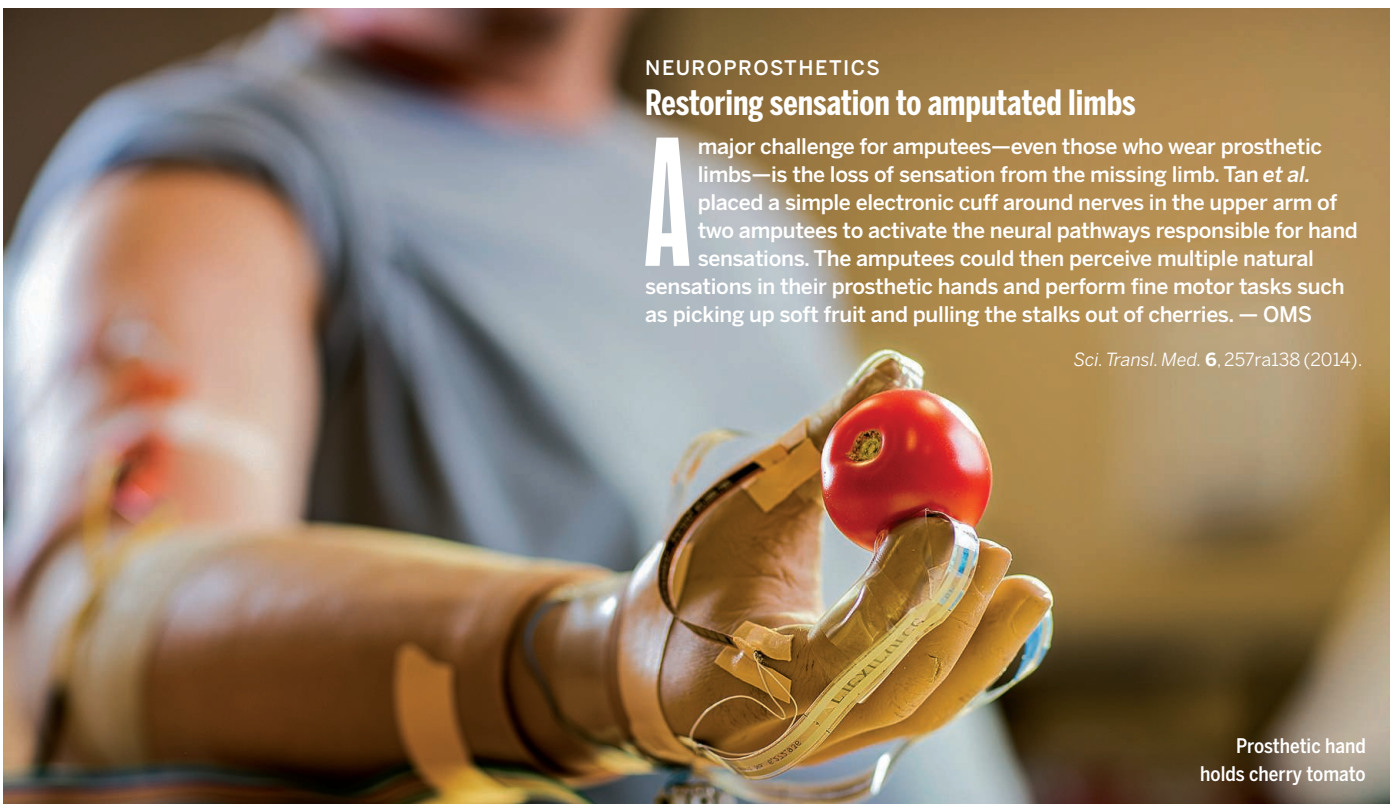
RESEARCH

Why sister chromatids comigrate in the first meiotic division
Sarangapani et al., *p. 248*



IN *SCIENCE* JOURNALS

Edited by **Stella Hurtley**



NEUROPROSTHETICS

Restoring sensation to amputated limbs

A major challenge for amputees—even those who wear prosthetic limbs—is the loss of sensation from the missing limb. Tan *et al.* placed a simple electronic cuff around nerves in the upper arm of two amputees to activate the neural pathways responsible for hand sensations. The amputees could then perceive multiple natural sensations in their prosthetic hands and perform fine motor tasks such as picking up soft fruit and pulling the stalks out of cherries. — OMS

Sci. Transl. Med. **6**, 257ra138 (2014).

Prosthetic hand holds cherry tomato

QUANTUM PROCESSING

A sound proposition for quantum communication

Quantum computers exploit the quantum-mechanical properties of materials to store and manipulate information stored in the quantum states of atoms or artificial atoms. Although there are a number of quantum platforms under investigation already, Gustafsson *et al.* present another, based on the propagation of sound waves on the surface of a crystal (see the Perspective by Ruskov and Tahan). The ability to tune the system and the slow propagation speeds of the acoustic waves offer new opportunities to control and process quantum information. — ISO

Science, this issue p. 207; see also p. 165

ANIMAL MOTION

What's that coming over the hill—is it a robot?

Crossing a slope can be difficult, particularly if it is made of sand. Sidewinder rattlesnakes manage to climb sandy hills by adjusting the length of their body in contact with the sand. Marvi *et al.* designed robots based on this idea to determine what affects climbing ability on sandy slopes (see the Perspective by Socha). Based on the behavior of the robots, the authors performed further animal studies, and used an iterative approach to improve the robots' capabilities and to better understand animal motion. — MSL

Science, this issue p. 224; see also p. 160

LUNG CANCER EVOLUTION

Space, time, and the lung cancer genome

Lung cancer poses a formidable challenge to clinical oncologists. It is often detected at a late stage, and most therapies work for only a short time before the tumors resume their relentless growth. Two independent analyses of the human lung cancer genome may help explain why this disease is so resilient (see the Perspective by Govindan). Rather than take a single "snapshot" of the cancer genome, de Bruin *et al.* and Zhang *et al.* identified genomic alterations in spatially distinct regions of single lung tumors and used this information to infer the tumor's evolutionary history. Each tumor showed tremendous spatial and temporal diversity in its mutational profiles. Thus, the efficacy of drugs may be short-lived because they destroy only a portion of the tumor. — PAK

Science, this issue p. 251, p. 256; see also p. 169

Downloaded from www.sciencemag.org on October 9, 2014

CREDITS: (TOP TO BOTTOM) V. ALTOUNIAN/*SCIENCE*; RUSSELL LEE/RUSSELL LEE PHOTO

Published by AAAS

PLANETARY DYNAMICS

Close planet friends get out of line

Some "warm" giant exoplanets orbit much closer to their star than do similar planets in our solar system. Dawson and Chiang argue that understanding how such orbits have evolved can answer an outstanding question: How do "hot" giant planets (which are more common than these "warm" ones) get so close to their host star? These planets frequently have giant companions. Numerical simulations revealed that planets with an eccentric giant companion may have just the right mutual inclination for the inner planet to be pushed slowly toward the star. This process could then produce systems with "warm" rather than "hot" Jupiters. — MMM

Science, this issue p. 212

CELL-FREE ASSAYS

Reconstituting the right stuff for division

Cytokinesis, when two daughter cells are physically separated from one another, is the final stage of cell division. How dividing cells assemble a cleavage furrow ready for cytokinesis has long interested cell biologists. A major stumbling block to probing the underlying mechanisms has been the lack of a cell-free and fully controllable experimental system. Now, Nguyen *et al.* have reconstituted cytokinesis organization outside living cells, using a system derived from frog eggs. In the cell-free system, the cell cycle state is "frozen," and the spatial scale is unusually large. The authors examined the biophysics involved in signaling during cytokinesis over many minutes and many micrometers using powerful imaging techniques. — SMH

Science, this issue p. 244

ADULT NEUROGENESIS

Astrocytes' hidden ability to generate neurons

New neurons could be useful in the brain to respond to damage done by disease, trauma, or just plain age. But the adult brain does not produce many new neurons. Working in mice, Magnusson *et al.* hunted for intrinsic genetic programs that can help adult brains produce replacement neurons. They found that astrocytes, spidery cells that are interspersed between neurons, carry a latent neurogenic program. The ability to entice astrocytes to replace neurons could obviate the need for neuronal replacement strategies. — PJH

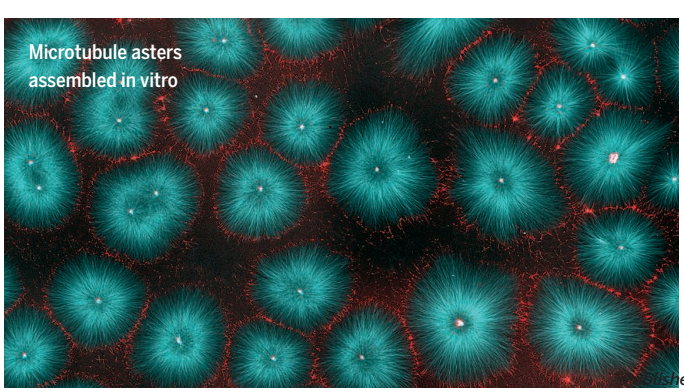
Science, this issue p. 237

ECONOMIC DEMOGRAPHY

Adjusting to fewer kids and more elderly

In many countries, populations are aging as retirees live longer, and the rates of population growth have declined as fewer babies are born. These demographic changes have evoked alarmist predictions that future retirement pensions will need to be curtailed, constraining future generations' purchasing power. Lee *et al.* point out that compensatory factors, such as more women working more years, along with a better educated workforce, may mitigate these demographic impacts (see the Perspective by Smeeding). — GJC

Science, this issue p. 229; see also p. 163



Microtubule asters assembled in vitro

PHOTOS: (LEFT TO RIGHT) PHUONG ANH NGUYEN; NASA/JPL-CALTECH/STSCI

IN OTHER JOURNALS

Edited by **Kristen Mueller** *and* **Jesse Smith**



ASTRONOMY

Do young star clusters follow the law?

One of the enduring puzzles of astrophysics is how mass is distributed among a population of stars at their birth. Astronomers currently use modified power-law functions in an attempt to describe the initial mass function (IMF), effectively a histogram of stellar masses. Sami Dib employed Bayesian statistics to find the probability distributions of IMF parameters for eight young star clusters with similar environments and ages, in order to discover if a universally descriptive IMF exists. Surprisingly, the resulting parameters did not overlap (within 1 sigma), suggesting that there is no universal description for young clusters. These findings demonstrate the power and necessity of Bayesian statistics in IMF studies as next-generation telescopes that can resolve stellar populations in many more clusters come online. — MMM

Mon. Not. R. Astron. Soc. 10.1093/mnras/stu1521 (2014).

TROPICAL FORESTS

Tree diversity benefits light capture

Higher plant diversity in ecosystems often benefits ecological processes such as nutrient cycling and rates of growth. To better understand how such improvements might work in tropical forests, Sapijajankas *et al*. set up experimental plantations in Panama using seedlings of native tree species and varied the number of species in the plots. Eight years later, they measured light penetrating through the tree canopy and found that plots with six species captured more light and grew taller than those with three species or only one. The researchers linked these effects to changes in tree

ished by AAAS

ALSO IN *SCIENCE* JOURNALS

Edited by **Stella Hurtley**

CONSERVATION

Needed: Better metrics, rigorously tested

News of species and ecosystems in peril abound around the world. Many governments have made commitments to protect biodiversity. But how well do we understand the changes in our natural environment? Different metrics, such as species abundance and extinction risk, can give very different impressions of conservation success. Collen and Nicholson argue that to be successful, conservation efforts require an agreed set of metrics of biodiversity change. These metrics may include existing as well as new ones and must undergo rigorous testing to ensure that they are suitable for the conservation target that they are used for. — JFU

Science, this issue p. 166

ORGANIC SYNTHESIS

Sceptrin goes through the looking glass

Marine sponges produce a trio of compounds—sceptrin, massadine, and ageliferin—that have intrigued chemists because they seemed to result from ring-forming reactions outside the standard repertoire of enzyme catalysis. Ma *et al.* now report laboratory syntheses of the first two compounds that uncover a surprising twist: It turns out the real structure of sceptrin is the mirror image of the originally reported structure. The work partially bolsters the prevailing biosynthetic hypothesis, though its revelation of enantiodivergence (the emergence of distinct mirror-image motifs in one compound class) is a rare event in natural product chemistry. — JSY

Science, this issue p. 219

WORLD POPULATION

Global population growth continuing

The United Nations released new population projections for all countries in July 2014. Gerland *et al*. analyzed the data and describe the probabilistic population projections for the entire world as well as individual regions and countries (see the Perspective by Smeeding). World population is likely to continue growing for the rest of the century, with at least a 3.5-fold increase in the population of Africa. Furthermore, the ratio of working-age people to older people is almost certain to decline substantially in all countries, not just currently developed ones. — BJ

Science, this issue p. 234; see also p. 163

EARLY UNIVERSE

A light leak to transform the universe

After the universe had cooled into an expanse of neutral gas after the Big Bang, how did the first starlight emerge from the dark? Borthakur *et al.* found a local starburst galaxy that leaks continuum radiation, which may provide some clues. Wind-generated gaps in the neutral gas enable large fractions of ionizing radiation to escape, possibly mimicking processes in the early universe. — MMM

Science, this issue p. 216

CONSERVATION TARGETS

Indicators of progress and decline

The targets set by the Convention on Biological Diversity in 2010 focused international efforts to alleviate global biodiversity decline. However, many of the consequences of these efforts will not be evident by the 2020 deadline agreed to by governments of 150 countries. Tittensor *et al.* analyzed data on 55 different biodiversity indicators to predict progress toward the 2020 targets—indicators such as protected area coverage, land-use trends, and endangered species status. The analysis pinpoints the problems and areas that will need the most attention in the next few years. — AMS

Science, this issue p. 241

YEAST MEIOSIS

Monopolin masterfully manages meiosis

Biologists have wondered for decades how replicated sister chromatids, which normally separate during mitotic cell division, instead comigrate during the first meiotic division, meiosis I. This process segregates chromosomal homologs and is needed to produce haploid gametes after the second, more mitosis-like, meiotic division. One hypothesis for sister chromatid comigration suggests that meiosis I–specific factors directly cross-link the sister kinetochores that attach each sister chromatid to dynamic microtubule tips. Yeast possesses a putative kinetochore cross-linker, known as monopolin, but monopolin's precise role during meiosis I is unknown. Sarangapani *et al.* isolated functional meiotic kinetochores from yeast cells. They reconstituted kinetochore activity in vitro and found that monopolin causes kinetochore fusion and underlies the sister chromatid comigration seen in meiosis I. — SMH

Science, this issue p. 248

NEUROSCIENCE

Enhancing pain with a growth factor

Muscle injury is associated with inflammation and pain and requires muscle growth to restore damaged tissue. Insulin-like growth factor 1 (IGF-1) stimulates muscle growth. Zhang *et al*. report that IGF-1 makes sensory neurons more sensitive to painful stimuli. IGF-1 increased the activation of a voltage-gated calcium channel through a G protein–dependent pathway in mouse sensory neurons, which increased neuronal activity. Blocking the G protein–dependent pathway or the calcium channel in sensory neurons prevented increased sensitivity to touch or heat in mice with chronic inflammation. Thus, targeting this pathway may be a therapeutic option for patients with chronic pain. — LKF

Sci. Signal. **7**, ra94 (2014).

Published by AAAS

RESEARCH ARTICLE

QUANTUM PROCESSING

Propagating phonons coupled to an artificial atom

Martin V. Gustafsson,[1,2]* Thomas Aref,[1] Anton Frisk Kockum,[1] Maria K. Ekström,[1] Göran Johansson,[1] Per Delsing[1]*

Quantum information can be stored in micromechanical resonators, encoded as quanta of vibration known as phonons. The vibrational motion is then restricted to the stationary eigenmodes of the resonator, which thus serves as local storage for phonons. In contrast, we couple propagating phonons to an artificial atom in the quantum regime and reproduce findings from quantum optics, with sound taking over the role of light. Our results highlight the similarities between phonons and photons but also point to new opportunities arising from the characteristic features of quantum mechanical sound. The low propagation speed of phonons should enable new dynamic schemes for processing quantum information, and the short wavelength allows regimes of atomic physics to be explored that cannot be reached in photonic systems.

The quantum nature of light is revealed and explored in its interaction with atoms, which can be either elemental or artificial. Artificial atoms typically have transition frequencies in the microwave range and can be designed on a microchip with parameters tailored to fit specific requirements. This makes them well suited as tools to investigate fundamental phenomena of atomic physics and quantum optics. In the form of superconducting qubits, they have seen extensive use in closed spaces (electromagnetic cavities), where they have ample time to interact with confined microwave radiation (*1*–*3*). These experiments have recently been extended to quantum optics in open one-dimensional (1D) transmission lines, where the atom interacts with itinerant microwave photons (*4*–*7*). We present an acoustic equivalent of such a system, where the quantum properties of sound are explored, rather than those of light.

At the intersection between quantum informatics and micromechanics, recent milestones include the coupling between a superconducting qubit and a vibrational mode (*8*, *9*), hybrids of mechanical resonators and electrical microwave cavities (*10*), and the use of mechanics to interface between microwaves and optical photons (*11*, *12*). The system we present here is another manifestation of mechanics in the quantum regime, but one that differs fundamentally from the suspended resonators mentioned above. In our case, the phonons are not bound to the eigenmodes of any structure but consist of surface acoustic waves (SAWs) that propagate freely over long distances, before and after interacting with an atom in their path.

[1]Microtechnology and Nanoscience, Chalmers University of Technology, Kemivägen 9, SE-41296 Göteborg, Sweden. [2]Department of Chemistry, Columbia University, NWC Building, 550 West 120th Street, New York, NY 10027, USA. *Corresponding author. E-mail: mg3465@columbia.edu (M.V.G.); per.delsing@chalmers.se (P.D.)

In the domain of quantum information, SAWs with high power have been used to transport electrons and holes in semiconductors (*13*–*15*). This stands in contrast with our use of SAWs, where the power is much too low to transport charge carriers, and we instead focus on the quantum nature of the phonons themselves.

We do this by coupling an artificial atom directly to the SAWs through piezoelectricity, so that this mode of interaction becomes the dominant one for the atom. This means that we can communicate with the atom bidirectionally through the SAW channel, exciting it acoustically as well as listening to its emission of propagating surface phonons.

The idea that this might be feasible was put forward in previous work (*16*), where the use of a single-electron transistor as a sensitive probe for SAWs was demonstrated. Earlier work on the interaction between phonons and two-level systems includes the demonstration of SAW absorption by quantum dots (*17*) and theoretical treatments of phonon quantum networks (*18*) and phononic coupling to dopants in silicon (*19*, *20*).

The acoustically coupled atom

Although there are several types of SAWs, we use the term to denote Rayleigh waves (*21*–*23*), which propagate elastically on the surface of a solid within a depth of approximately one wavelength. At and above radio frequencies (RF), the SAW wavelength is short enough that the surface of a microchip can serve as a medium of propagation. By use of a piezoelectric substrate, SAWs can be generated efficiently from electrical signals and converted back to the electrical domain after propagating acoustically over a long distance on the chip. This is used extensively in commercial applications such as microwave delay lines and filters (*22*–*24*).

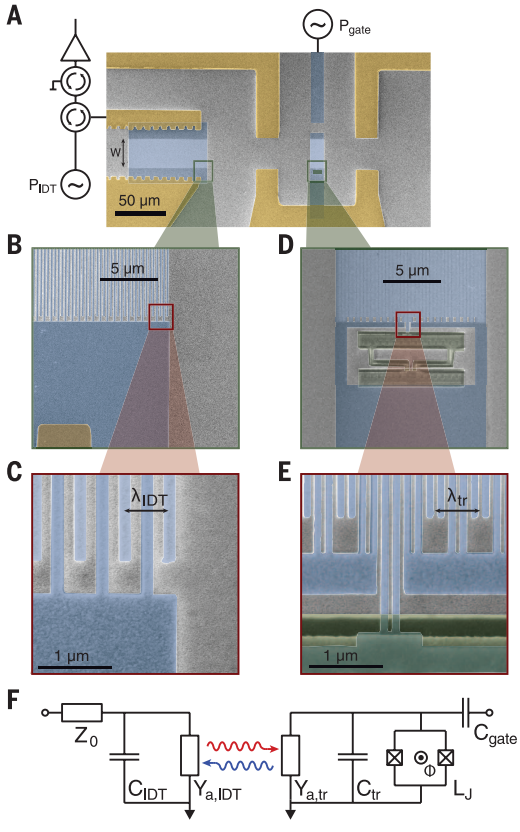


Fig. 1. Sample and experimental setup. (**A**) Electron micrograph of the sample (top view in false color). The IDT, shown to the left, converts electrical signals to SAWs and vice versa. It has $N_{IDT} = 125$ periods of fingers, each consisting of one finger from each electrode, with a periodicity of 600 nm. The width of the SAW beam is given by the overlap of the fingers, $W = 25$ μm. SAWs from the IDT propagate a distance of 100 μm before reaching the qubit, which is shown to the right. All electrodes without explicit connections are grounded. (**B** and **C**) Enlargements of the IDT. (**D** and **E**) Enlargements of the transmon qubit. The qubit has $N_{tr} = 20$ finger periods, with double fingers to suppress internal mechanical reflections (*22*, *23*, *26*). (**F**) Semiclassical circuit model for the qubit. C_{tr} is the geometric capacitance of the finger structure. It is shunted by a SQUID, which acts as a nonlinear inductance L_J that can be adjusted with a magnetic flux Φ. $Y_{a,tr}$ is the acoustic admittance element that can pick up a SAW from the IDT (red arrow) to produce electrical excitation in the qubit and regenerate it as a SAW with a phase shift (blue arrow) [(*27*), semiclassical and full quantum model]. In addition to SAWs from the IDT, radio-frequency signals applied through the gate capacitance C_{gate} can be used to address transitions in the qubit.

The primary component in a microelectronic SAW device is the interdigital transducer (IDT), which converts power from the electrical to the acoustic domain and vice versa. In its simplest form, it consists of two electrodes, each made of many long fingers deposited as thin films on a piezoelectric substrate. The fingers of the two electrodes are interdigitated so that an ac voltage applied between the electrodes produces an oscillating strain wave in the surface of the substrate. This wave is periodic in both space and time and radiates as a SAW away from each finger. The periodicity λ_{IDT} of the fingers defines the acoustic resonance of the IDT, with the frequency given by $\omega_{IDT} = 2\pi v_0/\lambda_{IDT}$ where v_0 is the SAW propagation speed. When the IDT is driven electrically at $\omega = \omega_{IDT}$, the SAWs emanating from all fingers interfere constructively, resulting in strong acoustic beams launching from the IDT in the two directions perpendicular to the fingers.

Our sample is fabricated on the (100) surface of a semi-insulating GaAs substrate, chosen for its piezoelectric and mechanical properties (Fig. 1A). The IDT is visible on the left side of the sample, with an enlargement in Fig. 1B. It has $N_{IDT} = 125$ finger pairs, with an overlapping width of W = 25 μm. The fingers, made of aluminum capped with palladium, are aligned so that the SAW propagates in the [011] direction of the crystal, at a speed $v_0 \approx 2900$ m/s.

In our case, the IDT makes use of internal reflections to achieve strong electro-acoustic power conversion that would otherwise be infeasible (*22*, *23*). This results in a narrow bandwidth of ~1 MHz around $\omega_{IDT}/2\pi = 4.8066$ GHz. The IDT is coupled to a low-noise cryogenic high-electron-mobility transistor amplifier via a circulator and an isolator. Through the circulator and the IDT, we can launch a SAW beam toward the artificial atom, which is shown to the right in Fig. 1A with enlargements in Fig. 1, D and E. Conversely, the IDT can pick up leftward-propagating SAW phonons emitted or reflected by the atom. All experiments were done in a dilution refrigerator with a base temperature of 20 mK, that is, with $k_B T \ll \hbar\omega_{IDT}$. At this low temperature, the charge carriers in the substrate are fully frozen out and the Bose-Einstein distribution gives a population of less than 10^{-4} thermal phonons per mode around ω_{IDT}.

The artificial atom in our setup is a superconducting qubit of the transmon type (*25*), positioned 100 μm away from the IDT (Fig. 1, A, D, and E). A transmon consists of a superconducting quantum interference device (SQUID) shunted by a large geometric capacitance C_{tr} with charging energy $E_C = e^2/(2C_{tr})$. The Josephson energy E_J of the SQUID can be tuned with a magnetic flux Φ. The Josephson inductance $L_J = \hbar^2/(4e^2E_J)$ forms a resonant circuit together with C_{tr}, and the nonlinearity of L_J gives rise to the anharmonic energy spectrum that is characteristic for an atom. The transmon is ideally suited for coupling to SAWs because the shunt capacitance can be designed as a finger structure, like an IDT. The charge on C_{tr} then relates directly to the mechanical strain of Rayleigh waves in the underlying substrate surface.

The periodicity of the capacitor fingers defines the resonance frequency where the acoustic coupling of the qubit is strongest. By design, the qubit and the IDT have the same acoustic resonance frequency, ω_{IDT}. The finger structure of the qubit has $N_{tr} = 20$ periods. In contrast with the IDT, each period of the qubit consists of four fingers, in a configuration that greatly diminishes internal mechanical reflections (*22*, *23*, *26*). This, along with the lower N_{tr} compared with N_{IDT}, means that the qubit has a much wider acoustic bandwidth than the IDT (~250 MHz). From the geometry and materials of the device, we estimate $C_{tr} = 85$ fF. In addition to the strong coupling to SAWs, the qubit couples weakly to an RF gate

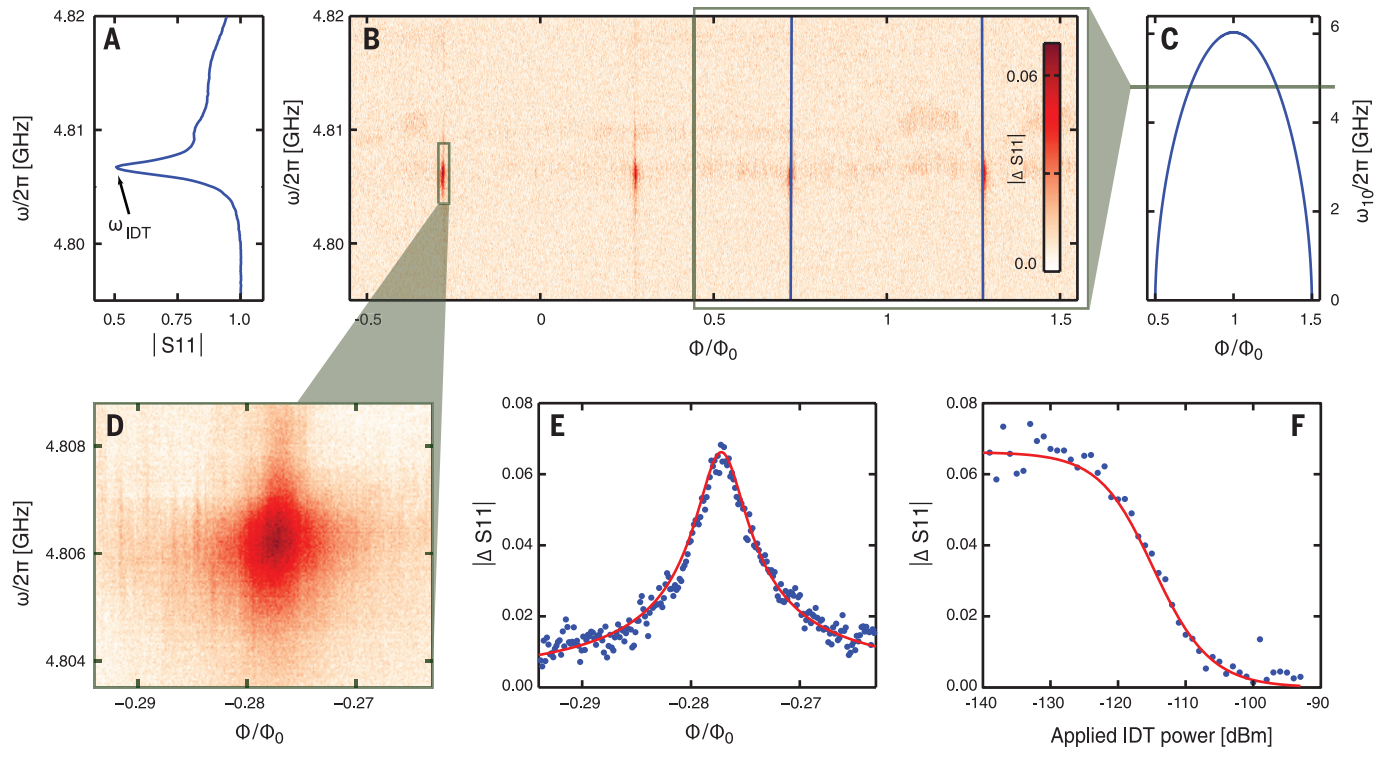


Fig. 2. Acoustic reflection measurements. (**A**) Reflection coefficient |S11| of the IDT versus frequency ω, with the qubit far detuned ($\omega_{10} \gg \omega$). The dip in the curve represents conversion of applied electrical power into SAWs. The complex background reflection acquired with the qubit far detuned has been subtracted from panels (B), (D), (E), and (F), which thus show the change |ΔS11| in total reflection coefficient caused by the qubit. (**B**) |ΔS11| versus frequency and qubit flux, Φ/Φ_0. As Φ/Φ_0 increases, the first transition frequency of the qubit, ω_{10}, periodically tunes in and out of the slim band where the IDT can address it acoustically. On resonance, the qubit reflects the incoming SAW beam. (**C**) Periodic modulation of ω_{10} with magnetic flux, fitted to the reflection peaks in (B). (**D**) Enlargement of one reflection peak from (B). (**E**) Cross section through (D) at $\omega = \omega_{IDT}$ (blue). A fit to the theoretical expression for the qubit reflection (red) gives the acoustic coupling rate, $\Gamma_{10}/2\pi = 38$ MHz. (**F**) Flux modulation of |ΔS11| versus power applied to the IDT (blue; theoretical fit in red). The rate at which the qubit reflects phonons from the incoming coherent beam is limited by the coupling rate Γ_{10}. Thus, the acoustic reflection coefficient of the qubit goes to zero for $P_{IDT}/\hbar\omega_{IDT} \gg \Gamma_{10}$, and the flux modulation vanishes. This saturation at the single-phonon level is evidence for the two-level nature of the qubit.

through a capacitance C_{gate}. The gate (in contrast with the IDT) has a high bandwidth, so we can use it to excite qubit transitions away from ω_{IDT} as well as to apply RF pulses.

The acoustic coupling rate of the qubit, Γ_{10}, is an important characteristic of the system, with $1/\Gamma_{10}$ representing the average time it takes the qubit to relax from the first excited state $|1\rangle$ to the ground state $|0\rangle$ by emitting an acoustic phonon at the transition frequency ω_{10}. The acousto-electric conversion of a finger structure is commonly represented as a complex and frequency-dependent acoustic admittance element Y_a, where electrical dissipation represents conversion to SAWs (*22*, *23*). By inserting this element into a semiclassical model of a transmon, we get the circuit shown in Fig. 1F. Here, the qubit is approximated as a harmonic oscillator, and the model is thus not valid for qubit states beyond the first excited one, $|1\rangle$. When L_J is adjusted so that the transition frequency ω_{10} between $|0\rangle$ and $|1\rangle$ resonates with ω_{IDT}, $Y_{a,tr}$ is real-valued and we get the coupling strength as the power loss rate of the parallel resonant circuit. Using this model, we find $\Gamma_{10} = c_g^2 N_{tr} K^2 \omega_{10}/\sqrt{2} = 2\pi \times 30$ MHz, where $c_g \approx 0.8$ is a geometry factor and $K^2 = 0.07\%$ is a material parameter that defines the strength of the piezoelectric coupling [(*27*), semiclassical model].

To analyze our system quantitatively, we have developed an extended model that takes the anharmonic nature of the qubit into account [(*27*), full quantum model] (*28*–*33*). A fully quantum mechanical model for the transmon (*25*) gives its energy levels as

$$E_n \approx -E_J + \sqrt{8E_J E_C}\left(n+\frac{1}{2}\right) - \frac{E_C}{12}(6n^2+6n+3)$$

In our extended model, we also need to account for the spatial extension of the qubit, because it interacts with SAWs over a distance of N_{tr} wavelengths. We do this by considering one interaction point per finger and accounting for the SAW phase shifts between the different points. However, we assume that the propagation time along the qubit is short compared with the inverse coupling frequency, $v_0/(N_{tr}\lambda) \gg \Gamma_{10}$. This means that each emitted phonon leaves the qubit entirely before the next one is emitted, an assumption that is valid in our experiments. It is interesting to note that the opposite limit can be reached, where dressed states should form between excitations in the qubit and phonons localized within its finger structure. Our model predicts the same nonlinear reflection for phonons that has previously been observed for photons (*4*, *5*), and we compare it with experimental data in Figs. 2, 3, and 5.

Acoustic reflection measurements

An atom in an open 1D geometry reflects weak resonant coherent radiation perfectly (in the absence of pure dephasing). This is also predicted both by our semiclassical and quantum mechanical models. However, at irradiation powers comparable to or larger than one photon per relaxation time, the $|1\rangle$ state of the qubit becomes populated to an appreciable degree, which reduces its ability to reflect phonons of frequency ω_{10} and leads to an increase in transmission (*4*, *5*, *7*, *34*). We measure the nonlinear acoustic reflection of the qubit by applying a coherent microwave tone of frequency ω to the IDT, which transmits part of the power in the form of a SAW propagating toward the qubit.

On IDT resonance ($\omega = \omega_{IDT}$), ~25% of the applied electrical power reflects against the IDT without converting to acoustic power (Fig. 2A). Here, the qubit is tuned off resonance so that $\omega_{10} \gg \omega$. Of the power that leaves the IDT in the form of SAWs, half is emitted in the rightward direction. With all losses accounted for, ~8% of the applied electrical power reaches the qubit in the form of a SAW [(*27*), extracted sample parameters]. Of the acoustic power that reflects against the qubit, an appreciable part converts back to electrical power in the IDT and can be detected.

The qubit resonance frequency ω_{10} is modulated by the magnetic flux Φ applied through the SQUID loop, with a periodicity $\Phi_0 = h/2e$. As we tune the flux, we observe an increase in the reflected SAW when ω_{10} coincides with ω_{IDT}. As shown in Fig. 2, B and C, we can fit the flux

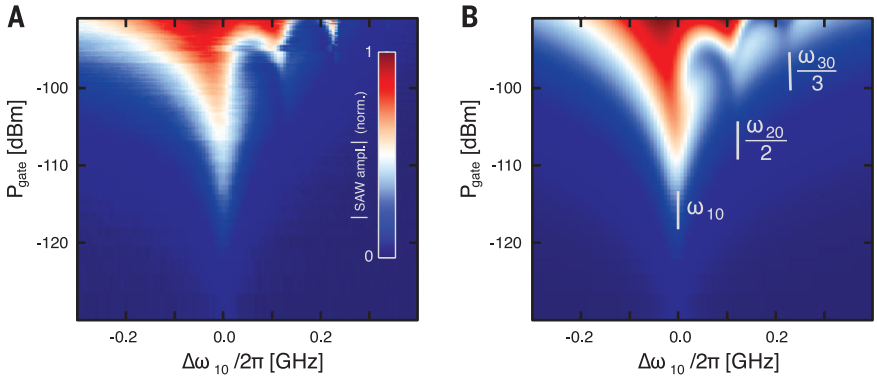


Fig. 3. Driving the qubit from the gate and listening to its acoustic emission with the IDT. (**A**) Transduction from the gate to the IDT versus driving power and qubit detuning. We apply a continuous RF signal to the gate at fixed frequency, $\omega = \omega_{IDT}$, and adjust the detuning of the first qubit transition from this frequency, $\Delta\omega_{10} = \omega_{10} - \omega_{IDT}$. The color scale shows the normalized coherent SAW amplitude detected by the IDT. No electrical signal is applied to the IDT. At low applied gate power, the qubit can only be excited at zero detuning, where it emits SAWs in proportion to the applied RF amplitude (constant |S12|). At higher power, two photons from the gate at $\omega = \omega_{20}/2$ can excite the $|2\rangle$ state of the qubit, which subsequently emits two phonons. For still higher power, photon-to-phonon conversions of increasingly higher orders are visible. (**B**) Theoretical simulation [(*27*), full quantum model]. The markup shows the values of $\Delta\omega_{10}$, where n photons at frequency ω_{n0}/n can excite the nth state of the qubit and give rise to the emission of n SAW phonons.

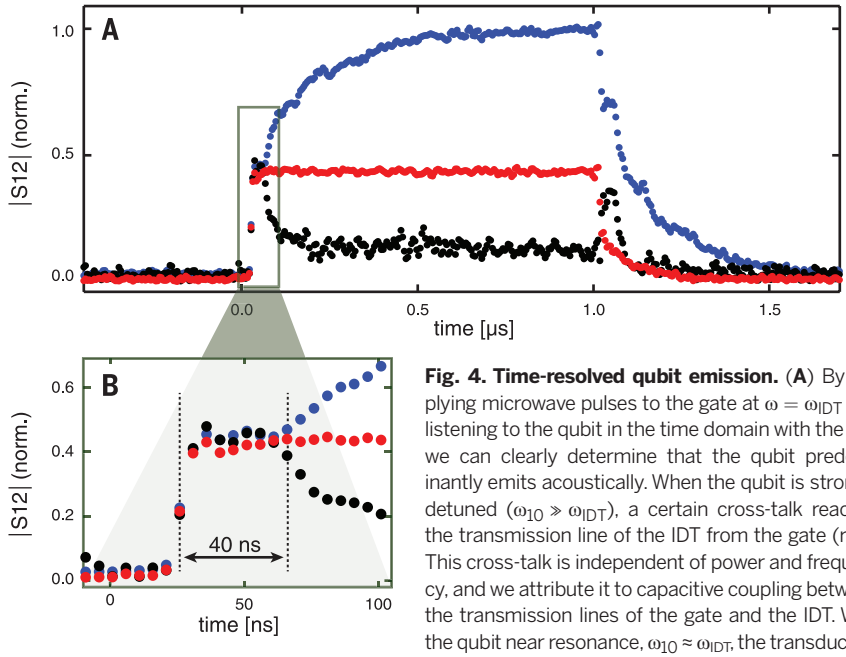


Fig. 4. Time-resolved qubit emission. (**A**) By applying microwave pulses to the gate at $\omega = \omega_{IDT}$ and listening to the qubit in the time domain with the IDT, we can clearly determine that the qubit predominantly emits acoustically. When the qubit is strongly detuned ($\omega_{10} \gg \omega_{IDT}$), a certain cross-talk reaches the transmission line of the IDT from the gate (red). This cross-talk is independent of power and frequency, and we attribute it to capacitive coupling between the transmission lines of the gate and the IDT. With the qubit near resonance, $\omega_{10} \approx \omega_{IDT}$, the transduction coefficient increases substantially above the cross-talk level when the acoustic signal adds in phase with the cross-talk (blue) and decreases when the SAW and the cross-talk have opposite phases (black). (**B**) Enlargement of (A). The emission from the qubit is observed ~40 ns after the onset of the cross-talk, which corresponds to the acoustic propagation time from the qubit to the IDT.

modulation $\omega_{10}(\Phi/\Phi_0)$ to these resonance points. The absence of reflection outside the frequency band of the IDT shows that acoustic coupling strongly dominates over any electrical cross-talk between the IDT and the qubit.

A key characteristic of reflection against an atom in one dimension is the nonlinear dependence of the reflection coefficient on the power of the applied coherent tone: Only when the flux of incoming phonons is much lower than one per interaction time, $P_{SAW}/\hbar\omega \ll \Gamma_{10}$, does the qubit produce full reflection. As the power increases, the $|1\rangle$ state of the qubit becomes partly populated, which reduces its ability to reflect phonons of frequency ω_{10} (*4*, *5*, *7*, *34*). This power-dependent saturation is shown in Fig. 2F. By fitting our theoretical model to these data, we find good agreement for $\Gamma_{10}/2\pi = 38$ MHz with negligible dephasing, which implies full reflection from the qubit in the low-power limit. All theoretical plots use the same values for the fitted parameters [(*27*), extracted sample parameters].

Electrical driving in the steady state

In addition to the acoustic excitation discussed above, we can address transitions in the qubit with the electrical gate and use the IDT to pick up the SAW phonons that the qubit emits. We expect the qubit to selectively emit one-phonon states when driven electrically on resonance, in a process similar to the nonlinear reflection observed under acoustic driving (Fig. 3A). With the frequency of the RF signal applied to the gate fixed at ω_{IDT}, we observe the dependence of the emitted phonon flux on the qubit detuning $\Delta\omega_{10} = \omega_{10} - \omega_{IDT}$ as well as the applied RF power P_{gate}. As P_{gate} increases from zero, we first see acoustic emission from the qubit at $\Delta\omega_{10} = 0$. At higher power, additional peaks show up for $\Delta\omega_{10} > 0$, which correspond to the excitation of higher states of the qubit by multiple photons, and subsequent relaxation into multiple phonons. The offsets between the peaks reflect the anharmonicity of the qubit. Fitting the positions of these multiphonon peaks allows us to determine the Josephson energy $E_{J0} = E_J(\Phi = 0)$ and E_C of the qubit to good accuracy. We find $E_{J0}/h = 22.2$ GHz and $E_C/h = 0.22$ GHz. This charging energy agrees well with our geometry-based estimate of the transmon capacitance.

Time domain experiments

The slow propagation of SAWs compared with electromagnetic waves allows us to clearly establish

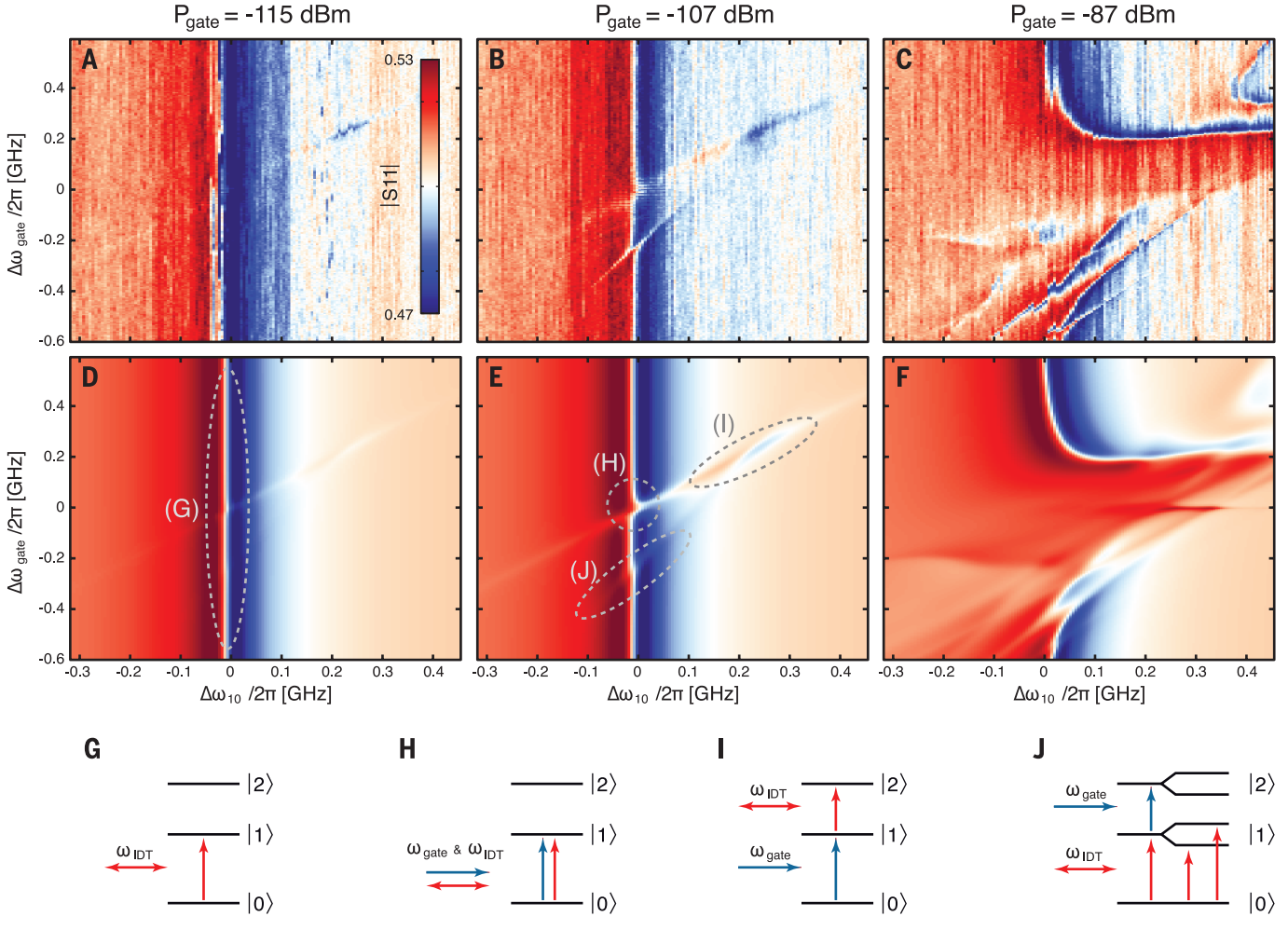


Fig. 5. Hybrid two-tone spectroscopy. We apply a continuous acoustic probe tone to the IDT with constant frequency ω_{IDT} and low power. At the same time, a continuous control tone with varying power P_{gate} and detuning from the probe, $\Delta\omega_{gate} = \omega_{gate} - \omega_{IDT}$, is applied to the gate. The color scale shows the electrical reflection coefficient |S11| of the IDT versus $\Delta\omega_{gate}$ and the qubit detuning $\Delta\omega_{10} = \omega_{10} - \omega_{IDT}$. (**A** to **C**) Experimental data for increasing P_{gate}. (**D** to **F**) Theoretical simulations corresponding to the experiments in (A) to (C). Selected features are highlighted and the corresponding qubit transitions illustrated in (G) to (J). (**G**) In the absence of a control signal on the gate, |S11| is modulated by the qubit flux, which is seen in (A) and (D) as a vertical feature at $\Delta\omega_{10} = 0$. (**H**) For $\Delta\omega_{gate} = \Delta\omega_{10} = 0$, a strong control tone contributes to the saturation of the first qubit transition. (**I**) Provided that the $|1\rangle$ state of the qubit is appreciably populated by the control tone, nonlinear acoustic reflection can occur also for $\omega_{21} = \omega_{IDT}$. We observe this when a moderately strong control tone is applied at $\omega_{gate} = \omega_{10}$. (**J**) For moderate to strong electrical driving of the $|1\rangle \rightarrow |2\rangle$ transition, Rabi splitting of the qubit energy levels gives rise to an Autler-Townes doublet (*35*, *36*). For very high control tone power [as shown in (F)], higher-order qubit states are populated and subject to Rabi splitting. This gives rise to a complex set of features that is well captured by the theoretical model [(*27*), full quantum model].

that the qubit couples to the IDT via phonons rather than photons. We do this by applying microwave pulses to the gate and studying the signal that reaches the IDT in the time domain. Figure 4 shows the results of such experiments using 1 μs long pulses with frequency ω_{IDT}. When the qubit is tuned far away from resonance ($\Delta\omega_{10} \gg \Gamma_{10}$), we see a cross-talk signal reaching the IDT from the gate. This is virtually independent of frequency, and we attribute it to stray capacitance between the electrical transmission lines.

Also, when the qubit is tuned close to its resonance, $\Delta\omega_{10} \approx 0$, the cross-talk signal is the first to rise above the noise floor. This leading edge serves as a time reference, showing the arrival of the electrical pulse to the gate. After the cross-talk edge, it takes another ~40 ns before we observe the emission from the qubit, which corresponds to the acoustic propagation time from the qubit to the IDT. This shows unequivocally that the signal from the qubit is phononic. The phase of the SAW phonons emitted coherently by the qubit is sensitive to $\Delta\omega_{10}$, and with small variations around $\Delta\omega_{10}$, we can go from the case where the qubit emission and the cross-talk interfere constructively (blue) to the case where they interfere destructively (black).

Because the IDT partly reflects phonons impinging on it from the qubit, additional features can be seen that correspond to acoustic round trips from the IDT to the qubit and back. These acoustic reflections add up gradually with time, superimposed on the transient response of the IDT, until the steady-state signal is established after ~1 μs. Just as in the steady-state experiments, the acoustic emission relative to the applied gate power increases with decreasing power P_{gate}, until it saturates at $P_{gate}/\hbar\omega \lesssim \Gamma_{10}$.

Hybrid two-tone spectroscopy

To characterize the dynamics of the phonon-qubit interaction in greater detail, we perform hybrid two-tone spectroscopy, where a continuous acoustic probe tone with low power is launched from the IDT toward the qubit at fixed frequency ω_{IDT}, and its reflection is measured. At the same time, we vary the qubit detuning $\Delta\omega_{10}$ and apply a continuous electrical control tone to the gate, with varying frequency ω_{gate} and power P_{gate}. When the qubit absorbs photons from the gate, we observe an impact on its reflection of phonons from the IDT (Fig. 5).

For low values of P_{gate}, the acoustic reflection is modulated only by the qubit detuning, as demonstrated in Figs. 2, B to E. For higher P_{gate} and when ω_{gate} coincides with ω_{10}, the control tone contributes to the population of the $|1\rangle$ state of the qubit. When the frequencies of the probe and control tones coincide, this results in saturation of the $|0\rangle \rightarrow |1\rangle$ transition, as seen in Fig. 2F. If the control tone is tuned to populate the $|1\rangle$ state of the qubit and the condition $\omega_{21} = \omega_{IDT} = 2\pi \times 4.8066$ GHz is fulfilled, the $|1\rangle \rightarrow |2\rangle$ transition exhibits nonlinear acoustic reflection.

For still higher control powers, we observe a rich set of spectral features, which agrees well with our model [(*27*), full quantum model]. Of particular interest is the Autler-Townes doublet, which is caused by Rabi splitting of the $|1\rangle$ state at strong electrical driving of the $|1\rangle \rightarrow |2\rangle$ transition (*35*, *36*).

Outlook and summary

Our SAW device occupies a middle ground between fixed mechanical resonators and transmission lines for free photons, and it is relevant to compare its features with both of these related systems.

Although their itinerant nature is an essential property of SAW phonons, they can also be confined into cavities by on-chip Bragg mirrors. Such cavities compare well with suspended resonators also in other respects than their natural integration with propagating waves: They can be fabricated for mode energies well above k_BT for temperatures attainable with standard cryogenic equipment, and because the motion takes place directly in the cooled substrate, thermalization is excellent. The few available studies also indicate that high-frequency SAW cavities can have comparatively high quality factors at low temperature (*37*, *38*).

In comparison to photons, SAW phonons have several striking features. Their speed of propagation is lower by a factor of ~10^5, and their wavelength at a given frequency is correspondingly shorter. The slow speed means that qubits can be tuned much faster than SAWs traverse inter-qubit distances on a chip. This enables new dynamic schemes for trapping and processing quanta.

SAW phonons furthermore give access to a regime where the size of an atom substantially exceeds the wavelength of the quanta it interacts with. This is the opposite of the pointlike interaction realized so far in photonics, cavity quantum electrodynamics (QED), and circuit QED (*28*). In our device, the qubit is a modest factor $N_{tr} = 20$ times longer than the SAW wavelength, but this can be extended substantially in a device designed for such investigations.

In the device presented here, the coupling strength between SAWs and the qubit is also moderate. This is necessary to discriminate between the different qubit transition energies due to the low anharmonicity of the transmon design. However, in a strongly piezoelectric material such as $LiNbO_3$, the many coupling points of an IDT-shaped qubit should make it possible to reach the regimes of "ultrastrong coupling" (*31*, *39*, *40*), $\Gamma_{10} \gtrsim \omega_{10}/10$ and even "deep strong coupling" (*41*), $\Gamma_{10} \gtrsim \omega_{10}$, which are difficult to access with the standard electrical dipole coupling of photonic systems.

In conclusion, we have demonstrated nonclassical interaction between surface acoustic waves and an artificial atom in the regime of strong coupling. Our experiments suggest that phonons can serve as propagating carriers of quantum information, in analogy with itinerant photons in quantum optics. The data are in good quantitative agreement with a theoretical quantum model, which captures the nonlinear acoustic reflection and relaxation of the atom. These results open up new possibilities in quantum experiments, because SAWs can reach regimes of coupling strength and time domain control that are not feasible with photons.

REFERENCES AND NOTES

1. A. Wallraff *et al.*, *Nature* **431**, 162–167 (2004).
2. M. Hofheinz *et al.*, *Nature* **459**, 546–549 (2009).
3. H. Paik *et al.*, *Phys. Rev. Lett.* **107**, 240501 (2011).
4. O. Astafiev *et al.*, *Science* **327**, 840–843 (2010).
5. I.-C. Hoi *et al.*, *Phys. Rev. Lett.* **107**, 073601 (2011).
6. C. Eichler *et al.*, *Phys. Rev. Lett.* **106**, 220503 (2011).
7. I.-C. Hoi *et al.*, *Phys. Rev. Lett.* **108**, 263601 (2012).
8. A. D. O'Connell *et al.*, *Nature* **464**, 697–703 (2010).
9. M. D. LaHaye, J. Suh, P. M. Echternach, K. C. Schwab, M. L. Roukes, *Nature* **459**, 960–964 (2009).
10. J.-M. Pirkkalainen *et al.*, *Nature* **494**, 211–215 (2013).
11. M. Eichenfield, J. Chan, R. M. Camacho, K. J. Vahala, O. Painter, *Nature* **462**, 78–82 (2009).
12. R. W. Andrews *et al.*, *Nat. Phys.* **10**, 321–326 (2014).
13. C. Barnes, J. Shilton, A. Robinson, *Phys. Rev. B* **62**, 8410–8419 (2000).
14. S. Hermelin *et al.*, *Nature* **477**, 435–438 (2011).
15. R. P. G. McNeil *et al.*, *Nature* **477**, 439–442 (2011).
16. M. V. Gustafsson, P. V. Santos, G. Johansson, P. Delsing, *Nat. Phys.* **8**, 338–343 (2012).
17. W. J. Naber, T. Fujisawa, H. W. Liu, W. G. van der Wiel, *Phys. Rev. Lett.* **96**, 136807 (2006).
18. S. J. M. Habraken, K. Stannigel, M. D. Lukin, P. Zoller, P. Rabl, *New J. Phys.* **14**, 115004 (2012).
19. Ö. O. Soykal, R. Ruskov, C. Tahan, *Phys. Rev. Lett.* **107**, 235502 (2011).
20. R. Ruskov, C. Tahan, *Phys. Rev. B* **88**, 064308 (2013).
21. L. Rayleigh, *Proc. London Math. Soc.* **s1-17**, 4–11 (1885).
22. S. Datta, *Surface Acoustic Wave Devices* (Prentice-Hall, Englewood Cliffs, NJ, 1986).
23. D. Morgan, *Surface Acoustic Wave Filters* (Academic Press, Amsterdam, ed. 2, 2007).
24. C. Campbell, *Surface Acoustic Wave Devices for Mobile and Wireless Communications* (Academic Press, San Diego, 1998).
25. J. Koch *et al.*, *Phys. Rev. A* **76**, 042319 (2007).
26. T. W. Bristol, W. R. Jones, P. B. Snow, W. R. Smith, in *1972 Ultrasonics Symp.* (IEEE, 1972), pp. 343–345.
27. Materials and methods are available as supplementary materials on *Science* Online.
28. A. Frisk Kockum, P. Delsing, G. Johansson, *Phys. Rev. A* **90**, 013837 (2014).
29. C. W. Gardiner, P. Zoller, *Quantum Noise* (Springer-Verlag, Berlin, 1991).
30. H. J. Carmichael, *Statistical Methods in Quantum Optics 1* (Springer-Verlag, Berlin, 1999).
31. B. Peropadre *et al.*, *New J. Phys.* **15**, 035009 (2013).
32. I. Rau, G. Johansson, A. Shnirman, *Phys. Rev. B* **70**, 054521 (2004).
33. R. Kubo, *J. Phys. Soc. Jpn.* **12**, 570–586 (1957).
34. J.-T. Shen, S. Fan, *Phys. Rev. Lett.* **95**, 213001 (2005).
35. S. H. Autler, C. H. Townes, *Phys. Rev.* **100**, 703–722 (1955).
36. I.-C. Hoi *et al.*, *Phys. Rev. Lett.* **111**, 053601 (2013).
37. A. El Habti, F. Bastien, E. Bigler, T. Thorvaldsson, *J. Ac. Soc. Am.* **100**, 272–277 (1996).
38. R. Manenti, thesis, University of Oxford, UK (2014).
39. T. Niemczyk *et al.*, *Nat. Phys.* **6**, 772–776 (2010).
40. P. Forn-Díaz *et al.*, *Phys. Rev. Lett.* **105**, 237001 (2010).
41. J. Casanova, G. Romero, I. Lizuain, J. J. García-Ripoll, E. Solano, *Phys. Rev. Lett.* **105**, 263603 (2010).

ACKNOWLEDGMENTS

We acknowledge financial support from the Swedish Research Council (VR), the Wallenberg Foundation, and the European Union through the European Research Council and the Scalable Superconducting Processors for Entangled Quantum Information Technology project. The samples were made at the Nanofabrication Laboratory at Chalmers. We acknowledge fruitful discussions with P. Leek, R. Manenti, and D. Niesner. M.V.G. acknowledges funding from the Wenner-Gren Foundations and support from X. Zhu and P. Kim during the manuscript preparation.

SUPPLEMENTARY MATERIALS

www.sciencemag.org/content/346/6206/207/suppl/DC1
Materials and Methods
Fig. S1
Table S1
References

10 June 2014; accepted 2 September 2014
Published online 11 September 2014;
10.1126/science.1257219

REPORTS

PLANETARY DYNAMICS

A class of warm Jupiters with mutually inclined, apsidally misaligned close friends

Rebekah I. Dawson* and Eugene Chiang

The orbits of giant extrasolar planets often have surprisingly small semimajor axes, large eccentricities, or severe misalignments between their orbit normals and their host stars' spin axes. In some formation scenarios invoking Kozai-Lidov oscillations, an external planetary companion drives a planet onto an orbit having these properties. The mutual inclinations for Kozai-Lidov oscillations can be large and have not been confirmed observationally. Here we present evidence that observed eccentric warm Jupiters with eccentric giant companions have mutual inclinations that oscillate between 35° and 65°. Our inference is based on the pairs' observed apsidal separations, which cluster near 90°. The near-orthogonality of periapse directions is effected by the outer companion's quadrupolar and octupolar potentials. These systems may be undergoing a stalled version of tidal migration that produces warm Jupiters over hot Jupiters, and they provide evidence for a population of multiplanet systems that are not flat and have been sculpted by Kozai-Lidov oscillations.

Planet-planet scattering (*1*), secular chaos (*2*), and Kozai-Lidov oscillations (*3*, *4*) induced by a stellar (*5*) or planetary (*6*) perturber are each capable of exciting the eccentricities of giant planets (*7*, *8*), of shrinking orbits by tidal friction to form close-in hot Jupiters [having semimajor axes a < 0.1 astronomical unit (AU)], and of tilting hot Jupiters' orbit normals away from their host stars' spin axes (*9*–*14*).

There are two outstanding issues with these models. First, they require or produce large inclinations between planetary orbits. These have not yet been observed. Most of the few systems with measured mutual inclinations are composed of planets on coplanar, low-eccentricity, mean-motion resonant orbits, such as GJ 876 (*15*) and Kepler-30 (*16*). This breed of system is thought to result from gentle disk migration (*17*), not from Kozai oscillations, planet scattering, or secular chaos. The two exceptions contain well-spaced (i.e., nonresonant) giant planets. Based on astrometry with the Hubble Space Telescope fine guidance sensor, a mutual inclination of 30° between Upsilon Andromeda c and d was inferred (*18*). From transit timing variations, a mutual inclination of $9°^{+8}_{-6}$ between Kepler-419 (KOI-1474) b and c was measured (*19*).

The second problem is that current models do not easily produce warm Jupiters, located exterior to hot Jupiters but interior to the pileup of giant planets at 1 AU (*20*). Although intrinsically rare, warm Jupiters promise to distinguish among models by serving as the exception that proves the rule. Many warm Jupiters have present-day eccentricities too high to have resulted from planet-planet scattering, because giant planets at small orbital distances collide and circularize before their velocity dispersions become too elevated (*21*). Yet most of their observed eccentricities are also too low to be easily accommodated within formation scenarios for hot Jupiters that invoke tidal migration (*22*), because warm Jupiters' current periapses are too far from their host stars for tidal friction to operate effectively.

One possibility (*23*) is that eccentric warm Jupiters are undergoing "slow Kozai" (*24*) migration driven by an external, mutually inclined companion. In this interpretation, warm Jupiters are observed today at the low-eccentricity phases of their secular Kozai cycles and only rarely attain eccentricities high enough for tidal friction to operate. For Kozai oscillations to not be quenched at these small semimajor axes by general relativistic precession, the external perturber must be nearby: It must be a "close friend" (*23*), in contrast to a "cold friend" (*25*). Supporting the possibility of migration driven by close friends, eccentric warm Jupiters orbit stars more enriched in metals—and therefore more likely to host multiple giant planets—than those of their circular counterparts (*26*). Indeed, the warm Jupiters known to have external giant planetary companions exhibit a broader range of eccentricities than solitary warm Jupiters (*23*). A key question is whether the mutual orbital inclination i_{mut} between warm Jupiters and their exterior companions exceeds 39.2°, the minimum angle required to excite Kozai oscillations in the quadrupole approximation (*3*, *4*). Unfortunately, nearly all of these planets are detected by

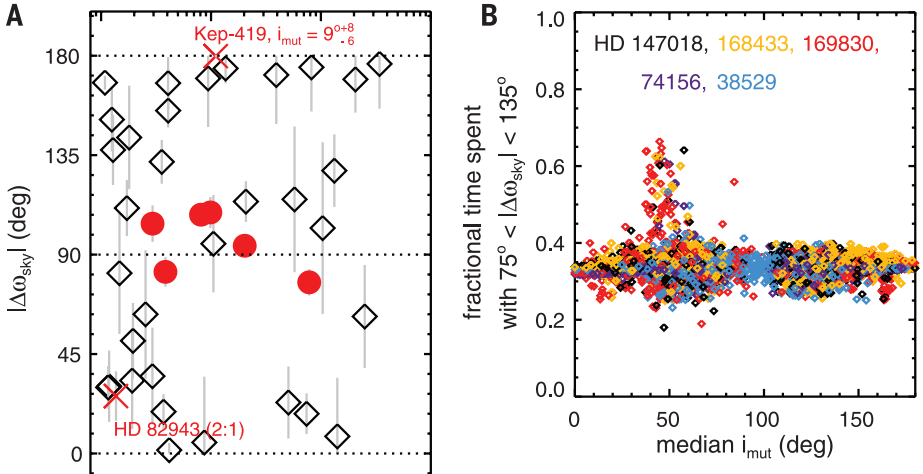


Fig. 1. Apsidal misalignments between pairs of planets and the large mutual inclinations implicated. (**A**) Sky-projected periapse separations $|\Delta\omega_{sky}|$ of planetary pairs, where $-180° < |\Delta\omega_{sky}| < 180°$. The sample includes all RV- and transit-discovered pairs with well-constrained (*30*) eccentricities and arguments of periapse. No mass or semimajor axis cut is made on the black diamonds. The red circles (corresponding to systems shown also in Figs. 2 and 3 and figs. S1 to S5) and crosses (HD 82943 and Kepler-419) represent warm Jupiters with only one known companion beyond 1 AU. All six of the red circles (*51*) lie close to $|\Delta\omega_{sky}| = 90°$; i.e., their apsides are strongly misaligned. For calculation of the abscissa values, the orbital angular momentum is evaluated as $m \sin i_{sky} \sqrt{a(1-e^2)}$. (**B**) Fraction of time that $|\Delta\omega_{sky}|$ spends near 90°, as a function of median mutual inclination, for stable simulations of systems corresponding to five of the six red circles (the same five are shown in Fig. 2). HD 202206 is omitted; its architecture and apsidal behavior differ from those of the five (fig. S5). Each simulation is consistent with the observed orbital elements, but only those with i_{mut} near 40° spend extra time at $|\Delta\omega_{sky}| \sim 90°$. The fractional time is evaluated for $75° < |\Delta\omega_{sky}| < 135°$; this window is centered on 105° instead of 90° because of general-relativistic precession.

Department of Astronomy, University of California, Berkeley, Hearst Field Annex 3411, Berkeley, CA 94720-3411, USA.
*Corresponding author. E-mail: rdawson@berkeley.edu

the radial velocity (RV) method, which does not yield i_{mut} directly but instead measures a given planet's a, eccentricity e, minimum mass m sin i_{sky} (where i_{sky} is the orbital inclination with respect to the sky plane), and argument of periapse ω_{sky} (referred to the sky plane).

However, the sky-projected apsidal separation of a planetary pair, $\Delta\omega_{sky}$, can be a clue to i_{mut} (*27*). In the invariable plane, the difference in apsidal longitudes $\Delta\varpi_{inv}$ (for which $\Delta\omega_{sky}$ is our observable proxy) is often found near 0° or 180° for pairs of coplanar planets, either in the secular limit (*28*) or in the 2:1 mean-motion resonance (*17*). In contrast, for highly inclined systems there is no such preference to find $\Delta\varpi_{inv}$ near 0° or 180°, at least for secular systems (*27*). The behavior of $\Delta\varpi_{inv}$ is directly reflected by its projection $\Delta\omega_{sky}$. Figure 1A displays $|\Delta\omega_{sky}|$ for RV-detected planetary pairs (*29*), some of which include warm Jupiters but most of which do not, with well-constrained (*30*) e and ω_{sky}, as a function of angular momentum ratio. Most systems with angular momentum ratio > ~3 have $|\Delta\omega_{sky}|$ near 0° and 180°. But some pairs with similarly large ratios are clustered near 90°.

The cluster of systems having $|\Delta\omega_{sky}| \sim 90°$ includes eccentric warm Jupiters with eccentric close friends. In fact, if we turn the problem around and consider only those systems with eccentric pairs consisting of one warm ($0.1 < a <$ 1 AU) and one "balmy" ($a > 1$ AU) Jupiter (defined as m sin $i_{sky} > 0.1\,M_{Jupiter}$) without regard for $|\Delta\omega_{sky}|$, then of the eight systems (*31*) so selected (red symbols in Fig. 1A), six (red circles) have $|\Delta\omega_{sky}|$ near 90° (HD 147018, HD 38529, HD 168443, HD 74156, HD 169830, and HD 202206). The two systems we know or expect to have low mutual inclinations (red crosses) are not among these six pairs with $|\Delta\omega_{sky}|$ clustered near 90°. HD 82943 (bottom red cross) is librating in the 2:1 mean-motion resonance (*32*), which interferes with the purely secular interactions we studied by driving apsidal precession on a shorter, resonant time scale. Another outlier is the transit-detected system Kepler-419 (top red cross), which was recently found to host an eccentric pair of one warm and one balmy Jupiter having a low ($9°^{+8}_{-6}$) mutual inclination and an apsidal separation of $|\Delta\omega_{sky}| = 179.8°^{+0.6}_{-0.7}$ (*19*). The orbital elements of all eight systems are listed in table S1.

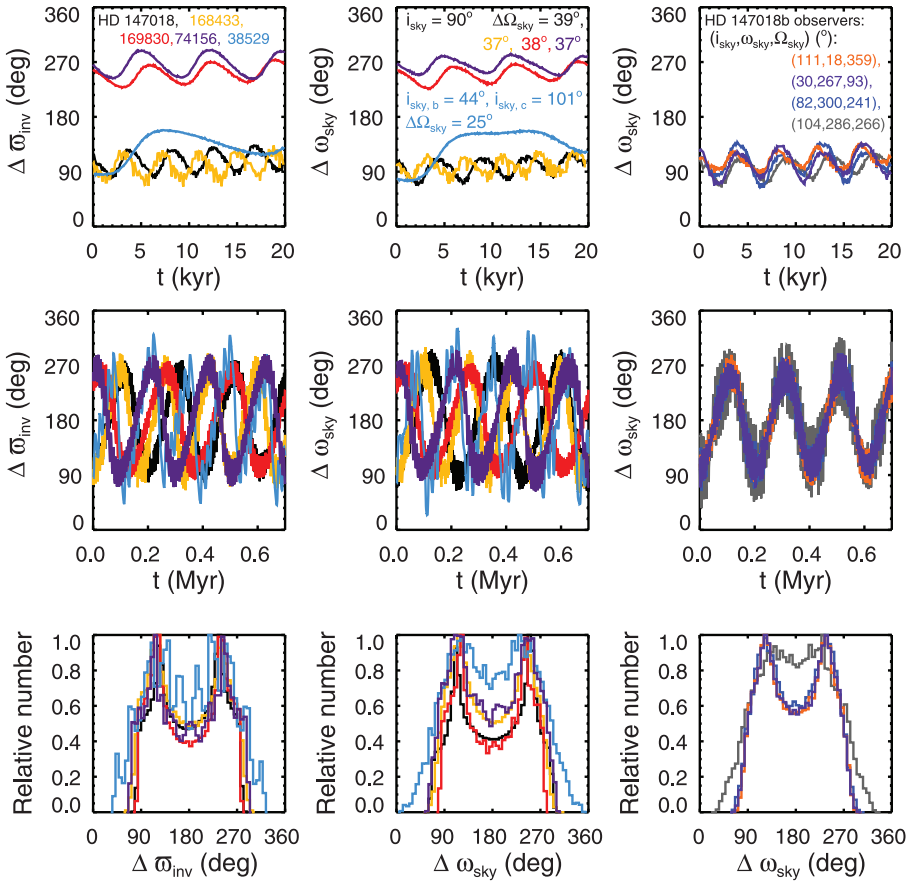


Fig. 2. Sample time histories of apsidal misalignment for five planetary pairs of warm Jupiters and their outer companions. Initial conditions are taken from table S1, with additional orbital angles indicated in the legend. For every history shown, the mutual inclination between the pair of planets varies within an interval that does not fall outside of 35° to 65°. (**Top**) On short time scales, the apsidal separation lingers near 90° or 270°. (**Middle**) Over longer time scales, the apsidal misalignment librates about 180° with an amplitude of 90°. (**Bottom**) Relative occurrence of either the apsidal separation evaluated in the invariable plane ($\Delta\varpi_{inv}$) or the sky-projected apsidal separation ($\Delta\omega_{sky}$), in uniformly spaced bins, indicating that these angles spend excess time near 90° and 270°. Because of the lower oscillation frequencies characterizing HD 38529 and HD 74156, for these two systems we plotted $t/3$ as the abscissa in both top and middle rows. Unlike the systems shown here, HD 202206 is situated near the 5:1 resonance, and its inner planet is almost certainly more massive than its outer planet (table S1); its dynamics is explored in fig. S5.

In Fig. 1B, we plotted the fraction of time that each simulated stable system spends having 75° < $|\Delta\omega_{sky}|$ < 135°, as a function of median mutual inclination, for five of our six systems (the sixth is a special case discussed below). A separation of $\Delta\omega_{sky}$ = 270° = –90° is equivalent to 90° in that both yield $|\Delta\omega_{sky}|$ = 90°. Each simulation was inspected by eye to ensure that the integration duration was long enough to sample the behavior of $\Delta\omega_{sky}$; integration durations range from 0.15 to 100 million years. A similar exploration of parameter space (*36*) was performed for two of our systems, HD 38529 and HD 168443, but without our aim of identifying regions of parameter space where $|\Delta\omega_{sky}|$ lingers near 90°. As illustrated in Fig. 1B, in the five systems we encounter configurations in which $|\Delta\omega_{sky}|$ spends excess time near 90°, but only for median $i_{mut} \sim 39°$, near Kozai's critical inclination. For such systems, $|\Delta\omega_{sky}|$ spends one-half to two-thirds of the time between 75° and 135°, depending on initial conditions. In comparison, uniform circulation of $|\Delta\omega_{sky}|$ gives a fractional time of one-third. Nearly coplanar systems for which $|\Delta\omega_{sky}|$ librates about 0° or 180° may spend no time at all in the desired range. Such realizations are inconsistent with the radial-velocity data and accordingly do not appear in Fig. 1B. The sixth system, HD 202206, is distinctive because its warm Jupiter is much more massive than the outer companion and because it lies near the 5:1 resonance. For this system, we still encounter configurations with $i_{mut} \sim 40°$ that

spend excess time with $|\Delta\omega_{sky}|$ near 90°, but not in the conventional range of 75° to 135°. An example is shown in fig. S5.

We reiterate that those integrations exhibiting libration of $|\Delta\omega_{sky}|$ about 90° all have i_{mut} close to 39.2°; typically, i_{mut} varies within an interval that does not fall outside 35° to 65° over the course of a given integration. In contrast, nearly coplanar, polar, or retrograde configurations consistent with the radial-velocity data have $|\Delta\omega_{sky}|$ circulating in the integrations we performed. Figure 2 shows examples of how the apsidal separation lingers near 90° and 270°, in the sky plane and invariable plane, over many secular oscillations. The desired libration of $|\Delta\omega_{sky}|$ does not require a finely tuned viewing geometry or set of initial conditions. Regarding viewing geometry, the libration of $|\Delta\omega_{sky}|$ is similar to that of $|\Delta\varpi_{inv}|$ for most observer orientations. Taking a single integration of HD 147018 for which $|\Delta\varpi_{inv}|$ spends 60% of its time between 75° and 135° in the invariable plane, we viewed this system from the vantage points of 500 isotropically distributed observers. We find that 60% (80%) of observers measure 75° < $|\Delta\omega_{sky}|$ < 135° at least 50% (40%) of the time. Measurements from four example observers are given in the right column of Fig. 2. Regarding initial conditions, we numerically integrated different realizations of the five systems shown in Fig. 2, ignoring all observational constraints on ω_{sky} and starting from various combinations of initial $\{\varpi_{inv,1}, \varpi_{inv,2}, i_{mut}\}$, with 35° < i_{mut} < 65°. To simplify and speed up these calculations, we approximated the inner planet as a test particle and integrated the secular equations of motion. Among the many realizations thus constructed (three are shown in fig. S6 along with accompanying surfaces of section), we find that it is not unusual for $\Delta\varpi_{inv}$ (and by extension $\Delta\omega_{sky}$) to linger near 90°/270°; i.e., it is not uncommon for $\Delta\varpi_{inv}$ to librate about 180° with a libration amplitude of 90°. Actually, depending on initial conditions, $\Delta\varpi_{inv}$ can librate about either 180° or 0° with a variety of amplitudes, as well as circulate, and we discuss later why warm Jupiters may prefer a libration amplitude near 90°.

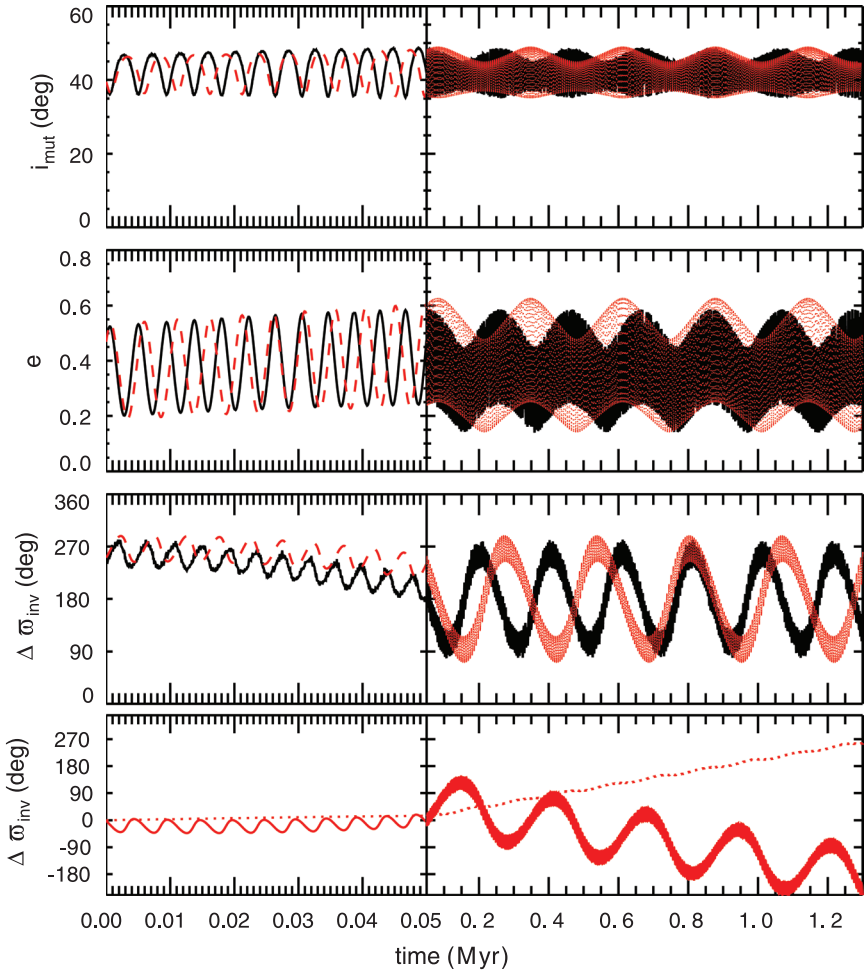


Fig. 3. Orbital evolution of HD 147018b, calculated using an *N*-body simulation and using a secular Hamiltonian expanded to octupolar order. Plotted are the time evolution of the mutual inclination (**row 1**), eccentricity of the inner warm Jupiter (**row 2**), apsidal separation (**row 3**), and near-canceling contributions to the apsidal separation from the quadrupolar and octupolar potentials (**row 4**). The simulation was performed in the invariable plane. Initial conditions were for the HD 147018 system (table S1) with i_{sky} = 90° and $\Delta\Omega_{sky}$ = 39°, corresponding to i_{mut} = 39° and to angles {i_1 = 35.6°, ω_1 = 66.0°, Ω_1 = 0°} and {i_2 = 3.4°, ω_2 = 136.9°, Ω_2 = 180°} in the invariable plane. All black curves in this figure are taken from the same Mercury6 *N*-body integration underlying the black curves in the left column of Fig. 2. Red curves are for a test particle integrated using Lagrange's equations of motion for the octupolar Hamiltonian (*39*). The bottom row is computed by separating the Hamiltonian into the quadrupolar terms (dotted line) and octupolar plus general-relativistic terms (solid line); by evaluating their respective contributions to ϖ_1 using Lagrange's equations of motion; and by integrating ϖ_1, setting the constant of integration to zero for simplicity. (The quantities *e* and i_{mut} are computed from the full Hamiltonian.) The sum of the dotted and solid curves in the bottom row equals the deviation of the red curve in the third row from its initial value. The secular behavior of the test particle reproduces qualitatively well that of the full *N*-body integration.

The apsidal libration we observed has been seen in other celestial mechanical contexts; it is qualitatively similar to the "artichoke-shaped" (*37*) libration exhibited by Saturn's irregular satellites Narvi (*38*) and, for some initial conditions, Pasiphae (*37*, *39*). Both Narvi and Pasiphae orbit Saturn with inclinations of ~140° with respect to the plane of Saturn's orbit about the Sun. In the context of triple stellar systems, "beatlike" patterns with superposed short– and long–time scale oscillations, similar to those shown in Fig. 2, were noticed in the modeled eccentricity variations of systems with i_{mut} ~ 40° and attributed to interference between the quadrupolar and octupolar potentials (*40*). The configurations of interest here do not lie near any border between circulation and libration; i.e., $\Delta\varpi_{inv}$ librates about 180° with an amplitude of 90°, not 180°. In particular, the dynamics responsible for how $|\Delta\varpi_{inv}|$ lingers near 90° is dissimilar from the "borderline" behavior of nearly coplanar systems in which $|\Delta\varpi_{inv}|$ speeds through 180° but does not linger near 90° (*41*, *42*).

We can reproduce the observed libration of $\Delta\varpi_{inv}$ by approximating a warm Jupiter as a test particle perturbed by an exterior body and solving Lagrange's equations of motion using a secular disturbing potential expanded to octupolar order (*39*), including general-relativistic precession of both planets' orbits (*35*). The octupolar potential plays an essential role in generating a precession rate $d\Delta\varpi_{inv}/dt$ that cancels, on average, the precession rate induced by the quadrupolar potential; the net result is that $\Delta\varpi_{inv}$ librates. Therefore, the perturber must not only be near enough to dominate general-relativistic precession (*5*, *23*) but must also be eccentric: The strength of the octupolar potential is proportional to the perturber's eccentricity. The importance of the octupolar potential has only recently been recognized in the exoplanet literature (*6*, *40*). A popular application has been to flip an interior body from a prograde to retrograde orbit at large eccentricities (*6*, *43*, *44*, *45*–*47*). A low mutual inclination, well below Kozai's critical angle, is sufficient to spur such a flip if the inner planet's eccentricity is high enough (*46*, *47*). The regime explored

here, which produces warm Jupiters with the observed clustering of $|\Delta\omega_{sky}|$ near 90°, is complementary: Both the inner and outer planets' eccentricities are too modest for the octupolar potential to effect flips, and i_{mut} remains near 40°, a prograde configuration. We deduced that our six systems with warm Jupiters and close friends are prograde, with $i_{mut} \sim 40°$ rather than retrograde with $i_{mut} \sim 140°$, because in the latter case $\omega_{sky,1} + \omega_{sky,2}$ would librate rather than $\omega_{sky,1} - \omega_{sky,2}$ (*39*).

It is no coincidence that our six warm Jupiter systems are all characterized by mutual inclinations abutting Kozai's minimum angle. In our regime in which the quadrupole potential still dominates and planetary eccentricities are low enough to avoid flips, 39° is the inclination that coincides with maximum eccentricity (minimum periapse) and hence maximum tidal dissipation. Orbital decay during this maximum-eccentricity, minimum-inclination phase of the Kozai cycle naturally leads to an abundance of tidally migrated warm Jupiters with i_{mut} near 39° to 65° (*48*). The octupolar potential is not strong enough for our systems to alter this feature of quadrupolar Kozai cycles (*6*, *48*). At the same time, the reason why warm Jupiters have not completed their migration to become hot Jupiters is because of the special octupole-modified nature of their eccentricity variations. The usual (quadrupole) Kozai oscillations of eccentricity, which occur over the short nodal precession period, are modulated by an octupole-induced envelope (*49*) of much longer period following that of apsidal libration (Fig. 3 and figs. S1 to S5). The envelope period is approximately $(a_2/a_1)\,(1 - e_2^2)/e_2$ longer than the Kozai time scale (*46*). This long-period modulation prevents eccentricities from surging too often and renders migration even slower than the "slow Kozai" migration described in (*24*). Such "super slow" evolution is similar to the "step" migration seen at high i_{mut} (*6*), except without the transition from prograde to retrograde orbital motion and the accompanying rapid tidal circularization. In the gentle and intermittent migration considered here, warm Jupiters reach the small periapses characterizing hot Jupiters only at the peaks of their eccentricity envelopes. As a proof of concept, we performed an integration of the secular equations of motion including tidal friction (Fig. 4). The warm Jupiter undergoes super slow tidal migration in which it librates apsidally and stalls in semimajor axis. A libration amplitude for $\Delta\varpi_{inv}$ near 90° enables super slow migration. If the libration amplitude were smaller, or if the apsidal separation were to circulate, then the envelope modulating the eccentricity would be less peaky, and the interior planet would spend more of its time near its maximum eccentricity. If the libration amplitude were larger, then not only would the apsidal separation be more prone to circulate given a small perturbation, but the system would also be more vulnerable to retrograde flips and concomitant eccentricity surges ($e \rightarrow 1$). The upshot of all these scenarios (fig. S7) in which $\Delta\varpi_{inv}$ does not librate with an amplitude of 90° is that tidal migration, once begun, would rapidly complete and spawn a hot Jupiter.

The class of warm Jupiters we have identified is similar to the predicted class of Kozai-oscillating warm Jupiters (*23*), except that here the octupolar field generated by the eccentricity of the exterior perturber plays a starring role in effecting the observed near-orthogonality of periapse directions and in braking tidal migration. The mutual inclination of $i_{mut} \sim 35°$ to 65° that we have inferred from the measured apsidal misalignment attests to how the Kozai mechanism, working between planets, has indeed shaped planetary systems. Although large inclinations between hot Jupiters' orbital planes and the equatorial planes of their host stars are well established, our finding provides evidence that pairs of more-distant giant planets are themselves highly mutually inclined (although still prograde), in stark contrast to the flatness of solar system planets. The origin of such large inclinations is a mystery; planet-planet scattering (*1*) or secular chaos (*2*) are possibilities.

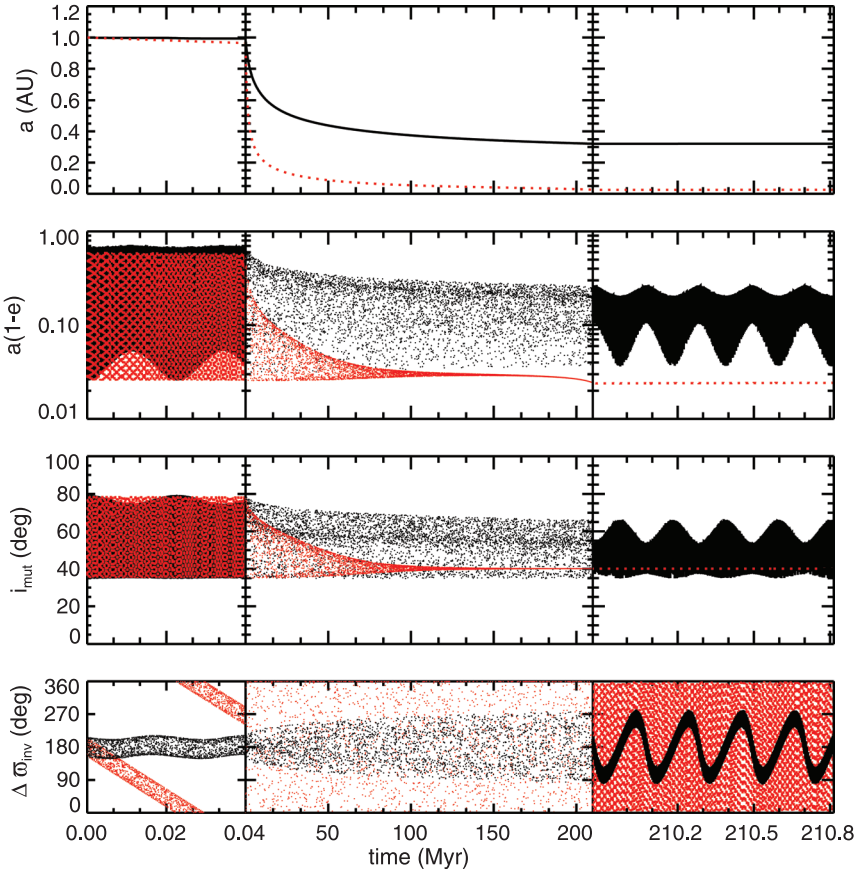


Fig. 4. Tidal migration under a secular potential expanded beyond quadrupolar order can produce a stalled warm Jupiter. Plotted are the time evolution of the inner planet's semimajor axis, periapse distance, mutual inclination with the outer planet, and apsidal separation, integrated using the test particle Hamiltonian expanded to hexadecapolar order (*39*); practically identical results are obtained with the octupolar Hamiltonian. Overplotted are results from the Hamiltonian including only up to quadrupolar terms (red dashed line) in which the inner planet fails to stall and instead becomes a hot Jupiter. General-relativistic precession is included for both planets (*35*). Tidal evolution was implemented using a constant tidal quality factor of 10^5, a Love number of 0.26, and a planetary radius of 1 Jupiter radius (*5*). Tides raised on the star are not included because they are weak compared to tides raised on the planet at these semimajor axes. The tidal forcing frequency is set to $\sqrt{\frac{G(M_* + m_1)}{|a_1(1 - e_1^2)|^3}}$ (*22*). The outer planet has $a_2 = 1.923$ AU, $e_2 = 0.133$, and $m_2 = 6.59\ M_{Jupiter}$, matching HD 147018c, and initial $\{i_2 = 0°, \omega_2 = 17.2°, \Omega_2 = 180°\}$. The inner planet (test particle) has initial $a_1 = 1$ AU, $e_1 = 0.9$, and $\{i_1 = 65°, \omega_1 = 38.4°, \Omega_1 = 0°\}$. With these choices, the eccentricity of the inner planet reaches a minimum of 0.33 at time = 220 years during the first Kozai cycle. The early tidal evolution, over the first ~20 million years, is subject to planet-planet scattering in a full *N*-body treatment; as such, the origin story portrayed in this figure is meant only to illustrate the concept of stalling, not to be definitive. This figure ends at ~200 million years, but similar histories spanning a few billion years are just as possible for different initial conditions or tidal efficiency factors.

REFERENCES AND NOTES

1. F. A. Rasio, E. B. Ford, *Science* **274**, 954–956 (1996).
2. Y. Wu, Y. Lithwick, *Astrophys. J.* **735**, 109 (2011).
3. Y. Kozai, *Astron. J.* **67**, 591 (1962).
4. M. L. Lidov, *Planet. Space Sci.* **9**, 719–759 (1962).

5. Y. Wu, N. Murray, *Astrophys. J.* **589**, 605–614 (2003).
6. S. Naoz, W. M. Farr, Y. Lithwick, F. A. Rasio, J. Teyssandier, *Nature* **473**, 187–189 (2011).
7. G. Takeda, F. A. Rasio, *Astrophys. J.* **627**, 1001–1010 (2005).
8. M. Jurić, S. Tremaine, *Astrophys. J.* **686**, 603–620 (2008).
9. D. Fabrycky, S. Tremaine, *Astrophys. J.* **669**, 1298–1315 (2007).
10. Y. Wu, N. W. Murray, J. M. Ramsahai, *Astrophys. J.* **670**, 820–825 (2007).
11. S. Chatterjee, E. B. Ford, S. Matsumura, F. A. Rasio, *Astrophys. J.* **686**, 580–602 (2008).
12. M. Nagasawa, S. Ida, *Astrophys. J.* **742**, 72 (2011).
13. T. D. Morton, J. A. Johnson, *Astrophys. J.* **738**, 170 (2011).
14. S. Naoz, W. M. Farr, F. A. Rasio, *Astrophys. J. Lett.* **754**, L36 (2012).
15. E. J. Rivera *et al.*, *Astrophys. J.* **719**, 890–899 (2010).
16. R. Sanchis-Ojeda *et al.*, *Nature* **487**, 449–453 (2012).
17. M. H. Lee, S. J. Peale, *Astrophys. J.* **567**, 596–609 (2002).
18. B. E. McArthur *et al.*, *Astrophys. J.* **715**, 1203–1220 (2010).
19. R. I. Dawson *et al.*, *Astrophys. J.* **71**, 89 (2014).
20. A. Cumming *et al.*, *Publ. Astron. Soc. Pac.* **120**, 531–554 (2008).
21. C. Petrovich, S. Tremaine, R. Rafikov, *Astrophys. J.* **786**, 101 (2014).
22. A. Socrates, B. Katz, S. Dong, http://arxiv.org/abs/1209.5724 (2012).
23. S. Dong, B. Katz, A. Socrates, *Astrophys. J. Lett.* **781**, L5 (2014).
24. C. Petrovich, http://arxiv.org/abs/1405.0280 (2014).
25. H. A. Knutson *et al.*, *Astrophys. J.* **785**, 126 (2014).
26. R. I. Dawson, R. A. Murray-Clay, *Astrophys. J. Lett.* **767**, L24 (2013).
27. E. I. Chiang, S. Tabachnik, S. Tremaine, *Astron. J.* **122**, 1607–1615 (2001).
28. T. A. Michtchenko, R. Malhotra, *Icarus* **168**, 237–248 (2004).
29. Queried from the Exoplanet Orbit Database (EOD) at exoplanets.org (*50*) on 8 April 2014.
30. Eccentricity was detected at two-sigma, and $\Delta\omega_{sky}$ was detected with an uncertainty of <40°.
31. We selected for eccentric warm Jupiters with only one known companion, because additional companions can disrupt Kozai oscillations. Our selection criterion thus excludes planetary pairs that are members of the 55 Cnc, upsilon Andromeda, mu Arae, HIP 14810, Kepler-9, and Kepler-30 systems. Moreover, each of these systems also has a close-in (a < 0.1 AU) planet that would be disrupted if the warm Jupiter were to attain periapse distances small enough for tidal circularization.
32. X. Tan *et al.*, *Astrophys. J.* **777**, 101 (2013).
33. For HD 202206c, modification of the semimajor axis from the best-fit value was required to avoid libration in the 5:1 resonance. See the supplementary materials for details.
34. J. E. Chambers, *Mon. Not. R. Astron. Soc.* **304**, 793–799 (1999).
35. D. C. Fabrycky, in *Exoplanets*, S. Seager, Ed. (Univ. of Arizona Press, Tuscon, AZ, 2011), pp. 217–238.
36. D. Veras, E. B. Ford, *Astrophys. J.* **715**, 803–822 (2010).
37. A. L. Whipple, P. J. Shelus, *Icarus* **101**, 265–271 (1993).
38. J. Correa Otto, A. M. Leiva, C. A. Giuppone, C. Beaugé, *Mon. Not. R. Astron. Soc.* **402**, 1959–1968 (2010).
39. T. Yokoyama, M. T. Santos, G. Cardin, O. C. Winter, *Astron. Astrophys.* **401**, 763–772 (2003).
40. E. B. Ford, B. Kozinsky, F. A. Rasio, *Astrophys. J.* **535**, 385–401 (2000).
41. R. Barnes, R. Greenberg, *Astrophys. J. Lett.* **659**, L53–L56 (2007).
42. E. B. Ford, *IAU Symp.* **249**, 441–446 (2008).
43. B. Katz, S. Dong, R. Malhotra, *Phys. Rev. Lett.* **107**, 181101 (2011).
44. Y. Lithwick, S. Naoz, *Astrophys. J.* **742**, 94 (2011).
45. S. Naoz, W. M. Farr, Y. Lithwick, F. A. Rasio, J. Teyssandier, *Mon. Not. R. Astron. Soc.* **431**, 2155–2171 (2013).
46. G. Li, S. Naoz, B. Kocsis, A. Loeb, *Astrophys. J.* **785**, 116 (2014).
47. G. Li, S. Naoz, M. Holman, A. Loeb, *Astrophys. J.* **791**, 86 (2014).
48. L. G. Kiseleva, P. P. Eggleton, S. Mikkola, *Mon. Not. R. Astron. Soc.* **300**, 292–302 (1998).
49. The eccentricity of HD 202206b does not have such an envelope (fig. S5), which may be due to its proximity to the 5:1 mean-motion resonance and the large relative mass of the inner planet.
50. J. T. Wright *et al.*, *Publ. Astron. Soc. Pac.* **123**, 412–422 (2011).
51. Among the black diamonds, the planetary pairs with $|\Delta\omega_{sky}|$ near 90° and large angular momentum ratios include giant planets in a five-planet system (55 Cnc), a pair of hot super-Earths (GJ 163), and a cold Jupiter partnered with a hot Neptune (HD 125612); it is unclear whether their orthogonal eccentricity vectors also signify large mutual inclinations. The transiting pair Kepler-30 c and d, which are near a 2:1 resonance, have $|\Delta\omega_{sky}|$ = 114°, an angular momentum ratio of 21, and a low mutual inclination (*16*).

ACKNOWLEDGMENTS

We gratefully acknowledge support from the Miller Institute for Basic Research in Science, the University of California (UC) Berkeley's Center for Integrative Planetary Science, the National Science Foundation, and the National Aeronautics and Space Administration. This research has made use of the Exoplanet Orbit Database at exoplanets.org. This research employed the SAVIO computational cluster provided by the Berkeley Research Computing program, which is supported by UC Berkeley's Chancellor, Vice Chancellor for Research, and Chief Information Officer. We thank four anonymous referees for constructive feedback and D. Fabrycky and J. Johnson for helpful comments.

SUPPLEMENTARY MATERIALS

www.sciencemag.org/content/346/6206/212/suppl/DC1
Figs. S1 to S7
Table S1
References (*52*–*63*)

4 June 2014; accepted 12 September 2014
10.1126/science.1256943

EARLY UNIVERSE

A local clue to the reionization of the universe

Sanchayeeta Borthakur,[1]* Timothy M. Heckman,[1] Claus Leitherer,[2] Roderik A. Overzier[3]

Identifying the population of galaxies that was responsible for the reionization of the universe is a long-standing quest in astronomy. We present a possible local analog that has an escape fraction of ionizing flux of 21%. Our detection confirms the existence of gaps in the neutral gas enveloping the starburst region. The candidate contains a massive yet highly compact star-forming region. The gaps are most likely created by the unusually strong winds and intense ionizing radiation produced by this extreme object. Our study also validates the indirect technique of using the residual flux in saturated low-ionization interstellar absorption lines for identifying such leaky galaxies. Because direct detection of ionizing flux is impossible at the epoch of reionization, this represents a highly valuable technique for future studies.

The reionization of the universe is a crucial event in cosmic history. Identifying the source(s) responsible for reionization will allow us to understand the underlying physics. Star-forming galaxies are the most likely candidates, but what is their nature? By what process does Lyman continuum radiation, capable of ionizing hydrogen atoms, escape the region of dense and cold gas from which the required population of hot massive stars forms?

Studies to date have had limited success at detecting such candidates. For example, Iwata *et al.* (*1*) found continuum leaking out of 17 galaxies from their sample of 198 star-forming galaxies [Lyman break galaxies (LBGs) and Lyα emitters (LAEs)], whereas Vanzella *et al.* (*2*) found only one such leaking galaxy out of 102 LBGs. Most of the high-redshift studies have resulted in only a handful of detections with substantial escape fractions (*3*, *4*). In some ways, the low incidence of such galaxies is not surprising. Hot massive stars are located in gas-rich regions with column densities ranging from 10^{21} to 10^{24} cm^{-2}. This is 4 to 7 orders of magnitude higher than the column density of H I required to produce an optical depth of unity at the Lyman edge ($N = 1.4 \times 10^{17}$ cm^{-2}). Therefore, extreme conditions may be required for a substantial fraction of the ionizing flux to escape from the galaxy.

Identifying local examples of such leaky galaxies will allow us to study in detail the processes that lead to the escape of Lyman continuum radiation. These local examples can also be used to validate indirect signatures of escaping ionizing flux that are based on the properties of the spectrum at wavelengths longer than the Lyman-α line (see below). This is invaluable, because the spectral region at shorter wavelengths is completely opaque at the epoch of recombination.

We previously uncovered a sample of relatively rare local (redshift $z \approx 0.2$) starburst galaxies whose overall properties [mass, metallicity, size, morphology, star formation rate, kinematics, dust attenuation, etc.] are very similar to those of the LBGs (*5*–*10*). These galaxies are termed Lyman break analog galaxies (LBAs). SDSS J092159.38+450912.3 (hereafter J0921+4509) is one such local LBA (z = 0.23499) that is producing stars at the rate of 50 solar masses ($M_\odot$) per year. It belongs to a special class of LBA where several billion solar masses of stars are produced in an extremely compact central region with a radius of ~100 pc (*11*). Such massive and highly

[1]Center for Astrophysical Sciences, Department of Physics and Astronomy, Johns Hopkins University, Baltimore, MD 21218, USA. [2]Space Telescope Science Institute, 3700 San Martin Drive, Baltimore, MD 21218, USA. [3]Observatório Nacional, Ministry of Science, Technology, and Innovation, Rio de Janeiro, Brazil.
*Corresponding author. E-mail: sanch@pha.jhu.edu

compact star-forming regions are referred to as dominant central objects (DCOs). Because of their compact nature, DCOs can generate extreme winds that were found to propel the surrounding interstellar neutral and ionized gas outward at velocities in excess of 1000 km s^{-1} (*9*).

Three independent but indirect lines of evidence were put forth by Heckman *et al.* (*9*) suggesting that a substantial amount of ionizing radiation could be escaping from this galaxy and others with DCOs. First, these authors found that the strongest interstellar absorption lines tracing the neutral phase of the interstellar medium (ISM) were optically thick (saturated) but still had a substantial residual flux in the line cores [~20 to 30%; see (*9*), figures 4 and 5]. This is an indication that the far-ultraviolet (UV) continuum source, the DCO, is only partially covered by optically thick neutral material. Second, they detected a substantial amount of blue-shifted Lyman-α emission, despite the presence of neutral gas seen in absorption at those velocities. This requires only partial coverage of the starburst region by the outflowing neutral gas. Third, the star formation rate estimated for this galaxy based on the extinction-corrected Hα emission line was smaller by a factor of 3 than the value based on the sum of the far-IR and far-UV continuum luminosities. This could indicate that some of the ionizing flux escapes the galaxy and thus does not produce Hα emission by photoionization and recombination. These properties led Heckman *et al.* (*9*) to speculate that the extreme feedback provided by an extraordinarily compact massive starburst (like a DCO) might be required to enable the escape of ionizing radiation from galaxies.

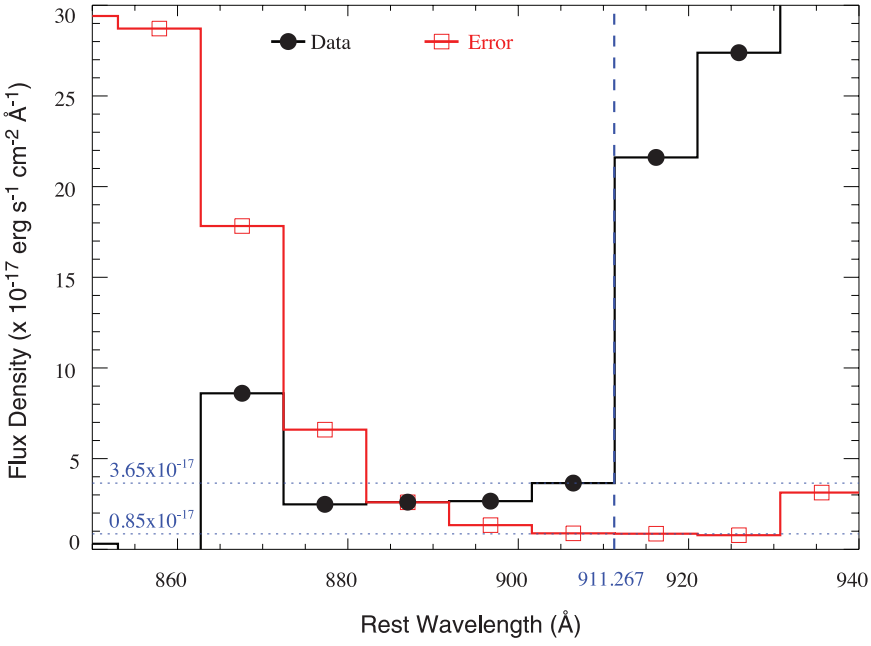


Fig. 1. COS spectra of J0921+4509. Flux density around the rest-frame wavelength 912 Å is shown in black (solid circles) and the associated errors in red (open squares). The flux density and errors were obtained by binning the COS pipeline data by 150 pixels (~10 Å) to increase the signal-to-noise ratio. The dashed blue line marks the position of the Lyman continuum break (≡ 13.6 eV). We detected Lyman continuum flux in the wavelength range 890 to 910 Å. The flux at 910 Å was measured to be 3.7 (±0.8) × 10^{-17} erg s^{-1} cm^{-2} $Å^{-1}$.

To directly confirm the inference of escaping ionizing radiation and compare it to that predicted by the residual flux technique, we conducted a program with the Cosmic Origins Spectrograph (COS) aboard the Hubble Space Telescope (HST) to obtain the spectrum of J0921+4509 below the Lyman edge at 912 Å in the rest frame of the galaxy. The data were obtained in two separate sets of observations (durations 4 and 5 orbits of HST, respectively), which were reduced using the standard COS data reduction pipeline (*12*). The final spectrum (Fig. 1) was produced by binning 150 pixels of the weighted average of the two data sets in order to improve the signal-to-noise ratio. The spectrum was corrected for the Milky Way's dust extinction in the direction of J0921+4509. We report a flux density detection of 3.7 (±0.8) × 10^{-17} erg s^{-1} cm^{-2} $Å^{-1}$ just below the Lyman edge. This corresponds to a luminosity λL_λ, at rest wavelength λ = 910 Å, of 5.0 × 10^{42} erg s^{-1}.

The young stars that produce the ionizing flux also produce strong stellar winds, which can be traced using transitions such as N V and C IV. These transitions are minimally contaminated by interstellar features and have the greatest diagnostic power to identify the underlying stellar populations. The strong P-Cygni profiles in these transitions (Fig. 2) clearly indicate the presence of young massive O stars capable of producing

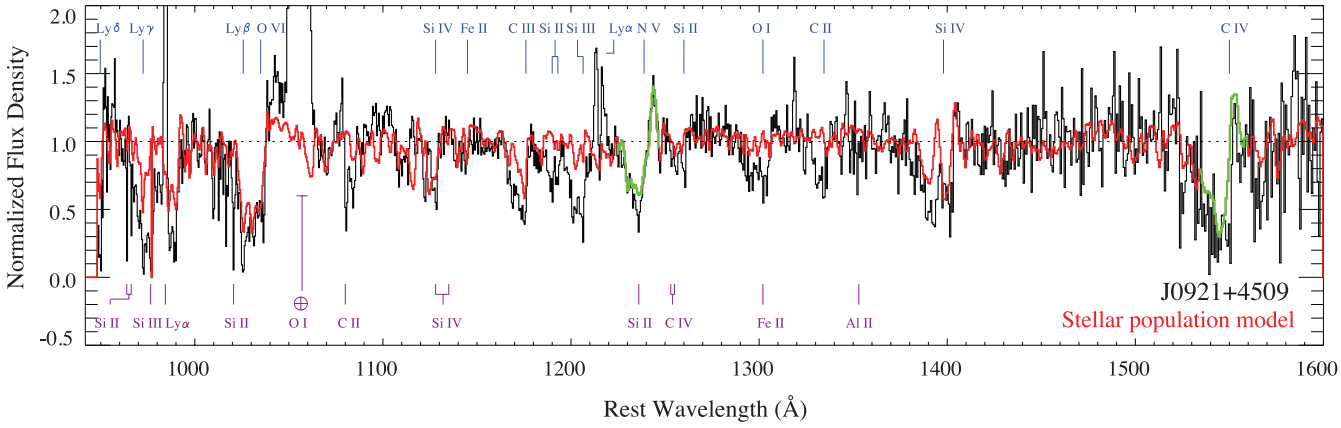


Fig. 2. Young stellar population in J0921+4509. Flux density–normalized combined spectrum from COS G140L (1040 to 1600 Å) and G130M (~950 to 1040 Å) of LBA J0921+4509 (black) overlaid with the best-fit stellar population model (Starburst99) of instantaneous star formation 3 million years ago, solar metallicity, and a Kroupa initial mass function (red). We fitted the high-ionization stellar wind transitions (shown in green) to evaluate the best stellar population model. The transitions associated with J0921+4509 are marked in blue above the spectrum; Milky Way and geocoronal features are marked in purple in the space below the spectrum. The J0921+4509 spectrum shows prominent P-Cygni profiles from the stellar winds (e.g., O VI λλ1032, 1038, N V λλ1239,1243, C IV λλ1548, 1551). This confirms the presence of a young stellar population with massive O stars in this galaxy.

substantial amounts of ionizing radiation. A stellar population model (*13*) of an instantaneous burst 3 million years ago and a Kroupa initial mass function describes our data best, thus suggesting that J0921+4509 has a large fraction of extremely young and massive stars.

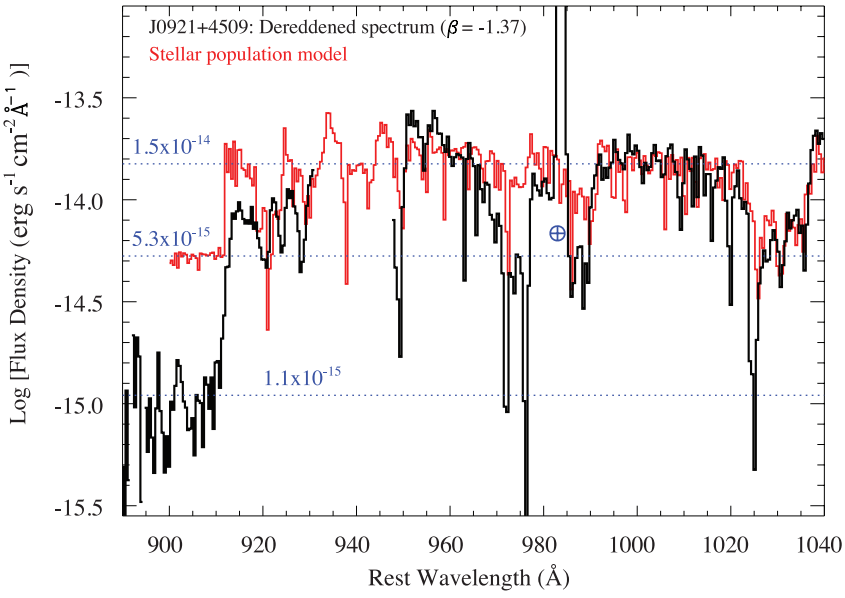


Fig. 3. Lyman continuum escape fraction. The black line denotes the COS spectrum of J0921+4509 between 890 and 1040 Å in the rest-frame of the galaxy. The spectrum was corrected for dust attenuation (*21*) corresponding to the observed UV slope of β = −1.37 in J0921+4509. The best-fit stellar population model is shown in red and has been normalized to match flux density of the data between 960 and 1040 Å. Dotted lines indicate the observed and predicted (by model) flux densities at the Lyman edge (900 to 910 Å) and at wavelengths between 1000 and 1020 Å. The ratio of strength of the observed drop to the theoretical drop represents the dust-free escape fraction.

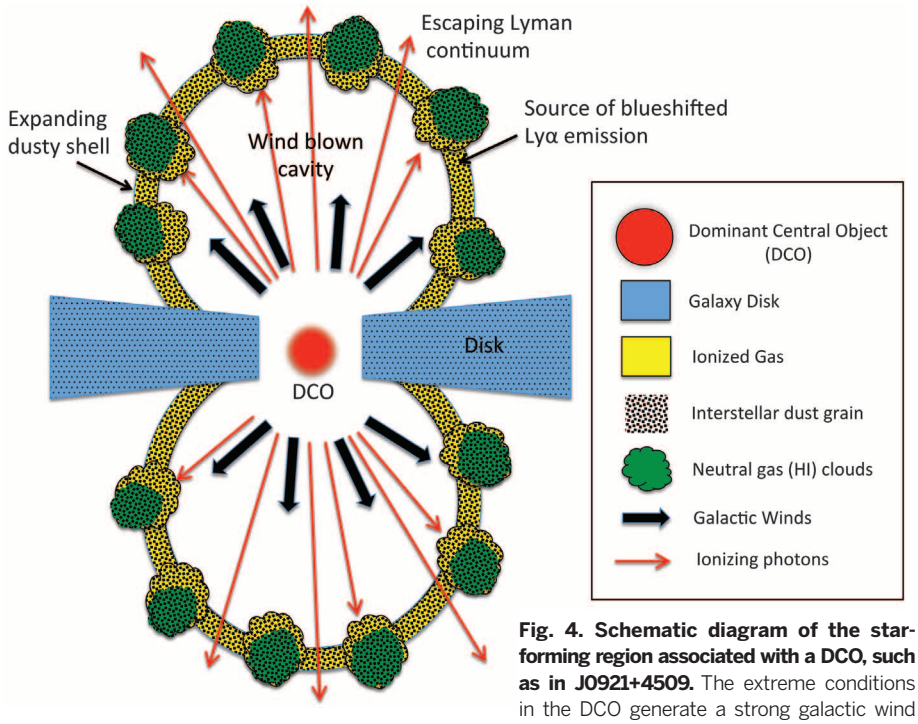


Fig. 4. Schematic diagram of the star-forming region associated with a DCO, such as in J0921+4509. The extreme conditions in the DCO generate a strong galactic wind and large quantities of ionizing flux that clear out a cavity (windblown cavity in the figure) and parts of the neutral gas cover. However, the entire region is covered by dust. The neutral gas cover contains gaps, where the gas becomes completely ionized and consequently has negligible optical depth due to photoelectric absorption of Lyman continuum photons by hydrogen. Thus, these gaps facilitate the escape of Lyman continuum and Lyman-α photons.

Before describing how we quantified the escaping ionizing radiation in this galaxy, it is important to distinguish between two sources of opacity provided by the galaxy's ISM. The first is the dust. Opacity due to dust suppresses the amount of escaping UV light by an amount that gradually and smoothly increases with decreasing wavelength. It therefore renders the UV continuum fainter and redder, but does not produce any signature across the Lyman edge at 912 Å. The second source of opacity is associated with photoelectric absorption by neutral hydrogen, which will produce a sharp drop in flux density at the Lyman edge. For simplicity, we describe these two sources of opacity separately.

First, we consider the effects of photoelectric absorption in the absence of dust (the dust-free case). The stellar population model predicts the intrinsic ratio of ionizing to nonionizing flux (i.e., the drop in flux at the Lyman edge in the absence of photoelectric absorption by the interstellar medium). A comparison of the drop in flux density between our observed data and the normalized best stellar population model describing the stellar wind lines (Fig. 3) gives us a measure of the fraction of Lyman continuum photons that suffer photoelectric absorption by atomic hydrogen in the ISM of the galaxy. In mathematical terms,

$$f_{\mathrm{esc}}^{\text{dust free}} = \frac{\left(\frac{F_{\lambda 912-}}{F_{\lambda 912+}}\right)_{\text{observed}}}{\left(\frac{F_{\lambda 912-}}{F_{\lambda 912+}}\right)_{\text{norm. model}}} \qquad (1)$$

where $F_{\lambda 912-}$ and $F_{\lambda 912+}$ are the fluxes below and above 912 Å. $F_{\lambda 912-}$ was measured by averaging the flux density over 10 Å below the Lyman break (Fig. 1). To avoid the effects of the confluence of the stellar and interstellar Lyman series absorption lines near the Lyman edge, we measured $F_{\lambda 912+}$ in a window between 1000 and 1020 Å (beyond Lyman γ). The observed drop in flux density relative to the stellar population model implies a value for $f_{\mathrm{esc}}^{\text{dust free}} \equiv 21 \pm 5\%$. The inferred incompleteness in coverage, f_{cov}, of the starburst region by optically thick neutral material predicts $f_{\mathrm{esc}}^{\text{dust free}} \equiv 1 - f_{\mathrm{cov}}$, which in turn is equal to the residual flux. Our measurement of $f_{\mathrm{esc}}^{\text{dust free}}$ is in good agreement with the estimate based on the residual flux (~20 to 30%) in the strongest interstellar absorption lines (*9*).

We can now consider the effect of dust absorption. Here we are concerned with estimating what we call the absolute escape fraction of Lyman continuum photons, attributable to the combined

Table 1. Properties of the target galaxy J0921+4509 (*7*).

Redshift	0.235
Stellar mass [log M_* ($M_\odot$)]	10.8
DCO mass [log M_* ($M_\odot$)]	9.0 to 9.2
Metallicity [12 + log(O/H)]	8.67
Star formation rate, Hα + 24 μm ($M_\odot$ year^{-1})	55.1
Dust content (β_{rest})	−1.37

effect of photoelectric absorption and dust extinction. Thus, we want to estimate the ratio between the observed luminosity of the escaping ionizing radiation and the intrinsic luminosity (in the absence of both dust and neutral hydrogen). The amount of dust absorption in the far UV is substantial in this galaxy: The ratio of UV to infrared (IR) flux is just ~10% (*7*). Assuming that the IR and UV luminosities dominate the bolometric luminosity ($L_{bol} \approx L_{UV} + L_{IR}$), we adopt the definition of the absolute escape fraction $f_{esc,abs}$ as described in (*14*):

$$f_{esc,abs} = \frac{L_{ioniz,esc}}{L_{UV} + L_{IR}} \left(\frac{L_{bol}}{L_{ioniz}} \right)_{intrinsic} \quad (2)$$

We estimate the escaping Lyman continuum luminosity $L_{ioniz,esc}$ from the data by measuring the parameter λL_λ just below the Lyman continuum break and correcting it by a factor as follows:

$$L_{ioniz,esc} = (\lambda L_\lambda)^{observed}_{\lambda=912\text{Å}} \left(\frac{L_{ioniz}}{(\lambda L_\lambda)_{\lambda=912\text{Å}}} \right)^{intrinsic} \quad (3)$$

The best-fit stellar population model predicts the intrinsic ratio L_{bol}/L_{ioniz} to be ~4, and the correction factor of Eq. 3 to be 0.9. This leads to an estimate of $f_{esc,abs} \approx 1\%$.

The difference between $f_{esc}^{dust\ free}$ and $f_{esc,abs}$ is due to the absorption of ionizing radiation by dust. It also indicates that the covering fractions of the neutral gas and the dust are not the same. Whereas the distribution of neutral gas evidently has gaps or holes, the dust almost fully covers the entire star-forming region. From this observation, we conclude that most of the dust absorption in this galaxy is associated with the ionized gas, consistent with the arguments given in (*9*). Thus, strong feedback from the starburst, in the form of ionizing radiation and shock heating by the galactic wind, is able to fully ionize holes in the distribution of neutral gas that envelops the starburst region. In these holes, the gas is fully ionized and allows the Lyman continuum photons to escape. However, the dust survives and is able to absorb both the ionizing and nonionizing UV photons (Fig. 4). The holes contain ionized gas with negligible optical depth due to photoelectric absorption for Lyman continuum photons, and also dust.

How relevant is the knowledge gained from J0921+4509 for understanding the sources responsible for reionization, given that it is highly obscured by dust? The good news is that the physics behind the creation of the holes that allow Lyman continuum to escape may be valid for any compact starburst. Such compact starburst galaxies are commonly seen at high redshifts (*15*). In fact, the highest-redshift galaxy known to date (z = 10.7) has a size (~200 pc) and stellar mass (10^8 to 10^9 $M_\odot$) (*16*) similar to the starburst in J0921+4509. On the other hand, mounting evidence from deep surveys of the early universe with the HST implies that the amount of dust absorption in star-forming galaxies is very small at the highest redshifts (*17*). This is most plausibly caused by the much lower metallicities (and hence lower dust-to-gas ratios) in these early galaxies. Recently, an intensely star-forming galaxy with very low dust and metals at $z \approx 7$ was discovered (*18*). Therefore, although dusty objects like J0921+4509 would not be good candidates for the population of galaxies that reionized the universe, similar analogs from the early universe that are compact but nearly dust-free would be excellent candidates.

It is important to reemphasize that the opacity due to neutral hydrogen in the intergalactic medium (IGM) during the epoch of reionization ($z \approx 6$ to 11) is so large that there is no hope of directly observing flux below the Lyman edge from these early galaxies and directly measuring the escape fraction. The idea that the amount of residual flux in the cores of saturated interstellar absorption lines that trace the neutral gas can serve as a proxy measurement of the escape fraction was proposed by Heckman *et al.* in 2001 (*19*), applied by Grimes *et al.* in 2009 (*14*) to a sample of local starbursts, and then applied by Heckman *et al.* (*9*) to a sample of LBAs. This idea has recently been extended to high-redshift galaxies by Jones *et al.* (*20*). Our study has validated this indirect technique. The direct value we measure for $f_{esc}^{dust\ free}$ in J0921+4509 is similar to the indirect estimate in (*9*).

REFERENCES AND NOTES

1. I. Iwata *et al.*, *Astrophys. J.* **692**, 1287–1293 (2009).
2. E. Vanzella *et al.*, *Astrophys. J.* **725**, 1011–1031 (2010).
3. D. B. Nestor, A. E. Shapley, K. A. Kornei, C. C. Steidel, B. Siana, *Astrophys. J.* **765**, 47 (2013).
4. R. E. Mostardi *et al.*, *Astrophys. J.* **779**, 65 (2013).
5. C. G. Hoopes *et al.*, *Astrophys. J. Suppl. Ser.* **173**, 441 (2007).
6. R. A. Overzier *et al.*, *Astrophys. J.* **710**, 979–991 (2010).
7. R. A. Overzier *et al.*, *Astrophys. J.* **726**, L7 (2011).
8. T. S. Gonçalves *et al.*, *Astrophys. J.* **724**, 1373–1388 (2010).
9. T. M. Heckman *et al.*, *Astrophys. J.* **730**, 5 (2011).
10. A. R. Basu-Zych *et al.*, *Astrophys. J.* **774**, 152 (2013).
11. R. A. Overzier *et al.*, *Astrophys. J.* **706**, 203–222 (2009).
12. D. Massa *et al.*, *COS Data Handbook, Version 2.0* (STScI, Baltimore, 2013).
13. C. Leitherer *et al.*, *Astrophys. J. Suppl. Ser.* **189**, 309–335 (2010).
14. J. P. Grimes *et al.*, *Astrophys. J. Suppl. Ser.* **181**, 272–320 (2009).
15. K.-H. Huang, H. C. Ferguson, S. Ravindranath, J. Su, *Astrophys. J.* **765**, 68 (2013).
16. D. Coe *et al.*, *Astrophys. J.* **762**, 32 (2013).
17. R. J. Bouwens *et al.*, http://arxiv.org/abs/1306.2950 (2013).
18. M. Ouchi *et al.*, *Astrophys. J.* **778**, 102 (2013).
19. T. M. Heckman *et al.*, *Astrophys. J.* **558**, 56–62 (2001).
20. T. A. Jones, R. S. Ellis, M. A. Schenker, D. P. Stark, *Astrophys. J.* **779**, 52 (2013).
21. I. C. Leitherer, I.-H. Li, D. Calzetti, T. M. Heckman, *Astrophys. J. Suppl. Ser.* **140**, 303–329 (2002).

ACKNOWLEDGMENTS

We thank A. Aloisi for assistance during the observations of this project, and the reviewers for their comments. S.B. is supported by a grant under program 12886 provided by NASA through a grant from the Space Telescope Science Institute, which is operated by the Association of Universities for Research in Astronomy Inc. under NASA contract NAS5-26555. Data used for this paper are publicly available in the Mikulski Archive for Space Telescopes (MAST) under programs 12886 and 11727.

1 April 2014; accepted 20 August 2014
10.1126/science.1254214

ORGANIC SYNTHESIS

Asymmetric syntheses of sceptrin and massadine and evidence for biosynthetic enantiodivergence

Zhiqiang Ma,[1]* Xiaolei Wang,[1]* Xiao Wang,[1] Rodrigo A. Rodriguez,[2] Curtis E. Moore,[3] Shuanhu Gao,[1] Xianghui Tan,[1] Yuyong Ma,[1] Arnold L. Rheingold,[3] Phil S. Baran,[2] Chuo Chen[1]†

Cycloaddition is an essential tool in chemical synthesis. Instead of using light or heat as a driving force, marine sponges promote cycloaddition with a more versatile but poorly understood mechanism in producing pyrrole–imidazole alkaloids sceptrin, massadine, and ageliferin. Through de novo synthesis of sceptrin and massadine, we show that sponges may use single-electron oxidation as a central mechanism to promote three different types of cycloaddition. Additionally, we provide surprising evidence that, in contrast to previous reports, sceptrin, massadine, and ageliferin have mismatched chirality. Therefore, massadine cannot be an oxidative rearrangement product of sceptrin or ageliferin, as is commonly believed. Taken together, our results demonstrate unconventional chemical approaches to achieving cycloaddition reactions in synthesis and uncover enantiodivergence as a new biosynthetic paradigm for natural products.

The dimeric pyrrole–imidazole alkaloids are structurally complex small molecules produced by marine sponges through reactions that are not well understood (*1*) (Fig. 1 and figs. S1 and S2). These natural products are highly polar, noncrystalline, redox labile, and pH sensitive because of their exceptionally high nitrogen content (~16% atomic composition or 15 to 30% by weight). The presence of multiple halogen atoms further contributes to their chemical instability and synthetic challenges (*2*–*21*). As depicted in Fig. 1, sceptrin (**1a**) (*22*), massadine (**2a**) (*23*, *24*), and ageliferin (**3a**) (*25*, *26*) are family members derived from formal

[2+2], [3+2], and [4+2] cycloaddition reactions of oroidin (**4a**), hymenidin (**4b**), or their congeners. Our previous studies on the de novo synthesis of ageliferins (**3**) (*4*, *14*, *15*) suggest that the biogenic dimerization of **4** is likely a radical reaction. We now describe the de novo syntheses of sceptrin (**1a**) and massadine (**2a**), using oxidative reactions that are suspected to be involved in their biosyntheses. These asymmetric syntheses along with two new crystal structures allow us to unambiguously assign the absolute stereochemistries of the pyrrole–imidazole dimers. We also demonstrate that the [3+2] dimers cannot be derived from the [4+2] or [2+2] dimers through a skeletal rearrangement reaction. Instead, a surprising enantiodivergent pathway must be involved in the biosynthesis of these alkaloids.

Sceptrin (**1a**) is the first dimeric pyrrole–imidazole alkaloid discovered in nature (*22*). Because there is insufficient light where the sponges live (20 to 30 m below the ocean surface), it is unlikely for hymenidin (**4b**) to undergo a photocycloaddition reaction to give **1a** biogenically (*2*, *22*). In addition, a [2+2] photocycloaddition reaction of **4b** would lead to the formation of racemic **1a,** whereas the isolated **1a** was optically active. Based on results of metabiosynthetic experiments, Molinski and Romo proposed an enzyme-promoted single-electron transfer (SET) mechanism for the biogenic dimerization of **4** (*27*). We believe that a SET oxidation of **4** would give radical cation $\mathbf{4}^{\bullet+}$ that is highly reactive toward [2+2] (path a) and [4+2] (path b) cycloaddition reactions to afford $\mathbf{1}^{\bullet+}$ and $\mathbf{3}^{\bullet+}$, correspondingly (Fig. 1). Subsequent back-SET would provide sceptrins (**1**) and "iso-ageliferins" (**5**) that tautomerize to ageliferins (**3**).

Massadine (**2a**) is a densely functionalized polycyclic [3+2] dimer that contains 8 contiguous stereocenters, 10 nitrogen atoms, and multiple sensitive functional groups. These structural features preclude the use of many traditional tools for its synthesis. Because enzymes that promote [3+2] cycloaddition reactions remain elusive, it is commonly believed that **2a** is derived from **5** through an oxidative skeletal rearrangement reaction (*13*, *28*, *29*). Oxidation of **5** would induce a ring-contraction reaction to give "pre-massadine" (**6**). Further oxidation of **6** would provide **2** and its congeners via different modes of cyclization (*1*, *30*). This oxidative rearrangement hypothesis was first proposed by Scheuer for palau'amine (*28*) and recently modified by us (*13*), Al-Mourabit, and Romo (*1*) to account for its revised relative stereochemistry. The chemical viability of this skeletal rearrangement through two-electron oxidation has also been demonstrated by Romo, Lovely, and us (*5*, *12*, *18*, *19*).

[1]Department of Biochemistry, The University of Texas Southwestern Medical Center, Dallas, TX 75390, USA. [2]Department of Chemistry, The Scripps Research Institute, La Jolla, CA 92037, USA. [3]Department of Chemistry and Biochemistry, University of California San Diego, La Jolla, CA 92093, USA.
*These authors contributed equally to this work †Corresponding author. E-mail: chuo.chen@utsouthwestern.edu

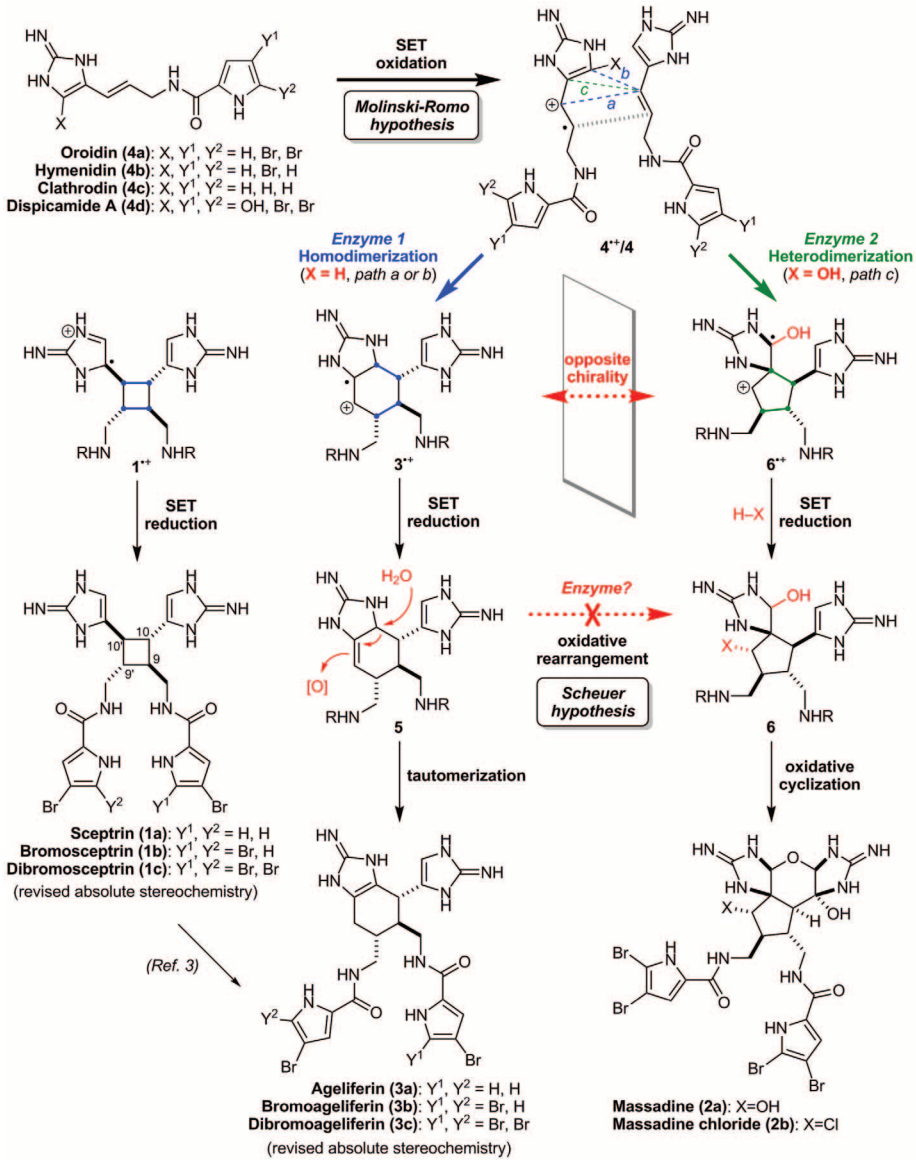


Fig. 1. The enantiodivergent biosynthetic pathways for the dimeric pyrrole-imidazole alkaloids. The biosyntheses of the [2+2] dimers sceptrins (**1**) and the [4+2] dimers ageliferins (**3**) involve a homodimerization of oroidin (**4a**) or hymenidin (**4b**). SET oxidation of **4** promotes a [2+2] cycloaddition reaction of $\mathbf{4}^{\bullet+}/\mathbf{4}$ to give $\mathbf{1}^{\bullet+}$ (path a), or a [4+2] cycloaddition reaction to give $\mathbf{3}^{\bullet+}$ (path b). Subsequent SET reduction yields **1** and **5** that aromatize to **3**. In contrast, the biosyntheses of the [3+2] dimers massadines (**2**) involve a heterodimerization of dispacamide A (**4d**) and oroidin (**4a**). SET oxidation of **4d** promotes a [3+2] cycloaddition reaction of $\mathbf{4d}^{\bullet+}/\mathbf{4a}$ to give $\mathbf{6}^{\bullet+}$. Subsequent SET reduction, protonation, and trapping with water or chloride provide "pre-massadines" (**6**). Oxidative cyclization of **6** gives massadines (**2**). The homodimerization (path a and b) and heterodimerization (path c) of **4** are enantiomeric pathways.

We were interested in using chemical synthesis to evaluate the Molinski-Romo and Scheuer biosynthetic hypotheses. The prior synthesis of sceptrin (**1a**) by Birman (*20*) and us (*2*, *4*, *5*) involved the construction of the cyclobutane ring by forming the C9/C10 and C9′/C10′ bonds using a [2+2] photocycloaddition reaction. The synthesis described herein involves the alternative formation of the C9/C9′ and C10/C10′ bonds (biogenic connection) via a SET-promoted [2+2] cycloaddition reaction (Molinski-Romo hypothesis). The synthesis of massadine (**2a**) has also been achieved by us, using an intramolecular aldol reaction (*8*) or a Pauson-Khand reaction (*10*) to construct the central cyclopentane ring. We now describe a complementary synthesis that involves an oxidative rearrangement (Scheuer hypothesis) of a dibromoageliferin derivative (*14*, *15*), using an oxidative radical cyclization reaction as the key step.

We first set out to develop an asymmetric synthesis of sceptrin (**1a**) using a SET-mediated [2+2] cycloaddition reaction to construct its core skeleton (Fig. 2). L-Glutamic acid (**7**) was used as the source of chirality to establish the absolute stereochemistry of our synthetic **1a**. Diazotization of **7** induced an anchimeric lactonization to give (*S*)-(+)-5-oxo-2-tetrahydrofurancarboxylic acid (**8**), a commercially available chiral building block. Dihydrofuran **9** was then prepared from **8** through reduction, silylation, and dehydration. Electrophilic selenation of **9** proceeded from the less hindered face, allowing alcohol **10** to approach from the more hindered face of **9** with excellent stereoselectivity. Subsequent oxidative elimination of the phenylselenyl group and reduction of the azido group provided **11** with *cis*-C8/C11 stereochemistry, setting the stage for the key [2+2] cycloaddition reaction.

Whereas treating **11** with a variety of single-electron oxidants (*31*) resulted in complete decomposition, the photoredox method developed by Yoon (*32*) promoted the reversible SET reactions of **11** smoothly. Irradiation of a solution of **11** with a catalytic amount of $Ir(ppy)_3$ induced the [2+2] cycloaddition to give **12** [diastereomeric ratio (d.r.) 1.8:1 at C10′]. Although this cycloaddition reaction could also proceed

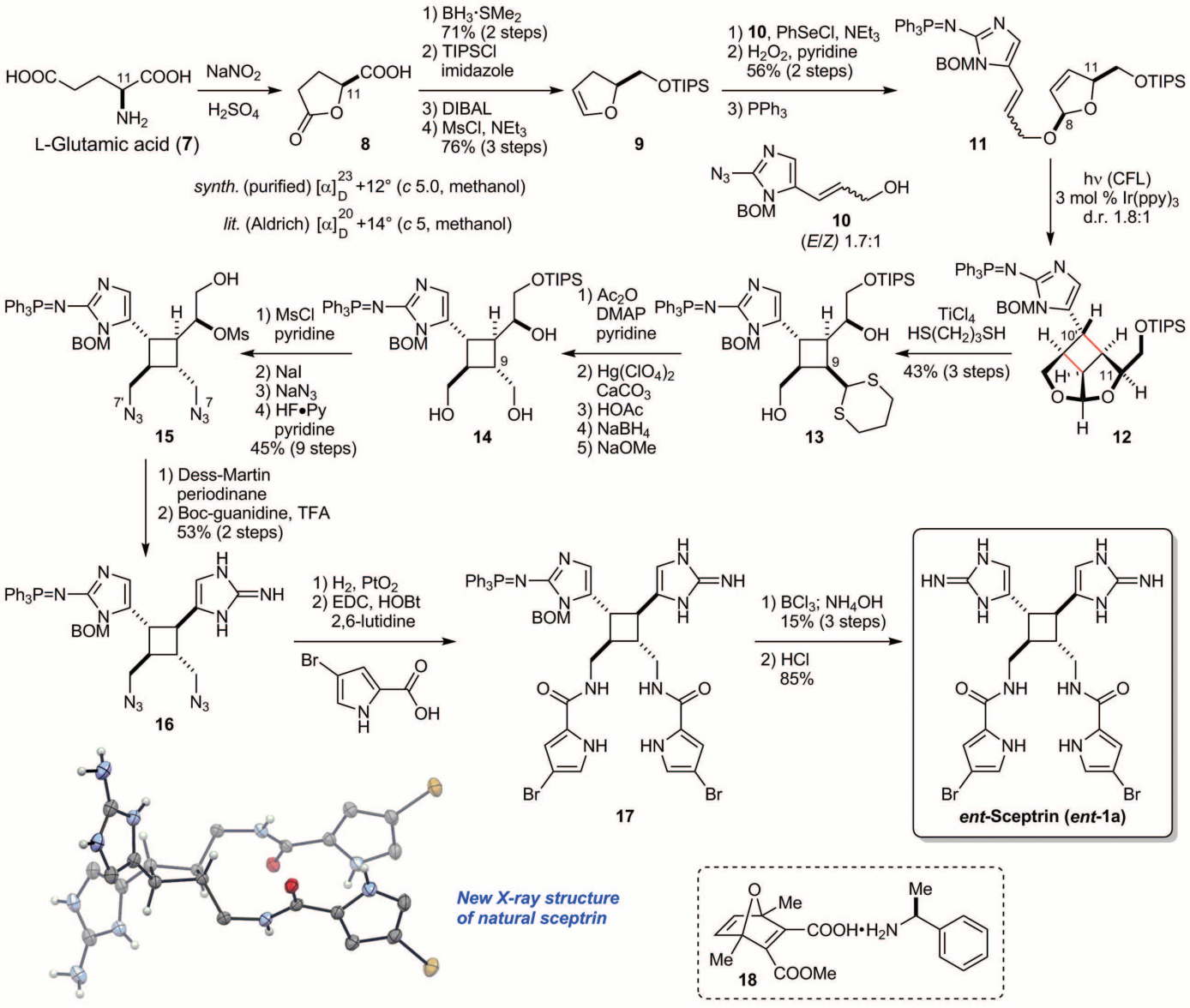


Fig. 2. Biomimetic synthesis of sceptrin and revision of its absolute stereochemistry. The key step involves a SET-mediated [2+2] cycloaddition reaction that mechanistically mimics the biogenic dimerization of hymenidin (**4b**). *ent*-Sceptrin was obtained while targeting the originally reported absolute stereochemistry. A new crystal structure of natural sceptrin (shown in ORTEP representation) confirms that its absolute stereochemistry needs to be revised. TIPS, triisopropylsilyl; DIBAL, diisobutylaluminium hydride; Ms, methanesulfonyl; BOM, benzyloxymethyl; CFL, compact fluorescent lamp; DMAP, 4-(dimethylamino)pyridine; Boc, *tert*-butyloxycarbonyl; EDC, 1-ethyl-3-(3-dimethylaminopropyl)carbodiimide; HOBt, 1-hydroxybenzotriazole.

through an energy transfer mechanism (*33*), 9-fluorenone, which has the same triplet energy (E_T = 55 kcal/mol) as $Ir(ppy)_3$ (*34*, *35*), could not catalyze this reaction. Therefore, we believe that the [2+2] cycloaddition of **11** was induced by reversible SET between $Ir(ppy)_3$ and the aminoimidazole group of **11**.

To complete the synthesis of sceptrin (**1a**), we used transthioketalization to reveal the cyclobutane core skeleton in **12**. The requisite all-trans configuration of the central cyclobutane core was furnished by epimerization of the C9 stereogenic center after protecting the hydroxyl groups and hydrolyzing the dithiane group of **13**. Subsequent reduction of the aldehyde group and deacetylation provided triol **14**. With the sceptrin core skeleton in hand, we then functionalized the side chains to install the second aminoimidazole group and the two pyrrole groups. The N7 and N7′ groups were introduced by sequential mesylation, iodination, and azidation. Subsequent desilylation gave bisazide **15**. The second aminoimidazole group was constructed by oxidizing the hydroxyl group of **15** and treating the resulting unstable mesyl aldehyde with Boc-guanidine. The azido groups of **16** were next reduced, and the pyrrole groups were introduced to give **17**. Removal of the protecting groups of **17** afforded sceptrin (**1a**) (0.4% yield from L-glutamic acid).

Although we targeted the synthesis of sceptrin in its presumed natural enantiomeric form, the circular dichroism (CD) spectrum of our synthetic sceptrin (fig. S3) was the reverse of the natural samples' spectrum (*4*, *36*). In our synthesis, the absolute stereochemistry of sceptrin was established by the intramolecular [2+2] cycloaddition reaction of **11**. The structure of the resulting pseudo-symmetric product **12** was determined by nuclear magnetic resonance (NMR) experiments. The rigid, cagelike structure of **12** rendered NMR a reliable tool for assigning its relative stereochemistry. We thus suspected that the original absolute stereochemistry of sceptrin was misassigned.

The absolute stereochemistry of sceptrin was determined in 1981 by Faulkner and Clardy through x-ray crystallographic analysis (fig. S1) (*22*). Although the Hamilton test favored *ent*-**1a**, the difference in the *R* factors was small (0.090 versus 0.094). In our previous synthetic study (*4*), a crystal of intermediate **18** was obtained from co-crystalization with (*S*)-α-methylbenzylamine. Although it supports the original assignment, the acid (**18**) used had only 75% enantiomeric excess. In light of our above-described findings, the ambiguity associated with enantio-impure sample of **18**, and the unconvincing x-ray data by modern standards, we recrystallized a natural sample of sceptrin and used anomalous dispersion to determine its absolute stereochemistry. A suitable crystal was obtained with a slowly evaporating (4°C) biphasic mixture of ethyl acetate and water (1:10). With a Flack factor of −0.002(5) for **1a**, we concluded that the previously reported absolute stereochemistry of sceptrin was incorrect. Because the absolute stereochemistry of ageliferin was determined based on that of sceptrin (*4*), this result suggests that a revision is also needed for ageliferin.

Previously, we targeted the synthesis of ageliferin via **19** using L-serine as the source of chirality (*14*, *15*). However, we obtained *ent*-ageliferin instead of the expected *nat*-ageliferin (figs. S4 and S5). In light of the revision of the absolute stereochemistry of sceptrin (**1a**), we reinvestigated the structural assignment of **19** (Fig. 3). Reduction of the azido and carbonyl groups of **19** followed by oxidation with dimethyldioxirane (DMDO) induced the Scheuer-type rearrangement (*5*, *12*, *18*, *19*) to give **20**. The absolute and relative stereochemistry of **20** was determined by x-ray crystallographic analysis of its crystalline derivative **21**. The C9/C10/C11 relative stereochemistry of **21** is consistent with that of **19** instead of **22**, a structure that would be consistent with the original *ent*-ageliferin (fig. S5). The absolute stereochemistry of **21** determined by anomalous x-ray scattering is also consistent with the chirality of L-serine. These experiments provide independent evidence that the absolute stereochemistry of ageliferin also needs to be revised.

After completing the biomimetic synthesis of sceptrin (**1a**), we turned our attention to the asymmetric synthesis of massadine (**2a**). We chose to carry out the Scheuer-type oxidation on **23**, a protected 10′-oxo-dibromoageliferin, to best mimic the putative Scheuer biosynthetic pathway (Fig. 4). Although we could induce the ring-contraction reaction with various oxidative methods, the undesired spiro-configuration was always obtained (*15*). We envisioned that the C10′ oxygen functionality of **23** could be used as a directing group (*37*) to reverse this stereoselectivity. Indeed, reduction of **23** with $LiBHEt_3$ gave **24** bearing the desired hydroxyl configuration. Oxidation of **24** with $Ti(O^iPr)_4$/TBHP induced the Scheuer-type ring contraction to give iminohydantoin **25** with the desired spiro configuration. This Ti(IV)-promoted oxidation was markedly chemo- and stereoselective. It only oxidized the more electron-rich aminoimidazole group in the presence of an unprotected aminoimidazole and two dibromopyrroles. It was also the only method that could provide the correct spiro configuration. Although alcohol **24** was

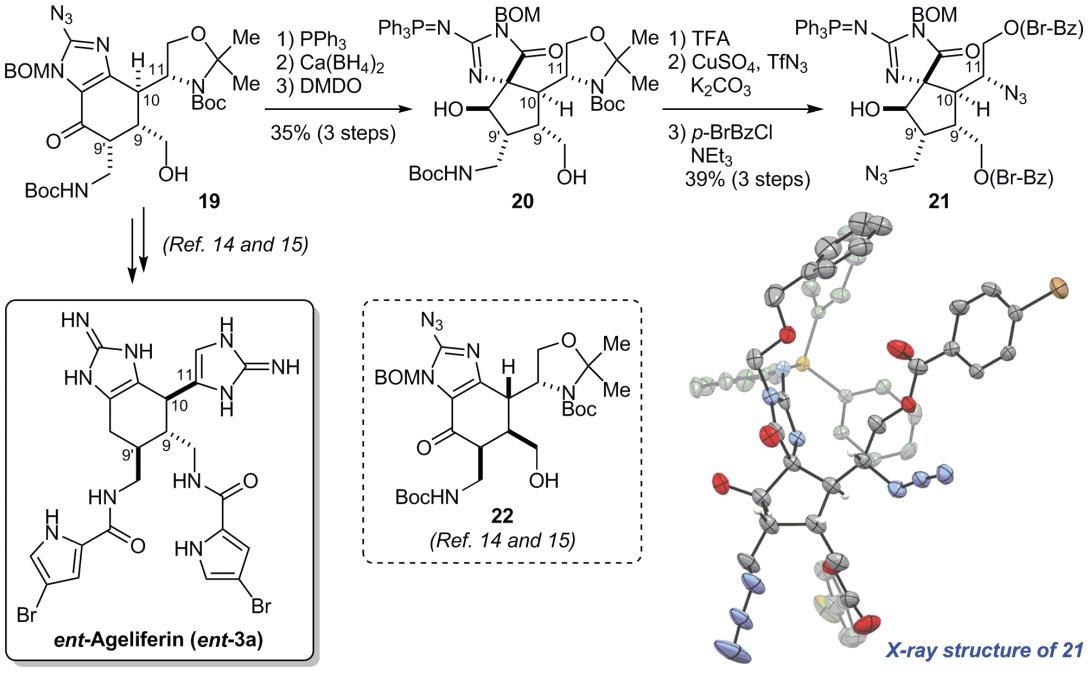


Fig. 3. Revision of the absolute stereochemistry of ageliferin (3a). Oxidative ring-contraction of **19**, the key intermediate in our ageliferin synthesis, gave **20** that bears a massadine core skeleton. The crystal structure of its crystalline derivative **21** (shown in ORTEP representation) confirms that the absolute stereochemistry of ageliferin needs to be revised. DMDO, dimethyldioxirane; TFA, trifluoroacetic acid; Br-Bz, 4-bromobenzoyl.

only stable as an acid salt, the $Ti(O^iPr)_4$/TBHP-oxidation reaction failed completely under even slightly acidic conditions. Therefore, we washed **24**•TFA with base and used it immediately to give **25** with good reproducibility. Without purification, **25** was reduced with $Ca(BH_4)_2$ to afford hemiaminal **26**. Subsequent removal of the protecting groups gave "pre-massadine" (**6**).

To complete the synthesis of massadine (**2a**), we would need to selectively oxidize the aminoimidazole group of **6** and promote the intramolecular cyclization to form the oxygen bridge between the two cyclic guanidine groups of **2a**. Both the oxidation and cyclization steps were pH-sensitive. Oxidation of **6** under acidic conditions resulted in considerable decomposition because the reactivity of aminoimidazole toward oxidation was suppressed when protonated and competing oxidation of other functionalities occurred. Although oxidation of **6** under neutral or slightly basic conditions proceeded more smoothly, the undesired *N*-cyclization occurred spontaneously to give the axinellamine skeleton (*8*). Eventually, we found that oxidation of **6** with *N*-bromosuccinimide (NBS) proceeded smoothly and cleanly in methanol to give a diastereomeric mixture of massadine-methanol adducts (*11*). Upon treatment with aqueous HCl, this mixture of oxidation products slowly converted into massadine (**2a**) (0.014% yield from L-serine) and 3,7-*epi*-massadine (**27**) (*8*).

The CD spectrum of our synthetic **2a** suggested that we had obtained the natural enantiomer of massadine (fig. S6), confirming the correct assignment of its absolute stereochemistry by Fusetani (*23*) and us (*11*) previously. Because of our revision of the absolute stereochemistry of ageliferins (**3**), **2** and **3** have mismatched absolute stereochemistries. To verify this surprising result, we repeated the syntheses of **2a** and **3c,** using the same batch of common intermediate **23**. We confirmed that oxidation and deprotection of **23** gave *nat*-**2a**, whereas deoxygenation and deprotection gave *ent*-**3c**. These experiments provided direct evidence that natural massadine (**2a**) and natural dibromoageliferin (**3c**) are antipodal, and an enantiodivergent pathway must be involved in their biosynthesis.

Sceptrins (**1**), massadines (**2**), and ageliferins (**3**) were previously thought to be derived from a common biosynthetic intermediate and have matched absolute stereochemistries (*11*). We have now shown that massadine (**2a**) and dibromoageliferin (**3c**) are antipodal. Therefore, **2a** cannot be produced from a biogenic oxidation of **3c** or **5**. Considering that both enantiomeric forms of phakellin, a monomeric pyrrole–imidazole alkaloid, have been found in nature (*38*), it is possible that sponges also produce both enantiomers of **1**–**3**. However, literature reports suggest that all the cyclic pyrrole–imidazole dimers exist in only one enantiomeric form. Because both the sign and magnitude of the optical rotation of **1**–**3** change with the salt form (*4*, *26*), CD spectroscopy is currently the only reliable method to study their absolute stereochemistries. Ageliferins isolated from different species of sponges (two *Agelas*, one *Astrosclera*, and one *Stylissa* sponge) in the Caribbean and Pacific oceans all have matched CD spectra (table S1). Similarly, massadines, stylissadines, axinellamines, and donnazoles isolated from different species of sponges (one *Agelas*, two *Axinella*, and two *Stylissa* sponges) in the Caribbean, Pacific, Indian, and Southern oceans all show a positive exciton splitting centered at ~275 nm (table S1). The only two reported CD spectra of sceptrin are also consistent with one another (*4*, *36*). Currently, there is no evidence that both enantiomers of cyclic pyrrole–imidazole dimers exist in nature, although it has also been shown that enantiomeric natural products can arise from a single species or from different genera and/or species (*39*). Because massadine (**2a**) and dibromoageliferin (**3c**) are antipodal, they have to be produced by independent biosynthetic pathways.

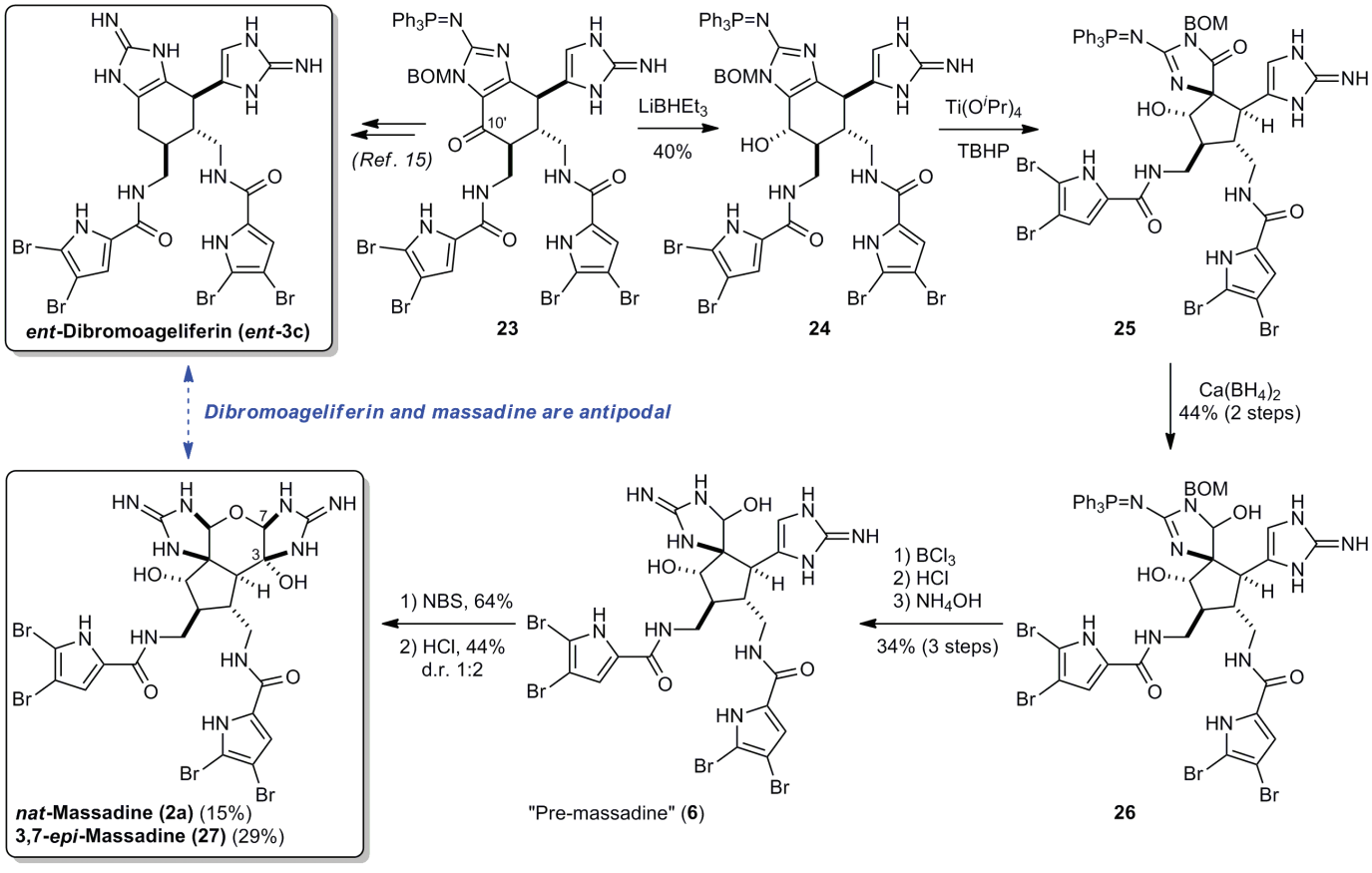


Fig. 4. Asymmetric synthesis of massadine and evidence against the Scheuer biosynthetic hypothesis. Deoxygenation and deprotection of 10′-oxo-dibromoageliferin (**23**) gave *ent*-dibromoageliferin (*ent*-**3c**) (the unnatural enantiomer), whereas skeletal rearrangement and oxidation of **23** provided *nat*-massadine (**2a**) (the natural enantiomer). TBHP, *tert*-butyl hydroperoxide; NBS, *N*-bromosuccinimide.

On the basis of our previous computational and experimental studies (*12*, *15*), we believe that sceptrin (**1a**) and ageliferin (**3a**) are derived from two hymenidin (**4b**, X=H) molecules whereas massadine (**2a**) is assembled from one oroidin (**4a**, X=H) and one dispacamide A (**4d**, X=OH) molecule (Fig. 1). The homodimerization (path a and b) and heterodimerization (path c) of **4** are enantiomeric pathways. The pathway selectivity is determined by the stability of the radical intermediates. The redox-neutral, reversible SET-promoted heterodimerization of **4a** and **4d** would give "pre-massadines" (**6**) with a C9 aminal group that is present in all [3+2] pyrrole–imidazole dimers (fig. S2). Although enantiomeric biosynthesis that produces both enantiomers of a natural product has been reported (*39*), enantiodivergent biosynthesis that produces opposite enantiomers of natural products as congeners described herein is unknown. This discovery may serve as a new guiding principle for protein engineering and catalyst design.

REFERENCES AND NOTES

1. A. Al-Mourabit, M. A. Zancanella, S. Tilvi, D. Romo, *Nat. Prod. Rep.* **28**, 1229–1260 (2011).
2. P. S. Baran, A. L. Zografos, D. P. O'Malley, *J. Am. Chem. Soc.* **126**, 3726–3727 (2004).
3. P. S. Baran, D. P. O'Malley, A. L. Zografos, *Angew. Chem. Int. Ed.* **43**, 2674–2677 (2004).
4. P. S. Baran, K. Li, D. P. O'Malley, C. Mitsos, *Angew. Chem. Int. Ed.* **45**, 249–252 (2005).
5. D. P. O'Malley, K. Li, M. Maue, A. L. Zografos, P. S. Baran, *J. Am. Chem. Soc.* **129**, 4762–4775 (2007).
6. J. Yamaguchi *et al*., *Angew. Chem. Int. Ed.* **47**, 3578–3580 (2008).
7. D. P. O'Malley, J. Yamaguchi, I. S. Young, I. B. Seiple, P. S. Baran, *Angew. Chem. Int. Ed.* **47**, 3581–3583 (2008).
8. S. Su, I. B. Seiple, I. S. Young, P. S. Baran, *J. Am. Chem. Soc.* **130**, 16490–16491 (2008).
9. I. B. Seiple *et al*., *Angew. Chem. Int. Ed.* **49**, 1095–1098 (2010).
10. S. Su, R. A. Rodriguez, P. S. Baran, *J. Am. Chem. Soc.* **133**, 13922–13925 (2011).
11. I. B. Seiple *et al*., *J. Am. Chem. Soc.* **133**, 14710–14726 (2011).
12. X. Tan, C. Chen, *Angew. Chem. Int. Ed.* **45**, 4345–4348 (2006).
13. Z. Ma, J. Lu, X. Wang, C. Chen, *Chem. Commun.* **47**, 427–429 (2011).
14. X. Wang, Z. Ma, J. Lu, X. Tan, C. Chen, *J. Am. Chem. Soc.* **133**, 15350–15353 (2011).
15. X. Wang *et al*., *J. Am. Chem. Soc.* **134**, 18834–18842 (2012).
16. L. E. Overman, B. N. Rogers, J. E. Tellew, W. C. Trenkle, *J. Am. Chem. Soc.* **119**, 7159–7160 (1997).
17. J. T. Starr, G. Koch, E. M. Carreira, *J. Am. Chem. Soc.* **122**, 8793–8794 (2000).
18. A. S. Dilley, D. Romo, *Org. Lett.* **3**, 1535–1538 (2001).
19. C. J. Lovely, H. Du, Y. He, H. V. Rasika Dias, *Org. Lett.* **6**, 735–738 (2004).
20. V. B. Birman, X.-T. Jiang, *Org. Lett.* **6**, 2369–2371 (2004).
21. H. Ding, A. G. Roberts, P. G. Harran, *Chem. Sci.* **4**, 303–306 (2013).
22. R. P. Walker, D. J. Faulkner, D. van Engen, J. Clardy, *J. Am. Chem. Soc.* **103**, 6772–6773 (1981).
23. S. Nishimura *et al*., *Org. Lett.* **5**, 2255–2257 (2003).
24. A. Grube, S. Immel, P. S. Baran, M. Köck, *Angew. Chem. Int. Ed.* **46**, 6721–6724; 8107 (2007).
25. J. Kobayashi *et al*., *Tetrahedron* **46**, 5579–5586 (1990).
26. P. A. Keifer *et al*., *J. Org. Chem.* **56**, 2965–2975 (1991).
27. E. P. Stout, Y.-G. Wang, D. Romo, T. F. Molinski, *Angew. Chem. Int. Ed.* **51**, 4877–4881 (2012).
28. R. B. Kinnel, H.-P. Gehrken, R. Swali, G. Skoropowski, P. J. Scheuer, *J. Org. Chem.* **63**, 3281–3286 (1998).
29. B. H. Northrop, D. P. O'Malley, A. L. Zografos, P. S. Baran, K. N. Houk, *Angew. Chem. Int. Ed.* **45**, 4126–4130 (2006).
30. M. Köck, A. Grube, I. B. Seiple, P. S. Baran, *Angew. Chem. Int. Ed.* **46**, 6586–6594 (2007).
31. N. L. Bauld, *Tetrahedron* **45**, 5307–5363 (1989).
32. T. P. Yoon, *ACS Catal.* **3**, 895–902 (2013).
33. Z. Lu, T. P. Yoon, *Angew. Chem. Int. Ed.* **51**, 10329–10332 (2012).
34. D. Valentine Jr., G. S. Hammond, *J. Am. Chem. Soc.* **94**, 3449–3454 (1972).
35. F.-C. Chen *et al*., *J. Polym. Sci., B, Polym. Phys.* **41**, 2681–2690 (2003).
36. J. Muñoz, C. Moriou, J.-F. Gallard, P. D. Marie, A. Al-Mourabit, *Tetrahedron Lett.* **53**, 5828–5832, 6865 (2012).
37. A. H. Hoveyda, D. A. Evans, G. C. Fu, *Chem. Rev.* **93**, 1307–1370 (1993).
38. J. T. Gautschi, S. Whitman, T. R. Holman, P. Crews, *J. Nat. Prod.* **67**, 1256–1261 (2004).
39. J. M. Finefield, D. H. Sherman, M. Kreitman, R. M. Williams, *Angew. Chem. Int. Ed.* **51**, 4802–4836 (2012).

ACKNOWLEDGMENTS

We thank M. Köck (Alfred Wegener Institute) for providing the natural samples of sceptrin and massadine, and J. Muñoz (Alfred Wegener Institute) for providing a copy of the CD spectrum of natural sceptrin•TFA. We also thank V. Lynch (University of Texas at Austin), J. Clardy (Harvard University), and T. Molinski (University of California, San Diego) for helpful discussions. The CD experiments were performed by H. Shi [University of Texas (UT) Southwestern]. Financial support was provided by NIH (NIGMS R01-GM079554 and R01-GM073949), the Welch Foundation (I-1596), and UT Southwestern. Metrical parameters for the structures of natural sceptrin (**1a**) and **21** are available free of charge from the Cambridge Crystallographic Data Centre under reference numbers CCDC-995387 (**1a**), 1014159 (**21**), and 1016848 (**21**).

SUPPLEMENTARY MATERIALS

www.sciencemag.org/content/346/6206/219/suppl/DC1
Materials and Methods
Figs. S1 to S10
Tables S1 to S5
References (*40*–*52*)
NMR spectra

6 May 2014; accepted 11 September 2014
10.1126/science.1255677

ANIMAL MOTION

Sidewinding with minimal slip: Snake and robot ascent of sandy slopes

Hamidreza Marvi,[1,2] Chaohui Gong,[3] Nick Gravish,[2] Henry Astley,[2] Matthew Travers,[3] Ross L. Hatton,[4] Joseph R. Mendelson III,[5,6] Howie Choset,[3] David L. Hu,[1,2,5] Daniel I. Goldman[2]*

Limbless organisms such as snakes can navigate nearly all terrain. In particular, desert-dwelling sidewinder rattlesnakes (*Crotalus cerastes*) operate effectively on inclined granular media (such as sand dunes) that induce failure in field-tested limbless robots through slipping and pitching. Our laboratory experiments reveal that as granular incline angle increases, sidewinder rattlesnakes increase the length of their body in contact with the sand. Implementing this strategy in a physical robot model of the snake enables the device to ascend sandy slopes close to the angle of maximum slope stability. Plate drag experiments demonstrate that granular yield stresses decrease with increasing incline angle. Together, these three approaches demonstrate how sidewinding with contact-length control mitigates failure on granular media.

The majority of terrestrial mobile robots are restricted to laboratory environments, in part because such robots are designed to roll on hard flat surfaces. It is difficult to systematically improve such terrestrial robots because we lack understanding of the physics of interaction with complex natural substrates such as sand, dirt, and tree bark. We are thus limited in our ability to computationally explore designs for potential all-terrain vehicles; in contrast, many of the recent developments in aerial and aquatic vehicles have been enabled by sophisticated computational-dynamics tools that allow such systems to be designed in silico (*1*).

Compared with human-made devices, organisms such as snakes, lizards, and insects move effectively in nearly all natural environments. In recent years, scientists and engineers have sought to systematically discover biological principles of movement and implement these in robots (*2*). This "bioinspired robotics" approach (*3*) has proven fruitful to design laboratory robots with new capabilities (new gaits, morphologies, and control schemes), including rapid running (*2*, *4*), slithering (*5*), flying (*6*), and swimming in sand (*7*). Fewer studies have transferred biological principles into robust field-ready devices (*4*, *8*) capable of operating in, and interacting with, natural terrain.

Limbless locomotors such as snakes are excellent systems to study to advance real-world all-terrain mobility. Snakes are masters of most terrains: They can move rapidly on land (*9*, *10*) and through water (*11*), burrow and swim through sand and soil (*12*), slither through tiny spaces (*13*), climb complex surfaces (*14*), and even glide through the air (*15*). Relative to legged locomotion, limbless locomotion is less studied, and thus broad principles that govern multi-environment movement are lacking. Recently

[1]School of Mechanical Engineering, Georgia Institute of Technology, Atlanta, GA, USA. [2]School of Physics, Georgia Institute of Technology, Atlanta, GA, USA. [3]Robotics Institute, Carnegie Mellon University, Pittsburgh, PA, USA. [4]School of Mechanical, Industrial, and Manufacturing Engineering, Oregon State University, Corvallis, OR, USA. [5]School of Biology, Georgia Institute of Technology, Atlanta, GA, USA. [6]Department of Herpetology, Zoo Atlanta, Atlanta, GA, USA.
***Corresponding author. E-mail: daniel.goldman@physics.gatech.edu**

developed limbless robotic platforms (*5*), based generally on the snake body plan, are appealing for multifunctional robotics study because they are also capable of a variety of modes of locomotion. These robots can traverse confined spaces, climb trees and pipes, and potentially dive through loose material. However, the gaits that carry these robots across firm ground can be stymied by loose granular materials, collections of particles that display solidlike features but flow beyond critical (yield) stresses.

A peculiar gait called sidewinding is observed in a variety of phylogenetically diverse species of snakes (*9*, *16*). Animals with excellent sidewinding ability—such as the North American desert-dwelling sidewinder rattlesnake (*Crotalus cerastes*) in Fig. 1, A and C—are often found in environments that are either composed of granular materials (such as sand dunes) or are smooth, such as hardpan desert. Sidewinding is the translation of a limbless system through lifting of body segments while others remain in static (in the world frame, locally rolling/peeling in the frame of the body) contact with the ground. Such interactions minimize shear forces at contact, and thus, sidewinding is thought to be an adaptation to yielding or slippery surfaces (*16*). Biological measurements (*17*, *18*) indicate that relative to lateral undulation, rectilinear locomotion, and concertina motion, sidewinding confers energetic advantages on hard surfaces, mainly through lack of slip at the points of contact. But although sidewinding motion of biological snakes has been extensively studied on hard ground, (*16*, *17*, *19*, *20*), only one study has reported kinematics on granular media (*9*).

An initial robotic version of the sidewinding gait has proven useful to enable snake robots to maneuver over flat and bumpy terrain (*21*). In a robotic sidewinding mode, the device maintains two to three static (locally rolling/peeling) contacts with the substrate at any moment (*22*). During this motion, individual segments of the robot are progressively laid into ground contact, peeled up into arch segments, and then transferred forward to become new ground contact segments (*16*, *22*). However, when in field tests a limbless robot [which we will refer to as the Carnegie Mellon University (CMU) robot (Fig. 1, B and D)] was confronted with even modest granular inclines (≈10°) far from the maximum angle of stability (≈30°), it failed to climb (either slipping or rolling downhill).

We posit that the study of success and failure modes in biological snakes can improve the mechanics and control of limbless robot performance, whereas study of success and failure modes of robots can give insight into important mechanisms that enable locomotion on loose material and perhaps explain why sidewinding has evolved in such organisms. This idea builds on recent work using biologically inspired robots as "physical models" of the organisms; such models have revealed principles that govern movement in biological systems, as well as new insights into low-dimensional dynamical systems [for example, (*8*) and references therein].

To discover principles of sidewinding in loose terrain, we challenged *C. cerastes* (n = 6 snakes, mass = 98 ± 18 g, body length, tip-to-tail, L = 48 ± 6 cm) (*23*) to climb loose granular inclines (table S2) (*28*) of varied incline angle, in a custom trackway housed at Zoo Atlanta (fig. S2A). The data comprised 54 trials: six snakes, three inclinations, three trials each. Before each experiment, air flow through a porous rigid floor fluidized the granular media and left the surface of the sand in a loosely packed state with a smooth surface (movie S4); details of this technique are described in (*24*). Three high-speed cameras tracked three-dimensional (3D) kinematics of 8 to 10 marked points on the body. For systematic testing, we chose three incline angles, θ = 0°, 10°, and 20°; the maximum angle of stability θ_0 of the loosely packed material, where local perturbations resulted in system-wide surface flows, was θ_0 = 27°.

As shown in Fig. 1, A and C, and fig. S1A and as previously noted (*9*, *16*), on level granular media the snake generated two contacts (as highlighted by dashed lines in Fig. 1A) with the substrate at each instant, similar to the movement on hard ground (*16*, *17*). As shown in Fig. 1E, the sidewinding pattern could be approximated by posteriorly propagating waves in both horizontal (*xy*) and vertical (*yz*) planes, with a phase offset

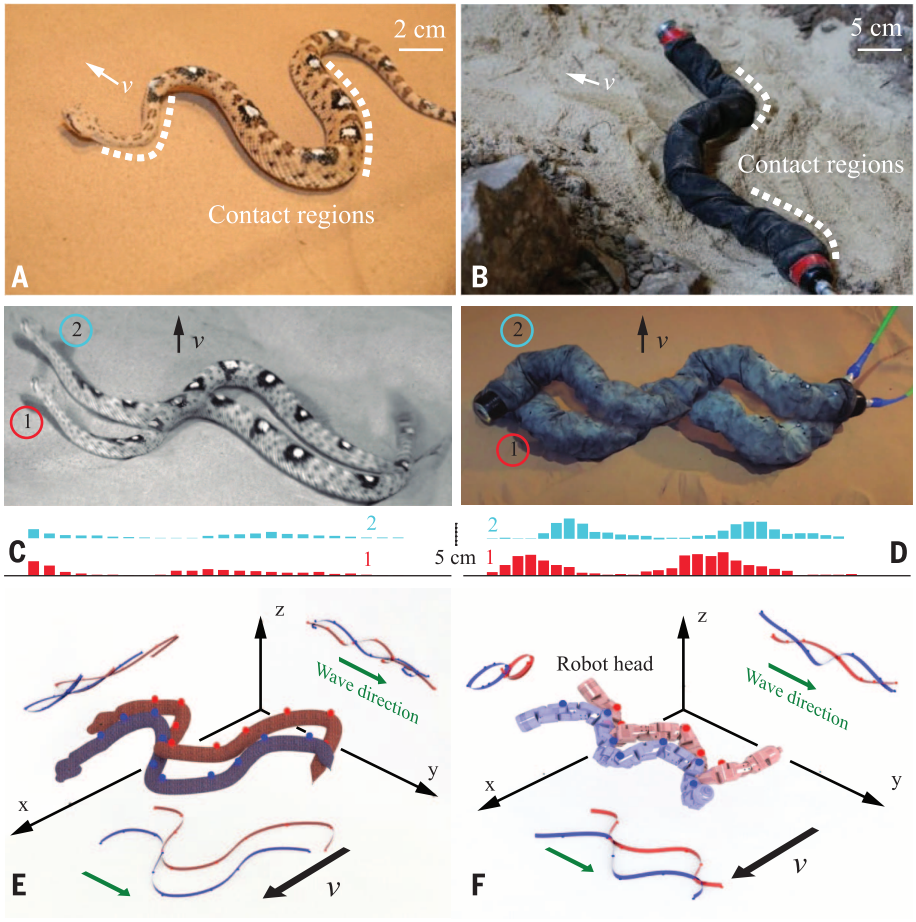


Fig. 1. Sidewinding locomotion on granular media. (**A**) A Sidewinder rattlesnake (*C. cerastes*) locomoting on a granular substrate of 20° inclination. (**B**) The CMU modular snake robot traversing granular media at ≈20° inclination. The arrow indicates the direction of motion. (**C** and **D**) Two superimposed snapshots of (C) a sidewinder and (D) the robot moving on level sand. The initial position is denoted by "1," and the successive position is denoted by "2." The time between snapshots in (C) and (D) is 0.2 and 3.1 s, respectively. The vertical bars beneath the images indicate vertical displacement along the body at the two times. (**E**) Two rendered snapshots of a snake sidewinding on level sand, with red indicating the initial time and blue a successive time; time between images is 0.2 s. The 3D configurations were reconstructed according to shape data collected from a sidewinder rattlesnake moving on level sand. Centerline projections of the 3D snake data are shown on three orthogonal planes. The z coordinates of the snake are scaled up four times to increase visibility in the yz and xz projections. The horizontal (xy) and vertical (yz) waves travel in the posterior direction of the snake with respect to a coordinate system rigidly attached to the animal (as shown by the green arrows). (**F**) Snapshots of the CMU snake robot executing a sidewinding gait on level sand and projections of the resultant body shapes onto three orthogonal planes. Red and blue indicate the initial and successive images, respectively. Time between images is 6.3 s. The horizontal and vertical waves travel in the posterior direction of the robot with respect to a body-fixed coordinate system (as shown by the green arrows).

of $\Delta\phi = 1.51 \pm 0.17$ rad. The position of contact points moved from head to tail, leaving pairs of straight parallel lines on the substrate. The angle between these lines and the direction of motion (fig. S4D) was $\alpha = 33 \pm 8°$ on granular media. The length of each track line was the same as snake body length; the spacing of tracks was thus determined by the spacing of contact points on the snake's body (fig. S4C) (*16*). As previously observed on hard ground (*17*), speed increased with frequency (defined here as the number of cycles per second) (fig. 2C, inset). The snake body intruded into sand by 1.4 ± 1.3 cm and created a hill of material at each contact point; details on penetration depth measurement are provided in (*23*).

We next examined the behavior of the animals as θ increased. A sidewinder climbing an inclination of θ = 20° is shown in fig. S1A and movie S1. Unlike the robot, the snakes were able to ascend the granular inclines without any axial or lateral slip (movie S1), indicated by the horizontal regions in Fig. 2B. In addition, increasing θ did not significantly change the penetration depth [analysis of variance (ANOVA), $F_{2,51} = 0.33$, $P = 0.72$], the angle between direction of motion and track lines (ANOVA, $F_{2,51} = 0.06$, $P = 0.81$), or the number of contacts. Instead, we observed that as θ increased, the length of the contact regions relative to the body length increased (ANOVA, $F_{2,51} = 48.99$, $P < 0.0001$); we refer to this quantity as l/L. To determine this quantity, we analyzed the 3D kinematics data to find the length of snake body in static (peeling) contact with sand in each cycle; details on contact length measurement are provided in (*23*). As shown in Fig. 2C, l/L increased by 41% as θ increased from 0° to 20°. At all θ, portions that were not in contact were lifted clear of the substrate. Wave frequency and climbing speed decreased with increasing θ (fig. S4, A and B) with effective step length S_t [defined as the distance the head moves forward in each period (fig. S4C)] remaining constant over all frequencies and θ. Further kinematic details of the movement are provided in the supplementary text.

To determine whether the ability to climb effectively on sandy inclines is common in closely related snakes, we examined the locomotor behavior of 13 species of pit vipers [subfamily Crotalinae (table S1)] in the collection of Zoo Atlanta on granular media. None of these species performed sidewinding in any conditions, instead using either lateral undulation or concertina, sometimes combined with rectilinear, gaits (table S1). On level sand, many species failed to achieve forward movement, and on sand slopes at θ = 10°, all but a single species failed to move uphill (Fig. 3C and movie S3). Yielding of the sand was accentuated by the failure of these species to lift portions of their body above the substrate (movie S3).

We hypothesize that the sidewinder rattlesnake's ability to move effectively on loose substrates (compared with the robot and the other closely related snakes) is made possible by neuromechanical control that generates appropriate contact length as sandy inclines become more susceptible to flow. To test this hypothesis, we next used the CMU robot as a physical model to study locomotor performance as a function of l/L for different θ (*23*). In particular, the CMU robot's ability to deform in arbitrary modes [using 17 modules (*23*), section 1.3], including a combination of traveling waves that generate sidewinding, makes it an attractive model on which to test the generality and efficacy of the contact length mechanism. And despite the differences in weight and size of the snake robot relative to the organism—as demonstrated in previous studies of fish, turtles, and cockroaches (*8*, *25*, *26*) (and shown below)—principles of small organism locomotor bio and neuromechanics can be deduced through systematic variation of parameters in larger-scale physical models.

To generate sidewinding in the robot, we controlled its modules (and joints) to generate two posteriorly directed traveling waves in the horizontal and vertical planes with a 1/4 period phase offset, $\Delta\phi = 1.57$ rad (comparable with that of the animal). These waves were generated so that dorsal and ventral surfaces maintained their respective orientations throughout the motion. This produced a pattern of undulation and lifting similar to that observed in the biological snakes (Fig. 1, E and F). When the traveling waves are approximated by using sinusoids, the resultant shape of the robot resembles an elliptical helix whose minor axis is perpendicular to the ground and major axis is aligned with the direction of motion. Similar to the biological snake, during a gait cycle each module (segment) traced an approximately elliptical trajectory (Fig. 1F). All experiments were performed at constant wavelength ($\lambda = 0.5L$) and at frequencies sufficiently low as to avoid motor angular position and speed error.

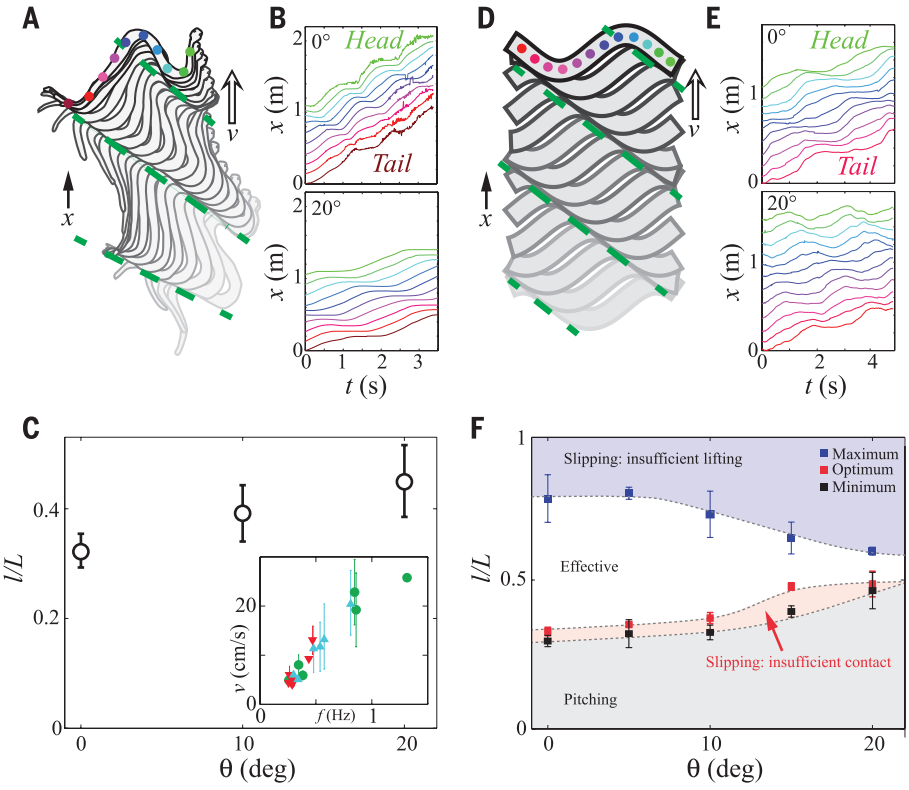


Fig. 2. Sidewinding motion at different granular incline angles θ. (**A**) Traces of the sidewinder rattlesnake (*C. cerastes*) sidewinding on level sand; green dashed lines indicate tracks that an animal leaves on sand. (**B**) Displacement versus time of the snake at θ = 0° (top) and 20° (bottom); colored lines correspond to colored dots on the snake in (A). Regions of each curve that have zero or near zero slope correspond to static contact with the granular medium. (**C**) Contact length l normalized by the body length L as a function of θ for sidewinder rattlesnakes. The data shown encompass six sidewinder rattlesnakes, with three trials per animal at each condition. (Inset) Snake forward speed v versus wave frequency f. Green circles, light blue triangles, and red upside down triangles correspond to θ = 0°, 10°, and 20°, respectively. Data are mean ± SD. (**D**) Illustration of the CMU snake robot sidewinding on level sand; green dashed lines indicate the tracks the robot leaves on the sand. (**E**) Displacement versus time of the robot at inclinations of 0° (top) and 20° (bottom); colored lines correspond to the colored dots on the robot in (D). The robot wave frequency in both of these plots was $f = 0.31$ Hz, and its normalized contact length was 0.53 ± 0.03 and 0.45 ± 0.05 for θ = 0° and 20°, respectively. (**F**) Minimum (black), optimum (red), and maximum (blue) normalized contact length l/L for successful robot climbs as a function of θ. The gray region below the minimum l/L corresponds to pitching failure. The pink region between the minimum and optimum l/L indicates slipping (but still maintains forward progress) due to insufficient contact, and the blue region above the maximum l/L indicates slipping failure due to insufficient lifting. Dashed lines are estimated boundaries of regions of different performance. The robot wave frequency for this plot was $f = 0.08$ Hz. l/L at several other wave frequencies are plotted in Fig. S6B. Data denote mean ± SD.

On level hard ground, a minor-to-major-axis aspect ratio of 0.9 produced steady motion at a speed of 0.03 m/s (at frequency f = 0.08 Hz). On hard surfaces at θ = 20°, decreasing the aspect ratio to 0.7 allowed the robot to climb without pitching or rolling down the hill and at comparable speeds as on level hard ground (*22*).

The waves that generated effective robot sidewinding on solid inclines were ineffective on granular media (movie S2). To improve the performance, we decreased the aspect ratio of the elliptical core, which increased the contact length in a manner analogous to the behavior observed in the biological snakes (fig. S6A). The minimum l/L needed for successful climbing (defined as ascending at positive forward speed without pitching; example traces are provided in Fig. 2D and tracked markers in Fig. 2E) increased by ≈70% as θ increased from 0° to 20°. Within the successful regions, we were further able to optimize the contact lengths to minimize slip and slightly improve the speed as compared with moving with the lower-bound of l/L. Details on robot contact length measurements are provided in (*23*). There was no dependence on frequency, indicating that body inertial forces were minimal and that granular frictional forces determined the resistive forces (*27*). Thus, despite the many differences between the biological and robot sidewinding, comparable performance was achieved through use of a similar strategy of increasing contact length with increases in θ. The elliptical helical gait is only one way to generate the traveling wave that propels the sidewinding in both hard ground and sand. Experimenting with helices of other cross-sections (such as oval shapes) led to similar results. Also, the maximum penetration depth d at the minimum l/L for successful climbing (at f = 0.08 Hz) decreased by ≈30% as θ increased from 0° to 20° (ANOVA, $F_{4,\ 10} = 9.03$, $P = 0.007$).

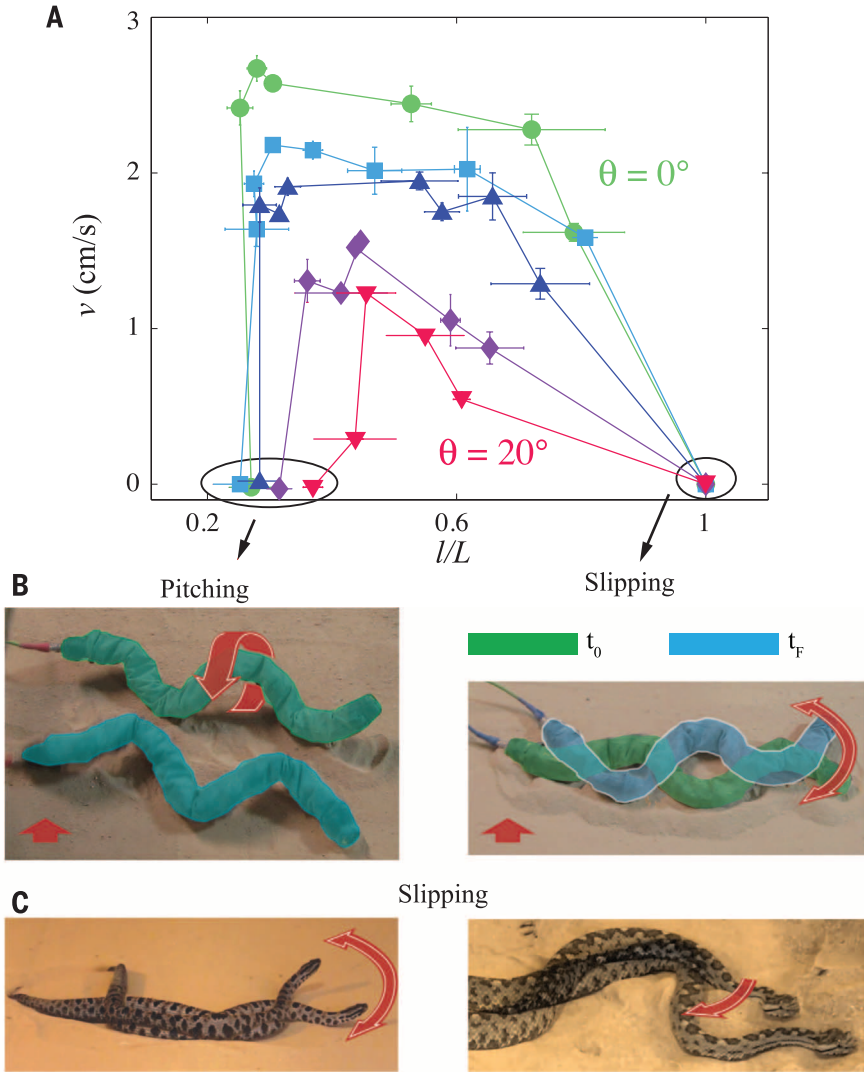


Fig. 3. Sensitivity of locomotor performance on granular media. (**A**) CMU snake robot speed versus l/L for inclination angles θ = 0° (green circles), 5° (light blue rectangles), 10° (dark blue triangles), 15° (purple diamonds), and 20° (red upside down triangles). Failure regimes due to pitching and slipping are circled in black. Three trials were performed at each condition. Data indicate mean ± SD. (**B**) Superimposed frames showing pitching and slipping failure modes in the robot ascending θ = 20° and 10° inclines, respectively. Uphill direction is vertically aligned with the page. t_0 and t_F represent the time at which each body configuration is captured. The time between two images in the pitching and slipping failure modes is 1.6 and 6.3 s, respectively. (**C**) Slipping failure of nonsidewinding snakes. Superimposed images show failed lateral undulation on level sand by *Sistrurus miliarius* (left, length 47 cm) and failed concertina locomotion on level sand by *Mixcoatlus melanurus* (right, length 47 cm). The time between two images of *S. miliarius* and *M. melanurus* is 0.5 and 9 s, respectively.

We next systematically studied how robot performance changed with l/L (Fig. 3A). As shown in Figs. 2F and 3A, the robot was able to ascend effectively for a given θ only within a range of l/L. The range narrowed as θ increased, indicating that for shallow slope angles, sidewinding performance was robust to variations in contact length, whereas for higher slope angles, the control effort must increase to target a narrower range of contact length. On inclinations of <15°, the robot exhibited high performance (speed) in a wide range of l/L until too large l/L produced slipping that decreased forward speed; this was related to an inability of the robot to lift itself sufficiently to avoid unnecessary ground contact (similar to the slipping failures observed in other snake species). At the other extreme, small l/L resulted in an insufficient supporting region, causing the robot to pitch down the slope. In the pink region between minimum and optimum l/L in Fig. 2F, the robot slipped due to insufficient contact but still made forward progress. For large θ, even within the band of effective ascent, performance was degraded because of downhill slip, which decreased the effective step length (fig. S6D).

The success of the robot and its similar performance to the biological sidewinder suggest the following picture of sidewinding on sandy slopes. First, the animal targets a neuromechanical control scheme consisting of two independently controlled and appropriately phased orthogonal waves (Fig. 1, E and F). Such a scheme satisfies the definition of a "template"—that is, a behavior "contains the smallest number of variables and parameters that exhibits a behavior of interest" (*4*). Discovery of templates is useful because they provide an organizing principle for the enormous number of degrees of freedom inherent in all organisms. Second, the robot experiments suggest that the two-wave template dynamics can be simply modified on sandy slopes so that the animal targets a pattern of l/L and body-segment lifting that minimizes slip and pitching.

Understanding the ground reaction forces responsible for the relevant interactions (for example, optimal l/L without slip) requires a model of the interaction of objects with granular media. However, there is no fundamental theory for bio- and robotically relevant interactions in granular media and a wider class of materials (mud, rubble, or leaf litter). In particular, despite recent discoveries in terradynamics (*28*), drag (*27*), and impact (*29*) on level dry granular media [and

theoretical approaches to characterize granular rheology (*30*)], none of these studies have investigated drag forces on granular inclines.

We therefore studied the physics of transient granular yield forces as a function of θ. For context, studies of steady-state drag on level granular surfaces reveal that force is proportional to plate width, w, and depth squared, d^2 (*31*). To make the first measurements of drag force F dependence on θ, d, and w, we performed drag force measurements on granular inclines (*23*). We inserted flat plates of different widths (w = 1.5 to 6 cm) to different depths (d = 1 to 2 cm) into the granular medium perpendicular to the slope plane and displaced the plate downhill 15 cm. Depths were chosen to bound the range of penetration depths observed in the animal experiments. Because we were interested in the yield behavior of the granular slope in the quasi-static limit (we assume inertial effects are small at speeds at which the snakes generally operate), we performed drag at slow speeds and studied the force increases under small displacements δ from rest.

As shown in Fig. 4B, force increased substantially for small displacements until it reached a saturation regime, after which there was a slower increase in force associated with the buildup of a granular pile in front of the plate. We refer to the regime of rapid rise as the "stiffness" of the sand (before large yielding) and denote it k (F/δ near $\delta = 0$). We estimated k by fitting a line to the first 17% of data (corresponding to a displacement 0.5 cm, before material yielded noticeably) presented in Fig. 4B, and we plot this in Fig. 4C. For fixed d, k decreased by ≈50% as θ increased from 0° to 20° (Fig. 4C). For a fixed θ, k increased quadratically with d and nearly linearly with w. This scaling indicates that in the limit of shallow drag and small displacements δ, $F \propto k\,\delta$ with $k \propto w^{0.8}\, d^2\cos\{[\pi/(2\theta_0)]\,\theta\}$, where the phenomenological cos term reflects the rapid decrease in force as θ approaches θ_0 [details on curve fitting are provided in (*23*)]. For θ = 0° and fixed δ, the dependence on w is similar to that previously observed (*31*), even though our depths are shallower.

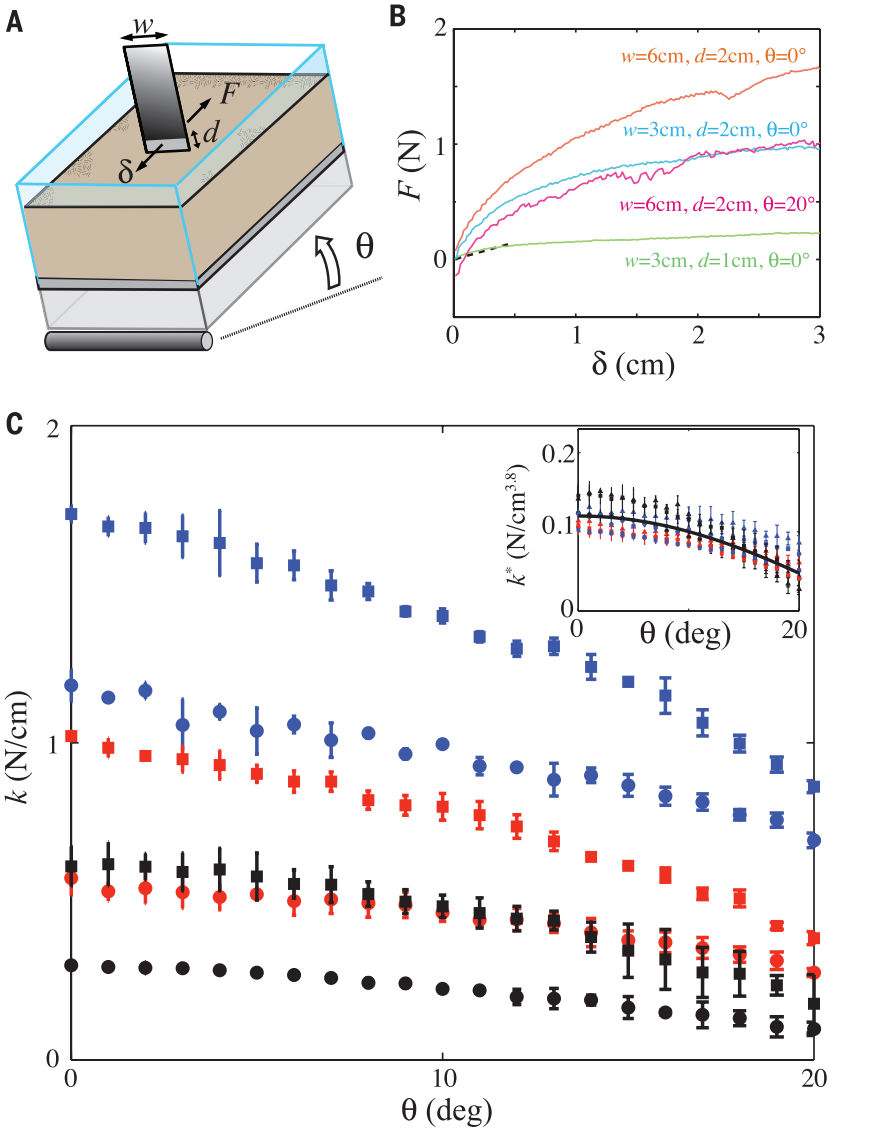


Fig. 4. Granular incline drag force experiments. (**A**) Schematic of drag force apparatus. (**B**) Drag force F versus horizontal displacement δ for different plate widths w and penetration depths d. The dashed line indicates the region used to calculate sand stiffness, k. (**C**) The fitted k versus inclination angle θ for different w and d. (Inset) The sand stiffness data collapse when normalized by $w^{0.8}d^2$; the thick black line is the fit function $0.12\cos([\pi/(2\theta_0)]\,\theta)$, with θ_0 = 0.47 rad (θ_0 = 27°). Triangles, circles, and squares represent w = 1.5, 3, and 6 cm, respectively. Black, red, and blue colors illustrate d = 1, 1.5, and 2 cm, respectively. Data denote mean ± SD.

The drag force measurements support our hypothesis of contact length control: As θ increases, effective sidewinding can be maintained by increasing the contact length to offset the decrease in yield forces. This allows the locomotor to maintain stresses below the yield stress, minimizing slip. Insights from the drag measurements also indicate why the appropriate amount of body lift and contact to be within the range of l/L is important. If lift is too small, other segments of the locomotor encounter drag forces that must then be offset by either increases in l/L, or potentially increasing intrusion depth. However, increases in l/L would decrease lift, resulting in greater drag. Increasing contact length relative to increasing intrusion depth has obvious benefits because intrusion into granular media requires yielding material, and the force to do so increases with depth [the challenges associated with penetration are described in (*32*)]. The energetic cost to vary l/L is small in comparison.

The contact length modulation strategy has benefits in terms of locomotor control: Once the animal or robot is moving using a sidewinding template (again, two independently controlled waves with phase difference of approximately π/2), slip and pitch mitigation in flowable substrates can be effected with relatively simple modulations of the basic template wave pattern. This control has features in common with our previous biological (*33*) and robotic (*24*, *26*) studies of relatively slow-legged movement on the surface of granular media, which also demonstrated that use of the solid features of granular media had benefits in certain locomotor regimes. We predict that other locomotors that move on granular surfaces could target movement patterns whose modulation can be used to achieve minimal-slip.

As expected, there were differences in the details between the sidewinding in the two systems. We view these differences, necessarily present because of the relative simplicity of the robot compared with the organism, as consequences of the different mechanisms that are used (biological complexity versus relative robot simplicity) as "anchors" of the templates, in the terminology discussed in (*8*). For example, the CMU robot has no compliance in its joints, many fewer degrees of freedom, and larger range of rotation (–90° to 90°) compared with those of biological snakes. Another interesting difference between a snake and the robot is that although both of them slowed as θ increased (figs. S4A and S6C), the snake's decrease in speed was correlated with

a decrease in frequency (indicating possibly either muscle limitations or active control to decrease inertial forces), whereas the robot speed decrease was largely determined by a decrease in spacing between tracks, as shown in fig. S6D. This decrease in effective step length was related to slipping of the robot at the highest θ. Comparative study of the anchoring mechanics is useful to learn about which lower-level mechanisms in the control hierarchy are critical, both to generate template dynamics as well as to understand neuromechanical control targets for the anchors.

REFERENCES AND NOTES

1. M. Costello, J. Sahu, *Proc. Inst. Mech. Eng. Part G J. Aerosp. Eng.* **222**, 1067–1079 (2008).
2. J. E. Clark *et al.*, *Proceedings of IEEE International Conference on Robotics and Automation* (2001), vol. 4, pp. 3643–3649.
3. B. Bhushan, *Philos. Trans. R. Soc. Math. Phys. Eng. Sci.* **367**, 1445–1486 (2009).
4. R. Playter, M. Buehler, M. Raibert, *Unmanned Ground Vehicle Technology VIII*, D. W. G. Grant R. Gerhart, Charles M. Shoemaker, Eds., vol. 6230 of *Proceedings of SPIE* (2006), pp. 6230201–6230206.
5. M. Tesch *et al.*, *Adv. Robot.* **23**, 1131–1158 (2009).
6. K. Y. Ma, P. Chirarattananon, S. B. Fuller, R. J. Wood, *Science* **340**, 603–607 (2013).
7. R. D. Maladen, Y. Ding, C. Li, D. I. Goldman, *Science* **325**, 314–318 (2009).
8. P. Holmes, R. J. Full, D. Koditschek, J. Guckenheimer, *SIAM Rev.* **48**, 207–304 (2006).
9. B. C. Jayne, *Copeia* **1986**, 915–927 (1986).
10. D. L. Hu, J. Nirody, T. Scott, M. J. Shelley, *Proc. Natl. Acad. Sci. U.S.A.* **106**, 10081–10085 (2009).
11. B. Jayne, *Copeia* **1985**, 195–208 (1985).
12. K. S. Norris, J. L. Kavanau, *Copeia* **1966**, 650–664 (1966).
13. H. Marvi, D. L. Hu, *J. R. Soc. Interface* **9**, 3067–3080 (2012).
14. G. Byrnes, B. C. Jayne, *J. Exp. Biol.* **213**, 4249–4256 (2010).
15. J. J. Socha, *Nature* **418**, 603–604 (2002).
16. W. Mosauer, *Am. Nat.* **64**, 179–183 (1930).
17. S. M. Secor, B. C. Jayne, A. F. Bennett, *J. Exp. Biol.* **163**, 1–14 (1992).
18. H. Marvi, J. Bridges, D. L. Hu, *J. R. Soc. Interface* **10**, 20130188 (2013).
19. J. Gray, *J. Exp. Biol.* **23**, 101–120 (1946).
20. B. C. Jayne, *J. Exp. Biol.* **140**, 1–33 (1988).
21. J. Burdick, J. Radford, G. Chirikjian, *Adv. Robot.* **9**, 195–216 (1994).
22. R. L. Hatton, H. Choset, *IEEE International Conference on Robotics and Automation* (2010), pp. 691–696.
23. Materials and methods are available as supplementary materials on *Science* Online.
24. C. Li, P. B. Umbanhowar, H. Komsuoglu, D. E. Koditschek, D. I. Goldman, *Proc. Natl. Acad. Sci. U.S.A.* **106**, 3029–3034 (2009).
25. S. Sefati *et al.*, *Proc. Natl. Acad. Sci. U.S.A.* **110**, 18798–18803 (2013).
26. N. Mazouchova, P. B. Umbanhowar, D. I. Goldman, *Bioinspir. Biomim.* **8**, 026007 (2013).
27. R. Albert, M. Pfeifer, A.-L. Barabási, P. Schiffer, *Phys. Rev. Lett.* **82**, 205–208 (1999).
28. C. Li, T. Zhang, D. I. Goldman, *Science* **339**, 1408–1412 (2013).
29. H. Katsuragi, D. J. Durian, *Nat. Phys.* **3**, 420–423 (2007).
30. D. L. Henann, K. Kamrin, *Proc. Natl. Acad. Sci. U.S.A.* **110**, 6730–6735 (2013).
31. D. J. Costantino, J. Bartell, K. Scheidler, P. Schiffer, *Phys. Rev. E Stat. Nonlin. Soft Matter Phys.* **83**, 011305 (2011).
32. A. G. Winter 5th, R. L. H. Deits, A. E. Hosoi, *J. Exp. Biol.* **215**, 2072–2080 (2012).
33. N. Mazouchova, N. Gravish, A. Savu, D. I. Goldman, *Biol. Lett.* **6**, 398–401 (2010).

ACKNOWLEDGMENTS

We thank M. Tesch, E. Cappo, J. Rembisz, and L. Li from Robotics Institute at Carnegie Mellon University for helping with the robot experiments; J. Brock, D. Brothers, R. Hill, L. Wyrwich, and B. Lock from Zoo Atlanta for helping with snake experiments; A. Young and K. Young for assistance with collecting snakes; D. Dimenichi, R. Chrystal, and J. Shieh from Georgia Institute of Technology for helping with construction and video analysis; T. Nowak and C. Hobbs for photography; V. Linevich for CAD drawings; P. Umbanhowar and A. Zangwill for helpful discussion; the National Science Foundation (NSF) (CMMI-1000389, PHY-0848894, PHY-1205878, and PHY-1150760); Army Research Office under grants W911NF-11-1-0514 and W911NF1310092; the Army Research Lab Micro Autonomous Systems and Technology Collaborative Technology Alliance under grant W911NF-08-2-0004; and the Elizabeth Smithgall Watts endowment, for financial support. D.I.G., H.C., and D.H. also acknowledge the Army Research Office and NSF Physics of Living Systems for supporting the Locomotion Systems Science Workshop in Arlington, Virginia, May 2012. The data collected for this study will be made available through the SMARTech data repository at Georgia Institute of Technology.

SUPPLEMENTARY MATERIALS

www.sciencemag.org/content/346/6206/224/suppl/DC1
Materials and Methods
Figs. S1 to S6
Tables S1 and S2
References (*34*–*38*)
Movies S1 to S5

7 May 2014; accepted 1 August 2014
10.1126/science.1255718

ECONOMIC DEMOGRAPHY

Is low fertility really a problem? Population aging, dependency, and consumption

Ronald Lee,[1]* Andrew Mason,[2,3]* members of the NTA Network†

Longer lives and fertility far below the replacement level of 2.1 births per woman are leading to rapid population aging in many countries. Many observers are concerned that aging will adversely affect public finances and standards of living. Analysis of newly available National Transfer Accounts data for 40 countries shows that fertility well above replacement would typically be most beneficial for government budgets. However, fertility near replacement would be most beneficial for standards of living when the analysis includes the effects of age structure on families as well as governments. And fertility below replacement would maximize per capita consumption when the cost of providing capital for a growing labor force is taken into account. Although low fertility will indeed challenge government programs and very low fertility undermines living standards, we find that moderately low fertility and population decline favor the broader material standard of living.

Economic behavior, abilities, and needs vary strongly over the human life cycle. During childhood and old age, we consume more than we produce through our labor. The gap is made up in part by relying on accumulated assets. It is also made up through intergenerational transfers, both public and private, that shift resources from some generations to others with no expectation of direct repayment. Private transfers occur when parents rear their children and when older people assist their adult children or receive assistance from them. Public transfers include public education, publicly funded health care, public pensions, and the taxes to pay for these programs. Because of these economic interdependencies across age, fertility rates that are falling or already low will drive rapid population aging in economies around the world. Forty-eight percent of the world's people live in countries where the total fertility rate (TFR) was below replacement, about 2.1 births per woman for 2005 to 2010. The TFR is 1.5 births per woman in Europe and 1.4 births per woman in Japan (*1*). With fertility this low, population growth will give way to population decline, and population aging will be rapid. The median age of the Southern European population, for example, is projected to reach 50 years of age by 2040 as compared to 41 in 2010 and 27 in 1950 (*1*). In 2013, governments in 102 countries reported that population aging was a "major concern," and 54 countries had enacted policies intended to raise fertility (*2*).

This is a remarkable reversal from decades of concern about the economic and environmental consequences of high fertility and rapid population growth (*3*). Should we now be alarmed about low fertility, population decline, and population aging? Should governments encourage their citizens to bear more children to balance the dramatic future increase in the number and proportion of elderly?

Identifying an optimal population policy is likely to be impossible for several reasons. First, children yield direct satisfaction and impose

[1]Department of Demography and Department of Economics, University of California, 2232 Piedmont Avenue, Berkeley, CA 94720, USA. [2]Department of Economics, University of Hawaii at Manoa, 2424 Maile Way, Honolulu, HI 96821, USA. [3]East-West Center, 1601 East-West Road, Honolulu, HI 96848-1601, USA.
***Corresponding author. E-mail: rlee@demog.berkeley.edu (R.L.); amason@hawaii.edu (A.M.)** †National Transfer Accounts (NTA) Network authors with their institutions appear at the end of this paper.

costs on parents that are difficult or impossible to measure. Second, the environmental consequences of continuing population growth are exceedingly complex and difficult to value or weigh against other costs and benefits of low fertility. Third, assessing the welfare consequences of differences in fertility requires comparing the welfare of those not yet born to those who will never be born.

Our goal is more modest: to examine how low fertility and population aging will influence the material standard of living. The analysis shows that relatively high fertility and young populations are favorable to public finances in rich countries because they have comprehensive systems of support for the elderly. A broader analysis that incorporates private intergenerational transfers and the capital costs of equipping each new generation shows that low fertility, older populations, and gradual population decline favor the material standard of living.

The implications of low fertility and population aging depend on the age patterns of labor income, consumption, and intergenerational transfers (*4*–*8*). However, estimates of economic life cycles and intergenerational transfers have not previously been available. The results presented here have their basis in estimates constructed by research teams in 40 countries following a common methodology: National Transfer Accounts (NTA) (*9*–*11*). NTA uses existing surveys, administrative data, and the United Nations System of National Accounts (SNA) to estimate the values of goods and services produced and consumed at each age and the intergenerational flows across ages through public and private transfers and assets. NTA incorporates the age dimension into SNA, thereby facilitating analysis of the macroeconomic implications of population change.

Estimated labor income by age includes wages, salaries, and fringe benefits as well as an estimate of the value of labor of those who are self-employed or unpaid family workers, all averaged across the entire population at each age. Consumption includes private expenditures and goods and services produced by governments (e.g., education and health care) imputed to different ages and averaged across all individuals at a given age.

NTA age profiles for the United States and Thailand illustrate the data used in the analysis (Fig. 1). In the United States, elderly consume far more than young adults and labor income falls off rapidly at older ages (Fig. 1A). Public transfer inflows to the elderly are generous, funded largely through public transfer outflows from the working ages (Fig. 1B). Familial transfers are important to some elderly, but on average the elderly give more than they receive at almost every age (Fig. 1C). In Thailand, elderly and young adults consume at similar levels. The elderly have somewhat higher labor income than in the United States (Fig. 1D). The public system for the elderly is very modest, with public transfer outflows from the elderly as great as public transfer inflows (Fig. 1E). Familial support is very important for the elderly, with private transfer inflows higher than private transfer outflows (Fig. 1F).

The differences in shapes of labor income and consumption by age, and in public and private transfers made and received, lead to differences in the impacts of population age distributions in the forty countries studied here. These differences are incorporated into two summary measures, the fiscal support ratio (FSR) and the support ratio (SR). Definitions are given below, but heuristically the FSR is the ratio of taxpayers to beneficiaries and the SR is the ratio of earners to consumers. Age profiles, FSR, and SR for all countries and complete definitions of variables are provided in the supplementary materials (*9*) (Table 1).

The FSR summarizes the influence of population age distribution on government budgets. The FSR is defined as the number of effective taxpayers, calculated by weighting the population in each age group by the average taxes paid by that age group in the base year, divided by the number of effective beneficiaries, calculated by weighting the population in each age group by per capita benefits received. A higher FSR is favorable for public finances allowing higher benefits at each age, lower taxes at each age, a smaller budget deficit, or some combination of the three. A population concentrated in high tax-paying ages leads to a high FSR. A population with many children, who pay little in taxes and receive education benefits, leads to a low FSR. Likewise, a population at older ages has a low FSR in rich countries, because they emphasize pensions and health care spending on the elderly.

The SR summarizes the effect of the population age distribution on income and outlays per person combining both the public and the private sectors. The SR is defined as the number of effective workers, the population weighted by per capita labor income at each age, divided by the number of effective consumers, the population weighted by per capita consumption at each age. A higher SR indicates proportionally higher resources available per person allowing for higher consumption, higher saving and investment, or some combination of the two. A population concentrated at ages where labor income is high and consumption is low leads to a high SR. A population concentrated at ages where labor income is low and consumption is high leads to a low SR.

The FSR and the SR provide distinctive perspectives because intergenerational transfers through the public and private sectors are very different. Especially in rich countries, public transfers are predominantly to the elderly, whereas private transfers go mostly to children. As a consequence, the age structure that favors public finances is much younger than the age structure that favors the combined finances of public and private sectors. Both a young, high-fertility, rapidly growing population and an old, low-fertility, rapidly declining population reduce the FSR and the SR. The central issue addressed here is what demographic conditions would be most favorable to public finances and standards of living in the long run.

The age structure of a population in the long run is determined by fertility, mortality, and migration.

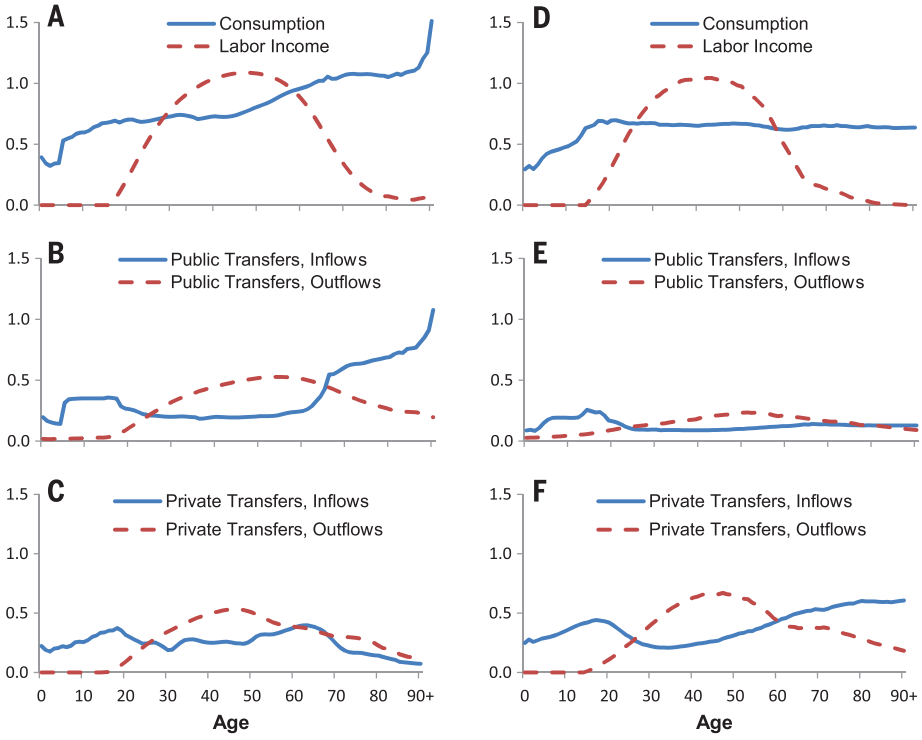


Fig. 1. Age profiles of economic flows. Per capita age profiles of consumption, labor income, and public and private transfers for the United States (2009) (**A** to **C**) and Thailand (2004) (**D** to **F**). Profiles are expressed relative to the mean labor income of persons 30 to 49 in each country.

Our analysis emphasizes fertility because it is an important determinant of age structure and because so many governments are encouraging higher fertility as a result of their concerns about population aging. Mortality decline also leads to older populations, but the effects are gradual, and no government has ever proposed slowing mortality decline to avoid population aging. Immigration is often suggested to help reduce the population aging that results from low fertility. Immigration does lead to a younger population in the short term, but it has a muted effect in the long term. Immigrants are relatively young on average when they arrive, but over time their age distribution tends to become similar to or older than the age distribution of the receiving population. This occurs because the immigrant populations age and because immigrant fertility rates typically converge toward the fertility rates of the receiving population (*12*–*14*). A summary of the literature concluded that "a steady stream of migrants almost always makes a population younger in the short-term but older in the long-term" (*13*). Net immigration also raises the population growth rate, which imposes capital costs, discussed below, that must be balanced against possible benefits from age structure.

Thus, we consider the effect of fertility given the level of mortality in a population closed to migration. Given mortality and in the absence of migration, the population growth rate is determined by fertility. What level of fertility and population growth rate would maximize the FSR and SR in the long run?

Given the NTA age profiles, we can easily find this level of fertility or growth rate by systematic numerical search. To gain analytic insight, we can also differentiate the log of the support ratio (ln *SR*) with respect to the population growth rate (n), finding that $\partial \ln SR/\partial n = A_c - A_{y_l}$ (see supplementary materials). Here, A_c is the average age of consuming in the population, and A_{y_l} is the average age of earning. The differentiation is across long-run age distributions with differing growth rates (steady-state age distributions or stable-population age distributions). When $A_c > A_{y_l}$ then earning occurs at a younger age than consumption, on average, so a younger population, achieved through higher fertility and more rapid population growth, would raise effective workers more than effective consumers, thereby raising the SR, and conversely. At the maximum long-run SR, these average ages are equal, and the derivative equals zero (*5*).

The SR is an intuitive and widely used indicator, but it has a serious limitation. Although higher fertility might push the SR higher, this could come at a cost: the increased saving and investment that would be required to provide capital for the growing labor force (*5*–*8*, *15*–*17*). This "capital cost" of higher fertility and additional population growth depends on the behavioral responses of households and firms and on public policies that influence saving and investment, for example, the extent of unfunded public pensions and health care. To deal with the uncertainty about future public policy, we consider two scenarios that in our view encompass the possible responses.

In one approach, the low capital cost case, we assume that the ratio of capital to output is constant and unaffected by changing demography. In the face of fertility decline, policies are implemented as needed to reduce saving rates to achieve this outcome. This case would be optimal for one variant of a well-known economic growth model (*9*, *18*, *19*). Between 1980 and 2004, the capital-output ratio was very stable for many Organization for Economic Cooperation and Development (OECD) countries, including the United States, with about three dollars of capital for each dollar of output produced (*20*). We use the average value of 3.0 to represent the low-capital-cost case.

For the second case, the high capital cost case, we rely on the most widely used model of economic growth, the neoclassical model. We will use an important, special case of this model in which policies are used to achieve the saving rate that leads to the economic growth path with the highest possible consumption per capita, called "golden rule" growth by economists. Under these conditions, capital per worker rises when fertility falls, as has been true in Japan, many OECD countries, and recently many other high-income countries (*21*). Under the high-capital-cost scenario, the capital-output ratio rises to higher levels than currently found in any country. The increase in capital because of low fertility is consistent with the view recently advanced by Piketty (*22*).

Again, the fertility rate that maximizes per capita consumption incorporating capital costs can be found by numerical search. For either of the cases, we can also differentiate across steady states, finding that the first order condition for maximum consumption is $d[\ln(\text{lifetime consumption})]/dn = A_c - A_{y_l} - K/C$, where K is capital and C is consumption. The SR effect is captured by $A_c - A_{y_l}$, whereas $-K/C$ captures the capital costs of higher fertility or more rapid population growth (*9*).

Table 2 reports the key results for 40 countries comparing each country's current fertility (column B) with the fertility rate that maximizes the FSR (column C), the SR (column D), and per capita consumption for the low- and high-capital-cost scenarios (columns E and F). Very low fertility does not adversely affect public finances in lower-income countries because public programs for the elderly are quite limited and the elderly do pay taxes. For every high- and upper-middle-income country except South Africa and Thailand, current fertility is below the fertility level that maximizes the FSR—3.0 and 2.9 births per woman, respectively, for upper-middle- and high-income countries. We expect that public transfer programs will become more generous in countries that have not yet embraced them, so that higher TFRs will maximize their FSRs in the future. At the same time, future pension and health care reform in rich industrial nations and many Latin American countries may well reduce the TFRs that maximize their FSRs.

The TFR that would maximize the support ratio (column D) is 1.8 births per woman in lower-income countries, 2.0 in upper-middle-income countries, and 2.3 in high-income countries. These values are lower than the FSR-maximizing values

Table 1. Key aging variables, definition, method of calculation, summary statistics, and sources. WPP is World Population Prospects 2012 Revision; NTA is from www.ntaccounts.org (accessed 10 July 2013). The range and mean values, except those for the TFR, are the stable values that would result if current age-specific fertility and mortality rates persist. See supplementary materials for detailed method of calculation.

Variable	Definition and sources	Range (mean)
FSR	Number of effective taxpayers per effective beneficiary determined by the population age distribution (WPP) and the age profiles of per capita taxes paid and benefits received for all in-kind and cash transfer programs, including education, health care, and pensions (NTA). All values expressed relative to the FSR for 2010.	0.70 to 1.09 (0.88)
A_C	Average age at which goods and services are being consumed. This is determined by the age distribution of the population (WPP) and the age profile of per capita consumption (NTA).	28.0 to 56.9 (44.5)
A_{y_l}	Average age at which goods and services are being produced by workers. This is determined by the age distribution of the population (WPP) and the age profile of per capita labor income (NTA).	35.2 to 47.4 (42.8)
SR	Number of effective producers per effective consumer determined by the population age distribution (WPP) and the age profiles of per capita consumption and labor income (NTA).	0.36 to 0.67 (0.49)
TFR	Number of births per woman over the reproductive span, given current age-specific birth rates (WPP).	1.1 to 5.6 (2.2)

because families bear most of the costs of child-rearing while governments, except in lower-income countries, are typically burdened more by the elderly. Still, one-third of the upper-middle-income countries and all high-income countries except Uruguay currently have fertility below the level that maximizes the support ratio. For high income countries, 2.3 births per woman would be "best," on average, as compared with a current value of 1.6 births per woman. Judged in this limited way, high-income countries would benefit from higher fertility.

The fertility rates that would maximize consumption, taking capital cost into account, are reported in columns E (low-capital-cost scenario) and F (high-capital-cost scenario). Using either of these measures, current fertility is higher than the consumption-maximizing level in every lower-income country except Vietnam and every upper-middle-income country except China, Hungary, and Thailand. In these four countries, fertility is too low with use of the low-capital-cost scenario and too high with use of the high-capital-cost scenario. However, we emphatically are not suggesting that these lower-income countries should be aiming for fertility as low as shown in Table 2. Development will likely lead to consumption and public support age profiles similar to those of richer countries.

The picture is mixed for the higher-income countries. Consider the nine countries with TFRs above 1.6 births per woman in 2005 to 2010 (Australia, Canada, Chile, Finland, France, Sweden, United Kingdom, United States, and Uruguay). In these countries, the TFR exceeds or is very close to the consumption-maximizing fertility level. Under any plausible assumption about the capital costs of higher fertility, these nine countries did not have fertility rates that were too low. For seven countries with TFRs ranging from 1.2 to 1.5 for 2005 to 2010 (Austria, Germany, Japan, Slovenia, South Korea, Spain, and Taiwan), higher fertility rates would result in higher consumption under any plausible scenario. For only one high-income country, Italy, is a definitive conclusion not possible.

Very low fertility results in lower living standards. Given current mortality rates, no immigration, and age profiles of high-income countries, an $n = -2\%$ per year ($TFR \simeq 1.1$) would reduce per capita consumption by 4% relative to consumption for $n = 0$ and TFR at replacement. Low fertility produces a smaller decline in consumption in lower- and upper-middle-income countries because elder consumption is not as high and because these countries have higher mortality rates (Fig. 2A). Given Japanese mortality rates, lost consumption would be greater for all income groups but especially for high-income countries—a 7.6% decline compared with consumption at replacement fertility (Fig. 2B). These costs of low fertility would be smaller for the high-capital-cost scenario.

The effects of having low fertility in 2005 to 2010 unfold gradually as the lower stable SR is reached. Among the high-income countries with TFRs of 1.6 or higher, the stable SRs are about 10% less than the 2010 SRs. For high-income countries with TFRs below 1.6, the stable SR is 80% of its 2010 level. For these, South Korea excluded, between 50 and 75% of the decline toward the stable SR would occur by 2030 (*9*)

Based on Japan, with the oldest population in the world, the effects of low fertility highlighted in this study are already beginning to emerge (*9*). Because of low fertility and long life, the population is aging rapidly, and the SR fell at 0.6% annually during the last decade, whereas the FSR fell even faster at 0.9%. However, slower and now negative labor force growth has led to

Table 2. Current TFRs and TFRs that maximize alternative objectives. Current TFRs are most recent estimates from the United Nations Population Division (*1*) and refer to the period of 2005 to 2010. All other values calculated by using methods described in detail in the supplementary materials. Income group based on World Bank classification for 2014 (http://data.worldbank.org/about/country-and-lending-groups); lower income includes low-income and lower-middle-income countries. Results were calculated by using the age profiles of economic flows estimated for each country, a depreciation rate of 5% per year, and exogenous labor-augmenting technological growth of 2% per year. na, not available.

Country/income group	TFR 2005–2010 (B)	TFR that maximizes each outcome			
		FSR (C)	SR (D)	Consumption, low-capital-cost scenario (E)	Consumption, high-capital-cost scenario (F)
All countries	2.44	2.56	2.05	1.54	1.24
Lower income	4.03	1.08	1.75	1.21	0.91
Cambodia	3.08	na	3.66	2.67	2.19
Ethiopia	5.26	na	1.40	0.91	0.62
Ghana	4.22	na	1.01	0.67	0.46
India	2.66	1.80	1.93	1.40	1.06
Indonesia	2.50	0.88	1.28	0.84	0.53
Kenya	4.80	1.12	2.07	1.54	1.26
Mozambique	5.57	1.30	1.61	1.12	0.89
Nigeria	6.00	na	0.96	0.54	0.29
Philippines	3.27	1.13	1.43	1.00	0.73
Senegal	5.11	0.25	1.32	0.67	0.28
Vietnam	1.89	na	2.60	1.99	1.67
Upper-middle income	2.09	2.96	2.01	1.51	1.20
Argentina	2.25	3.25	2.00	1.54	1.26
Brazil	1.90	5.45	2.29	1.82	1.50
China	1.63	2.64	2.17	1.65	1.34
Colombia	2.45	3.77	2.04	1.49	1.13
Costa Rica	1.92	3.85	2.31	1.77	1.42
Hungary	1.33	2.58	1.89	1.47	1.21
Jamaica	2.40	na	2.19	1.63	1.30
Mexico	2.37	2.83	1.98	1.47	1.14
Peru	2.60	3.45	2.17	1.61	1.26
South Africa	2.55	0.97	1.40	1.02	0.82
Thailand	1.49	0.79	2.00	1.55	1.28
Turkey	2.16	na	1.63	1.08	0.71
High income	1.65	2.94	2.27	1.78	1.48
Australia	1.89	na	2.70	2.06	1.70
Austria	1.40	3.74	2.44	1.90	1.58
Canada	1.63	na	1.96	1.55	1.26
Chile	1.90	3.63	2.20	1.69	1.36
Finland	1.84	2.92	2.30	1.83	1.54
France	1.97	na	2.41	1.92	1.61
Germany	1.36	3.33	2.55	2.00	1.65
Italy	1.38	na	2.11	1.65	1.34
Japan	1.34	2.70	2.33	1.88	1.57
Slovenia	1.44	3.25	2.21	1.78	1.52
South Korea	1.23	2.07	2.04	1.55	1.25
Spain	1.41	3.29	2.20	1.73	1.43
Sweden	1.89	3.07	2.15	1.76	1.49
Taiwan	1.26	1.85	2.15	1.70	1.43
United Kingdom	1.88	3.00	2.63	2.03	1.68
United States	2.06	2.16	2.33	1.84	1.50
Uruguay	2.12	3.22	1.90	1.47	1.19

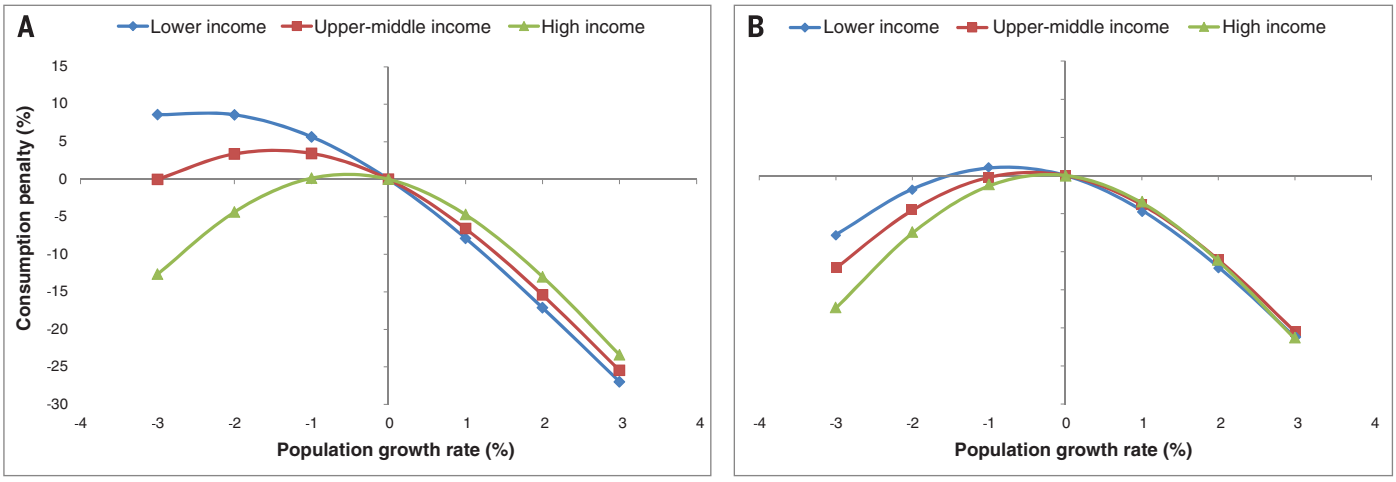


Fig. 2. Effect of population growth on consumption per equivalent adult as a percentage of consumption level for zero population growth. These data have their basis in the low-capital-cost case assuming that the saving rate adjusts to keep the capital-output ratio constant at 3.0 given own-country mortality rates (**A**) and 2009 Japanese mortality rates (**B**). Values are simple averages for countries in three groups: lower income, upper middle income, and high income. See Table 2 for countries in each group. Data sources are as follows: NTA (ntaccounts.org) for consumption and labor income profiles; United Nations Population Division (*1*) for age-specific mortality rates, except for age-specific survival rates for Japan in 2009, which were taken from the Human Mortality Database (www.mortality.org; accessed 16 October 2013).

reduced capital costs of equipping the new workers. Even with lower saving rates from 2000 to 2007 (the start of the global recession), the capital output ratio has risen, and, remarkably, consumption per capita also rose at more than 2% annually. It seems possible through developments in robotics that capital will be able to substitute for labor in elder care. It remains true, however, that a TFR of 1.34 (the average for 2005 to 2010) will impose considerable strain on public finances. Public debt is very high in Japan, making higher taxes and lower benefits a near certainty. But Japan is not experiencing economic decline, and standards of living continue to increase at favorable rates for an advanced economy—faster than long-term productivity growth.

Many factors will influence the economic effects of low fertility that are not part of the formal model used in the analysis. However, these additional considerations reinforce the basic conclusion that low fertility is not a serious economic challenge. The effect of low fertility on the number of workers and taxpayers has been offset by greater human capital investment, enhancing the productivity of workers (*23*). Targeted immigration policy might be helpful, although we are somewhat skeptical on this point (*9*). International capital flows, trade, and technological innovation may mitigate some adverse effects of population aging. Behavioral responses are likely: Changes in patterns of work and consumption are already occurring. Governments are scaling back systems that are not sustainable given any likely demographic scenario.

Fiscal pressures on public programs resulting from population aging are real and important. If the subreplacement fertility levels found in many countries persist, larger adjustments in public programs and retirement age will be required. The United States is exceptional with a TFR close to the level best for public finances. In a number of countries, particularly those with very low fertility, standards of living would be moderately higher if fertility increased. Fertility as low as 1.6 births per woman and possibly even lower should not in itself be a matter of concern. Fertility below replacement and modest population decline favor higher material standards of living.

REFERENCES AND NOTES

1. United Nations Department of Economic and Social Affairs, Population Division, *World Population Prospects: The 2012 Revision* (United Nations, New York, 2013).
2. United Nations Department of Economic and Social Affairs, Population Division, *World Population Policies Database* (United Nations, New York, 2013).
3. D. E. Bloom, D. Canning, J. Sevilla, *The Demographic Dividend: A New Perspective on the Economic Consequences of Population Change* (RAND, Santa Monica, CA, 2002).
4. W. B. Arthur, G. McNicoll, *Int. Econ. Rev.* **19**, 241–246 (1978).
5. R. J. Willis, in *Economics of Changing Age Distributions in Developed Countries*, R. D. Lee, W. B. Arthur, G. Rodgers, Eds. (Oxford Univ. Press, New York, 1988), pp. 106–138.
6. R. D. Lee, in *Demography of Aging*, L. G. Martin, S. H. Preston, Eds. (National Academy Press, Washington, DC, 1994), pp. 8–49.
7. R. D. Lee, *J. Human Res.* **29**, 1027–1063 (1994).
8. R. Lee, A. Mason, Eds., *Population Aging and the Generational Economy: A Global Perspective* (Edward Elgar, Cheltenham, UK, 2011).
9. Information on materials and methods is available on *Science* Online.
10. A. Mason, R. Lee, A.-C. Tung, M. S. Lai, T. Miller, in *Developments in the Economics of Aging*, D. Wise, Ed. (National Bureau of Economic Research Series The Economics of Aging, Univ. of Chicago Press, Chicago, 2009), pp. 89–126.
11. United Nations Department of Economic and Social Affairs, Population Division, *National Transfer Accounts Manual: Measuring and Analyzing the Generational Economy* (United Nations, New York, 2013).
12. T. J. Espenshade, L. F. Bouvier, W. B. Arthur, *Demography* **19**, 125–133 (1982).
13. J. R. Goldstein, in *International Handbook of Population Aging*, Peter Uhlenberg, Ed. (Springer, Dordrecht, Netherlands, 2009), pp. 7–17.
14. C. P. Schmertmann, *Demography* **29**, 595–612 (1992).
15. P. Samuelson, *Int. Econ. Rev.* **16**, 531–538 (1975).
16. P. Samuelson, *Int. Econ. Rev.* **17**, 516–525 (1976).
17. A. V. Deardorff, *Int. Econ. Rev.* **17**, 510–514 (1976).
18. G. Calvo, M. Obstfeld, *Econometrica* **56**, 411–432 (1988).
19. D. Cutler, J. Poterba, L. Sheiner, L. Summers, G. A. Akerlof, *Brookings Pap. Econ. Act.* **1990**, 1–73 (1990).
20. D. Backus, E. Henriksen, K. Storesletten, *J. Monet. Econ.* **55**, 48–61 (2008).
21. R. C. Feenstra, R. Inklaar, M. P. Timmer, The Next Generation of the Penn World Table, www.ggdc.net/pwt; accessed 22 June 2014.
22. T. Piketty, *Capital in the Twenty-First Century* (Harvard Univ. Press, Cambridge, MA, 2014).
23. R. Lee, A. Mason, *Eur. J. Popul.* **26**, 159–182 (2010).

ACKNOWLEDGMENTS

R.L.'s research for this paper was funded by the NIH, National Institute on Aging grant R37 AG025247, and R.L. and A.M.'s research was funded by the Bill and Melinda Gates Foundation through a grant provided to Johns Hopkins Bloomberg School of Public Health. Construction of NTA for many developing countries was possible due to the support of the International Development Research Centre (Canada). The content is solely the responsibility of the authors. The views expressed in this paper are those of J.B. and do not necessarily reflect those of the United Nations. We are grateful to D. Stojanovic for able research assistance. The data are available at http://ntaccounts.org/web/nta/show/Science.

NTA network authors

Eugenia Amporfu,[5] Chong-Bum An,[6] Luis Rosero Bixby,[7] Jorge Bravo,[8] Marisa Bucheli,[9] Qiulin Chen, [10] Pablo Comelatto,[11] Deidra Coy,[12] Hippolyte d'Albis,[13] Gretchen Donehower,[14] Latif Dramani,[15] Alexia Fürnkranz-Prskawetz,[16] Robert I. Gal,[17] Mauricio Holz,[18] Nguyen Thi Lan Huong,[19] Fanny Kluge,[20] Laishram Ladusingh,[21] Sang-Hyop Lee,[22] Thomas Lindh,[23] Li Ling,[24] Giang Thanh Long,[25] Maliki,[26] Rikiya Matsukura,[27] David McCarthy,[28] Iván Mejía-Guevara,[29] Teferi Mergo,[30] Tim Miller,[31] Germano Mwabu,[32] M.R. Narayana,[33] Vanndy Nor,[34] Gilberto Mariano Norte,[35] Naohiro Ogawa,[36] Olanrewaju Ademola Olaniyan,[37] Javier Olivera,[38] Morne Oosthuizen,[39] Mathana Phananiramai,[40] Bernardo Lanza Queiroz,[41] Rachel H. Racelis,[42] Elisenda Renteria,[43] James Mahmud Rice,[44] Joze Sambt,[45] Aylin Seçkin,[46] James Sefton,[47] Adedoyin Soyibo,[48] Jorge A. Tovar,[49] An-Chi Tung,[50] Cassio M. Turra,[51] B. Piedad Urdinola,[52] Risto Vaittinen,[53] Reijo Vanne,[54] Marina Zannella,[55] Qi Zhang[56]

[5]Kwame Nkrumah University of Science and Technology, Kumasi, Ghana. [6]Department of Economics, Sungkyunkwan University, Seoul, Republic of Korea. [7]San Jose, Costa Rica. [8]United Nations Department of Economic and Social Affairs–Population Division, New York, USA. [9]Department of Economics, Universidad de la

República, Montevideo, Uruguay. [10]Institute of Population and Labor Economics, Chinese Academy of Social Sciences, Beijing, China. [11]Centro de Estudios de Población–CENEP, Buenos Aires, Argentina. [12]Planning Institute of Jamaica, Kingston, Jamaica. [13]Paris School of Economics, University of Paris, Paris, France. [14]Demography Department, University of California, Berkeley, CA, USA. [15]Universite de Thiès/CREFAT, Dakar, Senegal. [16]Vienna University of Technology, Vienna, Austria. [17]Demographic Research Institute and TARKI Social Research Institute, Budapest, Romania. [18]UNESCO, Regional Bureau for Education in Latin America and the Caribbean, Santiago, Chile. [19]Institute of Labor Science and Social Affairs (ILSSA), Ministry of Labor, Invalids, and Social Affairs (MoLISA), Hanoi, Vietnam. [20]Max Planck Institute for Demographic Research, Rostock, Germany. [21]International Institute for Population Sciences, Mumbai, India. [22]Center for Korean Studies, University of Hawaii at Manoa, Honolulu, HI, USA. [23]Deceased. [24]National School of Development, Peking University, Beijing, China. [25]Institute of Public Policy and Management, National Economics University, Hanoi, Vietnam. [26]State Ministry of National Development Planning, Jakarta, Indonesia. [27]Nihon University Population Research Institute (NUPRI), Tokyo, Japan. [28]National Institute of Economic and Social Research (NIESR), London, UK. [29]Center for Population and Development Studies, Harvard School of Public Health, Cambridge, MA, USA. [30]University of California, Berkeley, CA, USA. [31]Economic Commission for Latin America and the Caribbean, Santiago, Chile. [32]University of Nairobi, Nairobi, Kenya. [33]Institute for Social and Economic Change, Bangalore, India. [34]National Institute of Statistics, Phnom Penh, Cambodia. [35]United Nations Population Fund (UNFPA), Maputo, Mozambique. [36]NUPRI, Tokyo, Japan. [37]Department of Economics, University of Ibadan, Ibadan, Nigeria. [38]Institute for Research on Socio-Economic Inequality, University of Luxembourg, Luxembourg. [39]School of Economics, University of Cape Town, Cape Town, South Africa. [40]Thailand Development Research Institute, Bangkok, Thailand. [41]CEDEPLAR–Department of Demography, Universidade Federal de Minas Gerais, Belo Horizonte MG, Brazil. [42]School of Urban and Regional Planning, University of the Philippines, Diliman, Quezon City, Philippines. [43]International Agency for Research on Cancer and Universitat de Barcelona, Barcelona, Spain. [44]Australian Demographic and Social Research Institute, Australian National University, Canberra, Australia. [45]Faculty of Economics, University of Ljubljana, Ljubljana, Slovenia. [46]Istanbul Bilgi University, Istanbul, Turkey. [47]Imperial College Business School, London, UK. [48]Department of Economics, University of Ibadan, Ibadan, Nigeria. [49]Department of Economics, Universidad de los Andes-Bogotá, Bogotá, Colombia. [50]Institute of Economics, Academia Sinica Taiwan, Taipei, Taiwan. [51]Department of Demography, Universidade Federal de Minas Gerais, Belo Horizonte MG, Brazil. [52]Department of Statistics, Universidad Nacional de Colombia-Bogotá, Bogotá, Colombia. [53]Finland Centre for Pensions, Helsinki, Finland. [54]Finnish Pension Alliance TELA, Helsinki, Finland. [55]Institute of Mathematical Methods in Economics, Vienna University of Technology, Vienna, Austria. [56]Department of Economics, University of Ottawa, Ottawa, Canada.

SUPPLEMENTARY MATERIALS

www.sciencemag.org/content/346/6206/229/suppl/DC1
Materials and Methods
Tables S1 and S2
References (*24*–*34*)

8 January 2014; accepted 26 August 2014
10.1126/science.1250542

WORLD POPULATION

World population stabilization unlikely this century

Patrick Gerland,[1]*† Adrian E. Raftery,[2]*† Hana Ševčíková,[3] Nan Li,[1] Danan Gu,[1] Thomas Spoorenberg,[1] Leontine Alkema,[4] Bailey K. Fosdick,[5] Jennifer Chunn,[6] Nevena Lalic,[7] Guiomar Bay,[8] Thomas Buettner,[9]‡ Gerhard K. Heilig,[9]‡ John Wilmoth[1]

The United Nations (UN) recently released population projections based on data until 2012 and a Bayesian probabilistic methodology. Analysis of these data reveals that, contrary to previous literature, the world population is unlikely to stop growing this century. There is an 80% probability that world population, now 7.2 billion people, will increase to between 9.6 billion and 12.3 billion in 2100. This uncertainty is much smaller than the range from the traditional UN high and low variants. Much of the increase is expected to happen in Africa, in part due to higher fertility rates and a recent slowdown in the pace of fertility decline. Also, the ratio of working-age people to older people is likely to decline substantially in all countries, even those that currently have young populations.

The United Nations (UN) is the leading agency that projects world population into the future on a regular basis (*1*). Every 2 years the UN publishes revised data of the populations of all countries by age and sex—as well as fertility, mortality, and migration rates—in a biennial publication called the *World Population Prospects* (*2*). In July 2014, probabilistic projections were released for individual countries to 2100. Unlike previous projections, these estimates allow us to quantify our confidence in projected future trends using established methods of statistical inference. These projections are based on recent data, including the results of the 2010 round of censuses and recent surveys until 2012, as well as the most recent data on incidence, prevalence, and treatment for the countries most affected by the HIV/AIDS epidemic (*3*), which had not been included previously.

Our analysis of these data shows that world population can be expected to increase from the current 7.2 billion people to 9.6 billion in 2050 and 10.9 billion in 2100 (Fig. 1A). These projections indicate that there is little prospect of an end to world population growth this century without unprecedented fertility declines in most parts of sub-Saharan Africa still experiencing fast population growth.

Traditionally, the UN has also provided high- and low-projection scenarios (shown in Fig. 1A), obtained by adding or subtracting half a child from the total fertility rate [(TFR) in children per woman] on which the main (or medium) projection is based, for each country and all future time periods. These scenarios have been criticized as having no probabilistic basis and leading to inconsistencies (*4*, *5*). For example, though it is plausible that fertility could exceed the main projection by half a child in a given country and year, it is unlikely that this would be the case for all countries and all years in the future, as assumed in the high projection.

In a methodological innovation aimed at overcoming this limitation, we derived new probabilistic projections based on probabilistic Bayesian hierarchical models for major components of demographic change—namely, fertility (*6*–*8*) and life expectancy (*9*, *10*). These models incorporated available data and take advantage of data from other countries when making projections for a given country. They also incorporated external information through Bayesian prior distributions, including an upper bound of 1.3 years per decade on the asymptotic rate of increase of life expectancy, based on historic data on life expectancy in leading countries (*11*) and on changes in the maximum age at death (*12*). The models included the assumption that the TFR for a country will ultimately fluctuate around a country-specific long-term average that is estimated from the data; these long-term averages are between 1.5 and 2 children per woman for most countries with high probability (*7*).

Probabilistic population projections were then obtained by inputting the output from the statistical models to the standard cohort component projection method (*4*, *13*). Aggregates were based on individual country projections and take into account the correlations between countries' fertility future trajectories (*8*). The models yielded probabilistic projections and, thus, probabilistic limits for future quantities of interest, responding to calls for probabilistic population forecasting (*5*). (See the supplementary materials and http://esa.un.org/unpd/ppp/ for summary tables, plots, assumptions, and methodology.) Here we summarize the overall trends and discuss their implications for world population in the future. The probabilistic projections of world population (Fig. 1A) provide a general statement of the confidence we can have in the projections. For example, there is a 95%

[1]Population Division, Department of Economic and Social Affairs, United Nations, New York, NY 10017, USA. [2]Departments of Statistics and Sociology, University of Washington, Seattle, WA 98195-4322, USA. [3]Center for Statistics and the Social Sciences, University of Washington, Seattle, WA 98195-4320, USA. [4]Department of Statistics and Applied Probability and Saw Swee Hock School of Public Health, National University of Singapore, Singapore 117546. [5]Department of Statistics, Colorado State University, Fort Collins, CO 80523-1877, USA. [6]James Cook University Singapore, 600 Upper Thomson Road, Singapore 574421. [7]Institutional Research, University of Washington, Seattle, WA 98195-9445, USA. [8]Latin American and Caribbean Demographic Center (CELADE), Population Division of the United Nations Economic Commission for Latin America and the Caribbean, Santiago, Chile. [9]Population Division, United Nations, New York, NY, USA.
*These authors contributed equally to this work. **†Corresponding author. E-mail: gerland@un.org (P.G.); raftery@u.washington.edu (A.E.R.)** ‡Retired.

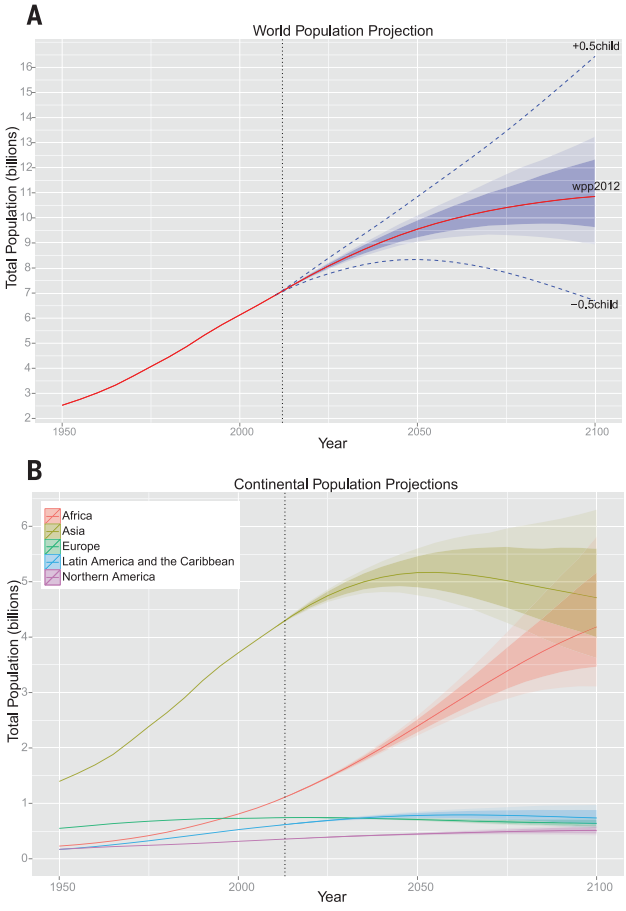


Fig. 1. World and continental population projections. (**A**) UN 2012 world population projection (solid red line), with 80% PI (dark shaded area), 95% PI (light shaded area), and the traditional UN high and low variants (dashed blue lines). (**B**) UN 2012 population projections by continent. In both panels, the vertical dashed line denotes 2012.

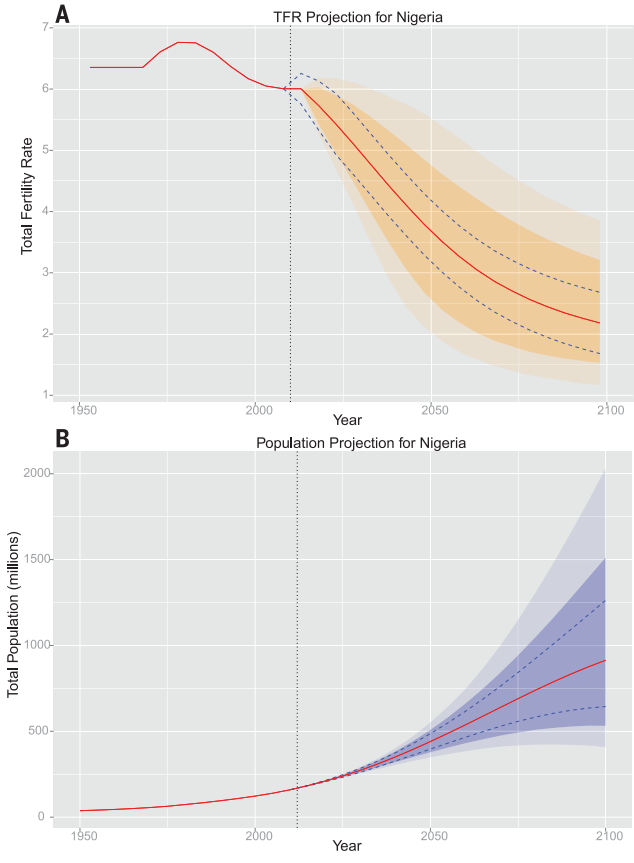


Fig. 2. TFR and population projections for Nigeria. UN 2012 projection of (**A**) TFR and (**B**) total population for Nigeria (solid red lines), with 80% PI (dark shaded areas), 95% PI (light shaded areas), and traditional UN high and low variants (dashed blue lines). In both panels, the vertical dashed line denotes 2012.

probability that world population in 2100 will be between 9.0 and 13.2 billion people. The projections also provide updated answers to long-standing questions about population change. Lutz *et al.* (*14*) gave an 85% probability that world population growth would end in the 21st century, but our probabilistic projection indicates that this probability is much lower, at only 30%. Lutz *et al.* (*15*) considered a doubling of world population from 1997 to 2100 to be unlikely, with a probability of one-third. We found a similar but slightly lower probability of 25%. The probabilistic intervals were much narrower than those between the traditional high and low scenarios, which seem to overstate uncertainty about future world population.

Figure 1B shows the projections of total population for each continent to the end of the century. Asia will probably remain the most populous continent, although its population is likely to peak around the middle of the century and then decline. The main reason for the increase in the projection of the world population is an increase in the projected population of Africa. The continent's current population of about 1 billion people is projected to rise to between 3.1 and 5.7 billion with probability 95% by the end of the century, with a median projection of 4.2 billion. Although this estimate is large, it does not imply unprecedented population density: Under this projection, Africa's population density would be roughly equal to that of China today.

The increase in the projected population of Africa is due to persistent high levels of fertility and the recent slowdown in the rate of fertility decline (*16*). Three-quarters of this anticipated growth is attributable to fertility levels above the replacement level, and the remaining quarter is due to mortality reduction and current youthful age structure (*17*). Since 1950, fertility has declined rapidly in Asia and Latin America and has also started to decline in Africa. Demographers had projected that fertility in African countries would decline at a rate similar to what has been observed in Asia and Latin America.

However, although fertility has been declining in Africa over the past decade, it has been doing so at only about one-quarter of the rate at which it declined in Asia and Latin America in the 1970s, when these regions were at a comparable stage of the fertility transition (*16*). Indeed, in some African countries, the decline seems to have stalled (*18*).

Bongaarts and Casterline (*16*) suggest two reasons for the slower fertility decline in sub-Saharan Africa. First, they note that despite declines in fertility desires in Africa, the most recent levels of ideal family size are still high, with a median of 4.6 children per woman. This is in line with prevailing family norms (*19*) and the fact that the TFR before fertility started to decline was higher in Africa (6.5) than in the other regions (5.8) (*20*, *21*). Second, the unmet need for contraception (the difference between the demand for contraception and its use) has remained substantial at ~25%, with no systematic decline over the past 20 years (*22*).

A stall in the decline in the past decade is apparent from the past and projected levels of TFR

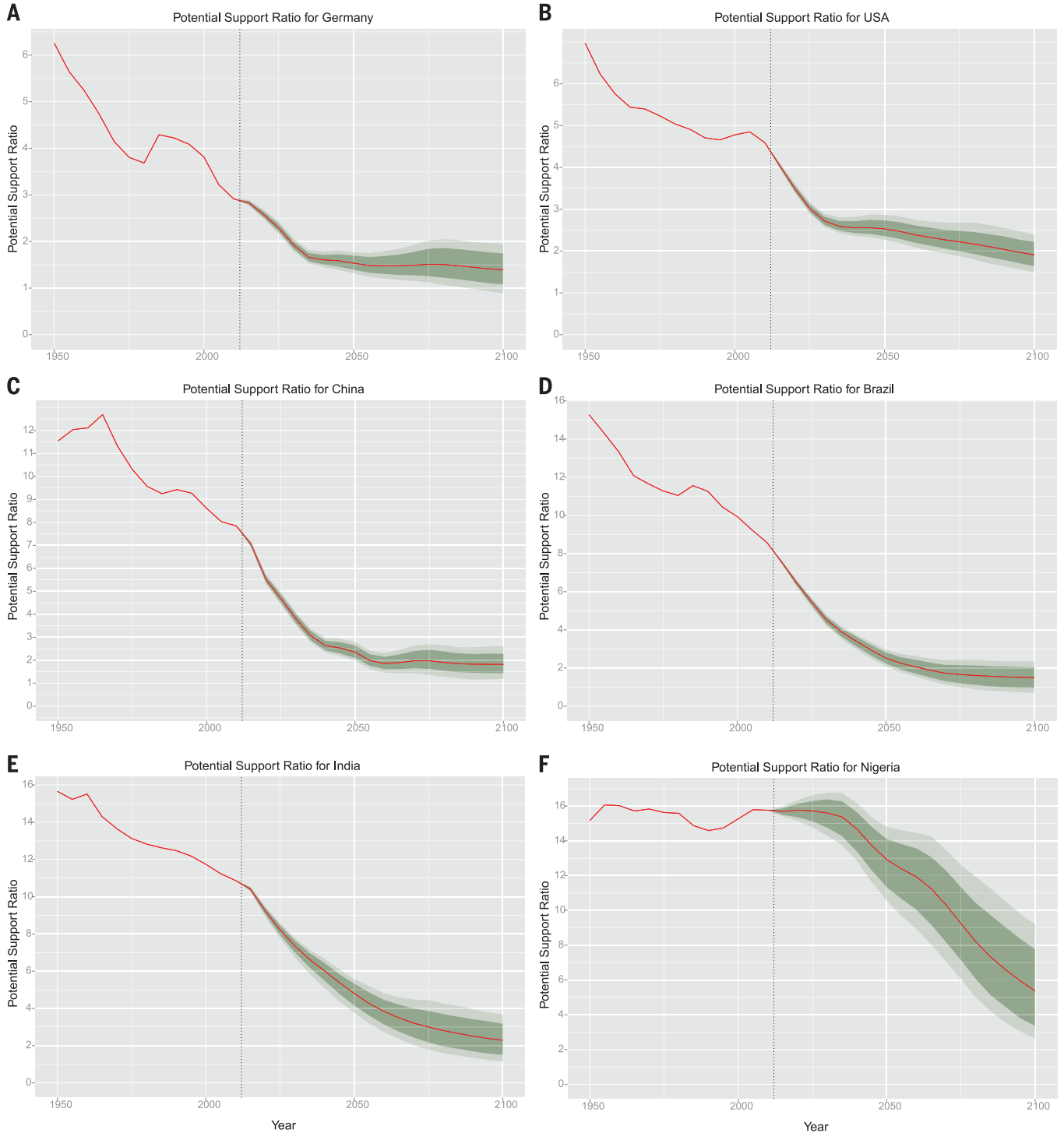


Fig. 3. PSR by country. (**A** to **F**) UN projections of PSRs, equal to the number of people aged 20 to 64 divided by the number of people aged 65 or over (solid red lines), with 80% PI (dark shaded areas) and 95% PI (light shaded areas) shown. In all panels, the vertical dashed line denotes 2012.

for Nigeria, the most populous country in Africa (Fig. 2A). The UN's projection continues to forecast a decline, but the uncertainty bands are wide, indicating that the stall could continue for a considerable time. This continued high fertility would result in a projected increase in total population of more than fivefold by 2100, from the current 174 to 914 million (Fig. 2B). There is considerable uncertainty about this projection, but there is still a 90% probability that Nigeria's population in 2100 will exceed 532 million, a more-than-threefold increase.

We also indicate the likely level of population aging in different countries. One measure of this is the potential support ratio (PSR), which is equal to the number of people aged 20 to 64 divided by the number of people 65 and over (Fig. 3). This can be viewed very roughly as reflecting the number of workers per retiree. Currently, the country with the lowest PSR is Japan, with 2.6.

Germany's PSR is currently 2.9 and is projected to decline rapidly at first, to 1.7 in 2035 and then to 1.4 by the end of the century. Although there is uncertainty about the level at the end of the century, with an 80% prediction interval (PI) of 1.1 to 1.7, it is likely that the German PSR will be well below the current Japanese ratio. The current

PSR in the United States is 4.6, and this is projected to decline to 1.9 by 2100 (80% PI: 1.6 to 2.2).

Whereas the population aging issues of developed countries have been widely discussed (*23*), the likely patterns in developing populations that currently have young populations are less well known. China's PSR is projected to decline to 1.8 (80% PI: 1.4 to 2.3) from the current high level of 7.8. Brazil's PSR is currently 8.6 and is projected to decline to 1.5 (80% PI: 1.0 to 2.0), which is well below the current Japanese level. India has a PSR of 10.9, but this is projected to decline to 2.3 (80% PI: 1.5 to 3.2) by the end of the century. The only country in Fig. 3 that is projected to have a PSR above 3 by the end of the century is Nigeria, whose PSR is currently at the high level of 15.8 and is projected to decline to 5.4 (80% PI: 3.4 to 7.8).

These results suggest some important policy implications. Rapid population growth in high-fertility countries can create a range of challenges: environmental (depletion of natural resources, pollution), economic (unemployment, low wages, poverty), health (high maternal and child mortality), governmental (lagging investments in health, education, and infrastructure), and social (rising unrest and crime) (*24*).

Among the most robust empirical findings in the literature on fertility transitions are that higher rates of contraceptive use and female education are associated with faster fertility decline (*25*). These suggest that the projected rapid population growth could be moderated by greater investments in family planning programs to satisfy the unmet need for contraception (*26*, *27*), as well as investments in girls' education. It should be noted, however, that the UN projections are based on an implicit assumption of a continuation of existing policies and reform efforts, but an intensification of current investments would be required for faster changes to occur. It should also be noted that the projections do not take into account potential negative feedback from the environmental consequences of rapid population growth. The addition of several billion people in Africa could lead to severe resource shortages that, in turn, could affect population size through unexpected mortality, migration, or fertility effects.

The implications are not all negative, however. Rapid fertility decline brings with it the prospect of a potential long-lasting demographic dividend in countries that currently have high fertility, such as Nigeria (see Fig. 3). Figure 3 also suggests that developing countries with young populations but lower fertility (e.g., China, Brazil, and India) are likely to face the problems of aging societies before the end of the century. This prediction suggests that these countries need to invest some of the benefits from their demographic dividends in coming decades in provisions for future seniors, such as social security, pension, and senior health care funds.

REFERENCES AND NOTES

1. W. Lutz, K. C. Samir, *Philos. Trans. R. Soc. London Ser. B* **365**, 2779–2791 (2010).
2. United Nations, *World Population Prospects: The 2012 Revision* (Population Division, Department of Economic and Social Affairs, United Nations, New York, 2013).
3. UNAIDS, *Global Report: UNAIDS Report on the Global AIDS Epidemic 2013* (UNAIDS, Geneva, 2013).
4. R. D. Lee, S. Tuljapurkar, *J. Am. Stat. Assoc.* **89**, 1175–1189 (1994).
5. National Research Council, *Beyond Six Billion: Forecasting the World's Population* (National Academy Press, Washington, DC, 2000).
6. L. Alkema *et al.*, *Demography* **48**, 815–839 (2011).
7. A. E. Raftery, L. Alkema, P. Gerland, *Stat. Sci.* **29**, 58–68 (2014).
8. B. K. Fosdick, A. E. Raftery, *Demogr. Res.* **30**, 1011–1034 (2014).
9. A. E. Raftery, J. L. Chunn, P. Gerland, H. Sevčíková, *Demography* **50**, 777–801 (2013).
10. A. E. Raftery, N. Lalic, P. Gerland, *Demogr. Res.* **30**, 795–822 (2014).
11. J. Oeppen, J. W. Vaupel, *Science* **296**, 1029–1031 (2002).
12. J. R. Wilmoth, L. J. Deegan, H. Lundström, S. Horiuchi, *Science* **289**, 2366–2368 (2000).
13. A. E. Raftery, N. Li, H. Ševčíková, P. Gerland, G. K. Heilig, *Proc. Natl. Acad. Sci. U.S.A.* **109**, 13915–13921 (2012).
14. W. Lutz, W. Sanderson, S. Scherbov, *Nature* **412**, 543–545 (2001).
15. W. Lutz, W. Sanderson, S. Scherbov, *Nature* **387**, 803–805 (1997).
16. J. Bongaarts, J. Casterline, *Popul. Dev. Rev.* **38** (suppl. 1), 153–168 (2013).
17. K. Andreev, V. Kantorová, J. Bongaarts, *Demographic Components of Future Population Growth* (Technical Paper no. 2013/3, Population Division, Department of Economic and Social Affairs, United Nations, New York, 2013).
18. United Nations, *Population Facts No. 2013/10, December 2013 - Explaining Differences in the Projected Populations Between the 2012 and 2010 Revisions of* World Population Prospects: *The Role of Fertility in Africa* (Population Division, Department of Economic and Social Affairs, United Nations, New York, 2013).
19. T. A. Moultrie, I. M. Timaeus, "Rethinking African fertility: The state in, and of, the future sub-Saharan African fertility decline," paper presented at the Annual Meeting of the Population Association of America, Boston, MA, 1 to 3 May 2014; http://paa2014.princeton.edu/abstracts/143218.
20. J. C. Caldwell, P. Caldwell, *Popul. Dev. Rev.* **13**, 409–437 (1987).
21. J. C. Caldwell, P. Caldwell, *Stud. Fam. Plann.* **19**, 19–28 (1988).
22. United Nations, *Model-Based Estimates and Projections of Family Planning Indicators: 2013 Revision* (Population Division, Department of Economic and Social Affairs, United Nations, New York, 2014).
23. National Research Council, *Aging and the Macroeconomy* (National Academy Press, Washington, DC, 2012).
24. J. Bongaarts, "Demographic trends and implications for development," paper presented at the International Union for the Scientific Study of Population 2013 Meeting, Busan, Republic of Korea, 26 to 31 August 2013; http://iussp.org/sites/default/files/event_call_for_papers/Session_071_01_Bongaarts.pdf.
25. C. Hirschman, *Annu. Rev. Sociol.* **20**, 203–233 (1994).
26. London Summit on Family Planning, Technical note: Data sources and methodology for developing the 2012 baseline, 2020 objective, impacts and costings (Family Planning Summit Metrics Group, London, 2012).
27. H. B. Peterson, G. L. Darmstadt, J. Bongaarts, *Lancet* **381**, 1696–1699 (2013).

ACKNOWLEDGMENTS

We thank the entire team involved in the production of the 2012 Revision of the *World Population Prospects*—in particular, K. Andreev and F. Pelletier. We also thank two anonymous reviewers for helpful comments. This work was supported by NIH grants R01 HD054511 and R01 HD070936. A.E.R.'s research was also supported by a Science Foundation Ireland ETS Walton visitor award, grant reference 11/W.1/I2079. Views expressed in this article are those of the authors and do not necessarily reflect those of NIH or the UN.

SUPPLEMENTARY MATERIALS

www.sciencemag.org/content/346/6206/234/suppl/DC1
Materials and Methods
Table S1
References (*28*–*47*)

16 June 2014; accepted 10 September 2014
Published online 18 September 2014;
10.1126/science.1257469

ADULT NEUROGENESIS

A latent neurogenic program in astrocytes regulated by Notch signaling in the mouse

Jens P. Magnusson,[1]* Christian Göritz,[1]* Jemal Tatarishvili,[2] David O. Dias,[1] Emma M. K. Smith,[3] Olle Lindvall,[2] Zaal Kokaia,[2] Jonas Frisén[1]†

Neurogenesis is restricted in the adult mammalian brain; most neurons are neither exchanged during normal life nor replaced in pathological situations. We report that stroke elicits a latent neurogenic program in striatal astrocytes in mice. Notch1 signaling is reduced in astrocytes after stroke, and attenuated Notch1 signaling is necessary for neurogenesis by striatal astrocytes. Blocking Notch signaling triggers astrocytes in the striatum and the medial cortex to enter a neurogenic program, even in the absence of stroke, resulting in 850 ± 210 (mean ± SEM) new neurons in a mouse striatum. Thus, under Notch signaling regulation, astrocytes in the adult mouse brain parenchyma carry a latent neurogenic program that may potentially be useful for neuronal replacement strategies.

Neurogenesis in the adult brain is largely restricted to the dentate gyrus and the subventricular zone lining the lateral ventricles. However, astrocytes close to a lesion can display neural stem cell properties when assayed in vitro (*1*–*3*), and astrocytes can be forced to either convert into (*4*, *5*) or produce neurons (*6*) when reprogrammed by ectopic expression of transcription factors in vivo.

To explore the in vivo neurogenic potential of astrocytes, we used Connexin-30–CreER (Cx30-CreER) transgenic mice (*7*) carrying a R26R–yellow

[1]Department of Cell and Molecular Biology, Karolinska Institute, SE-171 77 Stockholm, Sweden. [2]Lund Stem Cell Center, University Hospital, SE-221 84 Lund, Sweden. [3]Division of Translational Cancer Research, Lund University, SE-223 63 Lund, Sweden.
*These authors contributed equally to this work. **†Corresponding author. E-mail jonas.frisen@ki.se**

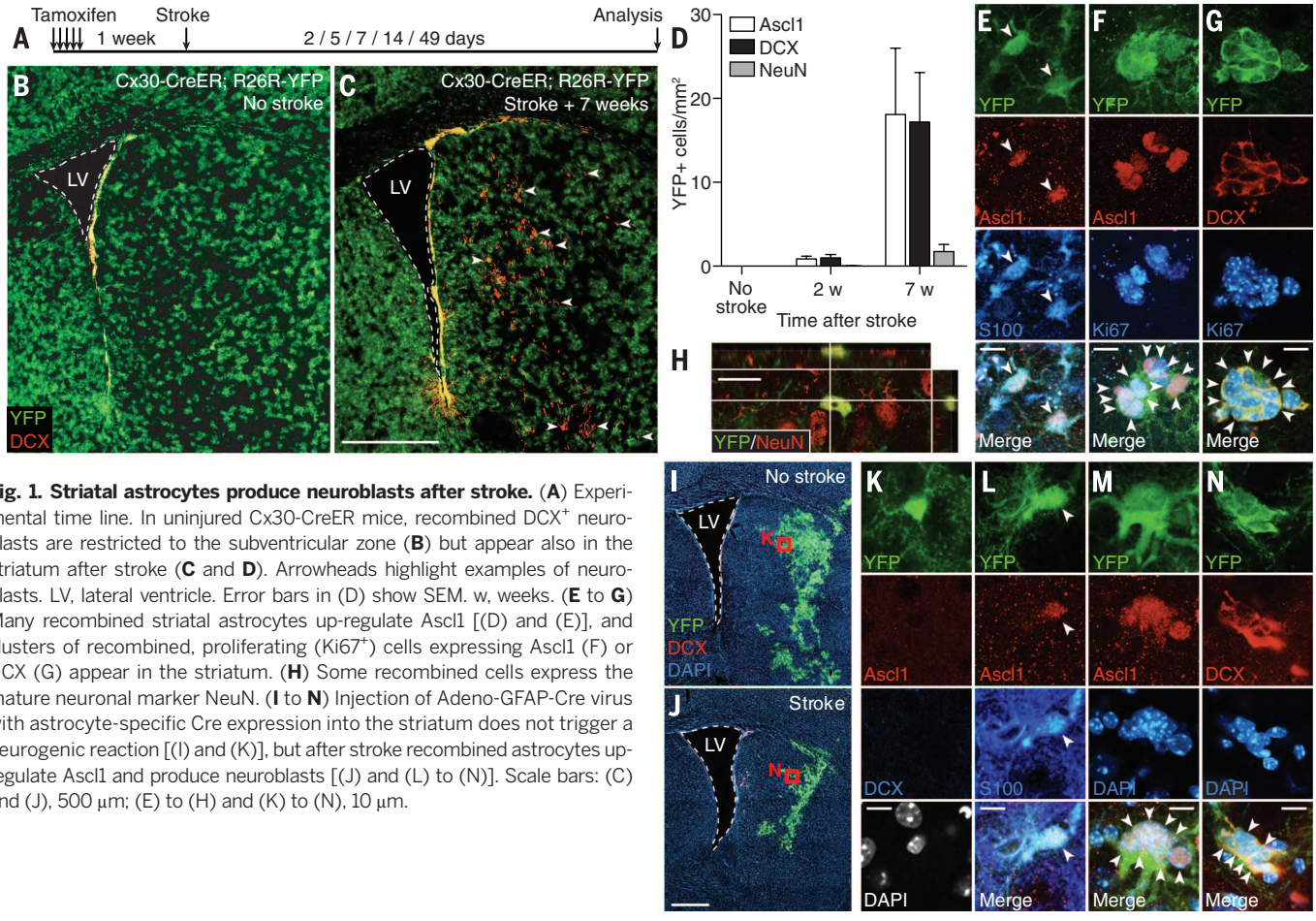


Fig. 1. Striatal astrocytes produce neuroblasts after stroke. (**A**) Experimental time line. In uninjured Cx30-CreER mice, recombined DCX$^+$ neuroblasts are restricted to the subventricular zone (**B**) but appear also in the striatum after stroke (**C** and **D**). Arrowheads highlight examples of neuroblasts. LV, lateral ventricle. Error bars in (D) show SEM. w, weeks. (**E** to **G**) Many recombined striatal astrocytes up-regulate Ascl1 [(D) and (E)], and clusters of recombined, proliferating (Ki67$^+$) cells expressing Ascl1 (F) or DCX (G) appear in the striatum. (**H**) Some recombined cells express the mature neuronal marker NeuN. (**I** to **N**) Injection of Adeno-GFAP-Cre virus with astrocyte-specific Cre expression into the striatum does not trigger a neurogenic reaction [(I) and (K)], but after stroke recombined astrocytes up-regulate Ascl1 and produce neuroblasts [(J) and (L) to (N)]. Scale bars: (C) and (J), 500 μm; (E) to (H) and (K) to (N), 10 μm.

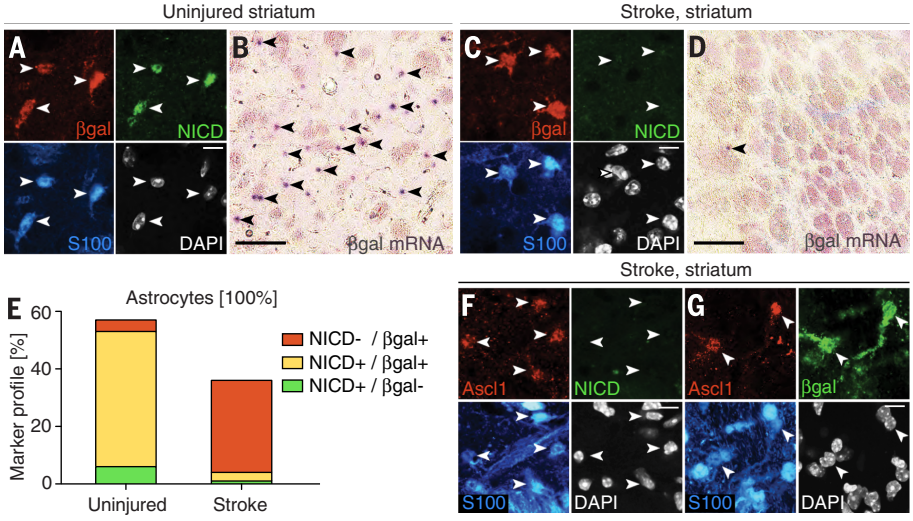


Fig. 2. Reduced Notch signaling in astrocytes that enter a neurogenic program. Many astrocytes in the uninjured striatum have active Notch1 signaling, as revealed by Notch1 activity–induced β-Gal expression and nuclear NICD protein (**A** and **B**). Two weeks after stroke in Notch1 reporter mice, cells in a large area of the injured striatum lack NICD protein (**C**) and β-Gal mRNA (**D**), but many still contain the long-lived β-Gal protein (C). (**E**) NICD and β-Gal in striatal S100$^+$ astrocytes. Most Ascl1-expressing astrocytes lack nuclear NICD in the injured striatum (**F**) but retain β-Gal protein (**G**). Arrowheads highlight individual cells. Scale bars: (A), (C), (F), and (G), 10 μm; (B) and (D), 100 μm. DAPI, 4′,6-diamidino-2-phenylindole.

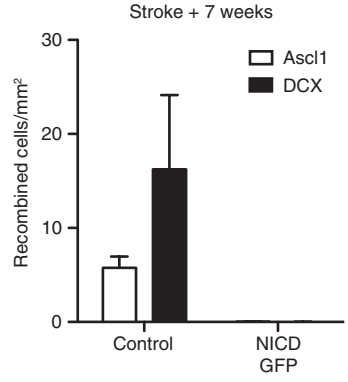


Fig. 3. Ectopic Notch1 activation in astrocytes inhibits stroke-induced neuroblast production. Ectopic Notch1 activation is sufficient to inhibit Ascl1 expression and neuroblast production by astrocytes after stroke. Error bars show SEM. GFP, green fluorescent protein.

fluorescent protein (YFP) reporter allele (*8*) for genetic fate mapping after experimental stroke. Stroke was induced by transient occlusion of the middle cerebral artery, a procedure that generated an ischemic lesion primarily in the striatum. We waited 1 week between giving tamoxifen and inducing the stroke, to allow for the tamoxifen to be eliminated and exclude the possibility of recombination in other cell types after stroke (Fig. 1A). The Cx30-CreER transgene allows specific recombination in a large subset of parenchymal astrocytes throughout the brain (37 ± 10% of glutamine synthetase$^+$, S100$^+$ cells in the striatum, mean ± SEM) (fig. S1), as well as in subventricular zone astrocyte-like neural stem cells (*9*).

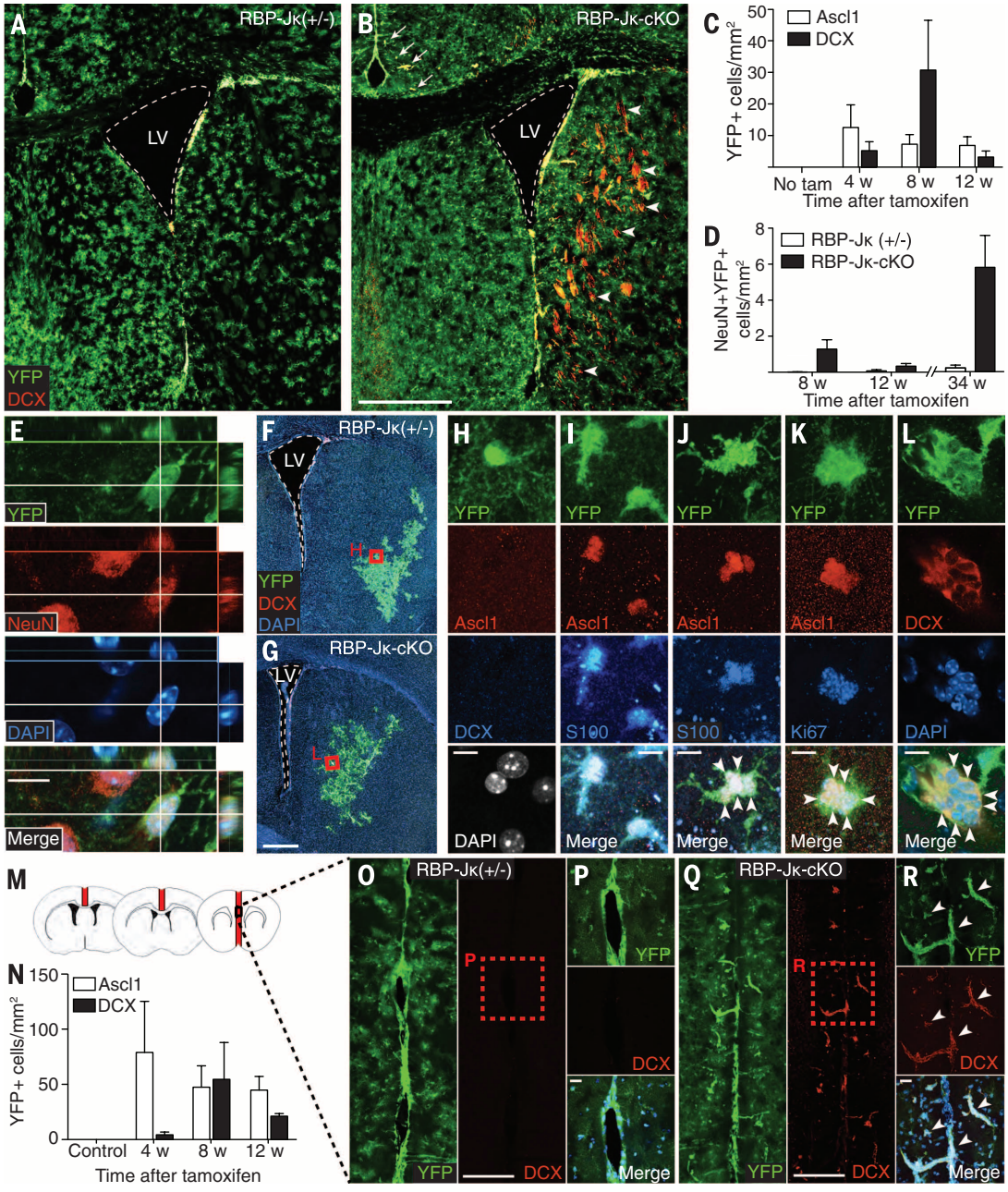


Fig. 4. Deletion of RBP-Jκ triggers neuroblast production by astrocytes in the striatum and medial cortex. (**A** to **C**) Deletion of RBP-Jκ in astrocytes of adult Cx30-CreER mice leads to the appearance of ectopic Ascl1$^+$ cells and DCX$^+$ neuroblasts in the striatum in the absence of injury. Arrowheads point to examples of neuroblasts. cKO, conditional knockout. (**D** and **E**) With time, some striatal neuroblasts mature into neurons. (**F** to **L**) Injection of Adeno-GFAP-Cre virus into the striatum of animals heterozygous for the mutated RBP-Jκ allele does not cause Ascl1$^+$ or DCX$^+$ cells to appear [(F) and (H)] but in homozygous animals induces astrocytes to up-regulate Ascl1 and produce neuroblasts [(G) and (I) to (L)]. Arrowheads in (J) to (L) highlight individual cells. (B) and (**M** to **R**) Cx30-CreER–mediated RBP-Jκ deletion triggers the appearance of Ascl1$^+$ cells and neuroblasts also in the superficial medial cortex [red areas in (M), arrows in (B)]. Arrowheads in (R) show cell clusters. Error bars in (C), (D), and (N) show SEM. Scale bars: (B) and (G), 500 μm; (E) and (H) to (L), 10 μm; (O) and (Q), 200 μm; (P) and (R), 25 μm.

As previously described, stroke triggered the appearance of many doublecortin-positive (DCX$^+$) recombined neuroblasts in the affected striatum (*10*, *11*) (Fig. 1, B to D) (n = 12 mice). We found signs that some of these neuroblasts might have been generated locally within the striatum, rather than having migrated from the subventricular zone. Beginning at 2 days after stroke, scattered astrocytes in the medial striatum expressed Ascl1 (Fig. 1E and fig. S2), a proneural transcription factor (*12*). At this time point, all S100$^+$,Ascl1$^+$ astrocytes proliferated (fig. S2, C to F) and subsequently formed clusters of recombined, proliferating Ascl1$^+$ cells (Fig. 1F), no longer expressing the astrocyte marker S100 (fig. S2, G and H). Up to ~70% of S100$^+$ astrocytes expressed Ascl1 in the most dense patches along the border of the lesion (fig. S3). Two weeks after the stroke, tightly packed clusters of recombined DCX$^+$,Ki67$^+$ neuroblasts appeared in the medial striatum; these neuroblasts were small and round and lacked the bipolar processes seen on migrating neuroblasts (Fig. 1G). All DCX$^+$ cells coexpressed polysialylated neural cell adhesion molecule (PSA-NCAM) (fig. S2I). The number of cells in the striatum expressing Ascl1 and DCX increased from 2 to 7 weeks (3900 ± 990 DCX$^+$ cells per lesion at 7 weeks, mean ± SEM) after the stroke (Fig. 1D) but maintained their general distribution (fig. S3). All described intermediate stages were continuously present, indicating that new astrocytes were being recruited for at least 7 weeks. Some of these neuroblasts developed into mature NeuN$^+$ neurons (340 ± 160 cells per striatum at 7 weeks after stroke, mean ± SEM) (Fig. 1, D and H)—of which several expressed neuronal nitric oxide synthase (nNOS), a marker for GABAergic medium-sized striatal interneurons—and formed synaptic connections (fig. S4).

Because Cx30-CreER mice also target cells in the subventricular zone, it was not possible to exclude a periventricular origin of these new cells. We specifically fate-mapped striatal astrocytes by injecting adenovirus expressing Cre under either the general cytomegalovirus (CMV) promoter or the astrocyte-specific human glial fibrillary acidic protein (GFAP) promoter in the striatum of R26R-YFP mice (94 to 99% specificity) (fig. S5). We used an oblique injection route, allowing local recombination of striatal astrocytes without transducing cells in the subventricular

zone or rostral migratory stream (Fig. 1, I and J, and fig. S6, A and B). The virus injection itself did not cause any ectopic Ascl1$^+$ or DCX$^+$ cells to appear (Fig. 1, I and K, and fig. S6, A and C). Animals were subjected to stroke and analyzed 7 weeks later. Many Ascl1$^+$ cells and DCX$^+$ neuroblasts, some of which expressed NeuN, expressed YFP in the virus-injected area of the striatum (Fig. 1, J and L to N, and fig. S6, B and D to G) (n = 6 mice), demonstrating that striatal astrocytes had generated neuroblasts after the stroke.

Seven weeks after stroke, 31 ± 4% (mean ± SEM) of recombined neuroblasts were found in clusters in Cx30-CreER mice, indicative of a local striatal origin. A fate-mapping study demonstrated that 33% of striatal neuroblasts derive from nestin-expressing subventricular zone stem cells after stroke (*13*), which suggests that approximately between one-third and two-thirds of the new neurons derive from striatal astrocytes after stroke.

Cx30-CreER–recombined striatal astrocytes in uninjured animals were negative for the neural stem cell marker nestin, whereas 95% were Sox2-positive (fig. S1, B, F, and H). In transgenic reporter mice where activation of the Notch1 receptor leads to expression of β-galactosidase (β-Gal) (*14*), β-*Gal* mRNA was abundant in the uninjured brain parenchyma, and half of all S100$^+$ striatal astrocytes were positive for the β-Gal protein (Fig. 2, A, B, and E) (n = 5 mice). The nuclei of these cells also contained the cleaved Notch1 intracellular domain (NICD), which is present in cells with active Notch signaling (Fig. 2, A and E).

Neural stem cell quiescence is regulated in part by Notch1 signaling (*12*, *15*). We found that stroke caused a reduction in the protein levels of Notch receptors 1, 2, and 3, as well as the Notch ligands Dll1, Jagged1, and Jagged2, whereas Dll3 levels were increased, in the affected striatum 3 days after stroke (fig. S7). Two weeks after stroke, both NICD protein and β-Gal mRNA in Notch1 reporter mice had become undetectable in a large area in the striatum, demonstrating that cells no longer had active Notch1 signaling (Fig. 2, C and D) (n = 6 mice). However, many NICD-negative astrocytes still contained detectable β-Gal protein (Fig. 2, C and E), probably due to a relatively high stability of this protein (*16*). Most Ascl1$^+$ astrocytes were located on the very border of the area devoid of NICD immunoreactivity and were negative for NICD (Fig. 2F). They did, however, still contain low levels of β-Gal protein 3 days and 2 weeks after stroke (Fig. 2G). The absence of NICD and presence of β-Gal protein suggested that Notch1 signaling was reduced as astrocytes entered the neurogenic program and that the astrocytes that up-regulated Ascl1 and produced neuroblasts after stroke were the ones that had been identifiable by having active Notch1 signaling before the injury (fig. S8).

To assess whether reduction of Notch1 signaling is required for triggering striatal astrocytes to enter the neurogenic program in response to stroke, we artificially maintained Notch1 signaling after stroke. We used Cx30-CreER mice homozygous for conditional NICD alleles, in which tamoxifen administration results in ectopic expression of NICD and green fluorescent protein (*17*). Seven weeks after stroke, Cx30-CreER;R26R-YFP control mice had recombined Ascl1$^+$ and DCX$^+$ cells in the striatum, as expected (6 and 16 cells/mm^2, respectively; n = 4 mice). However, virtually no recombined Ascl1$^+$ cells (0.04 cells/mm^2) or DCX$^+$ cells (0.02 cells/mm^2) were found in the striatum when NICD was ectopically expressed in astrocytes (n = 4 mice) (Fig. 3 and fig. S9). Thus, reduced Notch1 signaling is necessary for activation of the latent neurogenic program in the striatum.

We next asked whether experimental reduction of Notch signaling in striatal astrocytes could activate the latent neurogenic program, even in the absence of stroke. We deleted RBP-Jκ (CSL), an obligatory transcription factor for canonical Notch signaling that is present in all NICD$^+$ striatal astrocytes (fig. S10A), using Cx30-CreER;R26R-YFP mice homozygous for conditional *RBP-Jκ* null alleles (*18*). Abolishing Notch signaling in astrocytes largely phenocopied the effect of stroke (n = 20 mice) (Fig. 4, A and B, and fig. S10, B to F). Ascl1$^+$ astrocytes first appeared in the medial striatum 2 weeks after tamoxifen administration and 1 week later across the entire striatum. Proliferation was restricted to the S100$^+$,Ascl1$^+$ cells in the medial striatum (fig. S11). From 3 weeks after recombination, tightly packed clusters of recombined, proliferating cells expressing Ascl1 and DCX, or containing a mix of both, appeared in the same region (figs. S10, C to F; S11F; and S12). The vast majority of neuroblasts (83 ± 2%, mean ± SEM) were found in clusters in the striatum 3 weeks after tamoxifen administration, suggesting that striatal astrocytes represent the dominating source of neuroblasts after blocking Notch signaling. Whereas the number of striatal Ascl1$^+$ cells was highest 4 weeks after tamoxifen injection, neuroblast numbers increased with time, peaking at up to 17,000 cells per striatum 8 weeks after the administration of tamoxifen (6400 ± 3200 DCX$^+$ cells per striatum, mean ± SEM) (Fig. 4C). Even 34 weeks after tamoxifen administration, Ascl1$^+$ astrocytes and some DCX$^+$ cells were present in the striatum. If each cluster originated from a single astrocyte, we estimated that each Ascl1$^+$ astrocyte initiates a series of four to five cell divisions before differentiating into DCX$^+$ cells that divide once, resulting in ~40 neuroblasts. Over time, DCX$^+$ cells developed elaborate processes and neuronal morphology, and up to 1500 recombined cells per striatum expressed NeuN (850 ± 210 cells per striatum at 34 weeks, mean ± SEM) (Fig. 4, D and E), of which the majority were positive for nNOS and some had formed synaptic connections (fig. S13).

Deletion of RBP-Jκ exclusively in striatal astrocytes, using either the Ad-GFAP-Cre or Ad-CMV-Cre virus, caused up-regulation of Ascl1 in 43 ± 4% (mean ± SEM) of the recombined astrocytes and the generation of recombined neuroblasts (13 ± 5% of YFP$^+$ cells at 8 weeks after virus injection) in mice homozygous (n = 9 mice), but not heterozygous (n = 21 mice), for the conditional *RBP-Jκ* mutation (Fig. 4, F to L, and fig. S14, A to E). Some neuroblasts developed branched processes and up-regulated NeuN (fig. S14F). No migration of recombined neuroblasts was observed from the subventricular zone in these experiments, demonstrating the specificity of the recombination strategy to striatal astrocytes and corroborating on-site neurogenesis within the striatum.

We finally asked whether the Notch-regulated latent neurogenic program was restricted to astrocytes in the striatum. Analysis of the brains of Cx30-CreER;R26R-YFP mice in which *RBP-Jκ* had been ablated in astrocytes revealed a neurogenic potential of astrocytes also in the medial cortex (Fig. 4M). Ascl1-expressing astrocytes and cell clusters, as well as up to 2900 DCX$^+$ neuroblasts (1600 ± 530 DCX$^+$ cells 8 weeks after tamoxifen administration, mean ± SEM), were seen in the superficial cortex in all animals (n = 20 mice), in a band <200 μm on either side of the medial longitudinal fissure (Fig. 4, B and M to R, and fig. S15). DCX$^+$ cells in this area never acquired bipolar processes but were always small, round, and tightly clustered together. No ectopic DCX$^+$ cells were seen in other parts of the central nervous system. In mice in which astrocytes were targeted instead using a GLAST-CreER transgene (*7*), recombined ectopic Ascl1$^+$ and DCX$^+$ cells were generated in the same regions as in the Cx30-CreER mice, both after stroke (striatum; n = 9 mice) and after RBP-Jκ deletion (striatum and medial cortex; n = 6 mice) (fig. S16). Neither stroke nor deletion of RBP-Jκ resulted in generation of neuroblasts from oligodendrocyte progenitors (fig. S17).

Our results reveal a latent neurogenic potential in a population of astrocytes outside the neurogenic niches and delineate its molecular regulation. In contrast to other mammals, adult humans exhibit substantial neurogenesis in the healthy striatum (*19*). Our results raise the possibility that some new striatal neurons may derive from local astrocytes in the adult human brain, rather than from the adjacent subventricular zone. Neuronal loss in the striatum characterizes several neurological conditions. Blocking canonical Notch signaling resulted in a comparable density of new neurons (42 neurons/mm^3), as has been reported to have beneficial effects after interneuron transplantation (39 neurons/mm^3; see supplementary materials and methods) in an animal model of Parkinson's disease (*20*), suggesting that inducing endogenous generation of interneurons can be an attractive alternative to transplantation. Our findings of a latent neurogenic program within the striatum and the characterization of its molecular regulation point to a route for developing neuronal replacement therapies.

REFERENCES AND NOTES

1. S. Sirko *et al.*, *Cell Stem Cell* **12**, 426–439 (2013).
2. I. S. Shimada, M. D. LeComte, J. C. Granger, N. J. Quinlan, J. L. Spees, *J. Neurosci.* **32**, 7926–7940 (2012).
3. A. Buffo *et al.*, *Proc. Natl. Acad. Sci. U.S.A.* **105**, 3581–3586 (2008).

4. Z. Guo *et al.*, *Cell Stem Cell* **14**, 188–202 (2013).
5. O. Torper *et al.*, *Proc. Natl. Acad. Sci. U.S.A.* **110**, 7038–7043 (2013).
6. W. Niu *et al.*, *Nat. Cell Biol.* **15**, 1164–1175 (2013).
7. M. Slezak *et al.*, *Glia* **55**, 1565–1576 (2007).
8. S. Srinivas *et al.*, *BMC Dev. Biol.* **1**, 4 (2001).
9. T. Nomura, C. Göritz, T. Catchpole, M. Henkemeyer, J. Frisén, *Cell Stem Cell* **7**, 730–743 (2010).
10. A. Arvidsson, T. Collin, D. Kirik, Z. Kokaia, O. Lindvall, *Nat. Med.* **8**, 963–970 (2002).
11. J. M. Parent, Z. S. Vexler, C. Gong, N. Derugin, D. M. Ferriero, *Ann. Neurol.* **52**, 802–813 (2002).
12. I. Imayoshi, R. Kageyama, *Neuron* **82**, 9–23 (2014).
13. L. Li *et al.*, *Glia* **58**, 1610–1619 (2010).
14. E. Smith *et al.*, *Genesis* **50**, 700–710 (2012).
15. I. Imayoshi, M. Sakamoto, M. Yamaguchi, K. Mori, R. Kageyama, *J. Neurosci.* **30**, 3489–3498 (2010).
16. A. Varshavsky, *Genes Cells* **2**, 13–28 (1997).
17. L. C. Murtaugh, B. Z. Stanger, K. M. Kwan, D. A. Melton, *Proc. Natl. Acad. Sci. U.S.A.* **100**, 14920–14925 (2003).
18. K. Tanigaki *et al.*, *Nat. Immunol.* **3**, 443–450 (2002).
19. A. Ernst *et al.*, *Cell* **156**, 1072–1083 (2014).
20. V. Martínez-Cerdeño *et al.*, *Cell Stem Cell* **6**, 238–250 (2010).

ACKNOWLEDGMENTS

We thank E. Andersson, E.-B. Braune, J. Dias, S.-B. Jin, and U. Lendahl for valuable discussions. This study was supported by grants from the Swedish Research Council, the Swedish Cancer Society, the Karolinska Institute, Tobias Stiftelsen, The Swedish Heart and Lung Foundation, StratRegen, StemTherapy, European Union project TargetBraIn (279017), Torsten Söderbergs Stiftelse, and Knut och Alice Wallenbergs Stiftelse. D.O.D. was supported by the Portuguese government (SFRH/BD/63164/2009). C.G. is a Hållsten Academy and Wallenberg Academy fellow. We thank F. W. Pfrieger for providing Cx30 and GLAST transgenic mice through a material transfer agreement with the Institut Génétique Biologie Moléculaire Cellulaire (Strasbourg, France). Requests for mice should be directed to F. W. Pfrieger (CNRS, France). We declare no conflicts of interest. The supplementary materials contain additional data.

SUPPLEMENTARY MATERIALS

www.sciencemag.org/content/346/6206/237/suppl/DC1
Materials and Methods
Figs. S1 to S17
References (*21*–*25*)

23 June 2014; accepted 11 September 2014
10.1126/science.346.6206.237

CONSERVATION TARGETS

A mid-term analysis of progress toward international biodiversity targets

Derek P. Tittensor,[1,2]* Matt Walpole,[1] Samantha L. L. Hill,[1] Daniel G. Boyce,[3,4] Gregory L. Britten,[2] Neil D. Burgess,[1,5] Stuart H. M. Butchart,[6] Paul W. Leadley,[7] Eugenie C. Regan,[1] Rob Alkemade,[8] Roswitha Baumung,[9] Céline Bellard,[7] Lex Bouwman,[8,10] Nadine J. Bowles-Newark,[1] Anna M. Chenery,[1] William W. L. Cheung,[11] Villy Christensen,[11] H. David Cooper,[12] Annabel R. Crowther,[1] Matthew J. R. Dixon,[1] Alessandro Galli,[13] Valérie Gaveau,[14] Richard D. Gregory,[15] Nicolas L. Gutierrez,[16] Tim L. Hirsch,[17] Robert Höft,[12] Stephanie R. Januchowski-Hartley,[18] Marion Karmann,[19] Cornelia B. Krug,[7,20] Fiona J. Leverington,[21] Jonathan Loh,[22] Rik Kutsch Lojenga,[23] Kelly Malsch,[1] Alexandra Marques,[24,25] David H. W. Morgan,[26] Peter J. Mumby,[27] Tim Newbold,[1] Kieran Noonan-Mooney,[12] Shyama N. Pagad,[28] Bradley C. Parks,[29] Henrique M. Pereira,[24,25] Tim Robertson,[17] Carlo Rondinini,[30] Luca Santini,[30] Jörn P. W. Scharlemann,[1,31] Stefan Schindler,[32,33] U. Rashid Sumaila,[11] Louise S.L. Teh,[11] Jennifer van Kolck,[8] Piero Visconti,[34] Yimin Ye[9]

In 2010, the international community, under the auspices of the Convention on Biological Diversity, agreed on 20 biodiversity-related "Aichi Targets" to be achieved within a decade. We provide a comprehensive mid-term assessment of progress toward these global targets using 55 indicator data sets. We projected indicator trends to 2020 using an adaptive statistical framework that incorporated the specific properties of individual time series. On current trajectories, results suggest that despite accelerating policy and management responses to the biodiversity crisis, the impacts of these efforts are unlikely to be reflected in improved trends in the state of biodiversity by 2020. We highlight areas of societal endeavor requiring additional efforts to achieve the Aichi Targets, and provide a baseline against which to assess future progress.

Continued degradation of the natural world and the goods and services it provides to humankind has led to the adoption of numerous international agreements aimed at halting the decline of biodiversity and ecosystem services [e.g., (*1*)]. The Parties to the Convention on Biological Diversity (CBD) in 2002 committed to a significant reduction in the rate of biodiversity loss by 2010 (*2*), which, despite some local successes [e.g. (*3*)], did not lead to a reduction in the overall rate of decline (*4*, *5*). Renewed commitments were made in the Strategic Plan for Biodiversity 2011–2020 (*6*), which calls for effective and urgent action this decade. These goals are supported by 20 "Aichi Biodiversity Targets" to be met by 2020 at the latest (table S1), covering "pressures" on, "states" of, and "benefits" from biodiversity and "responses" to the biodiversity crisis [sensu (*4*, *7*); table S2]. Objectively quantifying progress toward these international environmental commitments is critical for assessing their impact and efficacy, yet as the midpoint of this 10-year period approaches, progress toward the Aichi Targets has not been quantitatively evaluated.

To address this gap, we assembled a broad suite of indicator variables to estimate historical trends and project to 2020 (*8*). Building on the CBD's indicative list (*9*), we performed a data scoping of more than 160 potential indicators and reviewed them against five criteria for inclusion, namely: (i) high relevance to a particular Aichi Target and a clear link to the status of biodiversity; (ii) scientific or institutional credibility; (iii) a time series ending after 2010; where unavailable but indicator fills a sizable gap, data ending as near to 2010 as possible; (iv) at least five annual data points in the time series; and (v) broad geographic (preferably global) coverage. Of the 163 potential indicators, 55 met these criteria (table S1), almost double the number used to test whether the 2010 target had been met (*4*). In total, we assembled indicators for 16 of the 20 targets (table S1), and progress to two more was measurable.

We fitted models to estimate underlying trends using an analysis framework adaptive to the highly variable statistical properties of the indicators. Dynamic linear models (*10*) were fitted to high-noise time series, while parametric multimodel averaging (*11*) was used for those with low noise. We projected model estimates and confidence intervals to 2020 to estimate trajectories and rates of change for each indicator (Fig. 1).

As most targets lack explicitly quantifiable definitions of "success" for 2020 (and those that have definitions for some components lack them for others), it was not generally possible to measure progress in terms of distance to a defined end point. Therefore, we assigned indicators as states, pressures, benefits, or responses and compared projected values in 2020 against modeled 2010 values (underlying trend estimates) for all indicators, while additionally measuring absolute progress where possible.

Societal responses to the biodiversity crisis generally showed improvements, with 21 of 33 response indicators (64%) projected to increase significantly by 2020, and most of the remainder having an increasing mean trend. Those increasing significantly included eight of nine indicators of protected area coverage, representativeness, and management (target 11) and all four indicators of sustainable management (fisheries and forest certification, organic farming, and conservation agriculture; targets 6 and 7), along with two of three indicators for research and data provision (Global Biodiversity Information Facility records, research into economic valuation of biodiversity; targets 2 and 19) and two of three indicators of biodiversity awareness (percentage of people who

have heard of biodiversity, percentage correctly defining biodiversity; target 1). However, none of the nine indicators of financial resources showed a significant increase by 2020 (though seven did show positive mean trends), nor did national legislation to prevent or control invasive species.

In contrast, for the underlying state of biodiversity and the pressures upon it, our projections indicate no significant improvement or a worsening situation by 2020, relative to 2010. Five of seven pressure indicators (71%) showed significant increases (a worsening situation), including those measuring consumption (ecological and water footprints, global fishing trawl effort), pollution (nitrogen surplus), and invasive species introductions. Recently emerging pressures (table S5) may also affect outcomes of targets. Among state and benefit indicators, 11 of 17 (65%) showed significant worsening trends, including two indicators of habitat loss (wetland extent and sea ice extent), two of three indicators of population abundance (Farmland Bird Index, Living Planet Index), all six indicators of species extinction risk [an aggregate IUCN Red List Index (RLI) along with disaggregated indices relevant to particular targets], and an indicator of domesticated breeds at risk. We caution, however, against overinterpreting the broader picture for benefits from only three indicators (Fig. 2).

Although some progress is evident across components of individual targets, including targets 1 (awareness), 11 (protected areas), and 19 (knowledge), if biodiversity and ecosystem services are to be maintained and extinction risk averted (targets 12, 13, and 14), additional effort is required to reduce pressures, particularly in relation to targets 4 (sustainable production and consumption), 5 (habitat loss), 8 (pollution), 9 (invasive species), and 10 (climate change impacts) (see fig. S54). For target components with specific numeric goals, we found a mixed picture, where measurable: On current trajectories, the rate of loss of natural habitats (target 5) will not be halved by 2020, all fish stocks will not be sustainably harvested (target 6), and the 10% marine area protection (target 11) will not be met, though taking into account targets set by the parties, actual progress on the latter could exceed extrapolated values (*12*). However, the 17% terrestrial protection component of target 11 is projected to be achieved; target 16 (Nagoya Protocol is in force and operational) and at least part of target 17 (development and adoption of national biodiversity strategy and action plans) are also likely to be met by 2015 (*8*). Although mobilization of financial resources appears to be generally accelerating, our analyses did not detect significant increases by 2020 (target 20); such increases will be needed to support progress toward other targets (*13*).

Comparing the aggregated differences between results for pressure, state, and benefit indicators with those for responses suggests a world in which increasing recognition of the biodiversity crisis is evident, and growing efforts are being made to address it, but one in which the effect of these efforts appears unlikely to be reflected in an improvement in the base state of biodiversity by 2020 (Fig. 2). However, when comparing estimated annual rates of change for each indicator between 2001 to 2010 and 2011 to 2020, our analyses suggest that whereas those for pressure, state, and benefit indicators remain largely unchanged during this period, many response indicators show a positively accelerating rate of change; i.e., a rapid or exponential growth rate (Fig. 3). Although the short post-2010 time span makes it difficult to resolve significant changes in velocity, particularly for financial indicators where there remains large uncertainty, this projected acceleration of response indicators without a comparable signal of their beneficial impacts on biodiversity states, benefits, and pressures by 2020 could be due to several factors. One

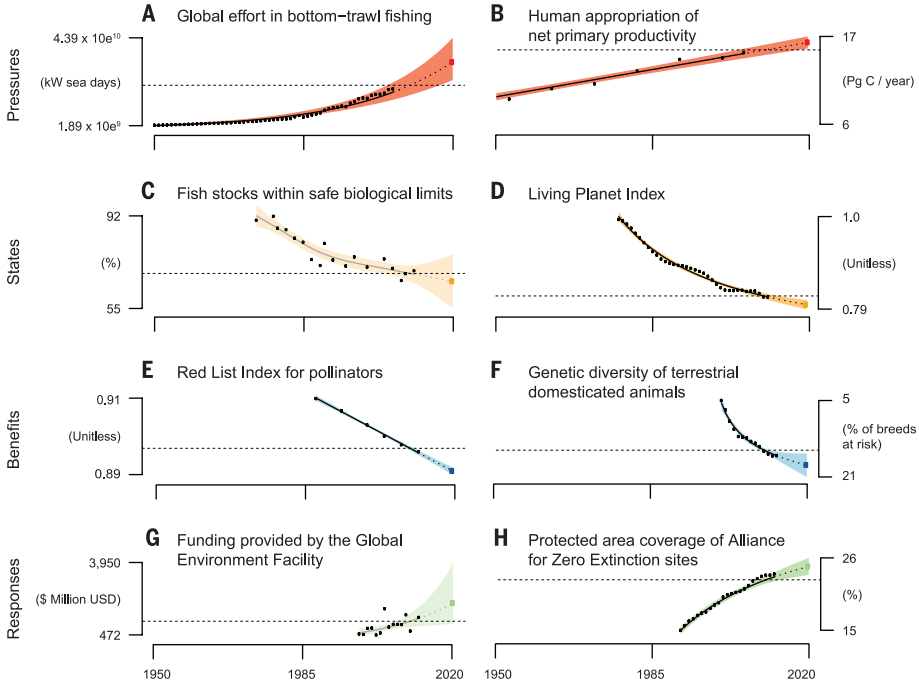


Fig. 1. Examples of model fits and projections for indicator data. Panels show selected pressure (**A** and **B**), state (**C** and **D**), benefit (**E** and **F**), and response (**G** and **H**) indicator data (black dots). Model fits (black and gray lines) and 95% confidence intervals (dark and light shading) indicate, respectively, significant and non-significant differences between 2010 (horizontal dashed line) and 2020 (colored square) estimates. (A) and (B) have been truncated at 1950 for visualization purposes. For fits to all 55 indicator time series, see fig. S54.

[1]United Nations Environment Programme World Conservation Monitoring Centre (UNEP-WCMC), 219 Huntingdon Road, Cambridge CB3 0DL, UK. [2]Department of Biology, Dalhousie University, 1355 Oxford Street, Halifax, NS B3H 4R2, Canada. [3]Department of Biology, Queen's University, Kingston, ON K7L 3N6, Canada. [4]Ocean Sciences Division, Bedford Institute of Oceanography, Post Office Box 1006, Dartmouth, NS B2Y 4A2, Canada. [5]Centre for Macroecology, Evolution and Climate, Natural History Museum, Copenhagen, DK-2100, Denmark. [6]BirdLife International, Wellbrook Court, Cambridge CB3 0NA, UK. [7]ESE Laboratory, Université Paris-Sud, UMR 8079, CNRS–Université Paris-Sud, 91405 Orsay, France. [8]PBL Netherlands Environmental Assessment Agency, Post Office Box 303, 3720 AH, Bilthoven, Netherlands. [9]Food and Agricultural Organization of the United Nations, Viale delle Terme di Caracalla, 00153 Rome, Italy. [10]Department of Earth Sciences–Geochemistry, Faculty of Geosciences, Utrecht University, Post Office Box 80021, 3508 TA Utrecht, Netherlands. [11]Fisheries Centre, The University of British Columbia, 2202 Main Mall, Vancouver, BC V6T 1Z4, Canada. [12]Secretariat of the Convention on Biological Diversity, 413, Saint Jacques Street, Suite 800, Montreal, QC H2Y 1N9, Canada. [13]Global Footprint Network, 7-9 Chemin de Balexert, 1219 Geneva, Switzerland. [14]Organisation for Economic Co-operation and Development, 2 rue André-Pascal, 75775 Paris Cedex 16, France. [15]RSPB Centre for Conservation Science The Lodge, Sandy, Bedfordshire SG19 2DL, UK. [16]Marine Stewardship Council, 1-3 Snow Hill, London EC1A 2DH, UK. [17]The Global Biodiversity Information Facility (GBIF) Secretariat Universitetsparken 15, 2100 Copenhagen, Denmark. [18]Center for Limnology, University of Wisconsin-Madison, 680 North Park Street, Madison, WI 53706, USA. [19]Forest Stewardship Council (FSC) International, Charles-de-Gaulle Strasse 5, 53113 Bonn, Germany. [20]DIVERSITAS, 57 rue Cuvier–CP 41, 75231 Paris Cedex 05, France. [21]University of Queensland, Diamantina National Park via Winton, QLD 4735, Australia. [22]Zoological Society of London, Regent's Park, London NW1 4RY, UK. [23]Union for Ethical BioTrade, De Ruyterkade 6, 1013 AA, Amsterdam, Netherlands. [24]German Centre for Integrative Biodiversity Research (iDiv) Halle-Jena-Leipzig, Deutscher Platz 5e, 04103 Leipzig, Germany. [25]Institute of Biology, Martin Luther University Halle-Wittenberg, Am Kirchtor 1, 06108 Halle (Saale), Germany. [26]Convention on International Trade in Endangered Species Secretariat, Maison internationale de l'environnement, 11-13 Chemin des Anémones, 1219 Châtelaine, Geneva, Switzerland. [27]Marine Spatial Ecology Lab, School of Biological Sciences, University of Queensland, St. Lucia Brisbane, Qld 4072 Australia. [28]The International Union for Conservation of Nature Species Survival Commission (IUCN SSC) Invasive Species Specialist Group, University of Auckland, Tamaki Campus, Auckland, New Zealand. [29]AidData, The College of William and Mary, Post Office Box 8795, Williamsburg, VA 23187-8795, USA. [30]Department of Biology and Biotechnologies, Sapienza–Università di Roma, Viale dell' Università 32, 00185 Rome, Italy. [31]School of Life Sciences, University of Sussex, Brighton BN1 9QG, UK. [32]Environment Agency Austria, Department of Biodiversity and Nature Conservation, Spittelauer Lände 5, 1090 Vienna, Austria. [33]University of Vienna, Department of Botany and Biodiversity Research, Division of Conservation Biology, Vegetation Ecology and Landscape Ecology, Rennweg 14, 1030 Vienna, Austria. [34]Microsoft Research, Computational Science Laboratory, 21 Station Road, Cambridge, CB1 2FB, UK.
***Corresponding author. E-mail: derek.tittensor@unep-wcmc.org**

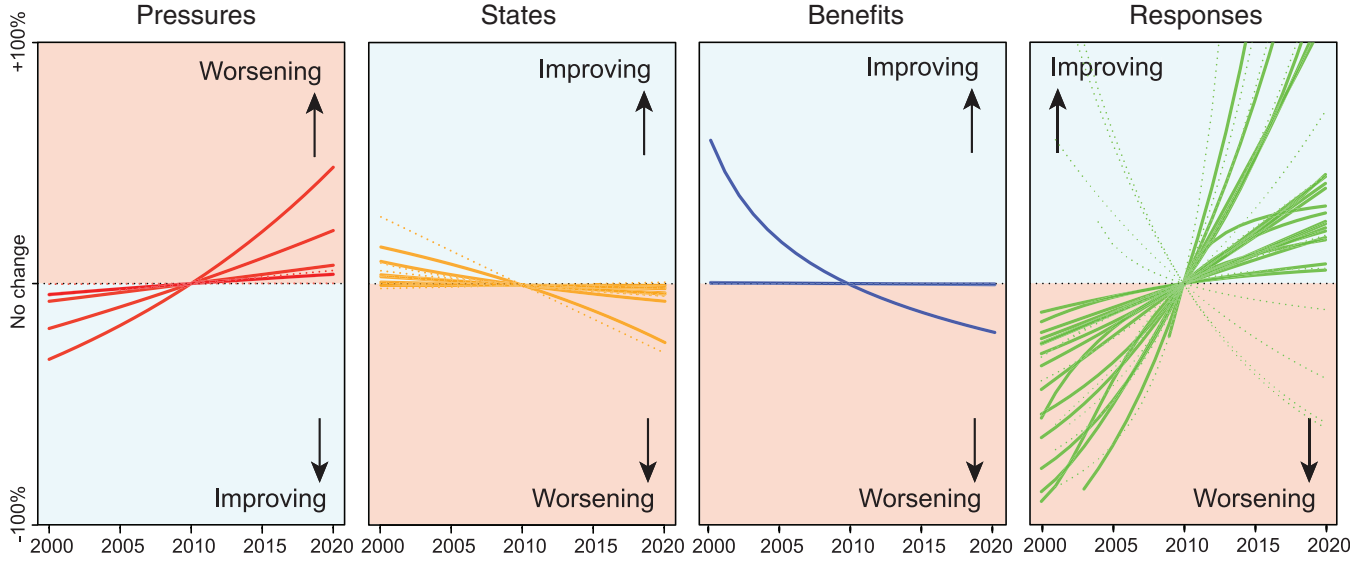


Fig. 2. Aggregated trends in pressures, states, benefits, and responses across all indicators and Aichi Targets. Lines represent significant (continuous) or nonsignificant (dotted) trends relative to 2010 modeled value (horizontal dotted black line). Indicators with very flat linear trends may be superimposed (e.g., two benefit indicators). An increase in states, benefits, and responses, or a decrease in pressures represents progress toward the targets. Some indicator trends (e.g., extinction rates) have been inverted to conform to this paradigm. Trends have been truncated before 2000 for visualization purposes.

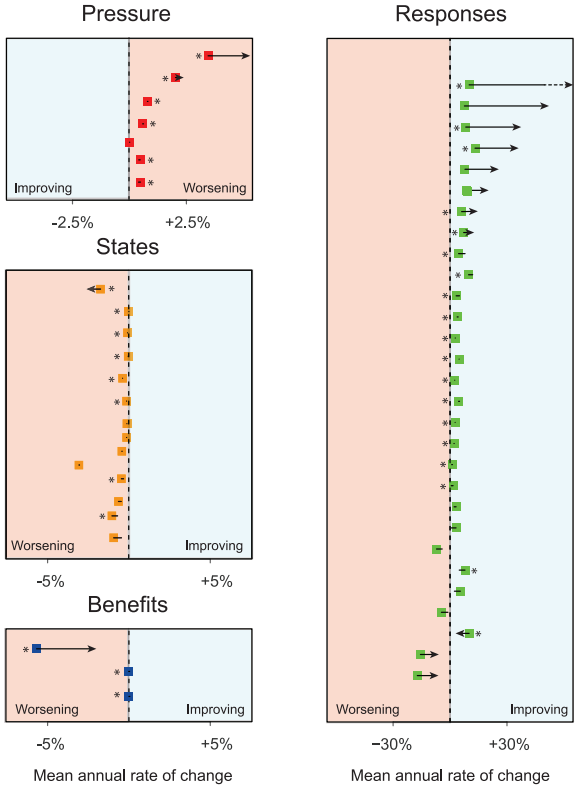


Fig. 3. Comparison between mean annual rates of change in indicators pre- and post-2010. Filled squares indicate estimated mean annual rate of change of indicator between 2001 (or earliest year if subsequent) and 2010. End points of arrows indicate estimated mean annual rate of change between 2011 and 2020. Indicators to the right of the vertical dashed line are increasing annually, whereas those to the left are decreasing. If arrows point toward the dashed line, then rate of change is slowing; conversely, if they point away, it is accelerating. Black asterisks indicate significant slopes for post-2010 mean rates of change, based on bootstrapped linear model fits. Dashed arrow indicates value beyond *x*-axis limit. Two state indicators for target 1 have been excluded because they only have a single year before 2010. For identification of each indicator, see table S8.

possibility is that there are substantial time lags before outcomes are detectable. That is, it may take years or decades before these increased responses translate to positive changes in the state of biodiversity or reduced pressures (*14*). Ecological theory and restoration ecology provide tangible evidence that supports this assertion (*15*–*17*), and a notable escalation of responses as implied here may signal improved progress toward targets over longer time scales; indeed, state, benefit, and pressure indicators already implicitly reflect prior conservation action. Alternatively, responses may be insufficient or inappropriate relative to pressures and fail to overcome the growing impacts of drivers that lead to biodiversity loss.

It is important to recognize that statistical extrapolations make the assumption of underlying processes remaining constant into the future, which may or may not hold, and should be viewed with this assumption clearly in mind. Our analyses are also inevitably incomplete. A global analysis will not reflect finer-scale spatial variation and local to regional improvements [e.g., (*3*, *18*)], and the taxonomic coverage is limited. Locating data that enable quantification of progress toward targets at a global scale is challenging (*19*, *20*), and some indicators are less well aligned with targets, leading to variable levels of coverage (fig. S53 and tables S3 and S4) (*21*). Indicators also have differing spatial, temporal, and/or taxonomic coverage (table S1), and for some individual target components (e.g., harmful subsidies for target 3, plant genetic resources for target 13), we were unable to locate indicators satisfying our criteria (table S3). Moreover, we could not locate any indicators meeting the criteria above to measure progress toward targets 15 (ecosystem resilience and contribution of biodiversity to carbon stocks) and 18 (integration of traditional knowledge and effective participation of indigenous and local communities). Investment in the development of novel indicators for unassessed targets or components remains an urgent priority, as does the development of indicators for "benefits" from ecosystems (*7*), of which we could only locate three. Novel data collection, data-sharing platforms, and support to developing nations in analytical capacities and training may help contribute to these goals, as may contemporary approaches to assessing the impact of interventions (*22*).

Despite these limitations, the rapid development of online databases, indicators, and indicator partnerships continues to improve our

ability to quantify progress toward targets (*23*). The benefits of maintaining biodiversity are well known (*24*). Our results provide a baseline against which to measure progress toward this objective in 2020 and suggest that efforts need to be redoubled to positively affect trajectories of change and enable global biodiversity goals to be met by the end of the current decade.

REFERENCES AND NOTES

1. United Nations, *Convention on Biological Diversity* (Rio de Janeiro, Brazil, 1992).
2. Secretariat of the Convention on Biological Diversity (SCBD), "Handbook of the Convention on Biological Diversity" (Earthscan, London, 2003).
3. B. Worm *et al*., *Science* **325**, 578–585 (2009).
4. S. H. M. Butchart *et al*., *Science* **328**, 1164–1168 (2010).
5. SCBD, "Global Biodiversity Outlook 3" (Montreal, 2010).
6. UNEP, CBD, "UNEP/CBD/COP/DEC/X/2 2010" (2010).
7. T. H. Sparks *et al*., *Oryx* **45**, 411–419 (2011).
8. See supplementary materials on *Science* Online.
9. UNEP, CBD, UNEP/CBD/COP/DEC/XI/3 2012 (2012).
10. J. Durbin, S. J. Koopman, *Time Series Analysis by State Space Methods* (Oxford Univ. Press, Oxford, 2001).
11. K. P. Burnham, D. R. Anderson, *Model Selection and Multi-Model Inference: A Practical Information-Theoretic Approach* (Springer, New York, ed. 2, 2002).
12. CBD, Programme of Work on Protected Areas (PoWPA), https://www.cbd.int/protected/implementation/actionplans/ (2013).
13. D. P. McCarthy *et al*., *Science* **338**, 946–949 (2012).
14. Furthermore, the ability of statistical models to react to recent changes in indicator trends will vary depending on, among other things, the length of the time series, the noise in the data, and the magnitude of departure from the previous trend.
15. J. M. Bullock, J. Aronson, A. C. Newton, R. F. Pywell, J. M. Rey-Benayas, *Trends Ecol. Evol.* **26**, 541–549 (2011).
16. J. P. Metzger *et al*., *Biol. Conserv.* **142**, 1166–1177 (2009).
17. M. Di Marco *et al*., *Conserv. Biol.* **28**, 1109–1118 (2014).
18. D. Nepstad *et al*., *Science* **344**, 1118–1123 (2014).
19. M. Walpole *et al*., *Science* **325**, 1503–1504 (2009).
20. H. M. Pereira, L. M. Navarro, I. S. Martins, *Annu. Rev. Environ. Resour.* **37**, 25–50 (2012).
21. It is also possible that the response, pressure, and state indicator framework is not tracking factors that are causally linked (*7*); use of this framework does not imply joined-up indicators.
22. M. Hoffmann *et al*., *Science* **330**, 1503–1509 (2010).
23. S. L. Pimm *et al*., *Science* **344**, 1246752 (2014).
24. B. J. Cardinale *et al*., *Nature* **486**, 59–67 (2012).

ACKNOWLEDGMENTS

We thank I. Arto, A. H.W. Beusen, C. Brown, L. Coad, L. Collette, R. de Groot, F. Essl, J. Geldmann, P. Genovesi, M. Harfoot, M. Hockings, I. Hoffmann, M. Hoffman, L. Joppa, D. Juffe-Bignoli, N. Kingston, F. Krausmann, V. Lam, B. MacSharry, M. McGeoch, L. McRae, H. Meng, B. O'Connor, D. Pritchard, W. Rabitsch, B. Russell, C. Smith, S. Stewart, P. Stoett, M van Oorschot, H. Visser, M. Wackernagel, A. Watkins, M. Wieczorek, B. Worm, and M. Zemp. A.G. acknowledges Global Footprint Network's Research team and MAVA Fondation pour la Nature. D.B. acknowledges support from NSERC Discovery grant to W.C. Leggett & K. T. Franmk. V.C. acknowledges support from the Natural Sciences and Engineering Research Council of Canada. W.C. acknowledges support from NF-UBC Nereus Program. S.R.J.H. acknowledges support from the National Science Foundation (DEB–1115025) and DIVERSITAS. S.C.B.D. and UNEP-WCMC acknowledge funding support from Canada, the European Union, Germany, Japan, Netherlands, the Republic of Korea, Switzerland, and the UK. All scripts and data used to conduct analyses are available at https://github.com/derekt/Aichi-2020-analysis.

SUPPLEMENTARY MATERIALS

www.sciencemag.org/content/346/6206/241/suppl/DC1
Materials and Methods
Supplementary Text
Figs. S1 to S55
Tables S1 to S8
References (*25*–*129*)

16 June 2014; accepted 15 September 2014
Published online 2 October 2014;
10.1126/science.1257484

CELL-FREE ASSAYS

Spatial organization of cytokinesis signaling reconstituted in a cell-free system

Phuong A. Nguyen,[1,2]* Aaron C. Groen,[1,2]* Martin Loose,[1] Keisuke Ishihara,[1,2] Martin Wühr,[1] Christine M. Field,[1,2]†‡ Timothy J. Mitchison[1,2]†

During animal cell division, the cleavage furrow is positioned by microtubules that signal to the actin cortex at the cell midplane. We developed a cell-free system to recapitulate cytokinesis signaling using cytoplasmic extract from *Xenopus* eggs. Microtubules grew out as asters from artificial centrosomes and met to organize antiparallel overlap zones. These zones blocked the interpenetration of neighboring asters and recruited cytokinesis midzone proteins, including the chromosomal passenger complex (CPC) and centralspindlin. The CPC was transported to overlap zones, which required two motor proteins, Kif4A and a Kif20A paralog. Using supported lipid bilayers to mimic the plasma membrane, we observed the recruitment of cleavage furrow markers, including an active RhoA reporter, at microtubule overlaps. This system opens further approaches to understanding the biophysics of cytokinesis signaling.

Actomyosin-based cleavage furrows in animal cells are positioned by signals emanating from microtubule assemblies formed shortly after anaphase onset (*1*). In typical somatic cells, the signaling complexes centralspindlin and the chromosomal passenger complex (CPC) accumulate at the center of the midzone (or central spindle), which forms in the space previously occupied by the mitotic spindle (*2*). It is unclear how the microtubules that position furrows are organized in much larger egg cells and how they signal to the cortex. We addressed these questions by developing a cell-free system to reconstitute the spatial signaling that is characteristic of cytokinesis in a large egg cell.

To reconstitute cytokinesis events, undiluted egg cytoplasm with intact actin (*3*), containing fluorescent probes and Aurora kinase A (AurkA)–based artificial centrosome beads (*4*), was treated with Ca^{2+} to mimic fertilization and immediately spread between two coverslips for imaging (fig. S1A). As the cell cycle progressed from metaphase to interphase (*5*), large microtubule asters grew out rapidly from each AurkA bead. Where the expanding edges of two neighboring asters met, antiparallel microtubule bundles formed in a boundary zone that we term the aster-aster interaction zone (AAIZ) (Fig. 1, A to C, fig. S1, and movie S1). In somatic cells, the CPC and centralspindlin complexes are recruited to the midplane in anaphase, where they specify the division plane by activating the small GTPase RhoA (*2*). We imaged endogenous complexes by adding labeled antibodies, and for the CPC we confirmed localization with a green fluorescent protein (GFP)–tagged DasraA subunit (*5*). CPC and the Kif23 subunit of centralspindlin were recruited to the AAIZ in a 5- to 15-μm-wide line bisecting the line between two AurkA beads (Fig. 1, B and C, and fig. S1). The AAIZ was wider than a somatic cell midzone and was hundreds of microns long. To evaluate its physiological relevance, we imaged the same proteins in *Xenopus* zygotes fixed between mitosis and cytokinesis, which takes place at interphase in early embryonic cells (Fig. 1D) (*6*). The morphology of the midplane in zygotes, as defined by microtubule morphology and CPC/centralspindlin localization, was strikingly similar to that of the AAIZ in extracts (Fig. 1, A to C).

To measure microtubule orientation at the AAIZ we tracked GFP-tagged end-binding protein 1 (EB1), which binds to growing microtubule plus ends (Fig. 1E, fig. S2, and movie S2) (*7*). Microtubules grew outward radially within each aster. At the AAIZ, EB1 comets from both directions entered antiparallel bundles, where they usually disappeared (Fig. 1E). We quantified the degree of interpenetration by categorizing EB1 comets based on their direction (fig. S3) (*5*). The AAIZ was characterized by a sharp change in directionality over ~20 μm, indicating a localized block to interpenetration between the asters (Fig. 1F).

Kinase activity of the Aurora kinase B (AurkB) subunit of the CPC is required to establish midzone morphology and for furrow ingression (*8*). We confirmed this in *Xenopus* eggs (fig. S4) (*5*). AurkB inhibition blocked recruitment of the CPC in our cell-free system (Fig. 1E) and caused much deeper interpenetration of microtubules (Fig. 1, E and F, and movie S3). Thus, AurkB activity was required to create a sharp boundary between asters.

CPC is proposed to be transported to the center of midzones along microtubules by a kinesin molecular motor (*9*), but transport has not been observed directly. Five plus-end–directed kinesins involved in cell division are candidates for CPC transport (*10*): Kif4A, Kif10 (also called CenpE),

[1]Department of Systems Biology, Harvard Medical School, Boston, MA 02115, USA. [2]Marine Biological Laboratory, Woods Hole, MA 02543, USA.
*These authors contributed equally to this work. †These authors contributed equally to this work. ‡Corresponding author. E-mail: Christine_Field@hms.harvard.edu

Kif11 (Eg5), Kif20A (Mklp2/Rabkinesin-6), and Kif23 (Mklp1, a subunit of centralspindlin). *Xenopus* eggs also contain an unusual kinesin 41% identical to Kif20A by sequence (*11*). This is likely to be an embryo-specific paralog, and we propose the name KIF20A embryonic, abbreviated KIF20AE. Small-molecule inhibition of Kif10 and Kif11, and depletion of somatic Kif20A and Kif23, had no effect on antiparallel microtubule bundling in the AAIZ or on CPC localization (Fig. 2, A and B, and figs. S5 and S6). Depletion of Kif4A did not block CPC accumulation or the assembly of antiparallel bundles, but increased the width of the CPC-positive zone; adding back recombinant Kif4A rescued this phenotype (Fig. 2A and fig. S6). Depletion of Kif20AE completely blocked CPC accumulation and disorganized the AAIZ (Fig. 2A). Thus, Kif20AE is absolutely required for CPC recruitment in eggs, presumably mirroring the Kif20A requirement in somatic cells (*9*), and Kif4A plays some role in focusing it.

Microtubule bundles in the AAIZ localized Kif20AE (Fig. 2C), Kif4A (Fig. 2D), and an embryonic paralog of PRC1 (PRC1E, an antiparallel microtubule crosslinker; fig. S1D), all of which have been shown to bind the CPC in pull-down experiments (*9*, *12*–*14*). Time-lapse imaging showed that CPC clusters moved to the center of the overlap zone at a rate of 10 to 25 μm/min, slowing as they reached the center (Fig. 2, E and F, fig. S7, and movie S4). Tubulin speckle imaging showed sliding of microtubules away from the overlap center at <5 μm/min (fig. S8 and movies S6 to S8). Thus, the observed CPC movement represents transport toward plus ends. The maximal transport rate was close to that of Kif4A in an isolated aster that was not part of an AAIZ (Fig. 2F, green line, and fig. S9) (*5*). Kif4A depletion blocked CPC movement, and addback of recombinant Kif4A rescued it (Fig. 2, E and F, fig. S10, and movie S5). Live imaging showed partial colocalization of CPC and Kif4A movement (fig. S11). Thus, the CPC is targeted to the AAIZ and transported to a narrow band by the combined action of Kif20AE and Kif4A. Transport probably slows as CPC engages binding sites in the AAIZ (*5*).

To test whether AAIZs in the cell-free system can signal to the cortex, we prepared supported lipid bilayers on glass coverslips, using lipids characteristic of the inner leaflet of animal cell plasma membranes, including phosphatidylinositol (PI) and phosphatidylinositol 4,5-bisphosphate [$PI(4,5)P_2$] (*5*, *15*). Protein recruitment was imaged

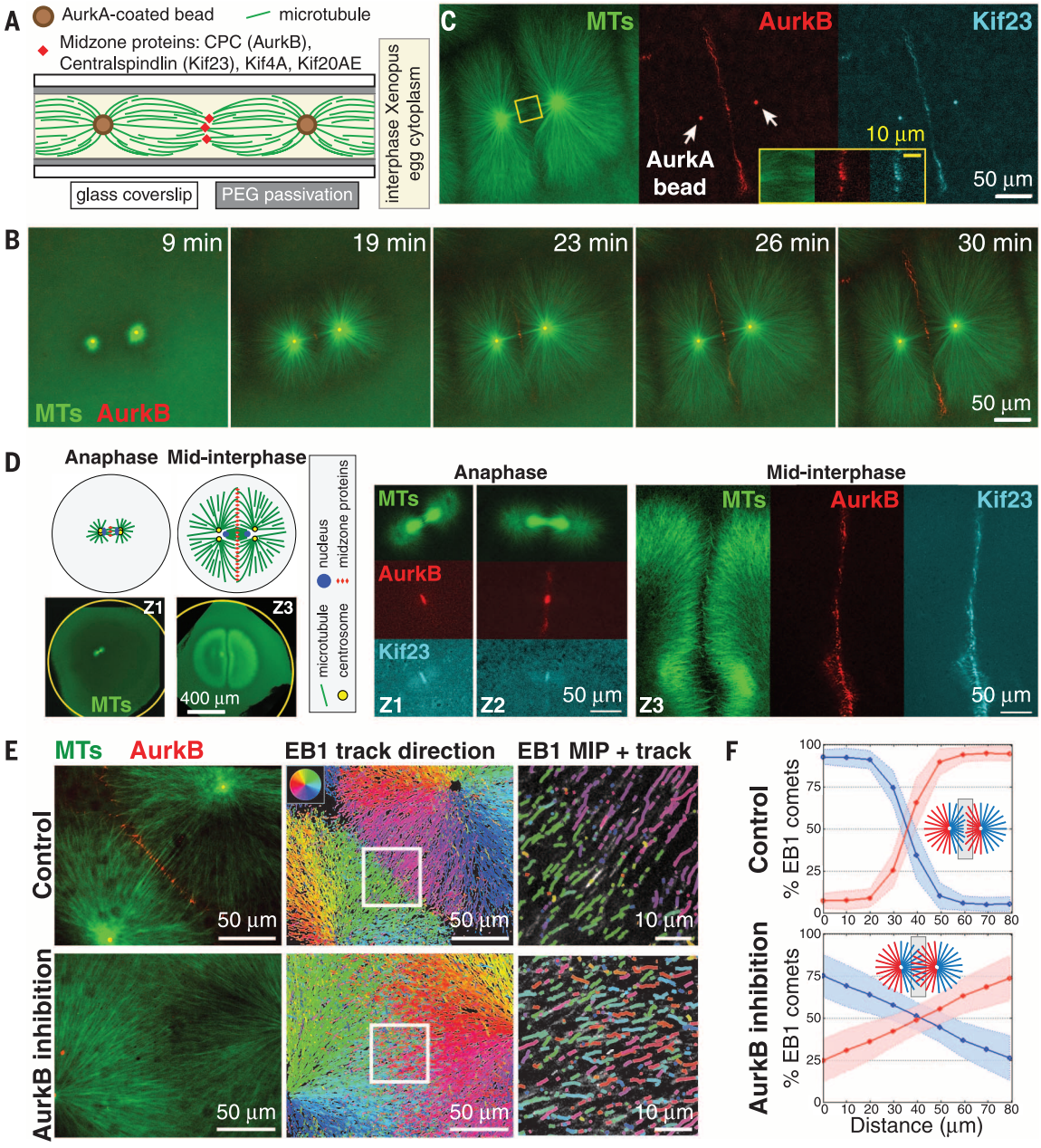
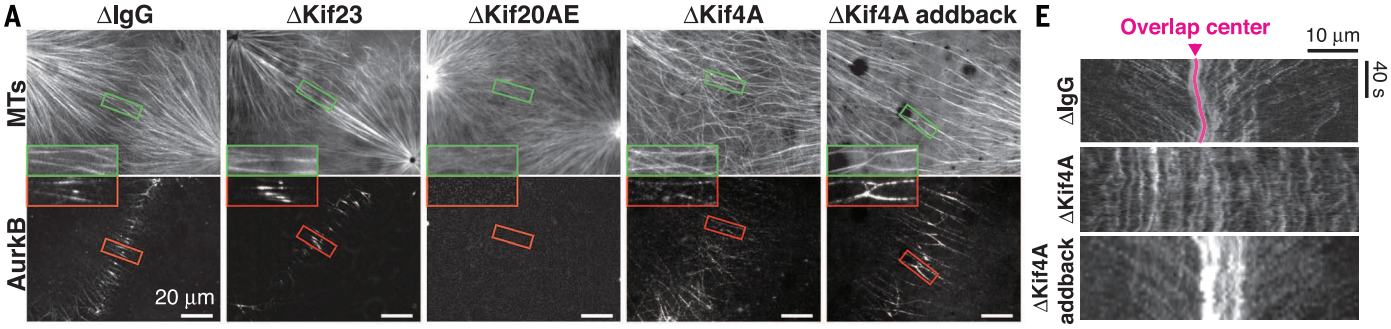
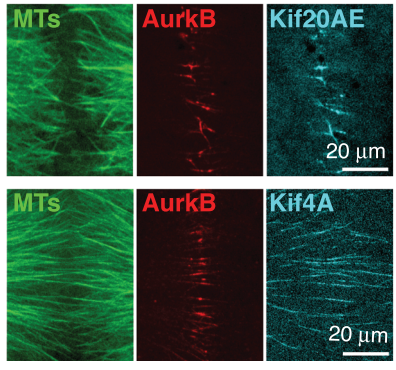


Fig. 1. Aster outgrowth and interaction in *Xenopus* egg cytoplasm. (**A**) Experimental setup. See (*5*) for methods and probes. (**B**) Widefield time-lapse images showing recruitment of AurkB (red) to an AAIZ. (**C**) AAIZ at 30 min (widefield) showing recruitment of AurkB (CPC subunit, red) and Kif23 (centralspindlin subunit, cyan). (**D**) Localization of microtubules (MTs) (green), AurkB (red), and Kif23 (cyan) in *Xenopus* zygotes fixed at consecutive stages of the first cell division (stages Z1 to Z3) imaged by laser scanning confocal microscopy (*5*). (**E**) Quantification of microtubule orientation using EB1 tracking. (Left) Spinning disc confocal images of control (top) and AurkB-inhibited (bottom) AAIZs. (Middle) Map of EB1-GFP trajectories over 2 min. (Right) ×4 zoom-up of square in middle panel with maximum intensity projection (MIP) of EB1 tracks over 15 s. (**F**) Spatial distribution of EB1 tracks at AAIZs classified by direction (shading indicates standard deviations determined from $n \geq 5$ zones). (See figs. S2 and S3 and (*5*) for data analysis.)



B

Kinesin candidate	Alternate names	Perturbation	CPC recruited	CPC focused
Control	NA	NA	+	+
Kif10	CenpE	inh	+	+
Kif11	Eg5	inh	+	+
Kif20A	Mklp2/rabkinesin-6	dep	+	+
Kif23	Mklp1/CHO1	dep	+	+
Kif4A	chromokinesin	dep	+	-
Kif20AE	NA	dep	-	-



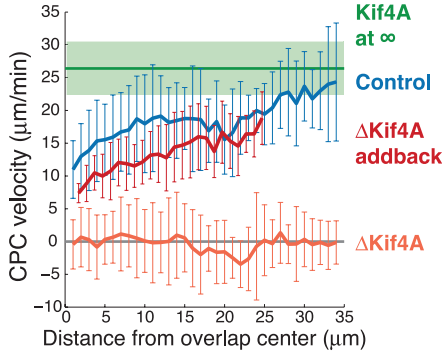
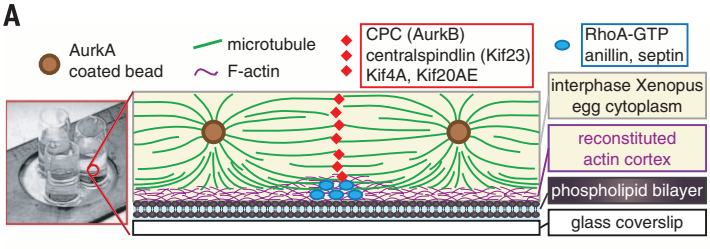
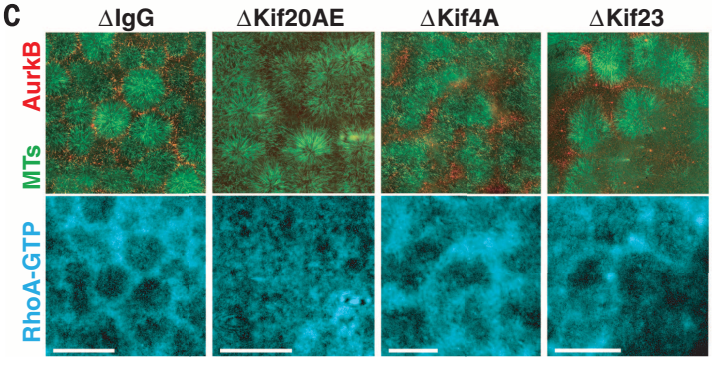


Fig. 2. Kinesin-dependent recruitment and motility of the CPC. (**A**) Representative spinning disc confocal images of microtubules and AurkB at AAIZs after kinesin immunodepletions, as labeled above. (**B**) Summary of kinesin perturbations using drug inhibition (inh) or immunodepletion (dep) (*5*). (**C** and **D**) Localization of Kif20AE and Kif4A at AAIZs (*5*). (**E**) Kymographs of CPC dynamics on individual microtubule bundles in AAIZs. (**F**) CPC velocity as a function of distance from the center of the AAIZ [error bars are standard deviations determined from $n \geq 3$ microtubule bundles (*5*)].





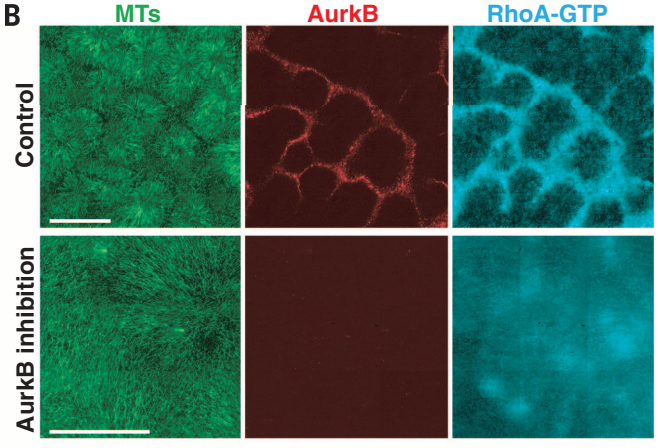


Fig. 3. Spatially localized recruitment of GTP-bound RhoA on model plasma membranes. (**A**) Drawing of experimental setup. See (*5*) for methods and probes. (**B** and **C**) Localization of a probe for RhoA-GTP (mCherry-rGBD; cyan) (*16*) and AurkB (red) at lipid bilayers proximal to AAIZs. TIRF images from 3 × 3 to 5 × 5 adjacent fields were corrected for uneven illumination and stitched (*5*). (B) Representative images of control and AurkB inhibition. (**C**) Representative images of kinesin immunodepletions, as labeled above. Scale bar, 200 μm.

using total internal reflection fluorescence (TIRF) microscopy (Fig. 3A). The small GTPase RhoA is thought to be the master organizer of the furrow (*16*). To localize active, GTP-bound RhoA we added an mCherry-tagged RhoA binding fragment of Rhotekin (mCherry-rGBD) (*16*). Using polyethylene glycol (PEG)–passivated coverslips, we saw no recruitment of RhoA-GTP. Using lipid bilayers, the RhoA-GTP reporter was enriched at the bilayer under AAIZs that recruited CPC and centralspindlin (Fig. 3B and fig. S12). Inhibition of AurkB or depletion of Kif20AE completely blocked AAIZ assembly and CPC localization as expected (*8*, *9*) and also blocked localized RhoA-GTP enrichment (Fig. 3, B and C). Kif4A depletion resulted in the broadening of both CPC and RhoA-GTP zones (Fig. 3C). Depletion of Kif23, a subunit of the centralspindlin complex, did not block AAIZ assembly or RhoA-GTP recruitment (Fig. 3C). Centralspindlin plays a central role in midzone assembly and signaling in many biological systems (*2*). Its dispensability in our system probably reflects functional redundancy among midzone factors and is consistent with its dispensability

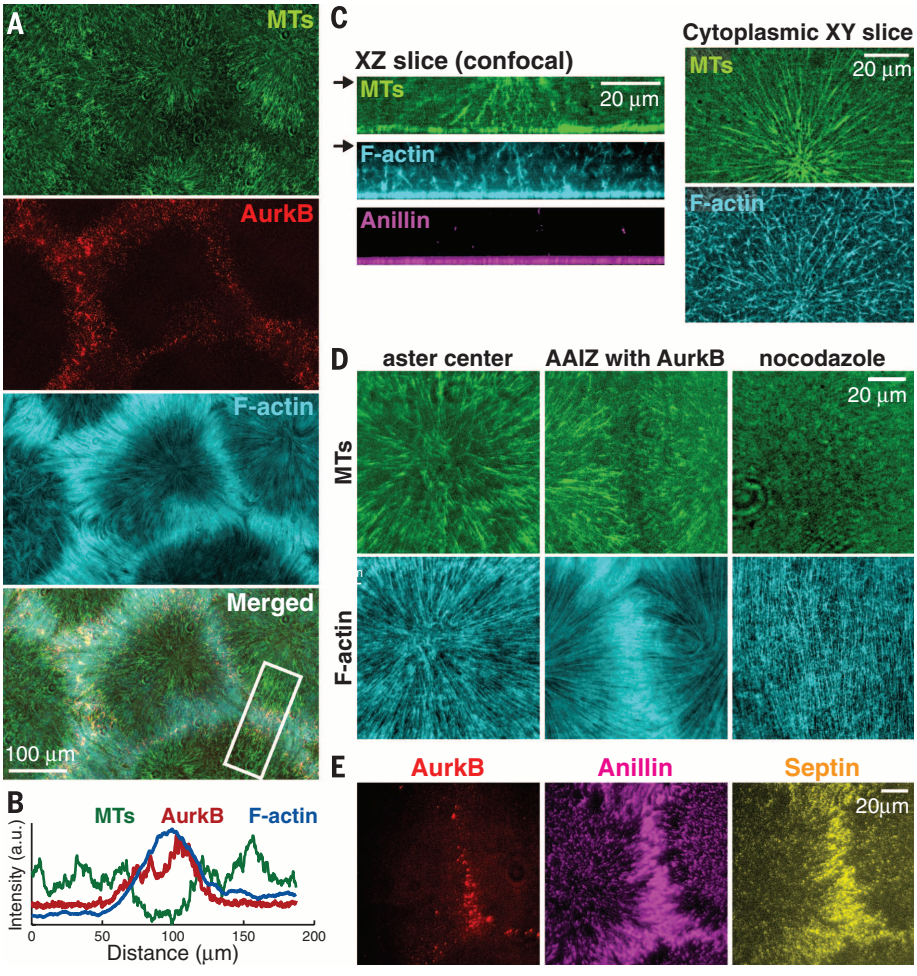


Fig. 4. Recruitment and organization of cortical cleavage furrow proteins. Experimental setup was as per Fig. 3A. (**A**) F-actin (TIRF image). Note the enrichment proximal to the CPC at AAIZs. (**B**) Intensity line scans across the AAIZ [boxed in (A)] show enrichment of AurkB and F-actin; a.u., arbitrary units. (**C**) XZ slices of three-dimensional reconstructions using spinning disc confocal microscopy, showing the organization of the microtubules, F-actin, and Anillin (left). XY slices of microtubules and F-actin at the plane marked by an arrow (right). (**D**) TIRF images of microtubules and F-actin at aster center (left) and an AAIZ (middle). The right shows a nocodazole-treated sample. (**E**) Anillin and septin on a bilayer (TIRF image) colocalize with the CPC at the AAIZ.

in *Xenopus* blastomere cytokinesis (*17*). We conclude that a CPC-positive AAIZ can locally activate RhoA in our system, although we cannot distinguish whether localized AurkB phosphorylation of cytokinetic factors or some specific organization of microtubules at the AAIZ is required for furrow signaling.

To probe cortical organization in our system, we visualized F-actin using Lifeact-GFP (Fig. 4) (*18*). F-actin was enriched at the lipid bilayer under AAIZs (Fig. 4, A and B). Above the cortical layer, F-actin organized into branched networks that showed only partial alignment with the microtubules (Fig. 4C). At the cortical layer, F-actin organized into long, uniformly spaced cables that aligned radially with microtubules (Fig. 4D, left and middle, and movie S9). The spacing between actin cables was 1.3 ± 0.5 µm (SD; n = 140), comparable to the spacing of actin-containing contractile bands on the cortex of live frog eggs (*19*). This organization was microtubule-dependent (Fig. 4D, right); we suspect it represents a configuration of actin bundles that normally precedes furrow ingression, because it has been noted in early anaphase in several systems (*5*). The furrow-selective actin bundling protein Anillin (*20*) colocalized with F-actin cables throughout the cortex and was enriched under AAIZs along with its binding partner septin complex (Fig. 4, C and E, and movie S10).

Summarizing, we have developed a cell-free system that recapitulates the hallmarks of spatially organized signaling characteristic of egg cytokinesis. Midzone proteins were recruited to the overlap zone between microtubule asters in egg extract, where they signaled to a nearby lipid bilayer to locally activate the RhoA pathway. Our system confirmed known mechanisms of spatially organized signaling (for example the AurkB activity requirement for cleavage furrow induction) and revealed new mechanistic aspects that were difficult to observe in living cells, notably transport of the CPC along microtubules toward the midzone in a process requiring two kinesins. Our data favor a model in which Kif4A is a transport motor for the CPC, and Kif20AE is required for it to bind microtubules, though not necessarily as a transporter. Future pure protein reconstitution experiments are required to conclusively determine the mechanism of CPC transport and the exact roles of these two kinesins.

Two factors facilitated imaging approaches in the cell-free system: the large spatial scale of the AAIZ (~20 µm) and its long time duration (>20 min). Both reflect the pre-cytokinesis organization of the large egg cell. In comparison, the microtubule overlap in somatic cell midzones is ~2 to 3 µm wide and lasts only ~3 min before being compressed by the furrow (*21*). Future studies will take advantage of these features and the experimental flexibility of an extract system to probe biophysical mechanisms involved in cytokinesis.

REFERENCES AND NOTES

1. R. Rappaport, *Cytokinesis in Animal Cells* (Cambridge Univ. Press, Cambridge, 1996).
2. M. Glotzer, *Science* **307**, 1735–1739 (2005).
3. C. M. Field, P. A. Nguyen, K. Ishihara, A. C. Groen, T. J. Mitchison, *Methods Enzymol.* **540**, 399–415 (2014).
4. M.-Y. Tsai, Y. Zheng, *Curr. Biol.* **15**, 2156–2163 (2005).
5. Supplementary materials are available on *Science* Online.
6. M. Wühr, E. S. Tan, S. K. Parker, H. W. Detrich 3rd, T. J. Mitchison, *Curr. Biol.* **20**, 2040–2045 (2010).
7. S. Petry, A. C. Groen, K. Ishihara, T. J. Mitchison, R. D. Vale, *Cell* **152**, 768–777 (2013).
8. H. Argiros, L. Henson, C. Holguin, V. Foe, C. B. Shuster, *Cytoskelet. Hoboken NJ* **69**, 840–853 (2012).
9. U. Gruneberg, R. Neef, R. Honda, E. A. Nigg, F. A. Barr, *J. Cell Biol.* **166**, 167–172 (2004).
10. R. A. Cross, A. McAinsh, *Nat. Rev. Mol. Cell Biol.* **15**, 257–271 (2014).
11. M. Wühr *et al.*, *Curr. Biol.* **24**, 1467–1475 (2014).
12. N. Ozlü *et al.*, *Mol. Cell. Proteomics* **9**, 336–350 (2010).
13. P. Bieling, I. A. Telley, T. Surrey, *Cell* **142**, 420–432 (2010).
14. T. J. Mitchison, P. Nguyen, M. Coughlin, A. C. Groen, *Mol. Biol. Cell* **24**, 1559–1573 (2013).
15. M. Loose, E. Fischer-Friedrich, J. Ries, K. Kruse, P. Schwille, *Science* **320**, 789–792 (2008).
16. W. M. Bement, H. A. Benink, G. von Dassow, *J. Cell Biol.* **170**, 91–101 (2005).
17. A. L. Miller, W. M. Bement, *Nat. Cell Biol.* **11**, 71–77 (2009).
18. J. Riedl *et al.*, *Nat. Methods* **5**, 605–607 (2008).
19. M. V. Danilchik, E. E. Brown, K. Riegert, *Development* **133**, 4517–4526 (2006).
20. A. F. Straight, C. M. Field, T. J. Mitchison, *Mol. Biol. Cell* **16**, 193–201 (2005).
21. D. N. Mastronarde, K. L. McDonald, R. Ding, J. R. McIntosh, *J. Cell Biol.* **123**, 1475–1489 (1993).

ACKNOWLEDGMENTS

We thank R. Ohi, D. Burgess, D. Miyamoto, and E. Tan for reagents; H. Basu for preliminary work; the Nikon Imaging Center at Harvard Medical School and Nikon at the Woods Hole Marine Biological Laboratory (MBL) for microscopy support; and the National Xenopus Resource at MBL for *Xenopus* animals and care. This work was supported by NIH grant GM39565 (T.J.M.); MBL fellowships from the Evans Foundation, MBL Associates, and the Colwin Fund (T.J.M. and C.M.F.); HFSP fellowship LT000466/2012-L (M.L.); and NIH grant GM103785 (M.W.).

SUPPLEMENTARY MATERIALS

www.sciencemag.org/content/346/6206/244/suppl/DC1
Materials and Methods
Supplementary Text
Figs. S1 to S13
Tables S1 to S2
References (*22–29*)
Movies S1 to S10

30 May 2014; accepted 12 September 2014
10.1126/science.1256773

YEAST MEIOSIS

Sister kinetochores are mechanically fused during meiosis I in yeast

Krishna K. Sarangapani,[1]* Eris Duro,[2]* Yi Deng,[1] Flavia de Lima Alves,[2] Qiaozhen Ye,[3] Kwaku N. Opoku,[1] Steven Ceto,[4]† Juri Rappsilber,[2,5] Kevin D. Corbett,[3,6] Sue Biggins,[4,7] Adèle L. Marston,[2]‡ Charles L. Asbury[1]‡

Production of healthy gametes requires a reductional meiosis I division in which replicated sister chromatids comigrate, rather than separate as in mitosis or meiosis II. Fusion of sister kinetochores during meiosis I may underlie sister chromatid comigration in diverse organisms, but direct evidence for such fusion has been lacking. We used laser trapping and quantitative fluorescence microscopy to study native kinetochore particles isolated from yeast. Meiosis I kinetochores formed stronger attachments and carried more microtubule-binding elements than kinetochores isolated from cells in mitosis or meiosis II. The meiosis I–specific monopolin complex was both necessary and sufficient to drive these modifications. Thus, kinetochore fusion directs sister chromatid comigration, a conserved feature of meiosis that is fundamental to Mendelian inheritance.

The hallmark of meiosis is a twofold reduction in ploidy, which occurs because one round of DNA replication is followed by two rounds of chromosome segregation. Sister chromatids distinctly comigrate during meiosis I, thereby enabling segregation of homologous chromosomes. During meiosis II, which resembles mitosis, the sister chromatids separate (fig. S1, A and B). It has been suggested that the comigration of sister chromatids during meiosis I depends on fusion of sister kinetochores in a range of organisms (*1*–*4*) (fig. S1C). Because fused sister kinetochore pairs would contain more microtubule-binding elements than individual kinetochores, we reasoned that they might form stronger attachments to microtubules. Alternatively, if one kinetochore within each sister pair was selectively inactivated during meiosis I (*5*, *6*), then the remaining active kinetochores would probably form attachments with similar strength relative to individual mitotic and meiosis II kinetochores.

To distinguish between the "fusion" and "one-sister shut-off" mechanisms, we purified native kinetochore particles from yeast cells arrested in metaphase of meiosis I (via meiosis-specific depletion of Cdc20) (*7*), using methods developed for the isolation of mitotic particles (*8*, *9*). The purified material contained essentially all known kinetochore components (table S1), and its bulk composition was very similar to material isolated from mitosis (Fig. 1A; fig. S2, A and B; and table S1). We used fluorescence- and laser trap–based assays to determine whether the meiosis I kinetochore particles remained functional in vitro. As shown previously for mitotic particles (*8*), fluorescently labeled particles isolated from meiosis I cultures bound specifically to microtubules and tracked processively with disassembling microtubule tips (Fig. 1B and movie S1). Furthermore, meiosis I kinetochore particles formed load-bearing attachments to microtubule tips, supporting forces up to 15 pN and persisting through "catastrophe" and "rescue" events, in which the filament switched from assembly to disassembly and vice versa (Fig. 1C). Thus, native kinetochore particles isolated from meiotic cultures are functional. The meiotic particles formed very-long-lived tip attachments with a mean lifetime of 52 ± 23 min at 7 pN of tension, double the lifetime measured previously for mitotic particles (26 ± 6 min) at a similar level of tension (7.2 pN) (*8*).

The long lifetimes of attachments formed by meiosis I kinetochore particles suggested that they may be stronger than particles from mitotic cells. To assess their strength directly, we attached the meiosis I kinetochore particles to growing microtubule tips and tested them using a force ramp, where force was increased at a constant rate until the attachments ruptured (Fig. 1D). Control kinetochore particles isolated from metaphase-arrested mitotic cells ruptured at an average force of 9.4 ± 0.4 pN (Fig. 2B), which is indistinguishable from the strength of particles harvested during vegetative (asynchronous mitotic) growth (*8*). Rupture strengths were unaffected by differences in ploidy and were relatively insensitive to the method of mitotic cell cycle arrest (fig. S3). Meiosis I particles, however, formed significantly stronger attachments, rupturing at forces ranging from 6.5 to 22 pN (i.e., up to the load limit of our laser trap), with an average of 13.1 ± 0.3 pN (Fig. 2, A and B, and table S2). Mean rupture forces for both meiosis I and mitotic particles remained invariant as the density of particles on the beads was reduced below the single-particle limit (fig. S4), indicating that higher strength is an intrinsic property of individual meiosis I kinetochore particles.

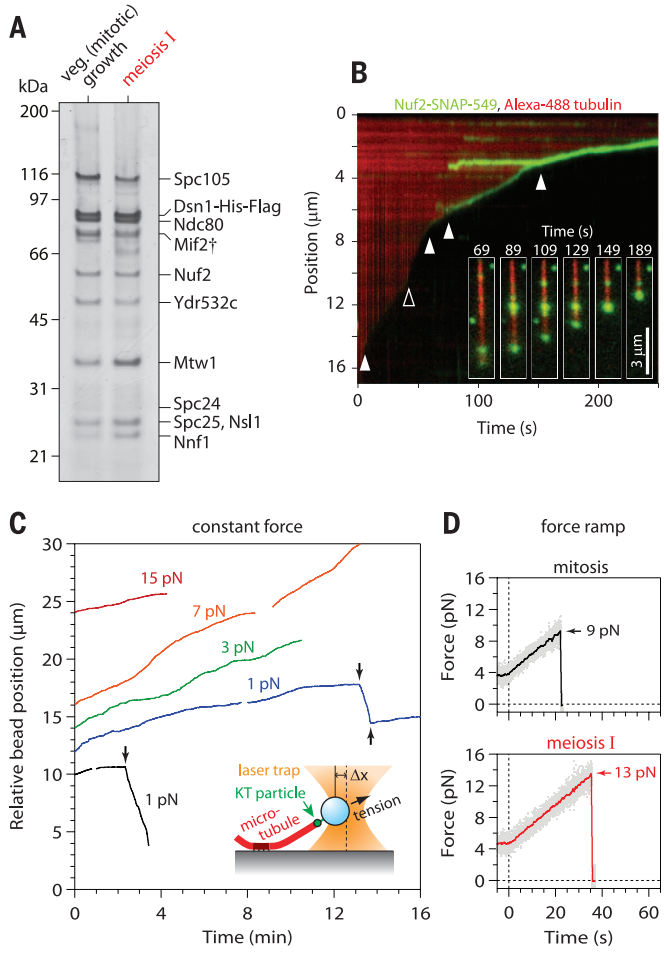
To determine whether the higher kinetochore attachment strength is specific to meiosis I or persists into meiosis II, we prepared synchronized meiotic cultures by releasing cells from a prophase I block (*10*, *11*). Particles harvested from synchronized metaphase I cells formed attachments that ruptured at 13.1 ± 0.6 pN, on average (Fig. 2, A and B, meiosis I*). However, particles from synchronized metaphase II cells ruptured at 9.3 ± 0.7 pN, on average (Fig. 2, A and B, meiosis II*). Thus, the higher intrinsic strength of kinetochore particles occurs specifically during meiosis I and returns to mitotic-like levels as cells progress into meiosis II.

If the particles isolated from meiosis I cells are fused sister kinetochore pairs, they should contain more microtubule binding elements than mitotic particles. We purified fluorescent particles doubly tagged with SNAP-549 on Nuf2 (a subunit of the microtubule-binding Ndc80 complex) and CLIP-647 on Mif2 (an inner kinetochore component orthologous to CENP-C). Spore viability was unaffected, and rupture strengths for the fluorescent particles were indistinguishable from untagged particles (fig. S5 and table S2), indicating no loss of functionality. The purified kinetochore material contained a mixture of dual-color particles carrying both Nuf2 and Mif2, plus subcomplexes lacking Nuf2 or Mif2 (Fig. 2C). Subcomplexes with just one detectable Nuf2 [identifiable by their single-step photobleaching behavior (fig. S6)] served as internal controls, allowing normalization of particle brightnesses into estimates for the approximate numbers of Nuf2 molecules associated with each particle. Dual-color particles from meiosis I cells carried more Nuf2 molecules, on average [6.5 ± 2.8 (mean ± SD from N = 4 preparations)], than those from vegetatively growing cells, which had 3.8 ± 1.3 (N = 4) (Fig. 2, D and E). The apparent Nuf2 content was variable and lower than in vivo estimates [which suggest 8 to 20 copies per mitotic kinetochore (*12*, *13*)]. However, consistent with the fusion model, Nuf2 content was significantly higher for dual-color meiosis I particles than for vegetative particles prepared in tandem, by a factor of 1.66 ± 0.26 (mean ± SD, N = 4 tandem pairs; P = 0.014 by t test).

If fusion of sister kinetochore pairs underlies the increased strength of meiosis I kinetochore particles, the increase should vanish if the particles are harvested from cells in which every kinetochore lacks a sister. We engineered cells to undergo meiosis without replicating their DNA [via meiosis-specific depletion of Cdc6 (*14*), part of the prereplicative complex (*15*)]. Because the lack of sister chromatids precludes homology-based DNA repair (*16*), we also deleted the Spo11 endonuclease, thereby avoiding high levels of DNA damage that might interfere with meiotic progression. Spo11 catalyzes formation of the chiasmata that link homologous chromosomes

[1]Department of Physiology and Biophysics, University of Washington, Seattle, WA 98195, USA. [2]Wellcome Trust Centre for Cell Biology, University of Edinburgh, Edinburgh, UK. [3]Ludwig Institute for Cancer Research, San Diego Branch, La Jolla, CA 92093, USA. [4]Division of Basic Sciences, Fred Hutchinson Cancer Research Center, Seattle, WA 98109, USA. [5]Institute of Bioanalytics, Department of Biotechnology, Technische Universität Berlin, Berlin, Germany. [6]Department of Cellular and Molecular Medicine, University of California, San Diego, La Jolla, CA 92093, USA. [7]Department of Biochemistry, University of Washington, Seattle, WA 98195, USA.
*These authors contributed equally to this work. †Present address: Department of Neurosciences, University of California, San Diego, CA 92093, USA. ‡Corresponding author. E-mail: casbury@u.washington.edu (C.L.A.); adele.marston@ed.ac.uk (A.L.M.)

(*17*), so its deletion (*spo11*Δ) enabled us to test whether tension across homologs is required for sister kinetochore fusion (*18*). Kinetochore particles from *spo11*Δ cells were identical in strength to those from wild-type cells, indicating that linkage between homologs (and, thus, spindle-generated tension across them) was dispensable for the high attachment strength of meiosis I kinetochores (Fig. 2, A and B, *no chiasmata*).



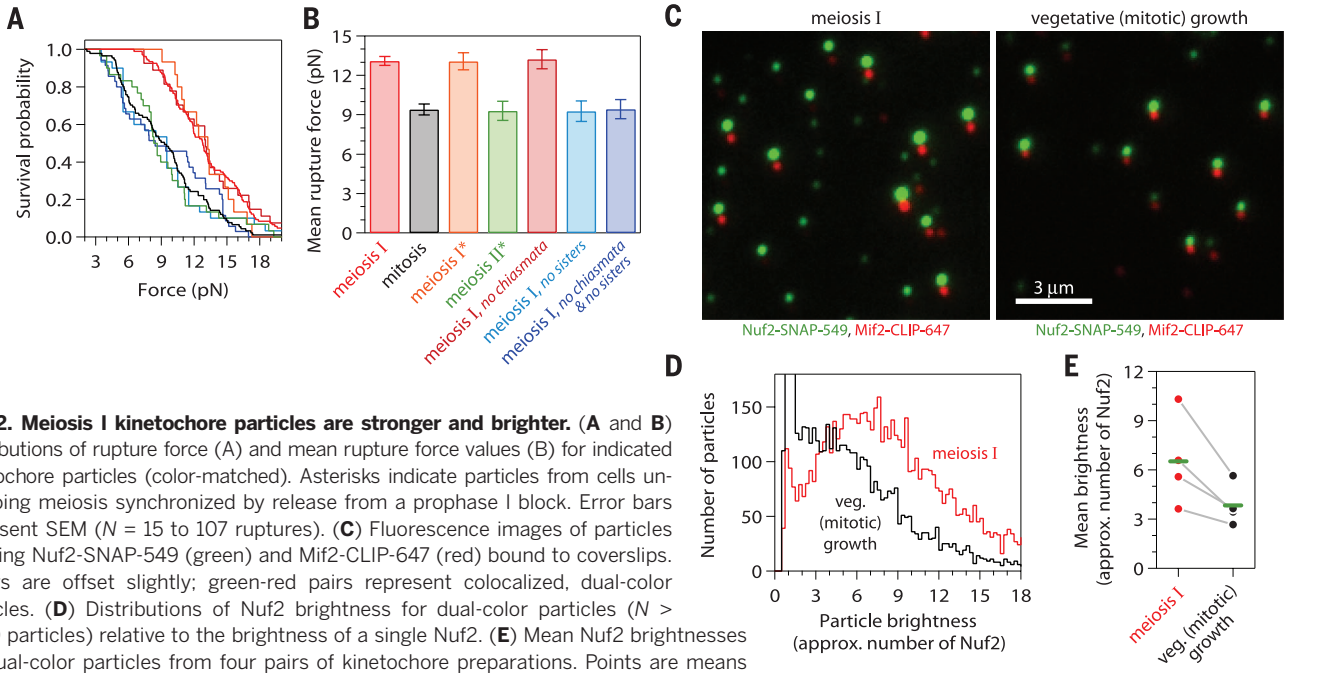


Fig. 1. Native kinetochore particles from meiotic cells recapitulate tip-coupling in vitro. (**A**) Core kinetochore proteins copurified from cells undergoing vegetative (mitotic) growth and cells arrested in metaphase I of meiosis, visualized by silver-stained SDS–polyacrylamide gel electrophoresis (*9*). Mif2 (†) comigrates with nonspecific background proteins (*8*). kDa, kilodaltons. (**B**) Kymograph showing movement of fluorescent meiosis I kinetochore particles (green) driven by a disassembling microtubule (red) (see movie S1). Filled arrowheads mark tip-particle encounters; the open arrowhead denotes particle release. Insets shows images at indicated times. (**C**) Position versus time for tip-attached meiosis I particles tested with a force clamp at indicated loads. Arrows mark catastrophes and rescue. Intervals when the laser trap was briefly shuttered (to clear debris) appear as gaps in the 1- and 7-pN traces. The inset shows a schematic of the assay (*9*). KT, kinetochore. (**D**) Tensile force versus time for indicated particles bound to assembling tips and tested with a 0.25–pN s^{-1} force ramp. Gray dots show raw data; colored traces show the same data after smoothing (500-ms sliding boxcar average). Dashed vertical lines mark the start of the force ramp. Arrows denote rupture.

Fig. 2. Meiosis I kinetochore particles are stronger and brighter. (**A** and **B**) Distributions of rupture force (A) and mean rupture force values (B) for indicated kinetochore particles (color-matched). Asterisks indicate particles from cells undergoing meiosis synchronized by release from a prophase I block. Error bars represent SEM (N = 15 to 107 ruptures). (**C**) Fluorescence images of particles carrying Nuf2-SNAP-549 (green) and Mif2-CLIP-647 (red) bound to coverslips. Colors are offset slightly; green-red pairs represent colocalized, dual-color particles. (**D**) Distributions of Nuf2 brightness for dual-color particles (N > 4900 particles) relative to the brightness of a single Nuf2. (**E**) Mean Nuf2 brightnesses for dual-color particles from four pairs of kinetochore preparations. Points are means from individual preparations. Gray lines connect means from particles prepared in tandem (*9*); green horizontal lines are means across all preparations.

However, high strength was lost when meiosis I particles were harvested from *cdc6-meiotic-null* cells (Fig. 2, A and B, *no sisters* or *no chiasmata & no sisters*). Thus, sister kinetochores are required for the increased strength of meiosis I kinetochore particles, as predicted by the fusion model.

The meiosis I–specific monopolin complex consists of four proteins (Mam1, Csm1, Lrs4, and Hrr25) (*5*, *19*–*21*) with twin kinetochore-binding sites that have been proposed to directly cross-link sister kinetochores in budding yeast (*1*, *5*, *20*, *22*). However, because the receptor for monopolin, Dsn1 (*1*, *23*), is present in multiple copies in the kinetochore (*12*), another possibility is that the twin monopolin sites bind to the same kinetochore and inactivate it, thereby shutting off one of the two sister kinetochores (fig. S1C) (*5*, *6*).

Monopolin was detectable at low levels in kinetochore material from meiosis I cultures (fig. S2C). To test the impact of monopolin on the behavior of kinetochore particles, we genetically disrupted its function in three ways (*mam1*Δ, *csm1-L161D*, and *dsn1-*Δ*N*), all of which disrupt sister comigration during meiosis I (*1*, *21*, *23*). In all cases, we found that the high 13-pN strength of meiosis I kinetochore particles was lost and their strength returned to mitosis-like levels (~9 pN) (Fig. 3), confirming that monopolin is required for high attachment strength. We also engineered cells to ectopically express monopolin during mitosis by inducing expression of *MAM1* together with *CDC5* (encoding Polo kinase), which caused erroneous co-orientation in 28% of cells (*5*). Kinetochore particles isolated from these cells gave a bimodal rupture force distribution (Fig. 3A) with an intermediate average strength of 11.2 ± 0.4 pN (Fig. 3B). This observation may be explained by the incomplete penetrance of monopolin induction in these cells (*5*).

To test whether kinetochores can be fused by monopolin in the absence of other cellular factors, we recombinantly expressed and purified the four-protein monopolin complex [containing a kinase-dead Lys^{38}→Arg^{38} mutant of Hrr25 (fig. S2D)] (*22*) and incubated it with isolated kinetochore particles. Incubation with recombinant monopolin was sufficient to strengthen mitotic particles and also particles from meiosis I cells in which monopolin was disrupted (*mam1*Δ or *csm1-L161D*), raising their mean rupture forces from ~9 to ~13 pN (Fig. 4, A and B) in a dose-dependent manner (Fig. 4C). However, the same treatment did not affect the strength of particles from cells lacking the monopolin binding site on Dsn1 (*dsn1-*Δ*N*) (Fig. 4, A and B). Likewise, monopolin addition did not strengthen particles (*mam1*Δ) prelinked to laser trapping beads (Fig. 4C), presumably because immobilization on beads prevented cross-linking of the particles. When fluorescent particles from vegetatively growing cells were incubated with increasing amounts of monopolin, their average brightness grew monotonically, and the approximate number of Nuf2 molecules associated with each particle increased twofold, from 4.8 ± 0.4 to 10.9 ± 1.5 (mean ± SD, $N \geq 2$ experiments) (Fig. 4D). Thus, monopolin alone is sufficient for fusion of kinetochore particles in vitro.

Sister chromatid comigration is a universal feature of meiosis I that governs Mendelian inheritance, and its failure is a major cause of birth defects and infertility (*24*). Here we have shown

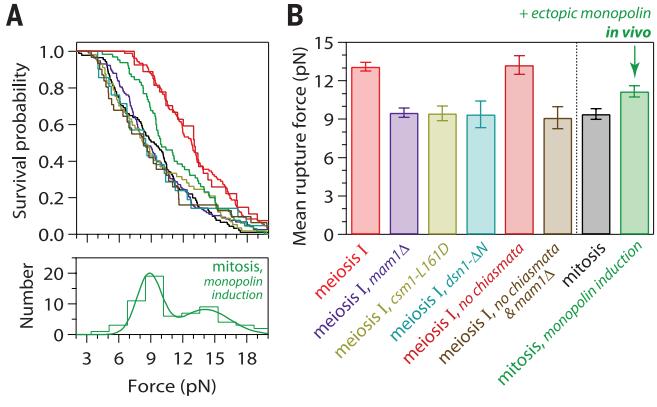


Fig. 3. Monopolin is necessary for the high strength of meiosis I kinetochore particles and is sufficient in vivo. (**A** and **B**) Distributions of rupture force (A) and mean rupture force values (B) for indicated kinetochore particles (color-matched). Data for particles from meiosis I (red), meiosis I without chiasmata (dark red), and mitosis (black) are replotted from Fig. 2, A and B, for comparison. Error bars represent SEM (N = 21 to 118 ruptures).

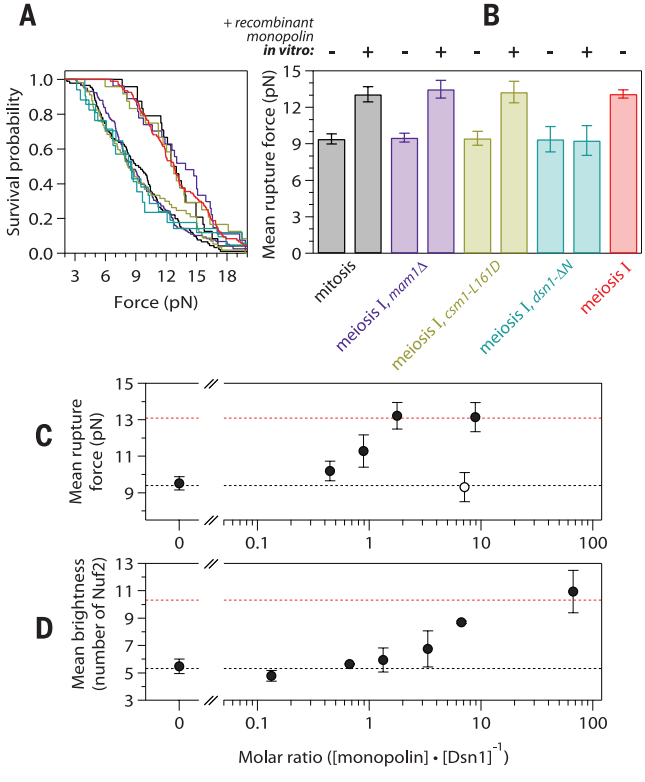


Fig. 4. Pure recombinant monopolin is sufficient to increase the strength and brightness of kinetochore particles in vitro. (**A** and **B**) Distributions of rupture force (A) and mean rupture force values (B) for kinetochore particles (color-matched) after incubation with recombinant monopolin [at molar ratio 1.8 versus Dsn1-His-Flag; "+" in (B)]. Data for particles without monopolin incubation ["-" in (B)] are replotted from Fig. 3, A and B, for comparison. Error bars represent SEM (N = 17 to 118 ruptures). (**C**) Mean rupture forces for meiosis I, *mam1*Δ kinetochore particles after incubation with indicated amounts of recombinant monopolin (*9*). Filled circles are data from particles preincubated with monopolin before linking to polystyrene laser trapping beads. The open circle shows control in which particles were first linked to trapping beads and subsequently incubated with monopolin. Error bars represent SEM (N = 28 to 118 ruptures). Dashed lines denote means for mitosis (black) and meiosis I (red) particles (from Fig. 2B). (**D**) Mean Nuf2 brightnesses for dual-color particles isolated from cells undergoing vegetative (mitotic) growth, incubated with indicated amounts of recombinant monopolin. Error bars represent SD (N = 2 or 3 experiments). Dashed lines represent mean brightnesses for dual-color vegetative (black) and meiosis I (red) kinetochore particles prepared on the same day, without monopolin incubation (from Fig. 2E).

that a meiosis I–specific factor from budding yeast, monopolin, generates kinetochores with more microtubule-binding elements and greater strength. These findings provide direct evidence that sister kinetochore fusion underlies the cosegregation of sister chromatids during meiosis I.

REFERENCES AND NOTES

1. K. D. Corbett *et al*., *Cell* **142**, 556–567 (2010).
2. X. Li, R. K. Dawe, *Nat. Cell Biol.* **11**, 1103–1108 (2009).
3. L. S. Goldstein, *Cell* **25**, 591–602 (1981).
4. L. V. Paliulis, R. B. Nicklas, *J. Cell Biol.* **150**, 1223–1232 (2000).
5. F. Monje-Casas, V. R. Prabhu, B. H. Lee, M. Boselli, A. Amon, *Cell* **128**, 477–490 (2007).
6. M. Winey, G. P. Morgan, P. D. Straight, T. H. Giddings Jr., D. N. Mastronarde, *Mol. Biol. Cell* **16**, 1178–1188 (2005).
7. B. H. Lee, A. Amon, *Science* **300**, 482–486 (2003).
8. B. Akiyoshi *et al*., *Nature* **468**, 576–579 (2010).
9. Materials and methods are available as supplementary materials on *Science* Online.
10. T. M. Carlile, A. Amon, *Cell* **133**, 280–291 (2008).
11. K. R. Benjamin, C. Zhang, K. M. Shokat, I. Herskowitz, *Genes Dev.* **17**, 1524–1539 (2003).
12. A. P. Joglekar, D. C. Bouck, J. N. Molk, K. S. Bloom, E. D. Salmon, *Nat. Cell Biol.* **8**, 581–585 (2006).
13. J. Lawrimore, K. S. Bloom, E. D. Salmon, *J. Cell Biol.* **195**, 573–582 (2011).
14. A. Hochwagen, W. H. Tham, G. A. Brar, A. Amon, *Cell* **122**, 861–873 (2005).
15. J. H. Cocker, S. Piatti, C. Santocanale, K. Nasmyth, J. F. Diffley, *Nature* **379**, 180–182 (1996).
16. T. Goldfarb, M. Lichten, *PLOS Biol.* **8**, e1000520 (2010).
17. S. Keeney, C. N. Giroux, N. Kleckner, *Cell* **88**, 375–384 (1997).
18. M. A. Shonn, R. McCarroll, A. W. Murray, *Science* **289**, 300–303 (2000).
19. M. Petronczki *et al*., *Cell* **126**, 1049–1064 (2006).
20. K. P. Rabitsch *et al*., *Dev. Cell* **4**, 535–548 (2003).
21. A. Tóth *et al*., *Cell* **103**, 1155–1168 (2000).
22. K. D. Corbett, S. C. Harrison, *Cell Reports* **1**, 583–589 (2012).
23. S. Sarkar *et al*., *PLOS Genet.* **9**, e1003610 (2013).
24. K. T. Jones, S. I. Lane, *Development* **140**, 3719–3730 (2013).

ACKNOWLEDGMENTS

We thank A. Hoskins, M. Miller, N. Umbreit, and E. Yusko for helpful comments. We thank A. Desai for providing antibodies and A. Hoskins for SNAPf and CLIPf plasmids. The Wellcome Trust supported this work through a Sir Henry Wellcome Fellowship to E.D. (096078), Senior Research Fellowships to A.L.M. (090903) and J.R. (084229), and two Wellcome Trust Centre Core Grants (077707 and 092076) and an instrument grant (091020). The work was also supported by NIH grants to C.L.A. (R01GM079373 and S10RR026406), S.B. (R01GM064386), and K.D.C. (R01GM104141) and by a Packard Fellowship to C.L.A. (2006-30521). K.D.C. also acknowledges support from the Ludwig Institute for Cancer Research and the Sidney Kimmel Foundation. Additional data described in this work can be found in the supplementary materials. E.D., K.K.S., S.B., A.L.M., and C.L.A. conceived the experiments. E.D. generated new yeast strains and isolated kinetochore particles. K.K.S. performed laser trap experiments. Y.D. performed the fluorescence measurements. F.d.L.A. and J.R. performed proteomics analysis. Q.Y. and K.D.C. purified monopolin. K.N.O. and S.C. optimized fluorescent labeling of kinetochore particles. E.D., K.K.S., A.L.M., and C.L.A. prepared the manuscript.

SUPPLEMENTARY MATERIALS

www.sciencemag.org/content/346/6206/248/suppl/DC1
Materials and Methods
Figs. S1 to S8
Tables S1 to S3
References (*25*–*42*)
Movie S1
Additional Data Tables S1 to S3

30 May 2014; accepted 1 September 2014
Published online 11 September 2014;
10.1126/science.1256729

LUNG CANCER EVOLUTION

Spatial and temporal diversity in genomic instability processes defines lung cancer evolution

Elza C. de Bruin,[1]* Nicholas McGranahan,[2,3]* Richard Mitter,[2]* Max Salm,[2]* David C. Wedge,[4]* Lucy Yates,[4,5]† Mariam Jamal-Hanjani,[1]† Seema Shafi,[1] Nirupa Murugaesu,[1] Andrew J. Rowan,[2] Eva Grönroos,[2] Madiha A. Muhammad,[1] Stuart Horswell,[2] Marco Gerlinger,[2] Ignacio Varela,[6] David Jones,[4] John Marshall,[4] Thierry Voet,[4,7] Peter Van Loo,[4,7] Doris M. Rassl,[8] Robert C. Rintoul,[8] Sam M. Janes,[9] Siow-Ming Lee,[1,10] Martin Forster,[1,10] Tanya Ahmad,[10] David Lawrence,[10] Mary Falzon,[10] Arrigo Capitanio,[10] Timothy T. Harkins,[11] Clarence C. Lee,[11] Warren Tom,[11] Enock Teefe,[11] Shann-Ching Chen,[11] Sharmin Begum,[2] Adam Rabinowitz,[2] Benjamin Phillimore,[2] Bradley Spencer-Dene,[2] Gordon Stamp,[2] Zoltan Szallasi,[12,13] Nik Matthews,[2] Aengus Stewart,[2] Peter Campbell,[4] Charles Swanton[1,2]‡

Spatial and temporal dissection of the genomic changes occurring during the evolution of human non–small cell lung cancer (NSCLC) may help elucidate the basis for its dismal prognosis. We sequenced 25 spatially distinct regions from seven operable NSCLCs and found evidence of branched evolution, with driver mutations arising before and after subclonal diversification. There was pronounced intratumor heterogeneity in copy number alterations, translocations, and mutations associated with APOBEC cytidine deaminase activity. Despite maintained carcinogen exposure, tumors from smokers showed a relative decrease in smoking-related mutations over time, accompanied by an increase in APOBEC-associated mutations. In tumors from former smokers, genome-doubling occurred within a smoking-signature context before subclonal diversification, which suggested that a long period of tumor latency had preceded clinical detection. The regionally separated driver mutations, coupled with the relentless and heterogeneous nature of the genome instability processes, are likely to confound treatment success in NSCLC.

Lung cancer is the leading cause of cancer-related mortality (*1*, *2*). Understanding the pathogenesis and evolution of lung cancer may lead to greater insight into tumor initiation and maintenance and may guide therapeutic interventions. Previous work characterizing the genome of non–small cell lung cancer (NSCLC) has demonstrated that NSCLC genomes exhibit hundreds of nonsilent mutations together with copy number aberrations and genome doublings (*3*–*9*). Although subclonal populations have been identified within single biopsies (*9*), the extent of genomic diversity within primary NSCLCs remains unclear. Moreover, although both exogenous mutational processes, such as smoking (*10*–*12*), and endogenous processes, such as up-regulation of APOBEC cytidine deaminases (*13*–*15*), have been found to contribute to the large mutational burden in NSCLC, the temporal dynamics of these processes and their contribution to driver somatic aberrations over time remain unknown.

To investigate lung cancer evolution, we performed multiregion whole-exome and/or whole-genome sequencing (M-seq WES/WGS) on a total of 25 tumor regions, collected from seven NSCLC patients who underwent surgical resection before receiving adjuvant therapy. The major NSCLC histological subtypes, including adenocarcinoma (LUAD) and squamous cell carcinoma (LUSC), were represented (table S1). Sequencing of tumor and normal DNA to mean coverage depths of 107× and 54× for M-seq WES and M-seq WGS, respectively (table S2), identified 1884 nonsilent and 76,129 silent mutations (*16*).

To evaluate the intratumor heterogeneity of nonsilent mutations, we classified each mutation as ubiquitous (present in all tumor regions) or heterogeneous (present in at least one, but not all, regions). Spatial intratumor heterogeneity was identified in all seven NSCLCs, with a median of 30% heterogeneous mutations (range 4

[1]Cancer Research UK Lung Cancer Centre of Excellence, University College London Cancer Institute, London WC1E 6BT, UK. [2]Cancer Research UK London Research Institute, London WC2A 3LY, UK. [3]Centre for Mathematics and Physics in the Life Science and Experimental Biology (CoMPLEX), University College London, London WC1E 6BT, UK. [4]Wellcome Trust Sanger Institute, Hinxton, CB10 1SA, UK. [5]University of Cambridge, Cambridge CB2 1TN, UK. [6]Instituto de Biomedicina y Biotecnología de Cantabria (CSIC-UC-Sodercan), Departamento de Biología Molecular, Universidad de Cantabria, Santander, Spain. [7]Department of Human Genetics, University of Leuven, 3000 Leuven, Belgium. [8]Papworth Hospital NHS Foundation Trust, Cambridge CB23 3RE, UK. [9]Lungs for Living Research Centre, University College London, London WC1E 6BT, UK. [10]University College London Hospitals, London NW1 2BU, UK. [11]Thermo Fisher Scientific, Carlsbad, CA 92008, USA. [12]Technical University of Denmark, 2800 Kongens Lyngby, Denmark. [13]Children's Hospital Informatics Program, Harvard Medical School, Boston, MA 02115, USA.
*These authors contributed equally to this work. †These authors contributed equally to this work. ‡**Corresponding author. E-mail: charles.swanton@cancer.org.uk**

to 63%) (Fig. 1A and fig. S1). In the adenosquamous tumor from patient L002, heterogeneous mutations separated concordant with LUAD (regions R1 and R2) or LUSC (regions R3 and R4) histopathologies (fig. S2). Patients L003 and L008 each presented with two tumors in separate lobes of the lung. M-seq WES revealed 74% ubiquitous mutations in the tumors from L008, which indicated a clonal origin. However, in L003, only a single mutation ($EGFR^{L858R}$, the epidermal growth factor receptor in which Leu^{858} is replaced with Arg) was detected in both tumors (Fig. 1A). Given that $EGFR^{L858R}$ is a highly recurrent mutation (*17*) and also that no silent mutations were shared, we concluded that the tumors in L003 were of independent clonal origin, with the evolution of identical oncogenic events in parallel.

To resolve the extent of genomic diversity in NSCLC and to infer the ancestral relations between tumor regions, we estimated the fraction of tumor cells within each region harboring each mutation (*16*, *18*). Almost all ubiquitous mutations (>99%) were classified as fully clonal within each region. Moreover, in most regions, the majority of heterogeneous mutations was clonal and, thus, present in all cells within the region (Fig. 1B and fig. S3). However, certain regions displayed considerable subclonal diversity. For example, >75% of heterogeneous mutations present in L004 R5 were subclonal (Fig. 1B), and this region consisted of two distinct subclonal populations. The subclonal structure of each tumor region was then used to construct phylogenetic trees, by using both maximum parsimony and unweighted pair-group methods. We also took into account regional copy number losses that resulted in shared truncal mutations becoming heterogeneous later in tumor evolution (*16*), such as a segment of chromosome 6 in LS01 (fig. S4) and the *PAX7* mutation in the lymph node of L001 (Fig. 1A). Notably, all seven NSCLCs showed evidence of branched tumor evolution (fig. S5).

We next evaluated the regional heterogeneity of potential NSCLC driver mutations, classified into three categories on the basis of current evidence supporting driver mutation status (*16*). Every tumor showed evidence for ubiquitous, as well as heterogeneous, driver mutations, many of which were clonally dominant in a subset of tumor regions and entirely absent in others (Fig. 1B, fig. S3, and table S3). Note that the probability of missing a category 1 "high-confidence" driver gene by analyzing a single region for each

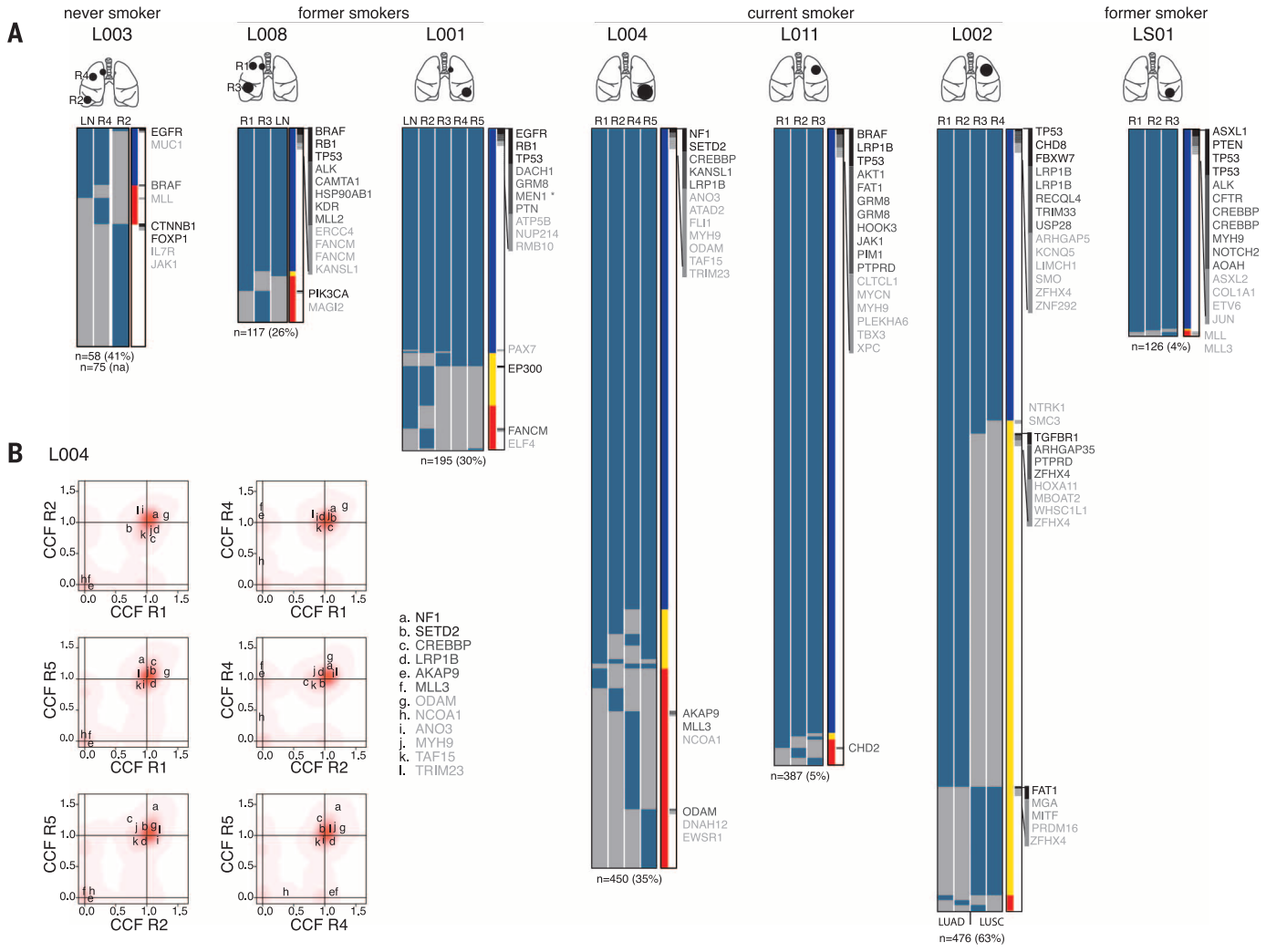


Fig. 1. Intratumor heterogeneity of somatic mutations in human NSCLC. (**A**) Heat maps show the regional distribution of all nonsilent mutations; presence (blue) or absence (gray) of each mutation is indicated for every tumor region. Cartoons depict the location of each tumor. Column next to heat map shows the intratumor heterogeneity; mutation present in all regions (blue), in more than one but not all (yellow), or in one region (red). Mutations are ordered on tumor driver category with categories 1 to 3 indicated in the right column in black, dark gray, and light gray, respectively (details in table S3). Total number of nonsilent mutations is provided below each tumor with percentage of heterogeneous mutations in brackets. In L001, the mutation marked by an asterisk (*) is additional to the germline MEN1 mutation. LN, lymph node; R, region. (**B**) Two-dimensional Dirichlet plots show the cancer cell fraction (CCF) of the mutations in all regions of tumors L004; increasing intensity of red indicates the location of a high posterior probability of a cluster. In region R5, the majority of heterogeneous mutations are subclonal, and a cluster of mutations with a CCF below 1 can be observed.

tumor was on average 42% (range 0 to 67%) and 83% (range 67 to 100%) for all potential driver genes (categories 1 to 3), which highlights the potential limitations of assessing single tumor regions. Nevertheless, category 1 and 2 driver mutations were significantly more often truncal compared with mutations in nondriver genes in our M-seq analysis ($P = 0.04$). Consistent with these data, in The Cancer Genome Atlas (TCGA) cohort, previously reported driver genes (*5*, *19*, *20*) were significantly enriched for clonal mutations ($P < 0.001$) (fig. S6). These data indicate that, in NSCLC, most known driver mutations occur early in tumor evolution.

To determine the intratumor heterogeneity of copy number aberrations, we estimated integer DNA copy numbers for each tumor region (*7*, *16*, *21*, *22*). A large fraction of the genome had undergone alterations in all tumors, and genomic profiles were more similar within tumors than between different tumors (fig. S7). To evaluate the spatial heterogeneity of potential tumor driver copy number aberrations, we explored the regional distribution of chromosomal segments identified as recurrently gained or lost in TCGA LUAD or LUSC tumors. Most segments were identified as aberrant in at least one tumor region, and many recurrent gains and losses were found to be heterogeneous in at least one tumor (Fig. 2A). For example, in L001, a focal EGFR amplification (chr7p11.2), as well as deletions of chromosomal segments harboring CDKN2A (chr9p21.3) and PTEN (chr10q23.31), was observed in all regions, whereas, in L008, we observed heterogeneous copy number losses involving CDKN2A and PTEN. In support of copy number aberrations occurring later in tumor development, we also identified subclonal copy number aberrations within tumor regions. For instance, more than 15% of the genome in region R1 of L008 was subject to subclonal copy number alterations (fig. S8). Consistent with evidence of subclonal copy number aberrations, centromeric fluorescence in situ hybridization analyses confirmed numerical chromosomal diversity within individual tumor regions (fig. S9), which suggested that chromosomal instability may provide a substrate for subclonal competition.

The high-coverage M-seq WGS (mean 96×) for L002 and L008 enabled us to investigate the regional separation of large-scale genomic events in these samples. For the adenosquamous tumor L002, we identified 30 structural variants, most of which were found either in the LUAD region R1 or the LUSC region R3, but not both (table S4), which suggested that they occurred after subclonal diversification (Fig. 2B). By contrast, for L008, 48 of the 52 identified structural variants were shared between the two tumor regions from different lobes of the lung, which suggested that the majority of these variants occurred before tumor metastasis to the other lobe (Fig. 2B). Notably, in L008, "chains" of translocations with highly clustered breakpoints were found between chromosomes 14 and 17, as well as chromosomes 17 and 19 (fig. S10 and table S4), which disrupted the *FANCM* and *NF1* tumor suppressor genes. Breakpoint homology profiling suggests involvement of either nonhomologous or alternative end-joining (*23*, *24*), indicative of double-strand break events. This lesion pattern is consistent with chromoanagenesis (*25*) and indicates a punctuated evolution pattern where multiple oncogenic events may have occurred simultaneously (*26*).

Four tumors displayed evidence for whole-genome–doubling events (*16*). In three tumors (L001, L004, and L008), the genome-doubling event was shared across every tumor region; it occurred before diversification, with the majority of truncal mutations (84 to 88%) present at ploidy ≥2, indicative of a large mutational burden before genome doubling. In one tumor, L002, the majority of heterogeneous mutations were also present at ploidy ≥2, indicative of two independent genome-doubling events: one in the LUAD region and one in the LUSC region (fig. S11). Notably, every truncal driver mutation likely occurred before genome doubling.

To further explore the dynamics of the mutational processes shaping lung cancer genomes over time, the spectra of point mutations in each tumor were temporally dissected. Early (truncal) mutations likely reflect processes involved before and during tumor initiation and early development, whereas late (branched) mutations

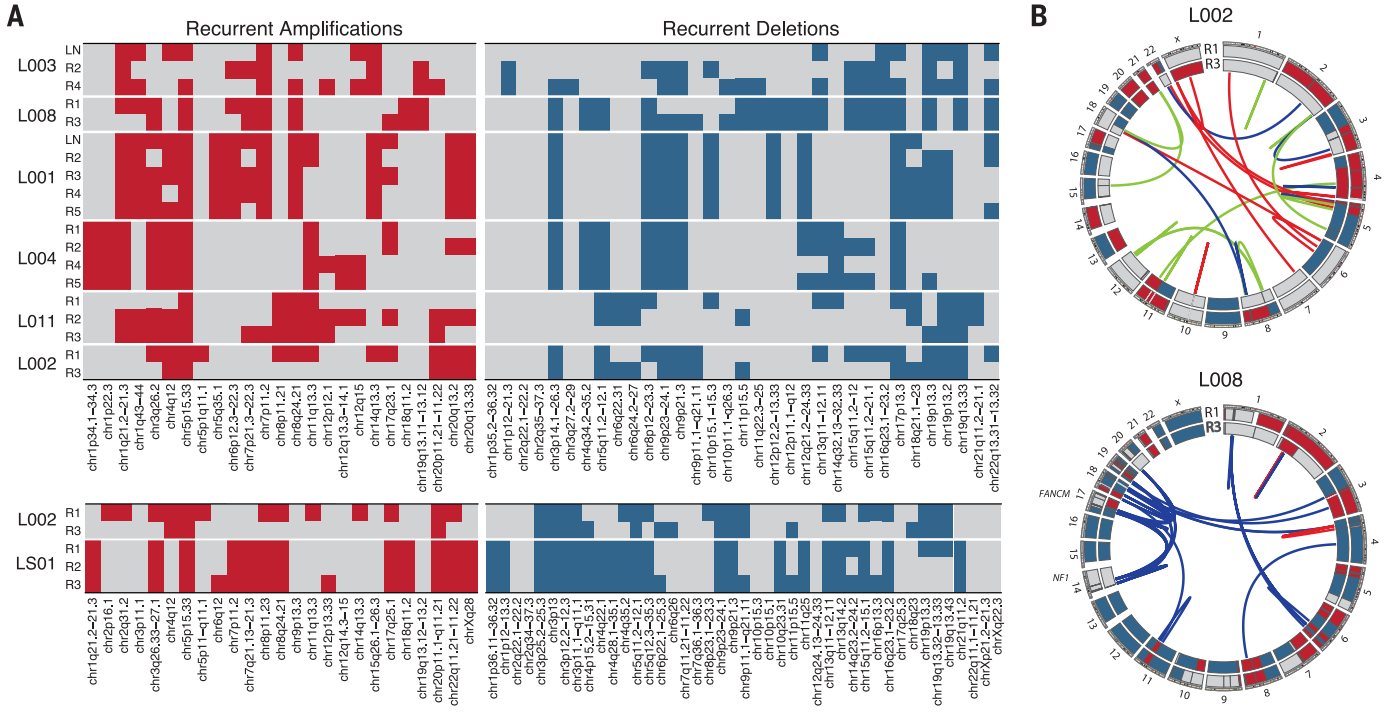


Fig. 2. Intratumor heterogeneity of chromosomal alterations in human NSCLC. (**A**) Distribution of potential tumor driver copy number alterations is indicated for each tumor region. The upper heat maps show the regional distribution of recurrently amplified (left) or deleted (right) chromosomal segments based on TCGA LUAD data, and the lower heat maps show the regional distribution of recurrently amplified or deleted chromosomal segments based on TCGA LUSC data. For each region, gain (red) or loss (blue) was determined relative to the mean ploidy. (**B**) Circos plots depicting inter- and intrachromosomal translocations, as well as deletions and insertions for regions R1 and R3 for L002 (upper) and L008 (lower); shared events are indicated in blue, events private to region R1 are indicated in red, and private to region R3 in green. The outer circle represents the integer copy number data for R1 and the inner circle for R3 for each tumor sample; copy number segments with an integer value greater than mean ploidy are in red and those less than mean ploidy in blue.

reveal mutational processes shaping the genome during tumor maintenance and progression, including those contributing to intratumor heterogeneity. For L002, we analyzed regions R1 and R3 separately to allow comparisons of LUAD and LUSC histologies within the same tumor.

In all tumors, we observed statistically significant shifts in the mutation spectra over time ($P < 0.05$ all cases) (Fig. 3A). Furthermore, every tumor exhibited a statistically significant decrease in the proportion of C>A transversions in late compared with early mutations ($P < 0.05$) (Fig. 3A), although this was more pronounced in the LUAD cases [mean odds ratio: LUAD 3.13 (range 2.07 to 5.55) and LUSC 1.34 (range 1.21 to 1.46)]. Because C>A transversions are associated with the mutagenic effects of tobacco smoke (*12*), a decrease in the proportion of C>A transversions indicates a relative decrease in the mutational burden attributable to smoking during LUAD development, in both former smokers and current smokers.

To validate these observations in a larger NSCLC cohort, mutations in TCGA LUAD and LUSC samples were temporally dissected (*16*). Consistent with our M-seq analyses, both TCGA LUAD and LUSC smokers and former smokers exhibited a decrease in the proportion of C>A transversions in late mutations (LUAD current smokers, $P < 0.0001$; former smokers, $P < 0.0001$; never-smokers, $P = 0.147$; LUSC current smokers, $P = 0.003$; former smokers, $P < 0.0001$; and never-smokers, $P = 0.673$) (Fig. 3B). Similarly, the least-pronounced decrease was observed in LUSC current smokers; 25% of LUSC displayed no decrease in C>A transversions, compared with less than 10% in LUAD. The mutational footprint of smoking exhibits a strand bias with C>A transversions accumulating preferentially on the transcribed strand (*10*, *12*). Both LUAD and LUSC former smokers revealed a statistically significant decrease in strand bias in late, compared with early, C>A transversions

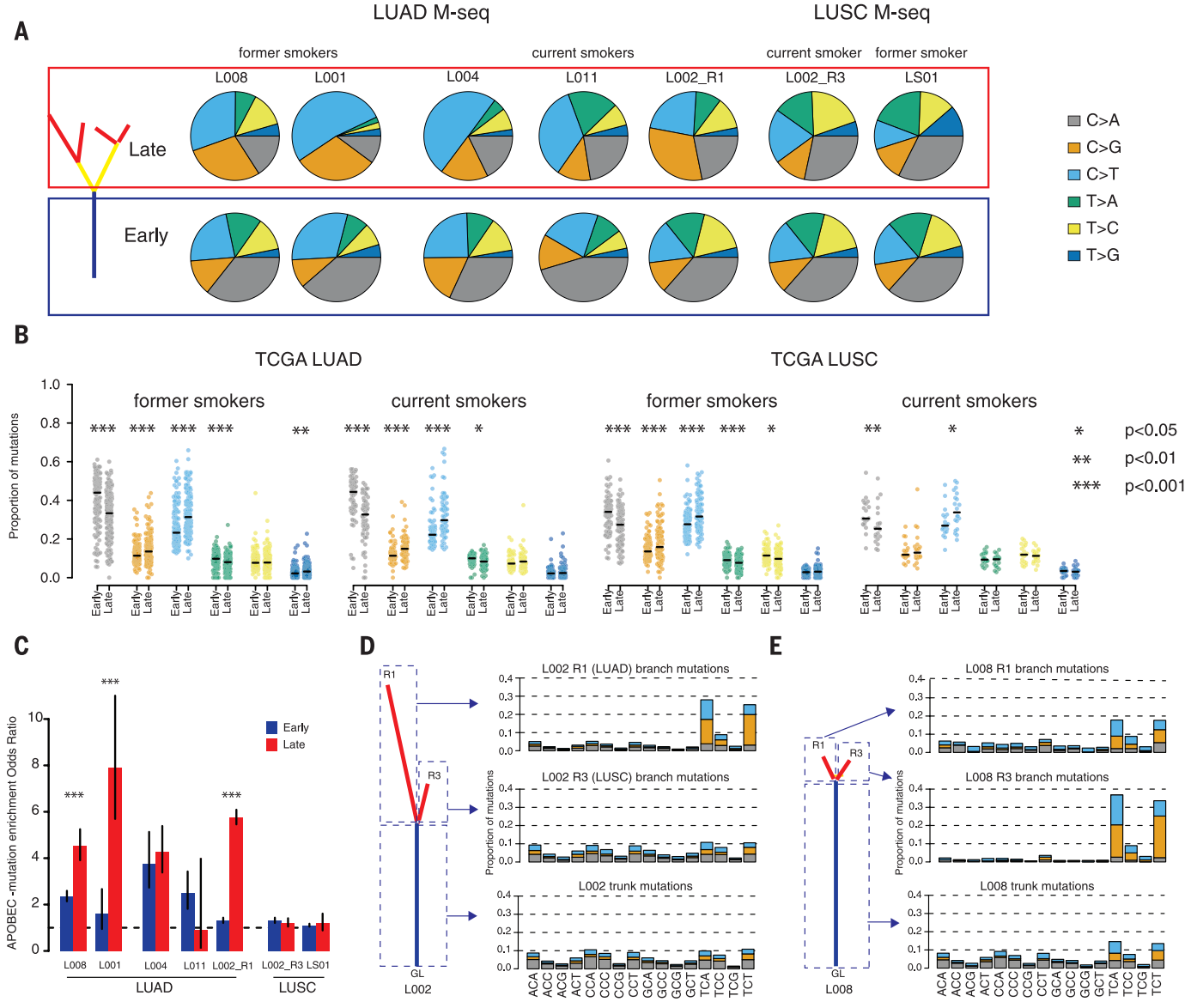


Fig. 3. Temporal and spatial dissection of mutation spectra in LUAD and LUSC samples. (**A**) Fraction of early mutations (trunk) and late mutations (branch) accounted for by each of the six mutation types in all M-seq samples. (**B**) Beeswarm plots showing the fraction of early mutations and late mutations accounted for by each of the six mutation types in every TCGA former smoker or current smoker with both early and late mutations. Significance is indicated. (**C**) APOBEC mutation enrichment odds ratio for early (trunk, blue bars) and late (branch, red bars) mutations for M-seq samples. The APOBEC signature encompasses C>T and C>G mutations in a TpC context (*16*). The 95% confidence intervals for Fisher's exact test are indicated. (**D** and **E**) Three mutation types (C>A; C>G and C>T) at all 16 possible trinucleotide contexts for L002 (D) and L008 (E). For both samples, trunk mutations as well as branch mutations from two regions are depicted.

(LUAD, P = 0.00354; LUSC, P = 0.046), consistent with an ancestral footprint of smoking on these genomes. Conversely, no statistically significant difference was observed between early and late mutations in current smokers (LUAD, P = 0.23; LUSC, P = 0.22).

In the majority of M-seq tumors, the decreased proportion of C>A mutations was accompanied by an increase in C>T and C>G mutations at TpC sites, indicative of APOBEC cytidine deaminase activity (*13*–*15*). Mutations consistent with APOBEC-mediated mutagenesis were more pronounced on the branches than the trunk in four out of five LUAD M-seq samples (Fig. 3C). On average 31% (8 to 41%) of nonsilent branch mutations occurred in an APOBEC-mutation context compared with 11% (7 to 16%) of truncal nonsilent mutations. Branched driver genes *PIK3CA*, *EP300*, *TGFBR1*, *PTPRD*, and *AKAP9* harbored mutations in an APOBEC context, which indicated a possible functional impact of APOBEC activity on subclonal expansion. Likewise, TCGA LUAD tumors with detectable APOBEC mutational signatures showed significant enrichment in late, compared with early, APOBEC mutations (P < 0.001) (fig. S12), and 20% of subclonal driver mutations were found to occur in an APOBEC context, compared with 11% of clonal driver mutations. However, for TCGA LUSC tumors with detectable APOBEC mutational signatures, temporal dissection of APOBEC mutations did not reveal such a clear trend (fig. S12), which indicated potential differences in the temporal dynamics of APOBEC-mediated mutagenesis between histological subtypes. In addition to temporal heterogeneity, spatial heterogeneity in both the proportion of APOBEC-associated mutations (Fig. 3, D and E) and APOBEC mRNA expression was observed in the M-seq tumors (fig. S13).

To gain a deeper understanding of NSCLC evolution, we focused on the two tumors with high-coverage M-seq WGS and temporally placed the genomic instability processes relative to the emergence of the most-recent common ancestor (Fig. 4). In patient L002, a current smoker, tobacco carcinogens played a significant role early in tumor development, with C>A transversions representing 39% of truncal mutations (Fig. 4A). Early mutations included multiple driver genes, such as *TP53* and *CHD8*. Upon diversification into a LUAD subclone and a LUSC subclone, copy number alterations (fig. S7) and driver mutations were acquired independently in both subclones, such as a stop-gain mutation in the tumor suppressor gene *FAT1* on the LUSC branch and mutations affecting *TGFBR1*, *ZFHX4*, *ARHGAP35*, and *PTPRD* in the LUAD region. APOBEC-associated mutations were elevated specifically in the LUAD region, which included the driver mutations in *TGFBR1* and *PTPRD*, and the highest *APOBEC3B* mRNA expression was detected in this region (fig. S13).

The tumors from patient L008 also displayed truncal C>A transversions and spatial heterogeneity in APOBEC enrichment, with a more pronounced APOBEC signature in the tumor of the middle lobe compared with the upper lobe (Fig. 4B). In L008, we gained further temporal resolution by exploring the mutations before and after the truncal genome-doubling event. All truncal driver mutations were found to occur before genome doubling. However, a tobacco smoke signature of C>A transversions was observed in more than 30% of truncal mutations both before and after doubling, and only in 21% and 9% of heterogeneous mutations in the two regions R1 and R3 from separate lobes of the lung. Because L008 ceased smoking more than 20 years before surgery (table S1), these data suggest that the genome-doubling event and truncal driver mutations occurred within a smoking carcinogenic context more than 20 years ago. Similarly, the genome-doubling event and truncal driver mutations in former smoker L001 also appeared to occur before smoking cessation more than 20 years before surgery (fig. S14). These data suggest a prolonged tumor latency period after genome doubling and before clinical detection in NSCLC.

Through sequencing multiple surgically resected tumor regions, we were able to unravel both the extent of genomic heterogeneity and the evolutionary history of seven NSCLCs. In contrast to the situation in clear cell renal cell carcinoma (ccRCC) (*27*, *28*), known driver mutations typically occurred early in NSCLC development, and the majority of high-confidence driver events were fully clonal. Conceivably, this explains the progression-free survival benefits associated with NSCLC oncogenic driver targeting (*29*). However, like ccRCC (*27*, *28*), all NSCLCs exhibited heterogeneous driver mutations and/or recurrent copy number aberrations and many heterogeneous mutations gave the "illusion of clonality," as they are present in all cells from certain regions but undetectable within other regions. Notably, although our multiregional sampling approach allowed us to evaluate spatial heterogeneity, only a small part of the entire tumor was sampled (on average <5%), which indicates that we might be underestimating the full extent of heterogeneity in these tumors.

Conceivably, intratumor heterogeneity may compromise the ability of a single biopsy to define all driver events comprehensively for optimal tumor control. For instance, L008 presented with an activating *BRAF* (G469A) mutation (*30*) in all regions and an activating *PIK3CA* (E542K) mutation (*31*) only in region R3. Thus, a biopsy taken from R3 might suggest treatment with an inhibitor of the phosphatidylinositol 3-kinase–mammalian target of rapamycin (PI3K/mTOR) signaling axis and combination therapy. Conversely,

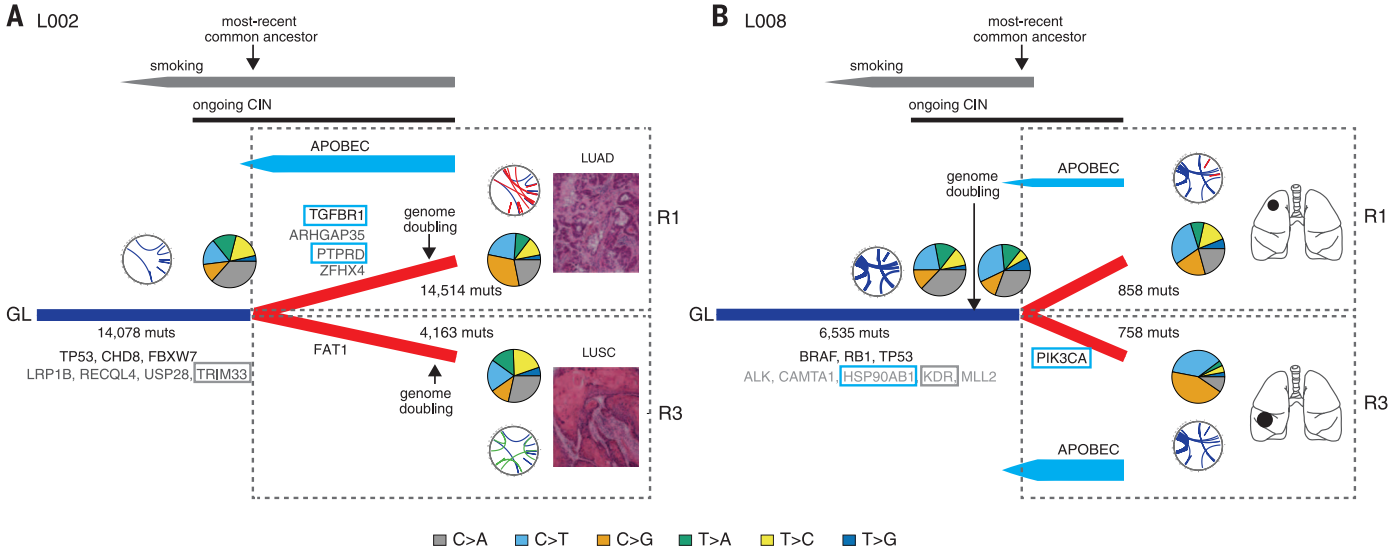


Fig. 4. A model of the evolutionary history of NSCLC. Evolutionary histories of tumors from patients L002 (**A**) and L008 (**B**) are depicted. Genomic instability processes defining NSCLC evolution have been placed on their phylogenetic trees. Driver mutations occurring in an APOBEC context are highlighted with a blue box, and those occurring in a smoking context with a gray box. In each case, the timing of genome-doubling events is indicated with an arrow. CIN, chromosomal instability; muts, mutations.

a single biopsy from any other region would suggest treatment with a BRAF inhibitor, for which the tumor cells from R3 might be resistant because of the *PIK3CA* mutation (*32*).

Our study also sheds light on the divergent genomic instability processes involved in NSCLC evolution and their dynamics over time. Evidence for spatial diversity in genomic instability processes suggests that opportunities to exploit such mechanisms therapeutically may be limited in this disease (*33*). In three tumors, we detected genome-doubling events occurring before subclonal diversification but after acquisition of driver mutations, consistent with findings in colorectal cancer that genome doubling may accelerate cancer genome evolution (*34*). The relation of chromosomal instability with drug resistance and early tumor recurrence (*35*, *36*) suggests that targeting truncal driver events may be compromised by the initiation of chromosomal instability later in tumor evolution. These results, coupled with the observation that NSCLC tumors may have prolonged latency periods, support continued efforts to optimize methods for earlier detection.

Unexpectedly, we found that despite continuous exposure to the mutagens in tobacco smoke, tumors from smokers showed evidence that an additional genomic instability process (APOBEC-associated mutagenesis) likely contributes to tumor progression. A large proportion of subclonal driver mutations were found to occur in an APOBEC context, which suggests that the differences in mutation spectra over time and space may reflect the activity of the process generating the mutations, as well as the selective advantage of the acquired mutations.

The presence of subclonal, regionally separated driver events, coupled with the relentless and dynamic nature of genomic instability processes observed in this study, highlight the therapeutic challenges associated with NSCLC. Engaging an adaptable immune system may present a tractable approach to manage the dynamic complexity in NSCLC (*37*). Longitudinal studies will be required to decipher drivers of subclonal expansion, identify the origins of subclones contributing to metastatic recurrence, and resolve the evolutionary principles that underpin the dismal outcome associated with this disease.

REFERENCES AND NOTES

1. World Health Organization, www.who.int/cancer/en/ (2013).
2. R. Siegel, D. Naishadham, A. Jemal, *CA Cancer J. Clin.* **63**, 11–30 (2013).
3. H. Tanaka *et al.*, *Cancer Res.* **67**, 6007–6011 (2007).
4. B. A. Weir *et al.*, *Nature* **450**, 893–898 (2007).
5. L. Ding *et al.*, *Nature* **455**, 1069–1075 (2008).
6. Z. Kan *et al.*, *Nature* **466**, 869–873 (2010).
7. S. L. Carter *et al.*, *Nat. Biotechnol.* **30**, 413–421 (2012).
8. T. I. Zack *et al.*, *Nat. Genet.* **45**, 1134–1140 (2013).
9. R. Govindan *et al.*, *Cell* **150**, 1121–1134 (2012).
10. E. D. Pleasance *et al.*, *Nature* **463**, 184–190 (2010).
11. W. Lee *et al.*, *Nature* **465**, 473–477 (2010).
12. G. P. Pfeifer, P. Hainaut, *Mutat. Res.* **526**, 39–43 (2003).
13. S. A. Roberts *et al.*, *Nat. Genet.* **45**, 970–976 (2013).
14. M. B. Burns, N. A. Temiz, R. S. Harris, *Nat. Genet.* **45**, 977–983 (2013).
15. L. B. Alexandrov *et al.*, *Nature* **500**, 415–421 (2013).
16. Detailed information on methods is available on *Science* online.
17. S. V. Sharma, D. W. Bell, J. Settleman, D. A. Haber, *Nat. Rev. Cancer* **7**, 169–181 (2007).
18. N. Bolli *et al.*, *Nat. Commun.* **5**, 2997 (2014).
19. M. Imielinski *et al.*, *Cell* **150**, 1107–1120 (2012).
20. M. S. Lawrence *et al.*, *Nature* **505**, 495–501 (2014).
21. P. Van Loo *et al.*, *Proc. Natl. Acad. Sci. U.S.A.* **107**, 16910–16915 (2010).
22. S. Nik-Zainal *et al.*, *Cell* **149**, 994–1007 (2012).
23. A. Malhotra *et al.*, *Genome Res.* **23**, 762–776 (2013).
24. S. F. Bunting, A. Nussenzweig, *Nat. Rev. Cancer* **13**, 443–454 (2013).
25. C. Z. Zhang, M. L. Leibowitz, D. Pellman, *Genes Dev.* **27**, 2513–2530 (2013).
26. S. C. Baca *et al.*, *Cell* **153**, 666–677 (2013).
27. M. Gerlinger *et al.*, *Nat. Genet.* **46**, 225–233 (2014).
28. M. Gerlinger *et al.*, *N. Engl. J. Med.* **366**, 883–892 (2012).
29. M. Reck, D. F. Heigener, T. Mok, J. C. Soria, K. F. Rabe, *Lancet* **382**, 709–719 (2013).
30. H. Davies *et al.*, *Nature* **417**, 949–954 (2002).
31. S. Kang, A. G. Bader, P. K. Vogt, *Proc. Natl. Acad. Sci. U.S.A.* **102**, 802–807 (2005).
32. H. Shi *et al.*, *Cancer Discov.* **4**, 80–93 (2014).
33. R. A. Burrell, N. McGranahan, J. Bartek, C. Swanton, *Nature* **501**, 338–345 (2013).
34. S. M. Dewhurst *et al.*, *Cancer Discov.* **4**, 175–185 (2014).
35. R. Sotillo, J. M. Schvartzman, N. D. Socci, R. Benezra, *Nature* **464**, 436–440 (2010).
36. A. J. Lee *et al.*, *Cancer Res.* **71**, 1858–1870 (2011).
37. J. C. Soria *et al.*, *Eur. J. Cancer* **49** (suppl. 2), 3408 (2013).

ACKNOWLEDGMENTS

E.B. is a Rosetrees Trust fellow; M.J.H. has a Cancer Research UK fellowship; N.Mu. received funding from the Rosetrees Trust; M.G. is funded by the UK Medical Research Council; I.V. is funded by Spanish Ministerio de Economía y Competitividad subprograma Ramón y Cajal; R.C.R. and D.M.R. are partly funded by the Cambridge Biomedical Research Centre and Cancer Research UK Cancer Centre; P.V.L. is a postdoctoral researcher of the Research Foundation—Flanders (FWO); S.M.J. is a Wellcome Senior Fellow in Clinical Science; and C.S. is a senior Cancer Research UK clinical research fellow and is funded by Cancer Research UK, the Rosetrees Trust, European Union Framework Programme 7 (projects PREDICT and RESPONSIFY, ID:259303), the Prostate Cancer Foundation, the European Research Council and the Breast Cancer Research Foundation. This research is supported by the National Institute for Health Research University College London Hospitals Biomedical Research Centre. We would like to thank Servicio Santander Supercomputación for their support. P.C. is a paid consultant for and holds equity in 14M Genomics Ltd. The results published here are in part based upon data generated by the Cancer Genome Atlas pilot project established by the National Cancer Institute and National Human Genome Research Institute, NIH. Information about TCGA and the investigators and institutions who constitute the TCGA research network can be found at http://cancergenome.nih.gov/. The data were retrieved through dbGaP authorization (accession no. phs000178.v5.p5). Sequence data have been deposited at the European Genome-Phenome Archive (EGA, www.ebi.ac.uk/ega/), which is hosted by the European Bioinformatics Institute (EBI), under accession numbers EGAS00001000809, EGAS00001000888 and EGAS00001000889.

SUPPLEMENTARY MATERIALS

www.sciencemag.org/content/346/6206/251/suppl/DC1
Materials and Methods
Figs. S1 to S14
Tables S1 to S4
References (*38*–*64*)

17 March 2014; accepted 4 July 2014
10.1126/science.1253462

LUNG CANCER EVOLUTION

Intratumor heterogeneity in localized lung adenocarcinomas delineated by multiregion sequencing

Jianjun Zhang,[1,2] Junya Fujimoto,[3] Jianhua Zhang,[4] David C. Wedge,[5] Xingzhi Song,[4] Jiexin Zhang,[6] Sahil Seth,[4] Chi-Wan Chow,[3] Yu Cao,[1] Curtis Gumbs,[1] Kathryn A. Gold,[2] Neda Kalhor,[7] Latasha Little,[1] Harshad Mahadeshwar,[4] Cesar Moran,[7] Alexei Protopopov,[4] Huandong Sun,[4] Jiabin Tang,[4]* Xifeng Wu,[8] Yuanqing Ye,[8] William N. William,[2] J. Jack Lee,[9] John V. Heymach,[2,10] Waun Ki Hong,[2] Stephen Swisher,[11] Ignacio I. Wistuba,[3] P. Andrew Futreal[1,12]†

Cancers are composed of populations of cells with distinct molecular and phenotypic features, a phenomenon termed intratumor heterogeneity (ITH). ITH in lung cancers has not been well studied. We applied multiregion whole-exome sequencing (WES) on 11 localized lung adenocarcinomas. All tumors showed clear evidence of ITH. On average, 76% of all mutations and 20 out of 21 known cancer gene mutations were identified in all regions of individual tumors, which suggested that single-region sequencing may be adequate to identify the majority of known cancer gene mutations in localized lung adenocarcinomas. With a median follow-up of 21 months after surgery, three patients have relapsed, and all three patients had significantly larger fractions of subclonal mutations in their primary tumors than patients without relapse. These data indicate that a larger subclonal mutation fraction may be associated with increased likelihood of postsurgical relapse in patients with localized lung adenocarcinomas.

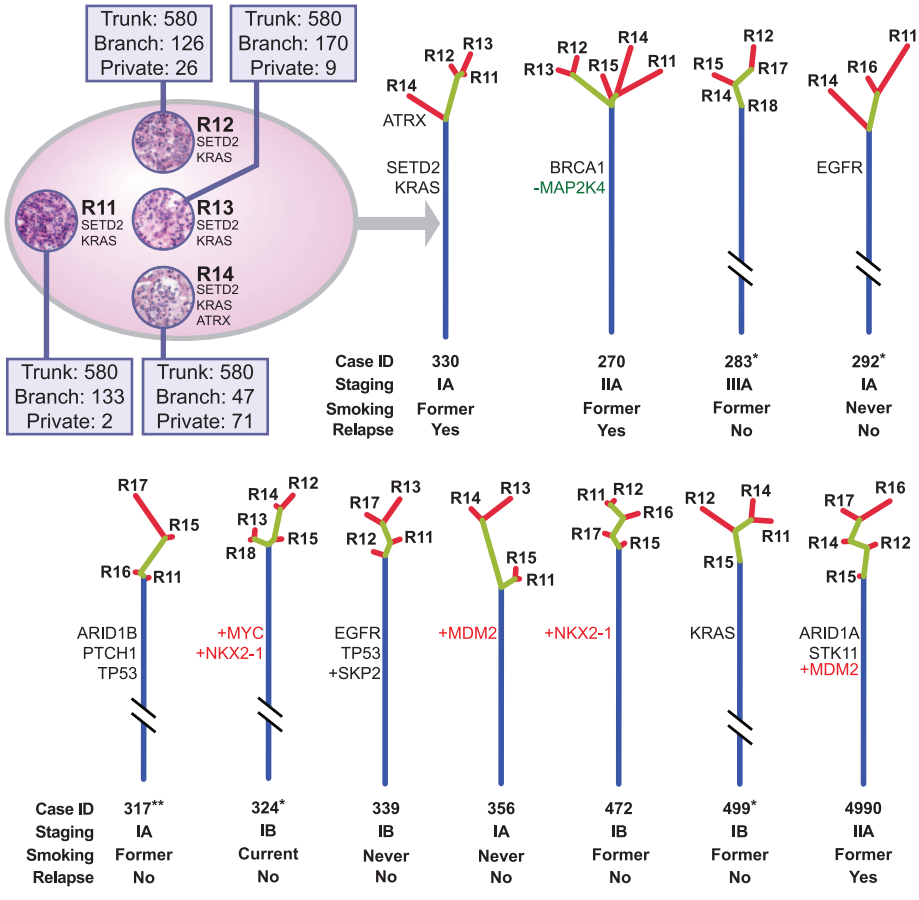
Intratumor heterogeneity (ITH) may have impacts on tumor biopsy strategy, characterization of actionable targets, treatment planning, and drug resistance (*1*–*6*). ITH has recently been elucidated in substantial detail in several cancer types with the use of next-generation sequencing (NGS) approaches (*7*–*14*). Recent evidence supports a model of branched evolution leading to variable ITH in different tumors (*9*, *13*, *15*, *16*). Studies in clear cell renal carcinoma

(ccRCC) have demonstrated substantial ITH, with the majority of mutations in known cancer genes confined to spatially separated tumor regions, except that *VHL* loss is a ubiquitous event (*16*, *17*). These data suggest that a single biopsy may be inadequate for identifying all cancer gene mutations from a tumor, as it presents an incomplete view of potential targets for therapy. Critically, the extent to which these observations in ccRCC apply to other solid tumors is currently not clear.

To characterize ITH in localized lung adenocarcinomas, we applied multiregion whole-exome sequencing (WES) on 48 tumor regions from 11 resected lung adenocarcinomas (eight stage I, two stage II, and one stage III tumors, tumor size 2 to 4.6 cm), all from patients who had surgery with curative intent (Fig. 1 and table S1). WES was conducted at a mean depth of 277×. In total, 7269 mutations were identified, and 7026 (97%) somatic mutations were validated by a separate bespoke capture sequencing experiment at mean depth of 863× (table S2). The numbers of mutations varied substantially between tumors (fig. S1), but no significant correlations were identified between mutation burden and age, gender, tumor size, lymph node status, or smoking status.

A useful approach when considering ITH is to depict a given tumor as a tree structure with the trunk representing ubiquitous mutations present in all regions of the tumor, branches representing heterogeneous mutations present in only some regions of the tumor, and private branches representing mutations that are present only in one region of the tumor—analogous to a phylogenetic tree. Placement of mutations on trunks versus branches reflects relative molecular time of acquisition, with branch mutations occurring, by definition, subsequent to trunk mutations. We applied this approach to multiregion sequencing data from these 11 lung adenocarcinomas. Evidence for ITH was found in each tumor studied. On average, 76% of all mutations were detected in all regions of the same tumors. However, the phylogenetic structure varied considerably between tumors (Fig. 1). We then characterized known cancer gene mutations, defined as nonsynonymous mutations identical to those previously reported in known cancer genes (*18*–*23*) or truncating mutations in known tumor suppressor genes, in the context of the derived phylogenetic tree structures. Thirteen of 14 known cancer gene point mutations were mapped to the trunks of the phylogenetic trees (Fig. 1 and table S3), which indicated that these mutations were acquired relatively early during evolution of these 11 tumors. In contrast to ccRCC, these data suggest that single-region sampling may be sufficient to identify the majority of known cancer gene mutations in localized lung adenocarcinomas.

We were also able to evaluate copy number changes relative to ITH. In contrast to ccRCC (*16*, *17*, *24*), we did not observe substantial differences in large-scale chromosome aberrations (fig. S2A), and the log2 ratio profiles were similar between different regions within the same tumors (fig. S2B and table S4). Furthermore, amplification or deletion of known cancer genes (*22*), as well as their relative placement on the phylogenetic trees, were delineated for these 11 lung adenocarcinomas. All of these events were mapped to the trunks of the phylogenetic trees (Fig. 1), which suggested that, like known cancer gene point mutations discussed above, amplification and/or deletion of known cancer genes were also early molecular events for these 11 tumors. Previous work in breast cancer also suggested that known cancer gene mutations were relatively early genetic events shared by all subclones of



© 2014 The University of Texas M.D. Anderson Cancer Center

Fig. 1. Assessment of ITH of 11 lung adenocarcinomas by multiregion sequencing. An example of regional mutation distribution (case 330) of resected tumors (represented by the ellipsis) is shown at the upper left corner. Mutated cancer genes are indicated to the right of representative hematoxylin and eosin–stained pathology image of each sequenced tumor region. Numbers of trunk, branch, and private branch mutations for each region are indicated in associated windows. A phylogenetic tree was generated from all validated mutations by using the Wagner parsimony method in PHYLIP. Blue, yellow, and red lines represent trunk, branch, and private branches, respectively. Trees are anchored at a germline DNA sequence obtained from peripheral blood of the relevant patients. Known cancer gene mutations are mapped to the trunks and branches as indicated. Point mutations, amplifications, and deletions of known cancer genes are presented as black, +red, and −green, respectively. Trunk and branch lengths are proportional to the numbers of mutations acquired on the corresponding trunk or branch. Note: Five tumors have their trunk lengths reduced to 10%* or 2%** of original length for visualization purposes.

[1]Department of Genomic Medicine, The University of Texas MD Anderson Cancer Center, 1515 Holcombe Boulevard, Houston, TX 77030, USA. [2]Department of Thoracic/Head and Neck Medical Oncology, The University of Texas MD Anderson Cancer Center, 1515 Holcombe Boulevard, Houston, TX 77030, USA. [3]Department of Translational Molecular Pathology, The University of Texas MD Anderson Cancer Center, 1515 Holcombe Boulevard, Houston, TX 77030, USA. [4]Applied Cancer Science Institute, The University of Texas MD Anderson Cancer Center, 1515 Holcombe Boulevard, Houston, TX 77030, USA. [5]Cancer Genome Project, Wellcome Trust Sanger Institute, Hinxton CB10 1SA, UK. [6]Department of Bioinformatics and Computational Biology, The University of Texas MD Anderson Cancer Center, 1515 Holcombe Boulevard, Houston, TX 77030, USA. [7]Department of Pathology, The University of Texas MD Anderson Cancer Center, 1515 Holcombe Boulevard, Houston, TX 77030, USA. [8]Department of Epidemiology, The University of Texas MD Anderson Cancer Center, 1515 Holcombe Boulevard, Houston, TX 77030, USA. [9]Department of Biostatistics, The University of Texas MD Anderson Cancer Center, 1515 Holcombe Boulevard, Houston, TX 77030, USA. [10]Department of Cancer Biology, The University of Texas MD Anderson Cancer Center, 1515 Holcombe Boulevard, Houston, TX 77030, USA. [11]Department of Thoracic and Cardiovascular Surgery, The University of Texas MD Anderson Cancer Center, 1515 Holcombe Boulevard, Houston, TX 77030, USA. [12]Honorary Faculty, Wellcome Trust Sanger Institute, Hinxton, UK CB10 1SA. *Present address: Center for Molecular Oncology, Memorial Sloan Kettering Cancer Center, 1275 York Avenue, New York, NY, 10065, USA. **†Corresponding author. E-mail: afutreal@mdanderson.org**

individual breast cancers (*13*). Taken together, these results indicate that different cancer types may have different relative timing of acquisition of cancer gene mutations. Further, the data would suggest in this subset of lung adenocarcinomas, there are likely mutations in noncanonical cancer genes that drive tumor development and subclonal divergence.

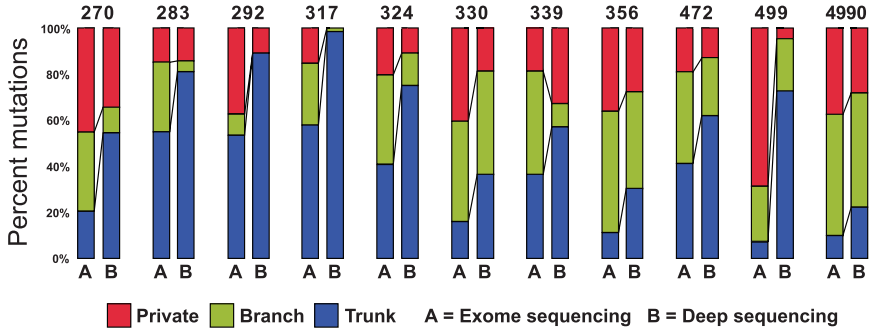
With a median follow-up of 21 months after surgery at the time of this report, three patients have had disease relapse. These three patients had a significantly larger proportion of subclonal nontrunk mutations (branch plus private branch mutations) in their primary tumors than patients without relapse (average 40% in relapsed patients versus 17% in patients without relapse, $P = 0.006$ by t test) (Fig. 1). Although the sample size is small, these findings suggest the possibility that subclonal mutations may be important for cancer progression and that larger subclonal mutation fraction may be associated with an increased likelihood of postsurgical relapse in this subset of lung adenocarcinoma patients.

Analysis of NGS data relies heavily on adequate sequencing depth to make high-accuracy consensus base calls. We compared our WES data (average sequencing depth 277×) with deep sequencing data (average sequencing depth 863×) to assess the effect of sequencing depth on detecting known cancer gene mutations. In tumor 499, a canonical *KRAS* p.G12C mutation was detected in only one of four tumor regions at exome depth but was detected in all four tumor regions at increased sequencing depth (table S2). Extending this analysis, we then compared deep sequencing data with WES data in defining ITH. The result showed many branch and private branch mutations defined by WES were detectable in all regions of individual tumors with increasing sequencing depth (Fig. 2). Taken together, these results indicate that considerable depth of sequencing will be necessary to detect cancer gene mutations and to accurately characterize ITH of lung adenocarcinomas.

Next, we analyzed the mutational spectrum of these 11 lung adenocarcinomas. Consistent with previous studies (*18*–*20*, *25*), different mutation spectra were observed in smokers and nonsmokers. Three never-smokers (cases 292, 339, and 356) showed C>T-predominant mutation profiles. Three former smokers who had quit more than 20 years before (cases 270, 472, and 4990) and one former smoker who had a 25 pack-year (pack-year = number of packs per day × number of years) history of smoking and quit 6 years ago (case 283) also showed C>T-predominant mutation profiles, as in nonsmokers. Two former smokers who had a >50 pack-year history of smoking and had quit 5 years before (cases 317 and 499) and one former smoker, who had a 25 pack-year history of smoking and had quit only 2.5 years before (case 330) showed C>A-predominant mutation profiles consistent with the mutation profile of cigarette smoke exposure. The only current smoker, who had a 20 pack-year history of smoking but had cut down to two cigarettes a day at the time of cancer diagnosis (case 324), showed an equivalent portion of C>T (26%) versus C>A (21%) substitutions in her tumor (Fig. 3A). These results indicate that tumor mutation spectra in former smokers reflect not only quantity of smoking exposure but also time since smoking cessation.

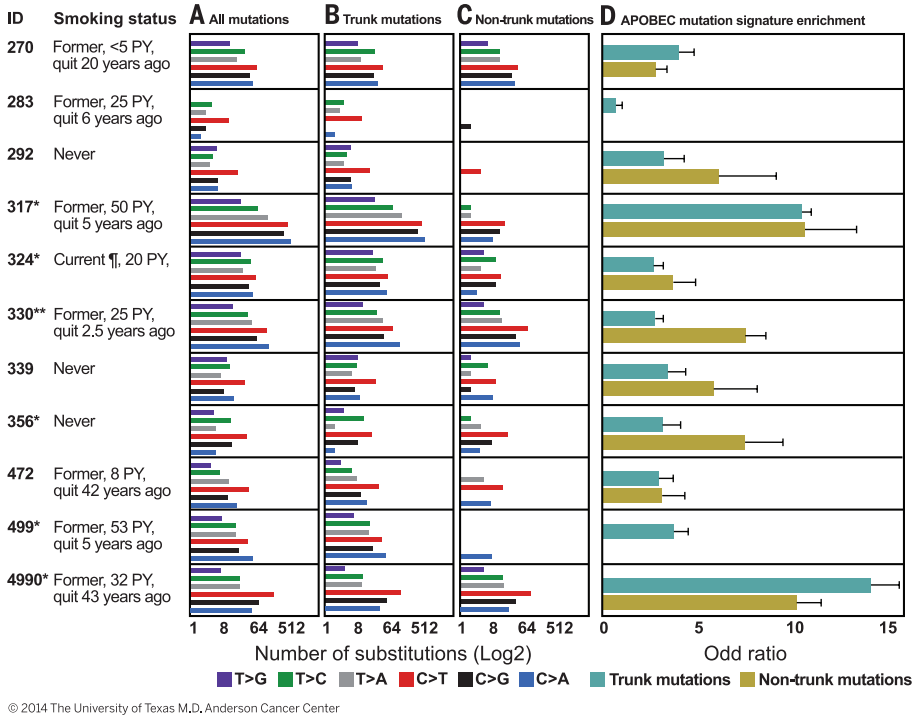
We next compared the mutational spectrum of trunk versus nontrunk mutations to explore the relative contribution of mutational processes over time. Significant differences in mutational spectrum were observed in six tumors, which indicated that specific mutational processes were likely operative at different times during development of these tumors (Fig. 3, B and C). Of interest, two former smokers (cases 317 and 330) and the current smoker (case 324) showed significant differences between trunk and nontrunk mutation spectrum with a shift from smoking-associated C>A transversions in trunk mutations to nonsmoker-associated C>T transitions in nontrunk mutations.

Recent evidence has suggested that APOBEC activity is a major source for C>T and C>G mutations



© 2014 The University of Texas M.D. Anderson Cancer Center

Fig. 2. Distribution of trunk, branch, and private branch mutations defined by exome sequencing (average sequencing depth of 277×) versus deep sequencing (average sequencing depth of 863×). Only validated mutations meeting the following criteria are included: total counts in tumor DNA ≥ 100; total counts in germline DNA ≥ 50; variant allele frequency (VAF) of ≥5% in tumor DNA, and VAF = 0 in germline DNA.



© 2014 The University of Texas M.D. Anderson Cancer Center

Fig. 3. Mutation spectrum of the 11 lung adenocarcinomas. (**A**) Mutation spectrum of all validated mutations. (**B**) Mutation spectrum of trunk mutations. (**C**) Mutation spectrum of nontrunk mutations. The difference of mutation spectrum between trunk and nontrunk mutations in each patient was evaluated with Fisher's exact test, and significant P values are shown as $^{*}P < 0.05$ and $^{**}P < 0.01$. (**D**) APOBEC mutation signature enrichment odds ratio for trunk and nontrunk mutations. The 95% confidence intervals for Fisher's exact test are indicated. PY, pack-year. ¶ indicates that the patient had cut down to two cigarettes a day at the time of cancer diagnosis.

(*12*, *26*). We therefore investigated whether there is evidence of an APOBEC mutational process in this subset of lung adenocarcinomas. On average, 28% of all mutations had a specific substitution pattern (C>T/G at TpCpW sites, where W is A or T), consistent with an APOBEC-mediated process (fig. S3). APOBEC mutation signature enrichment was found to be more pronounced for nontrunk mutations compared with trunk mutations in 7 of the 11 patients; however this difference was statistically significant only for case 330 (Fig. 3D). These data suggest that an APOBEC-like process is contributing substantially to the mutations found in this subset of lung adenocarcinomas and that the process tends to be more pronounced in later, subclonal mutations; this further highlights the dynamic nature of mutational processes in play.

Substantial variation in the allele frequency of somatic mutations within each individual tumor region from a given tumor was observed in this set of lung adenocarcinomas (fig. S4A). To more formally characterize subclonal fraction within each tumor region, we used the ABSOLUTE algorithm (*27*). These analyses demonstrated that at least 29 out of 48 individual tumor regions showed evidence of intraregional subclonal populations. The distribution of clonal and subclonal mutations was different among the sampled regions within the same tumors in some patients (fig. S4B), which suggests that single-biopsy analysis would be inadequate to fully represent ITH in these tumors.

To explore the possible implications of these data on translation to routine ITH assessment for in clinical practice, we repeated the ABSOLUTE analysis on the combined sequencing data from all tumor regions of each patient to assess the global ITH on a per-patient level, defined by the relative proportion of subclonal mutations. Similar to the phylogenetic analyses, all three patients with relapsed disease had larger subclonal fractions in their primary tumors (average 41% in patients with relapse versus 24% in patients without relapse, $P = 0.045$ by t test) (fig. S5A). Use of a complementary Bayesian Dirichlet process (*13*) on the per-patient combined data revealed the same trend (average subclonal mutations 66% in patients with relapse versus 36% in patients without relapse, $P = 0.035$ by t test) (fig. S5B). These results suggest that a measure of overall subclonal fraction may be of interest from a prognostic standpoint in this population of patients.

Resectable localized disease accounts for 30 to 50% of all non–small cell lung cancers, with increasing prevalence as screening is more widely implemented (*28*–*30*). Given that this subset of patients has tumors surgically resected as standard of care, there is an opportunity to confirm these preliminary observations by deep sequencing multiregion samples obtained from resected tumors. The questions of whether sequencing-targeted cancer gene panels versus WES will yield sufficient mutation data for meaningful analyses and the most appropriate algorithms for analyses will need to be addressed in order to fully test if the clinical correlation suggested in these data are borne out in larger patient cohorts.

Evidence of marked regional ITH in ccRCC suggested substantial challenges to personalized oncology based on single-tumor biopsy to portray the mutational landscape. This study, however, provides evidence that ITH patterns may be different between cancer types. With the caveat of limited sample size fully acknowledged, these data suggest that, although multiregion sampling is needed to fully assess ITH complexity, single-biopsy analysis at appropriate depth might be sufficient to identify the majority of known cancer gene mutations in this subset of lung adenocarcinomas. Studies in much larger cohorts, ideally with comprehensive clinical annotation and repeat biopsy at relapse, are needed to fully understand the clinical impact of ITH and insights afforded by these types of analyses. Furthermore, extension of research to epigenetic and phenotypic assessment through regional DNA methylation, chromatin state, and RNA and/or protein expression studies over time and under treatment is needed to fully understand the impact of ITH on the biology of the cancer itself and its impact on the clinical phenotype of cancer patients.

REFERENCES AND NOTES

1. T. A. Yap, M. Gerlinger, P. A. Futreal, L. Pusztai, C. Swanton, *Sci. Transl. Med.* **4**, 127ps10 (2012).
2. C. Swanton, *Cancer Res.* **72**, 4875–4882 (2012).
3. C. Swanton *et al.*, *Genome Med.* **2**, 53 (2010).
4. S. Horswell, N. Matthews, C. Swanton, *Cancer Lett.* **340**, 220–226 (2013).
5. R. Fisher, L. Pusztai, C. Swanton, *Br. J. Cancer* **108**, 479–485 (2013).
6. N. A. Saunders *et al.*, *EMBO Mol. Med.* **4**, 675–684 (2012).
7. N. Navin *et al.*, *Genome Res.* **20**, 68–80 (2010).
8. N. Navin *et al.*, *Nature* **472**, 90–94 (2011).
9. K. Anderson *et al.*, *Nature* **469**, 356–361 (2011).
10. A. Sottoriva *et al.*, *Proc. Natl. Acad. Sci. U.S.A.* **110**, 4009–4014 (2013).
11. P. J. Campbell *et al.*, *Proc. Natl. Acad. Sci. U.S.A.* **105**, 13081–13086 (2008).
12. S. Nik-Zainal *et al.*, *Cell* **149**, 979–993 (2012).
13. S. Nik-Zainal *et al.*, *Cell* **149**, 994–1007 (2012).
14. S. Yachida *et al.*, *Nature* **467**, 1114–1117 (2010).
15. S. P. Shah *et al.*, *Nature* **461**, 809–813 (2009).
16. M. Gerlinger *et al.*, *N. Engl. J. Med.* **366**, 883–892 (2012).
17. M. Gerlinger *et al.*, *Nat. Genet.* **46**, 225–233 (2014).
18. M. Imielinski *et al.*, *Cell* **150**, 1107–1120 (2012).
19. L. Ding *et al.*, *Nature* **455**, 1069–1075 (2008).
20. R. Govindan *et al.*, *Cell* **150**, 1121–1134 (2012).
21. I. R. Watson, K. Takahashi, P. A. Futreal, L. Chin, *Nat. Rev. Genet.* **14**, 703–718 (2013).
22. B. Vogelstein *et al.*, *Science* **339**, 1546–1558 (2013).
23. S. A. Forbes *et al.*, *Nucleic Acids Res.* **39** (Database), D945–D950 (2011).
24. P. Martinez *et al.*, *J. Pathol.* **230**, 356–364 (2013).
25. P. Hainaut, G. P. Pfeifer, *Carcinogenesis* **22**, 367–374 (2001).
26. L. B. Alexandrov *et al.*, *Nature* **500**, 415–421 (2013).
27. S. L. Carter *et al.*, *Nat. Biotechnol.* **30**, 413–421 (2012).
28. H. Bülzebruck *et al.*, *Cancer* **70**, 1102–1110 (1992).
29. P. J. Mahadevia *et al.*, *JAMA* **289**, 313–322 (2003).
30. T. R. Church *et al.*, *N. Engl. J. Med.* **368**, 1980–1991 (2013).

ACKNOWLEDGMENTS

This study was supported by the Cancer Prevention and Research Institute of Texas (R120501), the University of Texas (UT) Systems Stars Award (PS100149), the Welch Foundation Robert A. Welch Distinguished University Chair Award (G-0040), Department of Defense PROSPECT grant (W81XWH-07-1-0306), the UT Lung Specialized Programs of Research Excellence grant (P50CA70907), the MD Anderson Cancer Center Support grant (CA016672), NIH T32 Research Training in Academic Medical Oncology grant (CA-009666), the MD Anderson Institutional Support for the Center for Translational and Public Health Genomics, and the A. Lavoy Moore Endowment Fund. The authors thank L. Chin and R. Verhaak for constructive discussions. Sequence data have been deposited at the European Genome-phenome Archive (EGA, www.ebi.ac.uk/ega/), which is hosted by the European Bioinformatics Institute, under accession number EGAS00001000930.

SUPPLEMENTARY MATERIALS

www.sciencemag.org/content/346/6206/256/suppl/DC1
Materials and Methods
Figs. S1 to S6
Tables S1 to S4
References (*31*–*44*)

3 June 2014; accepted 29 August 2014
10.1126/science.1256930

High-Volume Microplates

Precisely manufactured to SLAS/ANSI specifications, Porvair Sciences' 24-well deep-well plates permit users to simply undertake multiple, high-volume (10 mL/well) experiments in a single unit maximizing both productivity and operational flexibility. The 24-well plates are constructed of high-grade, low extractable polypropylene, which imparts excellent temperature and chemical resistance making them the perfect tool for applications including serial dilution, mixing, reaction chemistry, and cell culture growth. The wells are square with a conical base to optimize sample concentration and recovery. The plate dimensions are precisely manufactured to SLAS/ANSI specifications making them compatible with automated liquid handling systems and other robotic sample processing equipment. To enable easy sampling access whilst maintaining sample integrity, Porvair high-volume deep-well plates may be securely sealed with a Santaprene piercable seal. The plates are also easily stackable economizing valuable space in low temperature storage (-80°C).

Porvair Sciences
For info: +44-(0)-1978-666239
www.porvair-sciences.com

Spectrometer

The new Epoch 2 Microplate Spectrophotometer is the first reader to combine a large touchscreen and full onboard data analysis software for simplified and efficient operation and reporting of absorbance-based detection workflows. The 10-inch color touchscreen interface offers an enhanced user experience, with intuitive navigation and a high-resolution display. On-board Gen5 Data Analysis Software provides quick analysis and flexible export and report options at the touch of a few buttons. Data export is expanded via WiFi, Bluetooth, and USB flash drive. To further maximize versatility, Epoch 2 features a spectral range from 200 to 999 nm, selectable in 1 nm increments for -single, -dual, and multi-wavelength measurements in end-point and kinetic read methods; and also offers spectral scanning and well area scanning. Compatible sample vessels include 6- to 384-well microplates, standard cuvettes, and 2 µL micro-volume samples via BioTek's Take3 Micro-Volume Plates.

BioTek Instruments
For info: 888-451-5171
www.biotek.com



Digital Water Baths

A new line of economical general purpose water baths that combine exceptional temperature control with full-featured digital functionality and ease of operation is now available. Designed to accommodate a wide variety of clinical and laboratory applications, these versatile water baths maintain bath temperatures from ambient +5°C to 99.9°C with ±0.1°C stability and ±0.2°C uniformity. They are available with 2, 5, 10, 20, or 28 L single chamber reservoirs. In addition to precise temperature control, PolyScience water baths feature a digital temperature readout that displays both the actual bath temperature and set point temperature simultaneously, three user-defined temperature preset buttons for the quick selection of frequently used temperature set points, and an integrated timer. For added operational convenience, all models include a steeply gabled tilting cover that accommodates glassware of varying heights and permits easy loading and removal of samples while allowing condensate to drain neatly back into the bath.

PolyScience
For info: 800-229-7569
www.polyscience.com

High-Resolution Spectrometer

A new high-resolution spectrometer system with picometer resolution capability is now available. The 1.3 m focal length McPherson Model 209 spectrometer with new micro-step drive can make wavelength steps as small as 0.1 pm. Software control is simplified since the wavelength steps are linear for uniform moves over thousands of nanometers free spectral range. The new models also support homing for wavelength calibration. With array detectors, spectral resolution is dictated by the sensors' pixel size and spectrometers focal length. Micro-step scans deliver superior performance and meet or exceed prior published specifications. All McPherson spectrometers are easy to use and can be systems' integrated. All are available with the special micro-step controller with an extensive software package. The step motor controller accepts ASCII commands. The user can specify speed, direction, and step size increment with software commands. LabVIEW libraries and program examples for text-based programming are available.

McPherson
For info: 978-256-4512
www.mcphersoninc.com

Row Dilution Plate Holder

A new Row Dilution Plate Holder accessory has been introduced for the VIAFLO 96 and 384 handheld benchtop pipettes. The new row dilution plate holder adds the functionality to perform serial dilutions in rows. The plate holder can easily be adapted to work with either 96- or 384-well plates. The ability to accurately and reproducibly produce dilution curves is essential to improving assay throughput and quality. The VIAFLO 96/384 offers high sample throughput without a robot. It is a handheld bench top pipette, capable of 96- and 384-well pipetting with a choice of various pipetting heads. The VIAFLO 96 benchtop electronic pipette offers an affordable solution to increase productivity when working with microplates. It closes the gap between traditional manual pipettes and robotic systems, allowing for accurate and reproducible 96-channel pipetting. The VIAFLO 384 is a more advanced system, which can work with both 96- and 384-channel pipetting heads to maximize productivity.

Integra Biosciences
For info: +41-(0)-81-286-9530
www.integra-biosciences.com

Electronically submit your new product description or product literature information! Go to www.sciencemag.org/products/newproducts.dtl for more information.

Newly offered instrumentation, apparatus, and laboratory materials of interest to researchers in all disciplines in academic, industrial, and governmental organizations are featured in this space. Emphasis is given to purpose, chief characteristics, and availability of products and materials. Endorsement by *Science* or AAAS of any products or materials mentioned is not implied. Additional information may be obtained from the manufacturer or supplier.

Downloaded from www.sciencemag.org on October 9, 2014



Science Careers Advertising

For full advertising details, go to ScienceCareers.org and click For Employers, or call one of our representatives.

Tracy Holmes
Worldwide Associate Director
Science Careers
Phone: +44 (0) 1223 326525

THE AMERICAS

E-mail: advertise@sciencecareers.org
Fax: 202 289 6742

Tina Burks
Phone: 202 326 6577

Nancy Toema
Phone: 202 326 6578

Marci Gallun
Sales Administrator
Phone: 202 326 6582

Online Job Posting Questions
Phone: 202 312 6375

EUROPE / INDIA / AUSTRALIA / NEW ZEALAND / REST OF WORLD

E-mail: ads@science-int.co.uk
Fax: +44 (0) 1223 326532

Axel Gesatzki
Phone: +44 (0) 1223 326529

Sarah Lelarge
Phone: +44 (0) 1223 326527

Kelly Grace
Phone: +44 (0) 1223 326528

JAPAN

Katsuyoshi Fukamizu (Tokyo)
E-mail: kfukamizu@aaas.org
Phone: +81 3 3219 5777

Hiroyuki Mashiki (Kyoto)
E-mail: hmashiki@aaas.org
Phone: +81 75 823 1109

CHINA / KOREA / SINGAPORE / TAIWAN / THAILAND

Ruolei Wu
Phone: +86 186 0082 9345
E-mail: rwu@aaas.org

All ads submitted for publication must comply with applicable U.S. and non-U.S. laws. *Science* reserves the right to refuse any advertisement at its sole discretion for any reason, including without limitation for offensive language or inappropriate content, and all advertising is subject to publisher approval. *Science* encourages our readers to alert us to any ads that they feel may be discriminatory or offensive.

Science Careers
From the journal *Science* AAAS

ScienceCareers.org

UNIVERSITY OF UTAH SCHOOL OF MEDICINE

Tenure-track Assistant or Associate Professor of Genetics/Genome Sciences

The Department of Human Genetics at the University of Utah School of Medicine (www.genetics.utah.edu) seeks outstanding applicants for tenure-track positions at the level of Assistant or Associate Professor. We are looking for a highly creative scientist who uses genetics to investigate fundamental biological problems. We especially encourage applicants whose research focuses on human and medical genetics using functional, computational, or evolutionary genomics and/or model organisms. As part of a vibrant community of collaborative faculty on campus, the Department of Human Genetics lies at the interface between basic and clinical sciences, creating ample opportunities for interdisciplinary studies (e.g., the newly formed Center for Genetic Discovery). Our institution is set in a unique recreational and geographical landscape that attracts a very diverse and productive scientific community. Successful candidates will receive a generous startup package and enjoy a stimulating research environment that places a strong emphasis on innovation and interaction.

Our submission deadline is **November 14, 2014**. To apply, please see the following website: **http://utah.peopleadmin.com/postings/35937**. For questions regarding this posting or your application, please contact Natalie Johnson at: **njohnson@genetics.utah.edu**

The University of Utah is an Affirmative Action/Equal Opportunity employer and does not discriminate based upon race, national origin, color, religion, sex, age, sexual orientation, gender identity/expression, status as a person with a disability, genetic information, or Protected Veteran status. Individuals from historically underrepresented groups, such as minorities, women, qualified persons with disabilities and protected veterans are encouraged to apply. Veterans' preference is extended to qualified applicants, upon request and consistent with University policy and Utah state law. Upon request, reasonable accommodations in the application process will be provided to individuals with disabilities. To inquire about the University's nondiscrimination or affirmative action policies or to request disability accommodation, please contact: Director, Office of Equal Opportunity and Affirmative Action, 201 S. Presidents Circle, Rm 135, (801) 581-8365.

The University of Utah values candidates who have experience working in settings with students from diverse backgrounds, and possess a [strong or demonstrated] commitment to improving access to higher education for historically underrepresented students.

The University of Utah Health Sciences Center is a patient-focused center distinguished by collaboration, excellence, leadership, and respect. The Health Sciences Center values candidates who are committed to fostering and furthering the culture of compassion, collaboration, innovation, accountability, diversity, integrity, quality, and trust that is integral to the mission of the University of Utah Health Sciences Center.

PURDUE UNIVERSITY

FIVE ASSISTANT PROFESSOR TENURE-TRACK POSITIONS CENTER FOR MOLECULAR AGRICULTURE

Purdue University, West Lafayette, Indiana, invites applications from outstanding basic scientists for five tenure-track assistant professor positions that will be part of a new Center for Molecular Agriculture. With the establishment of this Center, we aim to build a team of scientists that will cooperatively address grand challenges in plant biology including, but not limited to, the molecular basis of complex traits, genome interactions with the biotic and abiotic environment, the role of metabolic and cellular processes in determining phenotypes, and the molecular/genetic basis for developmental plasticity and adaptation in changing environments. We seek individuals with vigorous and innovative research programs that address fundamental questions in plant biology and who are eager to be part of an interdisciplinary team that will discover basic principles that may contribute to improving agricultural productivity and sustainability on regional, national, and international scales. Candidates utilizing computational/modeling approaches; biosensor/imaging technologies; and working on molecular, organismal or ecosystem levels are all encouraged to apply. The successful candidates will be expected to develop internationally recognized and extramurally funded scholarly research programs, interact with diverse faculty across the Purdue campus, teach undergraduate and graduate level courses and excel in doing so, and function as active and involved members of the Center. The Center is part of the Plant Sciences Research and Education Pipeline, which also includes facilities for genome editing, plant transformation, high-throughput phenotyping, and a plant commercialization incubator. This is an academic year appointment.

Applicants should have a Ph.D. in life, computational, or physical sciences, preferably with at least two years of post-doctoral experience or its equivalent, a strong publication record, the potential to develop a vigorous, extramurally funded research program, and a commitment to both hypothesis-driven research and teaching excellence. Applications should be submitted electronically to **molecularag@purdue.edu** and must include a cover letter, curriculum vitae, two-page summary of research interests, statement of teaching objectives/interests, and the names and contact information for three references. Screening of applications will begin **December 1, 2014** and will continue until the positions are filled. A background check is required for employment in this position.

Purdue University is an Equal Opportunity/Equal Access/Affirmative Action Employer fully committed to achieving a diverse workforce. All individuals, including minorities, women, individuals with disabilities, and protected veterans are encouraged to apply.

Ireland seeks World-class Research Talent

Science Foundation Ireland

INSPIRATION • INNOVATION • IRELAND

Ireland is building a reputation as a world leader in scientific research capability, continuously climbing the international citation and innovation rankings to be in the top 20 countries overall for citations, while achieving rankings of 1st, 3rd and 4th in Immunology, Nanoscience and Computer Science research respectively.

Ireland is a small English speaking technologically advanced country (population 4.5 million), home to leading multinational and indigenous companies, with a young growing population (the median population age is 35, the lowest in the EU), ranked 1st in Europe for completion of university education and in the top centile of Eurostat rankings for Innovation Output.

Ireland is committed to funding excellent and impactful research. In 2013 Science Foundation Ireland (SFI) invested, with industry, €300 million ($400 million) in 7 new cutting-edge research centres; funded over 300 new research awards; SFI supported researchers obtained over €125 million ($167 million) of additional research funding from the European Union, Charities and industry. SFI supports over 450 leading researchers who are involved in 2,000 national and international collaborations across 48 countries.

SFI also supports 100 outstanding young researchers at the early stages of their careers.

Ireland has now launched an integrated recruitment programme involving all the Irish Universities and the national science funding agency (SFI) to attract world-class researchers, with exceptional reputations, to assume leadership positions (e.g. Professorial Chairs) in key areas of national importance that include advanced manufacturing; bio-manufacturing; energy; marine; ICT; medical devices; agrifood; climate change; smart cities; ageing; connected health; and digital platforms, content and applications.



The SFI Targeted Research Professorship Programme 2014 will provide competitive research funding from SFI of up to €5 million ($6.7 million) in direct costs, salary and physical accommodation will be provided by the universities.

If you believe that you can inspire and build excellence with impact in a well-resourced research environment, please consult **www.sfi.ie** or email **researchprof@sfi.ie**

NUI Galway
OÉ Gaillimh

University of Limerick
Ollscoil Luimnigh

UCC
Coláiste na hOllscoile Corcaigh, Éire
University College Cork, Ireland

DCU

NUI Maynooth
Ollscoil na hÉireann Má Nuad

Trinity College Dublin
Coláiste na Tríonóide, Baile Átha Cliath
The University of Dublin

UCD Dublin

Science Careers online @sciencecareers.org

ETH zürich

Professor of Single Particle Cryo-electron Microscopy and Methods Development

→ The Department of Biology (www.biol.ethz.ch) at ETH Zurich invites applications for the above-mentioned position.

→ The successful candidate should use single particle electron microscopy to study the function and the molecular mechanism of biological complexes and large assemblies. Preferably, he or she is actively engaged in developing methods for high resolution structure determination by electron microscopy. The future professor will be expected to build an innovative and internationally competitive research program within the Institute of Molecular Biology and Biophysics (www.mol.biol.ethz.ch). The institute provides an excellent scientific environment and access to state-of-the-art equipment. The search is open to all research fields, although applications from candidates with a focus complementary to those already pursued at the Institute are encouraged. Transmission electron microscopes including a FEI Tecnai G2 cryo+ F20 and a FEI Titan Krios are available within the Electron Microscopy Center of ETH Zurich. The new professor will be expected to teach undergraduate level courses (German or English) and graduate level courses (English) and to actively contribute to the interactive, scientific environment at ETH Zurich.

→ **Please apply online at www.facultyaffairs.ethz.ch**

→ Applications should include a curriculum vitae, a list of publications, the names of at least three references, and a statement of future research and teaching interests. The letter of application should be addressed **to the President of ETH Zurich, Prof. Dr. Ralph Eichler. The closing date for applications is 30 November 2014.** ETH Zurich is an equal opportunity and family friendly employer and is further responsive to the needs of dual career couples. We specifically encourage women to apply.

W
UNIVERSITY of WASHINGTON

Faculty Position
Eukaryotic Cell Biology
Department of Biology

As part of a long-term strategy to enhance strengths in Cell Biology, the Department of Biology is searching to hire a full-time (9-month) Assistant Professor (Job class 0116) for a tenure-track faculty position in eukaryotic cell biology. We seek candidates who integrate perspectives from multiple disciplines, use quantitative approaches, and appreciate the breadth of research encompassed within the Department. We are especially interested in candidates using experimentally tractable plant, animal or protist systems to investigate fields including but not limited to cell homeostasis, signaling, polarity, proliferation, motility, membrane trafficking, interactions between cells and their environments, developmental cell biology, and evolutionary cell biology.

We are looking for individuals with a record of outstanding achievement or strong indications of outstanding future potential. Priority will be given to applications received by **3 November 2014** at: **http://www.biology.washington.edu/faculty/search/**. Applicants must have earned a doctorate by the date of appointment. All University of Washington faculty engage in teaching, research, and service.

The University of Washington is an Affirmative Action, Equal Opportunity Employer. All qualified applicants will receive consideration for employment without regard to, among other things, race, religion, color, national origin, sex, age, status as protected veterans, or status as qualified individuals with disabilities. The University is building a culturally diverse faculty and staff and strongly encourages applications from women, minorities, individuals with disabilities and covered veterans. The University is the 2006 recipient of the Alfred P. Sloan award for Faculty Career Flexibility, and is committed to supporting the work-life balance of its faculty. Our NSF-supported ADVANCE program http://advance.washington.edu/ is dedicated to increasing the participation of women in STEM disciplines.

Smithsonian
National Museum of Natural History

Research Zoologist
Department of Vertebrate Zoology

The Smithsonian's National Museum of Natural History seeks a zoologist to conduct an integrative, specimen- or collection-based research program in vertebrate evolution and biodiversity, in the disciplines of herpetology, ichthyology, mammalogy, and/or ornithology, particularly herpetology. The successful candidate is expected to develop an internationally recognized research program that makes important contributions to understanding vertebrate evolution and biodiversity through integrative research involving phylogenetics, anatomy, development, genomics, biogeography, conservation, informatics, or related fields. Frequent publication of highly regarded papers in competitive, peer-reviewed journals, curation of collections in specialty area, service to the scientific community in leadership capacities, acquisition of external funding, engagement in outreach activities, and mentorship of students are expected.

Full-time 4-year term appointment with full Government benefits to be filled at the GS-12 level; US citizenship required. The museum's authorized salary range for this position at this time is $75,621 – $80,662 per annum. **College transcripts and proof of U.S. accreditation for foreign study must be submitted online by the closing date of announcement or your application will be disqualified. For complete requirements and application procedures go to www.sihr.si.edu or www.usajobs.gov and refer to Announcement 14A-JW-299546-DEU-NMNH**. The announcement opens Monday, September 29, 2014. **Applications and all supporting documentation must be received on-line by Monday, October 27, 2014 and must reference the announcement number**. All applicants will be notified by email when their application is received.

The Smithsonian Institution is an Equal Opportunity Employer.

KOCH INSTITUTE
for Integrative Cancer Research at MIT

Faculty Position

The Koch Institute for Integrative Cancer Research at the Massachusetts Institute of Technology (http://ki.mit.edu) invites applications for a junior or senior faculty appointment. Appointments are expected to be in the MIT Department of Biology, but other departments will be considered if appropriate. The Koch Institute is an NCI-designated Cancer Center, which features research across a wide range of areas in basic cancer research and cancer-oriented engineering. This is an open search with regard to field of study and specific research focus, but cancer relevance will be a consideration. The candidate(s) will be expected to develop and lead an internationally competitive research program as well as participate in undergraduate and graduate teaching. The successful candidate(s) will have laboratory space in the Koch Institute.

Applicants should include curriculum vitae, brief summaries of past accomplishments and a description of future research plans. Letters of recommendation should be sent separately from three individuals able to evaluate the candidate's accomplishments and future potential for both research and teaching.

Please apply online at
https://academicjobsonline.org/ajo/jobs/4427

Complete applications are due
by November 1, 2014.

MIT is an Affirmative Action/Equal Opportunity employer, and we are actively committed to a diverse faculty. Women and members of underrepresented minority groups are strongly encouraged to apply.

Massachusetts Institute of Technology

Science Careers

Cernet

"《科学》职业" 已经与Cernet/赛尔互联开展合作。中国大陆的高校可以直接联系Cernet/赛尔互联进行国际人才招聘。



请访问
Sciencecareers.org/CER
点得联系信息。

Science

The University of Texas Medical Branch
Senior Faculty in Cryo-Electron Microscopy, X-ray Crystallography, and NMR
Sealy Center for Structural Biology & Molecular Biophysics

UTMB seeks senior faculty applicants in structural biology in the Sealy Center for Structural Biology and Molecular Biophysics (SCSBMB). The Center supports a graduate program in molecular biophysics and five well-run resource laboratories in Cryo-EM, NMR, X-ray, Computation and Solution Biophysics, each with an excellent PhD-level manager. For details see: http://www.scsb.utmb.edu/

The successful candidate must be a highly motivated individual with a PhD, MD or equivalent degree, a strong publication record, and a record of independent, well-funded grant support. The ideal candidate will have extensive experience in their specialty applied to the study of the structure, novel mechanisms, and functions of bio-macromolecules. Candidates for these positions will also hold appointments in the departments of Biochemistry and Molecular Biology and/or Pharmacology and Toxicology; they should also have or seek overlap with the highly collaborative, established biomedical research community in UTMB's basic science departments, and centers and programs of excellence. These include the Institute for Human Infections and Immunity, which includes the Galveston National Laboratory, Center for Tropical Diseases, Center for Biodefense and Emerging Infectious Diseases, and the Sealy Center for Vaccine Development. Outstanding collaborative research opportunities are also available through the Institute for Translational Sciences, the Sealy Center for Cancer Cell Biology, the Sealy Center for Environmental Health and Medicine, the Sealy Center on Aging, the George P. and Cynthia Woods Mitchell Center for Neurodegenerative Diseases, the Moody Center for Brain and Spinal Cord Injury Research, the Sealy Center for Molecular Medicine and the Chemical Biology Program. These and other entities provide a wide variety of core services in recombinant DNA, genomics, proteomics, high-throughput drug screening, mass spectrometry, membrane protein crystallization, and protein expression and purification. Excellent collaborative opportunities also exist through UTMB's participation in the Gulf Coast Consortia and the Keck Center for Interdisciplinary Bioscience.

Applicants are requested to submit electronically: a cover letter expressing interest in being considered, a curriculum vitae, current funding, a summary of research accomplishments, and future goals to mail to: **SCSBMB.recruiting@UTMB.edu**. Direct inquiries to **Dr. B. Montgomery Pettitt**, **mpettitt@utmb.edu**, **409-772-0723**.

UTMB Health strives to provide equal opportunity employment without regard to race, color, national origin, sex, age, religion, disability, sexual orientation, gender identity or expression, genetic information or veteran status. As a VEVRAA Federal Contractor, UTMB Health takes affirmative action to hire and advance women, minorities, protected veterans and individuals with disabilities

utmb Health

Science Careers online @sciencecareers.org

Director
Center for Neuropharmacology and Neuroscience
Albany Medical College

Albany Medical College invites applications for the position of Director of the Center for Neuropharmacology and Neuroscience (http://www.amc.edu/Research/CNN/). The successful candidate will qualify for appointment as a full professor with a PhD and/or MD degree. She/he will have outstanding research credentials, including an extramurally funded research program and track record of research productivity, a history of administrative leadership and/or significant evidence of potential for such leadership. Applicants who utilize integrated approaches involving translational models that address problems related to the pathophysiology of human disease are particularly encouraged to apply. The new Director is expected to provide research leadership and to promote career development for 17 existing faculty members with research interests in molecular neuropharmacology, neurodegenerative and neuropsychiatric diseases, nervous system development, synaptic plasticity, ischemic brain injury, pain and the neurobiology of drug and alcohol addiction. She/he also has responsibility for ensuring excellence of the CNN's graduate, post-graduate, and medical school teaching missions. To facilitate the new Director's vision for the Center a generous start-up package with two or more new faculty positions is planned. Newly recruited faculty, including the Director, will be able to receive joint appointments in an appropriate clinical department to encourage the development of physician-scientist collaborations.

The New York Capital Region provides a rich academic environment, research resources and extensive opportunities for collaborations with surrounding universities and centers. Albany Medical Center is a founding member of the New York State Capital Region (NYCAP) Research Alliance with Rensselaer Polytechnic Institute and the State University of New York (SUNY) at Albany. Other significant research partners include the SUNY Polytechnic Institute College of Nanoscale Science & Engineering, the New York State Department of Health Wadsworth Center for Research, Albany College of Pharmacy, the Neural Stem Cell Institute, and General Electric Health Care Research. The Albany area offers diverse cultural and recreational attractions with easy access to Boston, New York City, and the Adirondack, Catskill and Berkshire Mountains.

Consideration will be given to those applications received by December 5, 2014. A curriculum vitae, description of research interests, vision statement for building/maintaining a basic neuroscience center, and at least four letters of recommendation are required. Applications can be submitted by mail or e-mail to:

Harold A. Singer, PhD
Chair, CNN Search Committee
Albany Medical College (MC-8)
47 New Scotland Avenue
Albany, New York 12208
singerh@mail.amc.edu

Albany Medical College is an Equal Opportunity/Affirmative Action Employer. Women and minorities are encouraged to apply.

IPP International Postdoctoral Programme
cnic

Opportunities for POSTDOCTORAL RESEARCHERS in Biomedical Research at the Spanish National Centre for Cardiovascular Research CNIC, Madrid - Spain

The CNIC is dedicated to excellence in cardiovascular research and to translating new knowledge into real improvements in clinical practice.

The scientific project of the centre has been structured in three areas:
- Cardiovascular Development and Repair Department (CDR)
- Vascular Biology and Inflammation Department (VBI)
- Epidemiology, Atherothrombosis and Imaging Department (EAI)

To be eligible, candidates must:
- Hold a PhD degree that must have been awarded no more tan five years ago (exceptions will be made for documented career brakes and candidates with children)
- Have, at least, one publication as first author in an international peer reviewed journal
- Candidates must not have resided or carried out their main activity in Spain for more than twelve months in the last three years

The CNIC offers NINE (9) fellowships in this call:
- A 3-year contract
- An internationally competitive salary
- State of the art infrastructure and latest generation of technological equipment
- Scientific-technical support and complementary training

Deadline for submission of proposals: 14 November 2014

CNIC is an inclusive, equal opportunity employer, irrespective of nationality, ethnic origin, gender, marital or parental status, sexual orientation, creed, disability, age or political belief. Confidentiality is guaranteed throughout the selection process and all current regulations relating to the protection of personal data will be strictly adhered to.

For further information and applications, please, visit www.cnic.es

cnic

IBS Research Center Director Positions

Institute for Basic Science
at Gwangju Institute of Science and Technology, Gwangju, Korea

The Institute for Basic Science(IBS) at the Gwangju Institute of Science and Technology(GIST) invites applications for research center director positions at the **full tenured professor** level. Candidates' areas include basic science research in physics, chemistry(photochemistry, photobiophysics and etc.), life science (photobiophysics and etc.), or environmental sciences(global biogeochemical cycles, climate physics and etc.).

Qualifications include a Ph.D. degree and exceptional track record in world-leading research, and proven experiences in managing and directing a large-scale scientific research program.

Directors will be expected to work full time as both a tenured professor at GIST and the Director of an IBS research center. Research centers will pursue large-scale, longitudinal and team-based research which has not been explored at other universities or government-funded research organizations in Korea. Directors will have the authority for research team staffing, decision of specific research areas to explore, and budget allocation.

Evaluation of research centers will be conducted every three years to determine whether to provide continued support. This excludes the first evaluation which will take place five years after the opening of the research center.

GIST is a research oriented university which was established by the Korean Ministry of Science, ICT and Future Planning in 1993. In the QS World University Rankings 2014, GIST was ranked No. 4 in the world and No. 1 in Asia in "Citations per Faculty". For more information, please visit http://www.gist.ac.kr. Information on the IBS and specialized research areas for GIST is available at http://www.ibs.re.kr/eng.do and http://www.ibs.re.kr/eng/sub05_03_01.do.

Anyone interested in applying should contact the Section of Academic Affairs at GIST, at academy@gist.ac.kr (T. 82-62-715-2043).

university of groningen
2014 | 400 years

Are you the uniquely talented female researcher we are seeking?

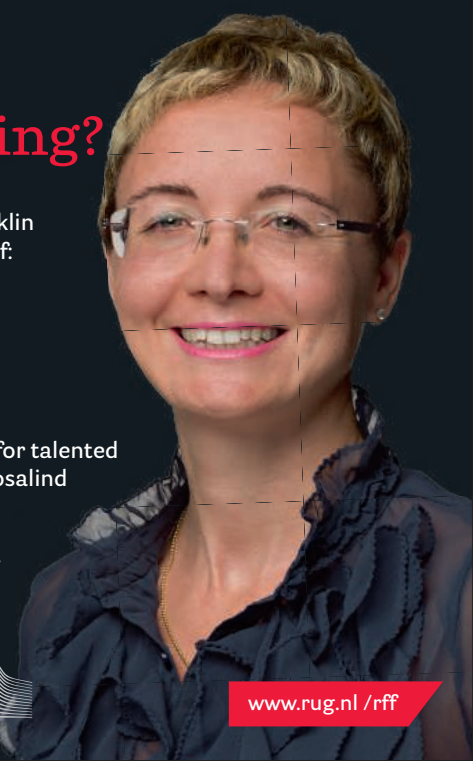
Your excellent research record may well earn you a position as a Rosalind Franklin Fellow at the University of Groningen and allow you to follow in the footsteps of:

Dr Angela Casini

› Expertise: Medicinal Inorganic and Bioinorganic Chemistry
› European Medal for Biological Inorganic Chemistry (EUROBIC11 Award)

The University of Groningen currently has 30 Tenure Track positions available for talented female researchers in various areas within the framework of the prestigious Rosalind Franklin Fellowship Programme. More information: www.rug.nl/rff

The University of Groningen (1614): an international top 100 research university in the North of the Netherlands.



layar Scan with Layar!

The RFF Programme is partly financed by the European Union

European Commission

www.rug.nl /rff

eli attosecond

ELI-HU Research and Development Non-Profit Limited Liability Company is looking for
DIVISION HEAD FOR THE SCIENTIFIC APPLICATION DIVISION OF THE ELI-ALPS RESEARCH INFRASTRUCTURE

The ELI Attosecond Light Pulse Source (ELI-ALPS)
research centre to be built in Szeged (Hungary) will be devoted to the study of ultrafast dynamics on the femto/attosecond timescale in atoms, molecules, plasmas and biological samples.

The Division Head is expected to be the driving force in the definition/selection of the research topics/activities and the formation/coordination of the research groups of the division that will pursue research in a broad spectrum of high harmonics, fast particle and laser applications at ELI-ALPS.

You are welcome to **submit your application** along with your detailed CV in English to **allas@eli-alps.hu**

SZÉCHENYI 2020
Hungarian Government
European Union
European Regional Development Fund
INVESTING IN YOUR FUTURE

UNIVERSITY OF CALIFORNIA
UC RIVERSIDE

PROFESSOR & CHAIR
Department of Bioengineering

The Department of Bioengineering invites applications for a senior faculty and department Chair position (full professor rank) beginning the 2015/16 academic year. Exceptional candidates in all areas of bioengineering will be considered.

The department offers BS, BS/MS, MS, and PhD degrees, with a current enrollment of approximately 100 graduate and 350 undergraduate students. Our graduate program is a gender-balanced blend of US and international students, with two-thirds of the PhD students being domestic, and of those, one-fourth are underrepresented minorities. Since 2011, ten PhD students have received the prestigious NSF Graduate Research Fellowship. The BS degree program is fully accredited by ABET since 2011.

The search committee seeks internationally recognized candidates in the field of Bioengineering/Biomedical Engineering, with distinguished record in academic scholarship, research, and leadership. The successful candidate will have the opportunity to enhance the existing and build new strengths in the department, and is expected to create research and educational opportunities with the new School of Medicine. UCR is entering a period of accelerated growth, with plans for hiring 300 new faculty members in the next 5 years and construction of new research facilities.

Full consideration will be given to applications received by **December 1, 2014**, but the search will continue until the position is filled. Inquiries should be directed to Professor Dimitrios Morikis at **dmorikis@ucr.edu**. Applications should be submitted via:
http://www.engr.ucr.edu/facultysearch/

The University of California is an Equal Opportunity/Affirmative Action/Disability/Veterans Employer.

http://www.bioeng.ucr.edu/

Smithsonian
National Museum of Natural History

SYSTEMATIC ENTOMOLOGIST

The Smithsonian's National Museum of Natural History seeks a systematic entomologist to conduct integrative, collections-based research focused on terrestrial arthropods or aquatic insects. The successful candidate is expected to develop an internationally recognized research program utilizing modern methods, which may include bioinformatics, in pursuing systematic research on a terrestrial arthropod or aquatic insect group with relevance to phylogenetics, genetics, evolution, morphology, behavior, biogeography, biodiversity, ecology, or related fields. Frequent publication of highly regarded papers in competitive, peer-reviewed journals, curation of collections in specialty area, service to the scientific community in leadership capacities, acquisition of external funding, engagement in outreach activities, and mentorship of students are expected.

This is a Federal Civil Service position for which U.S. citizenship is required. It will be filled at the GS-12 level ($75,621-$80,622 per year). **College transcripts and proof of U.S. accreditation for foreign study must be submitted online by the closing date of announcement or your application will be disqualified**. For application procedures go to www.sihr.si.edu and refer to Announcement 14A-JW-299547-DEU-NMNH. Applications and all supporting documentation must be received online by **Friday December 05, 2014** and must reference the announcement number. Applicants will be notified by e-mail when their applications are received.

The Smithsonian Institution is an Equal Opportunity Employer.

SCHOOL OF MEDICINE
INDIANA UNIVERSITY

Tenure Track Faculty Positions in Solid Tumors

Indiana University Melvin and Bren Simon Cancer Center and the Department of Biochemistry and Molecular Biology at Indiana University School of Medicine are jointly seeking applications for tenure track positions at all ranks to establish a rigorous research program focusing on solid tumors. Indiana University School of Medicine offers a highly interactive scientific environment with many multidisciplinary centers and state-of-the-art core facilities including transgenic, imaging, genomic, proteomic, and chemical genomics (http://www.medicine.iu.edu/research), as well as a one teraFLOP/s supercomputer that has time dedicated to bioinformatics computing, a Biobank with >2 billion medical records, active genomics projects, and a robust graduate training program. IU Simon Cancer Center is an NCI designated cancer center with basic and clinical programs ranging from understanding the basic biology of the normal organs to first-in-human clinical trials. The cancer center is also the home of Susan G. Komen normal breast tissue bank, which collects and stores breast tissue, serum, plasma, and DNA from healthy donors.

Candidates with research interests in solid tumors and programs complement or strengthen the existing research activities in the cancer center and the department, or who bring novel approaches and/or expertise in signaling mechanisms, systems biology, proteomics/genomics, bioinformatics, microRNA-mediated processes, epigenetics, metabolism, chemical biology, and genetic/disease model systems are encouraged to apply. Successful applicants are expected to develop innovative, independent and extramurally funded research programs and participate in the activities of the cancer center and the department. Highly competitive salary, start-up funds and laboratory space will be provided.

Minimal qualifications for the positions include an MD and/or PhD, post-doctoral experience, and clear evidence of research productivity for junior investigators, and a distinguished research/funding record for senior level positions. Interested candidates should send: (1) a curriculum vitae; (2) contact information for three references; and (3) a 1-2 page statement outlining the applicant's future research plans. Send all three as one PDF file by e-mail to **chasmill@iupui.edu** with **'Cancer Position'** as the subject of the message. Deadline for application is **December 12, 2014**.

Indiana University is an Equal Opportunity Employer committed to building a culturally diverse intellectual community and strongly encourages applications from women and minorities.

INSTITUT PASTEUR

Department of Parasites and Insect Vectors

FACULTY POSITIONS IN PARASITES AND INSECT VECTORS

The Institut Pasteur in Paris announces an international call for outstanding candidates at all levels to establish independent research groups in the Department of Parasites and Insect Vectors. Preference will be given to studies of trypanosomes/tsetse flies, *Leishmania*/sandflies, malaria/*Anopheles*, and *Toxoplasma*. We expect to recruit a new faculty member in each of the following areas: (i) field or clinical research emphasizing epidemiology, pathogenesis, intervention studies, transmission, or populations of parasites or vectors, and (ii) laboratory-based studies on all aspects of parasite or vector biology. Attractive start-up and ongoing support includes salary, equipment, and operating costs. In addition, Institut Pasteur provides access to state-of-the-art technology platforms, and to laboratories and research infrastructure in disease-endemic regions through the Pasteur International Network.

The application should comprise the following (in order) in a single pdf file: (i) A brief introductory letter, (ii) CV and full publication list, (iii) A description of past and present research activities (4-5 pages with 1.5 spacing), (iv) The proposed research project (8-10 pages with 1.5 spacing). Separately, provide the names of 3 scientists from whom letters of recommendation can be sought, together with the names of scientists with a potential conflict of interest from whom evaluations should not be requested.

Applications and requests for information should be addressed to **parasitology@pasteur.fr** by **15 January 2015**. Short-listed candidates will be invited for interviews in early 2015 and decisions will be announced by mid-2015.

UNIVERSITY OF DENVER
1 8 6 4

Department of Biological Sciences
Assistant Professor – Cellular Neuroscience

The Division of Natural Sciences and Mathematics at the University of Denver has been expanding our Molecular Life Sciences Initiative with 12 tenure-track hires in recent years. The Department of Biological Sciences invites applicants for a tenure track faculty position at the Assistant Professor level to begin September 1, 2015. We are seeking cellular neuroscientists that use biophysical methods to study basic questions in neurobiology that include but are not limited to the study of membrane trafficking and exocytosis, signal transduction, and cell physiology. Individuals applying advanced fluorescence imaging or electrophysiology are encouraged to apply as are individuals working with model organisms or in vitro culture systems. The successful candidate will have a Ph.D. and post-doctoral experience in an appropriate field, will develop an extramurally funded research program, will supervise Ph.D. and M.S. students and undergraduate research projects and will teach undergraduate and graduate courses in area of expertise. All candidates must submit their application through **https://dujobs.silkroad.com/**. Information on Departmental programs can be found at **http://www.du.edu/nsm/departments/biologicalsciences/**. Successful applicants will also be eligible to participate in the interdepartmental Molecular and Cellular Biophysics Ph.D. program **http://www.du.edu/nsm/departments/molecularandcellular/index.html**.

The online application should include: a curriculum vitae, and separate statements of research interests and teaching philosophy and two recent publications. In addition, at least three recommenders should email letters of reference to: Faculty Search Committee, University of Denver, Department of Biological Sciences at **biology.rec@du.edu**. The review of applications will begin **November 15, 2014** and continue until the position is filled. Contact Cedric Asensio at **cedric.asensio@du.edu** if you have questions regarding the search.

The University of Denver is committed to enhancing the diversity of its faculty and staff and encourages applications from women, minorities, members of the LGBT community, people with disabilities and veterans. The University is an Equal Opportunity/Affirmative Action Employer.

Southwest Jiaotong University, P.R.China Anticipates Your Working Application

Southwest Jiaotong University (SWJTU), founded in 1896, situates itself in Chengdu, the provincial capital of Sichuan. It is a national key multidisciplinary "211" and "985 Feature" Projects university directly under the jurisdiction of the Ministry of Education, featuring engineering and a comprehensive range of study programs and research disciplines spreading across more than 20 faculties and institutes/centers. Boasting a complete Bachelor-Master-Doctor education system with more than 2,500 members of academic staff, our school also owns 2 first-level national key disciplines, 2 supplementary first-level national key disciplines (in their establishment), 15 first-level doctoral programs, 43 first-level master programs, 75 key undergraduate programs, 10 post-doctoral stations and more than 40 key laboratories at national and provincial levels.

Our university is currently implementing the strategy of "developing and strengthening the university by introducing and cultivating talents". Therefore, we sincerely look forward to your working application.

More information available at http://www.swjtu.edu.cn/

I. Positions and Requirements

A.High-level Leading Talents

It is required that candidates be listed in national top talents programs such as ***Program of Global Experts, Top Talents of National Special Support Program, "Chang Jiang Scholars", China National Funds for Distinguished Young Scientists and National Award for Distinguished Teacher.***

Candidates are supposed to be no more than 50 years old. The limitation could be extended in the most-needed areas of disciplinary development.

Candidates who work in high-level universities/institutes and reach the above requirements are supposed to be no more than 45 years old.

B. Young Leading Scholars

Candidates are supposed to be listed in or qualified to apply for the following programs:

•National Thousand Young Talents Program

•The Top Young Talents of National Special Support Program(Program for Supporting Top Young Talents)

•Science Foundation for the Excellent Youth Scholars

Candidates should have good team spirit and leadership, outstanding academic achievements, broad academic vision and international cooperation experience and have the potential of being a leading academic researcher.

C. Excellent Young Academic Backbones

Candidates under 40 years old are expected to graduate from high-level universities/institutes either in China or other countries. Those who are professors, associate professors and other equal talents from high-level universities/institutes overseas could be employed as professors and associate professors as well.

D. Excellent Doctors and Post Doctoral Fellows

Candidates under 35 years old are supposed to be excellent academic researchers from high-level universities either in China or other countries.

II. Treatments

The candidates will be provided with competitive salaries and welfares that include settling-in allowance, subsidy of rental residence, start-up funds of scientific research, assistance in establishing scientific platform and research group as well as international-level training and promotion . As for outstanding returnees, we can offer further or specific treatments that can be discussed personally.

III . Contact us:

Contacts: Ye ZENG & Yinchuan LI Telephone number: 86-28-66366202 Email: *talent@swjtu.edu.cn*

Address: Human Resources Department of SWJTU, the western park of high-tech zone, Chengdu, Sichuan, P.R.China, 611756

http://www.swjtu.edu.cn/

北京大学 深圳研究生院 Peking University Shenzhen Graduate School

Five tenure-track positions at the Associate Professor level in the areas of Chemistry and Biology

The School of Chemical Biology and Biotechnology (SCBB) at Peking University Shenzhen Graduate School (PKUSZ) invites applications for five tenure-track positions at the Associate Professor level in the areas of Chemistry and Biology. Subfields of particular interest are biosynthesis, structural biology, cellular/molecular neuroscience, cancer biology and vascular or inflammation biology.

Located in Shenzhen, the SCBB of PKUSZ is dedicated to promote basic and applied research bridging chemistry and biology. Applicants with a strong interest and collaborative experiences in the interdisciplinary field of chemical biology are particularly encouraged to apply. Successful candidate shall complement and enhance the existing expertise of our faculty members, and is expected to establish an internationally competitive independent research program.

Applicants should hold a Ph.D. degree; have substantial postdoctoral training with a record of excellent research accomplishment. Complete application should include curriculum vitae, a 2-page description of research accomplishments, a 3-page description of future research directions, and three letters of recommendation. All application materials and enquires should be sent to:mengf @pkusz.edu.cn.

http://www.pkusz.edu.cn/

南京工业大学 NANJING TECH UNIVERSITY

海外领军人才招聘

Overseas Talents Recruitment

Nanjing Tech University, with a history of more than one hundred years, is a multidisciplinary university with a particular strength in engineering.

Aiming at excellence and innovation, Nanjing Tech University is set to become a first-class research university with a global vision. We are now seeking outstanding academic and research leaders in the following and related fields: Basic disciplines from within the Physical Sciences; Cutting edge disciplines from within the Life Sciences; Applied disciplines from within the Information Sciences; Humanities represented by Management Science.

Applicants should have a Ph.D. with at least 3-years research experience from leading universities or institutes. Candidates should demonstrate an internationally recognized research record and outstanding achievements. Successful candidates are expected to develop vigorous research programs and lead an independent research team. Successful candidates will be provided with a competitive relocation fee and salary package, generous start-up funds and spacious laboratories.

Interested candidates should visit **http://rczyb.njtech.edu.cn** for application details.

Phone: **Ms. Wang +86-25-58139148.**

E-mail: **job@njtech.edu.cn**

武漢大學

Faculty Positions Available at The IAS and The MRI, Wuhan University, Wuhan, China

Two newly founded institutes at Wuhan University in China, the Institute for Advanced Studies (IAS) and the Medical Research Institute (MRI), cordially invite applications for ~50 each, open-rank faculty positions in Biology, Chemistry, Physics, Material Sciences, and Medical Sciences.

All applicants must have a Ph. D or MD and a successful postdoctoral experience. Successful candidates will be expected to establish an active research program in relevant disciplines. We offer internationally competitive recruitment packages.

The applicants should submit, electronically, a full CV, a research statement and contact information of three referees in a single PDF file to wdgyy@whu.edu.cn (for IAS positions) or shuoffice@whu.edu.cn (for MRI positions).

Applications that apply for both institutes at the same time will not be accepted and further processed.

http://hr.whu.edu.cn/

UT SOUTHWESTERN MEDICAL CENTER

Hamon Center for Regenerative Science and Medicine

The Center in Regenerative Science and Medicine (CRSM) is a new initiative recently launched by UT Southwestern Medical Center, led by Eric N. Olson, Ph.D. and supported by an endowment from the Hamon Foundation. The CRSM incorporates discovery science, translational research, and clinical application, building on UT Southwestern's solid research foundation and clinical enterprise. The vision of CRSM is to decipher fundamental mechanisms of tissue formation and to pioneer new approaches to rejuvenate and regenerate damaged organs.

We are seeking to hire two new faculty members at the rank of Assistant or Associate Professor (tenure track). We are looking for accomplished research scientists with expertise in stem cell biology, iPS disease models, direct reprogramming, or tissue/bioengineering approaches. Preference will be given to those individuals examining the molecular mechanisms of human disease. Consideration will be given to individuals with a PhD, MD, or MD/PhD.

Attractive recruitment packages, including salary support, state-of-the-art core facilities, and exceptional laboratory space are available. UT Southwestern has a vibrant graduate program and an atmosphere of collegiality and collaboration.

Applicants should submit a curriculum vitae containing a summary of past research accomplishments, a statement of future objectives, and names of three references via email to:

Eric N. Olson, PhD
Hamon Center for Regenerative Science and Medicine
University of Texas Southwestern Medical Center
CRSM@UTSouthwestern.edu

UT Southwestern Medical Center is an Affirmative Action/Equal Opportunity Employer. Women, minorities, veterans and individuals with disabilities are encouraged to apply.

INSTITUTE OF BIOSCIENCES AND TECHNOLOGY
TEXAS A&M HEALTH SCIENCE CENTER

Faculty Positions in Biomedical/Health Science Research
Institute of Biosciences and Technology,
Center for Epigenetics & Disease Prevention

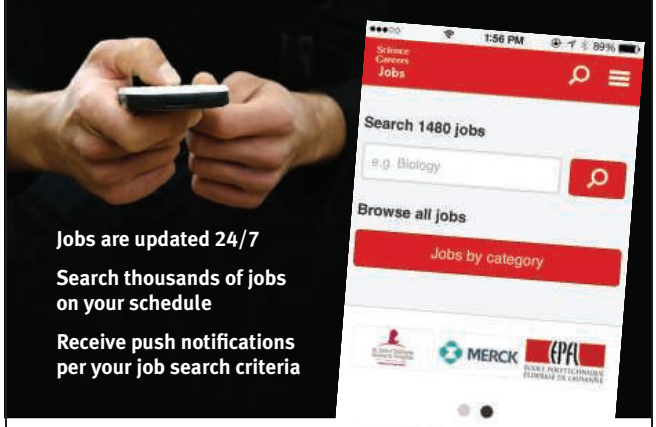
The Texas A&M Health Science Center **Institute of Biosciences and Technology** (IBT), http://ibt.tamhsc.edu/, is an internationally recognized leader in biomedical and health science research located at the Texas Medical Center in Houston, TX, with existing strengths in Epigenetics, Cancer/Stem Cell Biology, Infectious Disease, and Environmental Health.

The IBT is entering an expansion phase and will be recruiting faculty members into the new Center for Epigenetics & Disease Prevention (http://www.ibt.tamhsc.edu/research/cedp/). New hires will receive **highly competitive packages for salary, start-up, and support for graduate education, along with outstanding laboratory and office space** in the Texas A&M Health Science Center Alkek Building in the Texas Medical Center.

Applicants should have an M.D., Ph.D. or M.D./Ph.D. degree in biochemistry, cellular and molecular biology, genetics, or a related science, and an outstanding publication record in the epigenetics area (first or senior author in the highest impact journals relevant to the field). Applicants at the Assistant Professor level should have at least 3 years post-doctoral experience. Current/ongoing extramural funding would be viewed favorably during the review process. Successful candidates will be expected to establish an independent research group, conduct highly meritorious research, establish collaborations with other investigators in the Texas Medical Center and components in the Texas A&M University System, and to obtain significant extramural funding. Applications will be received and evaluated on a rolling basis, starting **November 3, 2014**. To apply, please send a cover letter, curriculum vitae, statement of research interests, copies of two key publications, and at least three reference letters to: **Dr. Roderick H. Dashwood, Search Committee Chair, Institute of Biosciences and Technology, 2121 W. Holcombe Blvd., Houston, TX 77030-3303; E-mail: rdashwood@ibt.tamhsc.edu**.

The Texas A&M Health Science Center is an Equal Opportunity/Affirmative Action/Veterans/Disability Employer.

Introducing the new
***Science* Careers Jobs app from Science**



Jobs are updated 24/7

Search thousands of jobs on your schedule

Receive push notifications per your job search criteria

Get a job on the go.
Search worldwide for thousands of scientific jobs in academia, industry, and government. Keep your finger on the pulse of your field—set up an alert for the type of job you are looking for and receive push notifications when jobs are posted that meet your criteria. The application process is seamless, linking you directly to job postings from your customized push notifications.

Scan this code to download app or visit **apps.sciencemag.org** for information.

Science Careers
From the journal *Science* AAAS
ScienceCareers.org

IOWA STATE UNIVERSITY

Tenure-Track Faculty Position in Population Biology

The Ecology, Evolution & Organismal Biology (EEOB) Department seeks a scholar employing theoretical or empirical approaches to understand the ecological or evolutionary dynamics of populations in response to abiotic or biotic stressors. Research may investigate the characteristics of individual or interacting species of any taxon in the context of population responses to environmental stress, broadly defined to include, for example, global climate change, habitat disturbance, or altered species interactions (invasive species, disease agents, predators, competitors, mutualists), among others. Successful candidates are expected to establish a vibrant, externally funded research program, demonstrate an ability to work collaboratively within existing research strengths at ISU (including a Presidential Translational Health Initiative), and teach undergraduate and graduate education courses, including courses in their area(s) of expertise.

Candidates must hold a Ph.D. by the time of appointment.

All applications must be submitted electronically at **www.iastatejobs.com** (vacancy **#400041**). Please be prepared to attach a letter of application, including concise teaching and research statements, curriculum vitae, and up to three reprints. Submission of three confidential letters of recommendation should be arranged as per instructions in the on-line application system. The positions will remain open until filled. Full consideration will be given to applications received by **6 November 2014**. For additional information please email **brent@iastate.edu**.

Iowa State University is an EO/AA Employer. All qualified applicants will receive consideration for employment without regard to race, color, religion, sex, national origin, disability, or protected Vets status. Iowa State University is an AAU-member comprehensive, land grant, Carnegie Doctoral/Research Extensive University with an enrollment of over 33,000 students. The university is located in Ames, IA, one of the nation's most highly rated metropolitan areas of its size (http://www.iastate.edu/about/ames.php) and is only 35 miles north of Des Moines. ISU is committed to achieving inclusive excellence through a diverse workforce and is dedicated to supporting work-life balance through an array of flexible policies.

Chief Executive Officer

Challenging opportunity for a respected senior scholar to lead South Africa's major research funding agency

The Board of the National Research Foundation invites nominations and applications for the position of Chief Executive Officer.

The National Research Foundation (NRF) is an autonomous statutory science council. In accordance with Act 23 of 1998, the NRF supports and promotes research, human resource development and the development of science infrastructure in order to facilitate the creation of knowledge, innovation and development in all fields of research, science and technology, including indigenous knowledge, thereby contributing to the improvement of the quality of life of all the people of the Republic of South Africa. As a statutory body its role is to stimulate research and promote the development of high-level human resources in the research system. The Foundation is also responsible for the operation of seven national research facilities and for the co-ordination of a range of regional and international collaborations.

The CEO of the NRF is its chief administrative and executive officer and is accountable to the Board of the NRF of which s/he is a member. The incumbent will represent the Foundation in its dealings with the community of scholars and researchers in higher education, research institutions, government, as well as the private and public sectors.

Since the NRF has significant global engagements, it will be necessary for the incumbent to operate effectively in this context.

The CEO of the NRF should be a distinguished scholar who is capable of providing strategic research management ability and intellectual leadership across the broad sweep of the natural, social, human, health, agricultural and engineering sciences. S/he must also have a proven and accomplished record in the management of a complex, multi-faceted organisation, including financial and human resources. This leadership would have to be a uniting and constructive force for change within the context of the reconstruction and development of the South African research and science capacity and society. In particular, s/he would have to be committed to the development of a set of imaginative and innovative programmes to deal with the vast race, gender and disciplinary imbalances that characterise the national science system.

Applications or nominations, including a statement of intent, a detailed CV which includes the names, addresses and contact numbers of at least three referees who are willing to provide a reference, should be submitted by 7 November 2014 in confidence to: nrf@humanjobs.co.za

Further information regarding the post and the selection procedures can be obtained from Mr PB Thompson, Group Executive: HR & Legal Services at +27 (12) 481 4073 or at patrick@nrf.ac.za

NRF website: www.nrf.ac.za

The NRF is committed to employment equity and redress.
Correspondence will be conducted with the short-listed candidates only.

NRF National Research Foundation

IOWA STATE UNIVERSITY

Tenure-Track Faculty Positions in Macroecology and Plant and Microbial Ecology

As part of a major interdisciplinary hiring initiative in the College of Liberal Arts and Sciences at Iowa State University (ISU), a new joint initiative by the Departments of Geological and Atmospheric Sciences; Ecology, Evolution and Organismal Biology; and Economics and the Greenlee School of Journalism and Communication aims to expand our capabilities for fundamental research on sustainable environmental systems. Multiple new hires in the field of Sustainability Science (http://www.las.iastate.edu/faculty-staff/faculty-careers/sustainability-science) are planned for the next 2-3 years and should expect to benefit from and contribute to the interaction and collaboration among these and other departments.

As part of this initiative, the Department of Ecology, Evolution and Organismal Biology invites applications for tenure-track faculty positions in macroecology and in plant and/or microbial ecology at the Assistant Professor level. These new faculty will have the opportunity to join a synergistic focal group in the area of Sustainability Science that will serve to facilitate team building and integrative research.

The **macroecology** hire will contribute to research examining integrated functioning of biological and physical components across multiple scales and the role of spatial and temporal patterns and processes as they relate to the development of sustainable environmental systems. Research could include state-of-the-art computational approaches, developing and applying ecological theory, and/or novel empirical analyses. This hire could also develop research that interprets and reports on large data sets across developing research networks spanning a range of scales.

The **plant or microbial ecology** hire will contribute to integrated research addressing biological and physical controls on material and energy fluxes in environmental systems. The person will examine plant and/or microbial processes or interactions, and might employ a spectrum of investigative tools and technologies across multiple scales.

Candidates must hold a Ph.D. by the time of appointment and are expected to establish successful, externally funded research programs and to teach at the undergraduate and graduate levels.

All applications must be submitted electronically at **www.iastatejobs.com** (**vacancy #: 400025 for macroecology** and **#400026 for plant and microbial ecology**). Please be prepared to attach a letter of application, including concise teaching and research statements, curriculum vitae, and up to three reprints. Submission of three confidential letters of recommendation should be arranged as per instructions in the on-line application system. The positions will remain open until filled. Full consideration will be given to applications received by November 21, 2014. For additional information please email macroeco@iastate.edu or plantmic@iastate.edu.

Iowa State University is an EO/AA Employer. All qualified applicants will receive consideration for employment without regard to race, color, religion, sex, national origin, disability, or protected Vets status. Iowa State University is an AAU-member comprehensive, land grant, Carnegie Doctoral/Research Extensive University with an enrollment of over 33,000 students. The university is located in Ames, IA, one of the nation's most highly rated metropolitan areas of its size (http://www.iastate.edu/about/ames.php) and is only 35 miles north of Des Moines. ISU is committed to achieving inclusive excellence through a diverse workforce and is dedicated to supporting work-life balance through an array of flexible policies.

Science Careers online @sciencecareers.org



Nontraditional Careers: Opportunities Away From the Bench

Webinar

Want to learn more about exciting and rewarding careers outside of academic/industrial research? View a roundtable discussion that looks at the various career options open to scientists and strategies you can use to pursue a nonresearch career.

Now Available On Demand
www.sciencecareers.org/webinar

Produced by the *Science*/AAAS Business Office.

Science Careers
From the journal *Science* AAAS

POSITIONS OPEN

CARNEGIE INSTITUTION FOR SCIENCE

TENURE-TRACK POSITION in Cellular/Molecular Neuroscience Carnegie Mellon University

The Department of Biological Sciences at Carnegie Mellon University seeks applicants for a tenure-track position, preferably at the assistant professor level. This search is associated with the BrainHub (**website: http://www.cmu.edu/research/brain/**), a campus-wide initiative to expand brain research across multiple disciplines within the university and with significant investment in facilities for imaging, animal handling, computing and high-throughput technologies. Applications are encouraged from outstanding individuals whose research addresses molecular mechanisms of neural function and disease including, but not limited to, the formation and function of neural circuits, synaptic biology, the molecular basis of neurological disease, and the application of new experimental technologies (e.g., imaging or sequencing tools for real-time analysis of neural function, protein localization, or gene expression in discrete neural subsets or individual cells). The Department of Biological Sciences provides a highly collaborative and interdisciplinary environment that integrates modern biological research at cellular and sub-cellular levels of organization (**http://www.cmu.edu/bio**). Successful candidates will have the opportunity to join the Center for the Neural Basis of Cognition, an interdisciplinary and collaborative group of neuroscientists from Carnegie Mellon and the University of Pittsburgh. Carnegie Mellon University offers highly competitive salaries and startup funding, and Pittsburgh is an urban environment that provides a high quality of life.

Review of applications will begin on November 1, 2014. Applications, including a cover letter, curriculum vitae, research and teaching statements and copies of no more than three relevant papers should be submitted electronically (in PDF format) to **https://apps.bio.cmu.edu/facultySearch/.** Applicants should also arrange for at least three reference letters (also in PDF format) to be sent directly to **e-mail: bio-facsearch@andrew.cmu.edu.**

Carnegie Mellon considers applicants for employment without regard to, and does not discriminate on the basis of, gender, race, protected veteran status, disability, or any other legally protected status.

AQUATIC ECOLOGY

The University of Arkansas Department of Biological Sciences seeks applicants for an **ASSISTANT PROFESSOR** nine-month tenure-track position in Aquatic Ecology (Position Y15932). Requirements: Ph.D. in ecology or related field, strong research record. Expectations: establish externally funded research program, contribute to undergraduate-graduate education, professional service. Application information **website: http://biology/uark.edu/News/Aquatic-Ecology.** Submit application (cover letter, curriculum vitae, research narrative, teaching statement, three reference letters) via Interfolio (**website: apply.interfolio.com/26778**) by 7 November 2014 for full consideration. Contact **Dr. Marlis Douglas** (**e-mail: aquaecol@uark.edu**). *Affirmative Action/Equal Opportunity Institution/Veterans/Disabled.*

The Singapore Centre on Environmental Life Sciences Engineering (SCELSE) at Nanyang Technological University is seeking candidates to work as **POSTDOCTORAL RESEARCHERS** investigating the structure-function activity and mechanisms of action of a potent class of antimicrobial polysaccharide molecules for the control of infections. Ph.D.s in Microbiology, Medicinal Chemistry, Molecular Biology, or relevant field with strong track record of publication in related disciplines are welcome to apply. Applicants should submit a cover letter describing their relevant research experience and career goals, as well as full curriculum vitae and the names of three references to **Prof. Kimberly Kline** at **e-mail: kkline@ntu.edu.sg.** Only successful applicants will be contacted.

POSITIONS OPEN

U.S. POSTAL SERVICE

Statement required by the Act of 12 August 1970, Section 3685, Title 39, United States Code, showing the ownership, management, and circulation of:

1–9. *Science*, Publication No. 0036-8075, is published weekly on Friday, except the last week in December, at 1200 New York Avenue, N.W., Washington, DC 20005. Date of filing: 22 September 2014. This is also the address of the publisher, the editor, and the managing editor, who are, respectively, Beth Rosner, Marcia McNutt, and Monica M. Bradford.

10. The owner is the American Association for the Advancement of Science, 1200 New York Avenue, N.W., Washington, DC 20005. Stockholders: None.

11. Known bondholders, mortgages, and other security holders owning or holding 1 percent or more of total amount of bonds, mortgages, or other securities: None.

12. The purpose, function, and nonprofit status of this organization and the exempt status for federal income tax purposes have not changed during the preceding 12 months.

13–15. The average number of copies of each issue during the preceding 12 months is (A) Total number of copies printed: 106,339; (B) Paid circulation: 84,361; (1) Paid/Requested outside-county mail subscriptions stated on form 3541: 71,462; (2) Paid/Requested in-county subscriptions stated on form 3541: 0; (3) Sales through dealers and carriers, street vendors, counter sales: 12,886. (4) Other classes mailed through USPS: 14; (C) Total paid circulation: 84,361; (D) Free distribution: samples, complimentary, and other free copies: 19,975; (1) Outside-county as stated on form 3541: 2,562; (2) In-county as stated on form 3541: 0; (3) Other classes mailed through the USPS: 1; (4) Free distribution outside of mail carrier or other means: 17,412; (E) Total free distribution: 19,975; (F) Total distribution: 104,336; (G) Copies not distributed: 2,003; (H) Total: 106,339; (I) Percent paid and/or Requested Circulation: 80.9%.

Actual number of copies of single issue (9/12/2014) published nearest to filing date are (A) Total number of copies printed: 271,450; (B) Paid circulation: 80,923; (1) Paid/Requested outside-county mail subscriptions stated on form 3541: 68,756; (2) Paid/Requested in-county subscriptions stated on form 3541: 0; (3) Sales through dealers and carriers, street vendors, counter sales: 12,153; (4) Other classes mailed through USPS: 10; (C) Total paid circulation: 80,923; (D) Free distribution: Samples, complimentary, and other free copies: 188,527; (1) Outside-county as stated on form 3541: 2,664; (2) In-county as stated on form 3541: 0; (3) Other classes mailed through the USPS: 1; (4) Free distribution outside of mail: Carrier or other means: 185,862; (E) Total free distribution: 188,527; (F) Total distribution: 269,450; (G) Copies not distributed: 2,000; (H) Total: 271,450; (I) Percent paid and/or Requested Circulation: 30.0%.

I certify that the statements made above are correct and complete. (signed) Beth Rosner, Publisher.

MARKETPLACE

PREMIUM REFURBISHED
GC/MS and LC/MS Systems
Save up to 50%
agilent.com/chem/refurbished
Agilent Technologies



AAAS is here –
helping scientists achieve career sucess.

Every month, over 400,000 students and scientists visit ScienceCareers.org in search of the information, advice, and opportunities they need to take the next step in their careers.

A complete career resource, free to the public, *Science* Careers offers hundreds of career development articles, webinars and downloadable booklets filled with practical advice, a community forum providing answers to career questions, and thousands of job listings in academia, government, and industry. As a AAAS member, your dues help AAAS make this service available to the scientific community. If you're not a member, join us. Together we can make a difference.

To learn more, visit
aaas.org/plusyou/sciencecareers

AAAS + U = Δ

UNIVERSITY OF CALIFORNIA
UCRIVERSIDE

DIRECTOR AND ENDOWED CHAIR
ENVIRONMENTAL DYNAMICS AND GEOECOLOGY INSTITUTE

The College of Natural and Agricultural Sciences (CNAS) invites applications for a tenured senior rank position for Director of the new Environmental Dynamics and GeoEcology (EDGE) Institute. The position will occupy a newly endowed chair and will include a tenured faculty position in one of the departments of CNAS. The successful candidate will lead a diverse group of faculty working in environmental change, global change biology, paleoecology, earth sciences, and conservation biology over both deep and contemporary time scales. The successful candidate will be expected to strengthen interdisciplinary collaborations, develop new funding initiatives, and become fully engaged in the research and teaching mission of the institute and the college.

The candidate is expected to develop an independent and innovative research program exploring the impacts and mechanisms of environmental change in arid or semi-arid regions. Appropriate areas of expertise include, but are not limited to: geological/geochemical approaches to address the patterns and drivers of climatic and paleoclimatic change, arid land dynamics, desertification or the global change processes related to arid land expansion, landscape ecology, biogeography or ecosystem ecology in the context of global change.

Applications must include a curriculum vita, statements of research and teaching interests, a perspective on leadership for a new institute, and full contact information for three to five referees. All application materials must be submitted through AP Recruit at: **https://aprecruit.ucr.edu/apply/JPF00236**.

For more information about the position, please contact **Prof. Mary Droser, Chair EDGE Institute Director Search, Department of Earth Sciences, University of California, Riverside, California. 92521**. E-mail contact: **mary.droser@ucr.edu**. Review of applications will begin **December 15, 2014** and will continue until the position is filled. Information about EDGE and the College of Natural and Agricultural Sciences at UCR is available at **http://edge.ucr.edu** and **http://cnas.ucr.edu**.

The University of California is an Affirmative Action/Equal Opportunity Employer. All qualified applicants will receive consideration for employment without regard to race, color, religion, sex, national origin, age, disability, protected veteran status, or any other characteristic protected by law.

Careers in Neuroscience

Special Career Feature

October 31, 2014

Reserve ads by October 14 to guarantee space
Ads accepted until October 27 if space is still available

There's only one **Science**



This feature examines the areas and regions where the career possibilities are expanding and offers advice for scientists building their career in neuroscience.

Why you should advertise in these issues of *Science*:
Reach: Your job ad is seen by 570,400 readers around the globe

Bonus distributions to:
Society for Neuroscience 15–19 November
Washington, DC

Science Careers
From the journal *Science* AAAS

Produced by the *Science*/AAAS Custom Publishing Office.

ScienceCareers.org

To book your ad:

advertise@sciencecareers.org

THE AMERICAS
202-326-6582

EUROPE/ROW
+44 (0) 1223 326500

JAPAN
+81 3 3219 5777

CHINA / KOREA / SINGAPORE / TAIWAN
+86 186 0082 9345

Science Careers online @sciencecareers.org

By **Ayanna Howard**

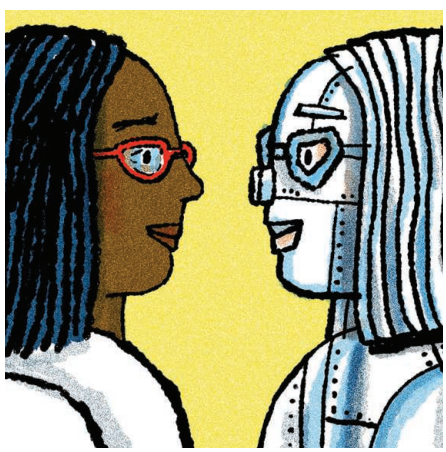
Building the Bionic Woman

I was shielded from stereotypes during my young and impressionable years. I didn't realize they existed until maybe middle school, and by then, I'd already decided I wanted to build the Bionic Woman. ¶ I was always drawn to 'techy' stuff, but I also liked what people would consider typical girly things. I would just as quickly ask for a RadioShack kit as a Betty Crocker oven, and get both. I learned to solder at the same time I was playing with dolls (not necessarily Barbie, although I did collect them for a while and have some that are quite valuable). In the third grade, I started programming in BASIC on a Commodore 64 computer in the basement.

My parents were large influencers in my life. From an early age, I loved math, puzzles, computers, and gaming, and I seemed to have a knack for them. I would watch anything that was science fiction. There was one show I particularly liked: *The Bionic Woman*.

Middle school was the time when everyone started to ask you, "What do you want to do in life? What do you want to be?" I wanted to build the Bionic Woman!

At first I wanted to be a doctor, like the ones who put Jaime—the Bionic Woman—together, but then I took biology and hated it. I believe it was a science teacher who suggested engineering—after all, doctors didn't build the bionic implants; they just did the operation.



"I wanted to build the Bionic Woman!"

College is when I learned about stereotypes. "The only reason you're here is because the school needs diversity." "Maybe you should think about applying to graduate school at XYZ University; they are trying to bump up their minority numbers." When you hear comments like that and you're no longer getting straight A's—and when you don't realize you're actually doing well because everyone else is barely passing—you begin to doubt yourself.

What kept me hopeful was a series of summer internships at NASA's Jet Propulsion Laboratory (JPL). I remember getting some simple, menial task that first summer. I rocked it in less than a week, and they gave me more challenging tasks. I kept hearing, "She can figure out anything. She's great; we'd better not lose her." After the summer I'd go back to college, sit in class, and feel dumb again.

I decided to work at JPL while going to graduate school because I knew I would need that ego boost. When I made a straight 4.0 GPA my first year, I thought I was lucky. When I received a Ph.D. fellowship, I thought I must have been the only one who applied.

I was 1 year out from earning my Ph.D. and had just won my first NASA grant. I arrived at my team-kickoff meeting to find one guy sitting in the room. "They moved the secretaries' meeting down the hall," he said. I held out my hand and said, "Oh, you must be so-and-so. I'm Dr. Howard. I'm running this meeting. Welcome to my team." I had my confidence back.

I started outreach programs for K-12 students and undergraduate women. Every summer, I hired and mentored undergraduate students at JPL; almost all of them continued on to graduate school. Students came to me and said, "I was about to drop out, but I think I can do it now," or "I want to grow up to be a scientist like you," or "You're the coolest." Such unbiased, unfiltered expressions of gratitude, hope, and admiration—they turned the tide for me. I'd never thought of myself as a mentor, but I realized that, just as past words had punched holes through my soul, I could patch holes for others through my own words. In return, my own holes were filled.

Today I'm a full professor, holding an endowed chair. I'm associate director of research for the robotics institute at Georgia Institute of Technology in Atlanta. I'm chief technology officer and founder of a startup. I still run outreach camps for K-12 students, even a robotics camp for children with disabilities. Every so often, in the dark of night, I still get those twinges of self-doubt. But now I can just close my eyes, breath deep, and tell my own self, "You're the coolest." ■

Ayanna Howard is the Motorola Foundation Professor in the School of Electrical and Computer Engineering at Georgia Institute of Technology in Atlanta. For more on life and careers, visit www.sciencecareers.org.

ILLUSTRATION: ROBERT NEUBECKER

Downloaded from www.sciencemag.org on October 9, 2014

Published by AAAS